DOE-BES PI Meeting

Physical Behavior of Materials

March 30 - April 1, 2015

Hilton Washington DC North/Gaithersburg

Program and Abstracts

Chairs: Mark Stockman (GSU), Christoph Boehme (Univ. Utah)

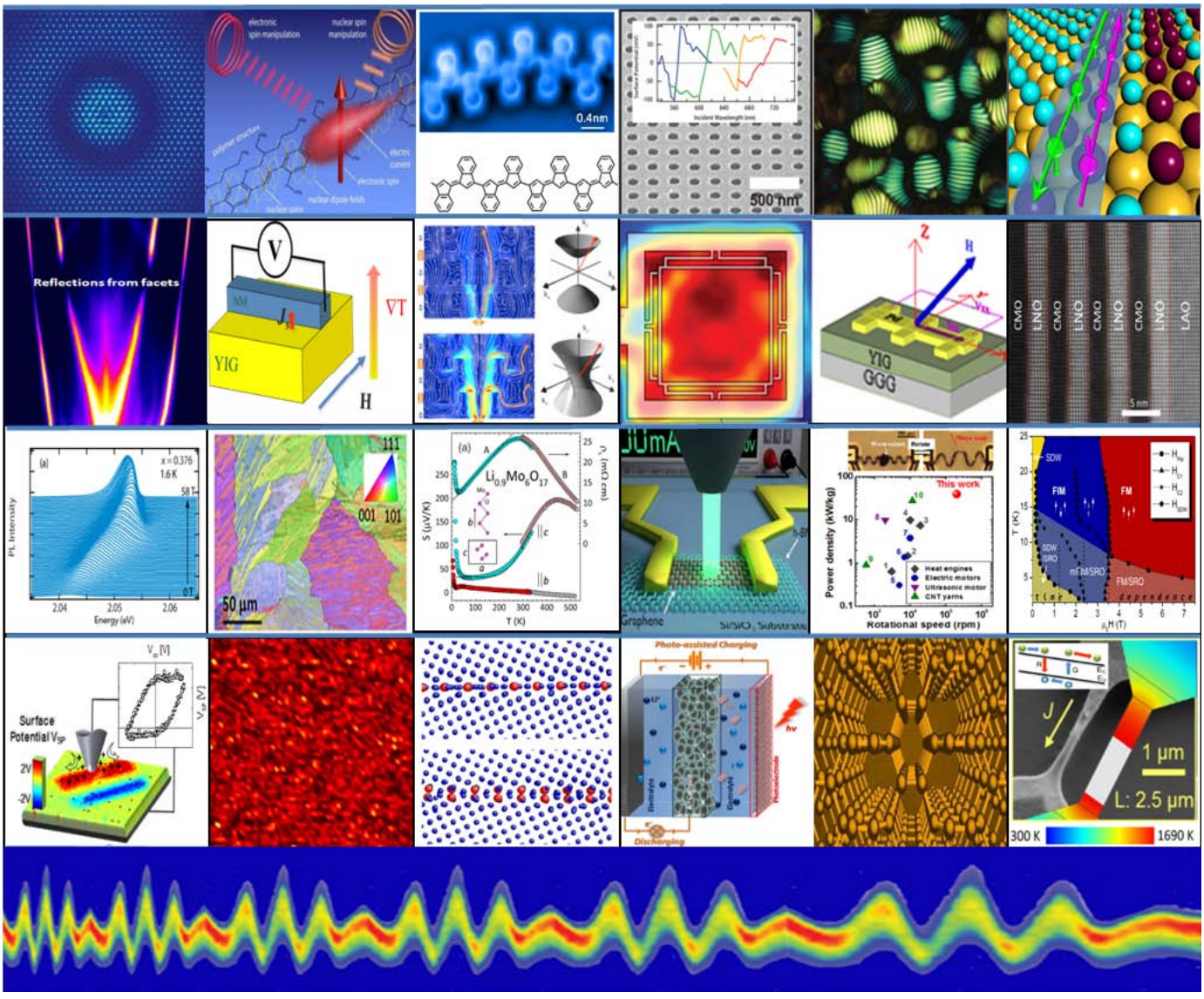

U.S. Department of Energy

Office of Science – Basic Energy Sciences

Division of Materials Sciences and Engineering

Cover Images:

1	2	3	4	5	6
7	8	9	10	11	12
13	14	15	16	17	18
19	20	21	22	23	24

1- Probing excitonic dark states in single-layer tungsten disulphide. (Xiang Zhang)
2- Room temperature coupling between electrical current and nuclear spins in organic light emitting diodes. (Christoph Boehme)
3- Single-bond Imaging Reveals New Molecular Self-assembly Process. (Michael Crommie)
4- Plasmoelectric Potentials in Metal Nanostructures. (Harry Atwater)
5- Orientationally Ordered Colloidal Co-Dispersions of Gold Nanorods and Cellulose Nanocrystals. (Ivan Smalyukh)
6- Large-gap Quantum Spin Hall State on Si Substrate. (Feng Liu)
7- Solid state catalysis mediated synthesis of superconductors. (Qiang Li)
8- A New Method for the Determination of Spin Hall Angle Θ_{SH} . (Chia Ling Chien)
9- Local field topology behind light localization and global metamaterial topological transitions. (Gang Chen)
10- Dynamic Manipulation of Infrared Radiation with MEMS Metamaterials. (Willie Padilla)
11- Spin-Dependent Phenomena in Heterostructures of Strong Spin-Orbit Coupling Metal and Magnetic Insulator. (Jing Shi)
12- Emergent Ferromagnetism at CaMnO3 interfaces. (Yuri Suzuki)
13- Magnetic field induced Direct-to-Indirect Crossover in $Al_xGa_{1-x}As$. (Angelo Mascarenhas)
14- Thin Film Vapor-Liquid-Solid Growth of Semiconductors. (Ali Javey)
15- Extreme Anisotropy of Seebeck Coefficient in a Quasi-one-dimensional Metal. (Joshua Cohn)
16- Thermal and Thermoelectric Transport across Graphene/BN Heterostructures. (Stephen Cronin)
17- Torsional Micro Muscles Activated by Phase Transition. (Junqiao Wu)
18- A new magnetic phase diagram for the quasi-one-dimensional (1D) spin chain $Ca_3Co_2O_6$. (Hariharan Srikanth)
19- New Method Probes Local Electrostatic Effects. (Nina Balke)
20- Terahertz-frequency electronic transport in grapheme. (Irena Knezevic)
21- Effect of Interface Phase Transformations on Diffusion. (Yuri Mishin)
22- Solar Battery: Integrating a Dye-sensitized Photoelectrode into a Li-O_2 Battery. (Yiying Wu)
23- Three-dimensional Metallic Carbon. (Puru Jena)
24- Crystallization and Thermoelectric Transport in Semiconductor Micro- and Nanostructures under Extreme Conditions. (Ali Gokirmak)

This document was produced under contract number DE-AC05-06OR23100 between the U.S. Department of Energy and Oak Ridge Associated Universities.

The research grants and contracts described in this document are supported by the U.S. DOE Office of Science, Office of Basic Energy Sciences, Materials Sciences and Engineering Division.

FOREWORD

This booklet is a summary of the scientific content of the 2015 Physical Behavior of Materials Principal Investigators' Meeting, sponsored by the Division of Materials Sciences and Engineering (DMS&E) of the Department of Energy, Office of Basic Energy Sciences (BES). The meeting was held on March 30 – April 1, 2015, at the Hilton Washington DC North/Gaithersburg, Maryland.

The primary purpose of the Principal Investigators' meetings is to provide an environment for the exchange of ideas and new knowledge among participants, and to foster synergistic activities among researchers in the Physical Behavior Program. For the grantees and BES, it facilitates an overview of the program useful to define future directions for the program and identify promising new research areas. These meetings are designed to stimulate crosscutting and inspiring of new ideas, as it brings together leading experts in diverse fields of interest to our program.

The Physical Behavior of Materials program supports a broad range of exciting research activities, many overlapping condensed-matter physics and materials sciences disciplines. The program has the mission to support fundamental science and use-inspired basic research that promise to bring a better understanding to fundamentals of material's physical behavior under external stimuli. Among the primary scientific interests of the program are electronic, electromagnetic, magnetic and thermal properties of materials that are relevant to the Basic Energy Sciences mission. The program has a rich portfolio in many ground-breaking, high-risk high-reward projects using both experimental and theoretical approaches.

This year's Principal Investigators' Meeting is chaired by Mark Stockman of the Georgia State University, and Christoph Boehme of the University of Utah, and is attended by over 80 scientists. There are 28 oral presentations in 10 oral sessions and over 45 presentations in two poster sessions. The oral presentations are organized to group similar topical research areas. The program includes two invited talks given by Dr. Alexander Efros (NRL) and Prof. Steven Anlage (University of Maryland). The titles of their talks are "A brief history of nanocrystals: Discovery, milestones, and the future" and "Nonlinear superconducting metamaterials," respectively.

We gratefully acknowledge the contributions of all the attendees participating at this meeting and sharing their ideas with other meeting participants. We also gratefully acknowledge the outstanding support of Tammy Click and Verda Adkins-Ferber from the Oak Ridge Institute for Science and Education, and Teresa Crockett of the DMS&E, and the staff of the Hilton Washington DC North/Gaithersburg.

Refik Kortan, Ph.D.
Program Manager
Division of Materials Sciences and Engineering
Office of Basic Energy Sciences
Department of Energy
March 2015

Table of Contents

Poster Abstracts

Physical Behavior of Materials Principal Investigators' Meeting
March 30 – April 1, 2015
Hilton Washington DC North/Gaithersburg MD

Meeting Chairs: Mark Stockman (Georgia State University) and Christoph Boehme (University of Utah)

Sunday, March 29, 2015	
	*** Dinner (On your own) ***
Monday, March 30, 2015	
7:30 – 8:30 am	*** Registration & Breakfast ***
8:30 – 8:40 am	**Welcome, *Meeting Chairs***
8:40 – 9:10 am	**"Division and Program Updates"** Linda Horton Director, Division of Materials Science and Engineering Refik Kortan Program Manager, Physical Behavior of Materials
Session I	***Chair: Christoph Boehme (University of Utah)***
9:10 – 9:40 am	Jing Shi *(University of California, Riverside)* *"Spin-dependent phenomena at magnetic/non-magnetic interfaces"*
9:40 – 10:10 am	Chia Ling Chien *(Johns Hopkins University)* *"Pure spin current phenomena"*
10:10 – 10:40 am	Joshua Cohn *(Miami University)* *"Novel transport and thermoelectric properties of quasi-one-dimensional Mo-oxides"*
10:40 – 11:00 am	*** Break ***
Session II	***Chair: Mark Stockman (Georgia State University)***
11:00 – 11:30 am	Harry Atwater *(California Institute of Technology)* *"Tuning of resonant optical absorption and emission in nanostructures"*
11:30 – 12:00 pm	Ivan Smalyukh *(University of Colorado)* *"Electrically and optically tunable plasmonic guest-host colloids with long-range ordered anisotropic nanoparticles"*

12:00 – 12:30 pm	Katherine Willets *(Temple University)* *"Visualizing electrochemical reactions on plasmonic nanoparticle electrodes"*
12:30 – 1:30 pm	*** Working Lunch (*poster introductions: Session I*) ***

Session III	***Chair: Mark Stockman***
1:30 – 2:30 pm	**Invited Talk: Dr. Alexander Efros *(U.S. Naval Research Laboratory)*** *"A brief history of nanocrystals: Discovery, milestones, and the future"*
2:30 – 3:00 pm	*** Break ***

Session IV	***Chairs: Stockman, Boehme***
3:00 – 5:30 pm	Poster Session I
5:30 – 6:30 pm	*** Dinner *(Scientific highlights of the day: Discussion and input from attendees)* ***

Session V	***Chair: Xiang Zhang (University of California, Berkeley)***
6:30 – 7:00 pm	Gang Chen *(Massachusetts Institute of Technology)* *"Photon thermodynamics and transport in near and far fields"*
7:00 – 7:30 pm	Zhifeng Ren *(University of Houston)* *"High performance thermoelectric materials and flexible transparent electrodes"*
7:30 – 8:00 pm	Evan Ma *(Johns Hopkins University)* *"Atomic structure and bonding in the two metastable states of GST that enable DVDs and phase-change memory devices"*
8:00 – 8:30 pm	Ragaiy Zidan *(Savannah River National Laboratory)* *"Hydrogen and hydrides interaction mechanisms with carbon nanostructures and the formation of novel energy storage and energy conversion systems"*

Session VI	***Chairs: Stockman, Boehme***
8:30 – 10:00 pm	Continuation of Poster Session I

Tuesday, March 31, 2015

7:30 – 8:30 am	*** Breakfast ***
Session VII	***Chair: Alain Karma (Northeastern University)***
8:30 – 9:00 am	Gerbrand Ceder *(Massachusetts Institute of Technology)* *"Similarity functions to datamine structural and chemical similarity between materials"*
9:00 – 9:30 am	Puru Jena *(Virginia Commonwealth University)* *"Penta-graphene: A new carbon allotrope"*
9:30 - 10:00 am	Dimitrios Maroudas *(University of Massachusetts, Amherst)* *"External-field-driven surface stabilization and patterning"*
10:00 – 10:30 am	Irena Knezevic *(University of Wisconsin)* *"Coupling electrons, phonons, and photons"*
10:30 – 11:00 am	*** Break ***
Session VIII	***Chair: Igal Brener (Center for Integrated Nanotechnologies)***
11:00 – 11:30 am	Steve Leone *(Lawrence Berkeley National Laboratory)* *"Charge state dynamics in Semiconducting Nanosystems"*
11:30 – 12:00 am	Mike Crommie *(Lawrence Berkeley National Laboratory)* *"Using Coulomb interactions and covalent coupling to control nanomachines at the single-molecule level"*
12:00 – 12:30 pm	Angelo Mascarenhas *(National Renewable Energy Laboratory)* *"Electronic Raman scattering as an ultra-sensitive probe of strain effects in semiconductors"*
12:30 – 1:30 pm	*** Working Lunch (*poster introductions: Session II*) ***
Session IX	***Chair: Christoph Boehme***
1:30 – 2:30 pm	**Invited Talk: Prof. Steven Anlage *(University of Maryland)*** *"Nonlinear superconducting metamaterials"*
2:30 – 3:00 pm	*** Break ***

Session X	***Chairs: Stockman, Boehme***
3:00 – 5:30 pm	**Poster Session II**
5:30 – 6:30 pm	*** Dinner *(Scientific highlights of the day: Discussion and input from attendees)* ***
Session XI	***Chair: Vitalij Pecharsky (Ames Laboratory)***
6:30 – 7:00 pm	Kirstin Alberi *(National Renewable Energy Laboratory)* *"Mechanisms of light-stimulated epitaxy of semiconductors"*
7:00 – 7:30 pm	Yoke Yap *(Michigan Technological University)* *"Electronics without semiconductors by functionalized boron nitride nanotubes"*
7:30 – 8:00 pm	Yuri Suzuki *(Stanford University)* *"Emergent magnetic phenomena at complex oxide interfaces"*
8:00 - 8:30 pm	Zhong Lin Wang *(Georgia Institute of Technology)* *"Updated progress in piezotronics and piezo-phototronics"*
Session XII	***Chairs: Stockman, Boehme***
8:30 – 10:00 pm	Continuation of Poster Session II

Wednesday, April 1, 2015

7:30 – 8:30 am	*** Breakfast ***
Session XIII	***Chair: Arto Nurmikko (Brown University)***
8:30 – 9:00 am	Stanislaus Wong *(Brookhaven National Laboratory)* *"Probing optical behavior in novel nanoscale heterostructures"*

9:00 – 9:30 am	Anton Malko *(University of Texas at Dallas)* *"Quantum-dots-on-silicon hybrids: Towards energy transfer based nanostructured photovoltaics"*
9:30 – 10:00 am	Shawn Yu Lin *(Rensselaer Polytechnic Institute)* *"Recent advances in 3D optical photonic-crystal: Light manipulation"*
10:00 – 10:30 am	*** Break ***

Session XIV	***Chair: Jeffrey Eastman (Argonne National Laboratory)***
10:30 – 11:00 am	Chris Van de Walle *(University of California, Santa Barbara)* *"First-principles calculations of nonradiative recombination in nitride light emitters"*
11:00 - 11:30 am	Shane Stadler *(Louisiana State University)* *"Pressure-induced modifications of magnetostructural transitions and corresponding enhanced magnetocaloric effects in MnNiSi-based systems"*
11:30 – 12:00 pm	Closing Remarks by Meeting Chairs and PM

Session I

Study of Materials and Interface Properties for High-Efficiency Spin Injection: Spin-Dependent Quantum Phenomena in Ferromagnetic Graphene

Jing Shi, Department of Physics and Astronomy, University of California, Riverside

Program Scope

The research program is focused on the study of thin film materials and interface properties for more efficient spin injection and spin-dependent transport. The material systems of particular interest include heterostructures of non-magnetic metals (e.g. Pt, Pd) or semimetals (e.g. topological insulators) with strong spin-orbit coupling and ferromagnet metals or insulators (e.g. NiFe or yttrium iron garnet: YIG), and carbon-based materials (e.g. graphene and organic semiconductors) interfaced with ferromagnetic insulators (e.g. YIG). The novel phenomena in those systems include the spin Seebeck effect, anomalous Hall effect, anomalous Nernst effect, and quantized anomalous Hall effect, etc.

Recent Progress

Recent progress include (a) a better understanding of the physical origin of the magnetoresistance phenomena in Pd(Pt)/YIG heterostructures and (b) the demonstration of the ferromagnetism in graphene in proximity with atomically flat YIG. In the former, the temperature dependence of the magnetoresistance effect is systematically studied in Pd(Pt)/YIG. Although the conventional anisotropic magnetoresistance is not observable at room temperature, it increases monotonically as the temperatures is lowered, indicating the importance of the proximity induced magnetization at the interface. In the meantime, the temperature dependence of the transverse magnetoresistance has a characteristic peak which is a consequence of the spin current effect in such heterostructures. This work appeared in PRL in 2014. More recently, ferromagnetism in graphene/YIG is demonstrated via the anomalous Hall effect measurements. Using atomically flat YIG film as substrate, electrons or holes in graphene acquire spin polarization in graphene/YIG, which is illustrated in its carrier type independence (Figure above). This work was published in PRL. The proximity induced exchange strength is recently shown to be higher than room temperature.

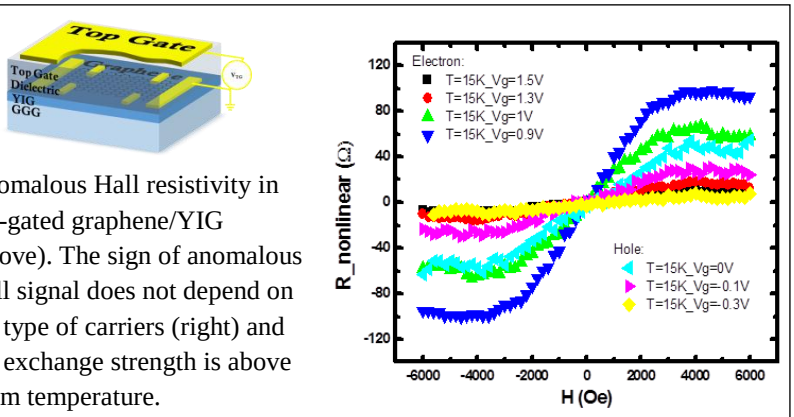

Anomalous Hall resistivity in top-gated graphene/YIG (above). The sign of anomalous Hall signal does not depend on the type of carriers (right) and the exchange strength is above room temperature.

Future Plans

The interface between graphene and YIG will be systematically characterized by HRTEM and its proximity coupling such as the exchange strength and the magnitude of the anomalous Hall effect will be investigated as a function of YIG orientation, pressure, and atomic terrace width of YIG. Disorder induced energy spread in the Dirac spectrum will be quantified and a much narrower energy spread will be achieved by significantly improving graphene mobility. In the meantime, stronger Rashba spin-orbit coupling will be systematically introduced and its strengthen will be tuned by controlling the sp^3 defects and using proximity coupling with another material with strong spin-orbit coupling.

Publications

1. X. He, W. Zhou, Z.Y. Wang, Y. N. Zhang, Jing Shi, R. Q. Wu, and J. A. Yarmoff, *Surface Termination of Cleaved Bi_2Se_3 Investigated by Low Energy Ion Scattering*, Phys. Rev. Lett. **110**, 156101 (2013).
2. T. Lin, C. Tang, H.M. Alyahayaei, and Jing Shi, *Experimental Investigation of the Nature of the Magnetoresistance in Pd/YIG Hybrid Structures*, Phys. Rev. Lett. **113**, 037203 (2014).
3. R. Sachs, Z.S. Lin, and Jing Shi, *Ferroelectric-Like $SrTiO_3$ Surface Dipoles Probed by Graphene*, Scientific Reports **4**, 3657 (2014). DOI: 10.1038/srep03657.
4. S.W. Jiang, D.J. Shi, L. Lin, Y.J. Shi, J. Shi, H.F. Ding, J. Du, M. Wang, and D. Wu, *Strong Asymmetrical Bias Dependence of Magnetoresistance in Organic Spin Valves: the Role of Ferromagnetic/Organic Interfaces*, New Journal of Physics **16**, 013028 (2014).
5. Z.Y. Wang, C. Tang, R. Sachs, Y. Balars, and Jing Shi, *Proximity-Induced Ferromagnetism in Graphene Revealed by the Anomalous Hall Effect*, Phys. Revi Lett. **114**, 016603 (2015).

Pure Spin Current Phenomena

C. L. Chien

Department of Physics and Astronomy, The Johns Hopkins University

Program Scope

Much attention has recently been focused on pure spin current, its generation, detection, and exploitation. In contrast to a spin-polarized current, a pure spin current delivers the same amount of spin angular momentum but with fewer charge carriers thus generating much less Joule heat. However, only a few mechanisms can generate a pure spin current, among them spin Hall effect (SHE), lateral spin valve, spin pumping, and longitudinal spin Seebeck effect (SSE). When a charge current density $\boldsymbol{J_S}$ passes through a metal with strong spin-orbit coupling (SOC), the SHE generates a pure spin current density in the transverse direction of $\boldsymbol{J_S} = \theta_{SH}(\hbar/2e)\,\boldsymbol{J_C} \times \boldsymbol{\sigma}$, where θ_{SH} is the spin Hall angle, σ the spin orientation, $\hbar$ the reduced Planck constant, and e the electronic charge. A pure spin current cannot be detected directly but by the inverse spin Hall effect (ISHE) using a strong SOC metal that converts it into a charge current and detected. The conversion of charge current and spin current thus far has involved mostly a few 5d non-magnetic metals, such as Pt, Au, W, and Pt. The most important quantity in pure spin current phenomena is the spin Hall angle θ_{SH}, which measures the efficiency of charge/spin current conversion. Unfortunately, the reported values of θ_{SH} for a metal (e.g., Pt, Au, Ta, W) can vary by as much as two orders of magnitude. The disparity in the values of θ_{SH} is one of the most outstanding issues in spin current phenomena.

Recent Progress

1. Observation of Inverse Spin Hall Effect in Ferromagnets: We have recently reported the first observation of inverse spin Hall effect (ISHE) in a ferromagnetic metal of permalloy (Py), the inverse effect of anomalous Hall effect.[1] The realization of ISHE in ferromagnetic metals with a sizable spin Hall angle θ_{SH} greatly expands the varieties of materials that can be exploited for spin current phenomena, including the use of inexpensive materials with efficient spin current conversion.

2. A New Method for Self-Consistent Determination of Spin Hall Angle: We recently demonstrate a self-consistent method to determine θ_{SH} by thermally injecting a spin current from the ferromagnetic insulator (YIG) into metals of different thicknesses and resistivity, and perform

full spin current analyses of the ISHE voltage.[2] Our self-consistently determined spin Hall angle values are in order of Pt, W, Au and Ta.

3. Physical Origins of the New Magnetoresistance in Pt/YIG: Recently, we have unconvered a new type of magnetoresistance (MR) in Pt/YIG with characteristics different from those of all other known MRs, including AMR, GMR, and CMR. There are several theoretical proposals for the mechanism of the new MR, including spin Hall MR (SMR) and magnetic proximity effect (MPE). By altering the interface thus blocking the pure spin current, we recently show most of the contribution for the new MR comes from MPE.[3]

Future Plans

Exploring prospects of inverse spin Hall effect in antiferromagetic metals, multilayers or alloys with exceptionally large spin Hall angle, switching using thermally injected spin current.

Publications

1. B. F. Miao, S. Y. Huang, D. Qu, and C. L. Chien, "Inverse Spin Hall Effect in a Ferromagnetic Metal", Physical Review Letters, **111**, 066602 (2013).

2. D. Qu, S. Y. Huang, B. F. Miao, S. X. Huang, and C. L. Chien, "Self-consistent determination of spin Hall angles in selected 5d metals by thermal spin injection," Physical Review B **89**, 140407 (R) (2014).

3. B. F. Miao, S. Y. Huang, D. Qu, and C. L. Chien, "Physical Origins of the New Magnetoresistance in Pt/YIG" Physical Review Letters, **112**, 236601 (2014).

Extreme Thermoelectric Behavior in Low-Dimensional Oxide Conductors

PI: Joshua L. Cohn, Department of Physics, University of Miami, P.O. Box 248046, Coral Gables, FL 33124

Contact:(305) 284-7123;cohn@physics.miami.edu

Program Scope

This program involves experimental transport studies of low-dimensional, bulk oxide conductors exhibiting extreme thermoelectric behavior. The investigations were motivated by preliminary research of the PI revealing a giant Nernst effect[1]at low T in quasi-one-dimensional (Q1D) $Li_{0.9}Mo_6O_{17}$ ("Li-purple bronze" or LiPB), and very large Seebeck anisotropy near room temperature in both LiPB and the Q1D perovskite-related compound, $Sr_5Nb_5O_{17}$. The novel characteristics of LiPB (Q1D electrons, large Fermi surfaces, bipolarity, low-D phonons, electron correlations) make it a model system for investigating the limits of conventional metals physics and the Nernst effect.

While these compounds have in common highly anisotropic electronic structures, other, as yet unknown, material characteristics are clearly important to their extreme thermoelectric behavior. For example, Seebeck anisotropy of the magnitude observed in LiPB is extremely rare in the many highly anisotropic bulk conductors that have been studied for decades (graphites, organics, other bronzes, cuprates, etc.). Insight from this work may help to inform the "rational design" of useful thermoelectric materials.

The physics and properties of the materials targeted for study overlap research interests in both the correlated-electron and thermoelectrics communities. Low temperature studies (to 0.3 K), made possible by a He-3 probe supported under this contract, are designed to provide new insight into the novel ground state of LiPB where possible triplet superconductivity[2] (at T< 2K) and unconventional charge-density wave order[3,4,5] appear to coincide.

Recent Progress

Extreme Seebeck Anisotropy and Transverse Peltier Effect in LiPB
[Phys. Rev. Lett. **112**, 186602 (2014)]

We completed a study of anisotropic transport within the most conducting *bc* planes of LiPB crystals, revealing remarkable Seebeck anisotropy (Fig. 1).For T≥400 K the interchain (c-axis) transport is determined by thermal excitation of charge carriers from a valence band ~0.14 eV below the Fermi level (Fig. 2), giving rise to a large, p-type thermopower that coincides with a small, n-type (metallic) thermopower along the chains. This dichotomy – semiconductor-like in one direction and metallic in a mutually perpendicular direction – gives rise to a substantial transverse Peltier effect (Fig. 3) and atransverse thermoelectric figure of merit among the largest known for a single compound, $Z_{\perp}T=0.024$.

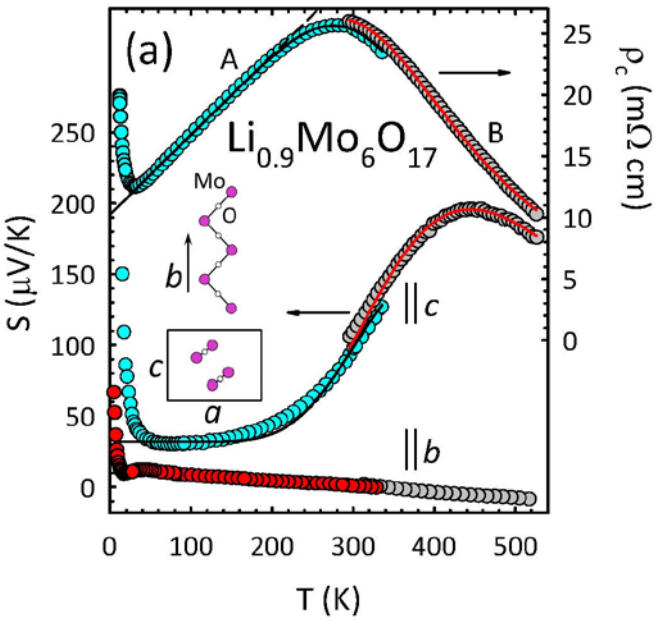

Fig. 1 LiPBinterchain (*c*-axis) thermopowers (left ordinate) and resistivities (right ordinate) for two crystals (labeled A and B), and intrachain (*b*-axis) thermopowers for two different crystals. Solid curves through the *c*-axis data are fits to a parallel conduction (2-band) model. Dashed line is a linear-least-squares fit to the low-T $\rho_c(T)$. Inset: orientation of the crystallographic axes with respect to the q1D Mo-O chains (2 per unit cell).

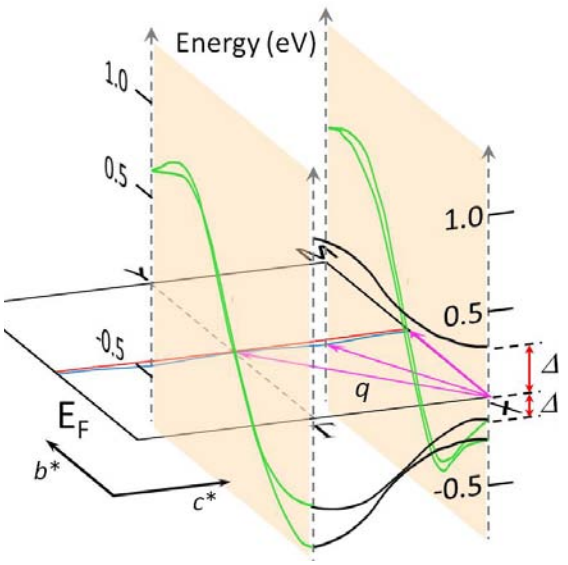

Fig. 2 Bands along main symmetry directions (green: along *b**, black: along *c**) and projected Fermi surface (red and blue curves) in the *b**-*c** plane for LiPB. Δ_V and Δ_C are excitation energies for valence- and conduction-band states, respectively, dispersing along *c** near the X-point of the Brillouin zone. Indirect transitions between these states and the Fermi surface are possible through thermal excitation and absorbtion of a phonon with sufficient momentum along *b** (wavevectors for excitation of valence-band states -- pink arrows).

$Li_{0.33}MoO_3$: a highly anisotropic, narrow-gap semiconductor[manuscript in preparation]

We are nearing completion of work on another highly anisotropic Mo-oxide with remarkable Seebeck anisotropy (Fig. 4). $Li_{0.33}MoO_3$, like LiPB, was first synthesized in the 1980s, but studied very little. Its crystal structure is triclinic,[6] differing from the alkali-metal "red bronzes" of the same formula, $A_{0.33}MoO_3$ (A=K, Rb, Cs, Tl). Electrical resistivity measurements[7] and tight-binding band calculations[8] confirming it to be an anisotropic, low-dimensional, narrow-gap (~0.2eV) semiconductor, are the full extent of prior work.

We have measured resistivity, thermopower and thermal conductivity along a, b* and c directions (b* is the stacking direction of the most conductive ac planes) of high-quality singlecrystals prepared by our collaborators.An electronic transition, evident in *ρ(T)*, *S(T)*near

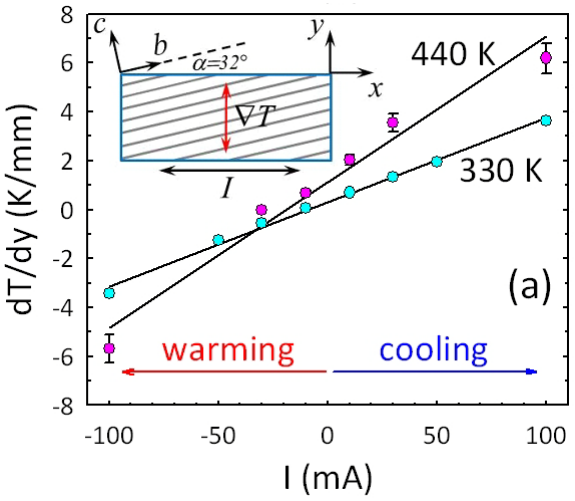

Fig. 3 Peltier-induced temperature gradient for a LiPB crystal at T = 330 K and 440 K. The inset shows the orientation of current and heat flow relative to the specimen (*x*-*y*) and crystallographic (*b*-*c*) axes.

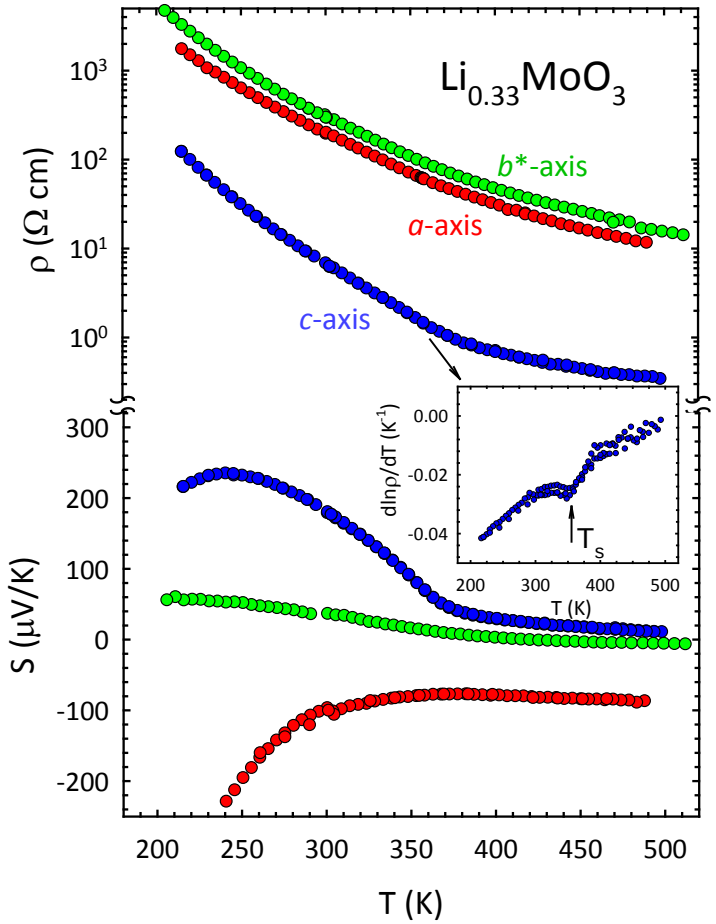

Fig. 4 Resistivity and thermopower for $Li_{0.33}MoO_3$. Inset: structural transition highlighted by a kink in the logarithmic derivative, dlnρ/dT, near 360 K.

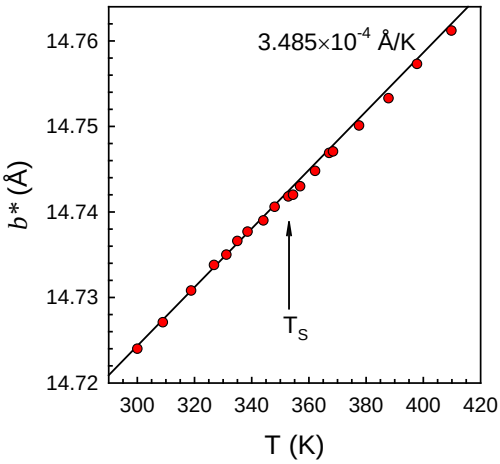

Fig. 5*b** lattice constant (perpendicular to the layers) *vs. T* for a $Li_{0.33}MoO_3$ crystal,

360 K (see inset)is associated with a small increase in the*b** lattice constant upon cooling (Fig. 5), consistent with an *increase* in the band gap.

The thermal conductivity of this compound is low, ~1.6 W/mK in the *ac* planes near 300 K and about 7-8 times smaller along the *b** direction.

Thermoelectric Coefficients and the Novel Ground State in LiPB

Shown in Fig. 6 are our first low-*T* measurements of thermopower and resistivity in LiPB. Most noteworthy: the $T \rightarrow 0$ limiting behavior of *S/T* in the field-supressed "normal state" at 5T implies a *very small* Fermi temperature, T_F~27K. This estimate for T_F comes from the expression for a free-electron gas, $\boldsymbol{S = \frac{\pi^2}{2}\frac{k_B}{e}\frac{T}{T_F}}$. How can such a small value for T_F be reconciled with ARPES and band structure determinations of T_F (~3000-5000 K)? Our Hall and Nernst measurements confirm that this small effective Fermi energy signals a very small density of mobile holes, $p_H \leq 8 \times 10^{18} cm^{-3}$. Indeed, the carrier density continues to decline well into the field-suppressed superconducting state, saturating only below 1K, and thus LiPB is among the most dilute superconductors known. This appears to be connected with a form of electronically-driven charge order that localizes most of the states at the Fermi level, and could have its origin in the physics of a crossover from Q1D Luttinger liquid behavior at high T to 3D Fermi liquid at low T (a prerequisite for the occurrence of superconductivity).

Future Plans

Further investigations of transport in LiPB to 0.3 K will clarify the nature of its low carrier density and effective Fermi temperature.

Transverse thermoelectric studies on miscut crystals of $Li_{0.33}MoO_3$ will be pursued to determine its viability for energy detection applications exploiting the transverse Seebeck effect.Attempts to grow epitaxial thin films of LiPB via pulsed-laser deposition are aimed at leveraging enhanced voltage readout in transverse Seebeck detectors.

Most recently we expanded our heat transport studies to include Q1D antiferromagnetic compounds with a goal to studymagnon-phonon interactions and spin-mediated heat conduction pursuant to spin caloritronic applications.

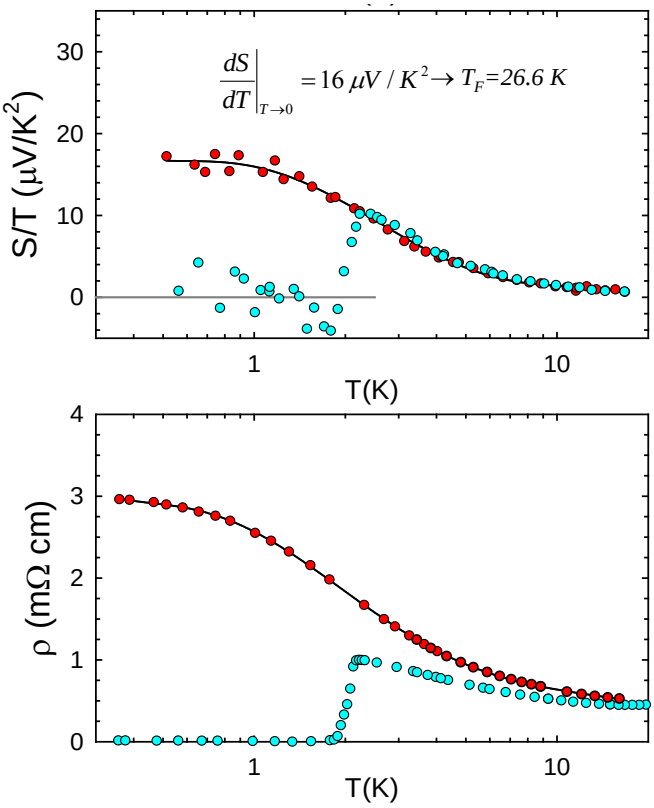

Fig. 6 S/T and ρ(T) along the b-axis with H=0, 5T applied along the *a* axis for a LiPB single crystal.

References

1. J. L. Cohn, B. D. White, C. A. M. dos Santos, and J. J. Neumeier, *Giant Nernst Effect and Bipolarity in the quasi-one-dimensional metal*, $Li_{0.9}Mo_6O_{17}$,Phys. Rev. Lett.**108**,056604 (2012).
2. J.-F. Mercure, A. F. Bangura, X. Xu, N. Wakeham, A. Carrington, P. Walmsley, M.Greenblatt, and N. E. Hussey, *Upper Critical Magnetic Field far above the Paramagnetic Pair-Breaking Limit of Superconducting One-Dimensional Single Crystals*, Phys. Rev. Lett. **108**, 187003 (2012).
3. J. Choi, J. Musfeldt, J. He, R. Jin, J. Thompson, D. Mandrus, X. Lin, V. Bondarenko, and J. Brill, *Probing localization effects in $Li_{0.9}Mo_6O_{17}$ purple bronze: An optical-properties investigation*,Phys. Rev. B **69**, 085120 (2004).
4. C. A. M. dos Santos, B. D. White, Y. K. Yu, J. J. Neumeier,and J. A. Souza, *Dimensional Crossover in the Purple Bronze*, $Li_{0.9}Mo_6O_{17}$Phys. Rev. Lett. **98**, 266405 (2007).
5. Xiaofeng Xu, A. F. Bangura, J. G. Analytis, J. D. Fletcher, M. M. J. French, N. Shannon, J. He, S. Zhang, D. Mandrus, R. Jin, and N. E. Hussey, *Directional Field-Induced Metallization of Quasi-One-Dimensional $Li_{0.9}Mo_6O_{17}$*, Phys. Rev. Lett. **102**, 206602 (2009).
6. P. P. Tsai, J. A. Potenza, M. Greenblatt, and H. J. Schugar, *Crystal Structure of $Li_{0.33}MoO_3$, a Stoichiometric, Triclinic, Lithium Molybdenum Bronze*, J. Sol. St. Chem. **64**,47-56 (1986).
7. B. T. Collins, K. V. Ramanujachary, M. Greenblatt, W. H. McCarroll, P. Mcnally, and J. V. Waszczak, *Substitutional Studies on the Anisotropic, Semiconducting, Molybdenum Bronze, $L_{0.33}MoO_3$*, J. Sol. St. Chem. **76**, 319-327 (1988).
8. EnricCanadell and Myung-Hwan Whangbo, *Semiconducting Properties of $Li_{0.33}MoO_3$*, Inorg. Chem. **27**, 228-232 (1988).

DOE-Supported Research Publications

1. J. L. Cohn, P. Boynton, J. S. Triviño, J. Trastoy, B. D. White, C. A. M. dos Santos, and J. J. Neumeier, *Stoichiometry, structure, and transport in the quasi-one-dimensional metal* $Li_{0.9}Mo_6O_{17}$,Phys. Rev.B**86**, 195143 (2012).
2. J. L. Cohn, S. Moshfeghyeganeh, C. A. M. dos Santos, and J. J. Neumeier,*Giant Nernst Effect and Bipolarity in the Quasi-One-Dimensional Metal* $Li_{0.9}Mo_6O_{17}$, Phys. Rev. Lett. **108**, 056604 (2012).
3. N. Prasai, A. Rebello, A. B. Christian, J. J. Neumeier, and J. L. Cohn, *Phonon-spin scattering and magnetic heat transport in the quasi-one-dimensional spin-1/2 antiferromagnetic chain compound* $CuSb_2O_6$,Phys. Rev. B**91**, 054403 (2015).

Session II

Electrochemical Potential Control of Mesophotonic Structures

Harry A. Atwater, California Institute of Technology, Thomas J. Watson Laboratories of Applied Physics, MS 128-95, Pasadena, CA 91125; **e-mail:**haa@caltech.edu

Program Scope

Control of the flow of light and heat is fundamental to the performance of optical materials in energy applications. For both natural materials and artificial materials, the optical properties are usually fixed at the time of synthesis, owing to either the atomic scale structure or mesoscale artificial structure, or both. However electrochemical driving forces can be used to dynamically alter the optical response of materials, especially for plasmonic materials. We are exploring the *relationship between the electrochemical potential and mesophotonic optical response* in plasmonic metamaterials. Our research has two broad objectives: 1) to understand how electrochemical potential modulation gives rise to striking changes in the optical properties of materials in the transition from plasmonic to dielectric behavior and 2) to understand the *plasmoelectric effect*, a newly discovered optoelectronic phenomenon in which resonant and nonresonant optical excitation of plasmons is found to alter the electrochemical potential state of plasmonic materials.

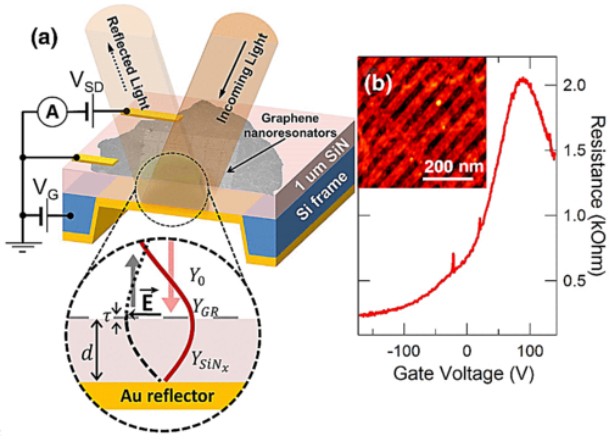

Figure 1. (a) Schematic device structure of graphene Salisbury screen. The inset illustrates the device with the optical waves at the resonance condition. (b) dc resistance of graphene as a function of the gate voltage. The inset is an AFM image of 40 nm nanoresonators.

Recent Progress

We have recently explored electrochemical potential control in plasmonic metamaterials by external gating in i) graphene nanostructures, and ii) hybrid graphene/metallic nanostructures. We have also investigated the plasmoelectric potential, a potential induced via resonant optical excitation of nanostructures. The optical absorption properties of periodically patterned graphene plasmonic resonators have been studied experimentally as the graphene sheet is placed near a metallic reflector(Fig. 1). By varying the size and carrier density of the graphene, the parameters for achieving a surface impedance closely matched to free-space(Z_0=377Ω)are determined and shown to result in 24.5% total optical absorption in the graphene sheet (Fig.2). Theoretical analysis shows that complete absorption is achievable with higher doping or lower loss. This geometry, known as a Salisbury screen, provides an efficient means of light coupling to the highly confined graphene plasmonic modes for future optoelectronic applications.

Future Plans

In the near future we will experimentally investigate tunable electronic control of blackbody emission from graphene plasmonic resonators on a silicon nitride substrate. We anticipatethat graphene resonators may be able to produce antenna-coupled blackbody radiation, manifest as narrow spectral emission peaks in the mid-IR. By continuously varying the nanoresonator carrier density, the frequency and intensity of these spectral features may be able modulated via an electrostatic gate, while the entire structural remains at a constant temperature. This work has opened the door for future approaches to control blackbody radiation at timescales beyond the limits of conventional thermo-optic modulation.

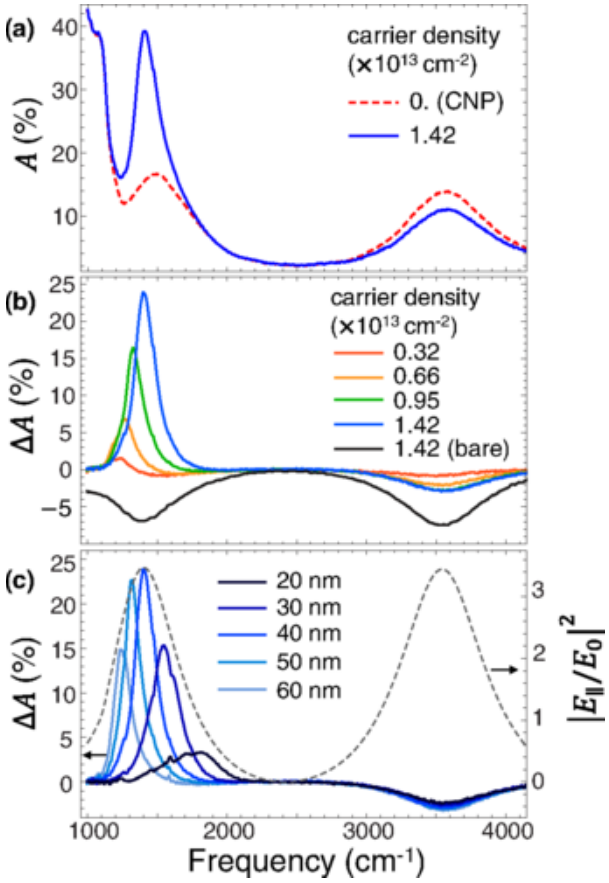

Figure 2. (a) The total absorption in the device for undoped (red dashed) and hole doped (blue solid) 40 nm nanoresonators. (b) The change in absorption with respect to the ab-sorption at the charge neutral point (CNP) in 40-nm-wide graphene nanoresonators at various doping levels. The solid black curve represents the absorption difference of bare (unpatterned) graphene. (c) Width dependence of the absorption difference with the carrier concentration of 1.42×1013cm−2. The resonator width varies from 20 to 60 nm. The dashed curve shows the theoretical intensity of the surface parallel electric field at the SiNx surface when graphene is absent.

Publications

1. "Plasmoelectric Potentials in Metal Nanostructures", M.T. Sheldon, J.van de Groep; A.M. Brown, A. Polman and H.A. Atwater, *Science*, **346**, 828 (2014).

2. "Tunable large resonant absorption in a midinfrared graphene Salisbury screen", M.S. Jang, V.W. Brar, M.C. Sherrott, J.J. Lopez, L. Kim, S. Kim, M. Choi, and H.A. Atwater, *Physical Review B*,**90**Article Number: 165409 (2014).

3. "Electrochemical Tuning of the Dielectric Function of Au Nanoparticles", A.M. Brown, M.T. Sheldon and H.A. Atwater, *ACS Photonics*, in press (2015).

Nanostructured colloidal self-assembly and controlled alignment of anisotropic nanoparticles

Ivan I. Smalyukh, University of Colorado at Boulder

Program Scope

Harvesting, storage, and conversion of energy among its different forms strongly depend on available materials and their properties. Self-assembly of nano-sized functional units is an exceptionally promising way of designing inexpensive artificial composite materials with new macroscopic physical behavior and properties. The main objective of this project is to explore self-organization of anisotropic nanoparticles into colloidal composites with tunable ordered structures. The research focuses on understanding and control of self-assembly of metal and semiconductor nanoparticles, as well as on material behavior arising from their ordered self-organization and alignment. Fundamental studies of shape-dependent colloidal interactions and ordering of quantum dots and plasmonic metal nanoparticles will reveal underpinning physical mechanisms that guide mesoscale morphology and ultimately determine material properties of the self-assembled composites. These properties are characterized and correlated with hierarchical structures and composition. Analytical and numerical modeling of colloidal interactions and material properties provides important insights. This research may lead to new, cheaper, and more efficient renewable energy technologies, a new breed of energy-efficient information displays and consumer devices, as well as a fertile ground for new basic science.

Recent Progress

According to the original plan of the proposal, we have focused on synthesis, dispersion, and both electrical and optical switching of various plasmonic metal nanoparticles and other nanoparticles in thermotropic liquid crystals(LCs). We have developed plasmonicnematic colloids with facile switching of ordered anisotropic metal nanoparticle ensembles by low-voltage fields and low-intensity light.

Macroscopic behavior of materials begins to manifest itself at the mesoscale, at which control of structure and composition is the emergence of engineering previously unrealized material functionality. Self-assembly of functionalnano-units, such as quantum dots,plasmonic, magnetic,and core-shell colloids, is an exceptionally promising approach to the design and scalable fabrication of these meso-structured materials. Furthermore, ordered assemblies of nanoparticles in LCs may enable composites with properties that can be tuned by fields, light, and other external stimuli. This may lead to cheaper and more efficient technology as well as a fertile ground for new fundamental science. However, practical realization of such tunable mesoscale LC composites is hindered by poor nanoparticle dispersion. Spontaneous alignment of dichroic and fluorescent dye molecules in LCs, which results from anisotropic molecular-scale interactions, is widely used in imaging of orientational ordering, defects, and structures well as in

"guest-host" devices. On the other hand, being much larger than molecules, microparticles locally distort the nematic alignment and induce topological defects, leading to assemblies that minimize their free energy cost.However, at mesoscopic scales between the size of molecules and hundreds of nanometers, behavior of solid inclusions in LCs is poorly understood and rarely controlledas they tend to aggregate. This is due to poorly controlled particle-induced elastic distortions that result in elasticity-mediated forces leading to minimization of the elastic free energy through "sharing" of distortions produced by different individual nanoparticles. Orientational switching of anisotropic nanoparticles in concentrated dispersions is also a challenge.Recently, we have developed(Fig. 1) long-range ordered LC dispersions of anisotropic colloids, such as gold, silver, and other metal nanoparticles, as well as semiconductor and dielectric nanoparticles, with facile response to low-voltage fields and low-intensity light. Nematic dispersions of these nanoparticles are obtained by polymer passivation of their surfaces to impose weak tangential boundary conditions for orientation of anisotropic host LC molecules. This allows us to mitigate elastic distortions imposed by surface boundary conditions on these nanoparticles, so that no additional elasticity-mediated interactions emerge polymer stabilization of GNPs works well not only in isotropic but also in mesomorphic phases of the LC hosts (Fig. 1). Similar to dichroic dye molecules in the guest-host LCs and displays, the GNPs follow

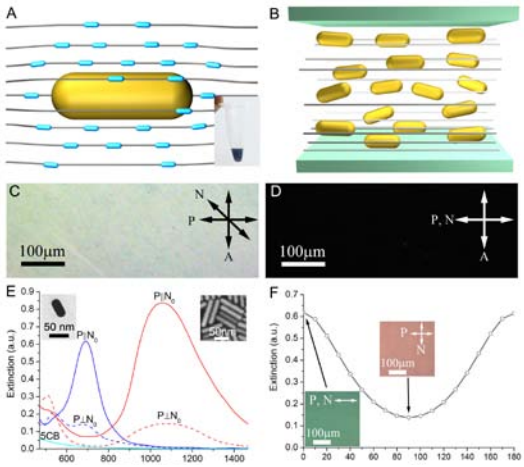

Fig. 1. Colloidal gold nanorods in a nematic LC. (**A**) Schematic of a nanorod with weak tangential boundary conditions for (cyan) LC molecules. The inset shows a vial with the dispersion. (**B**) Schematic of dispersed nanorods following director**N**. (**C**,**D**) POM micrographs of the composite with **N** at (**C**) 45°and (**D**) 0°to a polarizer**P**. (**E**) Extinction spectra of aligned short (blue curves) and long (red) gold nanorods in a nematic host for **N**parallel and perpendicular to **P**, with the spectrum of pure 5CB (cyan curve) shown for reference. Insets of (**E**) show nanorods. (**F**) Extinctionvs. angleφ between **N**&**P**.

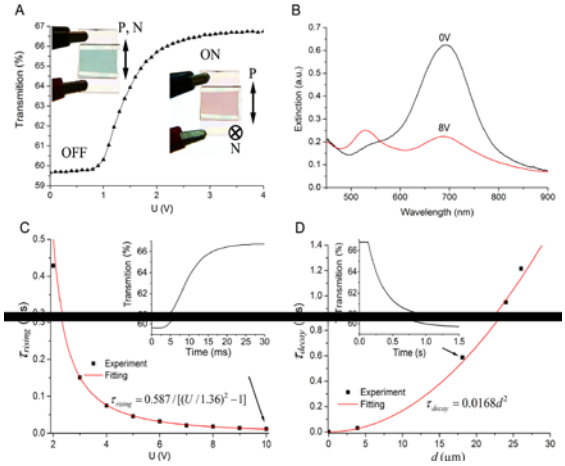

Fig.2. Electric switching of plasmonic guest-host LCs with gold nanorods.(**A**) Transmission vs. voltage voltage$U$. Insets showthe corresponding color change. (**B**) Voltage-dependent extinction spectra for polarizer**P** along the rubbing direction. (**C**) Rising time vs. U obtained from transmission vs. time curves, such as the one shown in the inset for glass cell thickness$d$=18μm and U=10V. (**D**) Decay time vs. d obtained from transmission vs. time (shown for$d$=18μm inthe inset).

switching of the LC director describing average local LC molecular orientations (Fig. 2). We quantitatively explained how this behavior arises from anisotropic colloidal surface interactions and leads to strong polarization-sensitive and voltage- or light-tunable surface plasmonresonance effects [1-4]. We also demonstrated that low-intensity light can allow for patterning of long-range ordering of anisotropic gold nanoparticle dispersions (Fig. 3). Our findings may enable composite materials with tunable properties emerging from combining switchable nanostructures of anisotropic fluids with surface plasmon resonance and other properties of anisotropic nanoparticles, new types of dynamic smart windows, as well as a new generation of energy-efficient guest-host LC displays.

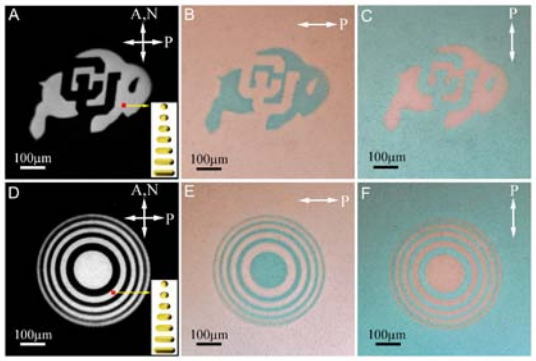

Fig.3. Optical realignment and patterning ofplasmonic guest-host LCs. (**A**) A POM micrograph of a "buffalo"-shaped twist domain in a uniformly aligned cellobtained by patterned illumination of the photo-alignment layer. (**B**,**C**)The corresponding brightfield micrographs for polarizations of incident light (**B**) perpendicular and (**C**) parallel to **N**. (**D**) POM and (**E,F**) brightfield micrographs of a Fresnel zone plate created by patterned illumination. Insets in (**A**,**D**)depicttheπ/2-twist of **N**and nanorods across the cell.

In addition to the dispersions of metal nanoparticle in thermotropic LCs [1-4], we also developed colloidal co-dispersions of cellulose nanocrystals and metal (gold and silver) nanoparticles as well mesostructured solid films with orientational ordering and controlled morphology [5,6]. These dispersions and films inherit plasmonic properties of the metal nanoparticles and also exhibit new material behavior arising from long-range orientational ordering and tunable periodic helicoidal structures [5,6]. We have discovered dynamic self-patterning of such LC forms of soft anisotropic matter arising from delicate interaction of low-intensity light & photosensitive azobenzene monolayers at confining surfaces [7]. In related studies of mesoscale ordering and new physical behavior arising from the interaction of colloids in structured LC host media, we have explored the role of chirality, surface topology and geometry of colloidal inclusions, and their combinations [8-12].

Future Plans

The PI is pursuing experimental realization and fundamental studies of dispersions of quantum dots and rods as well as upconversion nanoparticles in thermotropic and cellulose-based lyotropic LCs. Recent preliminary studies in the PI's group (unpublished) show that semiconductor nanoparticles dispersed in thermotropic LCs can self-assemble into colloidal crystals with different symmetries and tunable lattice parameters. The PI and his research group are conducting in-depth studies of how this mesoscale self-organization, which can yield centimeter-large mono-crystals of colloidal nanoparticles with tunable center-to-center separations, leads to new physical behavior and material properties arising from a combination of unique properties of nanoparticles as well as structural organization at nanometer to macroscopic scales. The PI is also planning to develop LC co-dispersions of quantum and plasmonic

nanoparticles. In these systems, he will probe how plasmon-exciton interactions can lead to new physical behavior when the nanoparticle-scale interactions are combined with different forms of long-range orientational and positional ordering that can be tuned by weak external stimuli applied to soft matter host media. More broadly, by exploiting unique properties of solid nanostructures in the forms of their colloidal dispersions and by combining them with the facile response of soft matter to external stimuli, the PI intends to develop a new breed of composites with novel physical behavior, pre-engineered properties, and facile response to external fields.

References (articles acknowledging the DOE award):

1. Y. Zhang, Q. Liu, H. Mundoor, Y. Yuan, and I. I. Smalyukh. "Metal nanoparticle dispersion, alignment and assembly in nematic liquid crystals for applications in switchable plasmonic color filters and E-polarizers."***ACS Nano***, published online, doi:10.1021/nn5074644 (2015).
2. Q. Liu, Y. Yuan, and I. I. Smalyukh."Electrically and Optically Tunable Plasmonic Guest-Host Liquid Crystals."***Nano Lett.*** 14, 4071–4077 (2014).
3. Q. Liu, J. Tang, Y. Zhang, A. Martinez, S. Wang, S. He, T. J. White, and I. I. Smalyukh. "Shape-dependent dispersion and alignment of non-aggregating plasmonic gold nanoparticles in lyotropic and thermotropic liquid crystals." ***Phys Rev E*** 89, 052505 (2014).
4. B. Senyuk, D. Glugla, and I. I. Smalyukh. "Rotational and translational diffusion of anisotropic gold nanoparticles in liquid crystals controlled by varying surface anchoring." ***Phys. Rev. E*** 88, 062507 (2013).
5. Q. Liu, M. Campbell, J. S. Evans, I. I. Smalyukh. "OrientationallyOrdered Colloidal Co-Dispersion of Gold Nanorods& Cellulose Nanocrystals." ***Adv. Materials*** 26, 7178–7184 (2014).
6. M. Campbell, Q. Liu, A. Sanders, J. S. Evans, I.I. Smalyukh. "Preparation of NanocompositePlasmonic Films Made from Cellulose Nanocrystals or Mesoporous Silica Decorated with Unidirectionally Aligned Gold Nanorods." ***Materials*** 7, 3021-3033 (2014).
7. A. Martinez and I.I. Smalyukh. "Light-driven dynamic Archimedes spirals and oscillatory patterns of topological defects in anisotropic soft matter." ***Optics Express*** 23, 4591-4604 (2015).
8. M.B. Pandey, P.J. Ackerman, A. Burkart, T. Porenta, S. Žumer, and Ivan I. Smalyukh. "Topology and Self-Assembly of Defect-Colloidal Superstructure in Confined Chiral Nematic Liquid Crystals." ***Phys Rev E*** 91, 012501 (2015).
9. M. Tasinkevych, M. Campbell, and I.I. Smalyukh."Splitting, linking, knotting, and solitonic escape of topological defects in homeotropicnematic drops with handles", ***Procs. Natl. Acad. Sci. USA***111, 16268-16273 (2014).
10. B. Senyuk, M. Varney, J. Lopez, S. Wang, N. Wu, and I. I. Smalyukh."Gourd-shaped colloidal particles in cholesteric liquid crystal."***Soft Matter*** 10, 6014-6023 (2014).
11. M. C. M. Varney, Q. Zhang, M. Tasinkevych, N. Silvestre, K. A. Bertness, and I. I. Smalyukh."Periodic dynamics, localization metastability, and elastic interaction of particles with confining surfaces and helicoidal structure of cholesteric liquid crystals."***Phys. Rev. E*** 89, 052505 (2014).

12. S. Copar, T. Porenta, P. J. Ackerman, M. B. Pandey, M. C. M. Varney, I. I. Smalyukh, and S. Žumer. “Topological Switching and Orbiting Dynamics of Colloidal Spheres Dressed with Chiral NematicSolitons.” ***Scientific Reports*** 4, 7337 (2014).

Optical readouts of electrochemical reactions on plasmonic nanoparticle electrodes

Katherine A. Willets

Department of Chemistry, Temple University, 1901 N. 13th St. Philadelphia, PA 19122

Program Scope

This program is focused on determining whether plasmon excitation in noble metal nanoparticle electrodes can impact electrochemical potentials of redox probes. Once a plasmon is excited in a metallic nanoparticle, it decays by (1) scattering light into the far field, (2) generating local heat at the surface, or (3) producing hot electrons (and corresponding hot holes). The latter two mechanisms could impact redox potentials of probe molecules, suggesting that plasmon excitation could lower energy barriers for important electrochemical reactions. This program is interested in determining both whether plasmon excitation changes the redox potentials of molecular probes, as well as what local structural features of the nanoparticles are linked to changes in electrochemical activity. To do this, optically active redox probes are used to determine the redox state of a molecule based on changes in the emission when the molecule is in its oxidized or reduced form.

Recent Progress

For our experiments, Nile Blue (NB) is used as an optically active redox probe. In its oxidized form, NB gives a strong surface-enhanced Raman scattering (SERS) signal when adsorbed to a nanoparticle electrode surface, while in its reduced form, the SERS signal reaches a minimum value. Figure 1A shows a representative SERS cyclic voltammogram (SERS-CV).

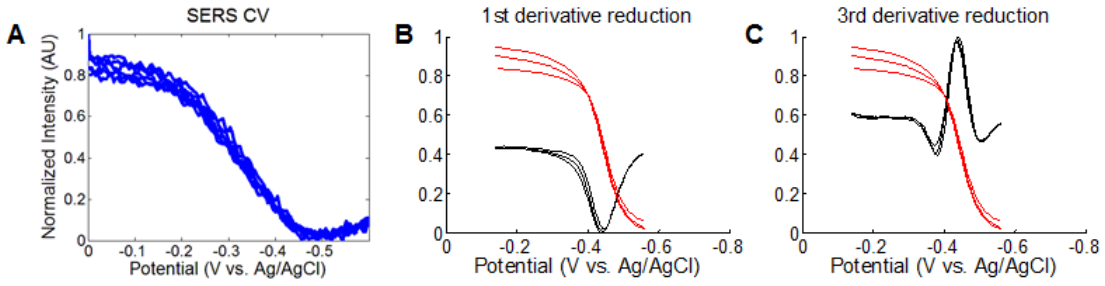

Figure 1. (A) SERS CV of Nile Blue. (B) 1st derivative analysis (black) of the reduction half-wave (red) to extract a SERS half-wave reduction potential. (C) 3rd derivative analysis (black) to extract the SERS reduction onset potential from a reduction half-wave (red).

To process these data, we use a derivative analysis to extract SERS analogs of the traditional electrochemical values for the half-wave potential and the onset potential. Given the non-uniform intensity enhancement of SERS, a derivative analysis was used to extract these parameters rather than arbitrary intensity thresholds. Figure 1B shows the first derivative calculations from three SERS reduction half-waves; the potential at which the inflection point (local minimum in the derivative) is observed is assigned as the SERS half-wave potential. Note that this parameter is distinct from a standard half-wave potential ($E_{1/2}$) used in traditional electrochemistry, but gives us a parametric handle with which to quantitate and compare subsequent measurements. Figure 1C shows the third derivative analysis, where the first local minimum corresponds to the "jerk" of the system (or a region of significant curvature change) which provides a value of the SERS reduction onset potential. Similar analyses can be performed to extract the SERS oxidation half-wave and onset potentials.

To determine the relationship between these extracted parameters and the plasmon resonance of a nanoparticle electrode, gold nanodisk arrays were fabricated using block copolymer lithography. Briefly, a poly(methyl methacrylate)-polystyrene (PMMA-PS) block copolymer is spin coated onto an indium tin oxide (ITO) coated glass slide and annealed at high temperatures, allowing the block copolymer to self-assemble into PMMA cylinders embedded in a PS matrix. Exposing the film to UV light cross-links the PS while chemically degrading the PMMA, allowing us to rinse the PMMA away and leaving us with a PS hole mask. By depositing the metal of interest through the mask and then removing the PS, we are left with small metal disks on the ITO surface (Figure 2A). The average diameter of the disks is controlled by the molecular weight of the copolymer (to date, we have prepared disks with diameters of 20, 40, and 80 nm) while the height of the disk is controlled by the metal deposition thickness. We can generate nanoparticle arrays on ITO that are broadly tunable across the visible spectrum, as shown in Figure 2B, with various metal compositions (e.g. silver or gold).

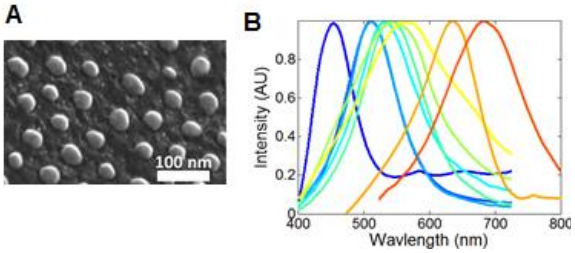

Figure 2. (A) Block-copolymer templated nanoparticle array. (B) LSPR spectra of arrays with different nanoparticle diameters and heights.

NB was tethered to the surface of the gold nanodisks by first functionalizing the gold with 3-mercapto-propionic acid (MPA), then reacting the free amine of the NB to the pendant carboxylic acid of the MPA using carbodiimide coupling chemistry. Next, SERS CVs were obtained and processed to extract the relevant electrochemical parameters associated with NB oxidation and reduction. SERS was excited using both 642 nm and 532 nm excitation; the red excitation is resonant with the absorption spectrum of the oxidized form of the NB which generates stronger overall SERS signals, although could also introduce resonance effects. Figure 3 shows the results of the SERS reduction and oxidation onset potentials for gold nanodisk

electrodes with differing plasmon resonances. The reduction onset potential (Figure 3A) shows a positive shift as the plasmon resonance is tuned to the red from 600 nm to 700 nm, then shifts back towards more negative values when the plasmon resonance is beyond 700 nm. This trend is observed with both excitation wavelengths, although the effect is more pronounced for red excitation than green excitation. In contrast, the oxidation onset potential (Figure 3B) does not show a clear trend with the plasmon resonance of the nanodisk array. The wavelength dependence of the reduction onset potential tracks with the fluorescence emission spectrum of NB, which peaks at ~670 nm, suggesting that the effect is due to coupling between the molecular resonance of the NB and the plasmon resonance of the array.

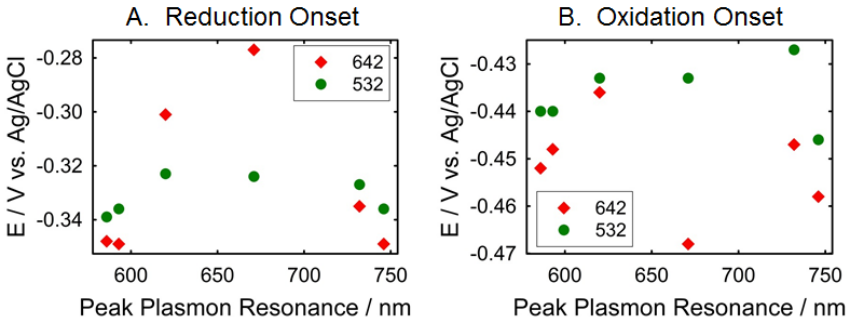

Figure 3. SERS onset potentials as a function of the plasmon resonance of a gold nanodiskarray electrode. Two excitation wavelengths were used: 642 nm (red) and 532 nm (green). Both (A) reduction and (B) oxidation SERS onset potentials are shown.

Despite the encouraging trends in the data, particularly for the reduction onset potential response to the plasmon resonance, we found several trends in control experiments that require us to be cautious when using optical readouts of electrochemical parameters. Figure 4 illustrates several of the issues that arose during our control experiments. In Figure 4A, SERS CVs are shown at different excitation intensities using MPA-tethered NB and gold island films deposited on ITO as a substrate. Gold island films are a faster means of generating plasmonic nanoparticle electrodes, although at the cost of a broadened plasmon resonance. Significant hysteresis and scan-to-scan variations are observed

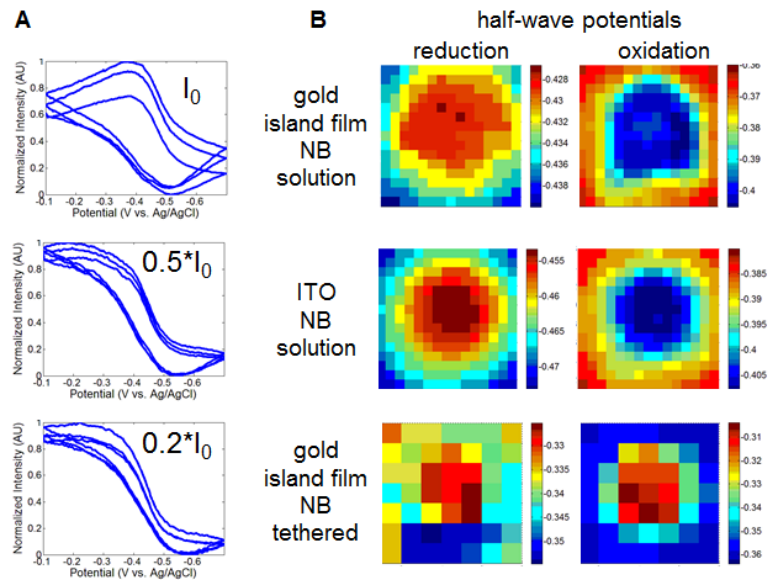

Figure 4. (A) SERS CVs of NB on gold island film electrodes using different excitation intensities as indicated. (B) Heat maps showing the spatial dependence of the SERS half wave potentials due to the intensity profile of the laser. Red values correspond to more positive potentials.

at the higher intensities (top panel, Figure 4A), while more consistent scan-to-scan and surface-tethered behavior is observed as the excitation intensity is lowered (bottom panel). A similar intensity dependence is observed across the laser excitation spot, as shown in Figure 4B. Here, the SERS half-wave potentials were calculated from the SERS CV data at different pixels of the CCD detector; the values change across the CCD and track with the Gaussian profile of the laser beam (note that larger bin sizes were required for the tethered NB case due to lower signal-to-noise). The spatial intensity dependence is observed on (from top to bottom) gold island films exposed to NB in solution, bare ITO exposed to NB in solution, and gold island films functionalized with NB. For both the gold island film and bare ITO substrates, the SERS reduction half-wave potentials are more positive at the center of the image where the excitation laser intensity is highest. On the other hand, the SERS oxidation half-wave potentials are more negative in the center when NB is in solution with both ITO and gold island film electrodes, but more positive when the NB is tethered to the surface on the gold island film. Current work is focused on trying to understand this bulk opto-electrochemical behavior in order to better calibrate the plasmon-dependent redox potentials using optically active redox probes.

Future Plans

Our future plans include understanding what experimental factors influence extracted electrochemical parameters using optical readouts. While single molecule experiments can solve this problem (since the molecule has a digital "on" or "off" response depending on its redox state), bulk experiments require careful controls that account for excitation intensity, analyte concentration, electrode active area, and analyte tethering strategy. As we develop insight into each of these factors, we will continue to probe how plasmon excitation impacts the electrochemical potentials, moving from the bulk electrodes described here to single nanoparticle electrodes. In particular, we wish to interrogate whether nanoparticle structural factors that generate enhanced plasmonic responses can also impact electrochemical potentials of redox probes, using the super-resolution SERS imaging techniques we have developed in recent work.

Publications

A.J. Wilson and K.A. Willets. " Visualizing site-specific redox potentials on the surface of plasmonic nanoparticles with super-localization SERS microscopy." *Nano Lett.* 14, 939-945 (2014).

Session III

A brief history of nanocrystals: discovery, milestones, and the future

Alexander L. Efros

Naval Research Laboratory, Washington, DC

Semiconductor nanocrystals are the most heavily studied of the nanoscale semiconductors. The size dependence of the nanocrystal optical properties was discovered independently more than 30 years ago in two different materials: in semiconductor-doped glasses by Ekimov et al,[1] who were working at the Vavilov State Optical Institute, and in aqueous solutions by Brus et al.,[2] who were with Bell Labs. There were many similarities in both discoveries. In both cases the growth of the NC is a result of the natural thermodynamic process of the microscopic phase separation of the supersaturated solution, and the nanocrystals are the nuclei of a new phase. The size of the nanocrystals is controlled by diffusion of the atoms or ions to the growing nuclei and by the degree of super-saturation. The final size of the nanocrystal is controlled by the duration of the phase separation process and is fixed at its interruption. This process is termed "arrested precipitation". In both cases the research was driven by the curiosity of Ekimovand Brus who tried to answer the question of what is determines the color of doped glasses and aqueous solutions. And in both cases the initial idea of why the NC color correlates to its size was stimulated by existing investigation of one-dimensionalsuperlattices. The size dependent optical properties of NCs was described theoretically by Efros[3]and Brus[4] and measured initially in NCs embedded in glass.[5] I will briefly discussed the history of the discovery, the main obstacles in the development of the field and the critical breakthroughs in establishing the field.

The 30 plus years of investigations of NCs got a critical burst when Brus' former postdoc, M. Bawendi, moved from Bell Labs to MITwhere, in 1993, he and two of his students, C. Murray and D. Norris, published a paper that providedthe first reliable technology of various colloidal nanocrystal growth.[6] The technology allows growth of almost monodisperse NCs in a wide range of sizes. The paper demonstrated the extremely narrow NC size dispersion with remarkable control of the CdSe NC size. Finally the authors showedthat various semiconductors could be grown in NC form.

Today, semiconductor NCs have become much more than objects of scientific curiosity. The demonstration of tunable, room-temperature lasing using NC quantum dot solids, the development of NC-based light-emitting diodes (LEDs) and photovoltaic cells, and the first commercial products in the area of NC bio-labeling are just a few illustrations of the broad technological potential of these materials. Periodic arrays of semiconductor NCs are emerging as a new class of solution-processable materials for low-cost, flexible, thin-film electronics after reports that these structures have a mobility of 25 $V/sm^{-1}s^{-1}$. Thus, in 2012 researchers

from Samsung Electronicsdemonstrated the first four inch full-color quantum-dot display, which is brighter than liquid-crystal displays and consumes less than a fifth of the power.

Many of these achievements become possible due to further development of the results of the C. Murray paper. In my talk I will discuss some of these developments. (i) Successful growth of core-shell structures.[7]This allows dramatically increased PL quantum yield. (ii) Doping of the NC with impurities.[8] (iii) Control of the colloidal NC shape: growth of CdSe nanorods[9] and growth of nanoplatelets[10], whicharefreestanding quantum wells. (iv) Finally, the growth ofa three dimensional periodic array of NCs.[11]Understanding of the physical processes responsible for the NC PL, which have been enhanced by a very strong spatial confinement of electrons and holes, also played a critical role in these developments. I am going to discuss briefly the dark exciton recombination mechanism and the enhancement of the nonradiative Auger recombination.

The NC quantum dot field continues its growth and development today; it has not yet achieved full maturity. Hundreds of scientists and engineers continue to work on creating novel NC structures, on improving NC transport and optical properties, and on developing numerous NC-based devices. Because of this work, it is difficult to predict where the fast developing field of NCs is going and what will be their most important applications. I will discuss just two of the most scientifically exciting developments.

The first development is connected with the fact that,electronically and mechanically, NCs can be considered as building blocks for the construction of more complex structures with long-range order (on a scale usually requiring lithography) and with new and potentially useful properties. The first three-dimensional periodic array of identical semiconductor NCs was grown by Murray et al1.[11]Much more complex meta-materials can be grown today—such as binary nanoparticle superlatticesin which two nanoclusters differing in both size and material composition are incorporated into a single ordered structure.[12] From the very beginning this research keep a great promise, because instead of the limited number of atoms which nature uses to create the solid state, one can use the unlimited number of various NC.Until recently, these super-crystals of NCs, however, have not shown any new physical properties. This is because NCs were only weakly coupled to each other like molecules in a van der waals crystal. There is huge progress, however, inthe development of strongly coupled NC arrays that have a collective band. I will discuss the potential for use of such NC superstructures.

Finally I am going to discuss the unique properties of the small size NCs that shouldhave a use for real-time visualization of electrical activity in single neurons as well as small networks of up to 100 neurons. Indeed, the NC typical size is somewhat smaller than the thickness of the neural membrane and the ability to conjugate the QDs to a number of membrane-specific peptides allows for the delivery of the QDs to specific regions of neuronal cells, including the outer surface of the membrane, the membrane bilayer and the cytosol. The

tunable, size-dependent PL of QDs allows for the selective marking of different neurons or their parts. QDs with different PL colors can be excited with a single excitation wavelength due to the very broad, continuous QD absorption spectra. Current nanocrystalline QDs have quite high PL quantum yields, up to 80% at room temperature. On top of this, the QDs have excellent optical stability, exhibiting very little photobleaching compared to organic dyes. Another outstanding characteristic of nanocrystalline QDs is their exceptionally large two photon absorption (TPA) coefficients, which are 10- to 100- times larger than those for organic molecules and fluorescence proteins. The large TPA coefficients utilize longer, tissue-penetrating excitation wavelengths that enable the investigation of subsurface neurons. The PL decay time of QDs is on the order of 20 ns, which is much shorter than the time scale of action potentials, therefore allowing for a faithful temporal representation of all of the neuronal transition processes which occur on a submillisecond time scale. Finally I will show that PL of NC is sufficiently sensitive to typical electric fields of the action potential in neuronal membrane.

References:

1. A. I. Ekimov, A. A. Onushchenko "Quantum size effect in three dimensional microscopic semiconductor crystals," JETP Letters **34**, 345 (1981).
2. R. Rossetti, S. Nakahara, and L. E Brus, "Quantum size effects in the redox potentials, resonance Raman spectra, and electronic spectra of CdS crystallites in aqueous solution," J. Chem. Physics **79**, 1086 (1983).
3. Al. L. Efros and A. L. Efros, "Interband absorption of light in semiconductor sphere," Sov. Phys. Semicond. **16**, 772 (1982).
4. L. E. Brus, "A simple model for the ionization potential, electron affinity, and aqueous redox potentials of small semiconductor crystallites," J. Chem. Phys. **79**, 5566 (1983)
5. A. I. Ekimov, Al. L. Efros, and A. A. Onushchenko "Quantum size effect in semiconductor microcrystals," Sol. St. Comm. **56**, 921 (1985).
6. C. B. Murray, D. J. Norris, and M. G. Bawendi "Synthesis and Characterization of Nearly MonodisperseCdE (E = S, Se, Te) SemiconductorNanocrystallites," J. Am. Chem. Soc. **115**, 8706 (1993).
7. M. A Hines&P. Guyot-Sionnest,"Synthesis and characterization ofstrongly luminescing ZnS-capped CdSe nanocrystals." J. Phys. Chem. **100**,468 (1996).
8. D. J. Norris, N. Yao, F. T. Charnock, T. A. Kennedy,"High-Quality Manganese-Doped ZnSe Nanocrystals", Nano Lett. **1** , 3 (2001).
9. X.G. Peng, L. Manna, W. Yang, J. Wickham, E. Scher, A.Kadavanich& A. P. Alivisatos"Shapecontrol of CdSe nanocrystals". Nature **404**, 59 (2000).
10. S.Ithurria,M.D.Tessier,B. Mahler,R.P.S.M. Lobo,B.Dubertret andAl.L.Efros, "Colloidalnanoplateletswithtwo-dimensionalelectronicstructure", Nature Material **10**,936 (2011)
11. C. Murray, C. Kagan, & M. Bawendi, "Self-Organization of CdSeNanocrystallites intoThree-Dimensional Quantum Dot Superlattices", Science **270**, 1335 (1995)
12. E.V. Shevchenko, D.V. Talapin, N.A. Kotov, S. O'Brien, C.B. Murray,"Structural diversity in binary nanoparticle superlattices", Nature **439**, 55 (2006).

Session V

Spectrally-Tunable Far-Field Thermal Radiation Extraction from Micro & Nanostructures

Gang Chen (PI) and Svetlana V. Boriskina (co-I), Mechanical Engineering Department, Massachusetts Institute of Technology, Cambridge, MA

Program Scope

The overall goal of this project is to explore a new approach towards radiative heat extraction from the near into the far field via morphology-mediated thermal emission (Fig. 1). Morphology-mediated engineering of optical density of states (DOS) in photonic structures has already been successfully used to manipulate light absorption, fluorescence rates, Raman scattering efficiency, etc. However, the broadband nature of thermal emission and the temperature dependence of the occupancy of available states make engineering the electromagnetic potential for heat extraction much more challenging. We seek to develop a general understanding and specific design rules for morphology-mediated radiative heat extraction. In particular, we investigate mechanisms of manipulating far-field thermally-emitted photons via engineering of local electromagnetic potentials are investigated, and probe limits of thermal radiation from (or via coupling to) micron and nanoscale structures into the far field. We also explore possibilities to convert low energy photons into high energy phonons via phonons in low-dimensional thermal absorbers/emitters.

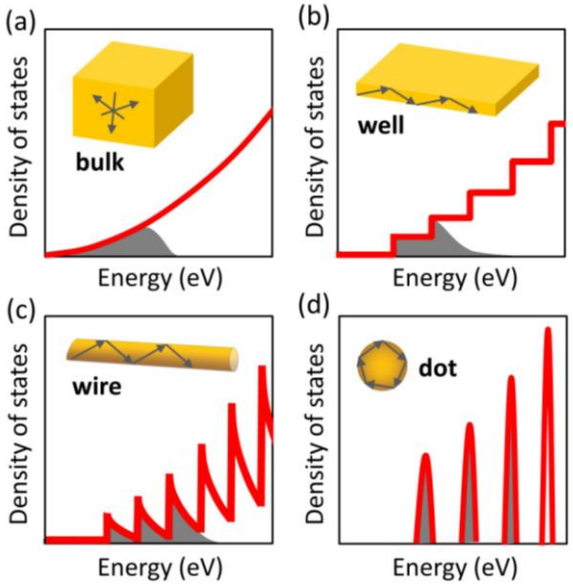

Figure 1. Spatial confinement concentrates photon states enhancing thermal emission at select frequencies. Red lines: density of optical states in the light-confining structures of various configurations; Shaded areas: thermal distribution of photons in (a) bulk material, (b) wells, (c) wires, and (d) dots.

Recent Progress

As a first step towards manipulating thermal emission via LDOS of confined photon states, we used fluctuational electrodynamics to study radiative heat transfer between thin films in the near and far field. Thin film thermal well structures act as photonic analogs to electrical quantum well structures and thus exhibit a photonic dispersion that deviates strongly from bulk systems as shown in Fig. 2a. By reducing the thickness of the emitter and the absorber, trapped waveguide modes are introduced which provide resonant enhancement to radiative transport for high energy photons while suppressing emission and absorption of low energy photons via mode cut-off frequencies. As shown in Fig. 2a, these effects lead to strong spectral shaping of radiative transfer between thermal wells. Such efficient spectral shaping of thermal emission shows great promise for thermophotovoltaics (TPV), and we theoretically predict order-of-magnitude efficiency enhancement of thermal well TPV platforms vs. their bulk counterparts[1].

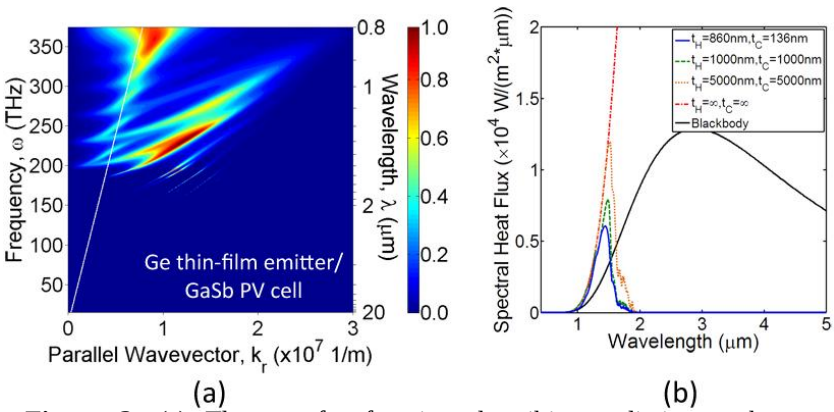

Figure 2. (a) The transfer function describing radiative exchange between two thermal wells (Ge emitter and GaSb absorber) in the energy-momentum domain. (b) Spectral radiative heat flux as a function of varying thicknesses of thermal wells on both hot and cold sides.

We also introduced a new concept of hybrid optical-thermal nanoantennas, which simultaneously provide intensity enhancement at the operating wavelength in the visible (e.g., for imaging or spectroscopy) and avoid overheating via a combination of reduced absorption and radiative cooling. The radiative heat extraction from plasmonic nanoparticles is achieved by using SiO_2 microspheres acting as thermal dots. We show that hybrid nanoantenna-thermal-dot structures enable two orders of magnitude enhancement of localized electric fields (Fig. 3a). At the same time, reduced absorption (Fig. 3b) and radiative cooling lower antenna temperature by several hundred degrees for the irradiance of 10^5-10^6 W/m^2 (Fig. 3c).

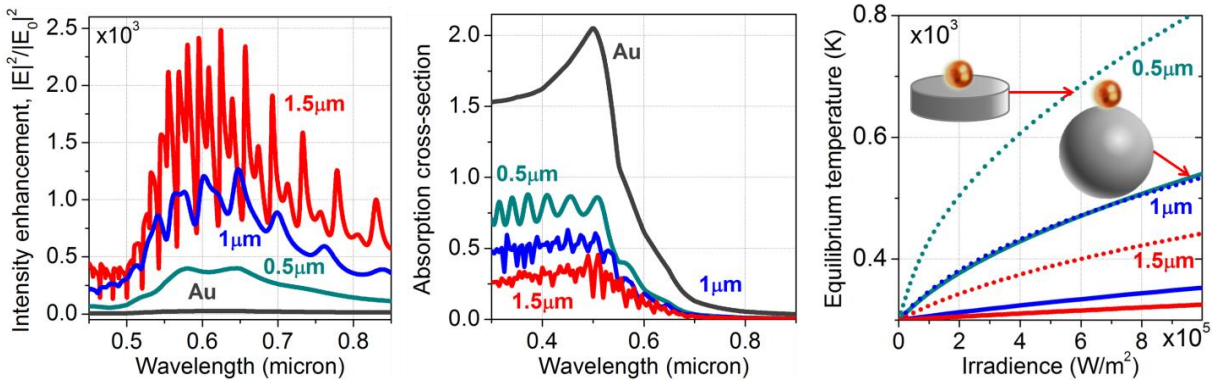

Figure 3. Hybrid nanoantennas enhance intensity by an order of magnitude and reduce temperature by several hundred degrees. (a) Local intensity enhancement (a) and absorption cross section (b) of a hybrid antenna composed of a 150nm-diameter Au nanoparticle and a SiO_2 microsphere with varying radius. (b) Equilibrium temperature under steady-state illumination with a frequency matching each antenna highest intensity peak.

We have also explored possible approaches to dynamically modulate thermal emittance over a broad wavelength range both in the near- and far field using phase-change materials and varied doping level. In particular, we explored vanadium dioxide (VO_2) and ferroelectric materials and metamaterials to tune and modulate both near- and far-field radiation. A tunable far-field metamaterial emitter design is illustrated in Fig. 4. At low temperatures, where VO_2 is an optically transparent dielectric, the structure acts as a mirror, while at high temperatures, where VO_2 becomes metallic, the layered metamaterial undergoes a transition into a hyperbolic regime, resulting in high thermal emittance. We further revealed that global topological transitions of photonic metamaterials are governed by the re-arrangement of local topological

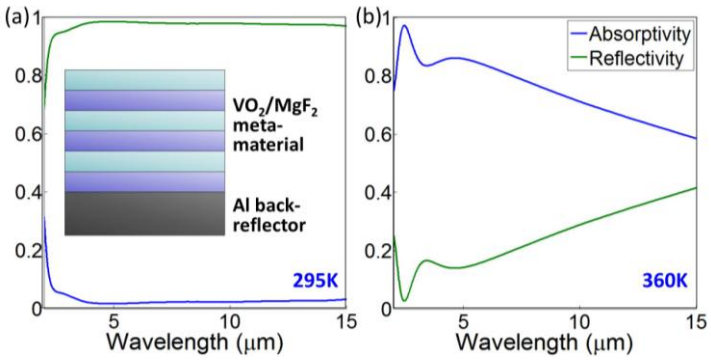

Figure 4. Optical properties of the photonic structure composed of VO2, MgF2, and an Al back-reflector. At low temperatures, the structure acts as a mirror (a), while at high temperatures it becomes an efficient and broadband metamaterial emitter.

features of the optical field, such as vortices and saddle points, which reconfigures global powerflow[2]. These new insights provide useful guidelines for the bottom-up design of artificial photonic materials with novel properties. We also explored ways to actively control near-field radiative heat transfer that relies on electrical tuning of phonon modes of ferroelectric materials[3].

We conducted measurements of surface-plasmon-polariton-mediated thermal emission. The plasmonic material we focused on was doped silicon. The plasma frequency of doped silicon can be tuned by changing the carrier concentration, hence, offering the mechanism to tune the near field radiative transfer. To probe this effect we measured near-field radiative transfer between a between a highly doped silicon sphere (75micron in radius) and silicon substrates with varied doping level. Preliminary experimental results showed good agreement with theoretical prediction for larger gaps, and at smaller gaps, deviated from theory due to the surface roughness of the sphere.

We developed an atomistic approach based on nonequilibrium Green's function and microscopic Maxwell equations to describe the transition from radiation in the far and near field to phonon heat conduction at contacts. For gaps larger than 1nm, the predicted conductance values are in excellent agreement with fluctuating electrodynamics. At sub-nanometer gaps, we find the conductance is enhanced up to 4 times compared to the continuum approach, while avoiding its prediction of divergent conductance at contact. This suggests that at gaps approaching the spacing between the atomic layers the continuum approach based on local bulk dielectric constant breaks down. In addition, our developed formalism provides insight about the *physical nature* of energy transfer at the nanoscale. Due to the presence of the vacuum gap, at large gaps, the far-field energy transfer is through photons. As the gap becomes smaller, the mediation shifts to surface phonon polaritons in the near-field regime (Fig. 6a). At sub-nanometer gaps, we find that there is tunneling of acoustic phonons, which provide additional channels of enhanced transport predicted by the atomic formalism (Fig. 6b). Finally, at contact, heat transfer is by phonon transmission or conduction. All these regimes are captured within a single formalism, demonstrating a

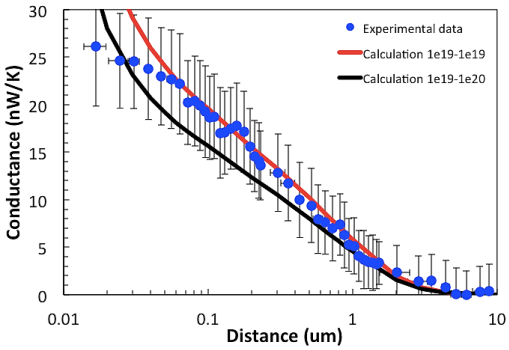

Figure 5. Measured near-field heat flux between a highly doped (10^{19}cm^{-3}) silicon sphere and a highly doped (10^{19} -10^{20}cm^{-3}) silicon substrate shows good agreement with theoretical predictions.

complete picture of the transition of radiation to conduction[4].

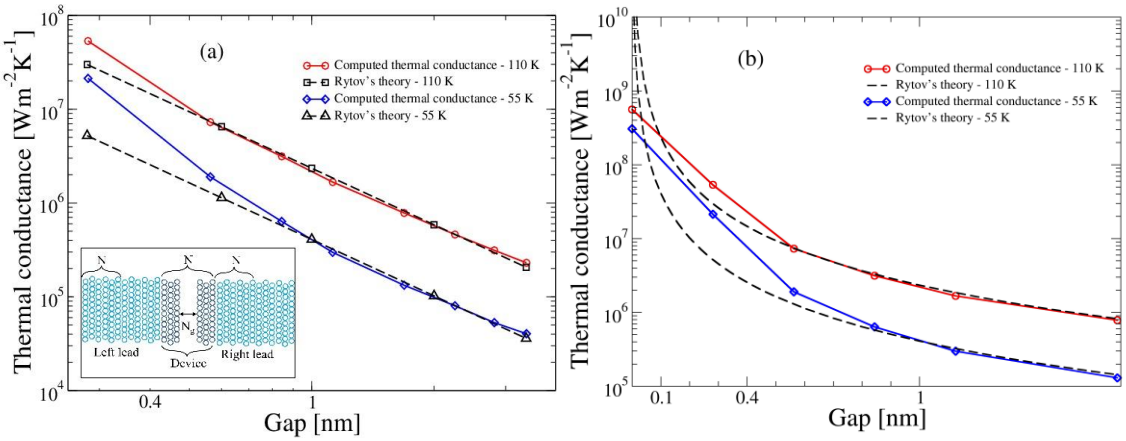

Figure 6. Comparison of thermal conductance with continuum and atomic approaches. Computed thermal conductance at few nanometer gaps in (a) log-log and (b) semi-log at 110 K and 55 K using atomistic formulations. The inset in (a) depicts a schematic of the system comprised of semi-infinite leads and a central device region, divided into two slabs with a finite gap separating the surfaces.

Finally, we considered thermodynamic properties of thermal radiation. Until today, there is no agreed way to define entropy flux of a thermally radiating surface. We clarified this confusion and derived the maximum efficiency that a heat engine can achieve through thermal radiation at a high temperature and rejecting the heat at a low temperature. This efficiency is lower than Carnot efficiency, but higher than the Landsberg limit. The new understanding will enable us to set proper limits for various photon-based energy conversion approaches.

Future Plans

We plan to further investigate theoretically and experimentally manipulation of thermal radiation via photon confinement effects. We will explore thermal down-conversion of absorbed photon energy and spectral shaping of infrared radiation by thermal wells (ultra-thin films) and thermal dots (sub-wavelength-size particles). We will also explore a new avenue of manipulating far-field thermal radiation by combining morphological effects with non-equilibrium excitation effects, such as via thermally modified luminescent emission from thermal wells and dots.

References

1. Tong, J. K., Hsu, W.-C., Huang, Y., Boriskina, S. V. & Chen, G. Thin-film "thermal well" emitters and absorbers for high-efficiency thermophotovoltaics. *to appear in Sci. Reports* (2015), http://arxiv.org/abs/1502.02061
2. Tong, J., Mercedes, A., Chen, G. & Boriskina, S.V. in *Singular and Chiral Nanoplasmonics* (Boriskina, S. V. & Zheludev, N. I.) (Pan Stanford, 2014).
3. Huang, Y., Boriskina, S. V. & Chen, G. Electrically tunable near-field radiative heat transfer via ferroelectric materials. *Appl. Phys. Lett.* **105,** 244102 (2014).
4. Chiloyan, V., Garg, J., Esfarjani, K. & Chen, G. Transition from near-field thermal radiation to phonon heat conduction at sub-nanometer gaps. *accepted for publication in Nat. Commun.* (2015).

Publications for the last 2 years

Book Chapter:

J. Tong, A. Mercedes, G. Chen, and S. V. Boriskina, "Local field topology behind light localization and metamaterial topological transitions," Ch. 8 of Singular and Chiral Nanoplasmonics, S. V. Boriskina and N. I. Zheludev, Eds. Pan Stanford, 2014.

Journal Publications

1. M. Krüger, V. A. Golyk, G. Bimonte, and M. Kardar, "Interplay of roughness/modulation and curvature for surface interactions at proximity," Europhysics Lett., vol. 104, no. 4, p. 41001, 2013.

2. S. V Boriskina, H. Ghasemi, and G. Chen, "Plasmonic materials for energy: from physics to applications," Mater. Today, vol. 16, pp. 379–390, 2013.

3. J. K. Tong, W.-C. Hsu, S. Eon Han, B. R. Burg, R. Zheng, S. Shen, and G. Chen, "Direct and quantitative photothermal absorption spectroscopy of individual particulates," Appl. Phys. Lett., vol. 103, no. 26, p. 261104, 2013.

4. V. A. Golyk, M. Krüger, and M. Kardar, "Linear response relations in fluctuational electrodynamics," Phys. Rev. B 88, 155117, 2013.

5. W.-C. Hsu, J. K. Tong, B. Liao, B. R. Burg, and G. Chen, "Direct and quantitative broadband absorptance spectroscopy on small objects using Fourier transform infrared spectrometer and bilayer cantilever probes," Appl. Phys. Lett., vol. 102, no. 5, p. 051901, Feb. 2013.

6. T. Luo and G. Chen, "Nanoscale heat transfer - from computation to experiment," J. Phys. Chem. Chem. Phys., vol. 15, 3389-3412, 2013.

7. Y. Huang, S.V. Boriskina, and G. Chen, "Electrically tunable near-field radiative heat transfer via ferroelectric materials," *Appl. Phys. Lett.* **105,** 244102, 2014.

8. J. K. Tong, W.-C. Hsu, Y.Huang, S.V. Boriskina, and G. Chen, "Thin-film "thermal well" emitters and absorbers for high-efficiency thermophotovoltaics," *to appear in Sci. Reports*, http://arxiv.org/abs/1502.02061, 2015

9. V. Chiloyan, J. Garg, K. Esfarjani, and G. Chen, "Transition from near-field thermal radiation to phonon heat conduction at sub-nanometer gaps," *accepted for publication in Nat. Commun.*, 2015.

High Performance Thermoelectric Materials and Flexible Transparent Electrodes

Zhifeng Ren
University of Houston

Recent Progress

Up to now, thermoelectric figure-of-merit (ZT) has been the most pursued parameter for any thermoelectric materials for possible high conversion efficiency. To achieve higher ZT, lowering the thermal conductivity by nanostructuring has been the major effort in the past a few years [1-6]. In this projectwe found that only high ZT is not good enough. We also need to have higher power factor in addition to higher ZT, in fact higher average ZT, not peak ZT. Fortunately we found some example materials to demonstrate that higherpower factor will result in higheroutput power [7].

In the second part, I will present our recent study on flexible transparent electrodes based on nanomesh of highly electrical conducting materials such as Au, Ag, Cu, Al, etc. We used a new technique to make such nanomesh. These nanomshes have sheet resistance as low as 10 ohms per square centimeter and transparency above 90%, and can be stretched for more than 200% [8]. We also found that these nanomeshes can go through tens of thousands of cycles under stretching of up to 150%.

Future Plans

We plan to further improve the thermoelectric performance of the existing thermoelectric materials and also search for new thermoelectric materials with higher ZT and power factor, and also improve the performance of the flexible transparent electrodes.

References

1. M. S. Dresselhaus, G. Chen, M. Y. Tang, R. G. Yang, H. Lee, D. Z. Wang, Z. F. Ren, J. P. Fleurial, and P. Gogna, “New Directions for Low Dimensional Thermoelectric Materials”, *Adv. Mater*. **19**, 1043 – 1053 (2007).
2. Bed Poudel, Qing Hao, Yi Ma, YuchengLan, Austin Minnich, Bo Yu, Xiao Yan, Dezhi Wang, Andrew Muto, DaryooshVashaee, Xiaoyuan Chen, Junming Liu, Mildred S. Dresselhaus, Gang Chen, and Z. F. Ren, “High-Thermoelectric Performance of Nanostructured Bismuth Antimony Telluride Bulk Alloys”, *Science***320**, 634 – 638 (2008).
3. D. Kraemer, B. Poudel, H.-P. Feng, J. C. Caylor, B. Yu, X. Yan, Y. Ma, X. W. Wang, D. Z. Wang, A. Muto, K. McEnaney, Q. Hao, M. Chiesa, Z. F. Ren, and G. Chen, “High-performance solar thermoelectric generators with flat-panel thermal concentration”, *Nature Materials***10**, 532-538 (2011).
4. Qinyong Zhang, Hengzhi Wang, Qian Zhang, Weishu Liu, Bo Yu, Hui Wang, Dezhi Wang, George Ni, Gang Chen, and Zhifeng Ren, “Effect of silicon and sodium on thermoelectric properties of thallium doped lead telluride based materials”, *NanoLetters***12**, 2324-2330 (2012).

5. Qian Zhang, Bolin Liao, YuchengLan, Kevin Lukas, Weishu Liu, KeivanEsfarjani, Cyril Opeil, David Broido, Gang Chen, and Zhifeng Ren, "High thermoelectric performance by resonant doping of indium in nanostructured SnTe", *PNAS***110**, 13261-13266 (2013).
6. Huaizhou Zhao, Jiehe Sui, Zhongjia Tang, YuchengLan, Qing Jie, Daniel Kraemer, Kenneth McEnaney, Arnold Guloy, Gang Chen, and Zhifeng Ren, "High thermoelectric performance of MgAgSb-based materials", *Nano Energy***7**, 97-103 (2014).
7. Weishu Liu, HeeSeok Kim, Shuo Chen, Qing Jie, Bing Lv, Mengliang Yao, Zhengsong Ren, Cyril P. Opeil, Stephen Wilson, Ching-Wu Chu, and Zhifeng Ren, "New n-type thermoelectric material $Mg_2Sn_{0.75}Ge_{0.25}$ for high power generation", *PNAS* (2015, www.pnas.org/cgi/doi/10.1073/pnas.1424388112).
8. ChuanFeiGuo,Tianyi Sun, Qihan Liu,ZhigangSuo, and Zhifeng Ren, "Highly stretchable and transparent nanomesh electrodes made by grain boundary lithography", *Nature Communications* **5**, 4121 (2014).

Publications in years from 2013 to 2015

1. Tianyi Sun,EserMetinAkinoglu,ChuanfeiGuo,TrilochanPaudel,JinweiGao,Yang Wang, Michael Giersig, Zhifeng Ren, and Krzysztof Kempa, "Enhanced broad-band extraordinary optical transmission throughsubwavelength perforated metallic films on strongly polarizable substrates", *Applied Physics Letters***102**, 101114 (2013).
2. ChuanFeiGuo, Tianyi Sun, Yang Wang, JinweiGao, Qian Liu, Krzysztof Kempa, and Zhifeng Ren, "Conductive black silicon surface made by silver nano-network assisted etching", *Small***9**, 2415-2419 (2013).
3. Xiao Yan, Weishu Liu, Shuo Chen, Hui Wang, Qian Zhang, Gang Chen, and Zhifeng Ren, "Thermoelectric property study of nanostructured p-type half-Heuslers (Hf, Zr, Ti)$CoSb_{0.8}Sn_{0.2}$", *Advanced Energy Materials***3**, 1195-1200 (2013).
4. EserMetinAkinoglu, Tianyi Sun, JinweiGao, Michael Giersig, Zhifeng Ren, and Krzysztof Kempa, "Evidence for critical scaling of plasmonic modes at the percolation threshold in metallic nanostructures", *Appl. Phys. Lett.* **103**, 171106 (2013).
5. V. G. Hadjiev, M. N. Iliev, B. Lv, Z. F. Ren, and C. W. Chu, "Anomalous Vibrational Properties of Cubic Boron Arsenide", *PRB***89**, 024308 (2014).
6. Longb Liao, Qiuhui Zhang, Zhihua Su, Zhongzheng Zhao, Yanan Wang, Yang Li, Xiaoxiang Lu, Dongguang Wei, GuoyingFeng, Qingkai Yu, XiaojunCai, Jimin Zhao, Zhifeng Ren, Hui Fang, Francisco Robles Hernandez, Steven Baldelli, and JimingBao, "High-efficiency solar water splitting using a nanocrystallineCoOphotocatalyst", *Nature Nanotechnology***9**, 69-73 (2014).
7. ChuanFeiGuo,Tianyi Sun, Qihan Liu,ZhigangSuo, and Zhifeng Ren, "Highly stretchable and transparent nanomesh electrodes made by grain boundary lithography", *Nature Communications* **5**, 4121 (2014).
8. ChuanFeiGuo, Tianyi Sun, Feng Cao, Qian Liu, and Zhifeng Ren, "Metallic nanostructures for light trapping in energy harvesting devices", *Light: Science & Applications***3**, e161 (2014).
9. M. H. Qin, S. Dong, H. B. Zhao, Y. Wang, J. -M. Liu, and Zhifeng Ren, "Magnetic orders in pnictide superconductors: effect of biquadratic interaction", *New Journal of Physics***16**, 053027(2014).

10. Huaizhou Zhao, Jiehe Sui, Zhongjia Tang, YuchengLan, Qing Jie, Daniel Kraemer, Kenneth McEnaney, Arnold Guloy, Gang Chen, and Zhifeng Ren, "High thermoelectric performance of MgAgSb-based materials", *Nano Energy***7**, 97-103 (2014).
11. ChuanFeiGuo and Zhifeng Ren, "Cold-welding of gold nanowires and conductance recovery offlexible transparent electrodes", *Nano Energy* (2014).
12. Tianyi Sun, ChuanFeiGuo, Feng Cao, EserMetinAkinoglu, Yang Wang, Michael Giersig, Zhifeng Ren, and Krzysztof Kempa, "A Broadband Solar Absorber with 12 nm Thick Ultrathin *a*-Si Layer by Using Random Metallic Nanomeshes", *Applied Physics Letter***104**, 251119 (2014).
13. Jing Shuai, HeeSeok Kim, YuchengLan, Shuo Chen, Yuan Liu, Huaizhou Zhao, Jiehe Sui, and Zhifeng Ren, "Study on thermoelectric performance by Na doping in nanostructured $Mg_{1-x}Na_xAg_{0.97}Sb_{0.99}$", *Nano Energy***11**, 640-646 (2015).
14. Jiehe Sui, Jing Shuai, YuchengLan, Yuan Liu, Ran He, Dezhi Wang, Qing Jie, and Zhifeng Ren, "Effect of Cu concentration on the thermoelectric properties of nanostructured p-type $MgAg_{0.97-x}Cu_xSb_{0.99}$", *ActaMaterialia***87**, 266-272 (2015).
15. Weishu Liu, Qing Jie, HeeSeok Kim, and Zhifeng Ren, "Current progress and future challenges in thermoelectric power generation: from materials to devices",*ActaMaterialia***87**, 357-376 (2015).

Atomic Structure in the Cubic Phase of the $Ge_2Sb_2Te_5$ Memory Alloy

E. Ma

Department of Materials Science and Engineering, Johns Hopkins University, Baltimore, MD 21218 ema@jhu.edu

Program Scope

The current phase of the DoE-BES funded project is entitled "evolution of atomic structure in the amorphous and crystalline states of the phase-change memory alloy $Ge_2Sb_2Te_5$". The multi-component chalcogenide $Ge_2Sb_2Te_5$ (GST) is a prototype alloy used as the media for high-density rewritable data storage. The amorphous (*a*-GST) and crystalline (*c*-GST) states possess significantly different optical and electronic properties, and at the same time, can be rapidly switched from one to the other (the crystallization of *a*-GST takes only several nanoseconds). Such characteristics are useful for not only rewritable optical data storage (CDs and DVDs), but also electronic phase-change memory. The latter can be a non-volatile memory that has faster data transfer rates and higher storage densities than the Flash memory.

The desirable behaviors of GST must originate from the internal atomic structures and chemical bonding in the *a*-GST and *c*-GST. Their reversible transformation involves easy atomic rearrangements, such that the phase change can be ultra-fast, while the changes in the chemical bonding are pronounced to produce a large contrast in optical and electronic properties. A thorough understanding of the atomic structure, bonding and their evolution is highly important to the science of phase-change materials. The structural variations also control the property range needed for future development of (e.g., multi-level) data storage applications.

This project builds on our previous success and experience in uncovering the atomic-level structure and poly(a)morphism [1,2] in *a*-GST. We will take advantage of our two-pronged computational/experimental approach, employing *ab initio* molecular-dynamics calculations and synchrotron X-ray and transmission electron microscopy experiments. Our goals are two-fold. 1) We aim to understand how the atomic structure and chemical bonding evolve in deeply supercooled GST, with emphasis on the temperature range from above the glass transition (and crystallization) temperature to room temperature. We will monitor the structural developments, especially the fraction of tetrahedrally coordinated Ge atoms and their stability (drift), the degree of Peierls-like distortion, and the fraction of homopolar bonds. 2) For the crystalline counterpart, the *c*-GST, we will determine the locations of Ge atoms, and assess the effects of defects/distortions on the degree of resonant bonding. In addition, we will characterize the defects induced by electrical current, to explore defect-triggered amorphization; this solid-state *c* to *a* collapse, in the absence of melting, would have implications for electrically-switched memories.

Recent Progress

Using DFT electronic structure calculations, previously we demonstrated dative bonds in the *a*-GST state at room temperature. The resulting *p* bonding profoundly influences the local atomic structure, leading to right-angled motifs. The dominance of *p* bonding is revealed by i) distributions of the coordination number

(CN) and the bond angle, for truly bonded atoms determined based on the electron localization functions (ELF), and ii) a direct evaluation of the *p* (and *s*) orbital occupation probability for the CN=3 Ge atoms that form 90° bonds with neighbors. This atomic structure is originated from the interaction between Ge and the lone-pair electrons of Te, which destabilizes the sp^3 hybridization and promotes *p* bonding among all the constituent species. As a result, the CNs of Ge and Te both shift towards 3, and the bond angles around Ge become dominated by ~90° [1].

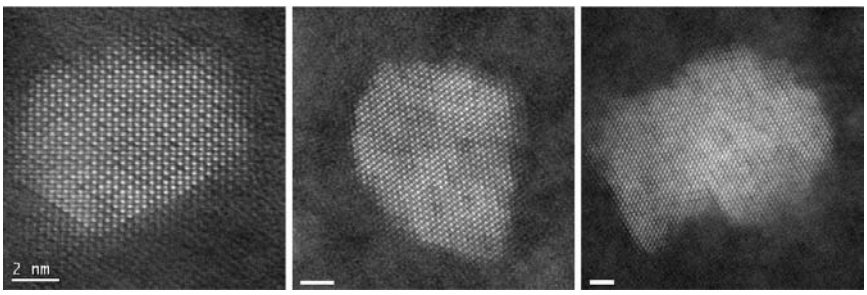

Fig. 1

TEM images of newly crystallized grains in *a*-GST samples obtained from three different sources (labs).

In this presentation we focus on the structure of the other state, the *c*-GST. As shown in Fig. 1, upon annealing at ~420 K (~150°C) for 1 min, the *a*-GST begins to crystallize into the metastable *c*-GST. X-ray diffraction (Fig. 2 left panel), electron diffraction and imaging showed an fcc structure. Experimentally, Data fitting and modeling suggested it is the rocksalt structure [3,4], composed of "Te taking one fcc sublattice, while Ge/Sb and vacancies taking the other". See Fig. 2 (right panel).

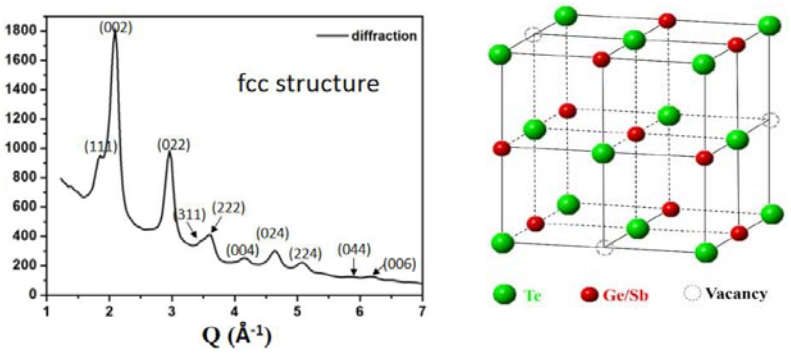

Fig. 2

Left panel: X-ray diffraction of the *c*-$Ge_2Sb_2Te_5$ phase.

Right panel: Commonly suggested structural model.

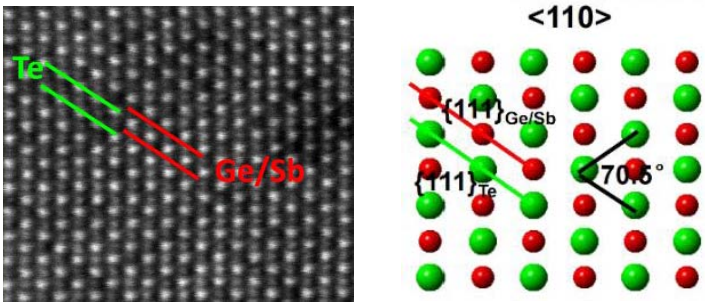

Fig. 3

Left panel: the <110> zone axis view.

Right panel: the actual HAADF-STEM image.

To determine how the three species and vacancies distribute on the lattices, we have carried out systematic atomic-resolution imaging and chemical analysis, using state-of-the-art aberration-corrected TEM. In the <110> zone axis, we see alternating close-packed plane of Te (green brighter dots) and Ge/Sb (red, dimmer spots), see Fig. 3. The challenge now is to create a spatial map of the species. To this end, we used atomic column EDX mapping. Under the strong e-beam in the HAADF-STEM mode, the e-beam effects need to be ruled out, which is demonstrated in Fig. 4 below.

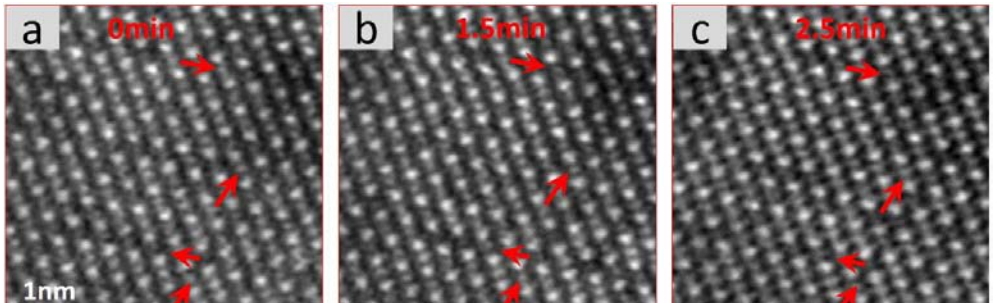

Fig. 4 The stability of the structure under HAADF-STEM was confirmed. The imaged features, such as the spots marked by red arrows, did not change after e-beam illumination (we also checked two e-beam voltages, 200 keV and 80 keV).

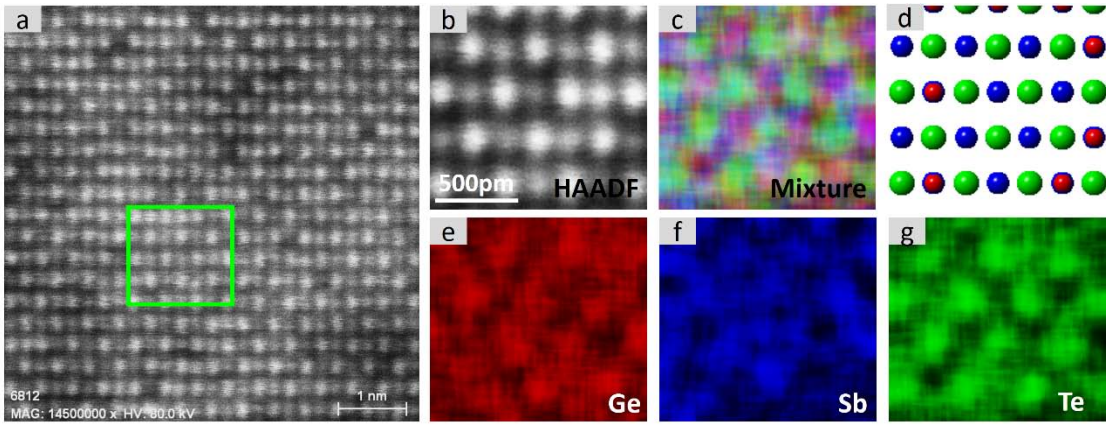

Figure 5. Structural and chemical maps of the GST cubic phase along the <110> zone axis. **a**, HAADF image. **b**, HAADF-STEM image, zooming into the green region marked in **a**. **c**, Composite elemental mapping of Ge/Sb/Te, **e**, **f**, **g** are the individual elemental mappings of Ge (red), Sb (blue), Te (green), respectively. **d** schematic showing the resultant atomic arrangement.

In the image in Fig. 5(a), some "dark" contrast in addition to the fcc planes reported above seem to be present. Zooming in, Fig. 6 demonstrates that locally there are "defects", due to vacancy ordering/clustering and corresponding depletion of Ge/Sb in the layer. Such defect ordering/clustering is expected to significantly change the resistivity of the cubic phase, potentially useful for multi-level memory.

Future Plans

We will continue to use state-of-the-art aberration-corrected TEM, especially the STEM mode for HAADF imaging and chemical mapping, to monitor the structural evolution, in particular the ordering of the vacancies, in the rocksalt GST at different stages of annealing. Presumably, with additional annealing at higher temperatures and/or longer times, the vacancies could order further, eventually into a "layer", which may be the precursor stacking before transition into the hexagonal phase of GST. The current multi-level memory cell (MLC) is achieved by tuning the ration between the amorphous and the crystalline portion of the phase change cell. The capacity suffers from resistance drift of the amorphous state. A new scheme would be to tune the state of the whole film, for example, inside the cubic, or hexagonal, phase of GST [5]. To this end, the understanding of the structure, particularly the distribution of species (Ge, Sb) and defects (vacancies and their clusters) on the sublattices, is essential before one can model and understand the electronic structure and resistivity behavior.

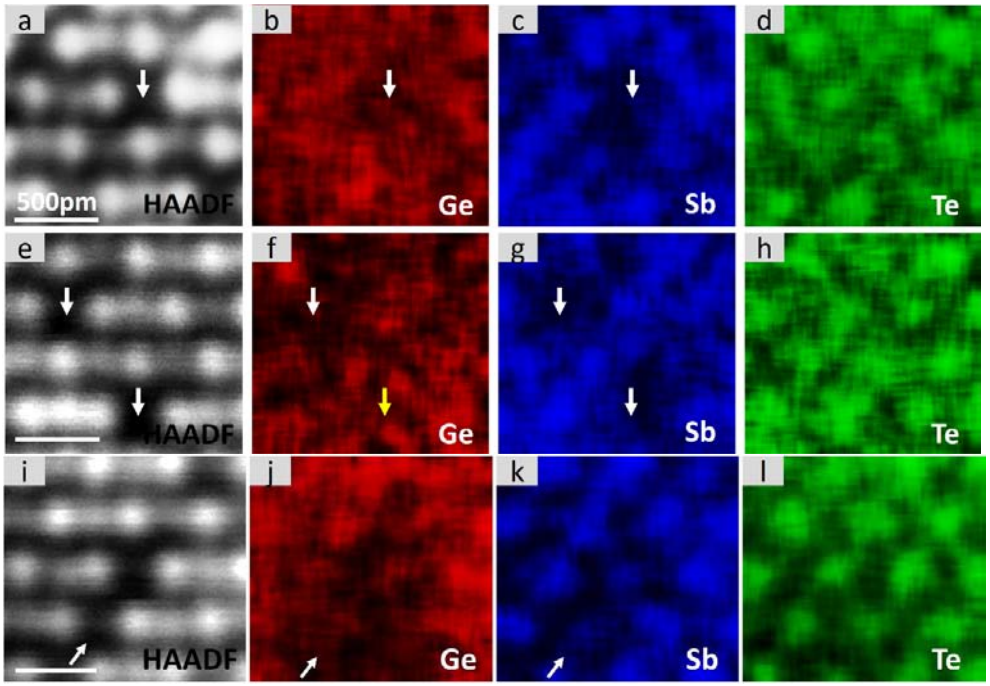

Fig. 6 Defects in the Ge/Sb/Vacancy layers. **a-d**, a darker spot; **e-h**, two adjacent dark spots; **i-l**, "short lines". The white arrows mark the shortage of Ge and Sb, due to enriched vacancies (possibly linked into strings in the through-foil direction). In 3D, the short-lines may be accumulated vacancies that have ordered into patches/clusters.

We also plan to use *ab initio* MD simulations to monitor the ABAB ring structure as well as cubes, Peierls-like distortion, homopolar bonding, tetrahedral Ge, etc. to figure out the structural origin of the fragile liquid behavior of GST [6,7]. We will examine the dynamic behavior (and heterogeneity), such as viscosity with temperature (there is no such study before in simulation). In the meantime, we have conceived an idea to develop an algorithm (a deletion-addition method for accelerated timescale simulations) to reach for a more stable configuration of *a*-GST. Regular *ab initio* molecular dynamics can only produce samples with cooling rates much higher than that in experiments (by at least 3-4 orders of magnitude). Our new approach may lead to a more stable and ordered configuration of *a*-GST that resembles real-world structure in actual device, and enable a more meaningful comparison with *c*-GST in simulated crystallization.

References

1. M. Xu, Y.Q. Cheng, H.W. Sheng and E. Ma, *Nature of atomic bonding and atomic structure in the phase-change $Ge_2Sb_2Te_5$ glass*, Phys. Rev. Lett. 103 (2009) Art. No.195502.
2. M. Xu, Y. Q. Cheng, L. Wang, H. W. Sheng, Y. Meng, W. G. Yang，X. D. Han, and E. Ma, *Pressure tunes electrical resistivity by four orders of magnitude in amorphous $Ge_2Sb_2Te_5$ phase-change memory alloy,* Proceedings of the National Academy of Sciences of the United States of America (PNAS), 109 (2012) E1055-E1062.
3. X.Q. Liu et al., *New Structural Picture of the Phase-Change GeSbTe Alloy*, Phys. Rev. Lett. 106 (2011) Art. No. 025501.
4. Y.Q. Cheng, M. Xu, H.W. Sheng, Y. Meng, X.D. Han and E. Ma, *A body-centered-cubic polymorph of the $Ge_2Sb_2Te_5$ phase-change alloy,* Appl. Phys. Lett. 95 (2009) Art. No. 131904.
5. W. Zhang, M. Muttig et al., Nature Mater. 11 (2012) 952.
6. J. Orava, A.L. Greer, B. Gholipour, D.W. Hewak, and C.W. Smith, Nature Mater. 11 (2012) 279–283.
7. Y.Q. Cheng and E. Ma, *Atomic-level structure and structure-property relationship in metallic glasses,* Progress in Materials Science, 56 (2011), pp. 379-473.

Publications

A list of the most recent (~ past 2 years) papers supported by DoE-BES is given in the following.

1) J. Ding, M. Xu, P.F. Guan, S.W. Deng, Y.Q Cheng and E. Ma.
Temperature effects on atomic pair distribution functions of melts
Journal of Chemical Physics 140 (2014) 064501.

2) J. Ding, Y.Q. Cheng and E. Ma.
Full icosahedra dominate local order in $Cu_{64}Zr_{34}$ metallic glass and supercooled liquid
Acta Materialia 69 (2014) 343–354.

3) J. Ding, S. Patinet, M.L. Falk, Y.Q. Cheng and E. Ma.
Soft spots and their structural signature in a metallic glass
Proceedings of the National Academy of Sciences of the United States of America 111 (2014)14052-14056.

4) L.H. Wang, J. Teng, P. Liu, A. Hirata, E. Ma, Z. Zhang, M.W. Chen and X.D. Han.
Grain rotation mediated by grain boundary dislocations in nanocrystalline platinum
Nature Communications 5 (2014) 4402.

5) M. Xu, J. Ding and E. Ma.
One-dimensional stringlike cooperative migration of lithium ions in an ultrafast ionic conductor
Appl. Phys. Lett. 101 (2012) 031901.

6) B. Zhang, X.D. Han, E. Ma et al.
Distribution of atomic species and defects in the rocksalt structure of the phase-change memory alloy $Ge_2Sb_2Te_5$
Nature Communications, submitted.

Elucidation of Hydrogen Interaction Mechanisms with Metal Doped Carbon Nanostructures

Ragaiy Zidan (PI), Joseph A. Teprovich Jr., Patrick A. Ward, Arron L. Washington

Savannah River National Laboratory, Aiken, SC 29808 **E-mail:** Ragaiy.Zidan@srnl.doe.gov

In Collaboration with

Puru Jena

Department of Physics, Virginia Commonwealth University, Richmond, VA 23284

Program Scope

This program continues to support the Office of Basic Energy Sciences (BES) mission through the development of a basic understanding of the formation and the physicochemical properties of carbon nanostructures, formed by the interaction of doped carbon nanomaterials with hydrides and/or hydrogen gas. For many years extensive work has been conducted on hydrogen interaction with metals and alloys forming hydrides. The research work on metal hydrides involved significant number of studies and characterization efforts, where chemical, electronic, optical and magnetic properties where determined. Our work continues to focus on the unique class of materials, metal-doped carbon nanostructure and their interaction with hydrogen. Our work will continue to focus on understanding the formation of these materials and on investigating their chemical, electronic, optical and magnetic properties when reacted with hydrogen. Previous work in our group through BES programs has led to advances in control over a material's properties at the electronic, molecular, and atomic level, which serve as the foundation of new energy technologies and can support other aspects of DOE missions. Our group has observed related properties in the materials such as hydrogen storage and luminescence with potential applications in clean energy and energy storage. However, developing customizable functional materials requires relating the microstructure of the materials to their physical properties. Our research activities will be aimed at developing and characterizing a novel class of hydride materials based on metal-carbon nanostructures. The current work will investigate different carbon materials utilizing their structure as building blocks for achieving unique properties based on zero, one and two dimension (0D, 1D, 2D) structures such as fullerenes, carbon nanotubes and graphene respectively.

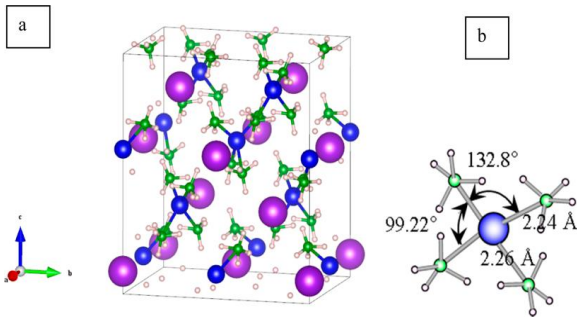

Figure 1. *(a) Crystal structure of $KAl(BH_4)_4$ viewed along the a-axis showing the coordination of the Al atoms (blue) by BH4− tetrahedral (green). (b) Structure of the $Al(BH_4)_4$− anion as was generated directly from the structural data of $K[Al(BH_4)_4]$.*

Recent Progress

Our work over the past two years has resulted in 12 publications, two of which were

published jointly with the experimental group of Dr. R. Zidan. The work covered a wide range of topics including the role of catalysts in the dehydrogenation of borohydrides to carbon-based nanostructures for hydrogen storage and the origin of the intermediate phases during decomposition of metal borohydrides. The joint experimental-theoretical work involved a novel bimetallic borohydride, namely $KAl(BH_4)_4$ which was identified as a "hypersalt" (**Figure 1**). We were able to demonstrate that highly volatile and pyrophoric $Al(BH_4)_3$ can be made safer if converting it into a hyper-halogen, $Al(BH_4)_4$ and reacting it with a K cation. This recipe can now be used to design and synthesize a large class of bimetallic borohydrides that are perovskite-like and have potential beyond hydrogen storage, for example as ferroelectrics and solar cell materials.

In another joint project between our groups, we built on our previous study of ionic mobility in a $LiBH_4$-C_{60} system, a series of electrochemical measurements were performed to quantify the lithium ionic mobility in the material under various conditions. This study also demonstrated that the material can be used as a solid electrolyte in an all solid-state lithium ion battery. Theoretical calculations by Prof. Jena's group indicated that the Li^+-BH_4^- bonding is perturbed in the presence of C_{60} resulting in a highly mobile Li ion due to the C_{60}-BH_4^- interaction (**Figure 2**). This suggests a nanoionic mechanism is responsible for the enhanced Li ion mobility due the formation of new interfaces at the nanoscale favoring the production of charge carriers.

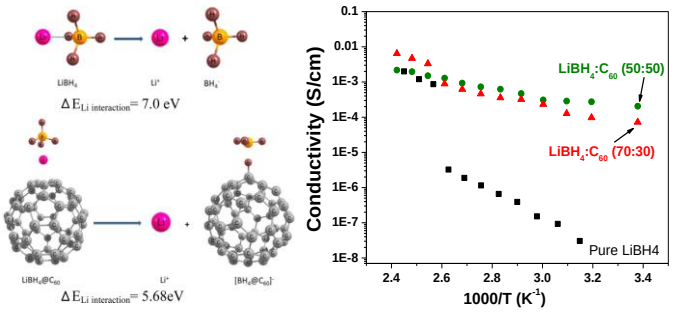

Figure 2. *(left) First-principles calculations of Li interaction in $LiBH_4$ with and without presence of C_{60}. (right) Comparison of the lithium ionic mobility in the $LiBH_4$-C_{60} nanocomposite versus pure $LiBH_4$.*

Further LDI-TOF-MS analysis of a sodium intercalated fullerene (Na_xC_{60}) in the hydrogenated state provided the first spectroscopic evidence for the formation of $C_{60}H_{60}$ among other highly hydrogenated fullerenes ($C_{60}H_{>36}$) (**Figure 3**). This finding was also confirmed through deuteration of the same material to form $C_{60}D_{60}$. Current efforts in this system are focusing on the

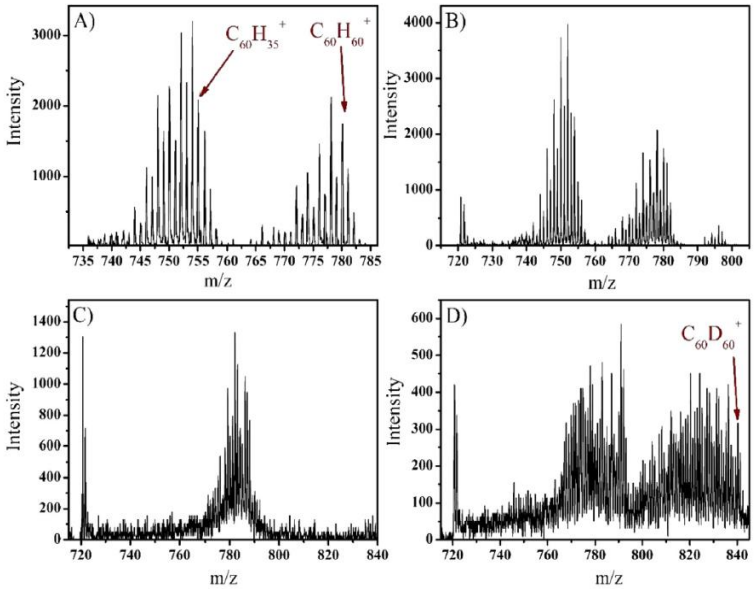

Figure 3. *Positive mode LDI-TOF-MS spectra of hydride doped Na_6C_{60} A) hydrogenated at 350°C and 100 bar H_2 B)hydrogenated at 350°C and 100 bar H_2 air exposed overnight C) deuterated at 290°C and 100 bar D_2 D) deuterated at 350°C and 100 bar D_2.*

isolation of the $C_{60}H_{60}$ from the other fulleranes for further analysis and characterization. Our current work is aimed at understanding how hydrogen interaction with C_{60} and other carbon nanomaterials can potentially lend itself to other energy storage systems and energy conversion devices.

Future Plans

Our future plan is to study systematically the interaction of hydrogen with C_{60}, namely $C_{60-x}H_x$ (x=1-60) to determine their electronic and optical properties. Preliminary experimental results on this system are already available in Dr. Zidan's group. The $C_{60}H_x$ system can potentially serve as a model system for understanding defect induced emission in carbon quantum dots (CQDs). We also plan to investigate the possibility of using BH_4^- anions in the formation of new perovskite-like phases. Until now, most perovskite structures have the formula ABO_3, where A and B are metal atoms. Having hydrides with perovskite structures will open a new field where their potential for ferroelectric and solar cell materials can be explored.

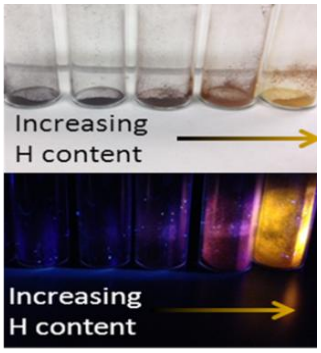

Figure 4. *(top) $C_{60}H_x$ with increasing values of x. (bottom) same samples exposed to UV-light.*

Some of our initial findings are shown in **Figure 4.** The amount of hydrogen present in the sample induces a visible color change in the material from black/brown at low hydrogen content to yellow at higher hydrogen content. The introduction of hydrogen defects in C_{60} also induces fluorescence in the visible spectrum. Additionally, we have been able to successfully incorporate the $C_{60}H_x$ material into a flexible polymer and still retain the photophysical properties of $C_{60}H_x$ when exposed to a UV source **Figure 5**.

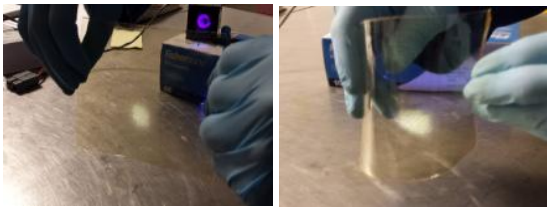

Figure 5. *$C_{60}H_x$ incorporated into a flexible polymer and exposed to a UV-source.*

Publications

[1] Paduani, C. and Jena, P.: "Role of Ti-based catalysts in the dehydrogenation mechanism of magnesium borohydride: A Cluster approach", Int. Journal of Hydrogen Energy 38, 2357 (2013)
[2] Wu, M., Wang, Q., Sun, Q., and Jena, P.: "Functionalized Graphitic Carbon Nitride for Efficient Energy Storage", J. Phys. Chem. C 117, 6055 (2013)
[3] Knight, D. A., Zidan, R., Lascola, R., Mohtadi, R., Ling, C., Sivasubramaniam, P. K., Kaduk, J. A., Hwang, S.-J., Samanta, D., and Jena, P.: "Stabilization of Hydrogen Rich, Yet Highly Pyrophoric $Al(BH_4)_3$ via the Synthesis of the Hypersalt $K[Al(BH_4)_4]$", J. Phys. Chem. C 117, 19905 (2013)
[4] Zu, G., Lu, K., Sun, Q., Kawazoe, Y., and Jena, P.: "Lithium-doped Triazine-based C_3N_4 Sheet for Hydrogen Storage at Ambient Temperature", J. Comp. Mat. Science 81, 275 (2014)

[5] Liu, Y., Giri, S., Zhou, J., and Jena, P.: "Intermediate phases during decomposition of metal borohydrides, $M(BH_4)_n$ (M=Na, Mg, Y)", J. Phys. Chem. C 118, 28456 (2014)
[6] Liu, Y., Zhou, J., and Jena, P.: "Electronic Structure and Stability of Mono- and Bi-metallic Borohydrides and Their Underlying Hydrogen-Storage Properties – A Cluster Study", J. Phys. Chem. C (in press)
[7] Knight, D.A., Teprovich Jr., J.A., Peters, B., Summers, A., Ward, P.A., Compton, R.N., Zidan, R.: "Synthesis, Characterization, and Reversible Hydrogen Sorption Study of a Sodium-doped Fullerene" Nanotechnology, 24, 455601 (2013)
[8] Paolone, A., Palumbo, O., Leardini, F., Cantelli, R., Knight, D.A., Teprovich Jr., J.A., Zidan, R.:"A Spectroscopic Investigation of Hydrogenated Li Doped Fullerane" J. Alloys and Compd., 580, S67-S69 (2013).
[9] Teprovich Jr., J.A., Knight, D.A., Peters, B., Zidan, R.: "Comparative Study of Reversible Hydrogen Storage in Alkali-Doped Fulleranes" J. Alloys and Compd. 580, S364-S367 (2013)
[10] Ward, P.A., Teprovich Jr., J.A., Peters, B., Wheeler, J., Compton, R.N., Zidan, R.: "Reversible Hydrogen Storage in a $LiBH_4$-C_{60} Nanocomposite" J. Phys. Chem. C, 117, 22569-22575 (2013)
[11] Teprovich Jr., J.A., Colón-Mercado, H.R., Ward, P.A., Peters, B., Giri, S., Zhou, J., Greenway, S., Compton, R.N., Jena, P., Zidan, R.: "Experimental and Theoretical Analysis of Fast Lithium Ionic Conduction in a $LiBH_4$–C_{60} Nanocomposite" J. Phys. Chem. C, 118, 21755–21761 (2014)
[12] Ward, P.A., Teprovich Jr., J.A., Compton, R.N., Schwartz, V., Veith, G.M., Zidan, R.: "Evaluation of the physi- and chemisorption of hydrogen in alkali (Na, Li) doped fullerenes" Int. J. Hydrogen Energy, 40, 2710-2716 (2015)

Session VII

DOE award DE-FG02-96ER45571**,** Massachusetts Institute of Technology

First principles prediction of structure, structure selectivity, and thermodynamic stability under realistic conditions

PI: Professor Gerbrand Ceder, Department of Materials and Engineering
Massachusetts Institute of Technology. gceder@mit.edu

Program Objectives

The objectives of this programare:

1) Develop adata-mining algorithm that can be combined with Density Functional Theory for the computationally efficient prediction of new crystal structures.
2) Develop a methodology for the calculation of surface energies as a function of adsorbates and pH in aqueous solutions.
3) Develop and test a formalism for the efficient calculation of charged surfaces.
4) Extend the existing Pourbaix formalism to calculate material stability as a function of pH, charge, size, and adsorbates, eventually leading to the ability to predict material synthesis pathways

Accomplishments

A distance semi-metric in compound space

The availability of large amounts of data generated by high-throughput computing or experimenting has generated interested in the application of machine learning techniques to materials science. Machine learning of materials behavior requires the use of feature vectors or descriptors that capture the essential compositional or structural information that is most likely to influence a property. While humans tend to use intuitive –and imprecise – ideas to evaluate whether two chemistries or crystal structures are the same, machine learning requires quantitative metrics to evaluate "similarity". Rigorous structure descriptions including concepts such as unit cells and symmetry, but chemists and materials scientists often use more intuitive and less well-defined terminology such as local environment, coordination, and polyhedral connectivity, to explain the properties of a compound. Indeed, unit cells and symmetry vary discontinuously with small changes in the atomic coordinates, and therefore do not provide a good set of descriptors in which to understand or expand materials properties. We have developed a mathematical description of structure and chemistry that can be used to create a distance semi-metric between compounds. This allows us to rigorously define *similarity* between compounds, and we expect this formalism to form the basis for machine learning approaches in materials science.

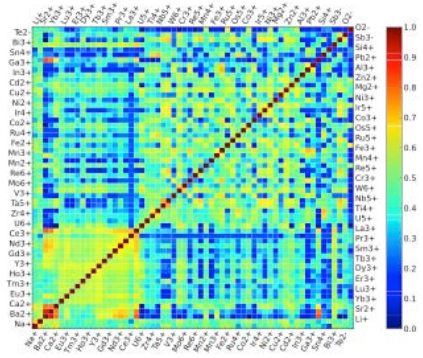

Figure 1: *Ionic similarity* indicates how likely two ions substitute for each other, thereby retaining

Our novel semi-metric captures both topological and chemical information of the local environment around atoms (i.e. an octahedral site formed by oxygen ions is

different from one formed by metal atoms). We combine a distance metric in chemical space (the *ionic similarity*) and in topological space (the *coordination similarity*), and coarse-grain the environment observed in known compounds (e.g. as documented in the ICSD database.

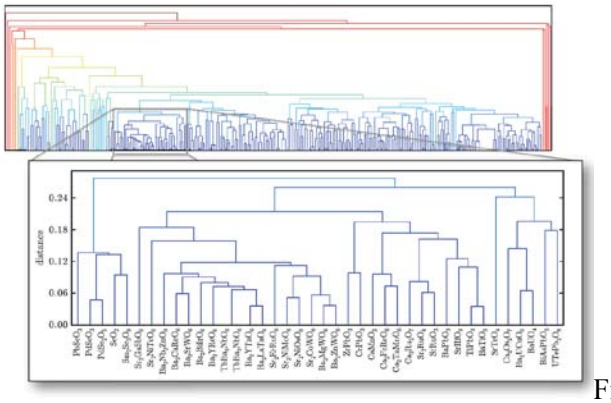

Figure 2: Dendogram showing which compounds are *similar* to each other

Figure 1 shows an *ionic similarity* metric. The matrix indicates how likely two elements are to substitute for each other in a given crystal structure. We have integrated this *ionic similarity* with a *topological similarity* between two atomic environments, e_i and e_j, obtained by creating a weighted Voronoi polyhedron as defined by O'Keefe.[i] From this construction, every ion i in a crystal structure X has a set of associated neighbors $\{n_i, w_i\}$, where n_i refers to a neighboring ion and w_i is its associated weight. A similarity score can then be defined as:

$$\text{score}\left(n_i \in e_i, n_j \in e_j\right) = \text{sim}_{\text{ion}}\left(n_i, n_j\right)\min\left(w_i, w_j\right)e^{-\frac{\left(w_i - w_j\right)^2}{2c^2}}.$$

The variable c tunes differences in topological or geometric similarity. The product of two atomic environments e_i and e_j, can then be defined via a one to one weighted bipartite graph matching between the vertices of $\{n_i\}$ to the vertices $\{n_j\}$. Each vertex in $\{n_i\}$ is matched to the vertex in $\{n_j\}$ that maximizes the sum of the similarity scores. If one neighborhood has more ions than the other, ions to complete the matching are inserted with similarities equal to zero:

$$\text{prod}\left(e_i, e_j\right) = \max_{\text{matchings}} \sum_{n_i, n_j \in \text{matchings}} \text{score}\left(n_i, n_j\right).$$

Finally, we define the similarity between two local environments:

$$\text{sim}_{\text{env}}\left(e_i, e_j\right) = \frac{\text{prod}\left(e_i, e_j\right)}{\sqrt{\text{prod}\left(e_i, e_i\right)\text{prod}\left(e_j, e_j\right)}}.$$

Figure 2 shows how our new distance measure can be used to construct a dendrogram, which groups compounds by similarity.

Predicting nucleation preferences

Predicting which phases can form and under which conditions they can form is one of the great unsolved problems of materials science, geology, and solid state chemistry. While it is amply clear that the lowest energy state for a given composition can easily form, no guidance exists as to how and when metastable polymorphs form instead. Solving this problem could lead to

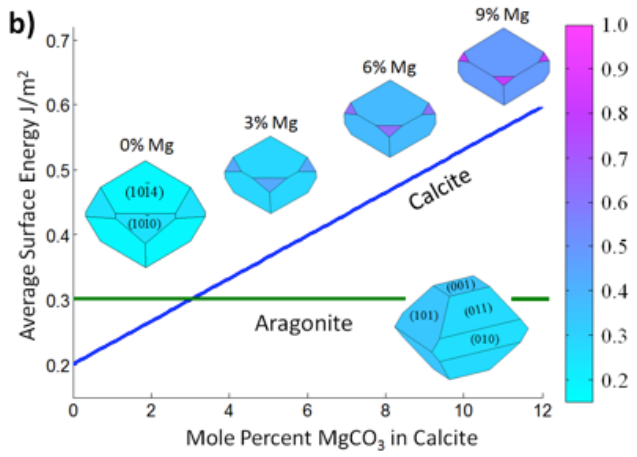

Figure 3: Surface energy of calcite and aragonite as function of Mg content

predictive and rational materials synthesis, and would significantly enhance the reach of computational materials development.

Metastable phases can form when they nucleate preferentially over the ground state phase. Predicting nucleation energies requires knowledge of relevant surface energies in the medium in which the phases form. In a first attempt to rationalize metastable phase formation we have studied the nucleation selection of the calcite or aragonite form of $CaCO_3$. This is an important problem in nature. Although calcite is the equilibrium phase under ambient conditions, metastable aragonite is the precipitated polymorph in modern seawater. Using *ab initio* density functional theory calculations, we demonstrated that in marine environments, calcite spontaneously incorporates Mg^{2+} in solid-solution, which increases its surface energy, and thus nucleation barrier, so that it greatly exceeds that of aragonite. Figure 3 shows the surface energy of both calcite and aragonite as a function of Mg concentration in the water the $CaCO_3$ precipitates from. Figure 4 shows the steady-state nucleation rates as function of supersaturation and Mg/Ca ratio in solution, clearly showing that aragonite is the preferred nucleation polymorph under high Mg/Ca ratios, including those that are found in modern seawater.

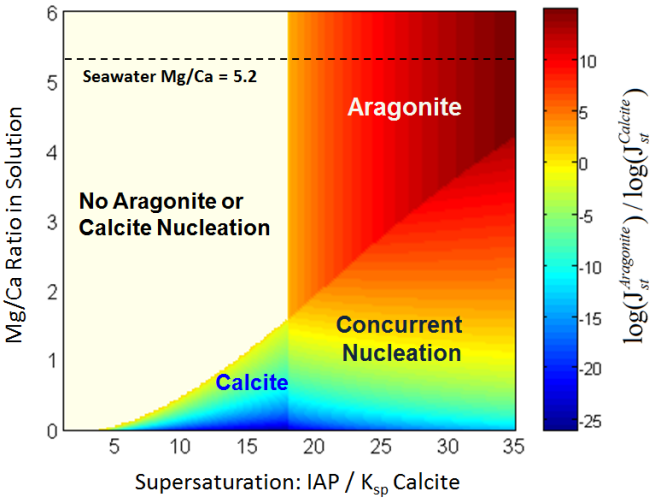

Figure 4: Nucleation preference as function of Mg/Ca ratio in solution and supersaturation

Plans for Next Year

We will continue to investigate the dependence of phase stability on size through careful modeling of surface energy as function of size. We expect that this will ultimately lead us to a predictive theory of polymorphism: i.e. can we predict which metastable structures can form, and under which conditions ?

Published and accepted Journal Publications of DOE sponsored research in 2013-2015

(1) S.P. Ong, W.D. Richards, A. Jain, G. Hautier, M. Kocher, S. Cholia, D. Gunter, V.L. Chevrier, K. Persson, G. Ceder, *Python Materials Genomics (Pymatgen): A Robust, Open-source Python Library for Materials Analysis,* Computational Materials Science, 68, 314-319 (2013).
(2) Y. Wu, P. Lazic, G. Hautier, K. Persson, G. Ceder, *First Principles High Throughput Screening of Oxynitrides for Water-Splitting Photocatalysts*, Energy & Environmental Science 6 (1), 157-168 (2013).
(3) A. Jain, S.P. Ong, G. Hautier, W. Chen, W.D. Richards, S. Dacek, S. Cholia, D. Gunter, D. Skinner,
(4) G. Ceder, K.A. Persson, *Commentary: The Materials Project: A Materials Genome Approach to Accelerating Materials Innovation,* APL Materials 1, 011002, 1-11 (2013).
(5) P. Lazic, R. Armiento, F.W. Herbert, R. Chakraborty, R. Sun, M.K.Y. Chan, K. Hartman, T. Buonassisi, B. Yildiz, G. Ceder, *Low Intensity Conduction States in FeS2: Implications for Absorption, Open-circuit Voltage and Surface Recombination,* Journal of Physics-Condensed Matter, 25 (46), 465801 (2013).
(6) W. Sun, G. Ceder, *Efficient Creation and Convergence of Surface Slabs*, Surface Science, 617, 53-59 (2013).
(7) Y. Wu, G. Ceder, *First Principles Study on Ta3N5:Ti3O3N2 Solid Solution as a Water-Splitting Photocatalyst*, Journal of Physical Chemistry, 117 (47), 24710-24715 (2013).
(8) L. Yang, G. Ceder, *Data-Mined Similarity Function Between Material Compositions*, Physical Review B, 88 (22), 224107 (2013).
(9) S.Y. Kang, Y.F. Mo, S.P. Ong, G. Ceder, *Nanoscale Stabilization of Sodium Oxides: Implications for Na-O-2 Batteries*, Nano Letters, 14 (2), 1016-1020 (2014).
(10) Wenhao Sun, S. Jayaraman, W.Chen, K.A. Persson, and G. Ceder, *Nucleation of metastable aragonite $CaCO_3$ in seawater*. Proceedings of the National Academyof Science, doi/10.1073/pnas.1423898112 (2015).

[i] M. O'Keeffe, "A proposed rigorous definition of coordination number," ActaCrystallographica A35, 772-775 (1979).

Abstract

PROJECT TITLE:"Bare, Coated, and Supported Clusters"

PI: Jena, Purusottam
Department of Physics, Virginia Commonwealth University, Richmond, VA 23284-2000
pjena@vcu.edu

PROGRAM SCOPE:

The objective of this project is to provide a fundamental understanding of the structure-property relationships of a novel class of highly electronegative clusters and superatoms in the gas phase, study their interaction with ligands, support, and counter-ions, and explore their potential as building blocks of materials with tailored properties.

The project exploits the unique size and composition specific properties of clusters and how they are affected by interaction with ligands and support. Using firstprinciples theory our goal is to design atom-by-atom a new class of negative ions suitable for forming salts with unusual properties, validate our predictions by working closely with experimentalists, and guide experiments in focused discovery of new materials. The project deals with three interrelated thematic areas: (1) Design unconventional superhalogen clusters whose electron affinities far exceed those of halogen atoms. Most superhalogens known thus far are composed of inorganic species. Our goal is to design super and hyperhalogens composed of organic species as well as metallo-fullerenes encapsulating rare-earth and actinide elements. Stability of a new class of Zintl ions composed of transition metal atoms embedded in Au cages is explored. Fundamental chemistry of the electrolytes in Li-ion batteries (LIBs) is studied with a view to creating halogen-free LIBs. (2) Study the effect of ligands on the magnetic properties of coated transition metal clusters. We focus on Mn based systems as the coupling between Mn atoms is very sensitive to inter-atomic distances and charge state. (3) Provide a fundamental understanding of cluster support interaction by focusing on bare superatom clusters and those supported on metal oxide, Au(111), and graphene substrates. The objective is to see if cluster-assembled materials composed of earth-abundant elements can mimic the properties of rare or costly elements. We also explore the possibility of creating low-dimensional materials with unusual stoichiometry and properties. The choice of the above systems is motivated not only by their rich physical and chemical properties, but also by a wealth of supporting experimental and theoretical data.

RECENT PROGRESS:

Research over the past two years has resulted in 49 publications,five of which are featured on the cover of the journals [1-5]. These are given in Figs. 1-5. Some of the papers are published in high-impact journals such as Proceedings of the National Academy of Sciences, Journal of the American Chemical Society, and Angew. Chem. Int. Ed. The papers cover a wide range of topics in structure-property relationships of zero-dimensional systems (clusters), one-dimensional systems (nano-wires and nano-ribbons), two-dimensional systems (graphene oxide, functionalized graphene, C-N sheets, MoS_2, and organic monolayers), and three-dimensional

metallic carbon and boron nitride. The works on clusters involve studiesfrom colossal magnetism in carbon and boron doped Mn systems to the design and synthesis of super- and hyper-halogen clusters whose electron affinities are far larger than those of halogen atoms. The work on nano-wires and mono-layers involve unusual magnetic and electronic properties. We also demonstrated that carbon and BN with interlocking hexagons can form a metastable phase that is metallic. Also published during this period are two invited perspectives in J. Phys. Chem. *Letters*[6, 7] and one invited retrospective inInternational Journal of Mass Spectroscopy [8].Eleven of the papers are published jointly with experimentalists.

Figs. 1-5 Covers of journals-ChemPhysChem, Phys. St. Sol., J. Chem. Phys., Angew. Chem., PCCP

It is impossible to cover in detailthe basic science addressed in all the papers published in the past two years.The presentation, therefore, will focuson specific topic, namely on a new carbon allotrope, penta-graphene, which is composed only of pentagons. This new two-dimensional (2D) metastable carbon allotrope [9] resembles the Cairo pentagonal tilingwhich is highlighted "In This Issue" of the proceedings of the National Academy of Sciences (Fig. 6).

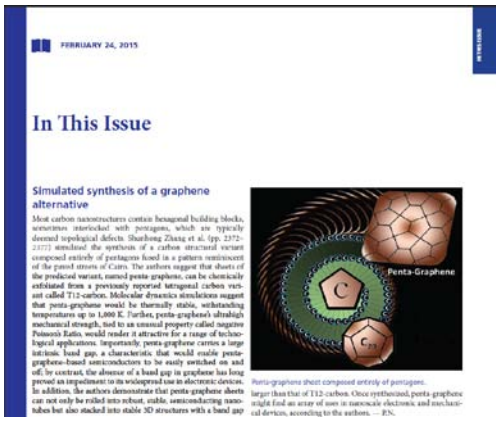

Fig. 6, Penta-graphene

Firstprinciplestheoretical calculations based on density functional theory confirm that the new carbon polymorph is not only dynamically and mechanically stable, but also can withstand temperatures as high as 1000 K. Due to its unique atomic configuration penta-graphene has an unusual negative Poisson's ratio (NPR) and ultra-high ideal strength that can even outperform graphene. Furthermore, unlike graphene that needs to be functionalized for opening a band gap, penta-graphene possesses an intrinsic quasi-direct band gap as large as 3.25 eV - close to that of ZnO and GaN. Equally important, penta-graphene can be exfoliated from T12-carbon.When rolled up, it can form pentagon-based nanotubes which are semiconducting, regardless of their chirality. When stacked in different patterns, stable 3D twin structures of T12-carbon are generated with band gaps even larger than that of T12-carbon. The versatility of penta-graphene and its derivatives are expected to have broad applications in nanoelectronics and nanomechanics.

FUTURE PLANS

Our future projects include studies of organic molecules that can have properties of superhalogens as well as superalkalies. Novel salts composed or organic cations and anions will be designed. We plan to work with experimentalists to synthesize such organic salts and study their properties. Second classes of problems will involve use of BH_4^- anions to create perovskite-like structures with potential applications in ferroelectric and solar cell materials. Magnetism of a new class of salt composed of alkalimetal cations (e.g. K^+) and Gd based superhalogens (e.g. $GdCl_3^-$) will be explored and the effect of Cl vacancies on the magnetic coupling will be investigated.

REFERENCES:

1. Wu, M. and Jena. P.: "Magnetic Hollow Cages with Colossal Moments", J. Chem. Phys. **139**, 044301 (2013)
2. Zhao, T., Li, Y., Wang, Q., and Jena, P.: "An All-Metal Cluster Mimicking the Chemistry of Halogens", Chem. Phys. Chem. **14**, 3227 (2013)
3. Mukherjee, P., Gupta, B., and Jena, P.: "Chain like structures of Gold supported by Silicon substrate", Physica Status Solidi B **251**, 913 (2014)
4. Zhao, T., Zhang, S., Wang, Q., Kawazoe, Q., and Jena, P.: "Tuning the Properties of Silicene with Magnetic Superhalogens", Phys. Chem. Chem. Phys. **16**, 22979(2014)
5. Giri, S., Behera, S., and Jena, P.: "Superhalogens as Building Blocks of Halogen-free Electrolytes in Li-ion Batteries", Angew. Chem. Int. Ed. **53**, 13916 (2014)
6. Jena, P.: "Beyond the Periodic Table of Elements: The Role of Superatoms", J. Phys. Chem. Letters **4**, 1432 (2013) (invited perspective)
7. Jena, P.: "Superhalogens: A Bridge Between Complex Metal Hydrides and Li-ion Batteries", J. Phys. Chem. *Letters* (invited perspective in press)
8. Jena, P. and Castleman, Jr., A. W.: "Mass spectrometry and its role in advancing cluster science", Int. J. Mass Spectroscopy (invited retrospective in press)
9. Zhang, S., Zhou, J., Wang, Q., Chen, X., Kawazoe, Y., and Jena, P.: "Penta-graphene: A New Carbon Allotrope" , Proc. Nat. Acad. Sci. (in press)

PUBLICATIONS in 2013-2015:

1. Gutsev, G. L., Weatherford, C. A., Jena, P., Johnson, E., and Ramachnadran, B. R.: "Competition between surface chemisorption and cage formation in $Fe_{12}O_{12}$ clusters", Chem. Phys. Letters **556**, 211 (2013).
2. Zhang, S., Zhou, J., Wang, and Jena, P.: "Structure, stability and property modulations of stoichiometric graphene oxide", J. Phys. Chem. C **117**, 1064 (2013).
3. Li, X., Zhou, J., Wang, Q., and Jena, P.: "Patterning C-N sheets to kagome lattice for magnetic materials", J. Phys. Chem. Letters **4**, 259 (2013).
4. Paduani, C. and Jena, P.: "Structure, stability and superhalogen properties of sodium and magnesium borohydrides", Chem. Phys. Lett. **556**, 173 (2013).
5. Li, Y., Zhang, S., Wang, Q., and Jena, P.: "Structure and Properties of Mn_4Cl_9: An Antiferromagnetic Binary Superhalogen", J. Chem. Phys. **138**, 054309 (2013).
6. Koirala, P., Pradhan, K., Kandalam, A., and Jena, P.: "Electronic and Magnetic Properties of Manganese and Iron Atoms Decorated with BO_2Superhalogens", J. Phys. Chem. A (invited) **117**, 1310 (2013)
7. Wu, M., Burton, J. D., Tsymbal, E. Y., Zheng, X., and Jena, P.: "Hydroxyl-decorated graphene systems as candidates for organic metal-free ferroelectrics, multiferroics, and high-performance proton battery cathode materials", Phys. Rev. B (Rapid Communication) **87**, 081406(R) (2013)
8. Wu, M. and Jena, P.: "Giant magnetic moments of B and C doped cubctohedral Mn_{13} clusters", Nanoscale, **5**, 2114 (2013)
9. Jena, P.: "Beyond the Periodic Table of Elements: The Role of Superatoms", J. Phys. Chem. Letters **4**, 1432 (2013) (invited perspective)
10. Gutsev, G. L., Weatherford, C. W., Belay, K. G., Ramachandran, B. R., and Jena, P.: "An all-electron density functional theory study of the structure and properties of the neutral and singly charged M_{12} and M_{13} clusters: M=Sc-Zn", J. Chem. Phys. **138**, 164303 (2013)
11. Wu, M. and Jena. P.: "Magnetic Hollow Cages with Colossal Moments", J. Chem. Phys. **139**, 044301 (2013)
12. Mukherjee, P., Gupta, B. C., and Jena, P.: "Electronic and magnetic properties of pristine and transition metal doped ZnTe nanowire", J. Phys. Condes. Matter. **25**, 266003 (2013)
13. Behera, S., Samanta, D., and Jena, P.: "Nitrate Superhalogens as Building Blocks of Hypersalts", J. Phys. Chem. A **117**, 5428 (2013)
14. Wu, M., Zheng, X. C., and Jena, P.: "Unusual Magnetic Properties of Functionalized Graphene Nanoribbons": J. Phys. Chem. Lett. **4**, 2482 (2013)
15. Zhang, X., Visser, B., Tschurl, M., Collins, E., Wang, Y., Wang, Q., Li, Y., Sun, Q., Jena, P.,Boesl, U., Heiz, U., and Bowen, K.: "Communication: In Search of Four-Atom Chiral Metal Clusters" J. Chem. Phys. (Commun.) 139, 111101 (2013)
16. Chen, H., Kong, X., Zheng,W., Yao, J., Kandalam, A. K., and Jena, P.: "Anomalous Property of $Ag(BO_2)_2$Hyperhalogen: Does Spin-Orbit Coupling Matter?" Chem. Phys. Chem. **14**, 3303(2013)
17. Zhao, T., Li, Y., Wang, Q., and Jena, P.: "An All-Metal Cluster Mimicking the Chemistry of Halogens", Chem. Phys. Chem. **14**, 3227 (2013)

18. Vetter, K., Proch, S., Ganetfor, G. F., Behera, S., and Jena, P.: "Hydrogen mimicking the properties of coinage metal atoms in Cu and Ag monohydrides clusters", Phys. Chem. Chem. Phys. **15**, 21007 (2013)
19. Kan, M., Zhou, J., Sun, Q., Kawazoe, Y., and Jena, P.: "Intrinsic Ferromagnetism in MnO_2 Monolayer", J. Phys. Chem. *Letters* **4**, 3382 (2013)
20. Zhang, S., Wang, Q., Chen, X., and Jena, P.: "Stable Metallic 3D Metallic Phase of Carbon with Interlocking Hexagons", Proc. Nat. Acad. Sci. **110**, 18809 (2013)
21. Zhang, S., Wang, Q., Kawazoe, Y., and Jena, P.: "Three Dimensional Metallic Boron Nitride", J. Am. Chem. Soc. **135**, 18216 (2013)
22. Zhu, G., Kan, M., Sun, Q., and Jena, P.: "Anisotropic Mo_2-phthalocyanine sheet: A new member of the organometallic family", J. Phys. Chem. A **118**, 304 (2014)
23. Kan, M., Wang, J. Y., Li, X. W., Zhang, S. H., Li, Y. W., Kawazoe, Y., Sun, Q., and Jena, P. : "Structural stability and induced phase transition of MoS_2 monolayer", J. Phys. Chem. C **118**, 1515 (2014)
24. Wang, H., Zhang,X., Jae Ko,Y., Grubisic, A., Li, X., Gantefoer, G., Schnoeckel,[2] H., Eichhorn, B. W., Lee, M. S., Jena,P., Kandalam, A., K., Kiran, B., and Bowen, K. H.: "Aluminum Zintl Anion Moieties within Sodium Aluminum Clusters", J. Chem. Phys. **140**, 054301 (2014)
25. Tao, K., Sun, Q., Wang, Q., Stepanyuk, V., and Jena, P.: "Self-consistent Determination of Hubbard U for Explaining the Anomalous Magnetism of Gd_{13} Cluster", Phys. Rev. B **89**, 085103 (2014)
26. Giri, S., Behera, S., and Jena, P.: "Superalkalis and Sueprhalogens as building blocks of Supersalts", J. Phys. Chem. A **118**, 638 (2014)
27. Child, B., Gronett, S., and Jena, P.: "Aromatic Superhalogens", Chemistry- A European Journal **20**, 4736 (2014)
28. Wang, H., Ko, Y-J., Zhang, X., Gantefoer, G., Schnoeckel, H., Eichhorn, B., Jena, P., Kiran, B., Kandalam, A., Bowen, K.: "The Viability of Aluminum Zintl Anion Moieties within Magnesium-Aluminum Clusters", J. Chem. Phys. **140**, 124309 (2014)
29. Behera, S., Samanta, D., King, N., and Jena, P.: "Potential for ZrO clusters as replacement Pd catalyst", J. Chem. Phys. 141, 034301 (2014)
30. Giri, S., Moore, C. H., Mcleskey, J. T., and Jena, P.: "Origin of Red-shift in the Photo absorption Peak in MEH-PPV Polymer", J. Phys. Chem. C **118**, 13444 (2014)
31. Awnehss, A., Behera, S., El-Kaderi, H., and Jena, P.: "New insights into Carbon dioxide interactions with benzimidazole-linked polymers", Chem. Comm. **50**, 3571 (2014)
32. Mukherjee, P., Gupta, B., and Jena, P.: "Chain like structures of Gold supported by Silicon substrate", Physica Status Solidi B **251**, 913 (2014)
33. Zhou, J., Giri, S., and Jena, P.: "18-electron rule inspired Zintl-like ions composed of all transition metals", Phys. Chem. Chem. Phys. **16**, 20241(2014)
34. O'Neal, K. R., Brinzari, T. V., Wright, J. B., Ma, C., Giri, S., Schlueter, J. A., Wang, Q., Jena, P., Liu, Z., and Musfeldt, J. "Pressure-Induced Magnetic Crossover Driven by Hydrogen Bonding in $CuF_2(H_2O)_2$(3-chloropyridine)", Scientific Reports **4**, 6054 (2014)

35. Zhao, H. M. Zhao, Lin, X., Li, Y., Wang, Q., and Jena,P.: "Structural, electronic and magnetic properties of neutral and anionic $Fe_2(BO_2)_n$ (n=1~3) clusters", Phys. Letters A **378**, 2959 (2014)
36. Giri, S., Child, B., and Jena, P.: "Organic Superhalogens", Chem. Phys. Chem. **15**, 2903 (2014)
37. Rao, B. K., Samanta, D., Joshi, S., Basu, K., Baldwin, S. D., Jha, A., Dukat, M., Glennon, R. A., and Jena, P.: "Receptor-Ligand Interaction at 5-HT_3 Serotonin Receptors: A Cluster Approach", J. Phys. Chem. A **118**, 8471(2014)
38. Graham,J. D. , Buytendyk, A. M., Zhang,X., Collins,E. L., Kiran,B., Gantefoer, Eichhorn,B. W., Gutsev,G. L., Behera, S., Jena,P., and Bowen,K. H.: "Alanate Anion, AlH_4^-: Photoelectron Spectrum and Computations", J. Phys. Chem. A **118**, 8158(2014)
39. Zhao, T., Zhang, S., Wang, Q., Kawazoe, Q., and Jena, P.: "Tuning the Properties of Silicene with Magnetic Superhalogens", Phys. Chem. Chem. Phys. **16**, 22979(2014)
40. Teprovich Jr., J, Colon-Mercado, H., Ward, P., Peters, B., Giri, S., Zhou, J., Greenway, S., Compton, R., Jena, P., and Zidan, R.: "Experimental and Theoretical Analysis of Fast Lithium Ionic Conduction in a $LiBH_4$-C_{60}Nanocomposite", J. Phys. Chem. C **118**, 21755 (2014)
41. Kong,X-Y., Xu,H-G., Koirala, P., Zheng,W-J., Kandalam,A. K., Jena, P.: "Identification of Hyperhalogens in $Ag_n(BO_2)_m$ (n=1-3, m=1-2) clusters: Anion Photoelectron Spectroscopy and Density Functional Calculations", Phys. Chem. Chem. Phys. **16**, 26067 (2014)
42. Zhou, J., Sun, Q., Wang, Q, and Jena, P.: "Tailoring Li Adsorption on graphene", Phys. Rev. B. **90**, 205427 (2014)
43. Pradhan, K. and Jena, P.: "$LiFe_2Cl_n$ (n = 4-6) Clusters: Double-exchange Mediated Molecular Magnets", Appl. Phys. Letters **105**, 163112 (2014)
44. Giri, S., Behera, S., and Jena, P.: "Superhalogens as Building Blocks of Halogen-free Electrolytes in Li-ion Batteries", Angew. Chem. Int. Ed. **53**, 13916 (2014)
45. Zhou,J., Zhang,S., Wang,Q., Sun,Q., Kawazoe,Y., and Jena, P.: "Self-assembly of Metal Atoms (Na, K, Ca) on Graphene", Nanoscale **7**, 2352 (2015)
46. Jena, P. and Castleman, Jr., A. W.: "Mass spectrometry and its role in advancing cluster science", Int. J. Mass Spectroscopy (in press)
47. Yu, J., Sun, Q., Kawazoe, Y., and Jena, P.: "Stability and properties of 2D porous nanosheets based on tetraoxa[8]circulene analogues", Nanoscale (in press)
48. Zhang, S., Zhou, J., Wang, Q., Chen, X., Kawazoe, Y., and Jena, P.: "Penta-graphene: A New Carbon Allotrope" , Proc. Nat. Acad. Sci. (in press)
49. Jena, P.: "Superhalogens: A Bridge Between Complex Metal Hydrides and Li-ion Batteries", J. Phys. Chem. *Letters* (in press)

External-Field-Driven Surface Stabilization and Patterning

Dimitrios Maroudas (maroudas@ecs.umass.edu)
Department of Chemical Engineering, University of Massachusetts, Amherst, MA 01003

Program Scope

This work is part of our research program on *Surface Engineering by Simultaneous Action of Multiple External Fields* (**Award No. DE-FG02-07ER46407**). This program aims at enabling surface engineering strategies based on the fundamental understanding and predictive modeling of the surface morphological response of solid materials subjected to the combined action of multiple external forces. We focus on the surface morphological evolution and stability of electrically conducting and semiconducting solids under the simultaneous application of mechanical stresses, electric fields, and temperature gradients; materials of interest include metals, such as Cu, Ag, and Al, and semiconductors, such as Si and chemically functionalized or defect engineered graphene-based metamaterials. We emphasize on: identifying the conditions under which the driven surface morphology is stable, exploring the complexity of the corresponding various morphologically stable surface patterns, and generating and controlling nanoscale patterns on surfaces. Specifically, we investigate the morphological response to the combined action of multiple external forces of bulk solid surfaces, surfaces of thin films grown epitaxially on thick or thin substrates, as well as nanoscale surface features such as coherently strained epitaxial islands on substrate surfaces. The analysis of complex pattern formation as a result of the driven evolution of surface features (directed assembly), including distributions of single-layer epitaxial islands and vacancy islands, offers new paradigms of multiply driven surface nanopatterning. The research is based on a modeling approach that combines theoretical analyses of surface/feature morphological stability with self-consistent dynamical simulations of driven surface/feature evolution based on properly parameterized continuum and multi-scale surface transport models that we develop. Employing these models, we conduct systematic studies of the effects of multiple forcing conditions, varied over a broad range of material and operating parameters, on surface morphological response.

Recent Progress

Stabilization of the Surface Morphology of Stressed Solids Using Simultaneously Applied Thermal Gradients and Electric Fields – Our early studies in this program had demonstrated that electric current, through surface electromigration, can stabilize the surface morphology of stressed crystalline elastic solids against crack-like surface instabilities [1]. In a recent study, we examined the surface morphological stability of bulk conducting face-centered cubic (fcc) crystalline elastic solids in uniaxial tension under (a) the action of a temperature gradient [2] and (b) the simultaneous action of an electric field and a temperature gradient [3]. The analysis was based on self-consistent dynamical simulations, in conjunction with linear stability theory, according to our well validated fully nonlinear surface mass transport model that accounts for surface electromigration and thermomigration induced by the externally applied fields, surface diffusional anisotropy, and the Arrhenius temperature dependence of surface diffusivity. Our simulation results validated the findings of linear stability theory and established that: (a) a properly directed thermal gradient of magnitude higher than a critical value (on the order of 100 K/cm under conditions typical of metallic thin-film interconnects) can stabilize the

planar surface morphology [2] and (b) the electric field and the thermal gradient, if properly directed, can work synergistically to stabilize the planar surface morphology against the Asaro-Tiller/Grinfeld (ATG) instability, as shown in Fig. 1, when the strength of the resulting effective external field is higher than a critical level [3]. We also showed that the temperature dependence of the surface diffusivity does not change the criticality criterion for surface stabilization but only affects the rate of growth or decay of the surface morphological perturbation from its planar state [3]. Furthermore, we established that, in fcc crystals, the morphological response of <111>-oriented surfaces is superior to that of differently oriented surfaces [3]. Our study provides an effective practical solution to inhibit the surface cracking of crystalline conducting solids based

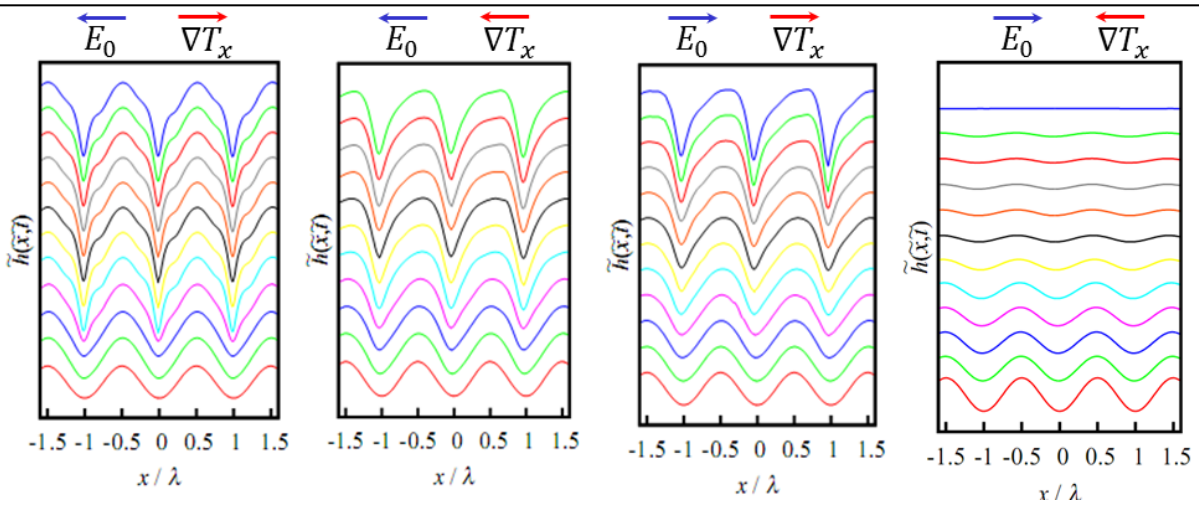

FIG. 1. Morphological evolution (from the bottom to the top profiles shown) of a <111>-oriented surface of a uniaxially stressed (along *x*) fcc metal, starting with a low-amplitude sinusoidal perturbation from a planar morphology and under different (shown) combinations of applied electric field and thermal gradient

on the optimal combination of the simultaneous action of externally applied electric fields and thermal gradients.

Nonlinear Analysis of Secondary Ripple Formation on Surfaces of Stressed Crystalline Solids – Self-consistent dynamical simulations of the surface morphological evolution of uniaxially stressed elastic crystalline solids have demonstrated that, in addition to ATG (surface cracking) instabilities, long-wavelength perturbations from the planar surface morphology can trigger a tip-splitting instability, which causes formation of a pattern of secondary ripples [4]. This type of surface pattern formation arises entirely due to the competition between surface energy and elastic strain energy and cannot be predicted by linear stability theory [4]. We have developed a weakly nonlinear theory, which can explain the occurrence of such secondary rippling instabilities and predict the number of secondary ripples that form on the surface as a function of perturbation wavelength [5]. We have also accounted in the theory for effects of surface diffusional anisotropy and of externally applied fields. The theory predicts the critical wavelength for the onset of secondary rippling and the external field strength required to stabilize the planar surface morphology [5]. The conclusions of the theory have been validated by systematic comparisons with results of self-consistent numerical simulations.

Current-Driven Complex Dynamics of Single-layer Epitaxial Islands on Substrates – We have conducted a systematic simulation study of the current-driven dynamics of single-layer

epitaxial islands on metallic crystalline substrates, which provides important guidance toward surface nanopatterning approaches based on the current-driven assembly of such islands. We have developed a fully nonlinear model for the islands' driven morphological evolution on elastic substrates of fcc crystals in the regime where diffusional mass transport is limited to the island edge [6] and validated the model by comparison of its predictions with experimental measurements [7]. We have discovered a transition in the asymptotic states reached by such driven island dynamics from steady to oscillatory, mediated by Hopf bifurcation, as shown in Fig. 2; this transition occurs at a larger-than-critical island size and at nonzero misorientation angles between the applied electric field direction and fast edge diffusion directions, other than 90°, 45°, and 30° for <110>-, <100>-, and <111>-oriented substrate surfaces, respectively. We have characterized the bifurcation and determined the dependence of the stable time-periodic state beyond the Hopf point on the misorientation angle, the strength of the edge diffusional anisotropy, and the island size. For islands larger than a critical size greater than that for Hopf bifurcation, depending on the orientation of the substrate surface, fingering and necking instabilities occur in the island morphology; for <100>- and <111>-oriented substrate surfaces at high misorientation angles, necking instabilities responsible for island breakup follow fingering instabilities.

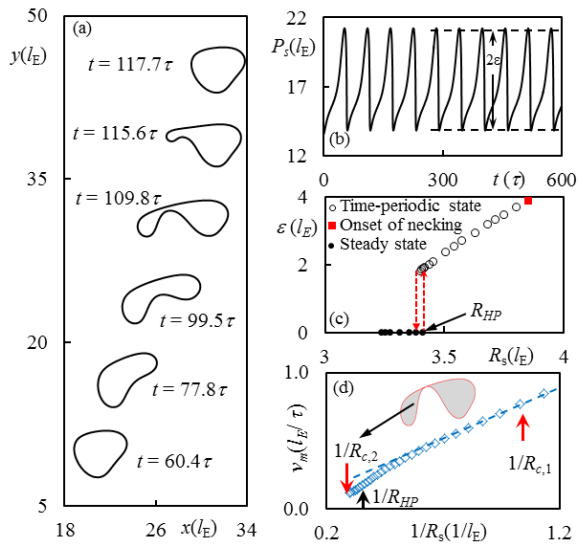

FIG. 2. (a) Current-induced morphological evolution of a single-layer homoepitaxial island (R_s = 3.81 l_E, where l_E is a characteristic length [6]) on a {110} surface at a misorientation angle of 45°. The island configurations have been displaced upwards (along y) over time. (b) Evolution of the island perimeter, P_s, for the island of (a). (c) Bifurcation diagram of the driven island morphological response, where the oscillation amplitude, ε, of the island perimeter at the asymptotic state is plotted as a function of island size, R_s. R_{HP} is the island size at the Hopf point. (d) Dependence of the island migration speed, v_m, on the inverse of the island size, $1/R_s$. The inset shows the island configuration at the onset of necking instability for $R_s = R_{c,2}$.

Surface Nanopatterning Using Electric-Field-Driven Assembly of Single-layer Epitaxial Islands – We have investigated an approach to surface nanopatterning based on electric-field-driven assembly of single-layer epitaxial islands on fcc crystalline substrates. We have used our validated fully nonlinear driven island evolution model, accounting for edge diffusional anisotropy, and a front tracking technique that can handle island coalescence and breakup phenomena. We have discovered the formation of complex

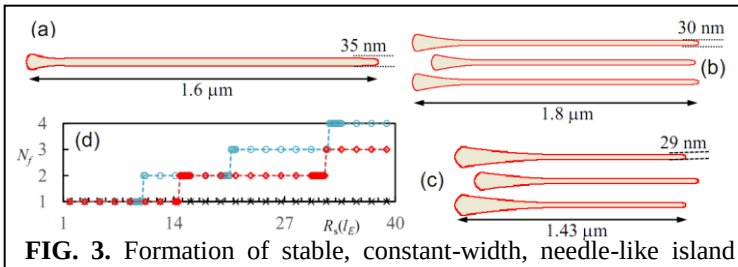

FIG. 3. Formation of stable, constant-width, needle-like island configurations as a result of current-induced fingering and necking instabilities undergone by large-size individual single-layer islands with the applied electric field oriented along the horizontal direction on (a) {110}, (b) {100}, and (c) {111} surfaces of Ag substrates at misorientation angles of (a) 90°, (b) 45°, and (c) 30°. (d) The number of such needle-like features, N_f, depends on the original island size, R_s, and the substrate surface orientation; ×-marks, open circles, and open diamonds are used to denote {110}, {100}, and {111} substrate surfaces, respectively.

nanopatterns on {110}, {100}, and {111} substrate surfaces, starting from either a single island with larger-than-critical size or an assembly of relatively small islands, which undergo a sequence of coalescence and breakup events [8]. For both initial configurations at all substrate surface orientations examined, important parameters that determine the nanopattern features include the misorientation angle between a fast edge diffusion direction and the applied electric field direction and the duration of application of the electric field. For assemblies of islands, we have also determined the resulting nanopattern dependence on the intrinsic geometrical parameters of the assembly [8]. Particularly notable is the formation of arrays of parallel needle-like island configurations of constant width (on the order of tens of nanometers), oriented along the electric field direction, as a result of fingering and necking instabilities undergone by the initial large-size single island configuration, as shown in Fig. 3, at misorientation angles of 90^o, 45^o, and 30^o for {110}, {100}, and {111} substrate surfaces, respectively. The number of finger-like features formed depends on the initial island size and the substrate surface orientation.

Future Plans

Our future research plans include: (1) Continuation of continuum-level analysis, dynamical simulation, and systematic parametric exploration of: (a) surface morphological instabilities and *external-field-driven stabilization* strategies of the stressed crystalline material systems within the program's scope; (b) driven dynamics of single-layer islands and vacancy islands and their assemblies toward developing systematic strategies for *physical nanopatterning of surfaces*; (c) external-field-driven highly complex (oscillatory, chaotic) dynamical response of surfaces and surface features. (2) Systematic, targeted atomic-scale computations of surface/edge properties, as well as their dependences on temperature and stress, and parameterization of surface/edge anisotropies for further incorporation of atomistic information into our continuum-level models toward continuous improvement of their predictive capabilities. (3) Development of coarse-grained (micromechanical/constitutive) models of strain relaxation based on analysis of molecular-dynamics simulations of material response to stress. (4) Development of multi-scale models of driven surface morphological evolution involving kinetic Monte Carlo simulations for atomic-scale modeling of surface/feature propagation toward fully quantitative predictions of physically driven nanopattering. (5) Continuation of our studies on directed assembly of colloidal-particle clusters and crystals, external-field-driven evolution of adsorbates on graphene, and physically driven patterning of graphene-based structures. (6) Development of experimental protocols to continue the validation of our models and test the modeling predictions for driven evolution of epitaxial film surfaces, epitaxial islands, and adsorbates on graphene.

References

1. V. Tomar, M. R. Gungor, and D. Maroudas, *Physical Review Letters* **100**, 036106/1-4 (2008).
2. L. Du, D. Dasgupta, and D. Maroudas, *Applied Physics Letters* **104**, 181901/1-4 (2014).
3. L. Du, D. Dasgupta, and D. Maroudas, *Journal of Applied Physics* **116**, 173501/1-11 (2014).
4. V. Tomar, M. R. Gungor, and D. Maroudas, *Applied Physics Letters* **94**, 181911/1-3 (2009); *Journal of Applied Physics* **109**, 053518/1-11 (2011).
5. L. Du, D. Dasgupta, and D. Maroudas, *Physical Review B*, submitted (2015).
6. D. Dasgupta, G. I. Sfyris, and D. Maroudas, *Surface Science* **618**, L1-L5 (2013).
7. C. Tao, W. G. Cullen, and E. D. Williams, *Science* **328**, 736-740 (2010).

8. D. Dasgupta and D. Maroudas, *Applied Physics Letters* **103**, 181602/1-4 (2013).

Publications of DOE sponsored research in 2013-2015

1. R. M. Sehgal, J. G. Cogan, D. M. Ford, and D. Maroudas, "Onset of the Crystalline Phase in Small Assemblies of Colloidal Particles," *Applied Physics Letters* **102**, Article No. 201905, 4 pages (2013).
2. G. I. Sfyris, D. Dasgupta, and D. Maroudas, "The Effect of a Thermal Gradient on the Electromigration-Driven Surface Morphological Stabilization of an Epitaxial Thin Film on a Compliant Substrate," *Journal of Applied Physics* **114**, Article No. 023503, 13 pages (2013).
3. D. Dasgupta, G. I. Sfyris, and D. Maroudas, "Current-Driven Morphological Evolution of Single-layer Epitaxial Islands on Crystalline Substrates," *Surface Science* **618**, L1-L5 (2013).
4. D. Dasgupta and D. Maroudas, "Surface Nanopatterning from Current-Driven Assembly of Single-Layer Epitaxial Islands," *Applied Physics Letters* **103**, Article No. 181602, 4 pages (2013).
5. R. M. Sehgal, D. Maroudas, and D. M. Ford, "Phase Behavior of the 38-atom Lennard-Jones Cluster," *Journal of Chemical Physics* **140**, Article No. 104312, 11 pages (2014).
6. L. Du, D. Dasgupta, and D. Maroudas, "Stabilization of the Surface Morphology of Stressed Solids Using Thermal Gradients," *Applied Physics Letters* **104**, Article No. 181901, 4 pages (2014).
7. R. M. Sehgal, D. Maroudas, and D. M. Ford, "Effects of the Attractive Potential Range on the Phase Behavior of Small Clusters of Colloidal Particles," *Journal of Chemical & Engineering Data* **59**, 3105-3112 (2014).
8. L. Du, D. Dasgupta, and D. Maroudas, "Stabilization of the Surface Morphology of Stressed Solids Using Simultaneously Applied Electric Fields and Thermal Gradients," *Journal of Applied Physics* **116**, Article No. 173501, 11 pages (2014).
9. L. Hu and D. Maroudas, "Thermal Transport Properties of Graphene Nanomeshes," *Journal of Applied Physics* **116**, Article No. 184304, 5 pages (2014).
10. M. A. Bevan, D. M. Ford, M. A. Grover, B. Shapiro, D. Maroudas, Y. Yang, R. Thyagarajan, X. Tang, and R. M. Sehgal, "Controlling Assembly of Colloidal Particles into Structured Objects: Basic Strategy and a Case Study," *Journal of Process Control*, in press (2015).
11. L. Du, D. Dasgupta, and D. Maroudas, "Weakly Nonlinear Theory of Secondary Rippling Instability in Surfaces of Stressed Solids," *Physical Review B*, submitted (2015).
12. R. M. Sehgal and D. Maroudas, "Equilibrium Shape of Colloidal Crystals," in preparation for submission to *Nano Letters* (2015).

13. D. Dasgupta and D. Maroudas, “Complex Oscillatory Dynamics of Current-Driven Single-layer Epitaxial Islands,” in preparation for submission to *Physical Review E* (2015).

14. A. Kumar, D. Dasgupta, C. Dimitrakopoulos, and D. Maroudas, “Current-Driven Dynamics of Large Single-layer Epitaxial Islands: An Approach to Surface Nanopatterning,” in preparation for submission to *Physical Review Letters* (2015).

Coupling Electrons, Phonons, and Photons for Nonequilibrium Transport Simulation

Irena Knezevic, University of Wisconsin – Madison

Program Scope

The objective of this project is to develop versatile computational tools for accurate simulation of the far-from-equilibrium and time-dependent quantum transport in realistic semiconductor nanostructures driven by high-intensity dc or ac electromagnetic fields. The key challenge in simulating nonequilibrium time-dependent transport is that one must capture the strong coupling between electrons, phonons, and electromagnetic fields in the same simulation, self-consistently and at every time step.

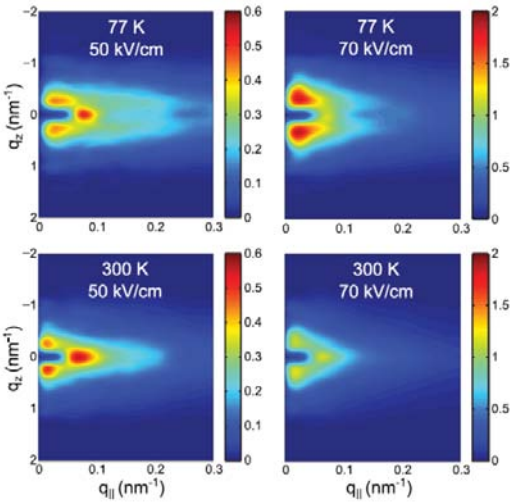

Figure 1.Nonequilibrium phonon occupation number (red – high, blue – low) at different fields and temperatures versus in-plane and cross-plane momentumin a GaAs-based midinfrared quantum cascade laser. The excess phonons exist only near the Brillouin zone center, but their population is drastically higher than in equilibrium. They strongly affect electronic transport, largely by amplifying electron scattering with phonon absorption. *From Shi and Knezevic, 2014* [2].

This project relates closely to experimental measurements of electronic, thermal, and optical properties of a variety of semiconductor nanostructures. For example, we predicted that uniformly doped double-barrier tunneling structures would act as emitters of THz-frequency radiation [1]; these are being fabricated by the PI's collaborators. The inclusion of nonequilibrium phonons affects measured performance of quantum cascade lasers (QCLs) in significant ways, leading to much better agreement between theory and experiment in the temperature performance [2]. Considering that QCLs are the highest-power coherent light sources at midinfrared and THz frequencies, this work significantly advances our understanding of the coupling between electrons and phonons in QCLs, aiding their widespread applications (Fig. 1).

Recent Progress

With high-intensity fields, considerable energy is pumped into the electron and hole systems, which relax by transferring much of it to the lattice; thereby, both electronic and lattice (phonon) systems are far from equilibrium. With high-frequency excitation, both interband and intraband electronic transitions potentially occur, and details of the interaction between the the electronic

systems and the fields are critical to capture. Three main directions have been undertaken during the course of this project (currently 2 years and 4 months in): a) high-frequency or time-dependent transport in nanostructures [1,3,4], b) nonequilibrium phonons in quantum cascade lasers (good example system for high-field dc transport) [2], and c) phonon transport in realistic confined structures of experimentally relevant sizes [5]. Under a), we calculated the ac conductivity, dielectric function and plasmon dispersion of graphene, with focus on the role of substrate impurities [3]. We also showed that self-sustained THz-frequency current oscillations occur in uniformly doped double-barrier tunneling structures, a phenomenon well documented at much lower frequencies in superlattices [1]. Under direction b), we demonstrated how critical it is to account for the coupled dynamics of electrons and phonons in far-from-equilibrium systems, especially at low temperatures. We have for the first time fully quantified the influence of nonequilibrium phonons on QCL operation (Fig. 1). Under c), we have developed a full-dispersion phonon Monte Carlo algorithms for 2D systems with hexagonal symmetry, like graphene nanoribbons, and elucidated the universal phonon transport features in nanowires with rough correlated surfaces (Fig. 2).

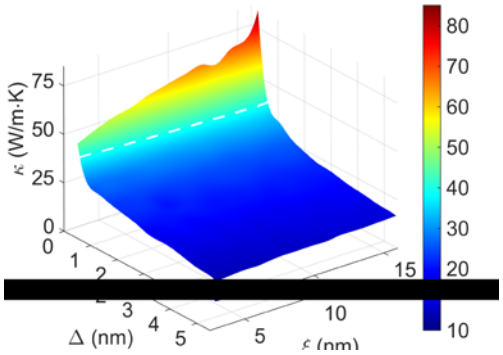

Figure 2. Thermal conductivity κ in 70-nm-wide Si nanowires with exponentially correlated real-space surface roughness of correlation length ξ and rms roughness Δ. The dashed line denotes the Casimir limit, the lower limit on thermal conductivity that is obtainable with the specularity model for phonon interaction with the boundaries. With real-space roughness, it is clear that a vast parameter space results in thermal conductivity below the Casimir limit, as seen in experiment. *From Maurer et al.* [5].

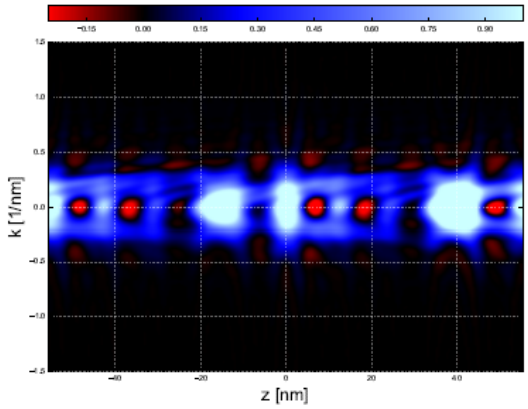

Figure 3.(*Preliminary data*)Wigner function (represented by color) versus position and wave vector for aTHz quantum cascade laser. Red denotes thenegative values of the Wigner function, which indicates coherent transport (tunneling). This type of simulation is computationally only marginally more intensive than semiclassical Monte Carlo, but captures coherent transport very well.*Jonassonand Knezevic*, in prep.

Future Plans

The work under a) and b) will merge as we include coherent tunneling effects with Wigner Monte Carlo along with nonequilibrium phonon effects for unprecedented accuracy in the modeling of heterostructures and superlattices far from equilibrium (Fig. 3). We will extend the effort to systems with 2D transport and look at how highly delocalized carriers, such as electrons in quantum point contacts at low temperatures, couple with light and how they respond to time-varying biasing. We will complete the work on the dielectric function and plasmons in graphene

nanoribbons and look into ways to "numerically" excite plasmons in graphene-based nanostructures with very accurate electronic and dielectric properties. Overall, during the next funding cycle, the PI will work on *three main thrusts*: 1. Far-from-equilibrium vertical quantum transport and optoelectronics in heterostructures,2. Microwave-driven quantum transport in 2DEG-based nanostructures at low temperatures, 3. Exciton dynamics and transport in low-dimensional nanostructures and nanostructured networks, as well as *two emergent thrusts*: 4. 2D materials and van der Waals heterostructures: electronic, thermal, and optical properties and 5. Coherent phonons in nanostructures). The PI will also work on releasing the codes developed during the current funding cycle.

References

[1] O. Jonasson and I. Knezevic, "Coulomb-driven terahertz-frequency intrinsic current oscillations in a double-barrier tunneling structure," Phys. Rev. B 90, 165415 (2014).

[2] Y. B. Shi and I. Knezevic, "Nonequilibrium phonon effects in midinfrared QCLs," J. Appl. Phys. 116, 123105 (2014).

[3] F. Karimi and I. Knezevic, "Dielectric function and plasmons in graphene: a self-consistent field calculation within a Markovian master equation formalism," submitted; N. Sule, K. J. Willis, S. C. Hagness, and I. Knezevic, "Terahertz-frequency electronic transport in graphene," Phys. Rev. B 90, 045431 (2014).

[4] I. Knezevic and B. Novakovic, "Time-dependent transport in open systems based on quantum master equations," J. Comput. Electron.12, 363-374 (2013).

[5] S. Mei, L. N. Maurer, Z. Aksamija, and I. Knezevic, "Full-dispersion Monte Carlo simulation of phonon transport in micron-sized graphene nanoribbons," J. Appl. Phys. 116, 164307 (2014); L. N. Maurer et al. "Universal features of phonon transport in nanowires with correlated surface roughness," submitted.

Publications

1. Y. B. Shi and I. Knezevic, “Nonequilibrium phonon effects in midinfrared quantum cascade lasers,”Journal of Applied Physics 116, 123105 (2014). [PDF]

2. O. Jonasson and I. Knezevic, “Coulomb-driven terahertz-frequency intrinsic current oscillations in a double-barrier tunneling structure,” Physical Review B 90, 165415 (2014). [PDF]

3. N. Sule, K. J. Willis, S. C. Hagness, and I. Knezevic, “Terahertz-frequency electronic transport in graphene,” Physical Review B 90, 045431 (2014). [PDF]

4. S. Mei, L. N. Maurer, Z. Aksamija, and I. Knezevic, “Full-dispersion Monte Carlo simulation of phonon transport in micron-sized graphene nanoribbons,” Journal of Applied Physics 116, 164307 (2014). [PDF]

5. I. Knezevic and B. Novakovic, “Time-dependent transport in open systems based on quantum master equations,” Journal of Computational Electronics 12, 363-374 (2013). [PDF]

6. L. N. Maurer, Z. Aksamija, E. B. Ramayya, A. H. Davoody, and I. Knezevic, “Universal features of phonon transport in nanowires with correlated surface roughness,” submitted.

7. O. Jonasson and I. Knezevic, “On the boundary conditions for the Wigner transport equation,” submitted.

8. F. Karimi and I. Knezevic, “Dielectric function and plasmons in graphene: a self-consistent field calculation within a Markovian master equation formalism,” submitted.

Session VIII

Physical Chemistry of Inorganic Nanostructures

Paul Alivisatos, Laboratory Director, Materials Sciences Division, Lawrence Berkeley National Laboratory Berkeley(LBNL)
Stephen Leone, Senior Faculty Scientist, Materials Sciences Division, LBNL
Peidong Yang, Senior Faculty Scientist, Materials Sciences Division, LBNL

Program Scope

Nanoscience offers unprecedented opportunities to studynovel materials and tailor their properties for applications such assolar energy conversion.Highly efficient energy conversion devices require an integrated system of nanomaterials, each of which is designed to perform a specialized function. Afundamental understanding of how light absorption, charge transfer and chemical reactions occur in individual and in-between components is crucial to design efficient integrated systems. Emphasizing the synthesis and integration of these inorganic nanomaterial components and the subsequent characterization of their physical properties, this program has several goals:1) advancement in the synthetic control of nanocrystals and nanowires for their use in integrated energy conversion systems; 2) establishment of experimental techniques and technology to measure charge generation and transport;3) measurement and interpretation of the electronic and chemical interactions of nanostructured materials at interfaces. To achieve these goals, physical measurements such as x-ray transient absorption spectroscopy and single-particle fluorescence are applied to synthetically controlled systems. Insight gained from these studies is used to develop fully integrated nanoscale devices for energy conversion applications. The combined expertise in synthesis, characterization, and device applications allows continuous feedback between materials development, fundamental insight, and device performance, providing rapid progress to be made toward more efficient devices for energy conversion applications.

Recent Progress

Cation exchange reactions are reactions in which cations ligated within a nanocrystal host lattice are substituted with those in solution. This is a powerful tool for obtainingacute control over composition and phase in nanocrystal synthesis and for making epitaxial semiconductor heterostructures often infeasible to obtain via traditional methods. The heterostructures include axial superlatticenanorods and core-shell nanocrystals and nanowires[1]. We are currently working towards understanding the mechanism of cation exchange in nanodots, nanorods, and nanowires. To this end, we have used isothermal titration calorimetry to probe the thermodynamics of CdSequantum dots (QD) exchanged with Ag, which shows a single phase transition and allows for the quantification of enthalpy and equilibrium constant of the reaction.Furthermore, we also conducted a study on the cation exchange in CdSnanowires to form

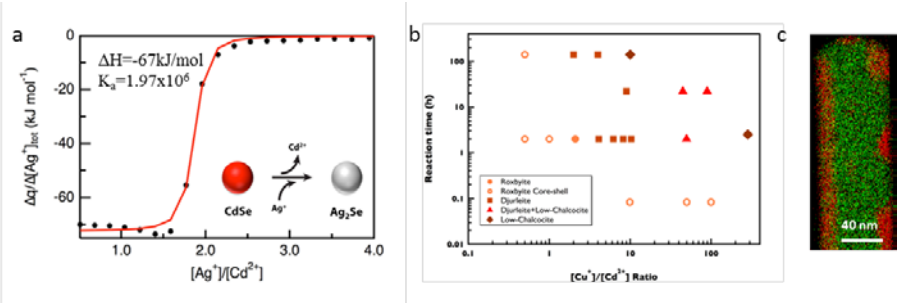

Figure 1.a. Isothermal calorimetry titration data for the exchange from CdSe QD to Ag_2Se QD. b. Cu_xS crystal structure as a function of time and cation ratios. c. partially converted Cu_2S/CdS nanowire

Cu_2S nanowires. Interestingly, the crystal phase of the resulting Cu_2S can be controlled via time and Cu^{2+} concentration as shown in figure 1b.Cation exchange in Figure 1c illustrates the finding that Cu_2S to CdS nanowires occur through island formation and coalescence.

In-situ liquid-cell TEM provides a unique and powerful tool to probe and visualize dynamic processes with nanometer resolution in a liquid environment, and represents one of the newly developed technologies under this program. Used initially to examine the electron beam-induced growth of Pt nanoparticles[2], the method has recently been extended to image the dynamics of soft materials, namely double stranded DNA connecting Au nanocrystals[3].

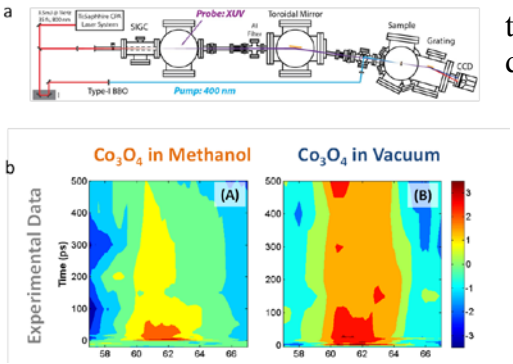

Figure 2.a. Transient X-Ray absorption setup . b. Transient cobalt M-edge absorption in methanol and in vacuum

Another developed technology is soft X-ray transient absorption spectroscopy, which can probe different oxidation and spin states for specific elements with femtosecond temporalresolution. Thisenables the study of charge transfer kineticsbetween various nanomaterial components. Using Co_3O_4, as an examplephotocatalystfor a model system, we found,after photo excitation, the $M_{2,3}$-edge of cobalt shows a significant 2 eV redshift, indicating a reduction of cobalt valence charge[4]. Attributed to a $O^{2-}(2p) \rightarrow Co^{3+}(e_g)$ charge transfer transition. A complementary study was further done to probe the charge transfer dynamics of this material at a catalyst-liquid interface[5]. In the presence of liquid methanol (Fig. 2), the photoexcited $M_{2,3}$-edge of Co_3O_4 thin film returns to the ground state with a time constant of 597 ± 37 ps, which is more than 3 times faster than the 1.95 ± 0.33 ns observed in vacuum, suggesting a hole transfer from O 2p orbital of Co_3O_4 to the adsorbed methanol layer.

Charge transfer at the semiconductor-ligand interface of quantum dots was investigated via ensemble and single particle fluorescence lifetime measurements to understand the charge transfer of quantum dots. A study of individual CdSe/CdS QDs and a new class of chalcogenidometalate (ChaM) ligands, specifically $Sn_2S_6^{4-}$ or $In_2Se_4^{2-}$.revealed an increased density of charge-trapping sites and an increased stabilization of surface-trapped charges for the ChaM-capped QDs as compared to the traditionaloleylamine-capped QDs[6]. Recently, ensemble studies of the quantum yield and luminescence lifetime of CdSe/CdS QDs as a function of the coverage of a hole-accepting ligand ferrocene were investigated. The driving force and coupling parameters in the Marcus charge transfer model were tuned by changing the redox potential of the hole acceptor andmodulating the thickness of the CdS energy.Results agree well with predicted models.

Future Plans

To probe the dynamics of cation-exchange reactions, the conversion of CdSenanocrystals into Ag_2Se will be investigated using the graphene liquid cell TEM technique. The Z-contrast difference between Ag_2Se and CdSe will differentiate the reactant and product species. A multichannel flow cell will enable several reactants to be introduced into the viewing area during imaging, enabling observation of the reaction's onset. We will also study how the effect of growth directions of CdS nanowires affects the cation exchange mechanism by conducting in situ solid statecation exchange within the TEM on CdS nanowires.Thegraphene liquid cell will

allow for the imaging of the same wire before, during and after the cation exchange reaction. Photoluminescence lifetime measurements will then be performed on devices processed using cation exchange chemistry to probe the dynamics of charge generation and transfer at the Cu_2S/CdS interface.

Transient X-ray absorption will be applied to probe real-time charge transfer across a semiconductor-semiconductor heterojunction such as TiO_2-Si and a semiconductor-catalyst heterojunction such as TiO_2-Co_3O_4. In the former system, electron-hole pairs will be generated in both semiconductors. It is anticipated that electrons will rapidly transfer from the n-$TiO_2$to the p-Si as a result of the p-n junction's built-in potential. In the TiO_2-Co_3O_4heterojunction, the electron/hole occupation levels on the Ti and Co atoms and their oxidation states can be measured simultaneously by following the M-edge absorption of Co and Ti.

Single particle fluorescence lifetime measurements will further elucidate the heterogeneity in fluorescence lifetimes of CdSe/CdS-ferrocenehole donor-acceptor system. Further studies on the effect of driving force will be investigated by examining the hole transfer rate from the quantum dot to a library of ferrocene ligands that span a range of redox potentials. From this systematic series of measurements, we will produce a Marcus parabola for charge transfer in colloidal semiconductor nanocrystals.

References

1. J. B. Rivest and P. K. Jain, “Cation Exchange on the Nanoscale: an Emerging Technique for New Material Synthesis, Device Fabrication, and Chemical Sensing,” ChemSoc Rev, 42, 89-96 (2013).

2. J. M. Yuk, J. Park, P. Ercius, K. Kim, D.J. Hellebusch, M.F. Crommie, J.Y. Lee, A. Zettl, A.P. Alivisatos, “High-Resolution EM of Colloidal Nancrystal Growth Using Graphene Liquid Cells,” Science, 336, 6077, 61-4 (2012).

3. Q. Chen, J. M. Smith, J. Park, K. Kim, D. Ho, H. I. Rasool, A. Zettl, and A. P. Alivisatos. “3D Motion of DNA-Au Nanoconjugates in Graphene Liquid Cell Electron Microscopy,” NanoLett, 13, 9, 4556-4561 (2013)

4. C.-M. Jiang, L. R. Baker, J. M. Lucas, J. Vura-Weis, A. P. Alivisatos, and S. R. Leone, “Characterization of Photo-induced Charge Transfer and Hot Carrier Relaxation Pathways in Spinel Cobalt Oxide (Co_3O_4),” J. Phys. Chem. 118, 22774-22784 (2014).

5. L. R. Baker, C.-M. Jiang, S. T. Kelly, J. M. Lucas, J. Vura-Weis, M. K. Gilles, A. P. Alivisatos, and S. R. Leone, “Charge Carrier Dynamics of Photoexcited Co_3O_4 in methanol: Extending High Harmonics Generation Transient Absorption Spectroscopy to Liquid Environments,” Nano Lett, 14, 5883-5890 (2014).

6. A. A. Cordones, M. Scheele, A. P. Alivisatos, and S. R. Leone,"Probing the Interaction of Single Nanocrystals with Inorganic Capping Ligands: Time-Resolved Fluorescence from CdSe-CdS Quantum Dots Capped with Chalcogenidometalates," J. Am. Chem. Soc. 134, 18366-18373 (2012)

Publications (2013-present)

1. Liu C, Dasgupta NP and Yang P. Semiconductor Nanowires for Artificial Photosynthesis. Chem. Mater., 2014, 26 (1), pp 415-422. Doi: 10.1021/cm4023198.
2. Resasco J, Dasgupta NP, Rosell JR, Guo J and Yang P. Uniform doping of metal oxide nanowires using solid state diffusion. J Am Chem Soc. 2014 Jul 23;136(29):10521-6. doi: 10.1021/ja505734s.
3. Sakimoto KK, Liu C, Lim J and Yang P. Salt-induced self-assembly of bacteria on nanowire arrays. Nano Lett. 2014 Sep 10;14(9):5471-6. doi: 10.1021/nl502946j.
4. Tarafder K, Surendranath Y, Olshansky JH, Alivisatos PA and Wang, L-W. Hole Transfer Dynamics from a CdSe/CdS Quantum Rod to a Tethered Ferrocene Derivative. JACS 2014, 136, 5121-5131. DOI: 10.1021/ja500936n.
5. Wittenberg JS, Miller TA, Szilagyi E, Lutker K, Quirin F, Lu W, Lemke H, Zhu D, Chollet M, Robinson J, Wen H, Sokolowski-Tinten K and Alivisatos AP, Lindenberg AM. Real-Time Visualization of Nanocrystal Solid-Solid Transformation Pathways. Nano Lett. 2014 Apr 9;14(4):1995-9. DOI: 10.1021/nl500043c.
6. Rao PM, Cai L, Liu C, Cho I, Lee C, Weisse JM, Yang P and Zheng X. Simultaneously Efficient Light Absorption and Charge Separation in WO3/BiVO4 Core/Shell Nanowire Photoanode for Photoelectrochemical Water Oxidation. Nano. Lett. 14, 1099, 2014. DOI: 10.1021/nl500022z.
7. Dasgupta NP, Sun J, Liu C, Brittman S, Andrews SC, Lim J, Gao H, Yan R and Yang P. Semiconductor Nanowires: Synthesis, Characterization, and Applications, Adv. Mater. 26, 2137, 2014 DOI: 10.1002/adma.201305929.
8. Goldstein AP, Andrews SC, Berger RF, Radmilovic VR, Neaton JB and Yang P. Zigzag inversion domain boundaries in indium zinc oxide-based nanowires: structure and formation. ACS Nano. 2013 Dec 23;7(12):10747-51. doi: 10.1021/nn403836d.
9. Jain PK, Manthiram K, Engel JH, White SL, Faucheaux JA and Alivisatos AP. Doped nanocrystals as plasmonic probes of redox chemistry. AngewChemInt Ed Engl. 2013 Dec 16;52(51):13671-5. DOI: 10.1002/anie.201303707.
10. Thoi VS, Kornienko N, Margarit CG, Yang P and Chang CJ. Visible-light photoredox catalysis: selective reduction of carbon dioxide to carbon monoxide by a nickel N-heterocyclic carbene-isoquinoline complex. J Am Chem Soc. 2013 Sep 25;135(38):14413-24. doi: 0.1021/ja4074003.
11. Manthiram K, Beberwyck B, Talapin DV and Alivisatos AP. Seeded Synthesis of CdSe/CdS Rod and Tetrapod Nanocrystals. J. Vis. Exp. 2013, 82, 50731. DOI: 10.3791/50731.
12. Vura-Weis J, Jiang CM, Liu C, Gao H, Lucas JM, F. de Groot FM, Yang P, Alivisatos AP and Leone SR. Femtosecond M2,3-Edge Spectroscopy of Transition-Metal Oxides: Photoinduced Oxidation State Change in alpha-Fe2O3. J. Phys. Chem. Lett. 2013, 4, 21, 3667-3671. DOI: 10.1021/jz401997d.
13. Beberwyck BJ, Surendranath Y and Alivisatos AP. Cation Exchange: A Versatile Tool for Nanomaterials Synthesis. J. Phys. Chem. C 2013, ASAP. DOI: 10.1021/jp405989z.
14. Britt DK, Yoon Y, Ercius P, Ewers TD and Alivisatos AP. Hexameric Octahedral Clusters of PbSeNanocrystals Grown from Amorphous Lead(II) Carboxylate Nanoparticles Chem. Mater., 2013, 25 (12), pp. 2544-2548. DOI: 10.1021/cm401083g.
15. Dasgupta NP, Liu C, Andrews S, Prinz FB and Yang P. Atomic layer deposition of platinum catalysts on nanowire surfaces for photoelectrochemical water reduction. J Am Chem Soc. 2013 Sep 4;135(35):12932-5. doi: 10.1021/ja405680p.

16. Sun Y, Sun J, Long JR, Yang P and Chang CJ. Photocatalytic generation of hydrogen from water using a cobalt pentapyridine complex in combination with molecular and semiconductor nanowire photosensitizers. Chem. Sci., 2013, 4, 118-124. doi: DOI: 10.1039/C2SC21163G.
17. Gao H, Fu A, Andrews SC and Yang P. "Cleaved-Coupled Nanowire Lasers", Proc. Natl. Acad. Sci. USA, 110, 865 (2013).
18. B Liu, H. M. Chen, C. Liu, S. C. Andrews,C. Hahn and P. Yang, "Large Scale Synthesis of Transition-metal Doped TiO_2 Nanowires with Low Overpotential," *J. Am. Chem. Soc.*, *135* (27), 9995–9998 (2013). DOI: 10.1021/ja403761s.
19. C.Liu, J. Tang, H. Chen, B. Liu and P. Yang "A Fully Integrated Nanosystem of Semiconductor Nanowires for Direct Solar Water Splitting", *Nano. Lett.*,*13*, 6, 2989–2992 (2013). DOI: 10.1021/nl401615t.
20. Cordones AA, Knappenberger KL Jr and Leone SR. Linking on-state memory and Distributed kinetics in single nanocrystal blinking. J PhysChem B. 2013 Apr 25;117(16):4241-8. DOI: 10.1021/jp3041549.
21. Cordones AA and Leone SR. Mechanisms for charge trapping in single semiconductor nanocrystals probed by fluorescence blinking. ChemSoc Rev. 2013 Apr 21;42(8):3209-21. DOI: 10.1039/c2cs35452g.
22. Hahn C, Cordones AA, Andrews SC, Gao H, Fu A, Leone SR and Yang P. Effect of Thermal Annealing in Ammonia on the Properties of InGaN Nanowires with Different Indium Concentrations. J. Phys. Chem. C., 117, 3627 (2013).DOI: 10.1021/jp311685x.
23. Chen HA, Hsin CL, Huang YT, Tang ML, Dhuey S, Cabrini S, Wu WW and Leone SR. Measurement of Interlayer Screening Length of Layered Graphene by Plasmonic Nanostructure Resonances. J. Phys. Chem. C., 117, 22211 (2013). DOI: 10,1021/jp312363x.
24. Polking MJ, Jain PK, Bekenstein Y, Banin U, Milio O, R. Ramesh R andAlivisatos AP. Controlling Localized Surface Plasmon Resonances in GeTe Nanoparticles Using an Amorphous-to-Crystalline Phase Transition, Phys. Rev. Lett., 111, 3 (7/2013). DOI: 10.1103/PhysRevLett.111.037401.
25. Baker LR, Jiang C-M, Kelly ST, Lucas JM, Vura-Weis J, Gilles MK,Alivisatos AP, and Leone SR, Charge Carrier Dynamics of Photoexcited Co_3O_4 in Methanol: Extending High Harmonics Generation Transient Absorption Spectroscopy to Liquid Environments, Nano Lett, 14, 5883-5890 (2014). DOI: 10.1021/nl502817a.
26. Jiang C-M, Baker LR, Lucas JM, Vura-Weis J, Alivisatos AP, andLeone SR.Characterization of Photo-induced Charge Transfer and Hot Carrier Relaxation Pathways in Spinel Cobalt Oxide (Co_3O_4),J. Phys. Chem. 118, 22774-22784 (2014).DOI: 10.1021/jp50711133.
27. Zhang D, Wong A,Yu Y,Brittman S, Sun J, Fu A, Berberwick B, Alivisatos AP, Yang P. Phase-selective Cation-exchange Chemistry in Sulfide Nanowire System, JACS,136(50), 17430–17433 (2014). DOI: 10.1021/ja511010q.
28. Liu B, C. Wu CH, Miao JW, Yang P. All Inorganic Semiconductor Nanowire Mesh for Direct Solar Water Splitting, ACS Nano. 8,11739, (2014). DOI: 10.1021/nl10066r.
29. Zhang L, Liu K, Wong AB, Kim J, Hong X, Liu C, Cao T, Louie SG, Wang F, Yang P. Three-Dimensional Spirals of Atomic Layered MoS_2, Nano Lett, 14 (11), 6418–6423 (2014).DOI: 10.1021/nl502961e
30. Liu K, Zhang L, Cao T, Jin C, Qiu D, Zhou Q, Zettl A, Yang P, Louie SG, Wang F. Evolution of Interlayer Coupling in Twisted Molybdenum Disulfide Bilayers, Nature Comm., 5, 4966, (2014).DOI:10.1038/ncomms5966.

31. Zhang L, Liu C, Wong AB,Resasco J, Yang P. MoS_2-Wrapped Silicon Nanowires for Photoelectrochemical Water Reduction, Nano Research (2015) DOI:10.1007/s12274-014-0673-y.
32. Ding TX, Olshansky JH, Leone SR, and Alivisatos AP, "Efficiency of Hole Transfer from Photoexcited Quantum Dots to Covalently Linked Molecular Species," J. Am. Chem. Soc. ASAP (2015). DOI: 10.1021/ja512278a.

Characterization of Functional Nanomachines

PI: Michael F. Crommie
Co-investigators: C. Bustamante, M. L. Cohen, S. G. Louie, G. Marriott, A. Zettl
UC Berkeley, Physics Department, 366 LeConte Hall #7300, Berkeley, CA 94720
Materials Sciences Division, Lawrence Berkeley National Laboratory
e-mail: crommie@berkeley.edu

Program Scope / Definition: The overarching goal of this program is to explore the fundamental science of nanomachines engineered at the atomic scale that have the ability to control energy and information through mechanical transduction processes. We are following two paths toward this goal. First, we are exploring naturally occurring biomotors that take advantage of the molecular mechanisms provided by Nature. Second, we are purposefully designing new synthetic molecular machines in a molecule-by-molecule fashion. This research helps to clarify the mechanisms by which nanomachines convert different forms of energy into directed mechanical activity, as well as how these processes are affected by different environmental dissipation mechanisms. The program is aimed at creating new categories of functional nanomachines, such as bottom-up fabricated synthetic molecular machines that operate on surfaces, top-down fabricated carbon-based nanomachines that exploit the electromechanical properties of nanotubes and graphene, and hybrid nanomachines composed of integrated synthetic and biological components. Fig.1 shows an example of a synthetic molecular machine scheme that is currently being explored. This nanomachine uses optically-actuated molecules (e.g., azobenzene and spiropyran) as the mechanical transducer building blocks that, when joined, enable new collective functionality. A major challenge to creating this type of nanomachine is to covalently couple the molecular building blocks in such a way that single-molecule-level interrogation can be performed at a surface.

This program has six co-investigators whose expertise span physics, chemistry, and biology. The experimental tools utilized by our collaboration range from synthetic chemistry, surface science, and scanned probe techniques (**Marriott** and **Crommie**), to photolithography, wet biology, and laser tweezers (**Zettl** and **Bustamante**). **Cohen** and **Louie** provide theoretical support through the use of *ab initio* density functional techniques and molecular dynamics calculations.

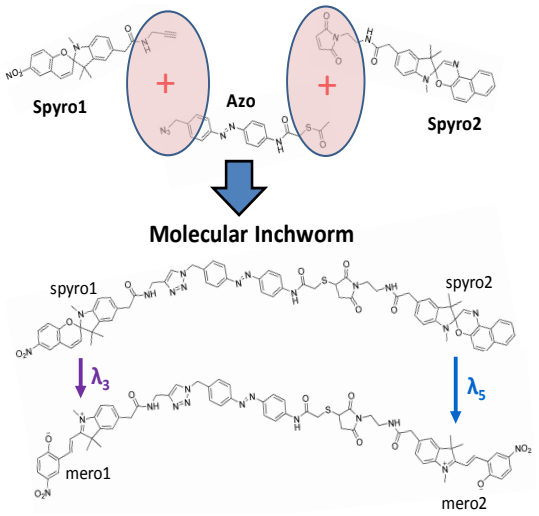

Fig. 1: Sketch of molecular building blocks for synthetic nanomachine (above), and scheme for coupling them into a functional assembly (below).

Recent Progress: Here I will highlight our activities within two subtasks of our overall program: *(A) Exploration of new covalent coupling mechanisms for molecules at surfaces*, and *(B) Exploration of a new Coulomb-induced electronic actuation mechanism for molecular machines*. Both of these subtasks involve single-molecule-level interrogation of molecular machine systems.

(A) New Mechanisms for Controlling Covalent Bonding Between Molecules at Surfaces: We have succeeded in the past at exploring individual molecules that can be stimulated (e.g., by photons or electric field) to elicit a mechanical response.[1] Coupling these molecules together into mechanically functional assemblies at surfaces, however, remains a challenge. Some of the difficulties faced here are that large, solution-grown assemblies are difficult to cleanly deposit onto surfaces so that single-molecule-resolved imaging is possible, and that surface-based covalent bonding techniques typically require metal surfaces to catalyze the reaction while such surfaces also quench photon-based and electrical-based mechanical actuation.[2]

In order to overcome these challenges, we are exploring new techniques for controllably coupling molecules in ways that might generalize to more photo- and electrically useful insulating surfaces. Two modalities that we have recently explored for this purpose are Bergman cyclization and alkyne coupling. Bergman cyclization is a well-known process in solution-phase reactions, but it is less well-understood for surface-based reactions. We have characterized enediyne molecules on surfaces in order to understand Bergman-cyclization-based coupling (Fig.2). Enediynes are hydrocarbons that exhibit alternating sequences of double and triple bonds (Fig. 2(a)). Under the right conditions the bonds will re-form (Fig. 2(b)) to create carbon rings (i.e., cyclization) that exhibit unpaired electrons at their edges (i.e., radicals). This is ideal for covalently coupling molecules together since the unpaired electrons induce polymerization between monomers (Fig. 2(c)).

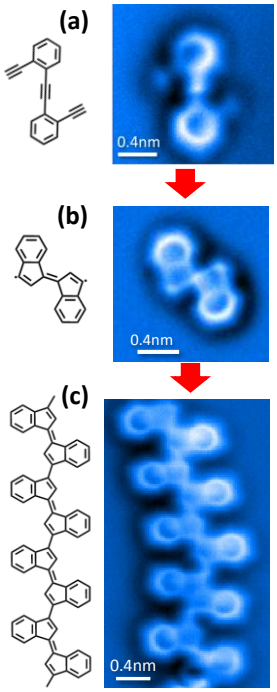

Fig. 2: Sketch and nc-AFM image of (a) enediyne monomer, (b) cyclized monomer, and (c) polymerized monomers. (Images taken at T=4K, Au(111) surface).

We have explored this process by depositing the molecule shown in Fig. 2(a) (fabricated by F. Fischer) onto a clean Au(111) surface at room temperature. We used a new cryogenic non-contact AFM-based (nc-AFM) imaging technique[3,4] to determine the precise bonding configuration of the molecules. Here a single CO molecule is adsorbed to the tip of the AFM which is connected to a quartz oscillator. The change in frequency of the oscillator is measured as the CO molecule is scanned over molecular nanostructures at the surface. Fig.2(a) shows an nc-AFM image obtained in this way for individual, isolated enediyne molecules on Au(111). The phenyl rings of the enediyne molecules are clearly resolved, as well as the bond order within the molecule. In order to induce Bergman cyclization and radical polymerization (i.e., covalent bonding) for these molecules, we heated the surface up to 160C and then cooled it back down to 4K and imaged it using nc-AFM. This allowed us to successfully induce Bergman cyclization (Fig. 2(b)) and subsequent polymerization of Bergman cyclized monomers (Fig. 2(c)).[5] Fig. 2(c) is the first single-bond-resolved image of Bergman-cyclization-induced polymerization, and it allows us to

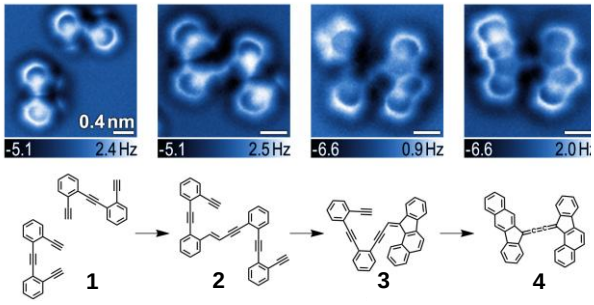

Fig. 3: Sketches and nc-AFM images of enediyne monomer (1), alkyne coupling intermediates (2,3), and final cyclized product after processing at temperatures 1 (room temperature), 2 (50C), 3 (75C), and 4(100C). (Images taken at T=4K, Ag(100) surface).

unambiguously determine the chemical route taken as enediyne monomers are covalently bonded to form extended molecular networks.[5]

We have also succeeded in exploring the chemical steps involved in performing alkyne coupling between two enediyne monomers. Alkyne coupling involves the conversion of two terminal triple bonds into a covalent link between two molecules, as shown in the sketches of Fig. 3. Single-bond-resolved alkyne coupling was achieved by depositing enediyne fragments onto a Ag(100) surface and slowly increasing the temperature (after each temperature increment the sample was cooled back to 4K for imaging). This allowed us to capture, for the first time, single-bond-resolved images of the intermediate steps of an alkyne coupling reaction.[6] Fig. 3 (1) shows an nc-AFM image of the unreacted molecules on Ag(100), while Figs. 3 (2-4) show how the dominant molecular species on the surface changes as the monomers undergo alkyne coupling and subsequent cyclization at different temperatures. This unprecedented high resolution imaging of intermediate steps in a reaction has allowed us to analyze alkyne reaction dynamics using combined tight-binding/molecular-dynamics theoretical simulations (A. Rubio). Comparison of theoretical results to our experimental data has allowed us to assess the relative importance of different dissipative processes that determine which intermediate states dominate the alkyne-coupling reaction pathway.[6]

(B) Coulomb-Induced Actuation of Single-Molecule Mechanical Motion: The Coulomb force between two charged objects is a powerful mechanical actuator, but controlled manipulation of the charge on nearby molecular objects remains a challenge. For example, optical ionization is difficult to reversibly control, electrochemical techniques involve complex ionic environments that are not amenable to single-molecule interrogation, and STM tip-induced ionization cannot easily be performed for multiple objects in parallel. A novel alternative is to use electrostatic gating to raise the Fermi level of the molecular substrate to an energetic level above the lowest unoccupied molecular orbital (LUMO). This causes charge to flow from the substrate into the LUMO state, thus giving each molecule a charge of Q = -e (Fig. 4(a)). If two molecules are placed near one another then this charging will cause a Coulomb repulsion between them that can push them apart. This effect will be controllable remotely by applying a potential to the gate electrode.

We have accomplished such Coulomb-induced mechanical actuation by placing F_4TCNQ molecules (Fig. 4(a)) at the surface of a graphene/boron-nitride field-effect transistor (Fig. 4(b)). The LUMO level of F_4TCNQ lies close to the Dirac point of graphene (Fig. 4(a)) and so it can be reversibly charge by gating the graphene Fermi level either below (for Q = 0) or above (for Q = -e) the LUMO level (Fig. 4(a)). We have observed that under the proper conditions F_4TCNQ molecules placed into the Q = -e charge state will mechanically repel each other. This can be seen in the "before" and "after" STM images of Fig. 4(c). Fig. 4(c) (left) shows a cluster of F_4TCNQ molecules in the neutral state with a gate voltage of $V_G = 0$ V. Fig. 4(c) (right), on the other hand,

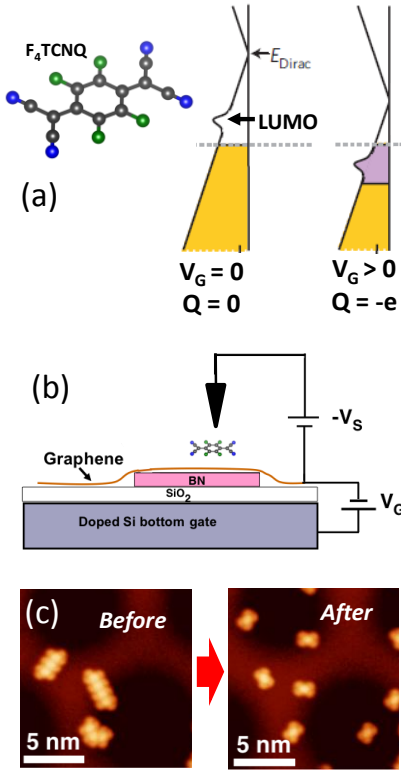

Fig. 4: Sketches of (a) F_4TCNQ molecule and charging of molecular orbital due to gating, and (b) graphene/BN FET device. (c) STM images of Coulomb-induced mechanical repulsion of F_4TCNQ molecules.

shows the same patch of molecules after applying (and then removing) a gate voltage of V_G = 50 V which induces Q = -e in each molecule. The molecules are seen to mechanically repel one another due to application of the gate voltage and subsequent generation of Coulomb forces, and then to stabilize once the gate voltage is reduced.

Future Plans: An important future goal for this subtask of our program is to create synthetic, controllable nanomachines at surfaces by coupling together chemically designed molecular building blocks. We intend to synthesize these on either graphene or insulating substrates in order to control them via photonic and/or electronic actuation. To accomplish this we will integrate new covalent coupling techniques with photo-active (azobenzene, spiropyran) and electrically active (F_4TCNQ) molecular building blocks on graphene and BN surfaces. We will use combinations of photonic and gate-induced actuation to mechanically control the resulting nanomachines, and we will characterize them at the single -molecule level. We will additionally explore the use of metallic nanostructures to both control surface electrostatic potentials and to focus light via plasmonic coupling to better control the mechanical response of surface-bound molecular machines.

References:

[1] M. J. Comstock, D. A. Strubbe, L. Berbil-Bautista, N. Levy, J. Cho, D. Poulsen, J. M.J. Fréchet, S. G. Louie, and M. F. Crommie, *Phys. Rev. Lett.* **104**, 178301 (2010).
[2] M.J. Comstock, N. Levy, A. Kirakosian, J. Cho, F. Lauterwasser, J.H. Harvey, D.A. Strubbe, J.M. Frechet, D.Trauner, S.G. Louie, and M.F. Crommie, *Phys. Rev. Lett.* **99**, 038301 (2007).
[3] L. Gross, F. Mohn, N. Moll, P. Liljeroth, G. Meyer, *Science* **325**, 1110 (2009).
[4] D. G. de Oteyza, P. Gorman,Y.C. Chen, S. Wickenburg, A. Riss, D. J. Mowbray, G. Etkin, Z. Pedramrazi, H.Z. Tsai, A. Rubio, M. F. Crommie, and F. R. Fischer, *Science* **340**, 1434 (2013).
[5] A. Riss, S. Wickenburg, P. Gorman, L. Z. Tan, H.-Z. Tsai, D. G. de Oteyza, Y.-C. Chen, A. J. Bradley, M. M. Ugeda, G. Etkin, S. G. Louie, F. R. Fischer, and M. F. Crommie, *Nano Lett.* **14**, 2251 (2014).
[6] A. Riss, A. Pérez Paz, S. Wickenburg, H. Tsai, D. G. de Oteyza, A. J. Bradley, M. M. Ugeda, A. Rubio, M. F. Crommie, and F. Fischer, submitted for publication (2015).

DOE Publications Relevant To This Subtask:

[1] X. Zhang, O. V. Yazyev, J. Feng, L. Xie, C. Tao, Y.-C. Chen, L. Jiao, Z. Pedramrazi, A. Zettl, S. G. Louie, H. Dai, and M. F. Crommie, *ACS Nano* **7**, 198 (2013).
[2] I. V. Pechenezhskiy, X. Hong, G. D. Nguyen, J. E. P. Dahl, R. M. K. Carlson, F. Wang, and M. F. Crommie, *Phys. Rev. Lett.* **111**, 126101 (2013).
[3] Y. Sakai, G. D. Nguyen, R. B. Capaz, S. Coh, I. V. Pechenezhskiy, X. Hong, F. Wang, M. F. Crommie, S. Saito, S. G. Louie, and M. L. Cohen, *Phys. Rev. B* **88**, 235407 (2013).
[4] A. Riss, S. Wickenburg, L. Z. Tan, H.-Z. Tsai, Y. Kim, J. Lu, A. J. Bradley, M. M. Ugeda, K. L. Meaker, K. Watanabe , T. Taniguchi, A. Zettl, F. R. Fischer, S. G. Louie, and M. F. Crommie, *ACS Nano* **8**, 5395 (2014).
[5] A. Riss, S. Wickenburg, P. Gorman, L. Z. Tan, H.-Z. Tsai, D. G. de Oteyza, Y.-C. Chen, A. J. Bradley, M. M. Ugeda, G. Etkin, S. G. Louie, F. R. Fischer, and M. F. Crommie, *Nano Lett.* **14**, 2251 (2014).
[6] Y.-C. Chen, T. Cao1, C. Chen, Z. Pedramrazi, D. Haberer, D. G. de Oteyza, F. R. Fischer, S. G. Louie, and M. F. Crommie, *Nature Nanotechnology* **10**,156 (2015).
[7] A. Riss, A. Pérez Paz, S. Wickenburg, H. Tsai, D. G. de Oteyza, A. J. Bradley, M. M. Ugeda, A. Rubio, M. F. Crommie, and F. Fischer, submitted for publication (2015).

DOE FWP # ERWER05, NREL

Electronic Raman Scattering as an Ultra-Sensitive Probe of Strain Effects in Semiconductors

PI: Angelo Mascarenhas
National Renewable Energy Laboratory
15013 Denver West Parkway, Golden, CO 80401-3305, angelo.mascarenhas@nrel.gov

Program Scope or Definition

Advanced energy technologies require high-performance materials, which in photovoltaics (PV) translates to new semiconductor materials to efficiently absorb sunlight, and in solid-state lighting (SSL), to new semiconductor alloys for direct conversion of electricity to white light. A goal of this project is fundamental materials research for the realization of semiconductors that transcend the existing limitations that constrain present PV and SSL technologies. It specifically addresses the current unavailability of efficient high bandgap (2.1 eV) and low bandgap (1 eV) absorbers for PV, and efficient amber emitters for SSL, via technologies based on GaAs substrates. The key to transcending the present limitations is understanding and controlling fundamental electronic and optical processes in semiconductor alloys. Towards this, the project will focus on the abnormal electronic structure and properties of isoelectronic dopants N and Bi in GaAs, the consequences of their isoelectronic co-doping, and the electronic behavior of alloys at the direct-indirect crossover. Additionally, it will address recent observations of electronic Raman Scattering as an ultra-sensitive strain measurement technique, and light scattering from high density plasmons in semiconductors. Through collaborative efforts, this project utilizes the high-magnetic field facility at the NHFML (Los Alamos) and growth facilities at the CINT (Sandia labs).

Recent Progress (on two themes)

1) **High magnetic field studies at the direct-indirect crossover in $Al_xGa_{1-x}As$.**

Understanding the nature of the direct-indirect crossover x_c is important, as it governs the electronic behavior of alloys with compositions near x_c. In particular, questions as to whether the crossover occurs at a well-defined critical composition and whether it is continuous or discontinuous remain.[i] Theoretical Monte Carlo simulations indicate that in analogy with temperature-induced phase transitions, the crossover approximates a first-order phase transition as a function of variation in the alloy composition.[i] However, experimental verification of this prediction is difficult because statistical fluctuations[ii] in alloy composition broaden the transition, and spectroscopic measurements of the radiative transition energy are representative of the mean value of the statistical distribution function.[iii] It is therefore important to elucidate the role that such fluctuations play on the direct–indirect crossover and how they influence the determination of x_c. We studied the nature of the direct-indirect crossover in $Al_xGa_{1-x}As$ by inducing it in a single sample with a pulsed magnetic field up to 60T.[iv] The crossover was accompanied by the onset of an asymmetric lineshape in the bound exciton PL peak, which results from the competition between the radiative recombination lifetime and the time for carriers to migrate to local minima in the alloy. This study using magnetic fields to systematically investigate the

direct–indirect crossover in $Al_xGa_{1-x}As$ provided strong evidence that the crossover is an alloy-broadened, first-order phase transition.

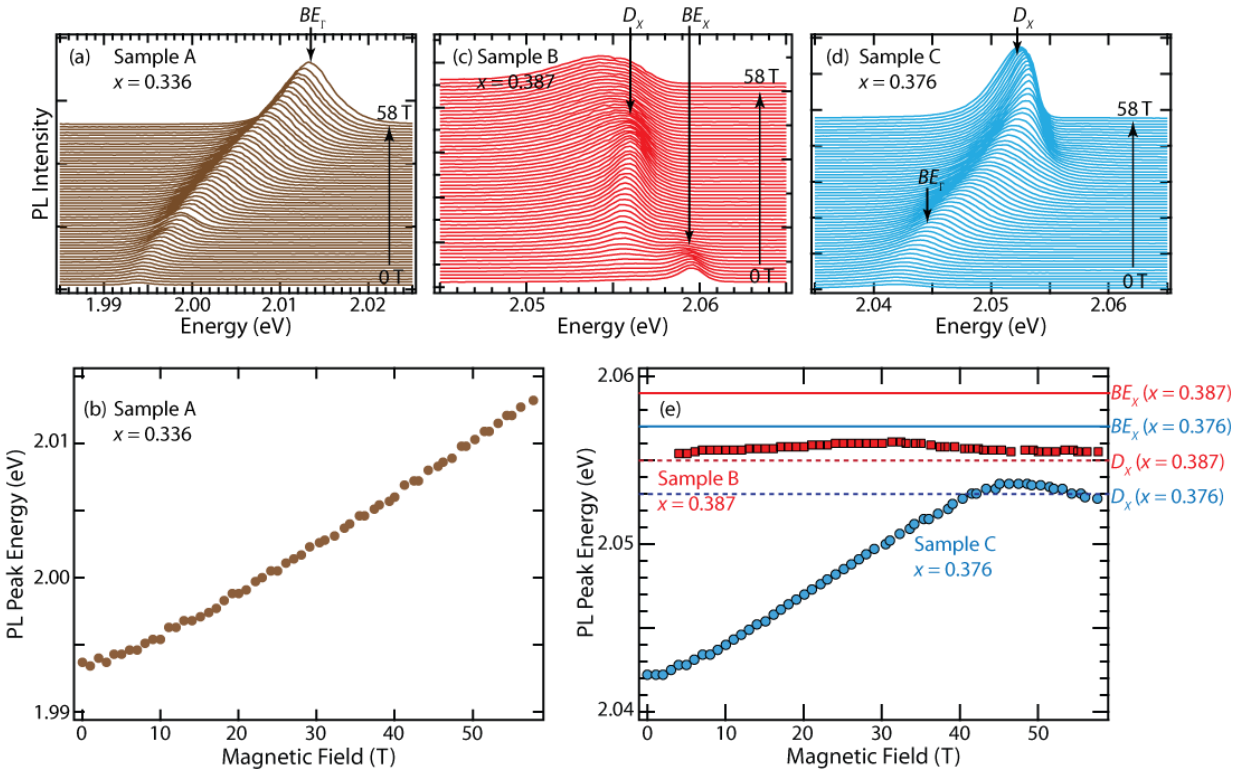

Fig. 1. Magneto-PL spectra for (a) direct gap $Al_xGa_{1-x}As$ (x = 0.336), (c) indirect gap $Al_xGa_{1-x}As$ (x = 0.387) and (d) $Al_xGa_{1-x}As$ undergoing a direct-indirect crossover at high magnetic fields (x = 0.376). (b) PL energy of the direct gap sample in (a) as a function of magnetic field. (e) PL peak energy as a function of magnetic field for the indirect (red squares) and crossover samples (blue circles).

2) **Electronic Raman Scattering as an Ultra-Sensitive Probe of Strain Effects in Semiconductors**.

Semiconductor strain engineering has become a critical feature of high-performance electronics due to the significant device performance enhancements it enables. These improvements that emerge from strain induced modifications to the electronic band structure necessitate new ultra-sensitive tools for probing strain in semiconductors. Using electronic Raman scattering, we recently showed that it is possible to measure minute amounts of strain in thin semiconductor epilayers. We applied this strain measurement technique to two different semiconductor alloy systems, using coherently strained epitaxial thin films specifically designed to produce lattice-mismatch strains as small as 10^{-4}. Comparing our strain sensitivity and signal strength in $Al_xGa_{1-x}As$ with those obtained using the industry-standard technique of phonon Raman scattering we found a sensitivity improvement of × 200, and a signal enhancement of 4 × 10^3 thus obviating key constraints in semiconductor strain metrology. The sensitivity of this approach rivals that of contemporary techniques and opens up a new realm for optically probing strain effects on electronic band structure.

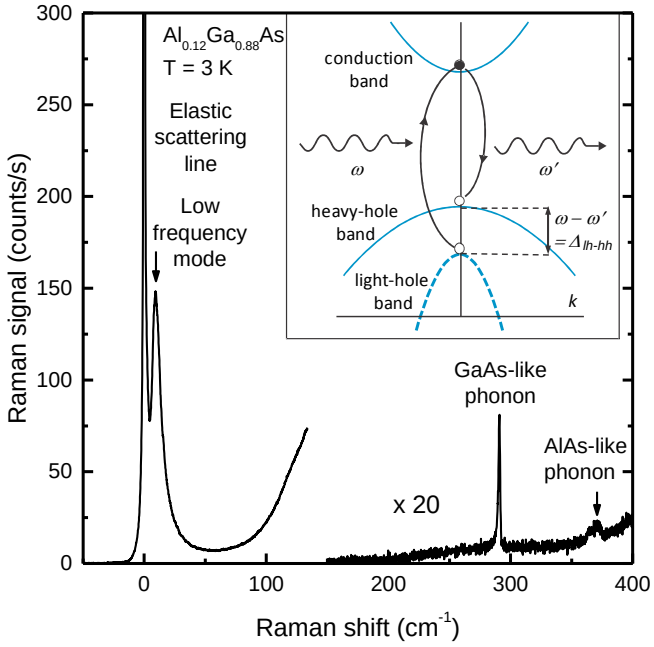

Fig. 2: Raman spectrum overview. The Raman scattering spectrum from the AlGaAs epilayer with 12% Al content grown on GaAs substrate is shown separately for the low frequency (electronic Raman scattering) and for the high frequency (phonon Raman scattering) regions. The low frequency spectral window recorded using laser excitation at 1.668 eV and 12 μW of power in the depolarized scattering geometry shows a low energy electronic Raman scattering feature close to the elastically scattered laser line. The high frequency region recorded using laser excitation at 1.745 eV and 2 mW of power in the polarized scattering geometry shows the GaAs-like phonon at 291 cm^{-1} and the AlAs-like phonon at 370 cm^{-1}. Inset: Schematic of intrinsic inter valence band electronic Raman scattering: The $Al_xGa_{1-x}As$ electronic bands participating in the three-band Raman scattering process are shown. Wavy lines denote the incoming, *w*, and outgoing, *w'*, photons. Thins solid lines denote the scattering of a hole from the heavy-hole band to the light-hole band via generation of an electron in the conduction band intermediate state. The Raman shift of the observed low frequency mode results from the biaxial compressive strain-induced splitting energy $D_{lh\text{-}hh}$.

The advent of silicon based photonics [v], III-V based nanoelectronics [vi] and integration of photonics and electronics[vii], requires new metrology tools [viii] for probing effects on the electronic band structure introduced either by design or process technology variation[ix]. The ultra-sensitivity to strain induced band structure changes demonstrated for the electronic Raman technique could make this a valuable tool for such applications. It could also be valuable for probing electronic structure changes due to single dislocations[x], strain engineering of ultra-thin semiconductor crystalline layers[xi], and unconventional approaches to hetero-epitaxy[xii].

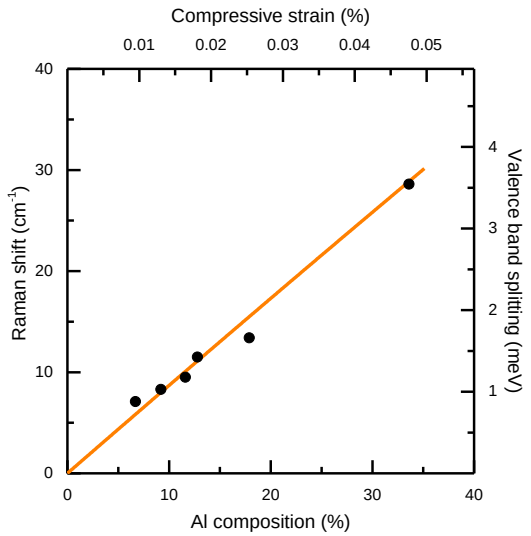

Fig. 3: Energy of the low frequency mode vs. theoretically predicted strain-induced valence bands splitting. Solid line displays the splitting between the light-hole and heavy-hole valence bands (see Fig.2) due to lattice mismatch between the AlGaAs epilayer on the GaAs substrate calculated using elastic moduli values at 0 K. Symbols show the energy of the low frequency mode averaged over the dispersion for the resonance profile.

Future Plans

We will investigate the applicability of the Electronic Raman strain measurement technique to epitaxial silicon, as this would potentially have a significant impact on current silicon technology. From a practical standpoint, our priority is on the direct gap where the strong resonance may be expected to provide a Raman signal in the very thin layers of strained silicon typically used in the electronics field. Although inapplicable to thin films, the indirect gap is also important to us, because it is known from the electron-hole liquid (EHL) work of the 1970s that an ERS signal from the strain-induced valence band splitting occurred there[xiii]. The indirect gap is also interesting because splitting may be expected both from the valence band and the multiple valleys of the conduction band. One approach will replicate the very high mechanically-applied stress first used for EHL. We have a similar apparatus used for creating exciton potential traps in GaAs systems, requiring only a simple modification to apply compressive instead of tensile stress.

References

[i] B. Koiller and R. B. Capaz, Phys. Rev. Lett. 74, 769 (1995).

[ii] E. F. Schubert and W. T. Tsang, Phys. Rev. B 34, 2991 (1986).

[iii] A. Müller and M. Grundmann, Phys. Rev. B 87, 035134 (2013).

[iv] K. Alberi, A.V. Mialitsin, B. Fluegel, S.A. Crooker, J.L. Reno and A. Mascarenhas, *Appl. Phys. Express*, **7**, 111201 (2014)

[v] Kimmerling, L.C., Kwong, D.-L & Wa, K. Scaling computation with silicon photonics. *MRS Bulletin* **39**, 687-695 (2014).

[vi] Riel, H., Wernersson, L.-H., Hong, M. & del Alamo, J.A. III-V compound semiconductor transistors-from planar to nanowire structures. *MRS Bulletin* **39**, 668-677(2014).

[vii] Beausoleil, R.G. Large Scale Integrated Photonics for Twenty-First Century Information Technologies. *Foundations of Physics* **44**, 856 (2014).

[viii] Wong, T.K. Semiconductor Strain Metrology: Principles and Applications. *www.benthamscience.com/ebooks/9781608053599*, (2012).

[ix] Kuhn, K.J. *et al*. Process Technology Variation. *IEEE Trans. Electron Devices*. **58**, 2197 (2011).

[x] Irmer, G. & Jurisch, M. Micro-Raman study of strain fields around dislocations in GaAs. *Phys. Stat. Sol*. (a) **204**, 2309 (2007).

[xi] Leite, M.S. *et al*. Wafer-Scale Strain Engineering of Ultrathin Semiconductor Crystalline Layers. *Adv. Mater*. **23**, 3801 (2011).

[xii] Falub, C.V. *et al.* Scaling Hetero-Epitaxy from Layers to Three-Dimensional Crystals. *Science* 335, 1330-1334 (2012).

[xiii] D. Guidotti, S. Lai, M.V. Klein, and J. P. Wolfe, *Phys. Rev. Lett*. **43**, 1950 (1979).

Publications (in last two years)

1. **"Doping dependence and anisotropy of minority electron mobility in molecular beam epitaxy-grown p type GaInP".** N. M. Haegel, T. Christian, C. Scandrett, A. G. Norman, A. Mascarenhas, P. Misra, T. Liu, A. Sukiasyan, E. Pickett, and H. Yuen. *Appl. Phys. Lett*. **105**, 202116 (2014).
2. "**Resonant state due to Bi in the dilute bismide alloy, $GaAs_{1-x}Bi_x$**". R. S. Joshya, A. J. Ptak, R. France, A. Mascarenhas, and R. N. Kini. *Phys. Rev. B* **90**, 165203 (2014).
3. "**Magnetic Field Induced Direct-Indirect Crossover in AlGaAs**". K. Alberi, A.V. Mialitsin, B. Fluegel, S.A. Crooker, J.L. Reno and A. Mascarenhas, *Appl. Phys. Express* **7**, 111201 (2014).
4. "**Carrier Decay and Diffusion Dynamics in Single-Crystalline CdTe as seen via Microphotoluminescence**". B. Fluegel, K. Alberi, M. J. DiNezza, S. Liu, Y.-H. Zhang, and A. Mascarenhas. *Phys. Rev. Applied* **2**, 034010 (2014).
5. "**Probing carrier lifetimes at dislocations in epitaxial CdTe**". K. Alberi, B. Fluegel, M.J. DiNezza, S. Liu, Y.-H. Zhang, A. Mascarenhas, *Appl. Phys. Express* **7**, 065503 (2014).
6. "**Effects of dislocation strain on the epitaxy of lattice-mismatched AlGaInP layers**". K. Mukherjee, D.A. Beaton, A. Mascarenhas, M.T. Bulsara, E.A. Fitzgerald, " *J. Crystal Growth* **392**, 74 (2014).
7. "**Coherent acoustic phonon generation in $GaAs_{1-x}Bi_x$**". R.S. Joshya, A.J. Ptak, R. France, A. Mascarenhas, R.N. Kini. *Appl. Phys. Lett.*, **104**, 091903 (2014).
8. **"Photoluminescence Imaging of Semiconductors"**. K. Alberi, B. Fluegel and A. Mascarenhas, *Microscopy and Microanalysis* **20**, suppl. S3, 532 (2014).
9. "**Determination of the direct to indirect bandgap transition composition in $Al_xIn_{1-x}P$**". D.A. Beaton, T. Christian, K. Alberi, A. Mascarenhas, K. Mukherjee, E.A. Fitzgerald, *J. Appl. Phys.*, **114**, 203504 (2013).
10. "**Measuring Long-Range Carrier Diffusion across Multiple Grains in Polycrystalline Photovoltaics**". K. Alberi, B. Fluegel, R. Dhere, S.A. Crooker, and A. Mascarenhas, *Nature Comm*. **4**, 2699 (2013).
11. "**Amber-green light-emitting diodes using order-disorder $Al_xIn_{1-x}P$ heterostructures**". T. Christian, D.A. Beaton, K. Mukherjee, K. Alberi, E.A. Fitzgerald and A. Mascarenhas, *J. Appl. Phys*. **114**, 4818477 (2013).
12. "**Raman Scattering Signature of a Localized-to-Delocalized Transition at the Inception of a Dilute Abnormal $GaAs_{1-x}N_x$ Alloy**". A.V. Mialitsin and A. Mascarenhas. *Appl. Phys. Express* **6**, 052401 (2013).
13. "**Growth, microstructure, and luminescent properties of direct-bandgap InAlP on relaxed InGaAs on GaAs substrates**". K. Mukherjee, D.A. Beaton, T. Christian, E.J. Jones, K. Alberi, A. Mascarenhas, M.T. Bulsara, E.A. Fitzgerald. *J. Appl Phys*. 113, 1183518 (2013).
14. "**Precise Determination of the direct-indirect bandgap energy cross-over composition in $Al_xGa_{1-x}As$**". D.A. Beaton, B. Fluegel, K. Alberi, A. Mascarenhas and J.L. Reno, *Appl. Phys. Express* **6**, 071201 (2013).
15. "**Magnetic field-induced delocalized to localized transformation in GaAs:N**". K. Alberi, S.A. Crooker, B. Fluegel, D.A. Beaton, A.J. Ptak, A. Mascarenhas. *Phys. Rev. Lett*. **110**, 156405 (2013).

Session IX

Nonlinear Macroscopic Quantum Superconducting Metamaterials

Steven M. Anlage

Center for Nanophysics and Advanced Materials, Physics Department, University of Maryland, College Park, MD 20742-4111 USA

Metamaterials represent an organizing principlefor developing artificial and engineered materials that create and enable unique interactions of matter with electromagnetic waves. Superconductors bring several unique advantages to the development of metamaterials, namely low loss, compact dimensions for the meta-atoms compared to other realizations, new opportunities for nonlinearity, tuning, and switching behavior, and finally new physics associated with macroscopic quantum phenomena, quantum interactions between photons and discrete energy states in the meta-atom, and strong diamagnetism. In this presentation I will discuss a new class of active metamaterials capable of quickly tuning their electrical and magnetic responses over a wide frequency range. The meta-atoms are rf superconducting quantum interference devices (SQUIDs) that combine two macroscopic quantum phenomena: magnetic flux quantization and the Josephson effect, making them extraordinarily tunable.The coupled rf SQUID metamaterial is thus a richly nonlinear effective medium. The coherent oscillation of all the meta-atoms is strongly sensitive to the environment and measurement conditions. In addition this metamaterial displays a self-induced broadband transparency due to a qualitatively novel nonlinear mechanism that is different from conventional electromagnetically-induced-transparency or its classicalanalogs. A near complete disappearance of resonant absorption under a range of incident power (rf flux) is observed experimentally and explained theoretically.

This work is supported by the NSF-GOALI and OISE Programs through Grant No. ECCS-1158644 and the Center for Nanophysics and Advanced Materials (CNAM).

Session XI

Light-Stimulated Epitaxy of Novel Semiconductor Alloys and Heterostructures

PI: Kirstin Alberi
National Renewable Energy Laboratory
15013 Denver West Parkway, Golden, CO 80401, Kirstin.Alberi@nrel.gov

Project Scope

Synthesis of semiconductor alloys and heterostructures often requires growth conditions that are far from equilibrium, yet such conditions can also enhance the incorporation of defects. The objective of this project is to explore light stimulation of growth surface as a means to selectively manipulate processes that enhance adatom kinetics and enable the growth of new semiconductor material systems. Absorption of light can affect the growth surface through three primary pathways: local enhancement of thermal energy, photo-dissociation of bonds and species, and generation of free carriers, which can influence the Fermi energy, bonding processes and surface reconstructions (Fig. 1).[1-5] Studies specifically focus on exploring the basic mechanisms through which photons and photogenerated carriers affect adatom mobility, doping processes, defect formation and interface formation at low growth temperatures. This information is used to tailor the growth of new semiconductor alloys and heterostructures that are difficult to synthesize by traditional techniques.

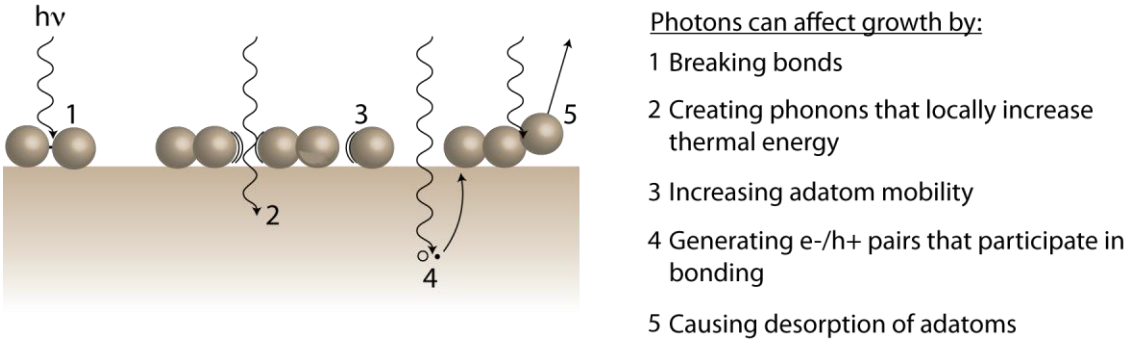

Figure 1. *Possible photo-assisted processes that affect the growth of a semiconductor.*

Recent Progress

We have explored the means by which photon irradiation affects growth processes through several focused studies. The results suggest that several mechanisms play a role, depending on the starting growth conditions. It should be noted that heating of the substrate under the flux of high-energy photons was substantially regulated during these experiments. While some elevated local surface heating is expected, the results largely contradict thermal heating effects and in many cases point toward electronic-related mechanisms instead.

Influence of Photon Irradiation on Adatam Mobility[6]

Previous investigations of light stimulated epitaxy on II-VI semiconductors suggested that the energy imparted by absorbed photons enhanced adatom diffusion and improved surface morphology, but no direct evidence of this was provided.[1] We determined the influence of broadband illumination on the adatom diffusion length in GaAs by measuring the substrate temperature at which the layer-by-layer island nucleation growth mode switches to step flow growth with reflection high energy electron diffraction (RHEED) oscillations.[7] *Contrary* to the previous reports on II-VI semiconductors, the growth mode transition temperature increased under illumination, suggesting that it causes the adatom diffusion length to decrease. Surface morphology measurements with atomic force microscopy (AFM) also show that broadband illumination roughens the surface. These changes are attributed to the blocking of adatom attachment sites at step edges by photogenerated carriers, which is similar to the reported role of hydrogen in GaAs growth.[8]

Adjustment of Fermi Level-Controlled Growth Processes by Photogenerated Carriers[9]

The Fermi level plays a significant role in epitaxial growth processes. The position of the Fermi level relative to the Fermi stabilization energy as well as Fermi level pinning are known to significantly influence dopant incorporation and diffusion, defect formation, surface reconstruction and growth processes governing surface morphology.[10,11] Consequently, free carriers generated under above bandgap illumination have the potential to influence the Fermi energy and alter these growth processes. To probe this effect, we have specifically studied the influence of ultraviolet (UV) photon irradiation on dopant surface segregation in heavily Si-doped GaAs. Dopant surface segregation can be enhanced by two effects: 1) drift of ionized dopant atoms in the electric field created by Fermi level pinning at the growth surface[12], and 2) diffusion aided by the presence of compensating defects.[13] Figure 2 shows that the degree of Si surface segregation and carry-forward into an adjacent undoped GaAs layer is reduced under increasing photon flux. These results can be explained by a reduction in the band bending and compensating vacancy formation caused by splitting of the quasi Fermi levels in the presence of photogenerated minority holes.[12,14] Light stimulated epitaxy therefore presents a practical method of mitigating undesirable growth processes associated with heavy doping.

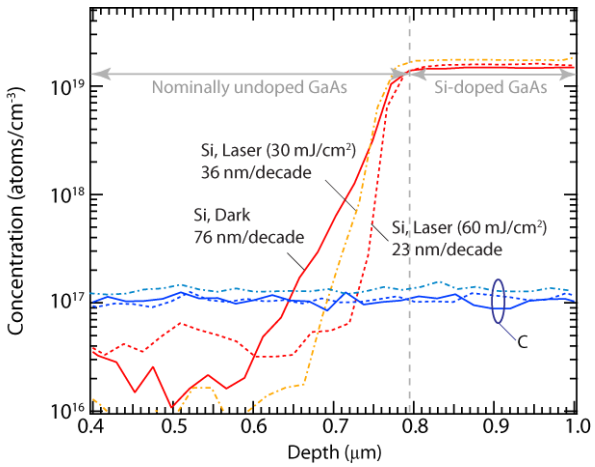

Figure. 2 *Si and C doping profiles in samples grown under dark conditions (solid lines), illumination with a laser fluence of 30 mJ/cm^2 (dash-dotted lines), and illumination with a laser fluence of 60 mJ/cm^2 (dashed line). The vertical dashed gray line demarks the point at which the Si flux was turned off.*

Improved Low Temperature Growth

Because of its large size, Bi tends to act as a surfactant and is incorporated into a growing crystal only at low temperatures. For example, $GaAs_{1-x}Bi_x$ is grown only at temperatures < 400 °C. Such conditions for dilute bismide alloy epitaxy tend to promote defect formation and excess group V incorporation if the V/III ratio is not carefully regulated. We have shown that the crystalline quality and optical properties of $GaAs_{1-x}Bi_x$ increases substantially under UV photon irradiation. These results are attributed in part to a decrease in the sticking of excess As adatoms, which reduces the concentration of As antisites. The concentration of other crystalline defects may also be reduced by a slight increase in the adatom mobility under photon flux. These results will help to guide the synthesis and exploration of other Bi-containing alloys.

Future Work

Ongoing research will continue to explore the light-stimulated growth mechanisms identified above with a combination of *in-situ* and *ex-situ* measurement techniques. We also plan to study the influence of photogenerated carriers on the formation of III-V/II-VI semiconductor heterostructures. Charge build-up at the heteropolar interface causes inter-diffusion between the layers and the formation of compensating defects. Photo-injection of free carriers may change the interface nucleation process and help to create high quality III-V/II-VI heterostructures with abrupt interfaces.

References

1. N. Matsumura, T. Fukada and J. Saraie, *J. Crystal Growth*, **101**, 61 (1990)
2. R.N. Bicknell, N.C. Giles, J.F. Schetzina and C. Hitzman, *J. Vac. Sci. Technol. A*, **5**, 3059 (1987)
3. J.D. Benson, D. Rajavel, B.K. Wagner, R. Benz II and C.J. Summers, *J. Crystal Growth*, **94**, 534 (1989)
4. Y. Marfaing, *Semicond. Sci. Technol.*, **6**, A60 (1991)
5. H.H. Farrell, R.E. Nahory and J.P. Harbison, *J. Vac. Sci. Technol. B*, **6**, 779 (1988)
6. D.A. Beaton, C.E. Sanders and K. Alberi, *J. Crystal Growth*, **413**, 76 (2015)
7. J.H. Neave, P.J. Dobson, B.A. Joyce and J. Zhang, *Appl. Phys. Lett.*, **47**, 100 (1985)
8. H. Asahi, T. Hisaka, S.G. Kim, T. Kaneko, S.J. Yu, Y. Okuno and S. Gonda, *Appl. Phys. Lett.*, **61**, 1054 (1992)
9. C.E. Sanders, D.A. Beaton, R.C. Reedy and K. Alberi, *submitted*.
10. W. Walukiewicz, *Appl. Phys. Lett.*, **54**, 2094 (1989)
11. S.B. Zhang, S.-H. Wei and A. Zunger, *J. Appl. Phys.*, **83**, 3192 (1998)
12. E.F. Schubert, J.M. Kuo, R.F. Kopf, A.S. Jordan, H.S. Luftman and L.C. Hopkins, *Phys. Rev. B*, **42**, 1364 (1990).
13. T.Y. Tan and U. Gosele, *Appl. Phys. Lett.*, **52**, 1240 (1988)
14. Z. Bryan, I. Bryan, B.E. Gaddy, P. Reddy, L. Hussey, M. Bobea, W. Guo, M. Hoffmann, R. Kirste, J. Tweedie, M. Gerhold, D.L. Irving, Z. Sitar and R. Collazo, *Appl. Phys. Lett.*, **105**, 222101 (2014).

Publications

1. "Effects of Incident UV Light on the Surface Morphology of MBE Grown GaAs," D.A. Beaton, C.E. Sanders and K. Alberi, *J. Crystal Growth*, **413**, 76 (2015)

2. "Magnetic Field Induced Direct-Indirect Crossover in AlGaAs"**.** K. Alberi**,** A.V. Mialitsin, B. Fluegel, S.A. Crooker, J.L. Reno and A. Mascarenhas**,** *Appl. Phys. Express*, **7**, 111201 (2014).

3. "Fermi Energy Tuning with Light to Control Doping Profiles During Epitaxy," C.E. Sanders, D.A. Beaton, R.C. Reedy and K. Alberi, *submitted*.

Electronics without Semiconductors by Functionalized Boron Nitride Nanotubes

Yoke Khin Yap

Department of Physics, Michigan Technological University, 1400 Townsend Drive, Houghton, MI 49931, USA.

Program Scope

The far reaching goal of this research project is to experimentally investigate single walled (SW) heterojunctions of boron nitride nanotubes and carbon nanotubes (BNNT/CNT junctions) with specific zigzag, armchair, or chiral structures. According to theory,[1-4]

- Zigzag BNNT/CNT junctions (Figure1a) are insulator/semiconductor junctions. They have flat band structures and tunable direct band gaps (~0.5 to 2.0 eV) at the interface. Thus these BNNTs/CNTs junctions can be used as nanoferromagnetic materials, spintronic and tunable photonic devices etc..
- Armchair BNNT/CNT junctions (Figure 1b) are insulator/semimetal junctions with tunable direct band gap, and applicable for Schottky devices, quantum dots, etc..

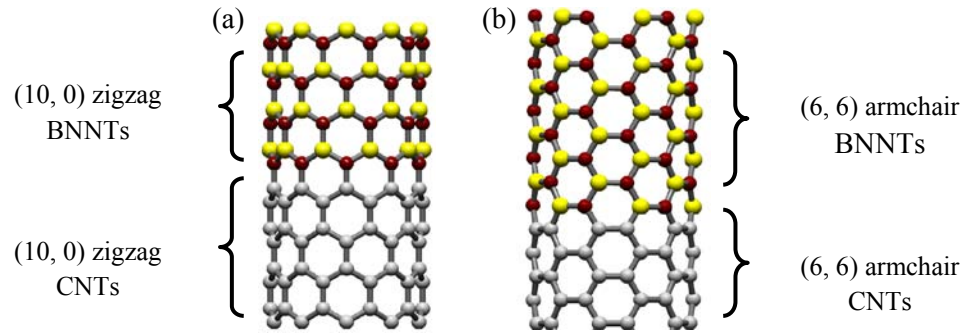

Figure 1. Ball-and-stick representations of (a) a zigzag (10, 0) and (b) an armchair (6,6) BNNT/CNT junctions.

This ultimate goal is currently not realistic because the science and engineering on chirality controls of both BNNTs and CNTs are not well established. In particular, technology to grow SW-BNNTs is still not fully achievable in the field.

Instead, the **major objectives of the current project are**to

1) Understand the science behind the synthesis of co-axial multiwalled (MW)BNNT/CNT junctions through a series of promising procedures that we have identified.
2) Investigate the novel physical properties of BNNT/CNT junctions, and their precursors that we have discovered during the pass funding period, including a) branching BNNT/CNT junctions, b) graphene-BNNT junctions, and c) quantum-dots functionalized BNNTs (QDs-BNNTs).

Recent Progress

1. Electronics without Semiconductor by Branching BNNT/CNT Junctions

As shown in Figure 2a, branching MW BNNT/CNT junctions have been synthesized and characterized.[5] As shown in Figure 2b, the transport property across the junction is different from the insulating BNNTs or metallic CNTs. We explain this by room-temperature electron tunneling across the junction when sufficient potential difference is applied across the junctions. Since this junction is branching and catalyst nanoparticles (NPs) may presented at the junctions. We are expecting better switching behaviors from seamless co-axial junctions, in which resistance and electron-phonon scattering are lower. We show that branching BNNT/CNT junctions could lead to new electronic devices without the use of semiconducting materials.

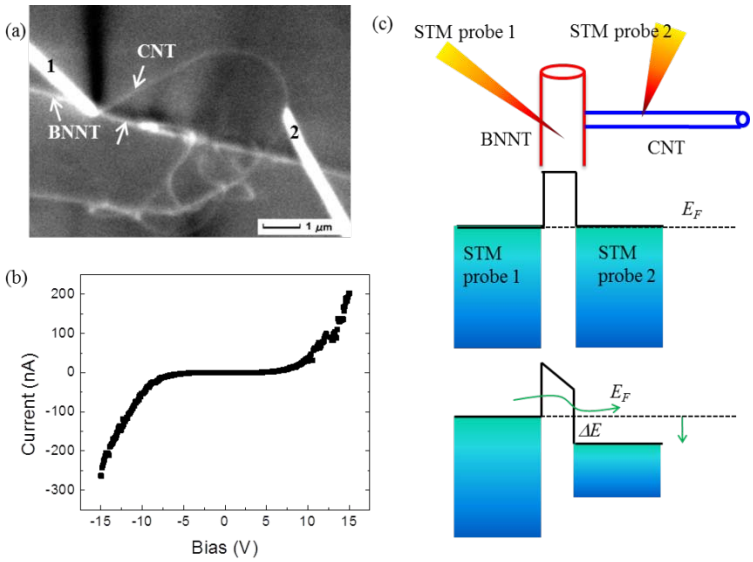

Figure 2. (a) Image of two STM probes on a branching CNT/BNNT hetero-junction. Probe 1 is on the junction (without shorting on CNT) while probe 2 is in contact with the CNT. (b) Current-voltage (I-V) character across the junction. (c) Schematic of the measurement and the related energy diagram before and after applying a bias voltage on the probes.

2. Electronics without Semiconductor by QDs-BNNTs

During the course of investigating the branching BNNT/CNT junctions, we have discovered a new class of functional materials: quantum-dots functionalized BNNTs (QDs-BNNTs).[6]As shown in Figure 3a, we have managed to deposit these crystalized gold NPs on one side of the BNNTs. These 1D arrays of NPs have diameters ranging from 3-10 nm and spacing of about 1-5 nm in between. At low bias voltages, this QDs-BNNT is insulating like pure a wide band gap

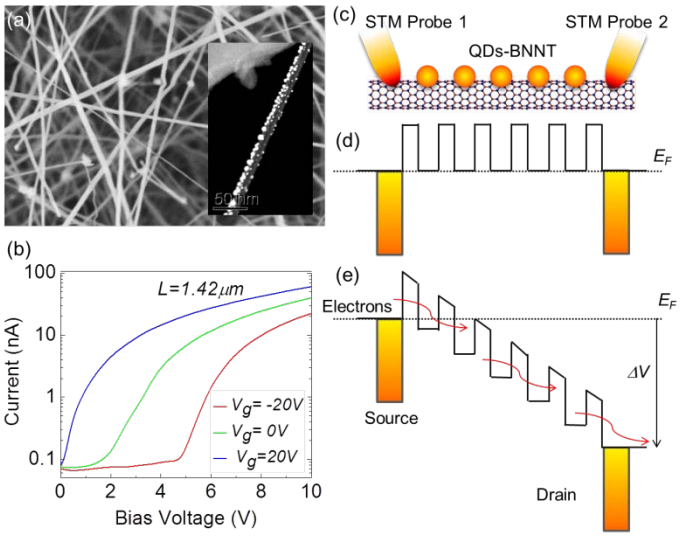

Figure 3.(a) Image of QDs-BNNTs and (b) the I-V characteristic at various gate potential (V_g). (c) Schematic of the tunneling channel at (d) off and (e) on states.

BNNT. By applying increasing bias voltages, this QDs-BNNT allowed current to flow along the nanotube (Figure 3b). The turn-on voltage (V_{on}) decreases with the shortening of the length between probes and is tunable by gate potential. We explain the detected switching behaviors by quantum tunneling across these NPs as also proven by a kinetic Monte Carlo simulation. Because of their function in facilitate the tunneling and single electron transport processes, we called these NPs as QDs.

3. Electronics without Semiconductor by Graphene-BNNTs

More recently, we have verified our new idea of forming carbon-BN hetero-junctions without using catalysts. Such a self-assembly process was first tested by using graphene sheets as the "substrates" for the growth of BNNTs. As shown in Figure 4a, BNNTs are selectively grown on the surfaces of graphene sheets. The stability of these hetero-junctions was also proven by total energy calculations performed by plane wave pseudopotential approach within the local density approximation (LDA) of density functional theory (DFT). Results indicate that these graphene-BNNT junctions are current rectifiers (Figure 4b and 4c), resembling a novel class of electronics without using semiconductors.

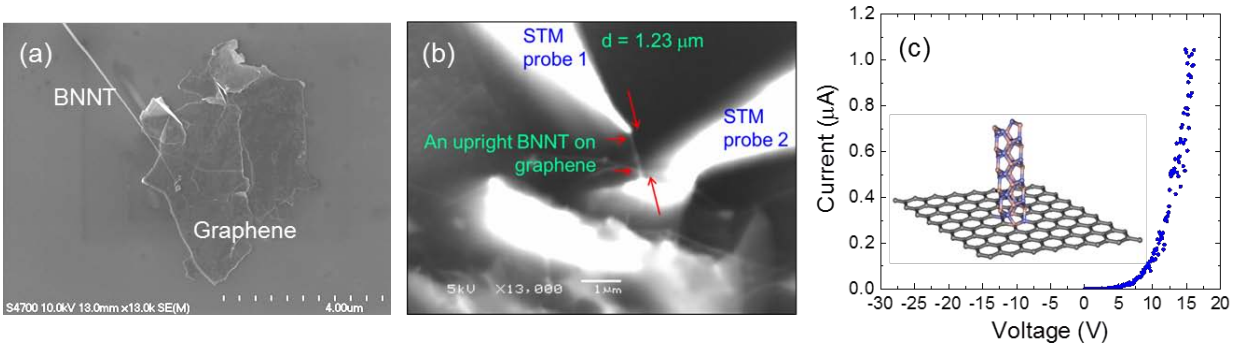

Figure 4.(a) SEM image of a BNNT grown selectively on graphene .(b and c) The formation and switching behaviors of these graphene-BNNT junctions are theoretically and experimentally proven.

Future Plans

Our theoretical results suggest that the tunneling behaviors on QDs-BNNTs resembled those of single electron transistors (SETs). This was proven with the detection of Coulomb staircases from out QDs-BNNTs at liquid helium (LHe) temperature. We are in the process to further understand this single electron transport behavior. Prior to this investigation, it is desired for us to refining the synthesis of QDs-BNNTs to improve their switching behaviors. This includes the control of the dot diameters, and dot separation. Recent results indicate that these modifications can enable the use of QDs-BNNTsin flexible electronics. In addition, we are interested to explore the possible plasmonic effects on these QDs-BNNTs. This will enable a novel class of SETs and even spintronic devices that can be modulated by surface plasmons at room temperature. Finally, experiments are now in progress to further understand the properties

of our branching BNNT-CNT junctions, as well as the graphene-BNNTjuctions. All these will enable us to understand the physical properties of MW BNNT-CNT junctions.

References

1 Blase, X., Charlier, J. C., DeVita, A. & Car, R. Theory of composite BxCyNz nanotube heterojunctions. *Appl Phys Lett***70**, 197-199 (1997).

2 Okada, S., Igami, M., Nakada, K. & Oshiyama, A. Border states in heterosheets with hexagonal symmetry. *Phys Rev B***62**, 9896-9899 (2000).

3 Okada, S. & Oshiyama, A. Magnetic ordering in hexagonally bonded sheets with first-row elements. *Phys Rev Lett***87**, 146803 (2001).

4 Choi, J., Kim, Y. H., Chang, K. J. & Tomanek, D. Itinerant ferromagnetism in heterostructured C/BN nanotubes. *Phys Rev B***67**, 125421 (2003).

5 Jiesheng Wang, C. H. L., Yoke Khin Yap. in *the 12th International Conference on the Science and Application of Nanotubes.* (2011).

6 Lee, C. H., Qin, S. Y., Savaikar, M. A., Wang, J. S., Hao, B. Y., Zhang, D. Y., Banyai, D., Jaszczak, J. A., Clark, K. W., Idrobo, J. C., Li, A. P. & Yap, Y. K. Room-Temperature Tunneling Behavior of Boron Nitride Nanotubes Functionalized with Gold Quantum Dots. *Adv Mater***25**, 4544-4548(2013).

Publications

1. Lee, C. H., Qin, S. Y., Savaikar, M. A., Wang, J. S., Hao, B. Y., Zhang, D. Y., Banyai, D., Jaszczak, J. A., Clark, K. W., Idrobo, J. C., Li, A. P. & Yap, Y. K. Room-Temperature Tunneling Behavior of Boron Nitride Nanotubes Functionalized with Gold Quantum Dots. *Adv Mater***25**, 4544-4548 (2013).

2. (Invited) Jaszczak, J. A., Savaikar, M. A., Banyai, D. A., Hao, B. Y., Zhang, D. Y., Bergstrom, P. L., Li, A-P., Idrobo, J-C., Yap. Y. K. "Simulation of Charge Transport in Disordered Assemblies of Metallic Nano-Islands: Application to Boron-Nitride Nanotubes Functionalized with Gold Quantum Dots" *Materials Research SocietyProceedings*, 1700, mrss14-1700-mm03-01 (2014) doi:10.1557/opl.2014.731.

Spin Polarized Functionality Through Complex Oxide Heteroepitaxy

PI: Yuri Suzuki
Department of Applied Physics, Stanford University
Geballe Laboratory for Advanced Materials
McCullough Room 341
Stanford University
Stanford, CA 94305-4665
ysuzuki1@stanford.edu

Program Scope

The *main research objective* of the proposed program is to develop novel paradigms for the generation of quasi-two dimensional magnetic functionality in complex oxide thin films and heterostructures. In this program, we focus on the development of novel complex oxide thin films and heterostructures with spin functionality where surfaces/interfaces and coherent epitaxial strain play a critical role in the realization of the long range magnetic order. Complex oxides exhibit a wide range of electronic, magnetic and optical properties that can be tuned by parameters such as lattice strain and substitution. The tunability combined with the ability to control complex oxide interfaces with atomic accuracy makes them ideally suited for the exploration of *new quasi-two dimensional, magnetically functional materials systems*.

Our focus is on two classes of materials based on *transition metal oxide compounds for*:

(a) heterostructures in which the interfaces gives rise to spin functionality not observed in the two constituent materials and engineered by *modulation doping of magnetic species, carrier mediated exchange interactions orvalence discontinuities at ferromagnetic interfaces.*

(b) thin films in which epitaxial strain can induce *spin-state transitions or metal-insulator transitions* to stabilize ferromagnetic and/or metallic ground states.

Recent Progress

Highlights of recent work include (i)demonstrating interfacial ferromagnetism in $LaNiO_3/CaMnO_3$superlattices, (ii) understanding the origin of modulated interfacial ferromagnetism in $CaRuO_3/CaMnO_3$superlattices and (iii) developing a comprehensive understanding of the origin of ferromagnetism in $LaCoO_3$,.

$CaRuO_3/CaMnO_3$superlattices. In our group, we have previously demonstrated the emergence of interfacial ferromagnetism in one single unit cell of $CaMnO_3$at each interface in $CaMnO_3/CaRuO_3$ superlattices.[1] These results are in agreement with density functional theory calculations that described the ferromagnetism to arise from a ferromagnetic double exchange interaction of the Mn ions due to the leakage of itinerant $CaRuO_3$ electrons into the $CaMnO_3$layer.[2]In the bulk,$CaMnO_3$is an antiferromagnetic insulator and $CaRuO_3$ is an itinerant metal. We have performed further studies on superlattices with larger periodicities, demonstrating conclusively by careful polarized neutron reflectivity measurements that interfacial ferromagnetism can only be attributed to one single unit cell of the $CaMnO_3$ at each

interface.[3]This result is rather surprising given that long-range ferromagnetic behavior is not observed in single unit cell thick films of bulk ferromagnets. Through exchange biased hysteresis loops, we have also determined that each $CaMnO_3$ layer is composed of single unit cell thick $CaMnO_3$ layers sandwiching a more bulk-like antiferromagnetic $CaMnO_3$ layer. Surprisingly this exchange bias field does not saturate with increasing $CaMnO_3$ layer thickness. However through neutron diffraction measurements, we have determined the antiferromagnetic correlation length along the growth axis direction to be greater than the sample thickness. In other words, all the $CaMnO_3$ layers in a superlattice can be thought to act as one large antiferromagnet. This long antiferromagnetic correlation length may account for the increasing exchange bias field that we observe as a function of increasing $CaMnO_3$ thickness in our superlattices.[3]

$LaNiO_3$/$CaMnO_3$ superlattices. One of our most important results has been to demonstrate that this emergent interfacial ferromagnetism that we observed in $CaMnO_3$/$CaRuO_3$ superlattices is a much more general phenomena.[4]We replaced the paramagnetic metallic $CaRuO_3$ with $LaNiO_3$. We find similar emergent behavior when we replace $CaRuO_3$ with $LaNiO_3$. Moreover $LaNiO_3$ undergoes a thickness dependent metal-insulator transition. When we vary the thickness of the $LaNiO_3$ layer from an insulator to a metal, we find that the interfacial ferromagnetism only appears when the $LaNiO_3$ layer is metallic. Therefore the leakage of itinerant electrons is essentialfor the interfacial ferromagnetism.

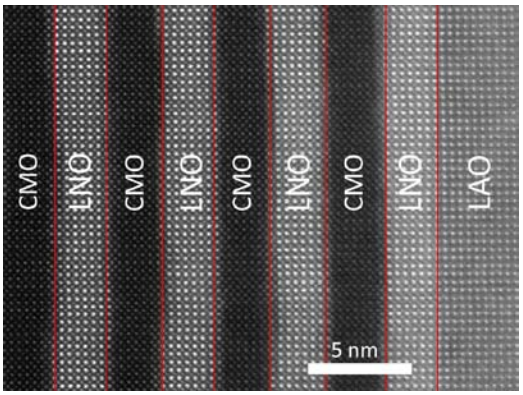

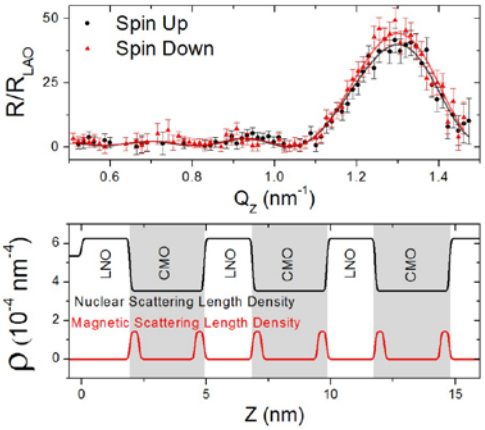

Figure 2. Polarized neutron reflectometry shows spin splitting of the Fresnel reflectivity (above) that is modeled best by a single antiferromagnetic layering of the individual $LaNiO_3$ and $CaMnO_3$ layers (below).

$CaMnO_3$ thin films. One of the outstanding questions in our study of the $CaMnO_3$ based superlattices has been the presence of weak ferromagnetism in $CaMnO_3$ possibly due to oxygen off-stoichiometry. Bulk studies have shown that there can be a small ferromagnetic contribution. We have demonstrated the synthesis of antiferromagnetic epitaxial $CaMnO_3$ thin films without any sign of weak ferromagnetism.[5]The highly crystalline CMO films in strain states ranging from fully relaxed to 1.6% coherently strained. X-ray diffraction indicates epitaxial growth with in-plane alignment with the underlying substrate. X-ray absorption spectroscopy (XAS) indicates a manganese valence of +4.0(1) to within the error of measurement. We find that the magnetic transition temperature of these films is suppressed from bulk with the amount of suppression increasing as a function of increasing strain. X-ray magnetic circular dichroism(XMCD) and SQUID magnetometry show no evidence for ferromagnetism in contrast to the bulk, thus confirming that the stabilization of antiferromagnetic CMO films with

negligible oxygen off-stoichiometry.

Long range ferromagnetic order in $LaCoO_3$ and the role of oxygen vacancies.We have developed a comprehensive picture of the origin of the long-range ferromagnetic order in epitaxial $LaCoO_3$(LCO) thin films.[6]Over the course of the last 8 years, there have been a number of studies demonstrating a ferromagnetic ground state in epitaxial LCO thin films but the explanation of the origin of ferromagnetism has remained controversial. Initial explanationsincluded epitaxial strain induced electronic structure modification but could not explain all of the data. More recently a superexchange interaction among high spin and low spin Co^{3+}based on correlated hopping has been cited as the origin of the long-range ferromagnetic order.

However we have found that such a superexchange mechanism cannot completely explain our experimental data. In collaboration with microscopists and theorists, we recently demonstrated the role of oxygen vacancies, induced by the underlying epitaxial strain, in explaining the stabilization of the long-range ferromagnetic order in epitaxial LCO films grown on $SrTiO_3$ (STO) substrates.[7]Through a combination of atomically resolved **Z**-contrast imaging, electron-energy-loss spectroscopy (EELS), and density functional calculations, we have demonstrated that, in epitaxial $LaCoO_3$ films, oxygen-vacancy superstructures release strainand produce the observed ferromagnetism via the excess electrons in the Co **d** states.The EELS data demonstrate unambiguously that there is a significant oxygen deficiency, which is responsible for the lattice relaxation and the ensuing dark stripes in the **Z**-contrast images; it also results in charge ordering within the Co sublattice. A theoretical model based on antiferromagnetically aligned high spin (HS) Co^{2+} states in the O-depleted planes and FM-ordered HS Co^{2+} ions explains the observed oxygen vacancy superstructure and ferromagnetic ground state. The calculated EELS spectra in the O-depleted and stoichiometric regions are in agreement with the measured spectra, confirming the present conclusions. In the absence of vacancies, large La-La displacements are not stable. Although oxygenvacancies typically dope a material n-type, we have found that ordered vacancies induce Peierls-like minigaps which, combined with strain relaxation, trigger a nonlinear rupture of the energy bands, resulting in insulating behavior.

Our comprehensive study of the combined effects of epitaxial strain and defects on the long range magnetic order in epitaxial LCO thin films has provided significant insight into the mechanism behind the long range order.[6]Through a comparative study of epitaxial LCO thin films grown on STO, LSAT and $LaAlO_3$ substrates, we find that the stabilization of HS Co^{2+} and Co^{3+} states combined with an ordered oxygen vacancy superstructure can account for a ferromagnetic exchange interaction observed in many of our LCO thin films. We have performed detailed structural characterization of the strain states of our samples using reciprocal space mapping in X-ray diffraction. Scanning transmission electron microscopy and EELS studies reveal oxygen vacancy ordering in our LCO samples on all three substrates to varying degrees. We have correlated these structural and vacancy ordering variations with the electronic structure and magnetism. Element specific XAS indicates that there are HS $Co,^{2+}$ LS Co^{3+} and HS Co^{3+} ions in the epitaxial films. SQUID magnetometry reveals ferromagnetic order primarily in the epitaxial LCO films under tensile strain. Element specific XMCD indicates that the long-range ferromagnetic order originates from HS Co^{2+} ions and HS Co^{3+} ions. By exploring the relationship between magnetism, strain, and stoichiometry in detail using microstructure and

electronic structure characterization, we have experimentally uncovered that both superexchange interactions among HS Co^{3+} and LS Co^{3+} based on correlated hopping and superexchange interactions among HS Co^{2+} and LS Co^{3+} based on oxygen vacancy superstructures are key in stabilizing the ferromagnetic ground state.

*Epitaxial $PrCoO_3$ thin films.*We have demonstrated that the long-range ferromagnetic order in $LaCoO_3$films can also be isolated in $PrCoO_3$ films. Since the bulk spin state transitions are at higher temperatures in $PrCoO_3$ compared to $LaCoO_3$, we expect the ferromagnetic transition temperatures to be lower in $PrCoO_3$ as observed.[8]Heteroepitaxial strain is foundto induce long-range ordering of the Co ions, which we deduce to be in a high-spin state. The ferromagneticordering of the CoO_6 array is accompanied by ordering of the Prsublattice in an antiparallel orientation to the Co. The ordering of the Prsublattice provides evidence for significant Co-Pr exchange likely facilitated by the presence of high-spin Co. The stabilization of ferrimagnetism and insulating behavior here presents a unique behavior not observed in other Pr-based perovskite oxides.

Future Plans

We plan to focus on some of the major challenges in the areas of oxide interfaces and coherent epitaxial oxide thin films. More specifically, we will explore(i) tuning (both statically and dynamically) the interfacial ferromagnetism at the interface of superlattices comprised of an itinerant metal and antiferromagnetic $CaMnO_3$ and(ii) exploring the role of spin state transition and the universality of the generation of ferromagnetism in the undopedcobaltites.

References

1. C. He,A.J. Grutter,M. Gu, N.D. Browning,Y. Takamura, B.J. Kirby, J.A. Borchers, J.W. Kim, M.R. Fitzsimmons, X. Zhai,V.V. Mehta,F.J. Wong, and Y. Suzuki, "Interfacial ferromagnetism and exchange bias in $CaRuO_3$/$CaMnO_3$superlattices," *Physical Review Letters***109** 197202 (2012).
2. B.R.K. Nanda, S. Satpathy and M.S. Springborg, "Electron leakage and double exchange ferromagnetism at the interface between a metal and an antiferromagnetic insulator: $CaRuO_3$/$CaMnO_3$," Phys. Rev. Lett. **98** 216804:1-4 (2007).
3. A.J. Grutter, A. Vailionis, J.A. Borchers, B.J. Kirby, C.L. Flint, C. He, W. Ratcliff III, Y. Suzuki, "Control of Magnetic Interfaces Through Structurally Induced Symmetry Mismatch in Complex Oxide Superlattices," to be published (2015).
4. A.J. Grutter, B.J. Kirby, M.R. Fitzsimmons, H. Yang, N.D. Browning, C.A. Jenkins, E. Arenholz, V.V. Mehta, U.S. Alaan, Y. Suzuki, "Interfacial Ferromagnetism in $LaNiO_3$/$CaMnO_3$," *Physical Review Letters***111** 087202 (2013).
5. C. L. Flint, A. J. Grutter, C. A. Jenkins, E. Arenholz, and Y. Suzuki, "Magnetism in $CaMnO_3$ Thin Films," *Journal of Applied Physics***115**17D712 (2014).
6. V.V. Mehta, N. Biskup, C. Jenkins, E. Arenholz, M. Varela, Y. Suzuki, "Long Range Ferromagnetic Order in $LaCoO_{3-\square}$epitaxial films due to the interplay of epitaxial strain and oxygen vacancy ordering," submitted to *Physical Review B* (2014).
7. NevenBiškup, Juan Salafranca, Virat Mehta, Yuri Suzuki, Stephen J. Pennycook, Sokrates T. Pantelides, and Maria Varela, "Insulating Ferromagnetic $LaCoO_{3-\delta}$ Films: A Phase Induced by Ordering of Oxygen Vacancies," *Physical Review Letters***112** 087202 (2014).

8. Virat V. Mehta, Shameek Bose, Jodi Iwata-Harms, ElkeArenholz, Christopher Leighton, Yuri Suzuki, "Ferrimagnetism un $PrCoO_3$ Epitaxial Films," *Rapid Communications Physical Review B***87** 020405 (2012). (2012).

Publications

- A. J. Grutter, F. J. Wong, E. Arenholz, A. Vailionis, and Y. Suzuki, "Evidence of high spin Ru and universal magnetic anisotropy in $SrRuO_3$ thin films," *Physical Review B***85** 134429 (2012).
- C. He, T. Sanders, M. Gray, F.J. Wong,V.V. Mehta, "Metal-insulator transitions in epitaxial $LaVO_3$ and $LaTiO_3$ films,"and Y. Suzuki, *Physical Review B***86** 081401 (2012).
- C. He,A.J. Grutter,M. Gu, N.D. Browning,Y. Takamura, B.J. Kirby, J.A. Borchers, J.W. Kim, M.R. Fitzsimmons, X. Zhai,V.V. Mehta,F.J. Wong, and Y. Suzuki, "Interfacial ferromagnetism and exchange bias in $CaRuO_3$/$CaMnO_3$superlattices," *Physical Review Letters***109** 197202 (2012).
- Virat V. Mehta, Shameek Bose, Jodi Iwata-Harms, ElkeArenholz, Christopher Leighton, Yuri Suzuki, "Ferrimagnetism un $PrCoO_3$ Epitaxial Films," *Rapid Communications Physical Review B***87** 020405 (2012). (2012).
- M.T. Gray, T.D. Sanders, F.J. Wong, A.J. Grutter, U.S. Alaan, C. He, E. Arenholz, C. Jenkins, Y. Suzuki, "Growth of Doped $LaAlO_3$ Thin Films for Modified Quasi-Two Dimensional Electron Gases," *Applied Physics Letters***102** 131601 (2013).
- A.J. Grutter, B.J. Kirby, M.R. Fitzsimmons, H. Yang, N.D. Browning, C.A. Jenkins, E. Arenholz, V.V. Mehta, U.S. Alaan, Y. Suzuki, "Interfacial Ferromagnetism in $LaNiO_3$/$CaMnO_3$," *Physical Review Letters***111** 087202 (2013).
- NevenBiškup, Juan Salafranca, Virat Mehta, Yuri Suzuki, Stephen J. Pennycook, Sokrates T. Pantelides, and Maria Varela, "Insulating Ferromagnetic $LaCoO_{3-\delta}$ Films: A Phase Inducedby Ordering of Oxygen Vacancies," *Physical Review Letters***112** 087202 (2014).
- C. L. Flint, A. J. Grutter, C. A. Jenkins, E. Arenholz, and Y. Suzuki, "Magnetism in $CaMnO_3$ Thin Films," *Journal of Applied Physics***115**17D712 (2014).
- V.V. Mehta, N. Biskup, C. Jenkins, E. Arenholz, M. Varela, Y. Suzuki, "Long Range Ferromagnetic Order in $LaCoO_{3-\square}$ epitaxial films due to the interplay of epitaxial strain and oxygen vacancy ordering," submitted to *Physical Review B* (2014).

Updated Progress in Piezotronics and Piezo-phototronics

Zhong Lin Wang

School of Materials Science and Engineering, Georgia Institute of Technology, Atlanta USA

Piezoelectricity, a phenomenon known for centuries, is an effect that is about the production of electrical potential in a substance as the pressure on it changes. For wurtzite structures such as ZnO, GaN, InN and ZnS, due to the polarization of ions in a crystal that has non-central symmetry, a piezoelectric potential *(piezopotential)* is created in the crystal by applying a stress. The effect of piezopotential to the transport behavior of charge carriers is significant due to their multiple functionalities of piezoelectricity, semiconductor and photon excitation. By utilizing the advantages offered by these properties, a few new fields have been created. Electronics fabricated by using inner-crystal piezopotential as a "gate" voltage to tune/control the charge transport behavior is named *piezotronics,* with applications in strain/force/pressure triggered/controlled electronic devices, sensors and logic units. This effect was also extended to 2D materials such as MoS_2. *Piezo-phototronic effect* is a result of three-way coupling among piezoelectricity, photonic excitation and semiconductor transport, which allows tuning and controlling of electro-optical processes by strain induced piezopotential. The objective of this talk is to introduce the fundamentals of piezotronics and piezo-phototronics and to give an updated progress about their applications in energy science (LED, solar) and sensors (photon detector and human-CMOS interfacing).

Acknowledgements. Research was supported by U.S. Department of Energy, Office of Basic Energy Sciences (Award DE-FG02-07ER46394).

[1] W.Z. Wu, X.N. Wen, Z.L. Wang "Pixel-addressable matrix of vertical-nanowire piezotronic transistors for active/adaptive tactile imaging", Science, 340 (2013) 952-957.

[2] C.F. Pan, L. Dong, G. Zhu, S. Niu, R.M. Yu, Q. Yang, Y. Liu, Z.L. Wang* "Micrometer-resolution electroluminescence parallel-imaging of pressure distribution using piezoelectric nanowire-LED array", Nature Photonics, 7 (2013) 752-758.

[3] Z.L. Wang "Piezopotential Gated Nanowire Devices: Piezotronics and Piezo-phototronics", Nano Today, 5 (2010) 540-552.

[4] Q. Yang, W.H. Wang, S. Xu and Z.L. Wang* "Enhancing light emission of ZnO microwire-based diodes by piezo-phototronic effect", Nano Letters, *11* (2011) 4012–4017.

[5] W.Z. Wu+, L. Wang+, Y.L. Li, F. Zhang, L. Lin, S. Niu, D. Chenet, X. Zhang, Y. Hao, T.F. Heinz, J. Hone, and Z.L. Wang "Piezoelectricity of single-atomic-layer MoS_2 for energy conversion and piezotronics", Nature, 2014, DOI: 10.1038/nature13792.

Session XIII

Program Title: **Synthesis and characterization of nanomaterial heterostructures and assemblies: investigation of charge and energy flow at nanostructured interfaces.**

Principal Investigator: **Stanislaus S. Wong, Brookhaven National Laboratory, CMPMSD Department, Building 480, Upton, NY 11973; Email: sswong@bnl.gov.**

Collaborators: **M.Y. Sfeir, R.M. Konik (BNL), J. Appenzeller (Purdue University)**
Unpaid Consultants: **Y. Zhu, J.A. Misewich (BNL)**

Program Scope: The ability to synthesize, functionalize, and purify nanomaterials and to understand their transport, optical and mechanical properties lies at the forefront of current materials science research. As shown in the DOE report on Basic Research Needs for Solar Energy Utilization, nanostructured materials offer several potential advantages for solar energy conversion by providing relatively high electron and hole transport efficiencies, excitation multiplication possibilities, high surface-to-volume ratios, and short electron-hole diffusion lengths to junctions.[1] However, the role of nanoscale heterojunctions in promoting exciton dissociation and charge separation is not understood. It is expected that junctions between low dimensional materials will behave differently as compared with bulk junctions. We will address the important question of the efficiency of charge separation versus recombination or trapping in prototypical heterogeneous nanomaterial systems: i.e. zero-dimensional (0d) – one-dimensional (1d) nanomaterial hybrids. We also expect to develop a fundamental emphasis on synthesizing and understanding more complex nanoscale materials, including metal-based heterostructures, of significance to the solar initiative. We have the ability to synthesize high quality samples and to study the properties and structure (both electronic and physical) of individual nanomaterial samples, thus eliminating the uncertainties in ensemble averaging over many structures. Working with our theoretical collaborators, these studies will clarify the potential of nanoscale heterojunctions and interfaces for charge separation in solar electric generation.[2]

Therefore, optimizing exciton harvesting through the mediation of well-defined nanoscale interfaces will be critical if the use of nanomaterials can result in an increased overall efficiency and integration into a real device for practical solar applications.[3] The overarching question that we seek to address in this work can be summarized as follows: *Can we design and synthesize well-controlled complex quantum-confined nanostructures so that we can manipulate the energy flow and charge transfer pathways in these materials in order to optimize not only the absorption of photons but also exciton harvesting for the production of useful work*? In order to answer this question, we have synthesized and structurally characterized a systematic series of model 0D/1D nanomaterials. In addition, we are also providing substantial insight into the transport and optoelectronic properties of these materials. In effect, correlating the intrinsic optical, transport, and opto-electronic properties with the structural characterization of these nanomaterial composite structures will allow us to unravel how competing pathways as well as the inherent properties of these materials in general depend on the nanoscale heterostructure's synthesis parameters, such as the 0D QD- 1D nanotube linker length as well as the chemical composition of the ligand field surrounding the QD itself.

Recent Progress: Several pathways for charge carrier relaxation in the semiconducting QDs are possible. In addition to the intrinsic QD relaxation processes (e.g. radiative recombination, electron/hole trapping, and Auger recombination), the 1D nanomaterial-CdSe QD composite will have additional quenching mechanisms including: (a) resonant energy transfer (RET) of both charge carriers through near-field dipolar coupling and (b) charge transfer (CT) of one charge carrier. These two additional pathways are illustrated in Figure 1 for a 0-dimensional/1-dimensional QD-NT system bound with a linker.

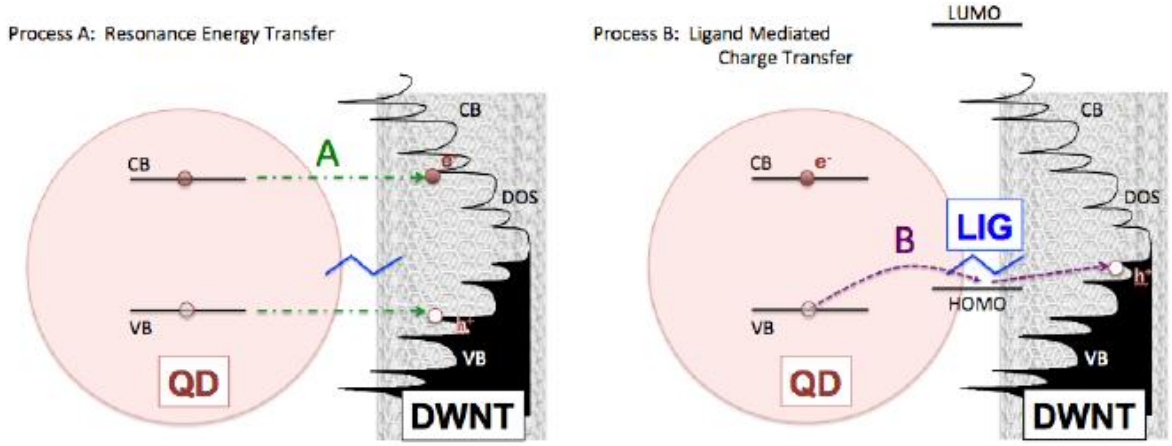

Figure 1. Schematic of energy and charge flow processes in ternary QD-LIGAND-NT heterostructures. In process A, both the photoexcited electron and hole are transferred simultaneously via near-field energy transfer. The ligand is a structural element only. In process B, the ligand is electronically active and functions to trap one of the carriers at the surface of the QD and tunneling (charge transfer) becomes the dominant kinetic interaction.

In *one manifestation* of this strategy[4] (Figure 2), double-walled carbon nanotube (DWNT) - CdSe heterostructures with the individual nanoscale building blocks linked together by 4-aminothiophenol (4-ATP) have been successfully synthesized using two different and complementary routes, i.e. covalent attachment and non-covalent π-π stacking, as confirmed by AFM height images. With DWNTs, consisting of two coaxial single tubes, we can potentially and selectively functionalize only the outer walls so as to enable selective chemical attachment of quantum dots without necessarily damaging and degrading the inner tubes, a consequence of which is that one can envision possibly retaining the desired electronic properties of the overall material. TEM and HRTEM images indicated that the non-covalent attachment was quantitatively more efficient in terms of coverage density of CdSe QDs on the DWNT surface. Furthermore, the non-covalent method is significantly more time-efficient, non-destructive, and facile as compared with analogous covalent attachment approaches. Moreover, the non-covalent π-π stacking method, taking advantage of the extended, delocalized conjugated π-electron system inherent to the NTs themselves, can be carried out using pristine DWNTs without additional surface functionalization, a favorable experimental outcome which can preserve the inherent electronic structure of the DWNTs. Additional acquisition of photoluminescence (including quantum yield data) as well as of Raman spectra strongly suggest that both covalent and non-covalent attachments of 4-ATP-functionalized CdSe QDs can lead to observable charge transfer behavior with the latter non-covalent protocols appearing to be more efficient, possibly due to the resulting higher coverage density of discrete QDs on the underlying DWNT surface.

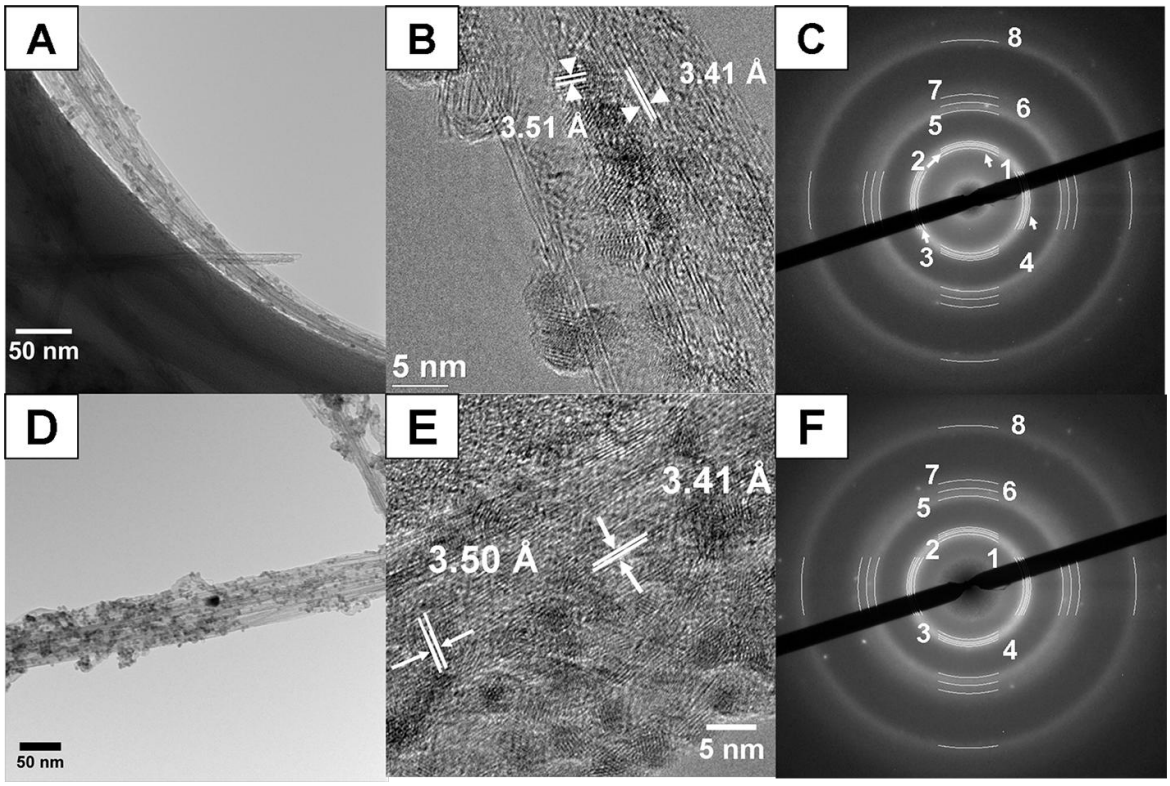

Figure 2. A, B, and C. TEM image, HRTEM image, and SAED pattern, respectively, of DWNT-4-ATP-CdSe heterostructures synthesized by covalent attachment. **D, E, and F.** TEM image, HRTEM image, and SAED pattern, respectively, of DWNT-4-ATP-CdSe heterostructures created through π-π stacking effects.

In a *second, more generalized approach* to this strategy, our team[5] has synthesized and characterized the structural and optical properties of novel heterostructures composed of (i) semiconducting nanocrystalline CdSe QDs coupled with (ii) 1D and 0D motifs of self-activated luminescent $CaWO_4$ metal oxides. Specifically, ~4 nm CdSe QDs have been anchored onto (i) high-aspect ratio 1D nanowires, measuring ~230 nm in diameter and ~3 μm in length, as well as onto (ii) crystalline 0D nanoparticles (possessing an average diameter of ~ 80 nm) of $CaWO_4$ through the mediation of 3-mercaptopropionic acid (MPA) as a connecting linker. Composite formation was confirmed by electron microscopy and spectroscopy (i.e. IR/Raman) data.

In terms of luminescent properties, our results show that our 1D and 0D heterostructures evince photoluminescence (PL) quenching and shortened PL lifetimes of $CaWO_4$ as compared with unbound $CaWO_4$. We propose that a photo-induced electron transfer process occurs from $CaWO_4$ to CdSe QDs, a scenario which has been confirmed by NEXAFS measurements and which highlights a decrease in the number of unoccupied orbitals in the conduction bands of CdSe QDs. By contrast, the PL signature and lifetimes of MPA-capped CdSe QDs within these heterostructures do not exhibit noticeable changes as compared with unbound MPA-capped CdSe QDs. The striking difference in optical behavior between $CaWO_4$ nanostructures and CdSe QDs within our heterostructures can be correlated with the relative positions of their conduction and valence energy band levels. In addition, the PL quenching behaviors for $CaWO_4$ within the heterostructure configuration were examined by systematically varying (i) the

quantities and coverage densities of CdSe QDs as well as (ii) the intrinsic morphology (and by extension, the inherent crystallite size) of $CaWO_4$ itself.

Building on this prior work,[6] coupled with either zero-dimensional (0D) CdS or CdSe quantum dots (QDs), we observed optimal charge transfer processes in 1D $CaW_{1-x}Mo_xO_4$: Eu^{3+} (‘*x’* = 0.8) – 0D QD composite nanoscale heterostructures. Our results show that $CaW_{1-x}Mo_xO_4$: Eu^{3+} (‘*x’* = 0.8) nanowires give rise to PL quenching when CdSe QDs and CdS QDs are anchored onto the surfaces of 1D $CaWO_4$ - $CaMoO_4$: Eu^{3+} nanowires. The optical behavior of 1D Eu^{3+} activated tungstate and molybdate solid solution nanowires as well as of the semiconducting 0D QDs within our heterostructures can be correlated with the relative positions of their conduction and valence energy band levels. We propose that the PL quenching can be attributed to a photo-induced electron transfer process from $CaW_{1-x}Mo_xO_4$: Eu^{3+} (‘*x’* = 0.8) to both CdSe and CdS QDs.

Future Plans: The key point to emphasize here is that core team members are actively involved with developing, optimizing, and cooperatively coordinating their part of the project, relevant to specific areas of expertise, whether it be ligand exchange, the development of relevant optical methods, theoretical modeling, tools for image interpretation in microscopy, or electronic device fabrication. The objective is to address the problem of energy and charge transfer in a consistent, uniform set of samples comprised of model nanoscale heterostructures through a comprehensive approach. In this light, additional goals include but are not limited to probing (a) the conjugation and characterization of nanotubes with surface-modified QDs of varying sizes and types, (b) the measurement of ensemble optical properties, (c) the generation and evaluation of hybrid nanocomposite devices, and (e) the theoretical limits of efficiency therein.

References: 1. Lewis, N. S.; Crabtree, G., *Basic Research Needs for Solar Energy Utilization: Report of the Basic Energy Sciences Workshop on Solar Energy Utilization, April 18-21, 2005*. Department of Energy, Office of Science: 2005; p 21.
2. Kamat, P. V., Meeting the clean energy demand: Nanostructure architectures for solar energy conversion. *Journal of Physical Chemistry C* **2007,** *111* (7), 2834-2860.
3. Giebink, N. C.; Wiederrecht, G. P.; Wasielewski, M. R.; Forrest, S. R., The Thermodynamic Efficiency Limit of Excitonic Solar Cells. *Phys. Rev. B* **2011,** *83*, 195326/1-195326/6.
4. Wang, L.; Han, J.; Hoy, J.; Hu, F.; Liu, H.; Gentleman, M. M.; Sfeir, M. Y.; Misewich, J. A.; Wong, S. S., Probing Differential Optical and Coverage Behavior in Nanotube-Nanocrystal Heterostructures Synthesized by Covalent versus Non-covalent Approaches. *Dalton Transactions* **2014,** *43* (20), 7480-7490.
5. Han, J.; McBean, C.; Wang, L.; Hoy, J.; Jaye, C.; Liu, H.; Li, Z.-Q.; Sfeir, M. Y.; Fischer, D. A.; Taylor, G. T.; Misewich, J. A.; Wong, S. S., Probing structure-induced optical behavior in a new class of self-activated luminescent 0D/1D $CaWO_4$ metal oxide – CdSe nanocrystal composite heterostructures. *Chem. Mater.* **2015,** *27* (3), 778-792.
6. Han, J.; McBean, C.; Wang, L.; Jaye, C.; Liu, H.; Fischer, D. A.; Wong, S. S., Synthesis of Compositionally-Defined Single-Crystalline Eu^{3+}-Activated Molybdate-Tungstate Solid Solution Composite Nanowires and Observation of Charge Transfer in a Novel Class of 1D $CaMoO_4$-$CaWO_4$: Eu^{3+} – 0D CdS/CdSe QD Nanoscale Heterostructures. *J. Phys. Chem. C* **2015**, *119* (7), 3826–3842.

Publications funded in part by Basic Energy Sciences (2013-present):

Publications intellectually led by this FWP

13. Robert M. Konik, Matthew Y. Sfeir, and James A. Misewich, "Predicting excitonic gaps of semiconducting single-walled carbon nanotubes from a field theoretic analysis", **91(7)**, 075417/1-10 (2015).

12. Jinkyu Han, Coray McBean, Lei Wang, Cherno Jaye, Haiqing Liu, Daniel A. Fischer, and Stanislaus S. Wong, "Synthesis of Compositionally-Defined Single-Crystalline Eu^{3+}-Activated Molybdate-Tungstate Solid Solution Composite Nanowires and Observation of Charge Transfer in a Novel Class of 1D $CaMoO_4$-$CaWO_4$: Eu^{3+} – 0D CdS/CdSe QD Nanoscale Heterostructures", *J. Phys. Chem. C*, **119(7),** 3826–3842 (2015).

11. Jinkyu Han, Coray McBean, Lei Wang, Jessica Hoy, Cherno Jaye, Haiqing Liu, Zhuo-Qun Li, Matthew Y. Sfeir, Daniel A. Fischer, Gordon T. Taylor, James A. Misewich, and Stanislaus S. Wong, "Probing structure-induced optical behavior in a new class of self-activated luminescent 0D/1D $CaWO_4$ metal oxide – CdSe nanocrystal composite heterostructures", *Chem. Mater.*, **27(3)**, 778–792 (2015).

10. Megan E. Scofield, Christopher Koenigsmann, Lei Wang, Haiqing Liu, and Stanislaus S. Wong, "Tailoring the Composition of Ultrathin, Ternary Alloy PtRuFe Nanowires for the Methanol Oxidation Reaction and Formic Acid Oxidation Reaction", *Energy & Environmental Sciences*, **8(1)**, 350-363 (2015).

9. Jonathan M. Patete, Jinkyu Han, Amanda L. Tiano, Haiqing Liu, Myung-Geun Han, J. W. Simonson, Yuanyuan Li, Alexander C. Santulli, M. C. Aronson, Anatoly I. Frenkel, Yimei Zhu, and Stanislaus S. Wong, "Observation of Ferroelectricity and Structure-Dependent Magnetic Behavior in Novel One-Dimensional Motifs of Pure, Crystalline Yttrium Manganese Oxides", *J. Phys. Chem. C*, **118(37),** 21695–21705 (2014).

8. Jinkyu Han, Lei Wang, and Stanislaus S. Wong, "Morphology and dopant-dependent optical characteristics of novel composite 1D and 3D based heterostructures of CdSe nanocrystals and $LaPO_4$: Re (Re = Eu, Ce, Tb) metal oxide nanowires", *RSC Advances*, **4(66)**, 34963-34980 (2014).

7. Haiqing Liu, Christopher Koenigsmann, Radoslav R. Adzic, and Stanislaus S. Wong, "Probing Ultrathin One-dimensional Pd-Ni Nanostructures as Oxygen Reduction Reaction Catalysts", *ACS Catalysis*, **4(8)**, 2544-2555 (2014).

6. Crystal S. Lewis, Lei Wang, Haiqing Liu, Jinkyu Han, and Stanislaus S. Wong, "Synthesis, Characterization, and Formation Mechanism of Crystalline Cu and Ni Metallic Nanowires under Ambient, Seedless, Surfactantless Conditions", *Crystal Growth and Design*, **14(8)**, 3825-3838 (2014).

5. Lei Wang, Jinkyu Han, Jessica Hoy, Fang Hu, Haiqing Liu, Molly M. Gentleman, Matthew Y. Sfeir, James A. Misewich, and Stanislaus S. Wong, "Probing Differential

Optical and Coverage Behavior in Nanotube-Nanocrystal Heterostructures Synthesized by Covalent versus Non-covalent Approaches", invited contribution, 'Organometallic and Coordination Derivatives of Nanocarbons' special issue, *Dalton Transactions,* **43(20)**, 7480 – 7490 (2014).

4. Jinkyu Han, Lei Wang, and Stanislaus S. Wong, "Observation of photoinduced charge transfer in novel luminescent CdSe quantum dot – $CePO_4$: Tb metal oxide nanowire composite heterostructures", *J. Phys. Chem. C*, **118(11)**, 5671-5682 (2014).

3. Lei Wang, Haiqing Liu, Robert M. Konik, James A. Misewich, and Stanislaus S. Wong, "Carbon Nanotube-based Heterostructures for Solar Energy Applications", invited contribution, *Chem. Soc. Rev.*, **42(20)**, 8134 – 8156 (2013).

2. Christopher Koenigsmann and Stanislaus S. Wong, "Tailoring Chemical Composition to Achieve Enhanced Methanol Oxidation Reaction and Methanol-Tolerant Oxygen Reduction Reaction Performance in Palladium-Based Nanowire Systems", *ACS Catalysis*, **3(9)**, 2031–2040 (2013).

1. Christopher Koenigsmann, Dara Bobb Semple, Eli Sutter, Sybil E. Tobierre, and Stanislaus S. Wong, "An Ambient Synthesis of High-Quality Ru Nanowires and the Morphology-Dependent Electrocatalytic Performance of Pt-decorated Ruthenium Nanowires and Nanoparticles in the Methanol Oxidation Reaction", *ACS Appl. Mater. Interf.*, **5(12),** 5518-5530 (2013).

Collaborative publications.

7. Erik Busby, Jianlong Xia, Jonathan Z. Low, Qin Wu, Jessica Hoy, Luis M. Campos, and Matthew Y. Sfeir, "Fast Singlet Exciton Decay in Push–Pull Molecules Containing Oxidized Thiophenes", *J. Phys. Chem. B*, in press.

6. Georgia C. Papaefthymiou, Arthur J. Viescas, Jean-Marie Le Breton, Hubert Chiron, Jean Juraszek, Tae-Jin Park, and Stanislaus S. Wong, "Mössbauer characterization of the magnetic properties of single crystalline sub-micron sized $Bi_2Fe_4O_9$ cubes", *Curr. Appl. Phys.*, **15(3)**, 417-422 (2015).

5. Fernando E. Camino, Chang-Yong Nam,Yutong T. Pang, Jessica Hoy, Matthew D. Eisaman, Charles T. Black, and Matthew Y. Sfeir, "Characterization of plasmonic hole arrays as transparent electrical contacts for organic photovoltaics using high-brightness Fourier transform methods, *Journal of Modern Optics*, **61(21),** 1735-1742 (2014).

4. Trevor A. Tyson, Tian Yu, Mark Croft, Megan E. Scofield, Dara Bobb-Semple, Jing Tao, Cherno Jaye, Daniel A. Fischer, and Stanislaus S. Wong, "Polar State in Freestanding $SrTiO_3$ Nanoparticles", *Appl. Phys. Lett.*, **105(9)**, 091901/1-5 (2014).

3. Katherine M. Dunnick, Melissa A Badding, Diane Schwegler-Berry, Jonathan M. Patete, Christopher Koenigsmann, Stanislaus S. Wong, and Stephen S. Leonard, "The effect of tungstate nanoparticles on reactive oxygen species and cytotoxicity in RAW

264.7 mouse monocyte macrophage cells", *Journal of Toxicology and Environmental Health, Part A*, **77(20)**, 1251-1268 (2014).

2. Kenneth R. O'Neal, Jonathan M. Patete, Peng Chen, Brian S. Holinsworth, Jacqueline M. Smith, Nara Lee, Sang-Wook Cheong, Stanislaus S. Wong, Carlos Marques, Meigan C. Aronson, and Janice L. Musfeldt, "Size-Dependent Vibronic Coupling in α-Fe_2O_3", *J. Chem. Phys.*, **141(4)**, 044710/1-5 (2014).

1. Bob C. Fitzmorris, Jonathan M. Patete, Jacqueline Smith, Xiomara Mascorro, Staci Adams, Stanislaus S. Wong, and Jin Z. Zhang, "Ultrafast Transient Absorption Studies of Hematite Nanoparticles: The Effect of Particle Shape on Exciton Dynamics", invited contribution, 'Shaping Nanostructures for Applications in Energy Conversion and Storage' special issue, *ChemSusChem*, **6(10),** 1907-1914 (2013).

Rational Design of Hybrid Nanocrystal/Silicon Architectures: From Fundamentals of Energy Transfer to Applications of Energy Sustainability

PI: Anton V. Malko, Co-PIs: Yves J. Chabal, Yuri N. Gartstein,
The University of Texas at Dallas, Departments of Physics and Materials Science,
800 W. Campbell Rd., Richardson, TX, 75080, anton.malko@utdallas.edu

Program Scope

This program is aimed to provide a *fundamental* understanding of processes and materials properties that would enable the operation of novel thin-film photovoltaic (PV) hybrid nanostructures based on *energy transfer* (ET)between light-absorbing colloidal nanocrystal quantum dots (NQDs) and high-mobility Si substrates. The solar light energy is initially absorbed by NQDs and then transferred, via radiative (RET) and non-radiative (NRET) energy transfer, into a thin flexible Si layer for further electron-hole separation and transport. The strength and novelty of this concept is in the separation of primary functionalities of the components of the hybrid augmented by the fact that NRET and RET are longer distance interactions as compared to standard charge transfer *and do not involve physical transfer of charge carriers across an interface*. Our approach is multi-pronged: We are developing a new class of NQDs with enhanced photophysical properties (superior photostability and long-lived multiexcitonic states) in the near-infrared spectral region necessary for efficient sunlight harvesting. We are developing methods to create think NQD multilayers of good optical quality. We are researching possibilities of various 3D geometrical structural arrangements in the hybrids and their optical and electrical characterization. Theexperimental efforts are supplemented by theoretical modeling of NRET and RET conditions as to achieve optimum efficiencies. Furthermore, we utilize ET-based platform as a testbed to study other advanced concepts for Si sensitization.

Recent Progress

a) Preparation of size-gradient nanocrystal multilayers for energy transfer applications

We have developed a comprehensive grafting approach to create dense, size-gradient NQD layers on Si surfaces. The first NQD layer is grafted to Si via amine-modified, self-assembled monolayer (SAM) of carboxylic ligands that passivate Si surface (very low number of surface traps, $N<10^{11}$ cm^{-2}) and provide anchoring to the nanocrystals. The consecutive NQD layers are linked via di-amine linker molecules (C_2 or C_6), which also serve dual role of surface passivation and layer attachment. Such linker assisted, layer-by-layer deposition strategy allows us to create tightly controlled, size-gradient NQD solids with directed energy transfer towards Si substrate as pictured in Fig.1. We have been developing an extension to this grafting strategy in which we first prepare Si substrate with the usual SAM linkers and then, using slow

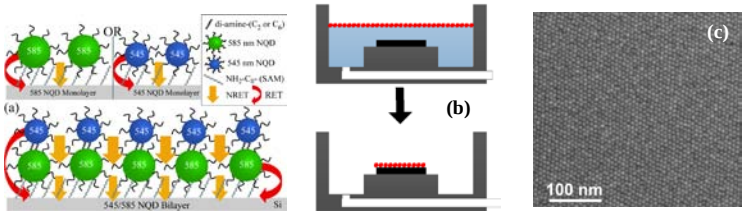

Figure 1. (a) Schematics of the monolayer and size-gradient bi-layer placement and relevant ET processes into Si substrate. (b) Slow evaporation/assembly schematics (c) SEM image of dense NQD layer on Si.

sedimentation/evaporation approach, slowly deposit NQDs onto it as illustrated in Fig. 1 (b). This approach results in very dense layer of NQDs that form nearly perfect close-packing arrangement. When chemically attached to SAMs, this approach is expected to result in robust dense surface coverage. We are currently assessing the absorption and luminescent properties of the mutilayered structures.

b) Detailed measurements of ET in bilayer NQD/Si hybrid structures

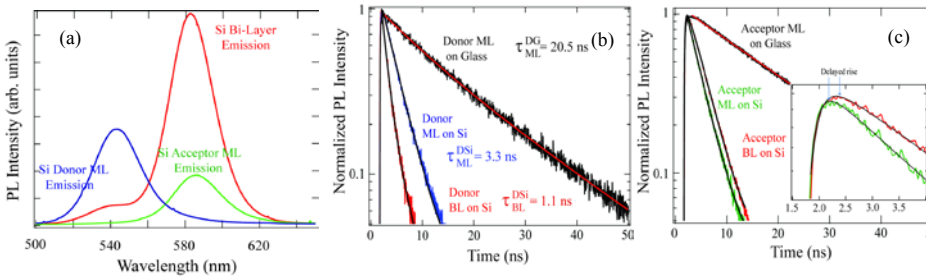

Figure 2. a) PL emission spectra of donor monolayer (blue), acceptor monolayer (green) and donor-acceptor bilayer (red) samples grafted on the Si substrates. b) Compared are the PL dynamics at the donor emission peak (545 nm) for the donor monolayer on SiO_2 (black trace), donor monolayer on Si (blue trace) and donor in the bilayer on Si (red trace) configurations. Traces are shown along with the fitting curves. c) Comparison of the PL kinetics at the acceptor emission peak (585 nm): acceptor monolayer on SiO_2 (black) trace), acceptor monolayer on Si (green trace), and acceptor in the bilayer on Si (red trace). The inset more clearly shows the delayed rise time and the fitting curves.

We performed measurements of energy relaxation pathways and energy transfer efficiencies between adjacent NQD layers and into Si substrates. Using time-resolved PL data, we have clearly delineated effects of nonradiative (NRET) and radiative (RET) energy transfer mechanisms in the overall excitonic energy transfer process. We found that NRET is primarily responsible for the very effective, ~90% efficient (due to the dense and accurate NQD layer positioning) interlayer transfer from smaller to larger size NQDs positioned closer to Si substrate. The RET, being comparatively longer ranged (50-60 nm effective distance), has been shown to couple excitations directly from the outermost NQD layer into Si substrate. Both NRET and RET effectively couple excitations from the bottom-most NQD layer into Si, thus completing energy "funneling" cascade through NQD layers. Overall transfer efficiency from the top NQD layer into Si through the combination of both ET processes approaches 90%. Importantly, experimental data agree well with theoretical calculations that only take into account energy transfer processes *without* the influence of any type of exciton scavenging/trapping mechanisms. Thus we were able to conclude that linker-assisted grafting strategy can provide defect-free NQD solids with high ET efficiency into underlying semiconductor substrate. [1]

c) Development of the near-infrared active, photostable nanocrystals

Within the scope of the project, we work with Dr. Jennifer Hollingsworth at Center of Integrated Nanotechnologies (CINT) at LANL to synthesize novel types of near infrared active (targeted to have around 1 μm PL emission wavelength), and photostable NQDs usable for grafting on Si surfaces. We are focusing on a new synthetic approach for shell growth that entails a two-step process by which a thin shell is first grown at low-temperatures by a partial cation exchange method. Then, a second, thicker-shell is grown at more ideal, higher temperatures by a successive ionic layer adsorption and reaction (SILAR) method. Several challenges are being met in attempting to apply true SILAR conditions for high quality shell growth to these lead chalcogenide QDs: namely, avoiding (a) particle ripening/coalescence, (2) core/shell de-wetting, and (3) formation of asymmetric shapes rather than core/shell structures, e.g., tetrapods. We have

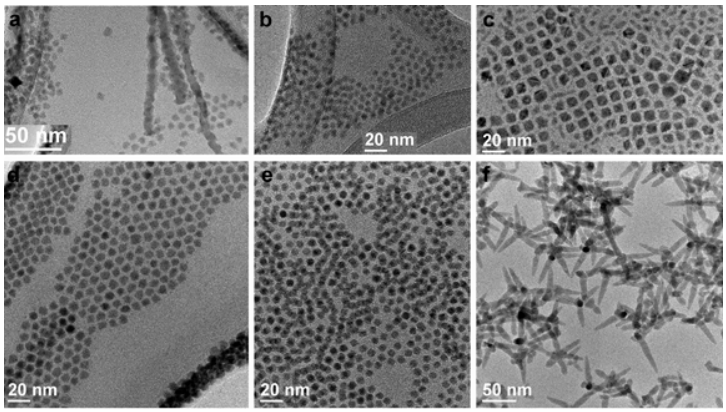

Figure 3. Transmission electron microscopy (TEM) images showing progression from PbSe QD cores (a and d) through PbSe/CdSe thin-shell core/shell QDs prepared using partial cation-exchange method (b and e) to either PbSe/CdSe thick-shell core/shell QDs (c) or PbSe/CdSetetrapods (f) resulting from attempted high-temperature SILAR shell growth.

found through the course of these studies that temperature, ligand choice, and even solvent choice can strongly influence the outcome of the SILAR process, both in terms of particle structure and quality of the photoluminescence. Importantly, the first shell-growth step using cation exchange was found necessary in order to avoid ripening during high-temperature SILAR growth. Direct SILAR shell growth onto bare PbSe cores resulted in uncontrolled particle coalescence. In contrast, by starting with a PbSe/thin-CdSe QD, we recently succeeded in growing a secondary thick CdSe shell onto PbSe QDs by SILAR. The key growth parameter in this case was the selection of the chalcogen precursor – phosphine-containing or phosphine-free. When trioctylphosphine-selenide (TOP-Se) was used, tetrapods were formed; whereas, when elemental Se was dissolved in octadecene and used as the precursor, shell growth was achieved. The figure shows the structural progress from PbSe core to PbSe/thin-CdSe core/shell to PbSe/thick-CdSe core/shell QDs compared to the distinctly non-shell growth obtained in the case of the phosphine containing reaction. In addition to the morphological variation, we observed by *powder x-ray diffraction* that the core/shell structures were characterized by a cubic crystal structure (a combination of rock salt PbSe and zinc blende CdSe), while the tetrapods were dominated by wurtziteCdSe arms. Thus, the presence of phosphines stabilized wurtziteCdSe and, thereby, prevented overgrowth of a cubic CdSe shell onto the cubic PbSe/thin-CdSe QDs. The novel thick-shell PbSe/CdSe QDs prepared thus far emit at 1300 nm. While this is too "red" for energy transfer to silicon, we can adapt the 2-step shell growth approach to either smaller PbSe starting cores or to PbS QDs, which afford easier access to sub-micron photoluminescence. To this end, we have already synthesized PbS/CdS thin-shell QDs that emit at ~900 nm, and will soon proceed to thick-shell growth.

d) Hybrid light sensors based on CdSe nanocrystals on ultrathin Si nanomembranes

In order study energy transfer effects via electrical characterization approach,we have prepared back-gated Si-nanomembrane (SiNM)field effect transistor (FET) devices functionalized with SAM and deposited thin layers of CdSe/ZnS nanocrystals by drop-coating. We observe a large photocurrent increase of several hundred nAs in NQD/SAM/SiNM compared to ~nAs levels in reference SAM/SiNM structures without NQDs. The observed photocurrent has a clear excitation-wavelength dependence that follows the NQD absorption profile, thus confirming its NQD-related origin. We observe that the presence of unintentional trenches at the border of the doped/undoped regions of the SiNM during the substrate preparation plays a crucial role in the photocurrent amplification. We propose two possible mechanisms to explain the observed large photocurrent increase: i) change in the electrostatic potential of the channel surface and ii) forward biasing of the junction by the minority carriers that leads to the current gain and amplification facilitated by the trench geometry. The observed photocurrent gain values

approach 0.1 A/W at the peak wavelength, comparable to the performance of the commercial bulk Si photodetectors despite the ultrathin Si nanomembrane thickness. These proof-of-concept results are very encouraging for the further development of the sensitive and versatile photodetectors by incorporating easily processable semiconductor NQDs with wide spectral response to the existing commercial Si technology. [3]

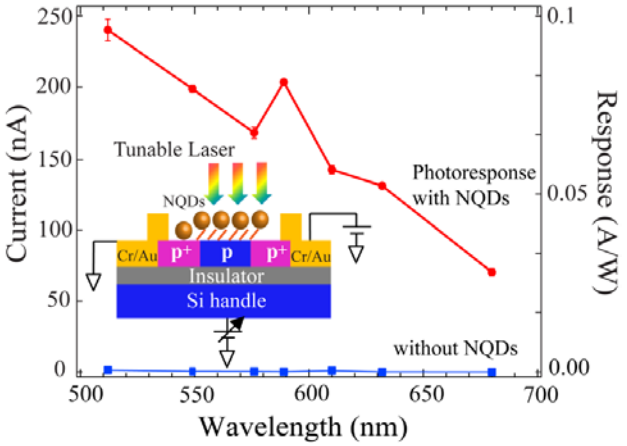

Fig. 4 Photocurrent response of the Si nanomembranes sensitized with CdSeNQDs.Inset: schematics of the FET structure.

Future Plans

In the next year of this project, we will continue to develop methods to assembly defect-free, dense, size-gradient NQD solids for ET applications. We will be using grafting and self-assembly methods to create optically thick, 100's of nm NQD solids on Si substrates. We will also continue to create textured, 3-dimensional Si substrates by creating Si nanopillar (nanowire) structures to enhance optical absorption and NQD packing density. Continuing collaboration with LANL, we will further develop infrared active NQDs (Pb and In based compounds) and methods of their grafting on Si surfaces. We will perform optical studies of these IR dots in order to record and explore multiexciton signatures. Based on the success of the synthesis, we are planning to study multiexciton transfer to Si. In electrical measurements, we will create doped, *p-i-n* junctions in 3D Si geometries and study NQD-induced photocurrent and photovoltaic performance. We will also attempt to explore other optically active materials to augment optical absorption and solar conversion performance, for example using perovskite materials that could be possibly used in conjunction with Si-based structures.

Published and accepted Journal Publications of DOE sponsored research in 2014-2015

[1] De Benedetti, W. J. I., Nimmo, M. T., Rupich, S. M., Caillard, L. M., Gartstein, Y. N., Chabal, Y. J. and Malko, A. V. (2014), "Efficient Directed Energy Transfer through Size-Gradient Nanocrystal Layers into Silicon Substrates" ***Advanced Functional Materials***, **24**, 5002–5010**,** (2014)

[2]B. D. Mangum, S. Sampat, Y. Ghosh, J. A. Hollingsworth, H. Htoon,andA. V. Malko, "*Influence of the Core Size on Biexciton Quantum Yield of Giant CdSe/CdS Nanocrystals*", ***Nanoscale,* 6 (7),** 3712 – 3720 (2014)

[3] W. Peng, S. Sampat, S. M. Rupich, B. Anand, H. M. Nguyen, D. Taylor, B. E. Beardon, Y. N. Gartstein, Y. J. Chabal and A. V. Malko, "*Hybrid light sensor based on ultrathin Si nanomembranes sensitized with CdSe/ZnS colloidal nanocrystal quantum dots*", ***Nanoscale***(2015), in press

[4] N. S. Karan, A. M. Keller, S. Sampat, O. Roslyak, A. Arefin,C. J. Hanson,J. L. Casson,A. Desireddy, A. Piryatinski, R. Iyer,H. Htoon, A. Malko and J. A. Hollingsworth, "*Plasmonic Giant Quantum Dots: Hybrid Semiconductor-Metal Nanostructures for Truly Simultaneous Optical Imaging, Photothermal Effect and Thermometry*", ***Chemical Science*** (2015), in press

Program Title: Light guiding, trapping and spectral shaping for maximizing solar energy conversion

Principle Investigators: Drs. Shawn-Yu Lin[1] and Sajeev John[2] , (1) Rensselaer Polytechnic Institute, Troy, NY 12180; (2) University of Toronto, Toronto, Canada

Program Scope: The key challenges for sunlight collection and conversion are to: (i) maximize solar trapping and absorption over a broad-θ and –λ range; (ii) minimize solar reflection over a broad-θ and –λ range; (iii) improve collection of photo-current; and lastly (iv) use less or, an ultra thin slab of, semiconductor material. Under this program, we proposed to explore a new optical effect, called "***parallel-to-interface refraction***", to be realized in a 3D simple-cubic photonic crystal (PhC). This class of 3D PhC can refract sun-ray into a plane parallel to a photovoltaic cell's surface over a broad wavelength and angle range. Another new trend in solar collection is to bend light by 90-degrees using advanced photonic structures. Under this program, we propose to use a holographic recorded film to diffract light by 90-degrees. Our goal is to realize a large-scale hologram that is capable of diffracting a wide spectrum of sunlight by 90-degrees. In doing so, sunlight may be better managed by the well-established planar optics to allow for a relatively easier guiding, concentration and conversion.

Recent Progress:

In this talk, I will describe two recent advances in 3D optical photonic-crystals (PhC). The ***first*** is the observation of anomalous light-refraction in a simple-cubic 3D PhC for visible light-trapping, guiding and near-unity absorption. This light trapping scheme is universal and can also lead to an efficient white light generation using an ultra-thin phosphors layer. The ***second*** is the observation of non-Planckian thermal radiation from a metallic 3D PhC composite that exhibits striking directionality, spectral selectivity and quasi-coherence. A summary of our experimental observation is illustrated in ***Figure 1***. A photo is also shown in ***Fig. 2*** to demonstrate efficient light-bending and concentration.

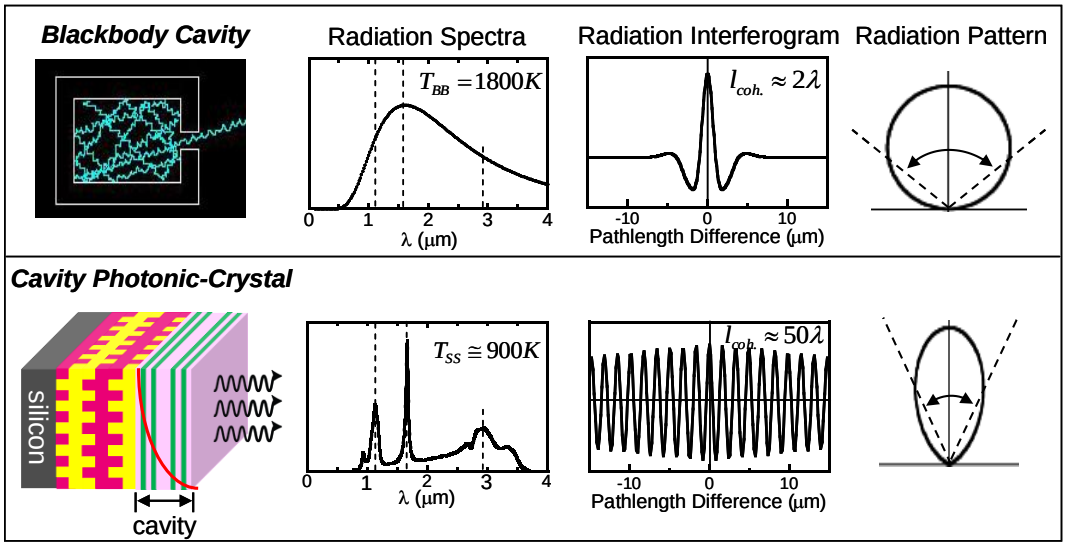

Fig.1: ***Emission Characteristic of a thermally excited metallic/ plasmonic 3D PhC. (top)*** a schematic of a blackbody-cavity and its radiation characteristics that include spectrum, temporal coherence and radiation pattern; ***(bottom)*** a schematic of our cavity-3D PhC composite structure and its corresponding, unconventional radiation characteristics.

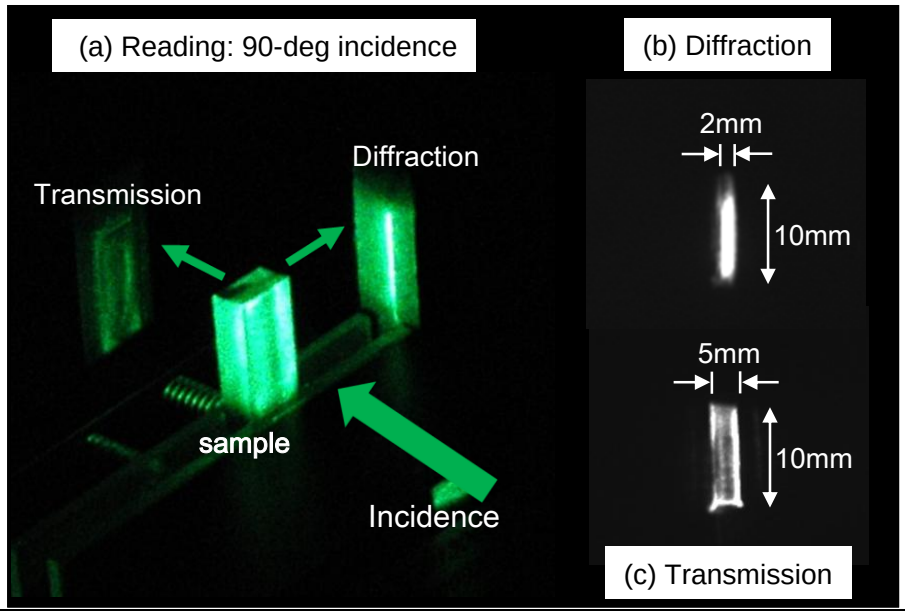

Fig.2: ***Lens-less light bending and area concentration by volume hologram. (a)*** *A photo of light-bending by 90-degrees due to a build-in holographic grating. While the transmitted beam is nearly invisible, the 90-degree diffracted beam is bright and well concentrated.* ***(b)*** *and* ***(c)*** *are CCD images of the transmitted and diffracted light, respectively. The diffracted beam exhibits 2.5-times narrower beam-width and is brighter than the incident beam.*

Future Plans:

The future research plan will be:
(i) ***Anomalous refraction for order-of-magnitude enhancement of optical-path-length.***
We will further our 3D simple-cubic PhC realization into a structure that is amenable to integration to a p-i-n type devices. This may be done by implementing a new open-structure design of a simple-cubic structure, namely "modulated nano-wire PhC". A preliminary structure design has been performed by Professor John and we, at RPI, is currently performing initial process characterization and sample fabrication.

(ii) ***Efficient 90-degree light-bending by volume hologram:***
With our recent success of demonstrating efficient 90-degree light bending by volume hologram at a wavelength of 633nm, we plan to extend our work to a broad spectral range, covering the entire visible spectrum. We also plan to increase angular acceptance of our hologram film to 45-60-degress using a "cylindrical recording scheme". Another important effort is to increase concentration factor from 2.5 times to 5-10 times. Finally, we plan to integrated our light-bending hologram film with a high efficiency PV cell, placed on the side output of the hologram film.

(iii) ***Spectral Shaping: non-Planckian thermal radiation from a 3D photonic-crystal.***
With the observation of discrete emission peaks and strong emission intensity, this work could open up many interesting energy applications. We plan to address the fundamental optical physics issues as well as its energy application possibilities. We plan to study

efficiency of energy concentration/conversion into these selective frequencies; we plan to implement a more reliable way to measure sample's surface temperature; we plan to fine-tune our cavity design to probe its role in radiation enhancement; we plan to work on theoretical understanding of our thermal/ plasmonic system and to provide evidence if "thermally stimulated-emission" plays a significant role in our metallic PhC system.

(iv) ***Photonic architectures for high-Temperature Bose-Einstein Condensation (BEC)***: A new trend in 3D active PhC is to enable simultaneously very strong exciton-photon coupling and long polariton lifetime. We plan to leverage our expertise in 3D PhC and explore such new physical phenomenon by working with Prof. John. Recent calculation by Prof. John theoretically illustrated such a possibility using a simple TiO2 based PhC sandwiching a planar quantum-well slab containing as few as three monolayers of MoSe2. This architecture provides a realistic route toward equilibrium polariton BEC above room temperature.

A list DOE sponsored publications:

1. B. Frey, P. Kuang, J.-H. Jiang, Sajeev John and Shawn-Yu Lin, "Large-scale fabrication of a simple-cubic photonic crystal for light trapping applications", ***J. of Vacuum Science and Technologies***, accepted for publication (March 2015).
2. ML Hsieh, H Y Chen, C.T. Peng and Shawn-Yu Lin, "Lens-less bending and concentration of light by volume hologram", submitted ***Optics Letters*** (Jan. 2015).
3. Abdullah Al-Rashid and Sajeev John "Optical Bio-sensing of Multiple Disease Markers in a Photonic Band Gap Lab-on-a-Chip: A Conceptual Paradigm,", ***Phys. Rev. Applied 3***, 034001 (2015).
4. ML Hsieh, H Y Chen and Shawn-Yu Lin," Observation of a large diffraction efficiency and efficiency enhancement of PQ/PMMA materials", ***Optics Communication*** **308,** p. 121-124 (Nov. 2014).
5. Alexei Deinega and Sajeev John, "Near perfect solar absorption in ultra-thin-film GaAs photonic crystals", Sergey Eyderman, , ***Journal of Materials Chemistry A***, DOI: 10.1039/c3ta13655h (2014).
6. Stephen Foster and Sajeev John, "Light trapping design for low band-gap polymer solar cells," ***Optics Express, Vol. 22***, Issue S2, pp. A465-A480 (2014).
7. Jian-Hua Jiang and Sajeev John, "Photonic Crystal Architecture for Room-Temperature Equilibrium Bose-Einstein Condensation of Exciton Polaritons,", ***Physical Review X 4***, 031025 (2014).
8. Jian-Hua Jiang & Sajeev John, "Photonic Architectures for Equilibrium High-Temperature Bose-Einstein Condensation in Dichalcogenide Monolayers,", ***Nature Magazine Scientific Reports 4***, 7432 (2014).
9. Ping Kuang, Alexei Deinega, ML Hsieh, Sajeev John and Shawn-Yu Lin, "Light trapping and near-unity absorption in a 3D optical photonic-crystal", ***Optics Letters 38***, 4200-2003 (Oct. 2013).
10. ML Hsieh, Ping Kuang, James A Bur, Sajeev John and Shawn-Yu Lin, "Review on Recent Progress of Three-dimensional Optical Photonic Crystal", ***American Institute of Physics Conference Proceeding***, ICN (accepted for publication, Sep. 2013).

11. Shawn-Yu Lin, Mei-Li Hsieh, J. Bur and R. Shenoi, "Observation of non-Planckian thermal radiation in a photonic crystal composite", submitted to ***Physical Review A***. (July 2014).
12. R. Shenoi, Shawn-Yu Lin, James Bur, D. Huang "Order-of-magnitude enhancement of infrared photo-response in a plasmonic-quantum dot system", ***Optics Letters 39***, 4454-4457 (Aug. 2014).
13. S. Eiderman, Sajeev John, A Deinega, "Solar light trapping in slanted conical pore photonic crystals: beyond statistical ray trapping" ***J. of Applied Physics***, **113**, 154315 (2013).
14. A. Deinega, Sajeev John, and S. Eiderman, "Coupled Electromagnetic and Electrical Modeling of Solar Cell based on Conical Pore Silicon Photonic Crystals" ***J. of Applied Physics*** 113, 224501 (2013); doi: 10.1063/1.4809982.
15. G. Alagappan, Sajeev John, E.P. Ling, "Macroscopic Response in Active Nonlinear Photonic Crystals", ***Optics Letters*** 38, No. 18, 3514 (2013)
16. Khai Q. Le and Sajeev John, "Synergistic plasmonic and photonic crystal light-trapping: Architectures for optical up-conversion in thin-film solar cells", ***Optics Express,*** Vol. 22, Issue S1, pp. A1-A12 (2014), DOI:10.1364/OE.22.0000A1

Session XIV

First-principles calculations of nonradiative recombination in nitride light emitters

Principal Investigator: Chris G. Van de Walle, University of California, Santa Barbara

Program Scope

Recent advances in the performance of solid-state light-emitting diodes (LEDs) and laser diodes (LDs) based on the III-nitride material system have resulted in commercial applications of these devices in high-efficiency general white lighting and display technologies. However, the widespread adoption and range of possible applications of nitride optoelectronics is still hindered by several nagging issues, including efficiency "droop" under high-current-density operating conditions, losses due to radiative and nonradiative recombination of carriers at defects, poor control of doping and transport in the *n*- and *p*-type layers, and the general exacerbation of these issues in green and UV (as opposed to blue) light emitters. Improved efficiency and performance of optoelectronic devices requires a comprehensive picture of carrier dynamics in the III-nitrides.

We address these issues using first-principles techniques based on density functional theory (DFT). Specifically, in the present phase of the project we focus on the effect of defects on the performance of light-emitting devices. Evaluation of such properties requires accurate band gaps and treatment of localized states; we therefore employ a hybrid functional in DFT [1], which has been demonstrated to provide accurate electronic and atomic structure of these materials, and allows quantitative comparison with experiment.

Recent Progress

A major goal of our project is to understand the microscopic origin of Shockley-Read-Hall (SRH) recombination centers in nitride light emitters. SRH recombination is proportional to the first power of the carrier density, and limits the peak efficiency in LEDs. Recombination consists of two nonradiative capture events: electron capture and hole capture; the latter is depicted schematically in Fig. 1. In the first phase of the project we have built on our experience with electron-phonon coupling in the context of the calculation of luminescence lineshapes [2] and developed a practical first-

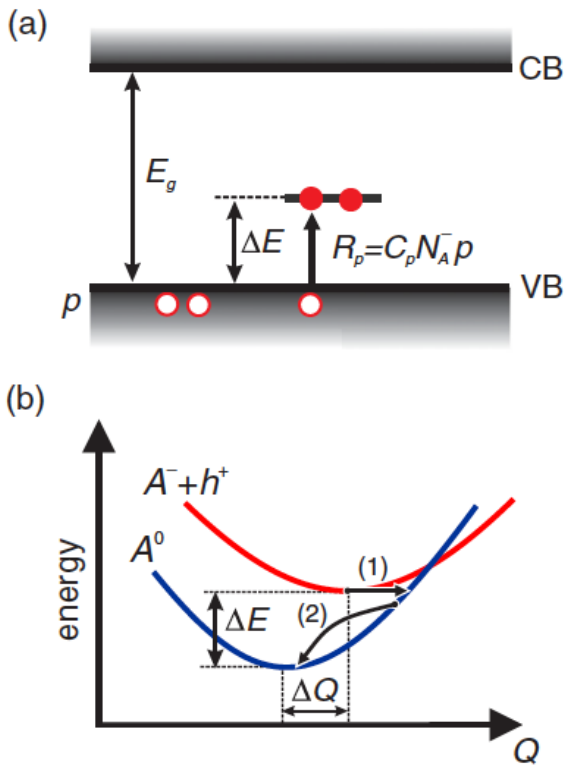

Figure 1: Nonradiative hole capture at a deep acceptor (with ionization energy ΔE) in two representations:
(a) band diagram and (b) configuration coordinate (energy vs. Q) diagram. Process (1) is the change of the electronic state due to electron-phonon coupling, process (2) is vibrational relaxation.

principles methodology to calculate carrier capture coefficients [P1]. As indicated in Fig. 1(b), this process involves a change in electronic states as a result of electron-phonon coupling, followed by a vibrational relaxation; the former process is the rate-limiting step, so we must calculate the electron-phonon matrix elements relevant to the transition. We have done this within a one-dimensional approximation, considering one special phonon mode that couples most strongly to the distortion between the electronic ground states. The accuracy of this approximation has been checked. The 1D configuration coordinate (CC) diagram of this special phonon mode for the example of a carbon impurity on a nitrogen site (C_N) in GaN is shown in Fig. 2. The CC diagram and all the ingredients for the theory, including vibrational frequencies and electron-phonon coupling constants, are determined consistently from hybrid functional calculations. In order to properly describe carrier capture processes at charged centers within the framework of supercell calculations, we also had to develop an approach to treat the effect of long-range Coulomb interactions on scattering states during a nonradiative capture process.

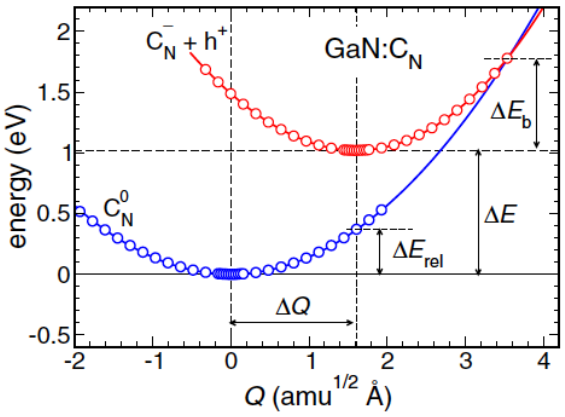

Figure 2: Calculated one-dimensional configuration coordinate diagram for hole capture at a C_N defect in GaN [process (1) in Fig. 1(b)]. ΔE_{rel} is the relaxation energy in the ground state and ΔE_b is the "classical" barrier for the nonradiative process.

The methodology has been applied to selected defects, including C_N in GaN and Li_{Zn} in ZnO, which were chosen as benchmark cases because reliable experimental results are available [3]. The agreement with experiment is excellent, as can be seen in Fig. 2 for C_N in GaN. The methodology is applicable to defects in other materials, and in addition provides insights in the physics of defects in wide-band-gap semiconductors, such as the impact of electron-phonon coupling and the role of different phonon modes.

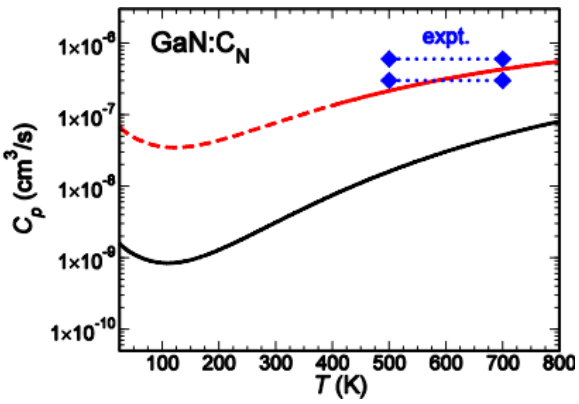

Figure 3: Black solid line: calculated nonradiative hole capture rate Cp at the C_N defect in GaN, as determined from our first-principles calculations. Red solid and dotted line: the same, but including the temperature effect on the band gap at high temperatures. Blue dotted horizontal lines and diamonds: experimental data from Ref. [3]; the latter were determined for several different samples in the temperature range 500–700 K.

In parallel to these studies of nonradiative recombination, we have also pursued our investigations of radiative recombination. The experimental study of radiative transitions provides a lot of useful information about defect geometries, vibrational properties, etc. However it is

often difficult to determine the chemical nature of defects responsible of a given experimental observation. Therefore, the ability to determine the luminescence properties of defects from first principles is a powerful tool for defect identification. Comparing with experiment for defects that *are* well characterized also serves as a further benchmark for the accuracy and reliability of our methodologies for treating electron-phonon interactions. Building on our development of a methodology to calculate luminescence lineshapes for defects with strong electron-phonon coupling [2], we have now developed an approach for studying defects with moderate coupling, a case in which luminescence lineshapes have more structure, and often many contributing phonon frequencies can be identified [P2]. As a test case, the methodology was applied to the nitrogen-vacancy (NV) center in diamond, a defect that serves as an excellent benchmark. Very good agreement was obtained, as evident in Fig. 4. This work also demonstrates the importance of using a hybrid functional for determining accurate vibronic properties of defects, as can be seen by comparing the blue line (hybrid functional [1]) and the red line (traditional DFT functional [4]) in Fig. 4.

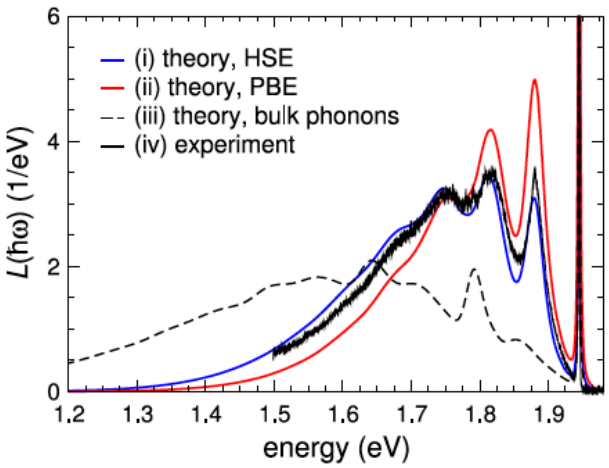

Figure 4: Measured (black solid line) and calculated (blue and red, and dashed lines) normalized luminescence lineshapes for NV centres in diamond in the energy range 1.5–2.0 eV. The blue line is calculated with a hybrid functional, the red line with a traditional DFT functional.

Future Plans

We will continue our study of the effect of defects on the properties of III-nitride devices. Using our methodology for calculating nonradiative capture coefficients [P1], we will survey a wide range of native defects and impurities to identify defects that may act as recombination centers for SRH in GaN and InGaN. Native defects to be studied include vacancies, antisites, and interstitials; impurities to be studied include Mg, Si, H, and O. Preliminary calculations also suggest that defect/impurity complexes may be important for this process.

We will also add to our defect identification tool kit by developing a methodology to determine rates of radiative capture at defects. The process involves the capture of a free carrier, with the energy being dissipated by a photon; this is often the mechanism for capture for very deep defects or at low temperatures, and the rate can be determined experimentally [3]. Such calculations provide an experimental signature without the need for a more involved calculation of the vibronic structure of the defect, as required for the lineshape. Preliminary calculations have benchmarked our technique on two well-characterized defects, C_N in GaN [3] and the V_{Ga}-Te_{As} complex in GaAs [5], demonstrating excellent agreement with experiment. We will now calculate capture coefficients for a variety of native defects and impurities.

Finally, we will turn our attention to another important limitation in III-nitride devices, the transport of holes. We will study activation and ionization of Mg acceptors in GaN, as well as interactions of holes with phonons and possible polaron formation in GaN and AlGaN.

References

[1] J. Heyd, G. E. Scuseria, and M. Ernzerhof, J. Chem. Phys. **118**, 8207 (2003); **124**, 219906 (2006).

[2] A. Alkauskas, J. Lyons, D. Steiauf, and C. Van de Walle, "First-Principles Calculations of Luminescence Spectrum Line Shapes for Defects in Semiconductors: The Example of GaN and ZnO," Phys. Rev. Lett. **109**, 267401 (2012).

[3] M. A. Reshchikov, "Carrier-capture characteristics of point defects in GaN and ZnO," in: Proceedings of the 27th International Conference on Defects in Semiconductors, ICDS-2013, **1583**, 127 (2014).

[4] J. P. Perdew, K. Burke, and M. Ernzerhof, "Generalized Gradient Approximation Made Simple," Phys. Rev. Lett. **77**, 3865 (1996).

[5] K. D. Glinchuk, A. V. Prokhorovich, V. E. Rodionov, and V. I. Vovnenko, "The scheme of electronic transitions via 0.94, 1.0, 1.2, and 1.3 eV radiative centres in n-GaAs," Phys. Status Solidi **41**, 659 (1977).

Publications

[P1] A. Alkauskas, Q. Yan, and C. G. Van de Walle, "First-principles theory of nonradiative carrier capture via multiphonon emission," Phys. Rev. B **90**, 075202 (2014).

[P2] A. Alkauskas, B. B. Buckley, D. D. Awschalom, and C. G. Van de Walle, "First-principles theory of the luminescence lineshape for the triplet transition in diamond NV centres," New J. Phys. **16**, 073026 (2014).

[P3] P. M. McBride, Q. Yan, C. G. Van de Walle, "Effects of In profile on simulations of InGaN/GaN multi-quantum-well light-emitting diodes," Appl. Phys. Lett. **105**, 083507 (2014).

Magnetocaloric and Multifunctional Magnetic Materials

Shane Stadler (Louisiana State University) and Naushad Ali (Southern Illinois University)

Program Scope

The Mn-based, orthorhombic ternary compounds MnTX (with T = Ni, Co and X = Si, Ge) are a class of materials that exhibit a variety of magnetic structures. For instance, MnCoGeassumes a collinear ferromagnetic structure, MnNiGe a spiral antiferromagnetic structure, and a non-collinear helical antiferromagnetic structure is observed in MnCoSi. Most of these systems have a second-order magnetic transition near room temperature, and stoichiometric MnNiGe and MnCoGe undergo a martensitic transition in the paramagnetic state. Some of the compounds (e.g., MnNiGe and MnCoGe) undergo a magnetostructural transition between two magnetic states, and exhibit large conventional and inverse magnetocaloric effects near room temperature as a result of the coincidence of magnetic and martensitic transitions.[1-3]Our aim is to develop newMnTX (T = Ni, Co, Cu and X = Si, Ge) systems, study the underlying physics of their phase transitions and magnetocaloric effects, and understand how their propertiesdepend onhydrostatic pressure, chemical composition, and stoichiometry.

Recent Progress

The Effects of Hydrostatic Pressure on the Phase Transitions and Magnetocaloric Properties of MnNiSi – Based Systems[4]

Recently there has been much interest inMnTX –based (T = Co, Ni, and X =Ge, Si) intermetallic compounds due to the temperature-induced magnetostructural transitions that are responsible for their shape-memory phenomena, giant magnetocaloric effects, and volume anomalies near room temperature. However, instead of a coupled magnetostructural transition (MST), the parent MnTX compounds exhibit second-order magnetic transitions at temperatures below the structural transitions, and undergo structural transitions from a low-temperature orthorhombic TiNiSi-type structure to a high-temperature hexagonal Ni_2In-type structure in the paramagnetic state. Considerable attention has been given to the MnCoGe-based system and its magnetocaloric effects (MCEs) due to the closely spaced magnetic ($T_C \sim 355$ K) and structural transitions ($T_M \sim 372$ K), and the potential to couple them through a single substitution, with the hope that the resulting MST will exhibit a large MCE at room temperature.

The MnNiSi system, however, is quite different than the abovementioned compounds in that it exhibits a structural transition at an extremely high temperature of about 1200 K, and T_C = 662 K. Therefore, reducing the structural transition at T_M so drastically in order to locate the MST near room temperature is a challenging task for which a single-element substitution is not sufficient. In the present study, it was found that isostructurally alloying MnNiSi with MnFeGe (which has a stable hexagonal structure with $T_C \sim 159$ K) stabilizes the hexagonal Ni_2In-type phase by sharply reducing the structural transition temperature from 1200 to less than 300 K. As

a result, coupled magnetostructural transitions have been realized in $(MnNiSi)_{1-x}$ $(MnFeGe)_x$ near room temperature.

Polycrystalline $(MnNiSi)_{1-x}(MnFeGe)_x$ (x = 0.52 and 0.54) samples were prepared by arc-melting the constituent elements of purity better than 99.9% in an ultrahigh purity argon atmosphere. The samples were annealed under high vacuum for 3 days at 750 °C, followed by quenching in cold water. Temperature-dependent X-ray diffraction (XRD) measurements were conducted on a Bruker D8 Advance diffractometer using a $CuK_{\alpha 1}$ radiation source (λ = 1.54060 Å) equipped with a LYNXEYEXE detector.

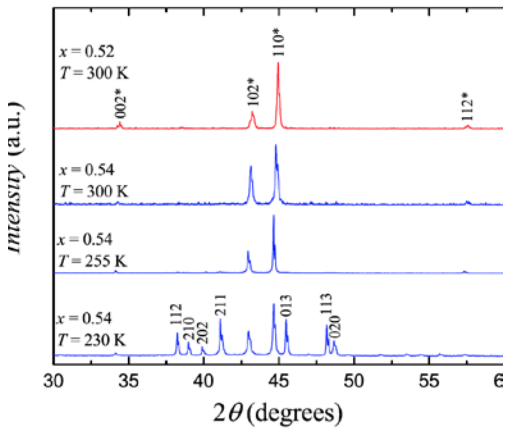

FIG. 1. Temperature-dependent XRD patterns for $(MnNiSi)_{1-x}(MnFeGe)_x$ with x = 0.54 and room-temperature XRD for x = 0.52. The Miller indices of the hexagonal and orthorhombic phases are designated with and without an asterisk (*), respectively.

The room-temperature x-ray diffraction (XRD) patterns of $(MnNiSi)_{1-x}(MnFeGe)_x$with x = 0.52 and 0.54 are shown in Fig. 1. A hexagonal Ni_2In-type crystal structure was detected at room temperature for both compositions. Structural refinement of the XRD data was carried out using the Rietveld profile refinement method, and the lattice parameters at roomtemperature were found to be a = 4.082 Å (4.092 Å) and$c$ = 5.294 Å(5.305 Å) for x = 0.52 (0.54), respectively.Therefore, the c/a ratio for x = 0.54 is slightly smaller thanthat for x = 0.52. In the orthorhombic crystal structure, thereduction of the lattice parametera_{ortho}distorts the geometry of the crystal structure in orthorhombic MnNiSi and, as aresult, the hexagonal structure is stabilized. Since the abovementioned orthorhombic lattice parameter is relatedto the hexagonal lattice parameter (a_{ortho}=c_{hex}), it is expectedthat a decrease in thec/a ratio tends to stabilize the hexagonalstructure. Furthermore,temperature-dependent XRD measurements have beenperformed to estimate the relative volume change associatedwith the structural transition for x = 0.54 (see Fig. 1). A large volume change of about 3.3% in the unit cell volume occursdue to the structural transition from the high-temperaturehexagonal phase to the low-temperature orthorhombic phase.

The temperature-dependent magnetization (M) data at ambient pressure for $(MnNiSi)_{1-x}$ $(MnFeGe)_x$ (x = 0.52, 0.54), as well as under the application of hydrostatic pressure for x = 0.54, measured during heating and cooling in the presence of a 1 kOe magnetic field, are shown in Fig. 2. A sharp change in magnetization was observed in the vicinity of the phase transition, indicating a magnetic transition from a lowtemperature ferromagnetic (FM) state to a high-temperature paramagnetic (PM) state. The observed thermal hysteresis between heating and cooling curves indicates that themagnetic and structural transitions coincide, leading to a single firstorder MST (at T_M) from a FM to a PM state. Increasing the level of substitution of hexagonal MnFeGe shifts $T_M$to lower temperature while maintaining the coupled nature of the MST. This coupling is maintained only in a narrow range of concentrations (0.50< x <0.56).

The application of hydrostatic pressure (P) also stabilizes the hexagonal phase at lower temperature, at a rate of $dT_M/dP = -4.5$K/kbar for the sample with x = 0.54 (see Fig. 2). This shift is likely associated with a distortion of the orthorhombic lattice that increases the stability of the hexagonal phase. The low temperature M(B) curves measured at T = 10 K show a shape typical for FM-type ordering. The value of the magnetization for 5T (M_{5T}) slightly decreases with increasing x. However, the pressure-induced change in $M_{5T}$is almost negligible, suggesting a minor variation of the FM exchange in the low-temperature orthorhombic phase that may be attributed to a slight modification of the electronic density of states at the Fermi level.

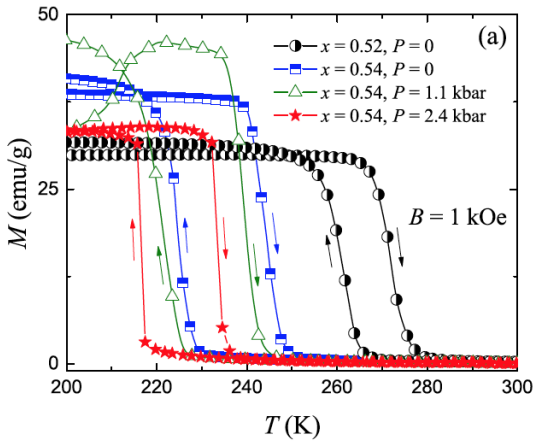

FIG. 2. Temperature dependence of the magnetization (M) in the presence of a 1 kOe magnetic field during heating and cooling for $(MnNiSi)_{1-x}(MnFeGe)_x$ as measured at ambient pressure for both compositions, and at different applied hydrostatic pressures (P) for x = 0.54. Arrows indicate the direction of change of temperature along the M(T) curves.

The maximum field-induced entropy change ($-\Delta S$) has been estimated using both the Maxwell relation and the Clausius-Clapeyron equation. The temperature dependence of ΔS, estimated using the integrated Maxwell relation $-\Delta S = \int(\partial M/\partial T)_B dB$, for a magnetic field change ΔB=1–5T, is plotted in Fig. 3for the compositions x = 0. 52 and 0.54, and was calculated from the isothermal magnetization curves.Alarge value of $-\Delta S$ has been observed at ambient pressure and is associated with the first-order MST.

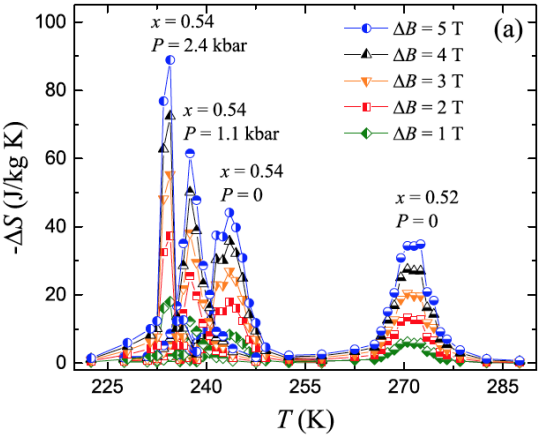

FIG. 3. Plot of the total isothermal entropy changes ($-\Delta S$) as a function of temperature for different magnetic field changes of ΔB = 1–5 T. The values were calculated using the Maxwell relation at ambient pressure for both compositions (x = 0.52 and 0.54), as well as under conditions of different applied hydrostatic pressures (P) for x = 0.54.

The most remarkable observation is that the application of relatively low hydrostatic pressure (~ 2.4 kbar) leads to a significant enhancement of $-\Delta S$, from ~44 J/kgK (ambient pressure) to 89 J/kgK (P = 2. 4 kbar), for a field change of 5 T (for x = 0. 54). It is also important to note the shift of $T_M$to lower temperature by -4.5 K/kbar with applied pressure, since it suggests a destabilization of the low-temperature phase, and also reveals a method by which the transition can be tuned in temperature.

The observed degree of enhancement of $-\Delta S$ with pressureis rare. Themaximum magnitude reaches a value of 89 J/kgKwith the application of P = 2.4 kbar for ΔB = 5T, whichexceeds that observed in other well-known giantmagnetocaloric materials. In this case, the

combined effect ofpressure and magnetic field could facilitate an improvementin the magnetocaloric working efficiency of the material.As the hydrostatic pressure increases, T_M decreases, and themaximum value of −ΔSincreases in a nearly linear fashionup to 2.4 kbar. A careful examination of the pressure-induced−ΔS(T) curves of Fig. 3 indicates that their shapeschange with increasing pressure.However, the area beneath the curves, which is a measure of the refrigeration capacity, remains constant.

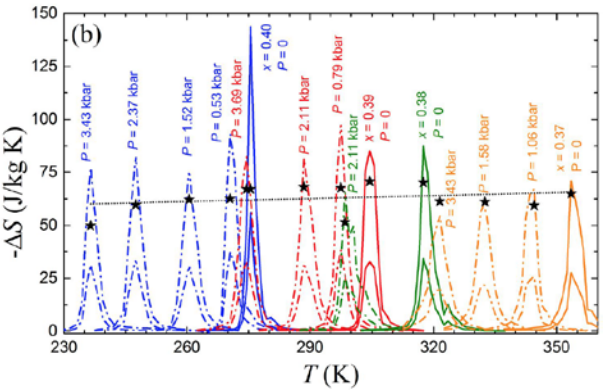

FIG. 4. The isothermal entropy changes (–Δ*S*) for $(MnNiSi)_{1-x}(CoFeGe)_x$ as a function of temperature were estimated using a Maxwell relation for magnetic field changes of Δ*B*= 5 T (upper curves) and 2 T (lower curves), measured at ambient pressure (solid lines) and at different applied hydrostatic pressures (broken lines). The "star" symbols inside each –Δ*S*(*T*) curve represents the corresponding total entropy change estimated by employing the Clausius-Clapeyron equation for Δ*B*= 5

A similar compound was studied following the same substitution scheme: $(MnNiSi)_{1-x}(CoFeGe)_x$. It shows even larger values of −ΔS (>140 J/kgK) and similar pressure dependence (see Fig. 4), but spans room temperature.Considering the higher degree of applicability (and reliability) of the Clausius-Clapeyron equation in the vicinity of discontinuous, first-order MSTs, the maximum value of −ΔS was also calculated using this method and shown in Fig. 4. The two methods are in reasonable agreement.

Together, the two compounds span temperatures from above the boiling point of water to below its freezing point.The large values of ΔS, and the pressure enhancements and shifts, make this an important class of materials to explore in the context of future magnetocaloric and, possibly, barocaloric technologies.

Future Plans

Due to the acute pressure sensitivity and large volume anomalies in these systems, we plan to investigate their barocaloric properties. Next, we will look for ways to reduce the thermal hysteresis (~10 K) by studying the effects of vacancies, trace doping (e.g., boron), and variation of synthesis parameters. Ideas for new compounds within this class will be explored.

References

[1] T. Samanta, et al., J. Magn. Mag. Mat. **330**, 88 (2013).
[2] T. Samanta, et al.,J. Appl. Phys. Lett.**100**, 052404 (2012).
[3] E. Liu, W. Wang, L. Feng, W. Zhu, G. Li, J. Chen, H. Zhang, G. Wu, C. Jiang, H. Xu, F. de Boer, Nature Commun. **3**, 873 (2012).
[4]T. Samanta, D. L. Lepkowski, A. Us Saleheen, A. Shankar, J. Prestigiacomo, I. Dubenko, A. Quetz, I. W. H. Oswald, G. T. McCandless, J. Y. Chan, P. W. Adams, D. P. Young, N. Ali, and S. Stadler, Phys. Rev. B**91**, 020401(R) (2015). DOI: 10.1103/PhysRevB.91.020401

Publications

[1] *Hydrostatic pressure-induced modifications of structural transitions lead to large enhancements of magnetocaloric effects in MnNiSi-based systems*, Tapas Samanta, Daniel L. Lepkowski, Ahmad Us Saleheen, Alok Shankar, Joseph Prestigiacomo, Igor Dubenko, AbdielQuetz, Iain W. H. Oswald, Gregory T. McCandless, Julia Y. Chan, Philip W. Adams, David P. Young, Naushad Ali, and Shane Stadler, Phys. Rev. B**91**, 020401(R) (2015). DOI: 10.1103/PhysRevB.91.020401

[2] *Asymmetric switching-like behavior in the magnetoresistance at low fields in bulk metamagneticHeusler alloys,* Tapas Samanta, Ahmad Us Saleheen, Daniel L. Lepkowski, Alok Shankar, Igor Dubenko, AbdielQuetz, Mahmud Khan, Naushad Ali, Shane Stadler. Phys. Rev. B **90**, 064412 (2014).

[3] *$Mn_{1-x}Fe_xCoGe$: A strongly correlated metal in the proximity of a noncollinear ferromagnetic state,* T. Samanta, I. Dubenko, A. Quetz, J. Prestigiacomo, P. W. Adams, S. Stadler, and N. Ali, Appl. Phys. Lett. **103**, 042408 (2013). [doi: 10.1063/1.4816381]

[4] *Enhancement of ferromagnetism by Cr doping in Ni-Mn-Cr-SbHeusler alloys, Mahmud Khan,* Igor Dubenko, Shane Stadler, J. Jung, S. S. Stoyko, Arthur Mar, AbdielQuetz, Tapas Samanta, Naushad Ali, and K. H. Chow, Appl. Phys. Lett. **102**, 112402 (2013). [doi: 10.1063/1.4795627

[5] *Evidence of martensitic phase transitions in magnetic Ni-Mn-In thin films,* A. Sokolov, LE Zhang, I. Dubenko, T. Samanta, S. Stadler, and N. Ali,Appl. Phys. Lett. **102**, 072407 (2013). [doi:10.1063/1.4793421]

[6] *Multifunctional properties related to magnetostructural transitions in ternary and quaternary Heusler alloys*, Igor Dubenko, AbdielQuetz, SudipPandey, Anil Aryal, Michael Eubank, Igor Rodionov, ValeriiPrudnikov, Alexander Granovsky, ErkkiLahderanta, Tapas Samanta, Ahmad Saleheen, Shane Stadler, Naushad Ali, J. of Mag. Mag. Mat., In Press, Corrected Proof, Available online 22 October 2014.

[7] *Asymmetric magnetoresistance in bulk In-based off-stoichiometric Heusler alloys*, Igor Dubenko, Tapas Samanta, AbdielQuetz, Ahmad Saleheen,,Valerii N. Prudnikov, Alexander B. Granovsky, Shane Stadler, and Naushad Ali, (accepted for publication in Physica Status Solidi (b) (2014)).

[8] *Phase Diagram and Magnetocaloric Effects in $Ni_{50}Mn_{35}(In_{1-x}Cr_x)_{15}$ and $(Mn_{1-x}Cr_x)NiGe_{1.05}$ alloys,* A. Quetz, B. Muchharla, T. Samanta, I. Dubenko, S.Talapatra, S. Stadler, and N. Ali, J. Appl. Phys. **115** 17A922 (2014). [http://dx.doi.org/10.1063/1.4866082]

[9] *Large magnetocaloric effects over a wide temperature range in $MnCo_{1-x}Zn_xGe$*, T. Samanta, I. Dubenko, A. Quetz, S. Stadler, and N. Ali, J. Appl. Phys. **113**, 17A922 (2013). [doi: 10.1063/1.4798339]

[10] *Thermoelectric Properties of Intermetallic Semiconducting $RuIn_3$ and Metallic $IrIn_3$,* N. Haldolaarachchige, W. A. Phelan, Y. M. Xiong, R. Jin, J. Y. Chan, S. Stadler, and D. P. Young, J. Appl. Phys. **113** (8), 083709 (2013). [DOI: 10.1063/1.4793493]

[11] *Magnetocaloric and magnetic properties of $Ni_2Mn_{1-x}Cu_xGa$ Heusler alloys: An insight from the direct measurements and ab initio and Monte Carlo calculations,* V. Sokolovskiy, V. Buchelnikov, K. Skokov, O. Gutfleisch, D. Karpenkov, Yu. Koshkid'ko, H. Miki, I. Dubenko, N. Ali, S. Stadler, andV. Khovaylo J. Appl. Phys. **114**, 183913 (2013). [doi: 10.1063/1.4826366]

[12] *Magnetic properties and phase transitions of gadolinium-infused carbon nanotubes*, AbdielQuetz, Igor Dubenko, Tapas Samanta, Herbert Vinson, SaikatTalapatra, Naushad Ali, and Shane Stadler, J. Appl. Phys. **113**, 17B512 (2013) [doi: 10.1063/1.4796151]

[13] *Phase diagram and magnetocaloric effects in aluminum doped MnNiGe alloys,*AbdielQuetz, Tapas Samanta, Igor Dubenko, Michael J. Kangas, Julia Y. Chan, Shane Stadler, and Naushad Ali, J. Appl. Phys. **114**, 153909 (2013). [doi: 10.1063/1.4826260]

[14] *Large magnetocaloric effects due to the coincidence of martensitic transformation with magnetic changes below the second-order magnetic phase transition in $Mn_{1-x}Fe_xCoGe$,* Tapas Samanta, Igor Dubenko, AbdielQuetz, Shane Stadler, and Naushad Ali, J. Magn. Magn. Mater. **330**, 88 (2013). [dx.doi.org/10.1016/j.jmmm.2012.10.040]

[15] *Phase Diagram and Magnetocaloric Effects in Ni1-xCrxMnGe1.05,* Anil Aryal, AbdielQuetz, SudipPandey, Michael Eubank, Tapas Samanta, Igor Dubenko, Shane Stadler, and Naushad Ali. (Accepted for publication in Journal of Applied Physics (2015))

[16] *Multifunctional properties related to magnetostructural transitions in ternary and quaternary Heusler alloys,*I. Dubenko, A. Quetz, S. Pandey, A. Aryal, M. Eubank, I. Rodionov, V. Prudnikov, A. Granovsky, A. Lahderanta, T. Samanta, A. Saleheen, S. Stadler, and N. Ali,*J. Mag. Mag. Mat*., In Press, Available online Journal of Magnetism and Magnetic Materials (2014), http://dx.doi.org/10.1016/j. jmmm.2014.10.

[17] *Influence of Copper substitution on the Magnetic and Magetocaloric Properties of NiMnInB Alloys,* SudipPandey, Anil Aryal, AbdielQuetz, Michael Eubank, Tapas Samanta, Igor Dubenko, Shane Stadler, and Naushad Ali. (Accepted for publication in Journal of Applied Physics (2015))

[18] *Magnetocaloric effect in $Ni_{50}Mn_{35}In_{15}$ in low and strong magnetic fields,*I.D. Rodionov, Yu.S.Koshkidko, A.Quetz, S.Pandey, A. Aryal, I. S. Dubenko, S. Stadler, N. Ali, J. Cwik, I. Titov, M. Blinov, M.V. Prudnikov, V.N. Prudnikova, E. Lähderanta, A.B. Granovskii.(Accepted for publication in JETP Letters (2015))

[19]*Effects of hydrostatic pressure on magnetostructural transitions and magnetocaloric properties in $(MnNiSi)_{1-x}(FeCoGe)_x$,*Tapas Samanta, Daniel L. Lepkowski, Ahmad Us Saleheen, Alok Shankar, Joseph Prestigiacomo, Igor Dubenko, AbdielQuetz, Iain W. H. Oswald, Gregory T.

McCandless, Julia Y. Chan, Philip W. Adams, David P. Young, Naushad Ali, and Shane Stadler. (Under Review/Resubmitted, Journal of Applied Physics (2015))

[20] *A New Class of Magnetic Refrigeration Materials:* $(MnNiSi)_{1-x}(FeCoGe)_x$ and $(MnNiSi)_{1-x}(MnFeGe)_x$, T. Samanta, S. Stadler, and N. Ali, Patent Application Number 62/062,0901, filed 18 July (2014).

Poster Sessions

Physical Behavior of Materials Principal Investigators' Meeting

POSTER SESSION I

Monday, March 30, 2015

1) **Sub-wavelength Metamaterial Design, Physics and Applications**
   Xiang Zhang, Lawrence Berkeley National Laboratory

2) **Quantum Nanoplasmonic Theory**
   Mark Stockman, Georgia State University

3) **Metamaterials**
   Costas M. Soukoulis, Thomas Koschny, Jigang Wang, Ames Laboratory

4) **Metamaterials as a Platform for the Development of Novel Materials for Energy Applications**
   Willie Padilla, Duke University

5) **Light-Matter Interaction Phenomena using Subwavelength Engineering of Material Properties**
   Igal Brener, Sandia National Labs & Center for Integrated Nanotechnologies

6) **Nanophotonics-Enhanced Solar Cells**
   Shanhui Fan, Stanford University

7) **Coherent Control of Spin-States in Organic Electronics**
   Christoph Boehme, University of Utah

8) **Probing Coherent States of Light and Matter in Two-Dimensional Semiconductors**
   Nathaniel Stern, Northwestern University

9) **Measurement of Near-Field Thermal Radiation Between Flat Surfaces with a Nanogap**
   Zhuomin Zhang, Georgia Tech Research Corp.

10) **Magnetization Dynamics and Cooperative Phenomena in Charge and Spin Frustrated Correlated Electron Materials**
    Hariharan Srikanth, University of South Florida

11) **Understanding the Spin-Lattice Coupling in Multiferroic Oxides**
    Trevor A. Tyson, New Jersey Institute of Technology

12) **Raman Spectroscopic Study of Coupling Between Magnetic and Ferroelectric Orders in Nanoscaled Thin Films Superlattices**
    Xiaoxing Xi, Temple University

13) **Extraordinary Responsive Magnetic Rare Earth Materials**
Vitalij Pecharsky, Ames Laboratory

14) **Structure-Optical-Thermal Relationships of Carbon Nanotubes**
Steve Cronin, University of Southern California

15) **Electrochemically-Driven Phase Transitions in Battery Storage Compounds**
Yet-Ming Chiang, Massachusetts Institute of Technology

16) **Towards Quantitative Understanding of Strain Induced Nanoscale Self-Assembly from Atomic-Scale Surface Energetics and Kinetics**
Feng Liu, University of Utah

17) **Atomistic and Mesoscopic Study of Metallic Glasses**
Takeshi Egami, Oak Ridge National Laboratory

18) **Designing Nanoparticle/Nanowire Composites and Nanotree Arrays as Electrodes for Efficient Dye-Sensitized Solar Cells**
Yiying Wu, Ohio State University Research

19) **Nanocrystal-Based Dyads for Solar to Electric Energy Conversion**
David Waldeck, University of Pittsburgh

20) **Diblock Copolymer Templated Two-Phase Inorganic Nano-Composites A Platform for Innovative Nano-Science**
Manfred Wuttig, University of Maryland

21) **Crystallization and Thermoelectric Transport in Silicon Microstructures and Nanostructures Under Extreme Electrical Stress**
Ali Gokirmak, University of Connecticut

22) **Superconducting Materials**
Qiang Li, Brookhaven National Laboratory

23) **High Performance Nano-Crystalline Oxide Fuel Cell Materials: Defects, Structures, Interfaces, Transport, and Electrochemistry**
Scott Barnett, Northwestern University

Physical Behavior of Materials Principal Investigators' Meeting

POSTER SESSION II

Tuesday, March 31, 2015

1) **Complex Hydrides - A New Frontier for Future Energy Applications**
   Vitalij Pecharsky, Ames Laboratory

2) **Thermodynamic and Kinetic Studies of High Temperature Proton Conductors (HTPC) Using Thin Films and Porous Bodies**
   Anil Virkar, University of Utah

3) **Proximity Effects in Conducting Oxide Heterostructures**
   Jeffrey Eastman, Argonne National Laboratory

4) **Dipolar Ferromagnets for Magnetocaloric Effect Nanocomposites**
   Sara Majetich, Carnegie Mellon University

5) **Functional Domain Walls as Active Elements for Energy Technology**
   Junqiao Wu, University of California, Berkeley

6) **Charge Transfer Across the Boundary of Photon-Harvesting Nanocrystals**
   Frank Wise, Cornell University

7) **Hybrid Inorganic Nitride Organic Semiconductor Heterostructures**
   Arto Nurmikko, Brown University

8) **Optical and Electrical Properties of III-Nitrides and Related Materials**
   Hongxing Jiang, Texas Tech University

9) **Evaluating the Oxidative, Photothermal and Electrical Stability of Colloidal Nanocrystal Solids**
   Matthew Law, University of California, Irvine

10) **Investigation of p-type Sb-doped ZnO Thin Films for Solid State Lighting**
    Jian Liu, University of California, Riverside

11) **Magnetic and Optical Properties of Ferromagnetic ZnO Nanoclusters**
    Matthew McCluskey, Washington State University

12) **Enhancement of the UV Luminescence and Defect Issues in ZnO Films**
    Leah Bergman, University of Idaho

13) **Exploring the Impact of the Local Environment on Charge Transfer States at Molecular Donor-Acceptor Heterojunctions**
Noel Giebink, Pennsylvania State University

14) **Exploring the Impact of the Local Environment on Charge Transfer States at Molecular Donor-Acceptor Heterojunctions**
Barry Rand, Princeton University

15) **Electronic Materials Programs**
Daryl C. Chrzan, Lawrence Berkeley National Laboratory

16) **Electronic Materials Programs**
Joel Ager, Lawrence Berkeley National Laboratory

17) **Structure-Optical-Thermal Relationships of Carbon Nanotubes**
Li Shi, University of Texas

18) **Fundamental Studies of Unconventional Sulfide Semiconductors for Cost- Effective and Environmentally Benign Thin Film Photovoltaics**
Michael Scarpulla, University of Utah

19) **Spatially Resolved Ionic Diffusion and Electrochemical Reactions in Solids: A Biased View at Lithium Ion Batteries**
Nina Balke, Oak Ridge National Laboratory

20) **Interfaces in Electronic and Structural Materials**
Yuri Mishin, George Mason University

21) **Prediction of Thermal Transport Properties of Materials with Microstructural Complexity**
Youping Chen, University of Florida

22) **Bridging Atomistic and Continuum Scales in Phase-Field Modeling of Solid-Liquid Interface Dynamics and Coalescence**
Alain Karma, Northeastern University

23) **Mesoscale Design of Magnetoelectric Heterostructures and Nanocomposites**
Dwight Viehland, Virginia Polytechnic Institute and Technology

Poster Abstracts

Spatially resolved ionic diffusion and electrochemical reactions in solids - a biased view at lithium ion batteries (ERKCZ12)

Nina Balke (PI)
Oak Ridge National Laboratory
1 Bethel Valley Road
P.O. Box 2008, MS-6487
Oak Ridge, TN 37831-6487
Email: balken@ornl.gov

Program Scope

The functionality of energy storage systems, such as Li-ion batteries, is based on and ultimately limited by the rate and localization of ion flows through the device on different length scales ranging from atoms over grains to interfaces. The fundamental gap in understanding ionic transport processes on these length scales strongly hinders the improvement of current and development of future battery technologies. The goal of this proposal is to create, through nanometer-resolution imaging of ionic flows, fundamental understanding of the local mechanisms which define a rechargeable battery. Using Electrochemical Strain Microscopy, which utilizes the intrinsic link between unit cell volume and Li-ion concentration, it is possible to separate and characterize transport processes in the electrodes and across electrode/electrolyte interfaces, allowing us to decipher the single stages of ionic transport through the battery. With this knowledge it will be possible to identify and overcome the bottlenecks which lead to predominant limitations in present battery technology such as low energy storage density or capacity loss during cycling.

Recent Progress

We developed Electrochemical Strain Microscopy (ESM) to detect ionic transport with nanometer resolution using strain generated through ion concentration change to explore structure-functionality relationships in Li-ion battery cathodes and anodes. Due to the nature of this experiment, not only Vegard-type volume changes, but also other electrochemical processes happening in the probed volume can contribute to the measured ESM signal, e.g. the formation of chemical dipoles. Therefore, it is crucial to discuss and explore all phenomena happening under the biased scanning probe microscopy (SPM) tip. We identified these processes and, based on their dependences on sample and experimental parameters, developed experimental techniques to differentiate between them. This is not only crucial for ESM but for any other type of SPM technique where local electrical biases are applied, e.g. ferroelectric materials. This effort led to the development of new characterization techniques which allow studying new phenomena previously unavailable to SPM research and knowledge of nanoscale functionality.

1. Electrochemical phenomena under a biased SPM tip

There is a range of physical and electrochemical phenomena which can be induced by a locally applied bias which are listed in Fig. 1 and which can result in contributions to the measured ESM signal.[1] On the right side are physical processes which do not necessarily involve ionic motion such as ferroelectricity and high currents which can result in Joule heating and thermal expansion of the sample. Electrochemical phenomena, including the formation of chemical dipoles, the change in surface potential due to charge injection from the tip or charge attraction/repulsion in the sample, and the volume expansion based on Vegard, are shown in the middle section of Fig. 1. Depending on the maximum bias applied, these processes are often reversible. Electrochemical processes which are mostly irreversible are listed on the right side of Fig. 1 and include deposition, vacancy ordering, and sample damage. Depending on sample and tip properties and the experimental conditions, different processes dominate the ESM signal or can be neglected. The goal is to identify how strong the single contributions are to pave the road to a more quantitative ESM signal interpretation.

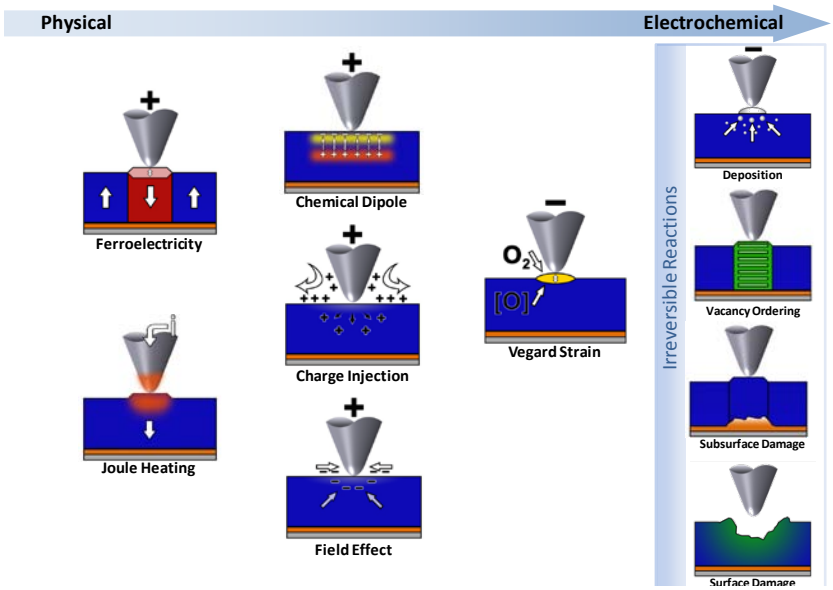

Figure 1: Summary of relevant physical and electrochemical processes happening under a biased SPM tip which can contribute to the measured ESM signal.[1]

2. Hidden information in electrostatic forces

SPM-type characterization techniques using biased probes are subject to electrostatic forces between the tip and sample. In the past, these forces have been ignored but they contain crucial information about mechanical and electrical properties of the sample and are highly sensitive to surface potentials. In order to test the strength of electrostatic interactions between the tip and the sample and to establish the contribution of surface potentials V_{SP} during ESM measurements, open-loop contact Kelvin Probe Force Microscopy (cKPFM) was developed. This technique allows the verification of the presence of electrostatic forces and the change of surface potential as function of bias applied to the tip. To demonstrate the technique, HfO_2 thin films were chosen as model systems since it is a well known charge trapping material and is not considered being an ion-conductor. In addition, the role of tip and electrical sample properties and their influence

on the observed signals were investigated. After the characteristic ESM loops from the presence of surface charges are established, extended ESM measurements and cKPFM experiments are repeated on two different $LiCoO_2$ films. The first film was uncharged after one electrochemical cycle and the second was charged, which means half of the Li is extracted from the cathode.

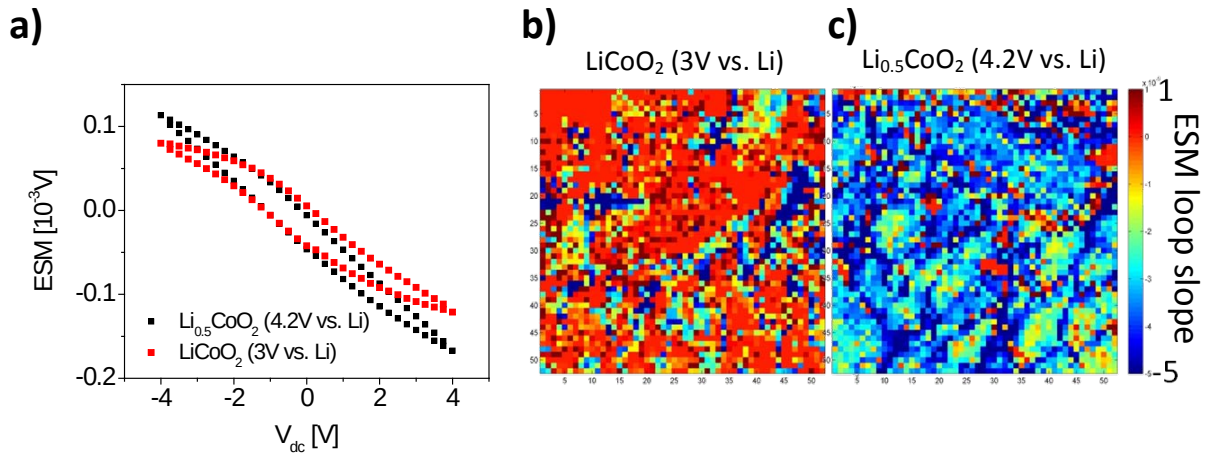

Figure 2: (a) Average ESM on-field loops over 50x50 measured points on charged und uncharged $LiCoO_2$. Map of ESM lope slope for an uncharged (b) and charged (c) $LiCoO_2$ thin film.

Figure 2a displays the averaged measured ESM curves. The hysteresis can be attributed to charge injection from the tip. Analysis of the slope of the remaining signal coming from electrostatic forces between tip and sample resolves strong differences in samples with different Li-content in magnitude and lateral variation (Fig. 2b, 2c). The negative slope increases and grain boundaries appear if half of the Li is electrochemically removed from $LiCoO_2$. This suggests that the ESM slope is related to the removal of Li-ions and that the removal of Li-ions does not happen homogeneously across the sample. The exact ion extraction mechanism and the correlation with macroscopic measurements and ionic mobility are ongoing.

3. Bias-induced Li-ion motion in solid electrolytes

When ESM is performed on solid electrolytes, it was found that the biased SPM tip can locally extract Li-ions from the electrolyte and forming Li-metal on the sample surface. The kinetics and reversibility of this phenomenon were studied. We were able to show that the bias needed to deposit Li metal on the sample surface is directly connected with the electrochemical potential by working with different bottom electrodes. This is an important step towards quantitative electrochemical measurements with the SPM tip. However, it was found that the process does not show a high degree of reversibility. Therefore, micron-scale Au current collectors were deposited and the in-situ formation of Li underneath the Au electrode was studied. The Li electrodes were shown to be highly cyclable (100% coulombic efficiency) after an initial

irreversible Li-plating in the first few cycles. This is a first step towards the production of highly scalable, secondary nano-battery arrays after capacity fading can be overcome.

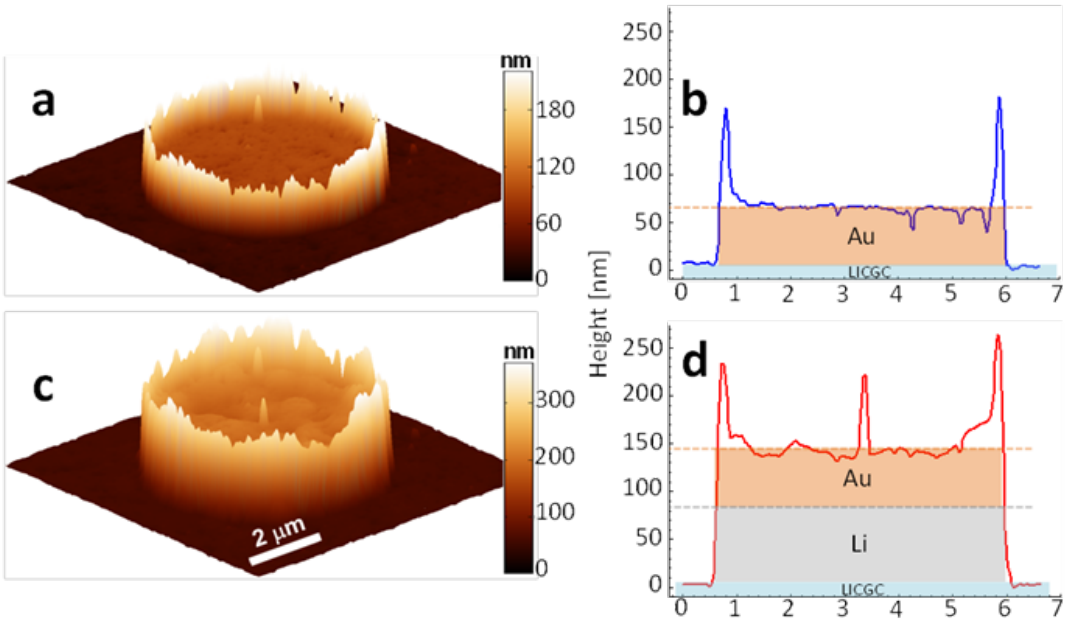

Figure 3. (a) Tapping mode AFM topography of an Au electrode on LICGC prior to potentiostatic cycling, (b) height profile of the same electrode in (a) sliced through the center of the electrode, (c) tapping mode AFM topography of the same Au electrode in (a) following 1000 cyclic voltammogram cycles (-5 V ≤ E ≤ 5 V vs. Cu), and (d) height profile for the same electrode shown in (c) sliced at exactly the same region as in (a).

Future Plans

In order to get closer to quantification of ionic transport through ESM measurements, several signal generating mechanism need to be considered. The difficulty is that some of the describing parameters have a unknown dependence on V_{dc} and multiple phenomena show the same characteristics. The key is to perform measurements on model systems showing only one dominant signal generating mechanism so their characteristics can be studied and compared to samples with unknown signal origin. This will be supported by collaborations with theoretical modeling to understand better contact mechanics of the SPM tip during the measurement. In addition, ESM is being extended to investigate other relevant cathode materials and additional electrochemical reactions.

References

[1] S.V. Kalinin, S. Jesse, A. Tselev, A. P. Baddorf, and N. Balke, ACS Nano 5, 5683 (2011).

Publications

1. L. Collins, S. Jesse, N. Balke, B. Rodriguez, S. Kalinin, and Q. Li, "Band Excitation Kelvin probe force microscopy utilizing photothermal excitation", *accepted to* **Appl. Phys. Letters** (2015).

2. Q. Li, S. Jesse, A. Tselev, L. Collins, P. Yu, I. Kravchenko, S.V. Kalinin and N. Balke, "Probing Local Bias-Induced Transitions Using Photothermal Excitation Contact Resonance Atomic Force Microscopy and Voltage Spectroscopy", **ACS Nano**, dx.doi.org/10.1021/nn506753u (2015).

3. N. Balke, S. Jesse, Q. Li, P. Maksymovych, M.B. Okatan, E. Strelcov, A. Tselev, and S.V. Kalinin, "Current and surface charge modified hysteresis loops in ferroelectric thin films", *accepted to* **J. Appl. Phys.** (2014).

4. N. Balke, P. Maksymovych, S. Jesse, I.I. Kravchenko, Q. Li, and S.V. Kalinin, "Exploring Local Electrostatic Effects with Scanning Probe Microscopy: Implications for Piezoresponse Force Microscopy and Triboelectricity", **ACS Nano** 8, 10229-10236 (2014).

5. E.A. Eliseev, A.N. Morozovska, A.V. Ievlev, N. Balke, P. Maksymovych, A. Tselev, and S.V. Kalinin, "Electrostrictive and electrostatic responses in contact mode voltage modulated scanning probe microscopies", **Appl. Phys. Lett**. 104, 232901 (2014).

6. L. Collins, S. Jesse, J.I. Kilpatrick, A. Tselev, O. Varenyk, M.B. Okatan, S.A.L. Weber, A. Kumar, N. Balke, S.V. Kalinin, and B.J. Rodriguez, "Probing charge screening dynamics and electrochemical processes at the solid–liquid interface with electrochemical force microscopy", **Nat. Commun.** 5, 3871 (2014).

7. T.M. Arruda, J.S. Lawton, A. Kumar, R.R. Unocic, I.I. Kravchenko, T.A. Zawodzinski, S. Jesse, S.V. Kalinin, and N. Balke, "In Situ Formation of Micron-Scale Li-Metal Anodes with High Cyclability", **ECS Electrochem. Lett.** 3, A4-A7 (2014).

8. J.M. Black, D. Walters, A. Labuda, G. Feng, P.C. Hillesheim, S. Dai, P.T. Cummings, S.V. Kalinin, R. Proksch, and N. Balke, "Bias-dependent molecular-level structure of electrical double layer in ionic liquid on graphite", **Nano Lett.** 13, 5954-5960 (2013).

9. T.M. Arruda, A. Kumar, S. Jesse, G.M. Veith, A. Tselev, A.P. Baddorf, N. Balke, and S.V. Kalinin, "Toward Quantitative Electrochemical Measurements on the Nanoscale by Scanning Probe Microscopy: Environmental and Current Spreading Effects", **ACS Nano** 7, 8175-8182 (2013).

High Performance Nano-Crystalline Oxide Fuel Cell Materials: Defects, Structures, Interfaces, Transport, and Electrochemistry

S.A. Barnett, L.D. Marks, T.O. Mason, K. Poeppelmeier, P.W. Voorhees
Northwestern University

Program Scope

This project addresses fundamental materials challenges in solid oxide electrochemical cells, devices that have a broad range of important energy applications. Although nano-scale mixed ionically and electronically conducting (MIEC) materials provide an important opportunity to improve performance and reduce device operating temperature, durability issues threaten to limit their utility and have remained largely unexplored. Our recent work has focused on both (1) understanding the fundamental processes related to oxygen transport and surface-vapor reactions in nano-scale MIEC materials, and (2) determining and understanding the key factors that control their long-term stability. Furthermore, materials stability is increasingly being explored under the "extreme" conditions encountered in many solid oxide cell applications, *i.e*, very high or very low effective oxygen pressures, and high current density.

Recent Progress

We have obtained important new results in several areas, including:

(1) Morphological stability of nano-scale electrode materials and prediction of long-term performance based on accelerated testing. *We believe that these results will lead to a new paradigm in the search for improved MIEC materials – one that includes not only anion (oxygen) transport but also the cation transport factors that determine stability;*
(2) New processing methods such as atomic layer deposition have been developed and are being explored to produce to more stable nano-electrode microstructures;
(3) Determination of oxygen reduction mechanisms on MIEC nano-scale electrodes using electrochemical impedance spectroscopy;
(4) Determination of the critical electrolysis current densities (overpotentials) where oxygen electrode degradation begins, *significant for development of materials whose properties can be tuned to yield optimal performance and stability;*
(5) Observation that an overpotential/current actually reduces the degradation of (La,Sr)(Co,Fe)$O_{3-\delta}$ electrodes associated with Sr surface segregation;
(6) Development and characterization of fuel electrode materials with tunable ability to form the oxygen vacancies that facilitate transport;
(7) Characterization of new fuel electrode materials that combine both mixed conducting behavior and self-assembly of nano-scale catalysts to achieve much-improved performance;
(8) Development of Ruddlesden-Popper MIEC materials such $Pd_2NiO_{4+\delta}$ that transport oxygen via interstitials, characterization of phase stability, development of the high-performance electrodes, and demonstration of a new method for measuring their transport properties.

($Sr_{0.5}Sm_{0.5}$)$CoO_{3-\delta}$ (SSC) is one of the highest performance fast oxygen transport MIEC materials – in prior work, we studied these properties in detail, and also produced nano-scale SSC oxygen electrodes with polarization resistance R_P amongst the lowest ever reported at target operating temperatures (~600^{o}C). We have now also carried out detailed electrochemical impedance spectroscopy studies that help elucidate the correlation between processing, electrode structure, materials' transport properties, and performance. Here the results on materials stability are highlighted.

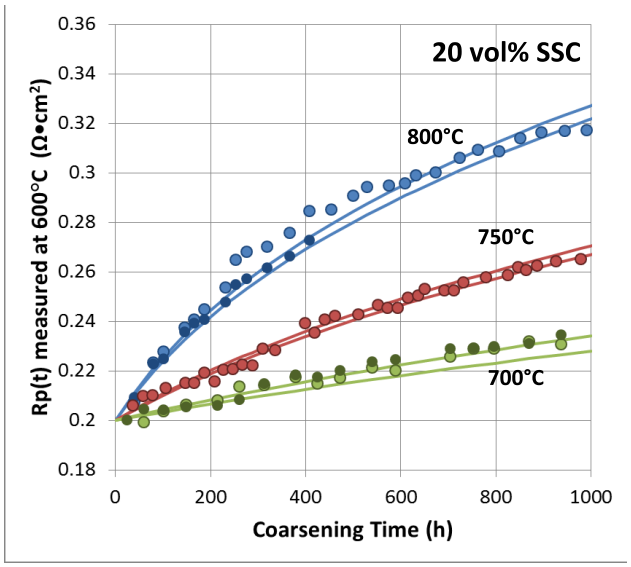

Figure 1. R_P measured at 600°C in air, versus time for $(Sm_{0.5}Sr_{0.5})Co_3$ nano-scale electrodes at various elevated temperature designed to accelerate degradation. Power-law coarsening fits are also shown.

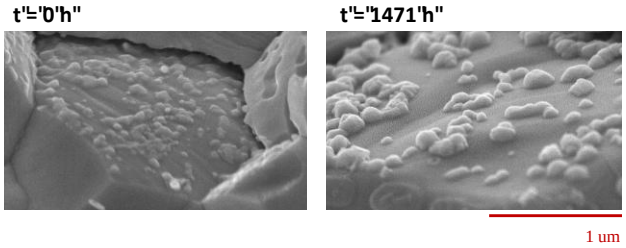

Figure 2. Scanning electron microscope images of nano-scale SSC on a Gd-doped Ceria (GDC) scaffold, before annealing and after 1471 h at 800°C.

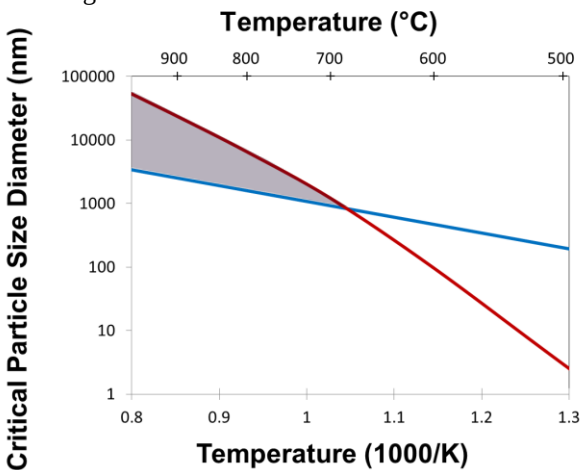

Figure 3. Critical particle size versus temperature. The blue line indicates the size above which the degradation rate over 40,000 h is < 0.2%/kh. The red line gives the size below which R_P is acceptable, < 0.2 Ω cm^2. The shaded indicates the particle size and temperature range where a stable low-R_P electrode is achieved.

The long-term stability of highly active nano-scale cathodes, such as SSC, has not previously been studied and remains a potential show-stopper (solid state ionic devices such as fuel cells that should operate at temperature for > 40,000 h). Figure 1 summarizes results from accelerated tests, showing more rapid R_P degradation with time at higher temperature. Figure 2 shows images indicating that a key change in the electrode after annealing is coarsening of SSC nano-particles. The results in Figure 1 were thus fitted using a model that accounts for power-law particle coarsening and its effect on R_P:

$$R_p = \left(Bexp(-E_D/kT_c)t + R_{p0}^n\right)^{1/n} \quad (1)$$

where t is time, $R_{P,0}$ is initial resistance, T_c is temperature, E_D is a diffusion activation energy, B includes a diffusion coefficient pre-factor and electrochemical terms, and n is the power law. After fitting the data with n = 4, corresponding to a surface diffusion process, eq. 1 is used to predict degradation rates for different particle sizes and temperatures. The results are summarized in Figure 3, which also shows the size below which R_P is suitably low. Unfortunately, the shaded region, indicating the particle size and temperature range where a stable low- R_P electrode is achieved, extends only down to ~ 700°C and ~ 1000 nm particle size! (Note, however, that a very stringent stability criterion was used here – relaxing this to 0.5%/kh, or 25% R_P increase over 40,000 h, extends this down to nearly 600°C and 100 nm.) There are two important implications of these results: (1) experimental work needs to focus on methods to improve stability, and (2) theoretical work, which to date has focused entirely on optimizing oxygen transport kinetics,[1,2] must also consider stability, *i.e.*, the cation diffusion processes that controls particle coarsening.

With these results in mind, initial experiments have been done to explore whether stability can be improved by altering the electrode morphologically. Initial experiments were carried out where a thin layer of a relatively stable material, ZrO_2, was deposited onto the SSC nano-particles using atomic layer deposition. The results in Figure 4 show that the coating yields an improvement in initial R_P as well as a reduced degradation rate, in basic agreement with an initial report on coated nano-electrodes.[3]

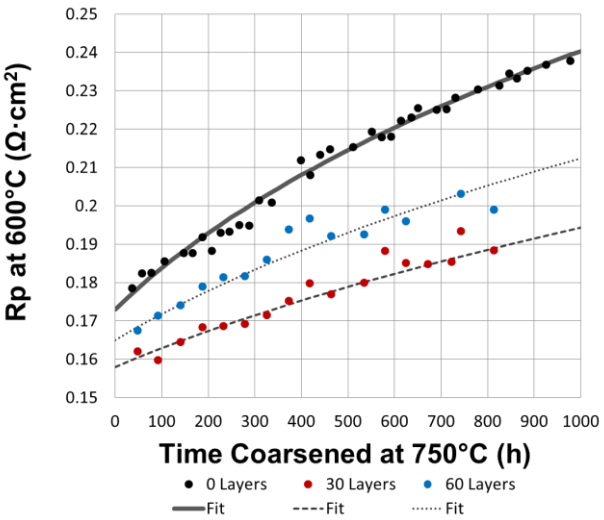

Figure 4. R_P versus time at 750°C for a conventional electrode and one coated with 5 nm (red) and 10 nm thick (blue) ZrO_2 layers by atomic layer deposition.

It is also important to understand the effects of cell operating conditions on stability – electrical potentials and currents yield high fields and large local swings in effective oxygen partial pressure, in many cases directly impacting materials stability and properties.[4,5] Figure 5 provides an example of LSCF electrodes where increasing the current density, and hence the electrode overpotential, increases degradation. The results suggest that degradation occurs when the overpotential exceeds ~ 300 mV, corresponding to any oxygen pressure > 1000 bar. Substantial changes in electrode microstructure are observed due to the high effective pressure.

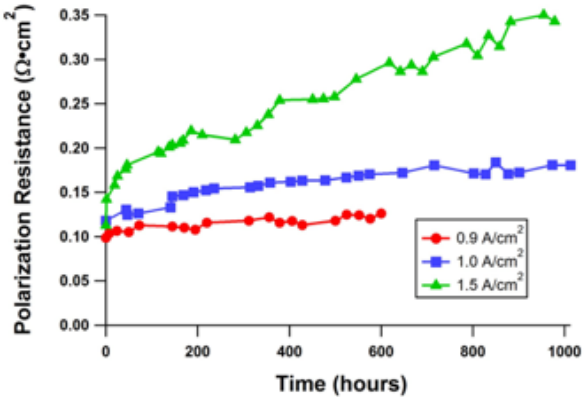

Figure 5. R_P versus time of an LSCF electrode during reversing-current life tests at current density values of 0.9, 1.0, and 1.5 A/cm^2.

Oxygen reduction kinetic parameters – oxygen ion diffusion D_δ and surface exchange coefficient k – were determined for porous $Nd_2NiO_{4+\delta}$ solid oxide cell electrodes as a function of temperature and oxygen partial pressure by analyzing electrochemical impedance spectroscopy data using the Adler-Lane-Steele model.[6] Three-dimensional electrode microstructural data were used in model. Figure 6 illustrates the measured transport coefficients obtained compared with prior measurements on bulk materials.

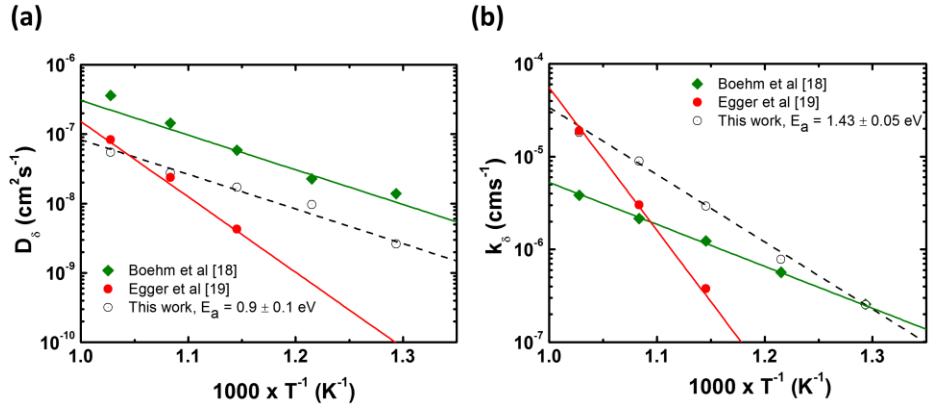

Figure 6. Comparison between D_δ (a) and k_δ (b) obtained in this work and those reported previously.

Figure 7 shows varying $La_{1-x}Sr_xCr_{1-x}Fe_xO_{3-\delta}$ (LSCrFe) fuel electrode compositions that were found to exhibit decreased R_P with increasing Fe and Sr content (x), which correlated with increase oxygen deficiency δ. For the conditions tested here – humidified hydrogen – LSCrFe with x = 0.4-0.7 yielded good performance and phase stability. However, in fuel cells and electrolysis cells the oxygen pressure may vary from ~ 10^{-14} to 10^{-30} bar – in this case, varying x in LSCrFe will provide a means to "tune" stability and properties (via oxygen deficiency) to best match a given operating condition.

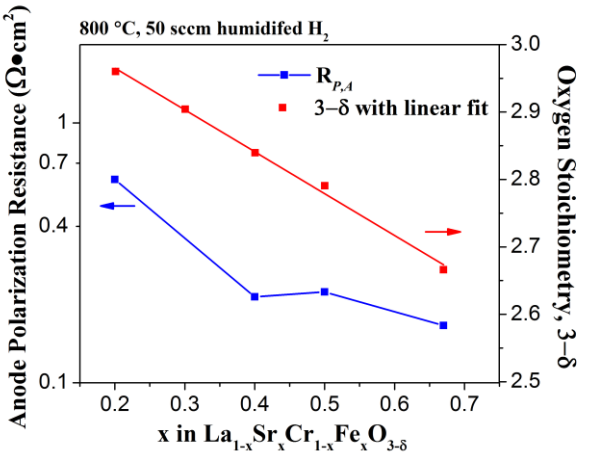

Figure 7. R_P and oxygen stoichiometry 3-δ versus composition x for $La_{1-x}Sr_xCr_{1-x}Fe_xO_{3-\delta}$ measured at 800°C in humidified H_2 fuel.

Future Plans

Future work will investigate the basic physical properties and transport kinetics of relevant materials under normal to extreme conditions, probed utilizing pressurization and/or applied electrochemical potentials. The thesis is that an improved understanding will allow "tuning" of properties for use in devices operating under various conditions. This will ultimately allow selection and development of materials and structures that can achieve the requisite performance and durability in different applications. A main emphasis will be on measurements, e.g., x-ray and neutron diffraction and impedance spectroscopy, done under cell operating conditions (*i.e.*, with applied current/potential) on materials in nano-scale electrodes.

References

1 Lee, Y.-L., Kleis, J., Rossmeisl, J., Shao-Horn, Y. & Morgan, D. Prediction of solid oxide fuel cell cathode activity with first-principles descriptors. *Energy & Environmental Science* **4**, 3966, doi:10.1039/c1ee02032c (2011).

2 Wang, L., Merkle, R., Mastrikov, Y. A., Kotomin, E. A. & Maier, J. Oxygen exchange kinetics on solid oxide fuel cell cathode materials—general trends and their mechanistic interpretation. *J. Materials Research* **27**, 2000-2008, doi:10.1557/jmr.2012.186 (2012).

3 Gong, Y. H., Palacio, D., Song, X. Y., Patel, R. L., Liang, X. H., Zhao, X., Goodenough, J. B. & Huang, K. Stabilizing Nanostructured Solid Oxide Fuel Cell Cathode with Atomic Layer Deposition. *Nano Letters* **13**, 4340-4345, doi:Doi 10.1021/Nl402138w (2013).

4 Chen, M., Liu, Y. L., Bentzen, J. J., Zhang, W., Sun, X., Hauch, A., Tao, Y., Bowen, J. R. & Hendriksen, P. V. Microstructural Degradation of Ni/YSZ Electrodes in Solid Oxide Electrolysis Cells under High Current. *Journal of the Electrochemical Society* **160**, F883-F891, doi:10.1149/2.098308jes (2013).

5 Knibbe, R., Traulsen, M. L., Hauch, A., Ebbesen, S. D. & Mogensen, M. Solid Oxide Electrolysis Cells: Degradation at High Current Densities. *Journal of The Electrochemical Society* **157**, B1209-B1217, doi:Doi 10.1149/1.3447752 (2010).

6 Lu, Y., Kreller, C. & Adler, S. B. Measurement and Modeling of the Impedance Characteristics of Porous La[sub 1−x]Sr[sub x]CoO[sub 3−δ] Electrodes. *Journal of The Electrochemical Society* **156**, B513, doi:10.1149/1.3079337 (2009).

Publications

1. Call, A. V. & Barnett, S. A. An Electrochemical Impedance Spectroscopy Study of (Sm,Sr)CoO_3 - Gd-Doped Ceria Electrodes, J. Electrochem. Soc. submitted (2015)
2. Gao, Z., Zenou, V. Y., Kennouche, D., Marks, L. D. & Barnett, S. A. Characteristics of Solid Oxide Cells with Zirconia/Ceria Bi-Layer Electrolytes Fabricated Utilizing Reduced-Temperature Firing. *Energy & Environmental Science* Submitted (2015).
3. Gao, Z., Mogni, L., Miller, E., Railsback, J. & Barnett, S. A. A Perspective On Intermediate-Temperature Solid Oxide Fuel Cells. submitted (2015).
4. Fowler, D., Messner, A., Slone, B., Poeppelmeier, K. & Barnett, S. A. Effect of Ru Substitution Into Mixed-Conducting (La,Sr)(Cr,Fe)O3 Solid Oxide Fuel Cell Anodes. Submitted, Chemistry of Materials.
5. Hughes, G. A., Railsback, J. G., Yakal-Kremski, K. J., Butts, D. M. & Barnett, S. A. Degradation of (La0.8Sr0.2)0.98MnO3-δ - Zr0.84Y0.16O2-γ Composite Electrodes During Reversing Current Operation. *Faraday Discussions* In press (2015).
6. Railsback, J.G., Gao, Z. & Barnett, S.A. Oxygen electrode characteristics of Pr2NiO4+δ-infiltrated porous (La0.9Sr0.1)(Ga0.8Mg0.2)O3. *Solid State Ionics* In press (2015).
7. Yakal-Kremski, K., Mogni, L. V., Montenegro-Hernández, A., Caneiro, A. & Barnett, S. A. Determination of Electrode Oxygen Transport Kinetics Using Electrochemical Impedance Spectroscopy Combined with Three-Dimensional Microstructure Measurement: Application to Nd2NiO4+δ. *J. Electrochem. Soc.* in press (2015).
8. Fowler, D. E., Haag, J., Boland, C., Bierschenk, D. M., Barnett, S. A. & Poeppelmeier, K. R. Stable, Low Polarization Resistance Solid Oxide Fuel Cell Anodes: La1-xSrxCr1-xFexO3-δ(x=0.2-0.67) *Chem Mater*, 140428025107009, doi:10.1021/cm500423n (2014).
9. Miller, E. C., Gao, Z. & Barnett, S. A. Fabrication of Solid Oxide Fuel Cells with a Thin (La0.9Sr0.1)0.98(Ga0.8Mg0.2)O3-δElectrolyte on a Sr0.8La0.2TiO3Support. *Fuel Cells* **13**, 1060-1067, doi:10.1002/fuce.201300155 (2013).
10. Cho, S., Fowler, D. E., Miller, E. C., Cronin, J. S., Poeppelmeier, K. R. & Barnett, S. A. Fe-substituted SrTiO3−δ–Ce0.9Gd0.1O2 composite anodes for solid oxide fuel cells. *Energy & Environmental Science*, doi:10.1039/c3ee23791e (2013).

DOE award # DESC0000909, University of Utah

Coherent control of spin states in organic electronic devices – Manipulation of electron-spin interactions for organic electronics and spintronics

PI: Christoph Boehme, co-PI: John M. Lupton
University of Utah, Department of Physics and Astronomy,
115S 1400E, Salt Lake City, Utah, 84112, boehme@physics.utah.edu

Program Scope or Definition

This research program builds on the experimental demonstration of electrically[1,2] and optically[3-5] detected coherent spin-motion in organic semiconductor materials which was accomplished in the course of the DOE supported project "Coherent control of spin states in organic electronic devices" (#DE-SC0000909) from 2009 to 2013. New, pulsed electrically and optically detected magnetic resonance techniques (pEDMR and pODMR, respectively)have proven to allow for the qualitative discrimination and individual quantitative determination of spin-exchange, spin-dipolar, hyperfine, and spin-orbit coupling involving spin states that influence optical and electrical materials properties. Based on these previous experimental breakthroughs, the research of this programfocuseson the systematic exploration of artificial pathways to the control of spin-coupling in organic semiconductors. The goal is to find ways to manipulate electrical and optical materials properties by adjustment of spin-coupling (type and magnitude) between electron spins as well as electron and nuclear spins. This work aims to achieve this by:

(i) **Control of spin interactions via materials structure and composition** which are explored by: (a) The investigation of novel organic and hybrid materials structures [3-5]; (b) The investigation of the morphological dependencies of spin-interactions, introduced by materials deposition techniques and parameters; (c) The investigation of isotopic dependencies of spin-interactions using isotopically modified organic semiconductors [6].

(ii) **Control of spin-exchange and spin-dipolar interactions [7] via electric fields**, which are explored through pEDMR experiments on organic field effect devices. The demonstration of an electric field control of exchange or dipolar coupling could lead to a fundamentally new class of spin-transistors whose characteristics are similar to existing (but still not technically feasible) inorganic spin transistor concepts, yet whose working principles depart radically from these existing approaches.

(iii) **Control of hyperfine coupled nuclear spin states via electric current**, utilizing Overhauser spin-transfer as well as electrically pumped polaron states with the goal of

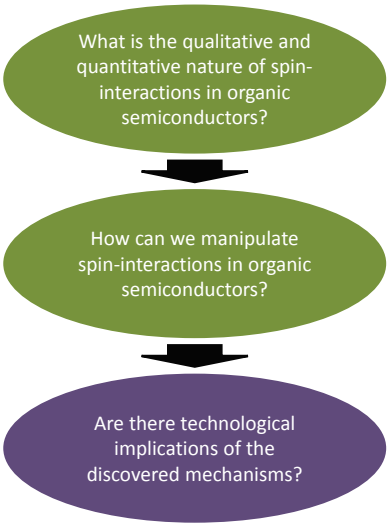

Fig. 1: The three main questions addressed: The two fundamental questions (green) are addressed first.The pursuit of applied device concepts (purple) will take place when microscopic processes with potentialrelevance for applications emerge from the investigations.

testing the suitability of hydrogen nuclei in organic semiconductors for nuclear quantum spin storage [6].

Methodologically, the different spin-spin coupling types are measured using pEDMR at magnetic fields and excitation frequencies covering 6 orders of magnitude (1MHz – 330GHz bands). This previously inaccessible frequency range isreached by utilization of the broadband low- to mid-frequency range pEDMR/pODMR facilities in the PI'slaboratoriesas well as in collaboration with the National High Magnetic Field Laboratory in Tallahassee, Florida.

Theresearch of this project aims to introduce a new parameter set (exchange, dipolar, spin-orbit, and hyperfine interactions) into organic semiconductor materials and device design. We aim to find new pathways for organic electronics and spin-electronics, including spin transistors, sensor concepts and organic microelectronic circuitry. In the long term, this fundamental research could also stimulate the development of initialorganic quantum information devices.

Recent Progress

In the course of the past year (2014) progress has been made on the experimental demonstration that the control of hyperfine coupling can directly affect recombination rates and thus the current in organic semiconductors [goal (iii)].

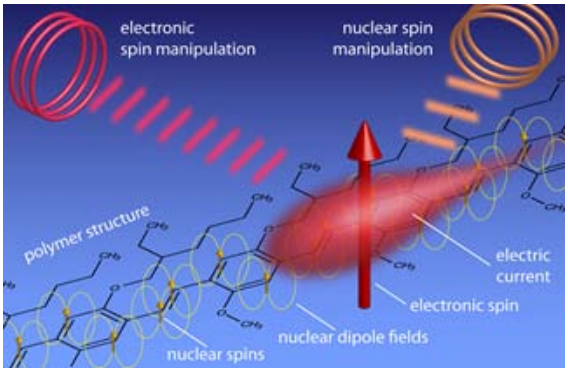

Figure 2: Illustration of the experiment that allows for the direct observation of nuclear-spin control of electric current in a polymer OLED. Charge carriers with an electron spin conduct electric current along polymer chains. The manipulation of the electron spin with microwaves leads to a change of the current. This change is further modulated when nuclear spins of the all-abundant hydrogen atoms are manipulated by application of radio-frequency radiation in an NMR experiment.

We have shown that a nuclear magnetic resonant (NMR) manipulation of proton spins can cause a change in conductivity. The technical challenge of such an experiment was to overcome the low polarization of proton ensembles at weakmagnetic fields and roomtemperature. We have achieved this in two ways, [6] as illustrated by the sketch in Fig. 2: First, by electrically measuring the effect of coherent nuclear spin motion on coherent electron spin motion through an electrically detected electron spin-echo envelope modulation (ESEEM) pulse scheme which projected Larmor oscillations of nuclear spins onto the electron-spin state of recombining charge carriers. Secondly, by employing an electrically detected electron-nuclear double (EDENDOR) resonance scheme which projected nuclear spin states after an NMR excitation onto the electric device current. Figure 3, taken from Ref. [6], displays some of the ESEEM data that was measured. It shows that under magnetic field conditions (~344mT) which fulfill magnetic resonance conditions for charge carriers, the current response of the OLED device shows an electron spin-echo decay which is modulated by the characteristic nuclear precession frequency (~14.5MHz). This apparent control of the room temperature device current was tested in two ways:

First, by repeating the experiments with the same polymer material (MEH-PPV) but substituted hydrogen isotopes where deuterium nuclei rather than protons where used on the 2-ethylhexyloxy side groups [6]. The results show qualitatively identical results – the Larmor precession of the nuclear spins modulates the charge carrier spin echo decay. However, in

contrast to polymers with hydrogenated side groups, the magnitude of the modulation frequency is only 2.3MHz as expected for the smaller deuterium magneton with only a very weak residual contribution remaining at 14.5MHz caused by the residual hydrogen of the polymer backbone. The second way to test nuclear spin control by electric currents was to directly observe current changes caused by application of nuclear magnetic resonance to the hydrogen spins of a polymer. Here, the problem of low nuclear spin polarization was overcome by application of highly selective off-resonant EDENDOR to the broad hyperfine resonance peaks of charge carriers in MEH-PPV. Due to the narrow excitation, the small subensemble of charge carrier pairs was selected for the measurement with distinct, very strong hyperfine fields, corresponding to exposure to a local nuclear spin ensemble with very high polarization. The NMR excitation was then performed on the selected subensemble and after the entire electron and nuclear spin-resonance pulse sequence, the device current transient was integrated in order to measure the charges ΔQ transmitted by the device due to the excitation. Due to the broad distribution of nuclear resonance frequencies (caused by the hyperfine-field distribution), any NMR

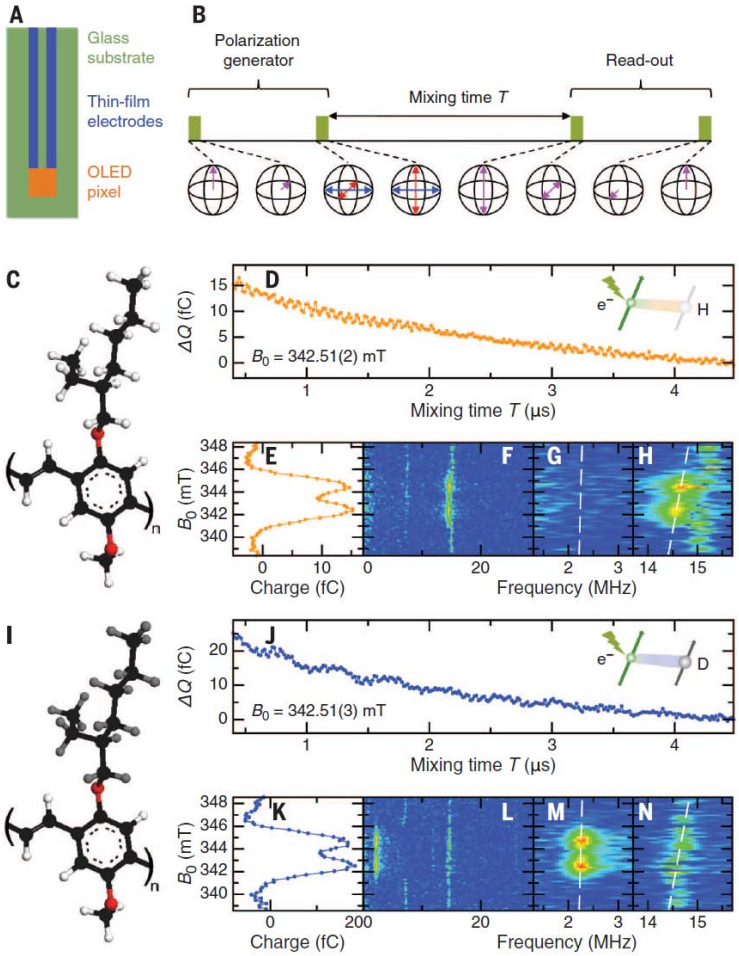

Figure 3: Isotopic fingerprinting of coherent electronic spin precession in the current of an OLED at room temperature, taken from Ref. [6]. (A) An ITO/PEDOT:PSS/MEH-PPV/Ca/Al OLED pixel was fabricated on an RF/microwave-compatible substrate with thin-film ITO and aluminum contact leads [ITO: indium tin oxide; PEDOT:PSS: poly(3,4-ethylenedioxythiophene):poly(styrene sulfonate)]. (B) Scheme for the electrical detection of ESEEM in a stimulated echo sequence. After electronic coherence is generated using a $\pi/2$-τ-$\pi/2$ ESR pulse sequence, electron and nuclear spins are allowed to mix for a time T before the read-out sequence $\pi/2$-τ-$\pi/2$ is applied. During T, the electron spins beat with the nuclear spins, imposing a periodic modulation on the spin-echo envelope, which is clearly seen. (C and I) Chemical structure of the hydrogenated and deuterated MEH-PPV polymers. Black, white, and gray spheres represent carbon, protium, and deuterium. (D and J) ESEEM signal as a function ofmixing time, T.The nuclear resonance signal is contained in the oscillations superimposed on the exponential decay of the current detected spin echo. The experiments were performed at a microwave frequency of 9.63 GHz. (E and K) B_0 dependence of the signal. (F and L) The ESEEM signal after background correction and Fourier transformation for different values of B_0 across the resonance. (G, H, M, and N) Magnified views around 2 and 15 MHz, the deuteron and proton matrix lines, respectively. The dashed lines indicate the anticipated frequencies of the proton and deuteron resonances.

excitation was also very selective. Thus, by essentially choosing a small subensemble of nuclear spins coupled to an already small subensemble of charge carrier pairs, the detected charges turned out to be very small (femtocoulomb range) requiring long measurement times (see Fig. 4). Nevertheless, clear proof of electrically detected NMR was given and comparison of the measured NMR line (which is affected by all hyperfine fields) with the ESEEM detected proton precession frequency (which is not affected by anisotropic hyperfine strength) allows for the determination of the strength and distribution of the different hyperfine couplings to charge carriers (isotropic and anisotropic) in the investigated material.

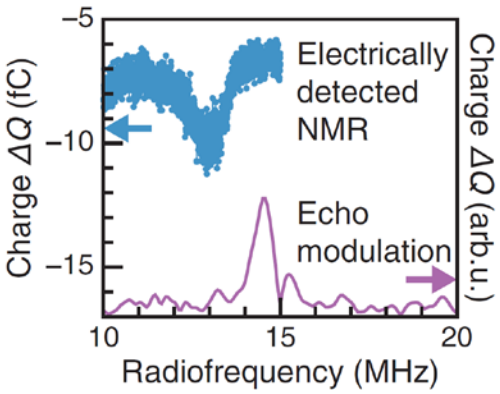

Figure 4: ENDOR spin-echo amplitude as a function of RF-frequency at B_0 = 344.1013 mT (blue) compared to the ESEEM spectrum from Fig. 2F (purple) shows direct control of OLED current by nuclear spin transitions. This figure has been taken from Ref. [6].

Future Plans

In the near future (the coming year) it is planned to focus on the exploration of electric field effects on spin-interactions [goal (ii)]. This will be accomplished by creating electric-field effect structures (electrically gated organic semiconductor films) which allow the execution of pulsed EDMR or ODMR experiments in the presence of very low charge carrier densities. Furthermore, it is planned to conduct high magnetic field pEDMR experiments at the National High Magnetic Field laboratory in Tallahassee, Florida,in order to complete the investigation of the influence of spin-orbit interactions on paramagnetic charge carrier states in organic semiconductors.

Published and accepted Journal Publications of DOE sponsored research in 2013-2015

[1] C. Boehme, J. M. Lupton, "Challenges for Organic Spintronics", Nature Nano.8, 612 (2013).
[2] K. J. van Schooten, C. Boehme, J. M. Lupton, “Coherent Magnetic Resonance of Nanocrystal Quantum-Dot Luminescence as a Window to Blinking Mechanisms”, *ChemPhysChem***15** ,9, 1737 (2014).
[3] K. J. van Schooten, J. Huang, W. J. Baker, D. V. Talapin, C. Boehme, J. M. Lupton, “Spin-dependent electronic processes and long-lived spin coherence of deep-level trap sites in CdS nanocrystals”,*Phys. Rev. B **87**, 125412* (2013).
[4] K. J. van Schooten, J. Huang, W. J. Baker, D. V. Talapin, C. Boehme, J. M. Lupton, “Spin-dependent exciton quenching and spin coherence in CdSe/CdS nanocrystals”,*Nano Letters***13**, 65 (2013).
[5] H. Morishita, W. J. Baker, D. P. Waters, R. Baarda, J. M. Lupton, and C. Boehme, “Spin-dependent dark conductivity mechanisms in films of a soluble fullerene derivative under bipolar injection”,*Phys. Rev. B***89**, 125311 (2014).
[6]H. Malissa, M. Kavand, D. P. Waters, K. J. van Schooten, P. L. Burn, Z. V. Vardeny, B. Saam, J. M. Lupton, C. Boehme, “Room-temperature coupling between electrical currents and nuclear spins in OLEDs”,*Science***345**, 1487 (2014).

[7] Kipp J. van Schooten, Douglas L. Baird, Mark E. Limes, John M. Lupton, Christoph Boehme, “Probing long-range carrier-pair spin-spin interactions in a conjugated polymer by detuning of electrically detected spin beating”,*NatureCommunications***6**, (2015), in press.

Light-matter interaction phenomena using subwavelength engineering of material properties

Igal Brener, Michael B. Sinclair
Sandia National Laboratories, Albuquerque, NM

Program Scope

The overarching goal of this project is to achieve fundamental understanding and control of light–matter interaction through engineering material properties at the subwavelength scale. Our approach involves the use of localized and propagating metamaterial photon modes coupled to semiconductor heterostructures. The metamaterials will allow tailoring of the photonic mode properties, while the semiconductor heterostructures will enable the production of electronic and vibrational transitions with desired characteristics. Two distinct classes of metamaterials will be utilized which will allow complementary aspects of the light–matter interactions to be investigated. One thrust will investigate strong coupling of the localized modes of planar metamaterial nanocavities to semiconductor transitions; while a second thrust will explore the coupling of the propagating modes of hyperbolic metamaterials to semiconductor transitions. The ultimate goal is to control the flow of energy between photons, phonons, and electrons in ways that are not possible with natural materials.

Recent Progress

1) Epsilon-Near-Zero (ENZ) modes using doped semiconductors

Physics of ENZ modes: The physics of the ENZ mode, which is supported by a nanolayer (Fig. 1(a)) at the frequency where the dielectric permittivity vanishes, has recently been a subject of debate. We thoroughly investigated and clarified the physics of this mode, providing its main characteristics and its domain of existence, demonstrating that: (i) The so-called ENZ mode is a part of the long-range surface plasmon mode, and is thus a transverse electromagnetic mode; (ii) for thicknesses much smaller than the skin depth, the dispersion relation can reach the plasma frequency ω_P (see Fig. 1(c)) and can then be approximated by a linear relation between the angular frequency ω and the wave vector $k_{//}$; (iii) the ENZ electric field inside the film increases when the thickness d decreases, and is proportional to $1/d$; (iv) these behaviors are rather robust, since we can find the same behaviors in very different geometries and for different materials, as for example a thin glass layer deposited on gold[1]; (v) the ENZ mode exists only for a given range of

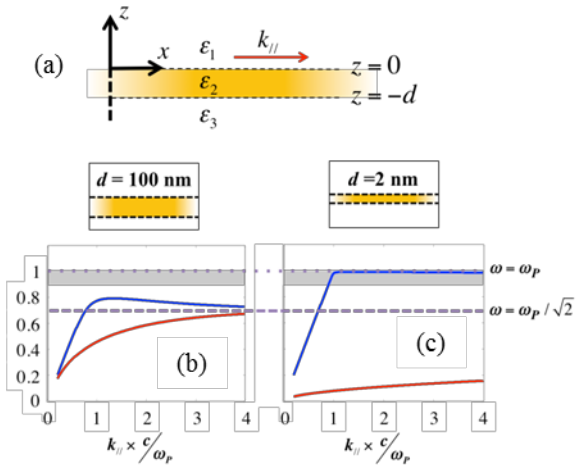

Fig. 1: (a) Thin film geometry. The intermediate layer and the surrounding semi-infinite media are characterized by their dielectric constants ε_2, and ε_1 and ε_3, respectively. (b, c) Dispersion relation for the short- (red) and long- (blue) range surface plasmons, for two different film thicknesses d. When d is much smaller than the skin depth, the dispersion reaches the plasma frequency. The gray area represents the frequency range where the mode presents a large, constant electric field inside the film. The dispersion relation becomes linear in this region.

thicknesses/frequencies (see Fig. 1(b, c)). A good rule of thumb is $d < \lambda_P/50$ where $\lambda_P = 2\pi c/\omega_P$is the plasma wavelength, or more generally, the wavelength for which the film dielectric constant vanishes.This can guide us towards the understanding of which material systems can support an ENZ mode.

Thermal emission: Control of thermal radiation using nanophotonic approaches is an important topic both from a fundamental scientific point of view and for applications such as thermophotovoltaics and infrared (IR) sources. Usually, spectrally selective and/or directional thermal emission requires some kind of surface patterning. We utilized the leaky waves in ENZ films (that correspond to what has been called Berreman modes[2]) to naturally out-couple thermal emission into free space without any surface patterning.Samples with a thin (60nm) n+ InAs top layer (doping concentrations of $1.1\text{x}10^{19}$ and $5.6\text{x}10^{18}$ cm^{-3}) were grown by molecular beam epitaxy. Weobtain absorptivity $A=1-R-T$by performinghemispherical directional reflectometer (HDR) measurements of reflectivity and transmitance at room temperature for different incident angles. We also measured calibrated thermal emission spectra as a function of angle at 140°C. In both cases, and for *p*-polarized light, a relatively sharp peak appears in the absorptivity and thermal emission spectra near the ENZ point for the two samples. This corroborates the flat dispersion of the Berreman modes for thin highly doped semiconductor layers.[3]

2) Control of strong light-matter coupling using the capacitance of metamaterial nanocavities

Metallic nanocavities with deep subwavelength mode volumes can lead to dramatic changes in the behavior of emitters placed in their vicinity, e.g. "strong coupling" behavior. The single bare cavity resonance splits into two resonances that can be measured experimentally in reflection or transmission (Fig. 2(c)). Intersubband transitions in semiconductor quantum wells (QWs) are an excellent system to study these interactions; a single dipole transition can be designed across most of the IRspectral region, using different III-V semiconductor heterostructures (e.g.: mid IR, ~4-15µm using InGaAs/AlInAsQWs, ~1.5-5µm using GaN/AlGaN QWs)[4]We studied the influence of the metamaterial nanocavity design on the type of strong light-matter interaction discussed above.[5] We model the bare metamaterial (bare cavity) as a simple RLC resonant circuit[6]. The strong light-matter coupling is added without free fitting parameters in the form of a dispersive capacitor (Fig. 2(a))[7]. Our model shows that the electrostatic capacitance of the

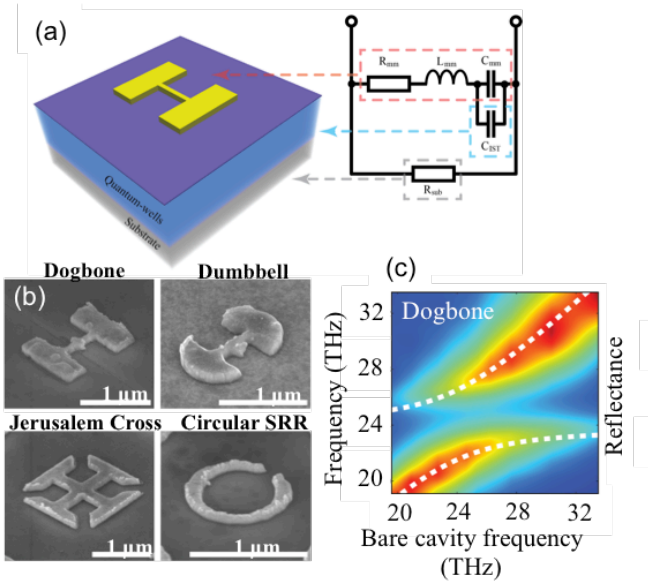

Fig. 2: (a) Schematic of the system used with its equivalent circuit. The strong coupling to the intersubband transitions is modeled by C_{IST}. (b) Electron micrographs of the different Au nanofabricated resonators. (c) Calculated reflectance spectra for the dogbone metamaterial resonator as a function of the bare cavity frequency. (White dashed lines: predicted polariton eigenfrequencies using a coupled oscillator model. Similar curves were measured experimentally)

metamaterial resonator is the key parameter that controls the light-matter coupling (or Rabi frequency)[7]. We verify the model experimentally using four metamaterial nanocavity geometries (Fig. 2(b)) atop the same wafer to exclude variations in the two-level system resonance frequency.[5]Such resonators display identical bare cavity resonances but different values for the capacitive, inductive, and ohmic components.

3) Semiconductor Hyperbolic Metamaterials.

At mid-infrared frequencies, highly doped semiconductor materials behave like metals. As a result, semiconductor hyperbolic metamaterials (SHMs) can be fabricated using alternate layers of doped and undoped semiconductor materials. Furthermore, semiconductor layers can easily be fabricated with nanometer scale layer thicknesses and, along with the mid-infrared (~10 μm) operating wavelengths, places SHMs well within the effective medium regime. Using full wave electromagnetic simulation, we have shown that SHMs exhibit superior properties when compared to metallic HMs, and that SHMs support high-quality, ultra-large photon momentum states.Furthermore, we have shown that SHMs offer opportunities for improved properties and can also allow for new phenomena such as *ultrafast transient creation of the hyperbolic manifold through optical pumping*. The design and growth of samples appropriate for these studies has been finished in this FY.Our plan is to: 1) experimentally demonstrate the unique electromagnetic properties of SHMs; and 2) to exploit the wide bandwidth, high density of states photon manifold to tailor light-matter interactions within the metamaterial.

Future Plans

1)Thermal emission

We aim to take advantage of the ENZ mode properties in 15 to 30 nm-thick films of n-doped GaAs or InGaAs to demonstrate the first fast and spectrally tunable thermal sources. The ENZ mode in these nanofilms appears around the plasma frequency, which depends on the doping. For high doping levels, ~$5x10^{18}$–10^{19} cm^{-3}, the ENZ mode takes place in the mid IRbetween 10 and 15 μm. An absorption/emissivity resonance is expected when the ENZ mode is excited[8]. The electron density can be changed using depletion[9], and thus the resonant-absorption wavelength can be shifted and electrically controlled. Numerical calculations are used to optimize the coupling of propagating waves to the ENZ mode. The highly doped layer is surrounded by a metallic grating,allowing the phase matching condition between free space and the large wave vectors of the ENZ mode. A metallic back reflector reinforces the absorption in the ENZ layer. A voltage can be applied between the grating and the back reflector to deplete the film and change the electron density.Fabrication and measurements are in progress.

2) Optical nonlinearities from strongly coupled metamaterials-intersubband transitions

Planar metamaterial resonators coupled to intersubband transitions in quantum wells can also be used for the manipulation and enhancement of nonlinearities. Resonant nonlinearities can be designed when multiple intersubband transitions overlap the photon energies of interest. [10] Metallic resonators with resonances at the fundamental and the second harmonic frequency can be used to enhance second harmonic generation (SHG). [11] Our preliminary results indicate that each resonator coupled to ISTs and excited at the fundamental frequency (~10um) behaves as a point source for SHG. A collection of such resonators can then be used to manipulate the far

field of the SHG light when arbitrary phase relationships are designed. In this coming year we will explore this emission form these phase-coherent arrays.

3) Transient excitation of SHMs

We plan to experimentally demonstrate thatSHMs enable ultrafast topological transitions between elliptical and hyperbolic dispersion. Using an ultrafast optical pump, we can rapidly produce a large density of photo carriers that will be trapped within the doped layers. In this manner the doped layers are rapidly switched from dielectric to metallic behavior at the frequencies of interest, and the superlattice structure will switch from elliptic to hyperbolic dispersion. Preliminary simulations predicta transition from elliptical to hyperbolic dispersion upon photo-pumping. After initial pumping, the superlattice will remain in the hyperbolic state for a brief period (~1 ns) before relaxation processes deplete the photo-carriers. This intriguing result suggests that transient excitation of SHMs might enable optical gating and modulation for many applications, such as imaging, lensing, and near-field energy transfer, as well as all-optical switching.

Publications

1) “Doping-tunable thermal emission from plasmonpolaritons in semiconductor epsilon-near-zero thin films”, YC Jun, TS Luk, AR Ellis, JF Klem, I Brener, Appl. Phys. Lett. **105**, 131109 (2014)

2) “Control of Strong Light–Matter Coupling Using the Capacitance of Metamaterial Nanocavities”, A. Benz, S. Campione, J.F. Klem, M.B. Sinclair, and I. Brener, Nano Letters Article ASAP, DOI: 10.1021/nl504815c (2015)

3) “Theory of epsilon-near-zero modes in ultrathin films”, Salvatore Campione, Igal Brener, and Francois Marquier, Physical Review B, Rapid Communications, accepted for publication, March 2015.

References

1. S. Vassant, J.-P. Hugonin, F. Marquier, *et al.*, Optics express **20** (2012).
2. D. W. Berreman, Physical Review **130**, 2193 (1963).
3. Y. C. Jun, T. S. Luk, A. R. Ellis, *et al.*, Applied Physics Letters **105** (2014).
4. A. Benz, S. Campione, S. Liu, *et al.*, Nature Communications **4**, 2882 (2013);A. Benz, S. Campione, M. W. Moseley, *et al.*, ACS Photonics (2014);A. Benz, I. Montano, J. F. Klem, *et al.*, Appl. Phys. Lett. **103**, 263116 (2013).
5. A. Benz, S. Campione, J. F. Klem, *et al.*, Nano letters (2015).
6. S. Y. Jun and K. Sarabandi, IEEE Antennas and Wireless Propagation Letters **11** (2012).
7. S. Campione, A. Benz, J. F. Klem, *et al.*, Phys. Rev. B **89** (2014).
8. S. Vassant, A. Archambault, F. Marquier, *et al.*, Physical review letters **109** (2012).
9. Y. C. Jun, J. Reno, T. Ribaudo, *et al.*, Nano letters **13** (2013).
10. C. Sirtori, F. Capasso, D. L. Sivco, *et al.*, Physical review letters **68** (1992).
11. S. Campione, A. Benz, M. B. Sinclair, *et al.*, Applied Physics Letters **104** (2014).

Compliant Substrate Epitaxy: Au on MoS_2

D. C. Chrzan,[1,2] J. W. Ager III,[1,2] E. E. Haller,[1,2] and A. Javey[1,3]
[1]Materials Sciences Division, Lawrence Berkeley National Laboratory, Berkeley, CA[2]Materials Science and Engineering, University of California, Berkeley, CA
[3]Electrical Engineering and Computer Science, University of California, Berkeley, CA

Program Scope

One of the goals of the Electronic Materials Program at LBL is to be able to be able to grow high quality nanostructures and thin films of any material on any other material. As a prototypical example, we are considering the growth of Au on MoS_2.

It has been known since the mid 1960's that using evaporative growth, Au grows epitaxially on MoS_2.[1-4]Nevertheless, this observation is surprising, since the nominal lattice mismatch between the two materials in the experimentally observed {111} oriented growth results in nearly an 8% biaxial strain. Even more surprising, is the fact that if Au were to grow with an {001} orientation, the elastic strain in the growing film would be much less than that expected for the {111} orientation.In fact, the {111}orientationpreference for Au growth remains unexplained. Given the technological promise of the transition metal dichalcogenides(and the need to make contacts for them) this problem is of technological interest, in addition to the more fundamental science issues it raises.

Accordingly, we are studying experimentally the growth of Au on MoS_2 using two approaches. In the first, we consider the evaporative deposition of Au, as was applied in the mid 1960's. In the second, we consider a wet chemistry approach that enables self-assembled epitaxial growth of Au nanowires at relatively low temperatures. Theoretical analysis relying on both continuum elasticity theory and density functional theory studies reveals the origin of the observed orientation in growth: MoS_2 is a example of a compliant substrate, able to relax during epitaxy to accommodate larger lattice mismatches than would otherwise be possible.In this case, despite the larger lattice mismatch, when one considers all the contributions to the energy, the {111} orientation is favored.

Recent Progress

Our work began with wet chemistry experiments aimed at growing Au epitaxially on MoS_2. To form Au nanowires on MoS_2, we cast a 30wt% $AuCl_3$ solution in dilutedHCl (Sigma-Aldrich) onto a mechanically exfoliated MoS_2 flake for 1 minute.The extra solution was blown from the film with N_2 gas, and the sample wasannealed at 150 °C for 2 min on a hotplate in an ambient environment. Given proper concentrations of solution, the Au atoms self-assemble into

nanowires (Fig. 1a). The nanowires are aligned preferentially along crystalline directions, suggesting an epitaxial relationship between the growing nanowires and the substrate. As noted above, this epitaxial relationship is remarkable because of the large lattice mismatch between the two materials.

In order to further explore the epitaxial Au growth mode, we evaporated a 2 nm thick film of Au onto a MoS_2 substrate and annealed at 400°C for two minutes. We then characterized the films using atomic force microscopy (AFM) and x-ray diffraction (Figs. 1b, 1c and 1d).AFM revealed that the film was not contiguous, but instead composed of flat islands, typically 50-80 nm wide and approximately 5 nm thick. There are some hints of faceting, suggesting an epitaxial relationship. X-ray diffraction studies indicate two orientations for the islands: {111} and {001} growth. The diffraction peak for the {111} spot is a bit more intense, suggesting that this is the predominant orientation. These results are similar to those that were seen in the earlier experiments.[1-4]

We discovered that the {111} growth orientation that we observe (both in nanowires and thin plates) can be understood if one considers the properties of the substrate. Within the most common models of epitaxial growth, the substrate is assumed to be infinitely thick, and therefore, infinitely rigid in comparison to the growing film. MoS_2, however, is a layered material that is only bonded between layers by van der Waals forces.

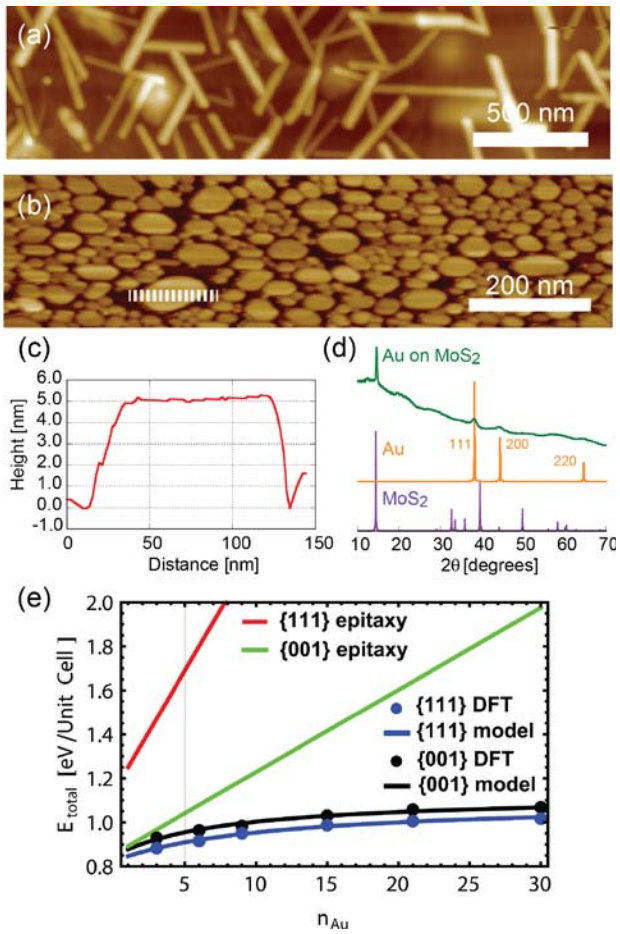

Figure 1. (a) Atomic force microscopy (AFM) image of Au nanowires grown as described in the text. (b) AFM image of Au islands grown through evaporation. (c) Profile of island marked by dashed line in (b). (d) X-ray diffraction of sample shown in (b). Note the presence of peaks corresponding to {111} and {001} epitaxy. (e) The predictions of the theory for excess energy associated with epitaxial growth as a function of the number of Au layers. The red and green curves are the excess energy per unit cell expected from epitaxial growth when the substrate is assumed infinitely rigid. Note that {001} epitaxy would be favored, but in all cases the excess energy is quite high. The solid symbols are the predictions of density functional theory for the total excess energy, and the solid curves are the predictions of the continuum elasticity theory. Note that the total energy is significantly reduced by the substrate relaxation, and that the {111} orientation is now preferred over the {001} orientation.

One consequence of this structure is that it may be possible for only the first layer of the substrate to deform in order to accommodate lattice mismatch within the growing film. This has the net effect of giving the substrate a markedly reduced stiffness, thus reducing the total elastic energy of the substrate and growing film. In addition, the interfacial energy and stresses are markedly different for the {111} orientation and the {001} orientation. Most notably, in the {111} orientation, every Au atom is bound to a S atom from the substrate. In contrast, in the {001} orientation, only every other S atom is bound to a Au atom. This results in a much lower energy for the {111} Au/MoS_2 interface vs. the {001} Au/MoS_2 interface.

We developed a model for the epitaxial growth within a continuum linear elasticity theory, and determined its parameters using density functional theory. The model focuses on the excess energy that the film and substrate have in comparison to their bulk materials. The predictions of the model are shown in Fig. 1e. This figure establishes two important points. First, in the case of traditional epitaxial growth, assuming a rigid substrate, the {001} orientation is preferred over the {111} orientation by a significant margin (though it is not clear that either should be experimentally observed due to their high energies per unit cell). The second point is that when substrate relaxation and interfacial/surface energies and strains are considered, the {111} orientation becomes the preferred epitaxial orientation, consistent with experimental observations.

Future Plans

Compliant substrate epitaxial growth was first proposed by Lo in 1991.[5] Lo argued that the substrate could be made more compliant by thinning it, using standard lithographic methods. Later, Jesser*et al.* proposed that a subsurface dislocation boundary might form a compliant substrate.[6]Our work suggests a new kind of compliant substrate: the van der Waals bonded layered substrate. Thisnew type of compliant substratepresents several interesting opportunities that we are pursuing in earnest.

First and foremost, we are developing a better understanding of the growth process itself. For example, misfit dislocations will undoubtedly be introduced within this epitaxial system and are likely to impact the growth of both plate-like films and nanowires. Second, the nanowire growth process itself is still not well understood. We need to develop a theory for the growth of the wires in order that we may exert more control over the process.

Looking forward, the compliance of the substrate during epitaxy presents the opportunity to use epitaxy as a means engineering strain within the substrate surface layer. In the present case, small epitaxial islands of Au (below the threshold at which misfit dislocations are introduced) will create “point” sources of compression in the substrate surface layer that will necessarily be accommodated by adjacent regions of tensile strain. Proper placement of these islands, using lithographic methods, can be used to generate tensile strain patterns within the substrate, thereby enabling engineering of the opto-electronic properties of the

dichalcogenides.These same islands might also be used to manipulate the MoS_2 itself.The islands bond covalently to the substrate. These covalent bonds, if sufficiently dense, could overwhelm the van der Waals bonding, and enable the islands to be used as grips for processing single layers of MoS_2. Finally, the idea of using van der Waals bonded solids as compliant substrates for epitaxial growth is more general, and can be applied to other systems as well. We are investigating this possibility as well.

References

[1] Honjo, G. & Yagi, K. Studies of Epitaxial Growth of Metallic and Nonmetallic Films by Means of High-Resolution Cine and Still-Electron Microscopy. *Journal of Vacuum Science & Technology* 6, 576-&, doi:Doi 10.1116/1.1315688 (1969).

[2] Jacobs, M. H., Pashley, D. W. & Stowell, M. J. Formation of Imperfections in Epitaxial Gold Films. *Philosophical Magazine* 13, 129-&, doi:Doi 10.1080/14786436608211992 (1966).

[3] Jesser, W. A. & Kuhlmann.D. Measurement of Elastic Strains in Small Gold Nuclei on Molybdenite Substrates as a Function of Nucleus Size and Misalignment. *Journal of Applied Physics* 38, 5128-&, doi:Doi 10.1063/1.1709289 (1967).

[4] Pashley, D. W., Jacobs, M. H., Stowell, M. J. & Law, T. J. Growth + Structure of Gold + Silver Deposits Formed by Evaporation inside Electron Microscope. *Philosophical Magazine* 10, 127-&, doi:Doi 10.1080/14786436408224212 (1964).

[5] Lo, Y. H. New Approach to Grow Pseudomorphic Structures over the Critical Thickness. *Applied Physics Letters* 59, 2311-2313, doi:Doi 10.1063/1.106053 (1991).

[6] Jesser, W. A., van der Merwe, J. H. & Stoop, P. M. Misfit accommodation by compliant substrates. *Journal of Applied Physics* 85, 2129-2139, doi:Doi 10.1063/1.369514 (1999).

Publications

Y. Zhou, D. Kiriya, E. E. Haller, J. W. Ager III, A. Javey and D. C. Chrzan, "Compliant Substrate Epitaxy: Au on MoS_2," to be submitted.

D. Kiriya, Y. Zhou, C. Nelson, M. Hettick, S. R. Madhvapathy, K. Chen, P. Zhao, A. Minor, D. C. Chrzan, and A. Javey, "Compliant Substrate Epitaxial Growth of Ordered Gold Nanowires on MoS_2," to be submitted.

DOE award #: DE-SC0006539

Methodology and Tool Development for Multiscale Simulation of Thermal Transport

Youping Chen, University of Florida, Gainesville, Florida 32611

Program Scope

A major obstacle standing in the way of progress in dynamic multiscale simulation is the lack of a concurrent atomistic-continuum method that allows waves, heat and defects to pass through the atomistic-continuum interface, since across this interface there is a change in system description and governing equations, and consequently a mismatch in the phonon representation, leading to phonon scattering or wave reflections at the artificial/numerical interface between the atomistic and continuum description. This in turn fundamentally alters the dynamic material behavior in the simulation, rendering most of the multiscale methods powerless in simulations of dynamic phenomena. The primary goal of this research is to establish a concurrent mutliscale methodology that can overcome this obstacle.

In pursuit of this goal, we reformulate the classical statistical mechanical theory of transport processes to unify atomistic and continuum descriptions of balance laws. We recast the mathematical form of the governing equations to facilitate finite element simulation of discontinuous materials behaviors. We then develop new numerical methods to establish a multiscale simulation tool. We test the accuracy and efficiency of the simulation tool through comparing the simulation results by the new tool with that by atomistic simulations at small scales and with experimental measurements at larger length scales. It is anticipated that this research will contribute to DOE a new simulation tool that expands current atomistic simulation-based predictive capability from the nanoscale to the mesoscale and that provides a unified treatment for microstructural, mechanical and thermal transport problems.

Recent Progress

In the past two years, our efforts have been devoted to two aims: to develop theoretical and numerical methods to establish a multiscale simulation tool, and to perform atomistic and multiscale simulation for understanding of the physics of dislocations, fracture, and phonon thermal transport. In this meeting we present our recent progress on the development of the simulation tool, including (1) a multiscale discretization scheme to concurrently model the multiple morphological length scales in materials with complex microstructure, (2) a new interpolation function to model the multiple length and time scale in phonon transport processes in the coarse-grained simulations, and (3) a phonon representation of heat pulse to mimic the coherent excitation of a non-equilibrium phonon population by ultrashort laser techniques.

(1) **A multiscale discretization scheme**. The efficiency and accuracy of the current version of the simulation tool, the concurrent atomistic-continuum simulator (CAC), in reproducing the multiscale microstructure and energetics has been tested through simulations of bicrystal and polycrystalline SrTiO3, single and polycrystalline Si, and SiGe superlattices. Simulation results show that the CAC simulation allows a smooth passage of defects (cracks and dislocations) through the atomistic-continuum interface without the need of additional constitutive rules; both the atomic-scale structures and the energies of the strontium titanate grain boundaries obtained

by CAC compare well with those obtained by existing experiments and Density Functional Theory calculations. Specifically, with 98.4% reduction in degrees of freedom, the CAC simulation results, including the stress and strain responses and the GB-defect interaction mechanisms, are comparable with that by atomistically resolved Molecular Dynamics simulation (MD). The accuracy and efficiency of CAC relative to MD have been tested and quantified. The effect of the size of the atomic resolution region to model the grain boundaries has been quantified with respect to MD. A CAC model of polycrystalline SrTiO3 in which the grain boundaries are modeled with atomic resolution while the ordered single crystalline regions are modeled with finite elements is shown in Fig. 1. The magnitude of the displacement difference between the CAC and MD simulation results is presented in Fig. 2, showing that when the size of the atomic-resolution region used to model the grain boundaries is larger than 2.62nm, the CAC and MD produce identical results for the displacement field.

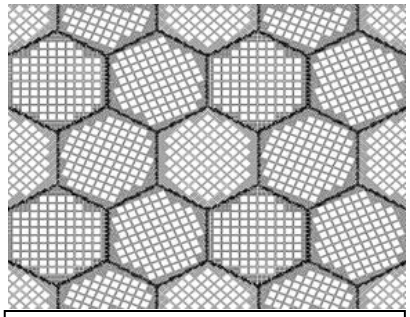

Fig. 1 A CAC model of polycrystal $SrTiO_3$ showing concurrent multiscale discretization.

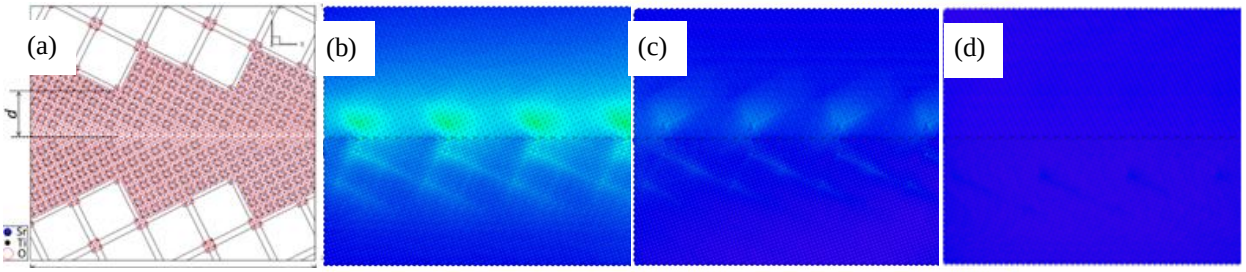

Fig. 2 The computer model (a) and the magnitude of atomic-level displacement discrepancy between CAC and MD simulation results with different *d* (the smallest distance between the atomic/continuum interface and the grain boundary): *d* = 7.0Å (b); *d* = 12.22Å (c); *d* = 26.2Å.

(2) **A new shape function**. The goal to develop a new shape function is to enable waves of all wavelengths to propagate across regions with different mesh size, e.g., from the atomic to the continuum region, without artificial wave reflections by the atomistic-continuum interface. In the conventional finite element (FE) method, there are two basic approximations: the displacement approximation (i.e., the shape function or interpolation function) and the numerical integration approximation. The usual linear shape functions cut off waves whose wavelengths are smaller than the element size[1, 2], resulting in wave reflections by the interface between regions of different mesh size, constituting one of unsolved problems in the FE method[2]. There are two issues with this problem: (1) artificial wave reflections by numerical interface alter the dynamics of the system and affect the simulation results, and (2) at small scale, temperature measured in the simulation is mesh size dependent, resulting in an inaccurate representation of temperature and heat.

The classical mechanics view of the motion of an atom is an irregularly fluctuating function of time. However, the motion of an atomistic system turns out to be most readily described not in terms of the individual atoms, but in terms of traveling waves[3-5]. These travelling waves are collective behavior of lattice at mesoscale. In the ordered region of a material, e.g., a single crystal grain, the freely propagating sound waves (i.e., acoustic phonons) have been

experimentally found to be omnipresent[6], suggesting that elastic waves can propagate phase-coherently. This phase coherence implies that a unique form of shape function can be derived to include small wavelength waves propagating within a finite element without the need of introducing additional parameters. We have formulated the shape function based on lattice dynamics by adding the displacements that are associated with the small wavelength waves to the displacement interpolated via the standard FE shape function. Using such an interpolation function, waves of all wavelengths are allowed to propagate across regions with different mesh size without artificial reflections. In Fig. 3 we present the simulation results of a wave packet transmission across the atomistic-continuum interface with the simulation tool that has implemented the new interpolation function.

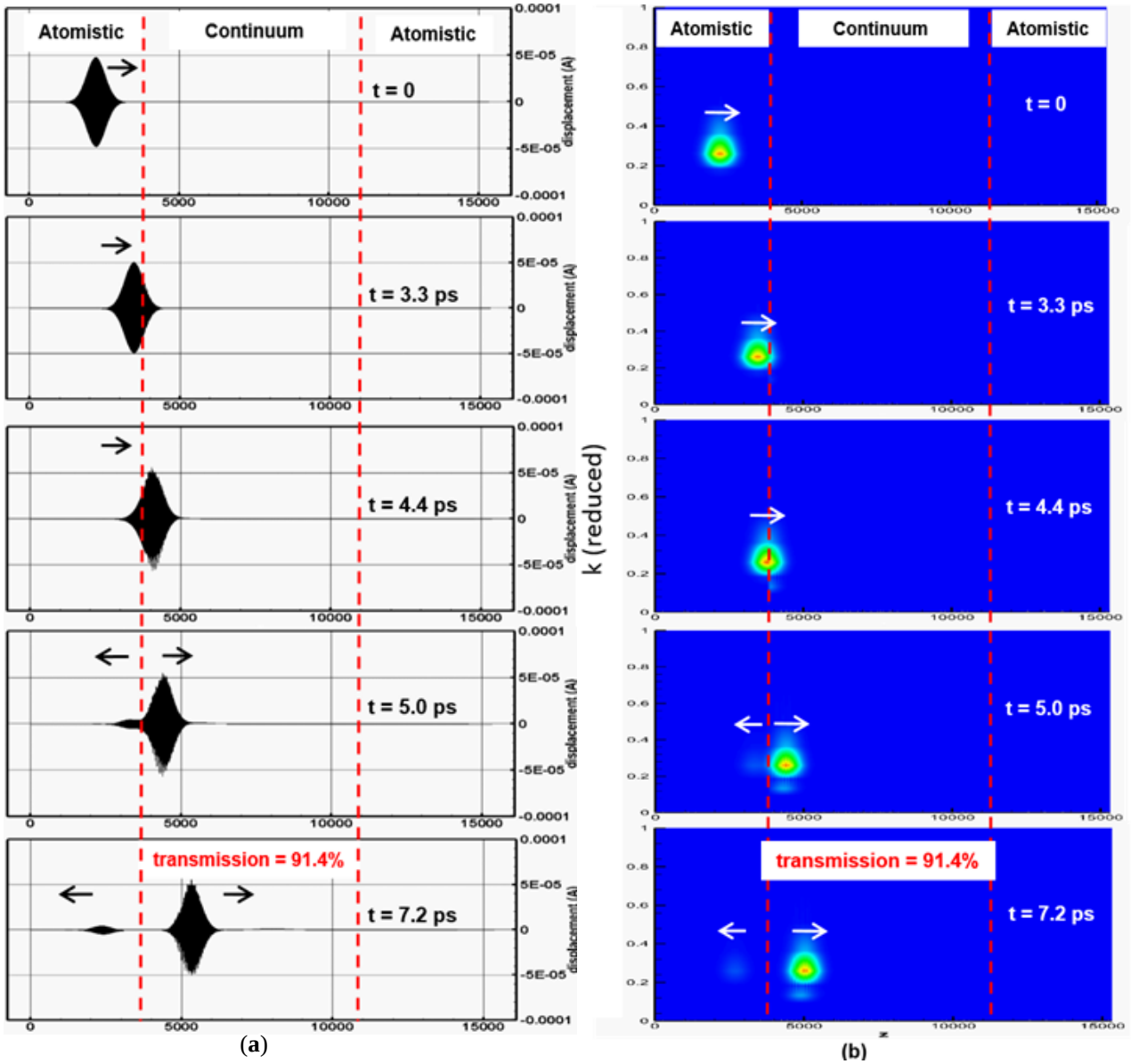

Fig. 3 A wave-packet (central wave vector $k = 0.25$) transmission across the atomistic-continuum interface with the new interpolation. (a) spatial distribution of the displacement presented in time sequence; (b) spatial distribution of the wave vector k presented in time sequence. The real space to reciprocal space transform is computed by a wavelet analysis. With a conventional linear shape function, the corresponding transmission is zero.

(3) **A new heat pulse model**. For the study of transient phonon thermal transport, we have developed a heat source model to mimic the coherent excitation of a non-equilibrium phonon population by ultrashort laser techniques. A heat pulse model is a key component in simulations that mimic the pump-probe experimental studies of phonon transport. There have been attempts to simulate the propagation of heat pulses in MD simulation using thermostat algorithms to model the heat source[7]. However, since thermostat algorithms mimic thermalizing events such as damping and dephasing of phonon waves[8], the phase information or the coherence of phonons excited by an ultrashort laser pulse is thus completely or partially destroyed. Therefore, they are not well suited for the simulation of the excitation and subsequently propagation of coherent phonons by femtosecond laser pulses. From a mathematical viewpoint, the spatial and temporal coherences of phonons can be represented by phonon wave packets. This leads to the construction of the phonon heat pulse model in terms of spatiotemporal Gaussian wave packets composed of allowed phonons modes of the materials. The number of phonons excited at temperature T is determined by the Plankian distribution[9]. A snapshot of phonon scattering by grain boundary is presented in Fig. 4, demonstrating the coexistence of coherent and incoherent phonon transport across the interface. Simulation results have shown that the heat pulse model facilitates not only quantitative measurement of phonon-interface scattering but also visualization and mechanistic understanding of the highly non-equilibrium process of heat conduction.

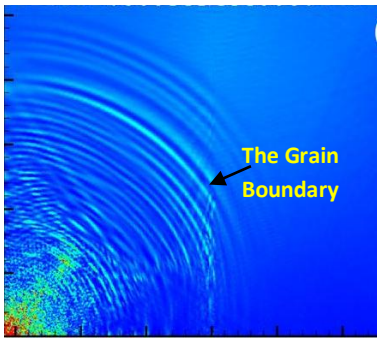

Fig. 4 Phonon scattering by a grain boundary in Si and by free surfaces, showing both the reflection and transmission of phonon waves at the interface.

Future Plans

In the next year, we will continue our work on (1) the theoretical formulation, numerical implementation, coding and code optimization to establish the simulation tool, including development of new integration scheme, new mesh refinement scheme, and optimization of the code, to enable mesoscale simulations of complex materials, and (2) atomistic and multiscale simulation to gain fundamental understanding of the physics of phonon thermal transport, defect dynamics, and the effect of static and mobile dislocations on thermal transport. Planned materials to be simulated include superlattices, polycrystalline materials, and phononic crystals.

References

1. Celep, Z.; Bažant, Z. P. *International journal for numerical methods in engineering* **1983,** 19, (5), 631-646.
2. Zienkiewicz, O. C. *International Journal for Numerical Methods in Engineering* **2000,** 47, (1-3), 9-28.
3. Born, M.; Heisenberg, W.; Jordan, P. *Z. Phys.* **1926,** 35, 557.
4. Born, M.; Huang, K., *Dynamical Theory of Crystal Lattices*. Clarendon Press: 1998.
5. Cochran, W., *The Dynamics of Atoms in Crystals*. 1973.
6. Percus, J. K.; Yevick, G. J. *Physical Review* **1958,** 110, (1), 1-13.
7. Tsai, D. H.; MacDonald, R. A. *Physical Review B* **1976,** 14, (10), 4714-4723.
8. Sääskilahti, K.; Oksanen, J.; Tulkki, J. *Physical Review E* **2013,** 88, (1), 012128.
9. Kittel, C., *Introduction to Solid State Physics*. **1967**.

Journal Publications resulting from work supported by the DOE grant (2013-2015)

1. Yang, S. and Y. Chen, *Concurrent atomistic and continuum simulation of bi-crystal strontium titanate with tilt grain boundary.* Proceedings of the Royal Society A:, 2015. **471**(2175).
2. Zheng, Z., X. Chen, B. Deng, A. Chernatynskiy, S. Yang, L. Xiong, and Y. Chen, *Phonon thermal transport through tilt grain boundaries in strontium titanate.* Journal of Applied Physics, 2014. **116**(7): p. 073706.
3. Chen, X., L. Xiong, A. Chernatynskiy, and Y. Chen, *A molecular dynamics study of tilt grain boundary resistance to slip and heat transfer in nanocrystalline silicon.* Journal of Applied Physics, 2014. **116**(24): p. 244309.
4. Xiong, L., S. Xu, D.L. McDowell, and Y. Chen, *Concurrent atomistic–continuum simulations of dislocation–void interactions in fcc crystals.* International Journal of Plasticity, 2015. **65**: p. 33-42.
5. Xiong, L., D.L. McDowell, and Y. Chen, *Sub-THz Phonon drag on dislocations by coarse-grained atomistic simulations.* International Journal of Plasticity, 2014. **55**(0): p. 268-278.
6. Xiong, L., X. Chen, N. Zhang, D.L. McDowell, and Y. Chen, *Prediction of phonon properties of 1D polyatomic systems using concurrent atomistic–continuum simulation.* Archive of Applied Mechanics, 2014. **84**(9-11): p. 1665-1675.
7. Yang, S., L. Xiong, Q. Deng, and Y. Chen, *Concurrent atomistic and continuum simulation of strontium titanate.* Acta Materialia, 2013. **61**(1): p. 89-102.
8. Deng, Q. and Y. Chen, *A Coarse-grained atomistic method for 3D dynamic fracture simulation.* International Journal for Multiscale Computational Engineering, 2013. **11**(3).
9 Xiong, L. and Y. Chen, *Coarse-grained atomistic simulations of dislocation and fracture in metallic materials*" in Handbook of Micromechanics and Nanomechanics, 2013 Pan Stanford Publishing Pte. Ltd.

DOE award # DE-SC0002626, Massachusetts Institute of Technology

Electrochemically-Driven Phase Transitions in Battery Storage Compounds

PI: Yet-Ming Chiang[1], co-PIs: W. Craig Carter[1], Ming Tang[2]
[1]Massachusetts Institute of Technology, Dept. of Materials Science and Engineering, Cambridge, MA 02139, ychiang@mit.edu
[2]Rice University, Dept. of Materials Science and Nanoengineering, 6100 Main Street, Houston, TX 77005

Program Scope or Definition

Compounds of interest for ion storage in advanced batteries frequently exhibit phase transformations as the working ion concentration varies. Under large electrochemical driving forces inherent to practical use, systems are often driven far from equilibrium. This program combines experiments and theory to develop a predictive understanding of the interaction between composition, transformation strain, crystallite size and shape, and the electrochemical conditions driving the phase transition. Behavior at nanoscopic to mesoscopic scale under electrical overpotentials that vary in magnitude and with time are studied. The systems to be studied have fundamental and practical interest, and include lithium and sodium transition metal olivines, AMPO4 (A = Li, Na; M = Fe, Mn, + additives) exhibiting a wide range of transformation strains. Phase-field modeling of phase stability and transformation pathways is combined with *operando*experiments in which electrochemical titration is conducted simultaneously with structure characterization at DOE facilities. Understanding of phase transformation pathways is expected to lead to new materials design concepts, and electrochemical duty cycles, that improve capacity utilization at high charge/discharge rates, control voltage and capacity hysteresis, and improve life by reducing cycling-induced mechanical fatigue. The main questions to be addressed are:

(i) How does the magnitude of the phase transformation strain, and the magnitude of the electrochemical driving force, dictate the phase transformation pathway?Our approach takes advantage of a unique series of olivines samples, developed over more than a decade [refs], in which the synthesis process and micro/nanostructure of the starting powders are held identical or nearly so, while the composition is widely varied in order to explore the existent range of phase diagrams and transformation strains. *Operando* synchrotron X-ray diffraction is used to study the transformation mechanisms and are coupled with phase field models to observe and interpret deviations from equilibrium transformation paths [1]. In general, it is found that large deviations from equilibrium are the rule rather than the exception.

(ii) What is the relationship between transformation strain and electrochemical performance? While it can be assumed that the rate-limiting kinetic steps and atomic species change with the transformation mechanism, it is not currently possible to predict electrochemical capacity and rate performance from basic structural knowledge. In the olivine family, we have systematically studied a wide range of compositions encompassing a sufficiently wide range of transformation strains that such correlations are now possible for the first time.

(iii) What is the role of plasticity? Behavior differs greatly between small-transformation-strain systems (i.e., olivine crystalline transformations with <10% volume differential) and in large-strain systems (e.g., Si with ~300% strain). Both have been studied under this program,

and elastic response dominates the former while plasticity and its consequences dominate the latter. Many materials of interest for energy storage fall in the middle – where strains are large enough that the elastic limit is surely exceeded, yet the parent/daughter phases remain structurally similar. The bridge between elastic and plastic response is being studied in this program experimentally and theoretically.

Recent Progress

Thephospho-olivine family$AMPO_4$(A=Li, Na and M=Fe, Mn, Ni, Co), spans a wide range of phase transition induced volume misfit, from as low as 1% for $LiMn_{0.4}Fe_{0.6}PO_4$ to about 5% for $LiFePO_4$ to 17% for $NaFePO_4$. During 2014 we conducted experiments which revealed that room temperature phase transitions occur by quite different mechanisms as transformation strain varies. Figure 1 shows a bird's-eye view of the (200) reflection in the three compositions during *operando* SR-PXD of an electrochemical cell (methodology developed in collaboration with the Structural Science Group, X-ray Science Division, at APS led by Dr. P. Chupas). It is immediately clear that the evolution of phase quantity (relative intensity) and composition (peak shift) follows a different path in each case. A large body of literature exists for $LiFePO_4$ (LFP), providing areasonably well-accepted picture that while micron sized particles are two-phase, nanoscale particles have binary states, being either mostly-lithiated or mostly-lithiated,. Our work has shown that this view, consistent with LFP results in Fig. 1,does not apply to olivines in general. For example, in the olivine of greatest interest for post-LFP applications, $LiMn_yFe_{1-y}PO_4$(LMFP), *operando* SR-PXD has shown a continuous transformation path through metastable phases (Fig. 2). We determined precisely the unit cell parameters of allcrystallinephases during electrochemical titration, and found three featuresthat indicatenonequilibriumbehavior: (a) During two-phase coexistence, the lattice dimensions, and therefore composition, of one or both phases change continuously, in violation of the Gibbs phase rule; (b) Significant hysteresis in phase behavior is observed between charge and discharge - clearly both cannot represent equilibrium; (c) Significant deviations in phase boundary compositions are observed*operando*.From these results, it is clear that nano-LMFP does not follow the "binary particle" model of nano-LFP but instead exhibits continuous transitions within single particles to minimize coherency strain energy. However, changes in mechanism do not necessarily correlate with faster electrochemical kinetics, and indeed, to now there has been no clear evidence that there is any correlation. Upon mapping results like Fig. 2 over a range of Mn content y in $LiMn_yFe_{1-y}PO_4$, we find for the first time a clear correlation between rate capability and transformation strain (Fig. 3). Note that the minimum in strain at y= .2-0.4 corresponds to a maximum in capacity at very high C-rates of 20C to 50C.

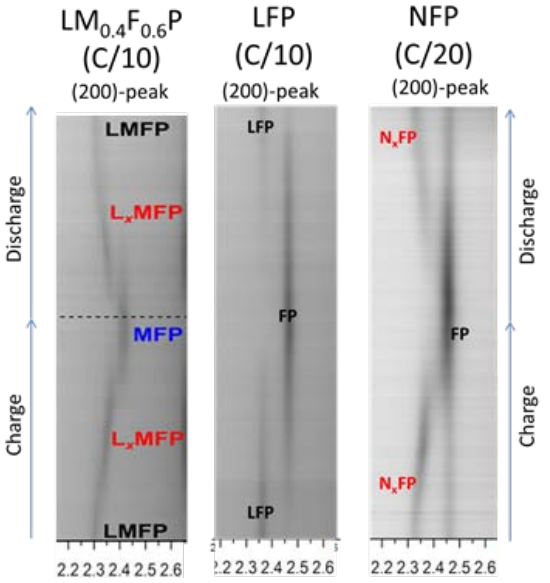

Fig. 1: Operando SR-PXD results showing evolution of the olivine (200) peak during a single charge-discharge (delithiation-lithiation) cycle.

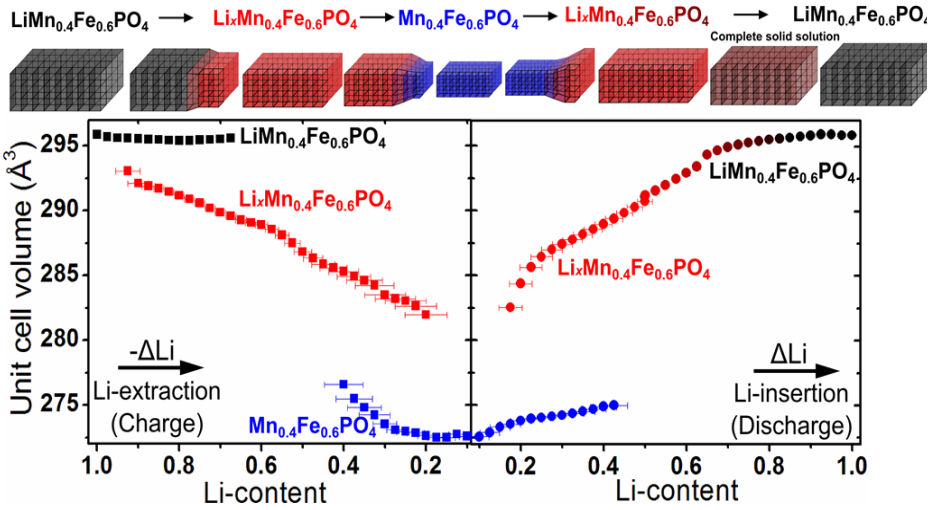

Fig. 2.Unit cell volumes determined by Rietveld refinement of operando SR-PXD data measured during Li extraction (charge) and insertion (discharge) at a C/10 rate of LMFP (52 nm particles), supporting a coherent transformation model as shown at top. Sample has 52nm averaae crvstallite size.

$NaFePO_4$ (NFP), having far higher transformation strain than either LFP or LMFP, has shown still a different response that is not yet understood in detail. The most striking difference is a cyclic loss of diffraction intensity during cycling that can only be interpreted as the creation of disordered, noncrystalline material.

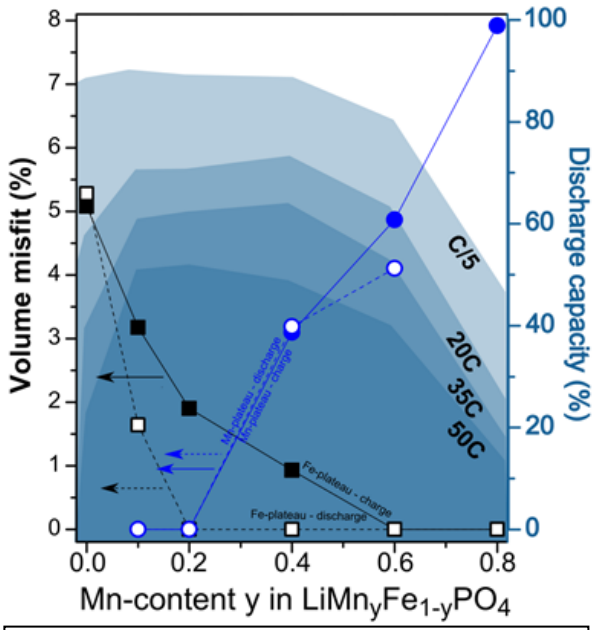

Fig. 3.Lattice misfit vs. discharge capacity at high C-rates in nanoparticulate LMFP.

Silicon is an ion-storage compound with such high strain (~300% expansion upon lithiation) that plasticity must play a role in any strain accommodation. We developed a mesoscale model for simulating concurrent phase transformation and plastic deformation in crystalline Si (c-Si) based on the front-tracking method, and used it to successfully reproduce the observed anisometric shapes of lithiated Si nanopillarsand nanowires of various crystallographic orientations. We also simulated for the first time the shape evolution of a three-dimensional Si particle upon lithiation, showing very good agreement (Fig. 4a) with experiment [5]. We also developed a novel strategy to mitigate lithiation-induced fracture in Si anodes through *morphological design*, choosing an anisometric Si shape to offset anisotropy in swelling to produce uniform volume expansion. Based on the design rules developed, optimal anisometric cross-section shapes are determined for Si pillars of different orientations (Fig. 4(b-f).

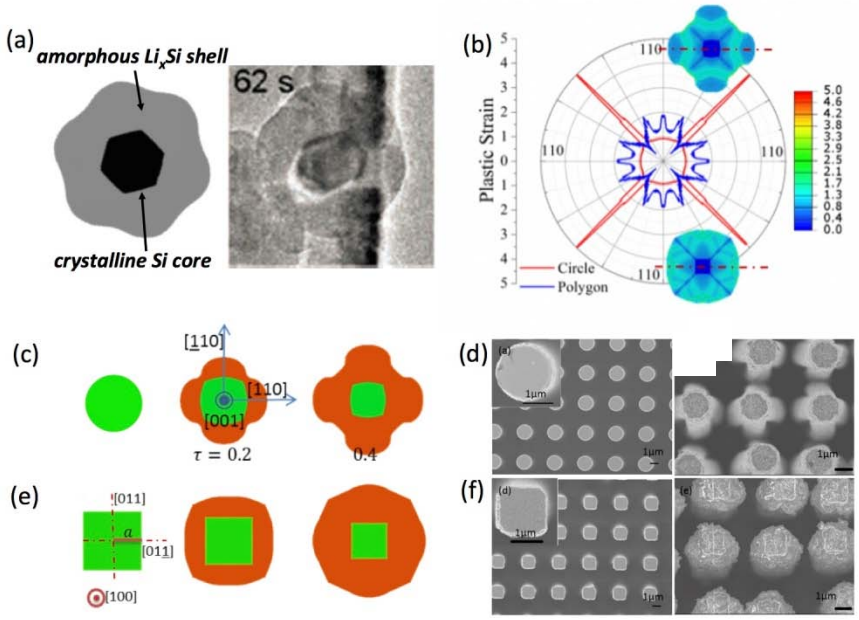

Figure 4 (a) Simulation of a partially lithiated spherical Si particle viewed along [111] axis (left) vs. experimental image (right, adapted from M.T McDowell et al., Adv. Mater. 24, 6034 (2012). (b) Comparison of the equivalent plastic strain distributions on surface of [001] Si pillars with circular (red curve) and square (blue curve) cross sections. Simulated shape evolution of [001] Si pillars with circular (c) and square (d) cross sections upon lithiation agrees well with experiments (d) & (f).

Future Plans

During 2015, we will investigate the NFP system experimentally and theoretically as a large strain intercalation compound that almost certainly exhibits plasticity, using compositional variations to systematically vary the transformation strain. The modeling methodology developed and demonstrated in silicon will be applied to NFP, towards the goal of generalizing design rules for morphological control of deformation in high transformation strain systems.

Published and accepted Journal Publications of DOE sponsored research in 2013-2015

1. D. B. Ravnsbæk, K. Xiang, W. Xing, O. Borkiewicz, K. Wiaderek, P. Gionet, K. Chapman, P. Chupas, W. C. Carter, Y.-M. Chiang, ”Extended solid solution behavior and coherent transformations in nanoscale olivine cathodes” *Nano Letters***2014**, *14*,1484–1491.
2. Z. Li, D. B. Ravnsbæk, K. Xiang, C. Carter, Y.-M. Chiang, ”$Na_3Ti_2(PO_4)_3$ as a sodium bearing anode for high energy density aqueous rechargeable sodium-ion batteries”,*Electrochem. Comm.***2014**, *44*,12–15**.**
3. J. Niu, A. Kushima, X. Qian, L. Qi, K. Xiang, Y.-M. Chiang, J. Li, "In situ observation of random solid solution zone in LiFePO4 electrode", *Nano Letters* **2014,** 14(7) pp. 4005-4010DOI: 10.1021/nl501415b.
4. P. R. Cantwell, M. Tang, S. J. Dillon, J. Luo, G. S. Rohrer, M. P. Harmer, "Grain boundary complexions", (invited review), ActaMaterialia 62, 1 (2014).
5. J. C. Ye, Y. H. An, T. W. Heo, M. M. Biener, R. J. Nikolic, M. Tang, H. Jiang, Y. M. Wang, “Enhanced lithiation and fracture behavior of silicon mesoscale pillars via atomic layer coatings and geometry design”, *Journal of Power Sources* **2014**, 248, 447 – 456.
6. Z. Li, K. Xiang, W. Xing, C. Carter, Y.-M. Chiang, "Reversible Aluminum-Ion Intercalation in Prussian Blue Analogs and Demonstration of a High-Power Aluminum-Ion Asymmetric Capacitor", *Advanced Energy Materials* **2014**.

Phonon and Electron Transport in Pristine Two-Dimensional Layered Nanostructures and Heterostructures

PI: Prof. Cronin (University of Southern California)
Co-PI: Prof. Li Shi (UT Austin)

Program Scope

This program is aimed at elucidating the transport and conversion processes of energy carriers (phonons and electrons) in a new class of 2D materials with novel structures, functionalities, and properties. The structure-property relationships resulting from the proposed research can serve as the basis for designing high-performance electronic devices and energy conversion devices employing these 2D materials.

Recent Progress

Thermal Interface Conductance across a Graphene/Boron Nitride Heterojunction

We have recently measured the thermal transport across a graphene/hexagonal boron nitride (*h*-BN) interface by electrically heating the graphene and measuring the temperature difference between the graphene and BN using Raman spectroscopy, as illustrated in Figure 1.[1] Because the temperature of the graphene and BN are measured optically, this approach enables nanometer resolution in the cross-plane direction. A temperature drop of 60 K can be achieved across this junction at high electrical powers (14 mW). Based on the temperature difference and the applied power data, we determine the thermal interface conductance of this junction to be 7.4 x 10^6 W/m^2·K, which is below the 10^7–10^8W/m^2·K values previously reported for graphene/SiO_2 interface. This discrepancy is likely due to the interfacial residue and lateral heat flow, which has been neglected in our analysis thus far.

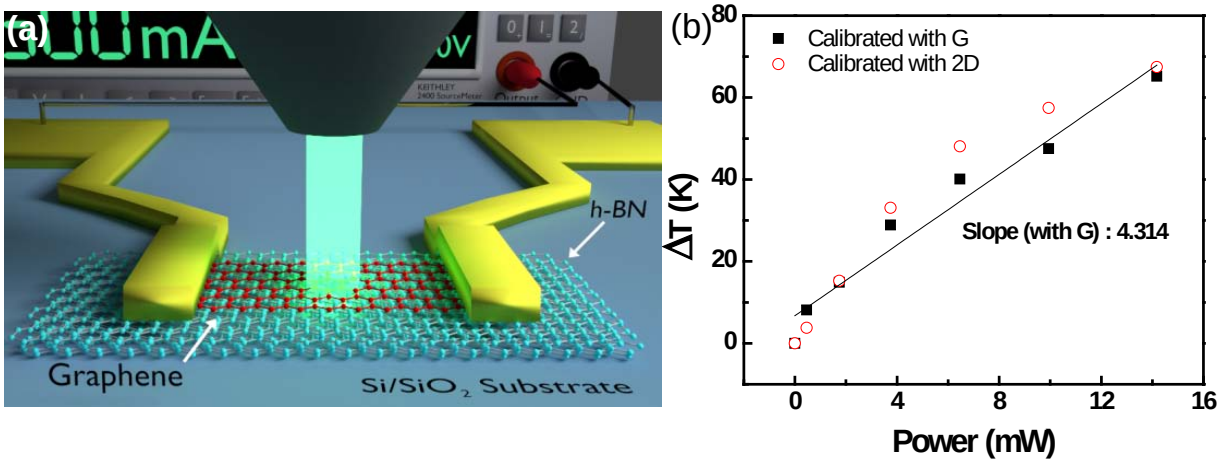

Figure 1. (a) Schematic diagram of the graphene/*h*-BN device and experiment setup. (b) Temperature difference across the interface of graphene/*h*-BN calibrated with the *2D*, *G* bands and BN optical phonon Raman frequencies plotted as a function of electrical heating power.

Thermoelectric Transport across Graphene/Boron Nitride/Graphene Heterostructures

We have also measured the thermoelectric transport across graphene/hexagonal boron nitride (*h*-BN)/graphene heterostructure devices.[2] Using an AC lock-in technique, we are able to separate the thermoelectric contribution to the *I*-*V* characteristics of these important device structures, as shown in Figure 2. The temperature gradient is measured optically using Raman spectroscopy, which enables us to explore thermoelectric transport produced at material interfaces, across length scales of just 1-2 nm. Based on the observed thermoelectric voltage (ΔV) and temperature gradient (ΔT), a Seebeck coefficient of 99.3 μV/K is ascertained for the heterostructure device. The obtained Seebeck coefficient can be useful for understanding the thermoelectric component in the cross-plane *I*-*V* behaviors of emerging 2D heterostructure devices. These results provide an approach to probing thermoelectric energy conversion in two-dimensional layered heterostructures.

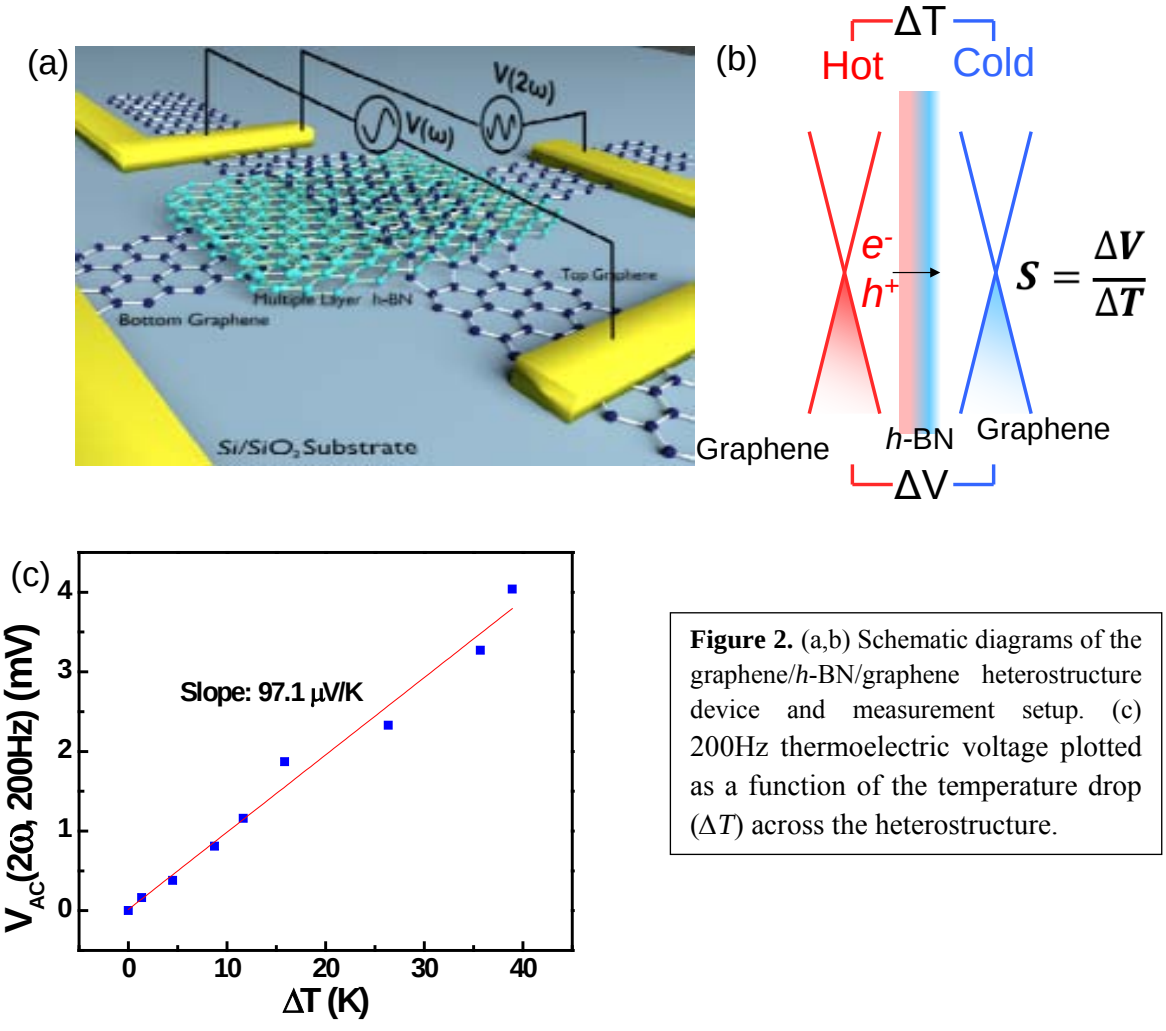

Figure 2. (a,b) Schematic diagrams of the graphene/*h*-BN/graphene heterostructure device and measurement setup. (c) 200Hz thermoelectric voltage plotted as a function of the temperature drop (Δ*T*) across the heterostructure.

Measurement of the Lateral Heat Flow in a Graphene/BN Heterojunction

For the graphene/BN device shown above in Figure 1, we assumed that the lateral heat flow was negligible and the primary heat dissipation was in the cross-plane direction because of the small vertical dimensions of the structure. However, Figure 3 shows the results of scanning thermal microscopy (SThM) of this device, which indicates that there is substantial heating extending laterally (~μm) beyond the edge of the graphene strip through the underlying BN flake. This extensive lateral transport arises because of the highly anisotropic thermal conductivities of the graphene and BN materials. In conjunction with thermal transport simulations, the obtained thermal images can be used to fully separate the vertical and in-plane heat transport in this system.

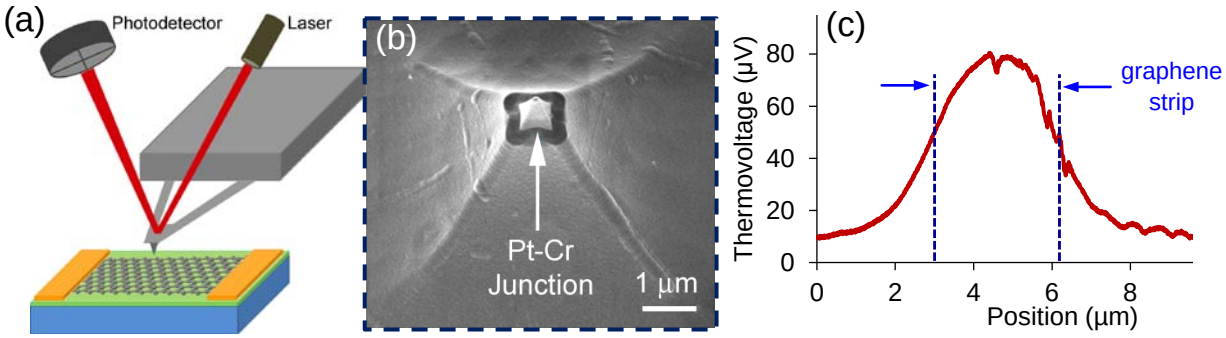

Figure 3: (a)Schematic diagram of scanning thermal microscope (SThM). (b) SEM image of SThM probe tip with nanoscale Pt-Cr thermocouple junction. (c) Thermovoltage measured across graphene strip under electrical heating conditions in BN substrate.

BulkDirect Band Gap MoS_2 by Plasma Induced Layer Decoupling

We have developed a robust method for engineering the optoelectronic properties of many-layer MoS_2 using a low energy oxygen plasma treatment.[3] Gas phase treatment of MoS_2 with oxygen radicals generated in an upstream N_2-O_2 plasma enhances the photoluminescence (PL) of many-layer, mechanically exfoliated MoS_2 flakes by up to 20 times, without reducing the layer thickness of the material, as shown in Figure 4. A blue shift in the photoluminescence spectra and narrowing of linewidth is consistent with a transition of MoS_2 from indirect to direct band gap material. Atomic force microscopy and Raman spectra reveal that the flake thickness actually increases as a result of the plasma treatment, indicating an increase in the interlayer separation in MoS_2. Ab-initio calculations reveal that the increased interlayer separation is sufficient to decouple the electronic states in individual layers, leading to a transition from an indirect to direct gap semiconductor. With optimized plasma treatment parameters, we observed enhanced PL signals for 32 out of 35 many-layer MoS_2 flakes (2-15 layers) tested, indicating this method is robust and scalable. Monolayer MoS_2, while direct band gap, has a small optical density, which limits its potential use in practical devices. The results presented here provide a

material with the direct band gap of monolayer MoS_2, without reducing sample thickness, and hence optical density.

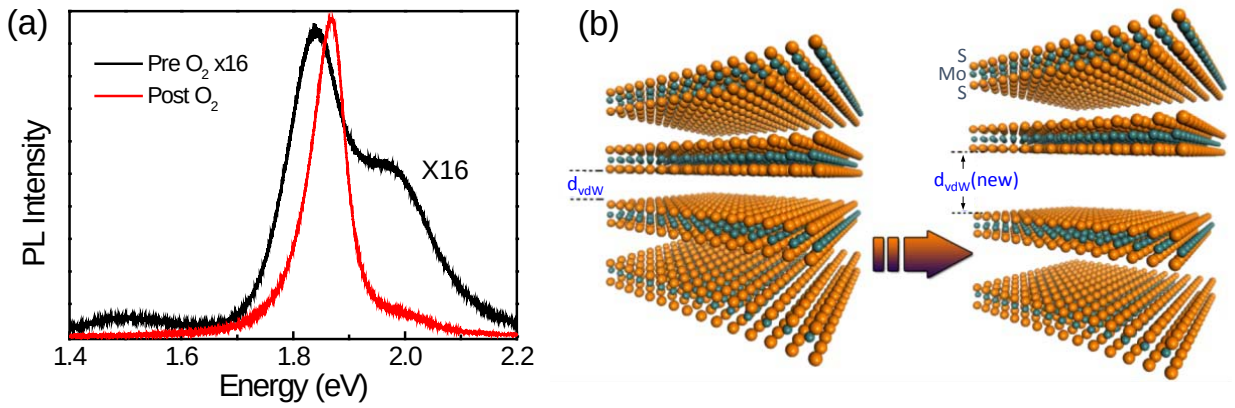

Figure 4.(a) Photoluminescence spectra before and after oxygen plasma treatment, plotted on different Y scales, highlighting the blue shift of the A exciton, the narrowing of the spectral linewidth, and the emergence of the asymmetry in PL lineshape after plasma treatment at 300K. (b) Atomistic structure of a bulk MoS_2 with the equilibrium vdW gap, d_{vdw}, and the modified vdW gap, d_{vdw} (new).

Future Plans

During the remaining funding period of this project, we will investigate non-equilibrium thermoelectric transport in graphene/transition metal dichalcogenide heterostructures. Thermal simulations will be carried out in order to separate the cross-plane and in-plane thermal transport characteristics from our experimental measurements.

References

1. Chen, C.-C., Z. Li, L. Shi and S.B. Cronin, *Thermal interface conductance across a graphene/hexagonal boron nitride heterojunction.* Applied Physics Letters, **104**, 081908 (2014).
2. Chen, C.-C., Z. Li, L. Shi and S.B. Cronin, *Thermoelectric Transport Across Graphene/Hexagonal Boron Nitride/Graphene Heterostructures.* Nano Research, **8**, 666 (2014).
3. Dhall, R., M.R. Neupane, D. Wickramaratne, M. Mecklenburg, Z. Li, C. Moore, R.K. Lake and S. Cronin, *Direct Band Gap Transition in Many-Layer MoS_2 by Plasma Induced Layer Decoupling* Advanced Materials, DOI:10.1002/adma.201405259 (2015).

Publications

"Direct Band Gap Transition in Many-Layer MoS_2 by Plasma Induced Layer Decoupling"
Rohan Dhall, Mahesh R. Neupane, Darshana Wickramaratne, Matthew Mecklenburg, Zhen Li, Cameron Moore, Roger K. Lake, and Stephen B. Cronin, *Advanced Materials*, DOI:10.1002/adma.201405259 (2015)

"Thermoelectric Transport across Graphene/Hexagonal Boron Nitride/Graphene Heterostructures"
Chun-Chung Chen, Zhen Li, Li Shi, and Stephen B. Cronin, *Nano Research*, 8, 666 (2014)DOI:10.1007/s12274-014-0550-8

"Clamping Instability and van der Waals Forces in Carbon Nanotube Mechanical Resonators"
Mehmet Aykol, Bingya Hou, Rohan Dhall, Shun-Wen Chang, William Branham, Jing Qiu, and Stephen Cronin, *Nano Letters*, 14, 2426-2430, (2014) DOI**:** 10.1021/nl500096p

"Enhanced photocurrent and photoluminescence spectra in MoS_2 under ionic liquid gating"
Zhen Li, Shun-Wen Chang, Chun-Chung Chen, and Stephen B. Cronin, *Nano Research*, 7, 973-980, (2014) DOI: 10.1007/s12274-014-0459-2

"Thermal interface conductance across a graphene/hexagonal boron nitride heterojunction"
Chun-Chung Chen, Zhen Li, Li Shi, and Stephen B. Cronin, *Applied Physics Letters*, 104, 081908 (2014) DOI: 10.1063/1.4866335

"Non-ideal Diode Behavior and Band Gap Renormalization in Carbon Nanotube P-N Junctions"
Shun-Wen Chang, Kevin Bergemann, Rohan Dhall, Jeramy Zimmerman, Stephen Forrest, Stephen Cronin, *IEEE Transactions on Nanotechnology*, 13, 41 (2014) DOI:10.1109/TNANO.2013.2287124

"Zener Tunneling and Photocurrent Generation in Quasi-Metallic Carbon Nanotube pn-Devices
Moh. R. Amer, Shun-Wen Chang, Rohan Dhall, Jing Qiu, and Stephen Cronin, *Nano Letters*, 13, 5129 (2013) **DOI:** 10.1021/nl402334e

"Evidence for structural phase transitions and large effective band gaps in quasi-metallic ultra-clean suspended carbon nanotubes"
Shun-Wen Chang, Rohan Dhall, Moh Amer, Kentaro Sato, Riichiro Saito, Stephen Cronin, *Nano Research*, 6, 736 (2013) DOI:10.1007/s12274-013-0351-5

Proximity Effects in Charged Oxide Heterostructures

PIs: J.A. Eastman, D.D. Fong, P.H. Fuoss, M.J. Highland, P. Zapol
Materials Science Division
Argonne National Laboratory
9700 S. Cass Ave., Bldg 241
Argonne, IL 60439
630-252-5141, jeastman@anl.gov

Program Scope: The goal of this program is to understand and thereby control defect behavior in oxide heterostructures. We perform *in situ* synchrotron x-ray studies of thin film synthesis and heterostructure behavior in controlled environments, complemented by first-principles simulations and multiscale computational theory to reveal the effects of interfacial proximity on defect behavior and the resulting electrochemical properties. In recent years, it has become clear that many of the remarkable properties discovered in the field of complex oxide heterostructures may be related to charged defects and their behavior at interfaces. Such phenomena, however, remain poorly understood due to the inherent difficulties in probing defect-interface interactions at the atomic-level and in the environments relevant to defect evolution. We address this problem by growing heterostructures with precise cation ordering and variable oxygen concentrations, enabling the systematic investigation of defect formation and migration behavior both during synthesis and while processing in different electrochemical environments. Throughout this program, the atomistic results are fed back to computational theory to gain insight into the mechanisms and the electronic and energetic processes taking place during defect structure evolution. Through this combined *in situ* x-ray / computational theory approach, our ultimate goal is to form a knowledge-basis of defect behavior, which will be analyzed for the discovery of descriptors that can enable large-scale predictions of interface-dependent defect transport kinetics and provide new insight for the design and synthesis of materials with tailored, tunable, and multifunctional defect-engineered properties.

Recent Progress: Our program is providing fundamental understanding in the areas of oxide thin film synthesis and defect interactions at charged surfaces and heterointerfaces. We recently designed and computationally tested model heterostructures with the potential to exhibit enhanced ionic conduction, with the results providing insight into the energetics that control ion distributions and the barriers to motion at heterointerfaces. Complementary experimental efforts using *in situ* synchrotron x-ray techniques to control and monitor epitaxial thin film heterostructure growth revealed remarkable effects of the chemical environment on thin film and surface phase transitions, and allowed an atomic-scale look into the mechanisms governing field-driven oxygen exchange behavior. In the following, we describe two brief highlights of recent growth studies, focusing in particular on investigating the effects of substrate surface polarity on the growth and properties of ferroelectric oxides, and on controlling and understanding the synthesis of layered oxide heterostructures by oxide molecular beam epitaxy.

Surface Polarity Effects on Epitaxial Thin Film Ferroelectric Behavior

The recent availability of new oxide single crystal substrates, exhibiting a wide range of lattice parameters, has resulted in exciting opportunities for tuning ferroelectric oxide thin film properties through control of the epitaxial strain. Theorists had previously predicted that the mechanical constraints imposed by different substrate lattice parameters result in large variations

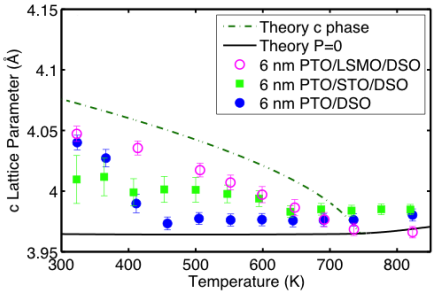

Fig. 1 *In situ* synchrotron X-ray observations revealed that the behavior of 6 nm thickness $PbTiO_3$ ferroelectric films depends strongly on the electrical boundary conditions imposed by the substrate surface.

in ferroelectric Curie temperatures, T_C, as well as ferroelectric domain structures below T_C, which have been confirmed experimentally. However, previous work had not considered the additional effects of substrate surface polarity on T_C and ferroelectric domain structure in films. We performed an *in situ* synchrotron X-ray study of epitaxial (001) $PbTiO_3$ (PTO) films grown on the polar (110) surface of $DyScO_3$ (DSO), with and without non-polar insulating or conducting intermediate layers chosen to systematically vary the electrical boundary conditions at the film-substrate interface. We discovered that the electrical boundary conditions imposed by the substrate surface result in different amounts of T_C suppression and different domain structures in 6 nm PTO films, as seen in Fig. 1 for 6 nm PTO films. The results were published in *Applied Physics Letters* [1]. The behavior we observed could significantly impact the performance of ferroelectric heterostructure devices, making it important to determine whether the behavior of ferroelectric films on DSO is general to all substrates with a polar bulk termination.

Dynamic Layer Rearrangement During Growth Of Layered Oxides by MBE

The $A_{n+1}B_nO_{3n+1}$ Ruddlesden-Popper compounds offer a wide variety of functionalities including dielectric, ferroelectric, magnetic and catalytic properties. Unfortunately, synthesis of such layered oxides has been a major challenge owing to the occurrence of growth defects that result in poor materials behavior. To understand the fundamental physics of layered oxide growth, we have developed an oxide molecular beam epitaxy system with *in situ* synchrotron X-ray scattering capability. We discovered that layered oxide films can dynamically rearrange during growth (Fig. 2(a,b)), leading to structures that are highly unexpected on the basis of the intended layer sequencing. Theoretical calculations indicated that such rearrangements can occur in many oxide systems and suggested a new strategy that may be essential for the construction of metastable Ruddlesden–Popper phases. We demonstrated the utility of the new-found growth strategy by performing the first atomically controlled

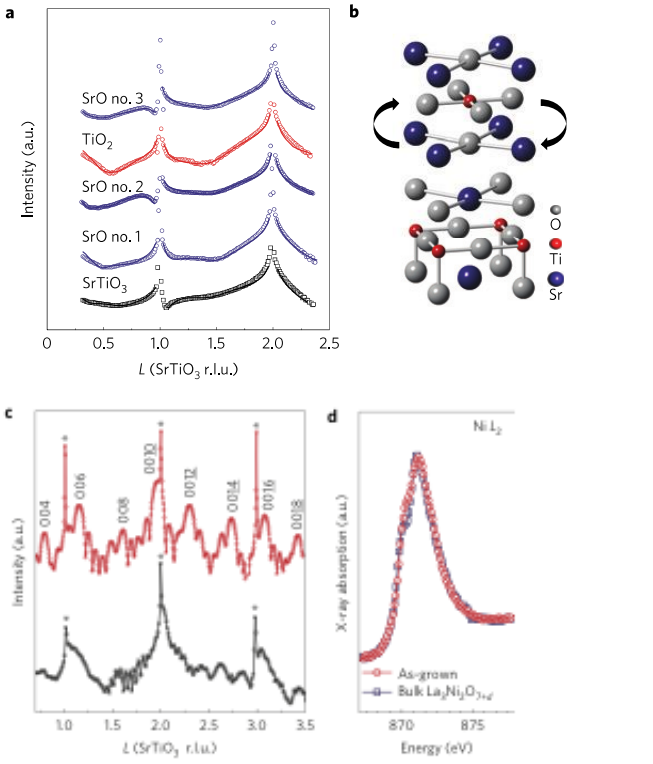

Fig. 2 (a) *In situ* surface X-ray diffraction measured after the growth of each atomic plane for Sr_2TiO_4. (b) Schematic illustrating the layer rearrangement. (c) $La_3Ni_2O_7$ grown using the new growth strategy accounting for layer rearrangement. (d) Near-edge absorption spectroscopy showing that Ni in the film has the proper oxidation state.

synthesis of single-crystalline $La_3Ni_2O_7$ (Fig. 2(c,d)). The results were published in *Nature Materials* [2]. The synthesis methodology used here, coupling quantitative *in situ* X-ray scattering with computational theory, is an approach that can be readily extended to the construction of a variety of new materials with enhanced properties.

Future Plans: Our planned research explores promising opportunities for creating and characterizing new oxide heterostructures possessing enhanced material properties through control of heterointerfacial charge. Two examples of planned and on-going research are briefly described in the following.

Oxygen exchange at surfaces and interfaces in epitaxial thin film oxide heterostructures

We are investigating the behavior of model mixed conducting epitaxial oxide thin film heterostructures, including ones comprised of $La_{1-x}Sr_xCo_xFe_{1-x}O_3$ (LSCF), Gd_2O_3-doped CeO_2 (GDC), and Y_2O_3-stabilized ZrO_2 (YSZ). These studies build on our previous *in situ* x-ray studies of such heterostructures, through which we were able to provide unique insight into rate-limiting oxygen exchange behavior [3]. We are focusing on elucidating the effects of variables such as temperature, oxygen partial pressure, water vapor partial pressure, epitaxial strain, field magnitude and direction, as well as coupled variable effects on defect-interface interactions.

Preliminary results from a synchrotron x-ray study illustrating transient behavior during field-induced oxygen transport through an ionically conducting heterostructure are shown in Fig. 3. With our *in situ* x-ray chamber, we measured changes in the LSCF out-of-plane lattice parameter and conductance with a time resolution of 100 ms for a LSCF/GDC/YSZ heterostructure under a cathodic potential. Analogous to electrical conductivity relaxation experiments, the transition from an initial state to a final (steady) state can be described with a characteristic time constant. Here, however, the dependent variable is the change in lattice parameter, which can be related to the average oxygen vacancy concentration through the chemical expansivity [4]. For a 60-nm-thick LSCF film, the time-dependent behavior can be attributed primarily to oxygen exchange behavior at the LSCF surface. From a fit to the transient data shown in Fig. 3, we determined a surface exchange coefficient of 1×10^{-5}cm/s, which is in reasonable agreement with values deduced by other methods [5]. Using these *in situ* techniques, we are probing how surface exchange behavior evolves in response to a variety of factors including oxygen partial pressure, surface adsorbates such as water vapor or other reactive gases, temperature, film thickness, epitaxial strain state, and film and surface composition.

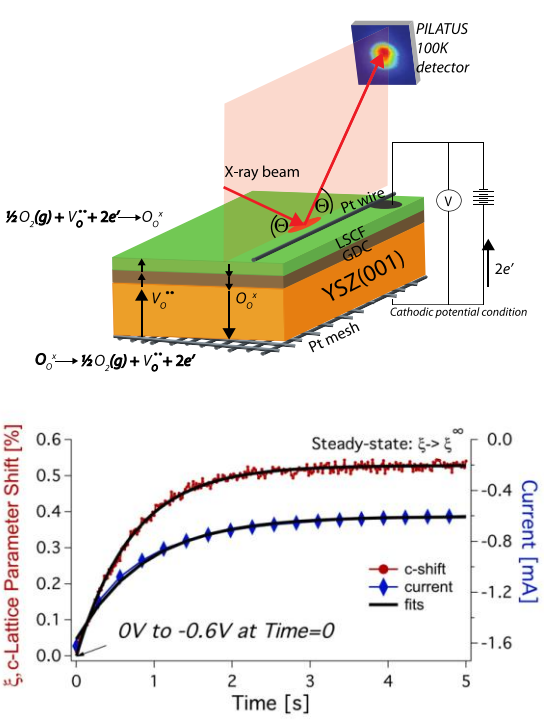

Fig. 3 (Top) Schematic of the sample and electrode configuration used for *in situ* x-ray studies of oxygen exchange behavior in thin film LSCF/GDC/YSZ heterostructures. (bottom) Out-of-plane lattice parameter shift and current transient in response to application of a 0.6 V cathodic potential at time = 0 with the sample at 500°C in a pO_2 = 15 Torr environment.

Reversible phase transitions in $SrRuO_{3-\square}$

We have also begun studies of the redox behavior of oxide surfaces in liquid environments, as necessary for understanding many electrocatalytic processes. The reactions of interest include the oxygen reduction reaction (ORR) and oxygen evolution reaction (OER), for which there is little understanding of the possible relationships between phase stability and activity. Since the reactions are electrochemically driven, the oxide must be at least partially conducting, and we have begun our studies by examining the behavior of single crystal surfaces of conducting $SrRuO_{3-\delta}$ and $LaNiO_{3-\delta}$ grown on conducting Nb-doped $SrTiO_3$ substrates. From our initial studies, we found that while both materials are electrocatalytically active for either OER or ORR, an equally important consideration is stability, as the activity tends to decrease with time, which is correlated with dissolution of the film [6]. As shown in Fig. 4, we also observe huge (~ 1% or larger, depending on conditions), reversible changes in lattice parameter with applied field, with an abrupt expansion along the out-of-plane direction occurring at -0.9 V. While some of the changes are due to electrostrictive effects, the time dependence indicates that much of it is due to ionic effects such as the reversible ejection and incorporation of oxygen from the anionic sublattice. In fact, we find that we can use ionic gating to reversibly drive a phase transition between $SrRuO_3$ and $SrRuO_{2.5}$ phases. We are carrying out a detailed study of these reversible effects at liquid-oxide interfaces, examining in particular the dynamics of oxygen exchange. Multiple *in situ* x-ray scattering and spectroscopic techniques are being used to isolate the mechanisms for both catalytic activity and instability. From these electrochemical studies, we will obtain a detailed understanding of the effects of redox processes on oxide surfaces and the atomistic mechanisms governing reversibility, stability, catalytic activity, and phase change behavior during field-driven defect exchange.

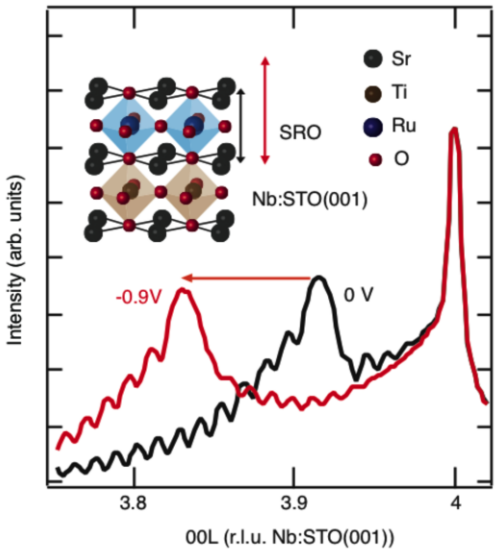

Fig. 4 Lattice modulation of SRO caused by ionic gating effect. The inset shows SRO structures at 0V (black) and -0.9 V (red).

References

1. M.J. Highland, D.D. Fong, G.B. Stephenson, T.T. Fister, P.H. Fuoss, S.K. Streiffer, Carol Thompson, M.-I. Richard and J.A. Eastman, *Appl. Phys. Lett.* **104**, 132901 (2014).
2. J.H. Lee, G. Luo, I.C. Tung, S.H. Chang, Z. Luo, M. Malshe, M. Gadre, A. Bhattacharya, S.M. Nakhmanson, J.A. Eastman, H. Hong, J. Jellinek, D. Morgan, D.D. Fong, J.W. Freeland, *Nature Materials*, **13**, 879 (2014).
3. B.J. Ingram, J.A. Eastman, K.-C. Chang, S.K. Kim, T.T. Fister, E. Perret, H. You, P.M. Baldo, P.H. Fuoss, *Appl. Phys. Lett.*, **101**, 051603 (2012).
4. X.Y. Chen, J.S. Yu, S.B. Adler, *Chem. Mater.*, **17**,4537 (2005).
5. A. Zomorrodian, H. Salamati, Z.G. Lu, X. Chen, N.J. Wu, A. Ignatiev, *Int. Jn. Hydrogen Energy*, **35**,12443 (2010).
6. S.H. Chang, N. Danilovic, K.-C. Chang, R. Subbaraman, A.P. Paulikas, D.D. Fong, M.J. Highland, P.M. Baldo, V.R. Stamenkovic, J.W. Freeland, J.A. Eastman, N.M. Markovic, *Nature Comm.*, **5**, 4191 (2014).

BES Sponsored Publications (2013-2015)

1) R. L. Johnson-Wilke, R.H.T. Wilke, C.B. Yeager, D. S. Tinberg, I. M. Reaney, I. Levin, D. D. Fong, and S. Trolier-McKinstry, "Phase transitions and octahedral rotations in epitaxial $Ag(Ta_xNb_{1-x})O_3$ thin films under tensile strain," (accepted for publication in J. Appl. Phys.)

2) H. Zhou and D. D. Fong, *In situ X-ray Scattering of Epitaxial Oxide Thin Films*, A chapter in Epitaxial Growth of Complex Metal Oxides, Eds. G. Koster, G. Rijnders, and M. Huijben, Woodhead Publishing (Elsevier) (2015).

3) B.W. Veal, P.M. Baldo, A.P. Paulikas, J.A. Eastman, "Understanding Artifacts in Impedance Spectroscopy," *J. Electrochem. Soc.*, **162**, H47 DOI: 10.1149/2.0791501jes (2015)

4) J.-H. Lee, G. Luo, I-C. Tung, S. H. Chang, Z. Luo, M. Malshe, M. Gadre, A. Bhattacharya, S. M. Nakhmanson, J. A. Eastman, H. Hong, J. Jellinek, D. Morgan, D. D. Fong, and J. W. Freeland, "Dynamic layer rearrangement during growth of layered oxide films by molecular beam epitaxy," Nature Mater. DOI: 10.1038/nmat4039 (2014).

5) S.-H. Chang, R. Subbaraman, K.-C. Chang, N. Danilovic, A. P. Paulikas, D. D. Fong, M. J. Highland, P. M. Baldo, V. R. Stamenkovic, J. W. Freeland, J. A. Eastman, and N. M. Markovic, Functional links between stability and reactivity of strontium ruthenate single crystals during the oxygen evolution, Nature Comm. **5**, 4191 DOI: 10.1038/ncomms5191 (2014).

6) K. Chen, W.J. Meng, J.A. Eastman, "Interface Development in Cu-Based Structures Transient Liquid Phase (TLP) Bonded with Thin Al Foil Intermediate Layers," Metal. Mater. Trans. A, **45A**, no. 9, 3892-3906, DOI: 10.1007/s11661-014-2339-5 (2014).

7) M.J. Highland, D.D. Fong, G.B. Stephenson, T.T. Fister, P.H. Fuoss, S.K. Streiffer, C. Thompson, M.I. Richard, J.A. Eastman, "Interfacial Charge and Strain Effects on the Ferroelectric Behavior of Epitaxial (001) $PbTiO_3$ films on (110) $DyScO_3$ Substrates," Appl. Phys. Lett., **104**, no. 13, 132901, DOI: 10.1063/1.4869579 (2014).

8) S.H. Chang, J. Kim, C. Phatak, K. D'Aquila, S.K. Kim, J. Kim, S.J. Song, C.S. Hwang, J.A. Eastman, J.W. Freeland, S. Hong, "X-ray Irradiation Induced Reversible Resistance Change in Pt/TiO_2/Pt Cells, ACS Nano, **8**, no. 2, 1584-1589, DOI: 10.1021/nn405867p (2014).

9) T.T. Fister, H. Zhou, Z. Luo, S.S.A. Seo, S.O. Hruszkewycz, D.L. Proffit, J.A. Eastman, P.H. Fuoss, P.M. Baldo, H.N. Lee, D.D. Fong, "Octahedral rotations in in strained $LaAlO_3$/$SrTiO_3$ heterostructures," *APL Materials*, **2**, 021102 (2014), DOI: 10.1063/1.4865160

10) R. Mishra, Y.-M. Kim, J. Salafranca, S. K. Kim, S. H. Chang, A. Bhattacharya, D. D. Fong, S. J. Pennycook, S. T. Pantelides, and A. Y. Borisevich, "Oxygen-vacancy-induced polar behavior in $(LaFeO_3)_2$/$(SrFeO_3)$ superlattices," *Nano Lett*. **14,** 2694 (2014), DOI: dx.doi.org/10.1021/nl500601d

11) T.M. McCleskey, P. Shi, E. Bauer, M.J. Highland, J.A. Eastman, Z.X. Bi, P.H. Fuoss, P.M. Baldo, W. Ren, B.L. Scott, A.K. Burrell, and Q.X. Jia, "Nucleation and growth of epitaxial metal-oxide films based on polymer-assisted deposition," *Chemical Society Reviews*, **43**, 2141 (2014), DOI:10.1039/c3cs60285k.

12) A. Rebola, R.F. Klie, P. Zapol, S. Ogut, "Phonon and thermal transport properties of the misfit-layered oxide thermoelectric $Ca_3Co_4O_9$ from first principles," *Appl. Phys. Lett.*, 251910, (2014), DOI: 10.1063/1.4885389

13) M. D. Biegalski, Y. Takamura, A. Mehta, Z. Gai, S. V. Kalinin, H. Ambaye, V. Lauter, D. D. Fong, S. T. Pantelides, Y. M. Kim, J. He, A. Borisevich, W. Siemons, and H. M. Christen, Interrelation between Structure-Magnetic Properties in $La_{0.5}Sr_{0.5}CoO_3$," *Adv. Mater. Interfaces* **1,** 1400203 (2014), DOI: 10.1002/admi.201400203

14) Z. L. Luo, H. Huang, H. Zhou, Z. H. Chen, Y. Yang, L. Wu, C. Zhu, H. Wang, M. Yang, S. Hu, H. Wen, X. Zhang, Z. Zhang, L. Chen, D. D. Fong, and C. Gao, "Probing the domain structure of $BiFeO_3$ epitaxial films with three-dimensional reciprocal space mapping," *Appl. Phys. Lett*. **104,** 182901 (2014), DOI: 10.1063/1.4875579

15) R.L. Johnson-Wilke, D.S. Tinberg, C. Yeager, W. Qu, D.D. Fong, T.T. Fister, S.K. Streiffer, Y. Han, I.M. Reaney, and S. Trolier-McKinstry, "Coherently strained epitaxial $Pb(Zr_{1-x}Ti_x)O_3$ thin films," *Journal of Applied Physics*, **114**, (2013), DOI:10.1063/1.4825215.

16) H. Jeen, W.S. Choi, M.D. Biegalski, C.M. Folkman, I.-C. Tung, D.D. Fong, J.W. Freeland, D. Shin, H. Ohta, M.F. Chisholm, and H.N. Lee, "Reversible redox reactions in an epitaxially stabilized $SrCoO_x$ oxygen sponge," *Nature Materials*, **12**, 1057 (2013), DOI:10.1038/nmat3736.

17) A. Rébola, D.D. Fong, J.A. Eastman, S. Öğüt, and P. Zapol, "First-principles study of compensation mechanisms in negatively charged $LaGaO_3/MgAl_2O_4$ interfaces," *Physical Review B*, **87**, 245117 (2013), DOI:10.1103/PhysRevB.87.245117.

18) Surface diffraction on a ψ-circle diffractometer using the χ-axis geometry, T.T. Fister, P.H. Fuoss, D.D. Fong, J.A. Eastman, C.M. Folkman, S.O. Hruszkewycz, M.J. Highland, H. Zhou, and P. Fenter, *Journal of Applied Crystallography*, **46**, 639 (2013), DOI:10.1107/S0021889813007693.

19) S. O. Hruszkewycz, M. J. Highland, M. V. Holt, D. Kim, C. M. Folkman, C. Thompson, A. Tripathi, G. B. Stephenson, S. Hong, and P. H. Fuoss, "Imaging Local Polarization in Ferroelectric Thin Films by Coherent X-Ray Bragg Projection Ptychography," *Phys. Rev. Lett.*, **110**, 177601 (2013), doi:10.1103/PhysRevLett.110.177601.

20) C.M. Folkman, M.J. Highland, E. Perret, S.K. Kim, T.T. Fister, H. Zhou, P.M. Baldo, S. Seifert, J.A. Eastman, P.H. Fuoss, and D.D. Fong, "Modular instrument mounting system for variable environment in operando X-ray experiments," *Review of Scientific Instruments*, **84**, 025111 (2013), DOI:10.1063/1.4791799.

21) E. Perret, C. Park, D.D. Fong, K.-C. Chang, B.J. Ingram, J.A. Eastman, P.M. Baldo, and P.H. Fuoss, "Resonant X-ray scattering studies of epitaxial complex oxide thin films," *Journal of Applied Crystallography*, **46**, 76 (2013), DOI:10.1107/S0021889812047620.

Atomic and Mesoscopic Study of Metallic Glasses

T. Egami (egami@utk.edu)
Joint Institute for Neutron Sciences, University of Tennessee, Knoxville, TN 37996
Oak Ridge National Laboratory, Oak Ridge, TN 37831

Program Scope

The overarching goal of this project is to gain a fundamental understanding of metallic liquids and glasses that will enable the development of new bulk metallic glasses (BMG) with superior properties. Metallic glasses have exceptionally high strength owing to the strongly disordered atomic structure, and they have excellent potential for improving the efficiency of energy production, storage and utilization when applied as structural materials. However, the basic science of metallic glasses at the atomistic level remains poorly developed. In this program we establish a fundamental understanding of atomistic mechanisms which control the structural and dynamic properties of metallic liquids and glasses through combination of tightly coupled simulation, theory and experiment. We use a novel approach, based upon the concept of atomic-level stresses and fluctuations in the local topology of atomic connectivity network. The computational effort includes classical and first-principles molecular dynamics (MD) simulation. Experimental studies include neutron and synchrotron x-ray scattering and nanoscale mechanical testing. Based upon our recent breakthrough in understanding the origins of mechanical properties of liquids and glasses we develop a general atomistic theory of deformation, dynamics and the glass transition in metallic glasses, which will guide us to the development of metallic glasses with superior properties, including high ductility. Our long-range goal is to ultimately contribute to the development of the general physics of liquids and glasses.

Recent Progress

1. Elementary Excitation and Origin of Viscosity in Liquid

Viscosity is a most fundamental property of a liquid. Yet, its atomistic origin has not been well understood. Through molecular dynamics (MD) simulations we discovered that the origin of viscosity is the fluctuations in local topology of atomic connectivity. We found that for high-temperature metallic liquids the Maxwell relaxation time, $\tau_M = \eta/G_\infty$, where η is viscosity and G_∞ is the high-frequency shear modulus, is equal to τ_{LC},the time for an atom to lose or gain one neighbor [P2]. This equality was confirmed by classical as well as quantum mechanical MD for various compositions (Fig. 1). Because phonons are overdamped in liquids the action of losing or gaining one neighbor, thus changing the topology of atomic

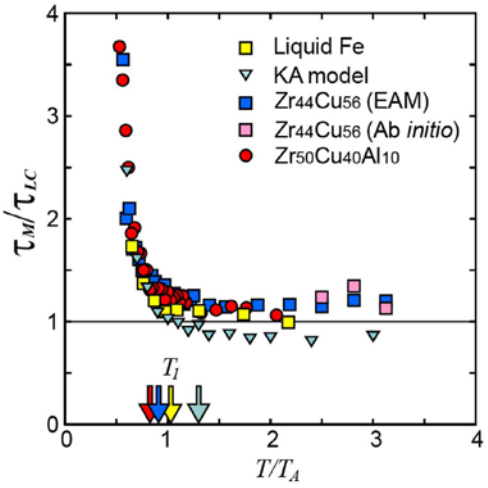

Fig. 1 The ratio of the Maxwell relaxation time, τ_M, to the time for an atom to lose or gain one neighbor, τ_{LC}, against T/T_A where T_A is the crossover temperature, showing $\tau_M = \tau_{LC}$for $T>T_A$ [P2].

connectivity network, is the elementary excitation in the high-temperature liquid. We named this excitation "anankeon" [P17] after Ananke, Greek Goddess of force, constraint and destiny. The equality, $\tau_M = \tau_{LC}$, is valid only above the crossover temperature $T_A$where phonons are localized due to dynamic disorder [P2]. Below $T_A$anankeons are no longer independent and interact through the stress field [P21]. Consequently τ_M/τ_{LC} is greater than unity and viscosity rapidly increases, resulting in the glass transition. The stress correlation function has the symmetry of the Eshelby field for elastic inclusion [1], except that it is characterized by oscillations similar to the atomic pair-density function (PDF)(Fig. 2). Now the Eshelby field has the $1/r^2$ dependence on r, the distance from the center of the inclusion. However, the stress correlation is screened in the form of

$$A(r) = (1/r^2)\exp(-r/\xi) \quad (1)$$

whereξ is the screening length which depends on temperature as

$$\xi(T) = \xi_0 \left(T_0/(T-T_0)\right)^{-\nu} \quad (2)$$

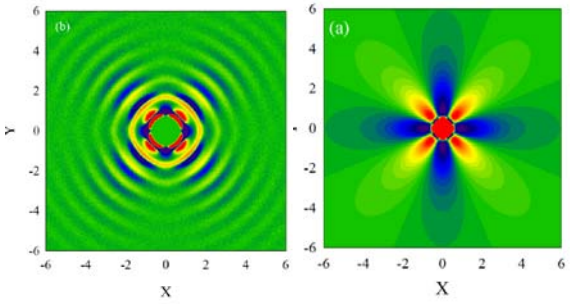

Fig. 2 Anisotropic correlation function of the atomic-level shear stresses(left) and the Eshelby field due to elastic inclusion (right) [P21].

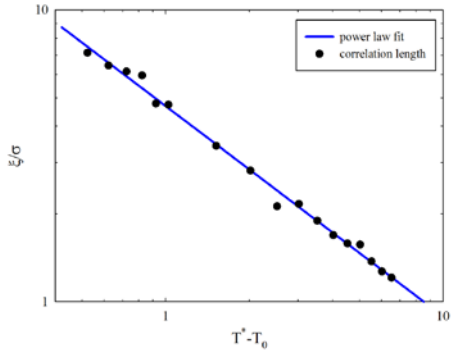

Fig. 3 Temperature dependence of the stress field screening length, ξ [P21].

whereT_0 is close to the glass transition temperature T_g(Fig. 3) [P21]. The results suggest that the Eshelby field adds to the driving force to form medium-range order which contributes to the increase in viscosity. We are studying the nature of such medium-range order.

2. Trigger Mechanism of Mechanical Deformation

Mechanical deformation in crystals occurs due to the motion of structural topological defects such as dislocations. However, in metallic glasses defects cannot be defined topologically because the local topology of a glass is open. Instead, some localized atomic rearrangements, called shear-transformation-zones (STZs) [2,3], are supposed to induce local plastic deformation. However, the nature of STZs has been controversial. For instance the estimate of its size ranges from 20 to 300 atoms. We used the activation-

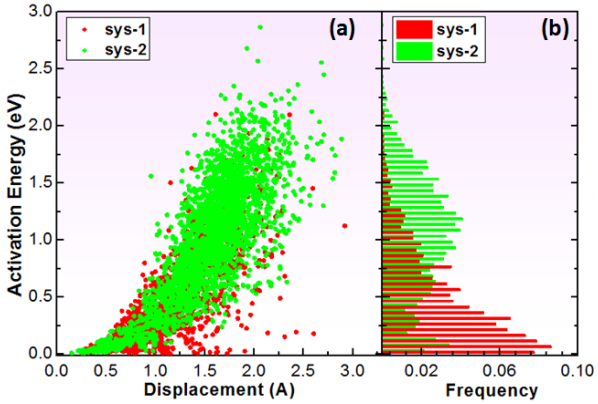

Fig. 4The ratio, τ_M/τ_{LC}, is nearly unity for $T>T_A$, suggesting that the LCE determines the viscosity of a liquid [P14].

relaxation technique (ART) to simulate the STZ, focusing on the state at the saddle point of the potential energy landscape (PEL) [P14]. We prepared two model systems of Cu-Zr glass, an unstable system prepared by rapid quench from the liquid state (Sys-1) and a more stable system obtained by slow cooling (Sys-2). Sys-1 showed a continuous spectrum of activation energies, whereas Sys-2 had a pseudo-gap in the activation energy spectrum (Fig. 4 (b)). But they were characterized by the identical quadratic relation between the activation energy and the maximum displacement, suggesting that the elastic self-energy accounts for the activation energy (Fig. 4 (a)). They also had the same distribution of the number of atoms involved, averaging only *about five* (Fig. 5). These results suggest that some universal mechanism, independent of thermal history, is in operation, and the only difference among samples is the density of the STZs [P13].

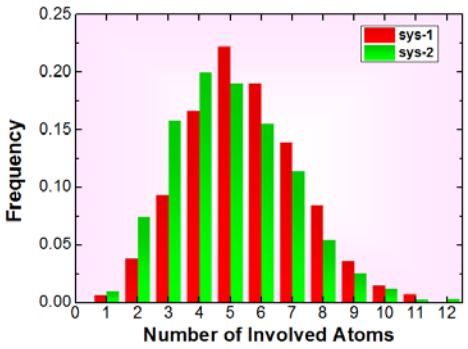

Fig. 5The distribution of the number of atoms involved in the STZ [P14]. For definition see P14.

3. Universal Mechanism of Thermomechanical Creep Deformation

Similar universality was observed also for thermo-mechanical creep measurement using high-energy x-ray diffraction [P22]. The structure function of a sample subjected to creep deformation is anisotropic,

$$S(\boldsymbol{Q}) = \sum_{\ell,m} S_\ell^m(Q) Y_\ell^m(\boldsymbol{Q}/Q) \quad (3)$$

where Y_ℓ^m is the spherical harmonics, due to internal anelastic deformation. We found that the anisotropic $S(Q)$ has the universal shape, regardless of the length of time, stress, and the direction of deformation (tensile or compressive) as shown in Fig. 6. This suggests the presence of a universal mechanism of anelastic deformation. We are working to identify such a mechanism by simulation.

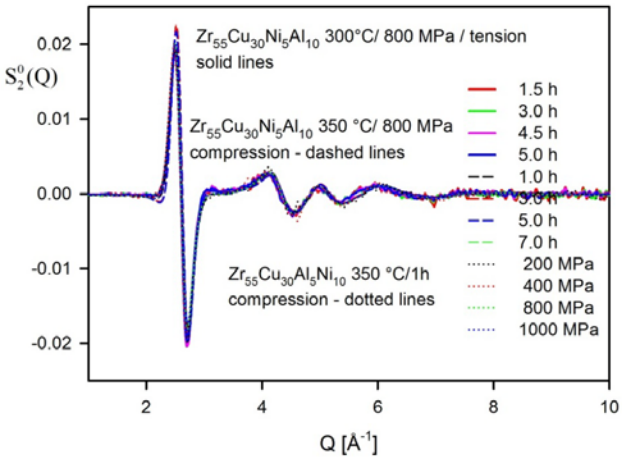

Fig. 6 Anisotropic structure function $S_2^0(Q)$ for BMG after creep at various lengths of time, stress and tension/compression [P22].

4. Nano-mechanical Probing of Structural Heterogeneity

A lack of macroscopic ductility and brittle fracture presents the major barrier for wide-spread application of metallic glasses. We employed nano-mechanical testing to investigate structural information for a metallic glass and developed a stochastic model to describe the structural heterogeneity ("defect" strength and distribution) in BMG [P6]. From more than 100 nano-indentation pop-in tests in each sample, the cumulative pop-in probability curves were generated as a function of the maximum shear stress, τ_{max}, as shown in Fig. 7. The metallic glass annealed

at 300 °C has the narrowest distribution of τ_{max}, whereas the as-cast samples have the τ_{max} values more widely distributed. We proposed a structural model of the metallic glass consists of a relaxed glass matrix with randomly distributed defects [P6]. In our model we quantify the structural heterogeneity by the defect density ρ_{def}. We find that ρ_{def} decreases by almost two orders of magnitude with the structural relaxation. We will relate this defect density to the STZ density and the effective temperature.

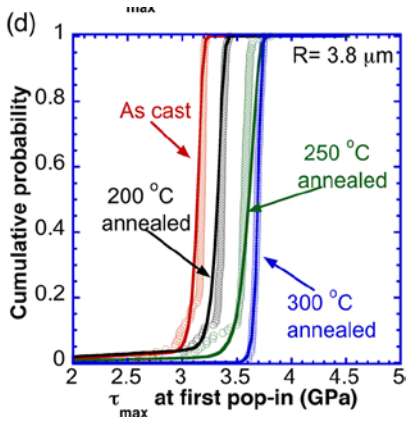

Fig. 7Cumulative pop-in probability vs. τ_{max} curve. Open circles: experimental measurements, solid curves: theoretical prediction [P6].

Future Plans

Our work on the stress correlations in the liquid suggests the growing medium-range order as a liquid is supercooled. We suspect a strong similarity of this medium-range order to the polar nano-regions (PNRs) which develop in relaxor ferroelectrics [4]. Even though the metallic liquids are non-polar, local nematic order could develop. We will identify such an order by simulation, and determine it by diffraction experiment using coherent x-rays. We also will work on identifying the universal mechanism of deformation suggested by our work. We recently discovered a surprising relationship between mechanical ductility and the structural response of BMG to applied tensile or compressive stress, determined by high-energy x-ray diffraction using the anisotropic PDF analysis. The deviation in the anisotropic PDF from the affine behavior describes anelastic response [5]. We discovered that the intensity of deviation, thus the intensity of anelasticity, is related to ductility; higher the anelasticity more ductile it is.We are now studying what feature contributes most to anelasticity, such as covalency (Poisson's ratio), atomic size ratio, effective temperature, etc., and are trying to design more ductile glasses. Because the lack of ductility is the greatest drawback of BMG overcoming this problem is an important task. We are also expanding the work on stress correlations to multi-component glasses and trying to find medium-range order that relates to the increase in viscosity with lowering temperature.

References

1. J. D. Eshelby, "The determination of the elastic field of an ellipsoidal inclusion, and related problems", *Proc. Roy. Soc. LondonA***241**, 376 (1957).
2. A. S. Argon, "Plastic deformation in metallic glasses", *Acta Metall.***27,** 47 (1979).
3. M. L. Falk and J. S. Langer, "Dynamics of viscoplastic deformation in amorphous solids", *Phys. Rev. E***57,** 7192 (1998).
4. I.-K. Jeong, T. W. Darling, J. K. Lee, T. Proffen, R. H. Heffner, J. S. Park, K. S. Hong, W. Dmowski and T. Egami, "Direct Observation of the Formation of Polar Nanoregions in $Pb(Mg_{1/3}Nb_{2/3})O_3$ using Neutron Pair Distribution Analysis", *Phys. Rev. Lett.,***94**, 147602 (2005).
5. W. Dmowski, T. Iwashita, C.-P. Chuang, J. Almer and T. Egami, "Elastic Heterogeneity in Metallic Glasses", *Phys. Rev. Lett.***105,** 205502 (2010).

Publications (’13 - ’15)

P1. T. Egami, T. Iwashita and W. Dmowski, “Mechanical properties of metallic glasses”, *Metals***3,** 77 (2013).

P2. T. Iwashita, D. M. Nicholson and T. Egami,“Elementary excitations and crossover phenomenon in liquids”, *Phys. Rev. Lett.*,**110,** 205504 (2013).

P3. V. A. Levashov, J. R. Morris and T. Egami, “The origin of viscosity as seen through atomic level stress correlation function”, *J. Chem. Phys.* **138,** 044507 (2013).

P4. J. S. Langer, “Ising model of a glass transition”, *Phys. Rev. E***88,** 012122 (2013).

P5. D. M. Nicholson, Madhusudan Ojha and T. Egami, “First principles local stress in crystalline and amorphous metals”, *J.Phys.: Condens. Matt.*, **25,** 435505 (2013).

P6. W.D. Li, H. Bei, Y. Tong, W. Dmowski and Y. F. Gao, "Structural heterogeneity induced plasticity in bulk metallic glasses: From well-relaxed fragile glass to metal-like behavior", *Appl. Phys. Lett.***103,** 171910 (2013).

P7. T. Egami, “Angell dynamics of liquids”, *Fragility of Glass-forming Liquids*, ed. A. L. Greer, K. F. Kelton and S. Sastry (Hindustan Book Agency, Gurgaon, India, 2013), pp. 117.

P8. P. You, Y.C. Chen, J. P. Chu, S. Y. Chang, H. Bei, J.S.C. Jang, C.H. Hsueh, "Rapid Relacation and embrittlement of Xr-based bulk metallic glasses by electropulsing", Intermetallics, **34**, 43-48 (2013).

P9. U. Dahlborg, M. J. Kramer, J. R. Morris and M. Calvo-Dahlborg, “Atomic dynamics in molten AlCu alloys of different compositions and at different temperatures by cold neutron scattering,” *Physica B***412**, 50-60 (2013).

P10. U. Dahlborg, M.J. Kramer, M. Besser, J.R. Morrisand M. Calvo-Dahlborg, “Structure of molten Al and eutectic Al-Si alloy studied by neutron diffraction,” *J. Non-Cryst. Solids* **361,** 63-69 (2013).

P11. B-G Yoo, J-Y Kim, Y-J Kim, I-Ch Choi, S. Shim, T.Y. Tsui, H. Bei, U. Ramamurty, J-I Jang, "Increased time-dependent room temperature plasticity in metallic glass nanopillars and its size-dependency", *International Journal of Plasticity*, **37,** 108-118 (2012).

P12. Bin Wu, Yun Liu, Xin Li, Eugene Mamontov, Alexander I. Kolesnikov, Souleymane O. Diallo, Changwoo Do, Lionel Porcar, Kunlun Hong, Sean C. Smith, Li Liu, Gregory S. Smith, Takeshi Egami and Wei-Ren Chen, “Charge-dependent dynamics of a polyelectrolyte dendrimer and its correlation with invasive water”, *J. Amer. Chem. Soc.*, **135,** 5111 (2013)

P13. Y. Fan, T. Iwashita and T. Egami, “Potential energy landscape and spatial variation of shear modulus in metallic glass”, *Phys. Rev. E,***89,** 062313 (2014).

P14. Y. Fan, T. Iwashita and T. Egami, “How thermally activated deformation starts in metallic glass”, *Nature Communications,***5,** 5083 doi: 10.1038/ncomms6083 (2014).

P15. T. Iwashita and T. Egami, “Local energy landscape in simple liquids”, *Phys. Rev. E,* **90,** 052307 (2014).

P16. J. Wang, P. Apte, J. R. Morris and X. C. Zeng, "Freezing Point and Solid-Liquid Interfacial Free Energy of Stockmayer Dipolar Fluids: A molecular dynamics simulation study," *J. Chem. Phys.***139**, 114705 (2013).

P17. T. Egami, "Elementary excitation and energy landscape in simple liquids", *Mod. Phys. Lett. B*, **28,** 1430006 (2014).

P18. O. Haruyama, T. Mottate, K. Morita, N. Yamamoto, H. Kato and T. Egami, "Structural relaxation in $Pd_{42.5}Cu_{30}Ni_{7.5}P_{20}$ BMG below the glass transition", *Mater. Trans. JIM*, **55,** 466 (2014).

P19. X. Li, L. E. Sánchez-Diáz, B. Wu, L. Porcar, P. Falus, Y. Liu, C. Do, G. S. Smith, T. Egami and W.-R. Chen, "Dynamical Threshold of Diluteness of Soft Colloid", *ACSMacro Lett.*,**3,** 1271 (2014).

P20. Y. Tong, T. Iwashita, W. Dmowski, H. Bei, Y. Yokoyama and T. Egami, "Structural Rejuvenation in Bulk Metallic Glasses", *Acta Mater*. **86,** 240 (2015).

P21. B. Wu, T. Iwashita and T. Egami, "Anisotropic Stress Correlations in 2D Liquids", *Phys. Rev. E*,**91,** 032301 (2015).

P22. W. Dmowski, Y. Tong, T. Iwashita, Y. Yokoyama and T. Egami, "Universal Mechanism of Thermo-Mechanical Deformation in Metallic Glasses", *Phys. Rev. B*, **91**(2015), in press.

DOE award # DE-FG02-07ER46426, Stanford University

Nanophotonics-enhanced solar cells

PI: Shanhui Fan, co-PI: Mark Brongersma
Stanford University, Department of Electrical Engineering,
Spilker Building, Room 314, CA 94305, shanhui@stanford.edu

Program Scope or Definition

The overall emphasis of the program is to develop a fundamental understanding of nanophotonic structures for light trapping purposes, and a practical strategy in using nanophotonic structures to enhance solar cell performance. Towards this goal, we are undertaking substantial efforts on understanding the fundamental limits of light trapping in solar cells, on numerical design in seeking to achieve absorption enhancement over the entire solar spectrum, as well as efforts in understanding some of the basic properties of high-index resonant dielectric structures in the context of solar cell light trapping.

Below we review some of the major progress [1-9] made in this report period.

Recent Progress

Review in Nature Materials On High-Index Nanostructures for Light Management in Solar Cells. Brongersma and Fan wrote a review for Nature Materials on the use of high-index nanostructures for light management in solar cells [4]. Whereas high-index materials in a planar form tend to produce a strong, undesired reflection of sunlight, high-index nanostructures afford new ways to manipulate light at a subwavelength scale. For example, nanoscale wires, particles, and voids support strong optical resonances that can enhance and effectively control light absorption and scattering processes (Figure 1). As such, they provide ideal building blocks for novel, broadband antireflection coatings, light-trapping layers, and superabsorbing films. The review discusses some of the recent developments in the design and implementation of such photonic elements in thin film PV cells.

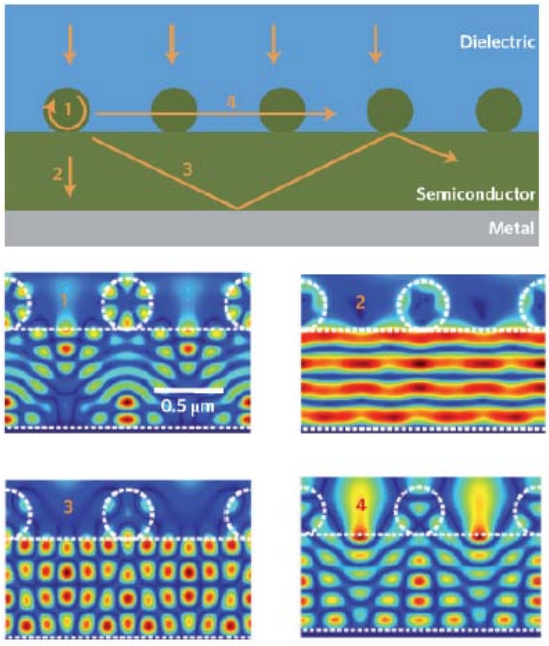

Figure 1. Various photonic mechanisms for enhancing solar cell performance in dielectric nanophotonic structures

*Detailed balance limit of single-nanowire solar cells*Semiconductor nanowire-based solar cells have been shown to be promising candidates for third-generation photovoltaics. Compared with traditional thin-film solar cells, the advantages of the nanowire cells include easily scalable manufacturing, lower cost, efficient charge separation, and tunable optical absorption. From the optical physics point of view, the nanowire geometry is interesting in that it

supports a variety of optical resonances, each with a spectral peak location that directly depends on the wire's diameter. In particular, a properly designed nanowire can support optical resonances with an absorption cross-section that is many times larger over the nanowire's geometrical cross-section. Accordingly, there has been a strong interest in engineering the location of these optical resonances of the nanowire in order to enhance its optical absorption and therefore its short-circuit current performance. However, in order to understand the fundamental limiting performance of a nanowire solar cell, these studies on the nanowire's output current behavior need to be complemented with a better understanding of the nanowire's intrinsic voltage behavior.

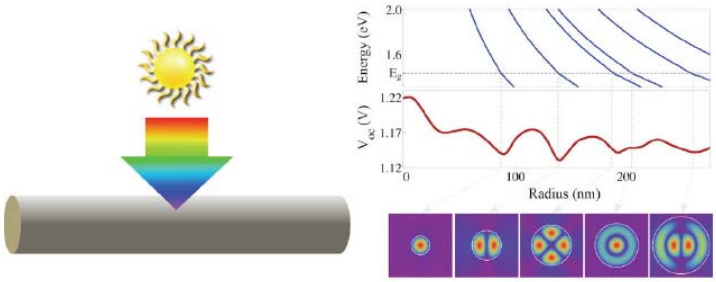

Figure 2. Left panel: A solar cell consisting of a single nanowire. Right panel: The nanowire supports resonances with different modal patterns. The energy of these resonances decreases as the radius increases. The open circuit voltage dips each time one of these resonances cross the semiconductor band edge.

We present a detailed balance analysis of current density−voltage modeling of a single-nanowire solar cell [3]. Our analysis takes into account intrinsic material non-idealities in order to determine the theoretical efficiency limit of the single-nanowire solar cell. The analysis only requires the nanowire's absorption cross-section over all angles, which can be readily calculated analytically. We show that the behavior of both the current and voltage is due to coherent effects that arise from resonances of the nanowire (Figure 2). In addition, we elucidate the physics of open-circuit voltage enhancement over bulk cells in nanowires, by showing that the enhancement is related to the removal of resonances in the immediate spectral vicinity above the bandgap.

Exceeding Shockley-Quiesser limit with a single-band gap semiconductor. Ever since the seminal work of Shockley and Queisser, there have been significant efforts aiming to overcome the Shockley−Queisser limit for solar energy conversion. The vast majority of these works aim to use materials or devices with electronic properties that are significantly different from the single bandgap semiconductors assumed in the original Shockley-Queisser analysis. These include the commercially available approach of multijunction solar cells, which utilizes multiple semiconductors with different band gaps, as well as more exploratory approaches such as hot-electron cells, multiple exciting generations, and inter-subband solar cells.

In contrast to all these works, we propose and analyze an alternative scheme for overcoming the Shockley−Queisser limit based purely on photonic engineering [2]. A single material can show different effective bandgap, set by its absorption spectrum, which depends on its photonic structure. In a tandem cell configuration constructed from a single material, one can achieve two different effective bandgaps, thereby exceeding the Shockley−Queisser limit.

Optical impedance transformation for ultra-thin transparent electrodes.Transparent conducting electrodes are important components in a variety of optoelectronic devices such as solar cells, light-emitting diodes, touch screens, and smart windows. A fundamental limitation of transparent

conducting electrode design is thought to be the trade-off between photonic and electrical performances: To achieve high optical transmission, one typically would reduce the material optical loss by, for example, reducing the carrier density, which then leads to lower electrical conductivity.

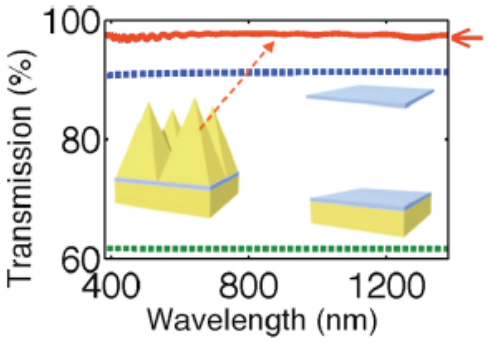

Figure 3. Transmission spectra of a transparent electrode consisting of four-layers of graphene. Blue curve: the electrode in air. Green curve: the electrode placed on the index between an high index substrate (n=4) and air. Red curve: the electrode placed in an optical impedance transformer consisting of nanopyramids placed on top of the electrode. Surrounding the electrode with high index materials reduce the optical impedance resulting in the suppression of optical absorption. The use of nanopyramid enables a gradual impedance transformation without reflection. The combination of these two effects result in strongly enhanced transmission.

We note, however, that the transmission property of a transparent conducting electrode is not intrinsic, but rather depends critically on the electromagnetic environment where the electrode is located (Figure 3). In this work, we develop the concept of optical impedance transformation and use this concept to design nanophotonic structures that provide broadband and omnidirectional reduction of optical loss in an ultrathin transparent conducting electrode, without compromising its electrical performance [6].

Fano interference leading to ultra-high efficiency solar cells.The Brongersma and Fan groups collaborated on exploring the light absorption and scattering properties of individual semiconductor nanostructures [7]. Control over these optical properties of individual particles can lead to improved control over the light trapping properties of the nanostructure arrays explore in this proposal. We discovered that judiciously-shape high index Si nanobeamscan support optical Fano resonances. Such resonances result from interference between direct and indirect, resonance-assisted pathways the light can take through the structure. In the nanophotonics field, Fano effects have been observed in a wide variety of systems, including metallic nanoparticle assemblies, metamaterials and photonic crystals. Their unique properties find extensive use in applications, including optical filtering, polarization selectors, sensing, lasers, modulators, and non-linear optics. We reported on the first observation of a Fano resonance in a single semiconductor nanostructure and published on it in a recent issue of Nature Materials [7]. As the Fano resonances can significantly alter the way in which light is absorbed and scattered by a nanoparticle, this opens up intriguing opportunities for their use in solar cells and active photonic devices.

Future Plans

In the near future (the coming year)we plan to focus on continued efforts towards understanding dielectric nanophotonic structures for enhancement of solar cell performance. This includes efforts that seek to further enhance the performance of nanowires through the use of co-axial structures, as well as the use of nanophotonic structures to enhance ultra-thin solar cells, such as solar cells based on two-dimensional semiconductors.

Published and accepted Journal Publications of DOE sponsored research in 2013-2015

[1] R. Pala, J. Liu, E. Barnard, D. Askarov, E. Garnett, S. Fan and M. Brongersma, "Optimization of non-periodic plasmonic light trapping layers for ultra-thin solar cells", *Nature Communications*, vol. 4, art. No. 2095 (2013).
[2] Z. Yu, S. Sandhu and S. Fan, "Achieving efficiency above the Shockley-Queisser limit using a single band gap material in a tandem configuration", *Nano Letters*, vol. 14, pp. 66-70 (2014).
[3] S. Sandhu, Z. Yu, and S. Fan, "Detailed balance analysis and enhancement of open circuit voltage in single nanowire solar cells", *Nano Letters*, vol. 14, pp. 1011-1015 (2014).
[4] M. L. Brongersma, Y. Cui and S. Fan, "Light Management for Photovoltaics Using High-Index Nanostructures", *Nature Materials*, vol. 13, pp. 451-460 (2014) (Invited Review).
[5] Y. Zhang, N. Stokes, B. Jia, S. Fan, and M. Gu, "Towards ultra-thin plasmonic silicon wafer solar cells with minimized efficiency loss", *Scientific Reports*, vol. 4, art. No. 4939 (2014).
[6]K. Wang, J. R. Piper and S. Fan, "Optical impedance transformer for transparent conducting electrodes", *Nano Letters*, vol. 14, pp. 2755-2758 (2014).
[7] P. Fan, Z. Yu, S. Fan, and M. Brongersma, "Optical Fano Resonance of an Individual Semiconductor Nanostructure", *Nature Materials*, vol. 14, pp. 471-475 (2014).
[8] K. Wang, Z. Yu, V. Liu, A. Raman, Y. Cui and S. Fan, "Light trapping in photonic crystals", *Energy and Environmental Science*, vol. 7, pp. 2725-2738 (2014).
[9]K. Wang, Z. Yu, S. Sandhu, V. Liu, and S. Fan, "Condition for perfect antireflection by optical resonance at material interface", *Optica*, vol. 1, pp. 388-395 (2014).

Project Title: Crystallization and thermoelectric transport in semiconductor micro- and nanostructures under extreme conditions

PI: Ali Gokirmak, co-PI: Helena Silva,
University of Connecticut, Department of Electrical and Computer Engineering
371 Fairfield Way, Storrs CT 06269

Program Scope

The objective of this project is to investigate non-equilibrium thermoelectric transport, and crystallization and amorphization dynamics in semiconductors. Self-heated micro- and nano-structures by electrical pulses form the core of the studies, focusing on the following aspects:

(1) Crystallization of Si micro wires by electrical stress, either by growing single crystal from melt by self-heating [1] or maintaining a super-heated / super-cooled state in non-equilibium.

(2) Theoretical understanding of thermoelectric effects (Seebeck, Peltier, or Thomson) which arise due to the exchange of energy between the lattice and charge carriers in motion. We have identified *electronic convective heat flow* (for semiconductor and metals) and *generation–transport–recombination (GTR) of minority carriers* (for semiconductor and insulator) as the two distinct components of Thomson heat in strong thermal gradient [1].

(3) Characterization of temperature dependent material parameters, such as: Seebeck coefficient, thermal conductivity, carrier mobility etc. up to high temperature.

(4) Develop a simulation framework to capture nucleation, growth and amorphization processes in equilibrium and non-equilibrium conditions incorporating semiconductor physics with generation and recombination of carriers.

Recent Progress

Thermoelectric transport in self-heated semiconductors

Current-carrying conductors self-heat due to conversion of electrical potential energy (V) to heat through scattering events (Joule heating). The Peltier coefficient (Π), represents the sum of kinetic and chemical potential energy of the charge carriers and the effect of energy exchange between the material and charge carriers in motion can be observed as Seebeck, Peltier or Thomson effects. We have been investigating the underlying physical mechanisms that give rise to Thomson heat, specifically in the case of self-heated semiconductors. We have identified *electronic convective heat flow* and *generation–transport–recombination of minority carriers (GTR)* as the two distinct components of Thomson heat. The GTR process is only present in material with a band-gap (semiconductors, and insulators) while electronic convective transport takes place in both semiconductors and metals. These two electro-thermal processes have a net effect if there is a thermal gradient present in the current carrying materials, and their contributions are in the opposite polarity. In the case of degenerately doped silicon, GTR dominates at elevated temperatures ($T > 1100$ K). The drift-diffusion of carriers in self-heated structures and the details of the GTR process are explained using experimental and computational studies in our recent publication in Nature's *Scientific Reports* [1]. Strong electric field and thermal gradients also lead to significant variations in free hole (broken bond) density.

This leads to electronic softening of the material on one side and hardening on the other side as the holes are swept from one part to the other, reinforcing the asymmetry in crystallization.

Progress in Modeling

The models used in [1] have some practical assumptions (such as assuming equilibrium carrier concentrations) and use some parameters extrapolated from measured quantities (such as thermal conductivity at elevated temperatures). The upgraded model we are constructing dynamically calculates the free carrier concentrations (n, p) and the electric potential (ψ) self-consistently by solving the current continuity equations (1, 2) and the Poisson's equation (3) (rather than using pre-calculated equilibrium electron and hole concentrations and solving Ohm's law as in previous model):

$$\frac{\partial n}{\partial t} = \frac{1}{q}\left(\nabla.\bar{J}_n\right) - U_n, \quad \frac{\partial p}{\partial t} = -\frac{1}{q}\left(\nabla.\bar{J}_p\right) - U_p \tag{1, 2}$$

$$\nabla.\left(\varepsilon\nabla\psi\right) = -q\left(p - n + N_D{}^{+} - N_A{}^{-}\right) \tag{3}$$

The net recombination rates are represented with U_n, U_p, current densities are J_n, J_p, and active dopant concentrations are N_D and N_A. This more rigorous approach gives a more complete understanding of the transient dynamics of the system and does not require the effective media approximation that we have been using so far. Accounting for local charging and non-uniformities allows us to calculate charge accumulation or depletion in any part of the structure at a given time and gives us a better understanding of the nano-scale non-equilibrium processes.

The electron and hole currents are calculated from the gradient of the respective quasi Fermi levels (F_n, F_p). This approach of calculating current has the advantage of using this model to semiconductor hetero-structures as different materials can be characterized using the material dependent parameters such as: electron affinity (χ), bandgap (E_g), effective density of states at the conduction and valence band (N_c and N_v), electron and hole mobilities (μ_n, μ_p). Mobility models that include phonon and impurity scattering, carrier-carrier scattering, surface scattering, and/or high field scattering can be incorporated. In the new model, we have incorporated the dynamic recombination rate to calculate the net recombination heat. So far, Shockley-Read-Hall (SRH) and Auger recombination models have been incorporated. Recently we have augmented our semiconductor model so that it can handle electric potential and current inside metals. Inclusion of impact ionization, the impact of which is dominant at high carrier density, in the model will also be considered.

Crystal Nucleation and Growth Model

The drive to scale conventional CMOS devices down to < 10 nm has led to a technology which enables fabrication of new devices that complement CMOS, such as phase change memory (PCM). PCM is a high-density high-speed non-volatile memory that utilizes a class of materials - $Ge_2Sb_2Te_5$ (GST) being the most common - that can be rapidly and reversibly switched between a highly resistive amorphous (reset) state and a conductive crystalline (set) state. Unlike conventional electronic devices, PCM utilizes heating to crystallize (set), and melting and resolidification to amorphize (reset). Hence, the material in the active region changes dynamically along with the thermal profiles in a non-equilibrium condition which makes it harder to construct SPICE models. Effective media approximations [1-5] using Arrhenius models are relatively efficient but cannot capture local stochastic variations and granularity [6].

Models that incorporate classical nucleation and growth theory do capture discrete nucleation, and can differentiate between grains. However, majority of these models do not run within electrothermal simulations of individual devices and cannot capture non-equilibrium processes. We have constructed a comprehensive phase change / electrothermal model for PCM devices based on our electro-thermal models. In this model nucleation, growth and amorphization processes are locally calculated using a temperature dependent rate expression.

New additions to the model include discrete grain orientation, grain boundary resistance using a temperature dependent activation model, heat of crystallization physics and incubation time for nucleation. An example of this unique grain orientation model for one reset and three different set states of a PCM mushroom cell is shown in Figure 1.

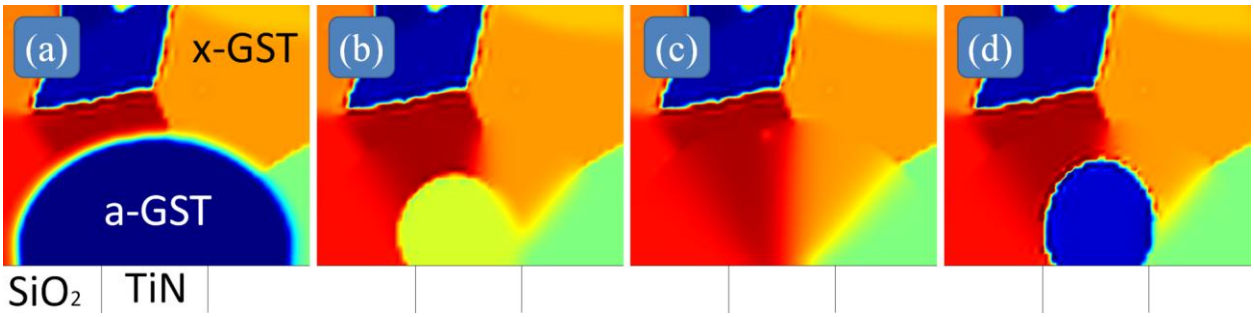

Figure 1. Crystal grain maps for reset state (a) and three different set states (b-d) of a simple mushroom cell device. Each color represents a different crystal grain with a unique orientation, while the labeled blue in (a) is the amorphous dome covering the TiN dome.

Experimental Materials Characterization

Chalcogenide materials such as GST provide a rich platform to understand the behavior of materials at various crystallinity states by annealing at various temperatures. We have performed experimental studies on electrical conductivity and Seebeck coefficient on thin-film (~50 nm) samples of $Ge_2Sb_2Te_5$ as a function of temperature and identified a correlation between the two (Figure 2). All cases show positive dS/dT slopes, the fit of the S-T curves meet at the S=0 at T=0 K with less than 1% standard error in their slopes. Small activation energy (E) for various annealing temperatures suggests that the material is polycrystalline and transport is limited by the grain boundaries.

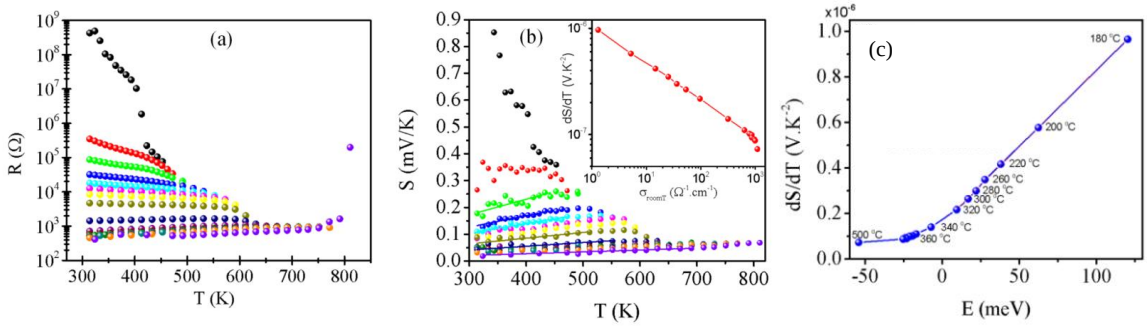

Figure 2. Simultaneously measured R-T (a) and S-T (b) on 50 nm GST film using 10 K steps in temperature. The inset is constructed using the slopes of the linear parts in S-T as a function of room temperature electrical conductivity of the sample at the beginning of each cycle. Correlation between *dS/dT* and activation energy (*E)*.

Future Plans

- Non-homogeneous materials under extreme thermal gradients: Combine our models capturing the dynamic nucleation, growth and amorphization processes as a function of temperature (induced by ambient temperature or joule heating) with semiconductor models to capture charging, depletion and generation and recombination heat. This will allow electro-thermal modeling of non-homogeneous materials (e.g. nano-crystalline materials) with homo and hetero-junctions.
- Detailed characterization of the amorphous phase of GST and crystallization dynamics.
- Extraction of thermal conductivity under large thermal gradients, as a function of structure size (hence thermal gradient) to study ballistic thermal transport (expected at ~ 1 K/nm and larger),
- Short range (~10 nm) electrothermal effects at interfaces: traps, bilayers, thermal boundary resistances,
- Non-equilibrium amorphization and crystallization processes including electronic softening and hardening and the combined effect of asymmetric thermal profile due to reneration-transport-recombination processes.

Published and accepted Journal Publications of DOE sponsored research in 2013-2015

1. G. Bakan, N. Khan, H. Silva, A. Gokirmak, "High-temperature thermoelectric transport at small scales: generation, transport and recombination of minority carriers," *Nature Publications, Scientific Reports* 3, 2724, doi:10.1038/srep02724 (2013) ***(major contribution to date)***.

2. G. Bakan, A. Gokirmak, H. Silva, "Suppression of thermoelectric Thomson effect in silicon microwires under large electrical bias and implications for phase-change memory devices," *Journal of Applied Physics* 116, 23, 234507 (2014)

3. F. Dirisaglik, G. Bakan, A. Faraclas, A. Gokirmak, H. Silva, "Numerical Modeling of Thermoelectric Thomson Effect in Phase Change Memory Bridge Structures," *Inter. J. High Speed Electr. and Sys.*, 23, 01n02 (2014)

4. A. Faraclas, G. Bakan, L. Adnane, F. Dirisaglik, N. Williams, A. Gokirmak, H. Silva, "Modeling of thermoelectric effects in phase change memory cells," *IEEE Trans. On Electronic Devices, 61, 2, 372-378 (2014)*

5. S. Muneer, A. Gokirmak, H. Silva, "Vacuum Insulated Self-Aligned Nanowire Phase-change Memory Devices," *IEEE Transactions on Electron Devices* (Accepted for publication, 2015).

6. S. Fischer, C. Osorio, N. Williams, S. Ayas, H. Silva, A. Gokirmak, "Percolation transport and filament formation in nanocrystalline silicon nanowires," *Journal of Applied Physics* 113, 16, 164902 - 164902-5 (2013).

Future Plans

- Non-homogeneous materials under extreme thermal gradients: Combine our models capturing the dynamic nucleation, growth and amorphization processes as a function of temperature (induced by ambient temperature or joule heating) with semiconductor models to capture charging, depletion and generation and recombination heat. This will allow electro-thermal modeling of non-homogeneous materials (e.g. nano-crystalline materials) with homo and hetero-junctions.
- Detailed characterization of the amorphous phase of GST and crystallization dynamics.
- Extraction of thermal conductivity under large thermal gradients, as a function of structure size (hence thermal gradient) to study ballistic thermal transport (expected at ~ 1 K/nm and larger),
- Short range (~10 nm) electrothermal effects at interfaces: traps, bilayers, thermal boundary resistances,
- Non-equilibrium amorphization and crystallization processes including electronic softening and hardening and the combined effect of asymmetric thermal profile due to reneration-transport-recombination processes.

Published and accepted Journal Publications of DOE sponsored research in 2013-2015

1. G. Bakan, N. Khan, H. Silva, A. Gokirmak, "High-temperature thermoelectric transport at small scales: generation, transport and recombination of minority carriers," *Nature Publications, Scientific Reports* 3, 2724, doi:10.1038/srep02724 (2013)***(major contribution to date)***.

2. G. Bakan, A. Gokirmak, H. Silva, "Suppression of thermoelectric Thomson effect in silicon microwires under large electrical bias and implications for phase-change memory devices," *Journal of Applied Physics* 116, 23, 234507 (2014)

3. F. Dirisaglik, G. Bakan, A. Faraclas, A. Gokirmak, H. Silva, "Numerical Modeling of Thermoelectric Thomson Effect in Phase Change Memory Bridge Structures," *Inter. J. High Speed Electr. and Sys.,* 23, 01n02 (2014)

4. A. Faraclas, G. Bakan, L. Adnane, F. Dirisaglik, N. Williams, A. Gokirmak, H. Silva, "Modeling of thermoelectric effects in phase change memory cells," *IEEE Trans. On Electronic Devices, 61, 2, 372-378 (2014)*

5. S. Muneer, A. Gokirmak, H. Silva, "Vacuum Insulated Self-Aligned Nanowire Phase-change Memory Devices," *IEEE Transactions on Electron Devices* (Accepted for publication, 2015).

6. S. Fischer, C. Osorio, N. Williams, S. Ayas, H. Silva, A. Gokirmak, "Percolation transport and filament formation in nanocrystalline silicon nanowires," *Journal of Applied Physics* 113, 16, 164902 - 164902-5 (2013).

Thin Film Vapor-Liquid-Solid Growth of Semiconductors

A. Javey,[1,2] J. W. Ager III,[1,3] and D. C. Chrzan[1,3]
[1]Materials Sciences Division, Lawrence Berkeley National Laboratory, Berkeley, CA
[2]Electrical Engineering and Computer Science, University of California, Berkeley, CA
[3]Materials Science and Engineering, University of California, Berkeley, CA

Program Scope

The development of low cost solar cells requires low cost processing routes capable of yielding high quality films. With this aim in mind, we sought to develop processing approaches capable of yielding thin films with large grain sizes without ultra-pure starting materials, and expensive processing steps.

Often, the grain size within a film is comparable to the thickness of the film. The implication is that for a 3 μm thick film, the typical grain size will be approximately 3 μm, and this results in an extremely high density of defects that serve as a detriment to performance of the optical device.

Under typical growth conditions, the grain size of the semiconductor is controlled by the number of nuclei during growth. Therefore, it is reasonable to expect that control of the nucleation rate within the film is essential to the control of the grain size. Controlling nucleation within a thin film environment, however, is difficult, as there is an abundant opportunity for heterogeneous nucleation to dominate the growth process: In the initial stages, the film is essentially all surface.

To circumvent this difficulty, we have introduced a new growth process, thin film vapor-liquid-solid (thin-film VLS) growth.[1] In this process, a substrate is chosen, and a precursor to the desired film is deposited on the substrate. The precursor is then capped by a layer chosen to be permeable to the other component of the film, but one in which the permeability can be controlled through film thickness and/or quality. The capped film is then exposed to the second precursor, and the temperature is controlled so that the desired film develops.

Recent Progress

We have explored thin-film VLS using the growth of InP as a prototypical example. Using Mo foil as a substrate, we deposited from 200 nm to 2 μm thick films of In using either e-beam evaporation or electroplating. We then evaporated a 50 nm thick film of SiO_x as the capping layer. The Mo/In/SiOx stack is then heated in hydrogen to a growth temperature of 450° –800° C, which is above the melting point of indium (157° C). The thin SiO_x capping layer enables the liquid indium to maintain a planar geometry by preventing it from dewetting. After

temperature stabilization, phosphorous vapor is introduced into the chamber, either by PH3 gas or a heated red phosphorous solid source. The diffusion of phosphorous vapor through the capping layer and dissolution in the liquid indium results in the precipitation of solid InP crystals as predicted by the indium-phosphorus phase diagram. The growth process is depicted in Fig. 1.

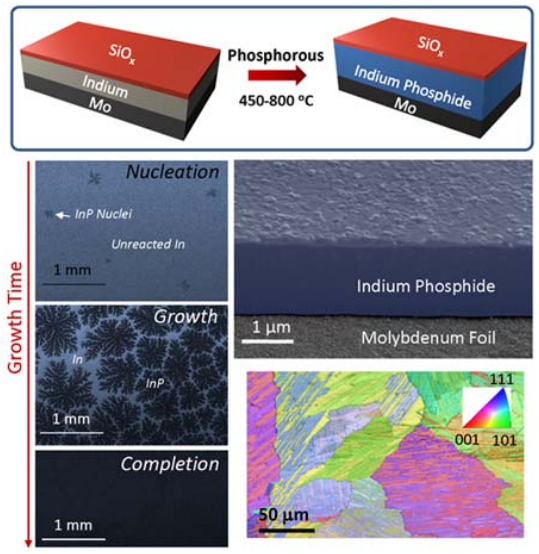

Figure 1. The thin-film vapor-liquid-solid growth process for InP thin films. The starting point is a Mo foil-Indium-SiO_x stack. This stack is then exposed to phosphorous gas and elevated temperatures in order to convert the In to InP. The capping layer controls the rate at which P enters the In, and thereby enables fine tuning of the P supersaturation with the In metal during growth. The result is very precise control of the nucleation density, and a resulting film structure that is approximately 3 µm thick, while have grain sizes that exceed 100 µm. The electronic and optical properties of these InP are exceptional given that the precursor materials are not ultra-high purity.

Nucleation in this growth process is controlled by the capping layer and the temperature. More specifically, the flow of phosphorous into the In is restricted by the capping layer. When combined with the temperature control afforded by the fact that the In is constrained from dewetting by the same capping layer, one can experimentally control the P supersaturation in the liquid In, and thereby control the nucleation rate. Control of nucleation is further aided by the fact that InP nucleates on Mo foil much more easily than on SiO_x. Using a simple model for nucleation, we argued that the number of nuclei within the liquid can be controlled by varying the flux of P. This was borne out by experiment.

Using thin-film VLS, optical quality InP thin films were produced. These films were typically 3 µm thick, but had grain sizes of the order of 100 µm in diameter. Note that these films do not grow epitaxially and consequently the suitable substrates are not constrained by lattice mismatch. Moreover, the electronic and optical quality of the films was very good: Carrier densities were below $8x10^{16}/cm^3$, despite the fact that we did not use an ultra-high purity Mo foil or source of In. Electron mobilities are reasonable in comparison to bulk values. Photoluminescence spectra were very similar to that obtained from bulk single crystal InP. Moreover, the films display an effective Fermi level splitting of 0.94 eV, a splitting that exceeds that in copper indium gallium selenide (CIGS) thin films.[2]

In subsequent work, we were able to show that nucleation during thin-film VLS could also be seeded. Specifically, we noted that MoOx could be used to seed the growth of thin films, and showed that nucleation could be controlled to the point that films with grains approaching millimeter diameters could be fabricated using the process.[3]

Future Plans

The notion of using control of nucleation via a capping layer to synthesize high quality films is more broadly applicable. In the case of InP, both the binary phase diagram and the temperature enable control of the grain sizes within the films. This suggests several questions for further research. For example, is it possible to grow high quality single component semiconductor films using a similar approach? Can nucleation be controlled sufficiently through judicious choice of substrate and capping layer materials? Is there a lower limit on film thickness, or can films thinner than 200 nm be fabricated by this method? Is there an upper limit on film thickness? We intend to explore these possibilities theoretically and experimentally in our future work.

References

[1] Kapadia, R. *et al.* A direct thin-film path towards low-cost large-area III-V photovoltaics. *Scientific Reports* **3**, doi:Artn 227 Doi 10.1038/Srep02275 (2013).

[2] Bauer, G. H., Bruggemann, R., Tardon, S., Vignoli, S. & Kniese, R. Quasi-Fermi level splitting and identification of recombination losses from room temperature luminescence in Cu(In(1-x)Ga(x))Se(2) thin films versus optical band gap. *Thin Solid Films* **480**, 410-414, doi:Doi 10.1016/J.Tsf.2004.11.061 (2005).

[3] Kapadia, R. *et al.* Deterministic Nucleation of InP on Metal Foils with the Thin-Film Vapor-Liquid-Solid Growth Mode. *Chemistry of Materials* **26**, 1340-1344, doi:Doi 10.1021/Cm403403v (2014).

Publications

R. Kapadia, Z. Yu, H.-H. H. Wang, M. Zheng, C. Battaglia, M. Hettick, D. Kiriya, K. Takei, P. Lobaccaro, J. W. Beeman, J. W. Ager, R. Maboudian, D. C. Chrzan, A. Javey, "A direct thin-film path towards low-cost large-area III-V photovoltaics", *Scientific Reports*, 3, 2275; DOI:10.1038/srep02275, 2013.

R. Kapadia, Z. Yu, M. Hettick, J. Xu, M. S. Zheng, C.-Y. Chen, A. D. Balan, D. C. Chrzan, A. Javey, “Deterministic nucleation of InP on metal foils with the thin-film vapor-liquid-solid growth mode”, *Chemistry of Materials*, 26 (3), 1340–1344, 2014.

P. Lobaccaro, A. Raygani, A. Oriani, N. Miani, A. Piotto, R. Kapadia, M. Zheng, Zhibin Yu, L. Magagnin, D. C. Chrzan, R. Maboudian, A. Javey, "Electrodeposition of High-Purity Indium Thin Films and Its Application to Indium Phosphide Solar Cells", *Journal of The Electrochemical Society*, 161 (14) D794-D800, 2014.

Epitaxial growth and fundamental properties of hexagonal boron nitride

Hongxing Jiang, Texas Tech University

Project Scope

Among the members of the III-nitride system, boron-nitride (BN) having a band gap comparable to AlN (E_g ~ 6.4 eV), is the least studied and understood. Its applications range from deep ultraviolet photonic devices to neutron detectors. The technical objectives of this project include: (1) Investigate the growth processes for obtaining high crystalline quality hexagonal BN (h-BN) epilayers by metal organic chemical vapor deposition; (2) Probe the optical properties and detailed band structures near the fundamental band edge; (3) Investigate the mechanisms of the formation and elimination of native defects during MOCVD growth; (4) Study the 2D optical and transport properties of semiconducting h-BN epilayers.

Recent Progress

MOCVD growth of h-BN epilayers with improved crystalline quality

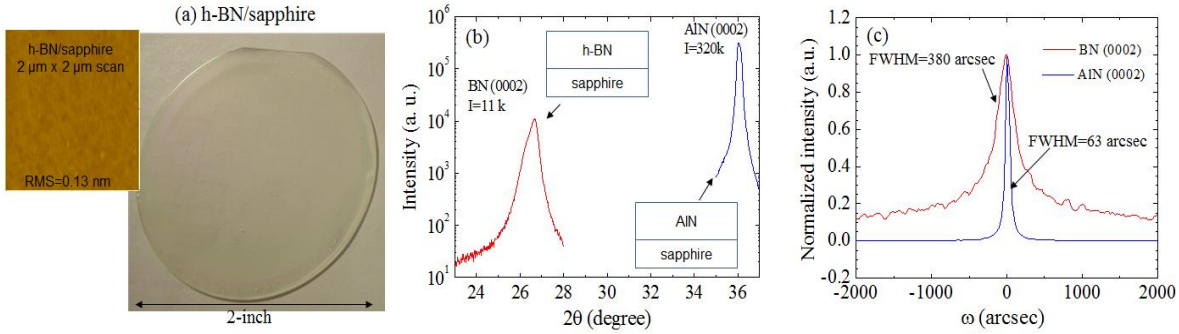

Figure 1. (a) Optical image of a 2-inch wafer of *h*-BN epilayer deposited on sapphire and the inset shows an AFM image of a thin *h*-BN epilayer over a 2 x 2 μm^2 area scan. (b) XRD θ-2θ scans of h-BN and AlN epilayers. (c) XRD rocking curves of the (0002) reflection peaks of h-BN and AlN epilayers [Publication #3].

Hexagonal BN epitaxial layers were synthesized by MOCVD using triethylboron (TEB) source and ammonia (NH_3) as B and N precursors, respectively. For h-BN epilayer growth, the surface migration of boron atoms is poor because the B-N bond is strong and the parasitic pre-reaction between TEB and NH_3 is severe. The by-products of the pre-reaction deposited on the wafer cause a rough surface and high crystalline defect density. We have employed modulation pulsed growth with alternating supplies of group III (TEB) and group V (NH_3) precursors to reduce the parasitic reactions in the gas phase and to improve the crystalline quality of h-BN. An optical image of a 2-inch wafer of *h*-BN epilayer is shown in Fig. 1(a). To evaluate the crystalline quality, we compare in Fig. 1(b) the x-ray diffraction (XRD) characterization results for AlN and h-BN epilayers deposited on sapphire substrates. It can be seen that the XRD intensity of the (0002) peak of h-BN is about 30 times lower than that of AlN epilayer with the same thickness. As shown in Fig. 2(c), thin h-BN epilayers exhibit an excellent surface morphology. However, the surface morphology of h-BN epilayers becomes poorer with an increase in the h-BN epilayer thickness and requires further improvement. The XRD rocking curve of the h-BN (0002) diffraction peak has a full width at half maximum (FWHM) of ~380 arcsec, which is comparable to those of typical high quality GaN epilayers deposited on sapphire [1], but is still much broader than the typical FWHM of high quality AlN epilayers of <60 arcsec

[2]. These results signify that it is feasible to obtain h-BN epilayers with high crystalline quality by MOCVD and that the development of epitaxial layers of h-BN is in its early stage.

Probing 2D exciton parameters in h-BN

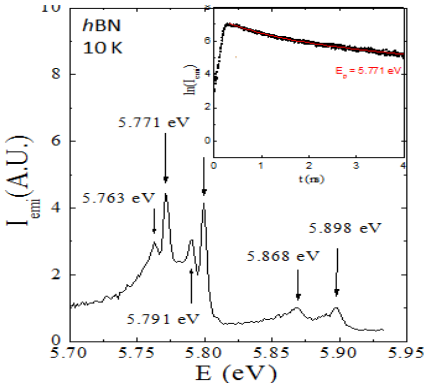

Figure 2. Exciton emission spectrum in *h*-BN. Inset is the PL decay kinetics measured at the main exciton peak, 5.771 eV. The measured exciton lifetime exhibits a minimum at T*, where T* = $\hbar s/ka_B$ [1] and the measured T*≈175 K and s = 2.2 x 10^6 cm/s in *h*-BN [Publication #8].

Table 1. Fundamental parameters in *h*-BN
Bandgap (E_g), Exciton binding energy (E_b) and Bohr radius (a_B), and effective masses (m_e and m_h)

E_g (eV)	E_b (meV)	a_B (nm)	m_e/m_h (m_o)
6.5	740	0.8	0.54/0.54

As illustrated in Fig. 2, we have probed the recombination processes of excitons in h-BN using time-resolved photoluminescence (PL). It was found that the theory [3] for 2D exciton recombination describes well the exciton dynamics in layer structured *h*-BN. The exciton Bohr radius and binding energy deduced from the temperature dependent exciton recombination lifetime is around 8 Å and 740 meV, respectively. The measured exciton binding energy of 740 meV represents the largest value ever reported for inorganic semiconductors. We have derived a generalized dispersion relation, which provides a direct relationship between the bandgap and effective mass for 2D semiconductors. The effective masses of electrons and holes in 2D h-BN deduced from the generalized relativistic dispersion relation of 2D systems are $0.54m_o$, which are remarkably consistent with the exciton reduced mass deduced from the temperature dependence of the exciton lifetime. The observed fundamental parameters of h-BN are summarized in Table 1. Our results explain that the origin of the extremely high optical efficiency of *h*-BN is due to its large exciton binding energy and layered structure and that *h*-BN represents an ideal platform to probe fundamental optical properties of 2D material systems.

The origin of deep-level impurity transitions in hexagonal boron nitride

The physical origins of various commonly observed deep level impurity related emission lines in h-BN are not yet fully understood due to the lack of tunability in growth parameters in synthesizing bulk and powder-like h-BN in the past. A comprehensive study on the properties of the impurity transitions in h-BN grown under controlled conditions is necessary to provide not only a better understanding of its optical properties, but also input for approaches towards the improvement of material quality and elimination of undesired impurities or defects as well as the design of particular device structures.

During the supporting period, we have successfully grown a set of h-BN epilayers by MOCVD under different ammonia (NH_3) flow rates to allow the investigation of the role of nitrogen vacancies (V_N) in the deep impurity level related donor-acceptor pair (DAP) transition in h-BN. Figure 3(a) shows the room temperature PL spectra of *h*-BN epilayer samples grown under varying NH_3 flow rates. The three peaks observed are related to a DAP related transition (zero-phonon emission line at 4.12 eV and its phonon replicas). Figure 3(b) plots the integrated emission intensity of the 4.12 eV transition line as a function the NH_3 flow rate (R_{NH3}), which

clearly demonstrates that the measured emission intensity decreases exponentially with increasing NH_3 flow rate (R_{NH_3}). As the NH_3 flow rate increases, more N atoms are supplied to the reaction zone and hence the concentrations of nitrogen vacancies (V_N) and its related defects in the samples are decreased. Our results provide a clear evidence that the DAP transition near 4.1 eV is associated with the presence of V_N or its related defects.

The temperature-dependent PL spectra were measured from 10 K up to 800 K, which

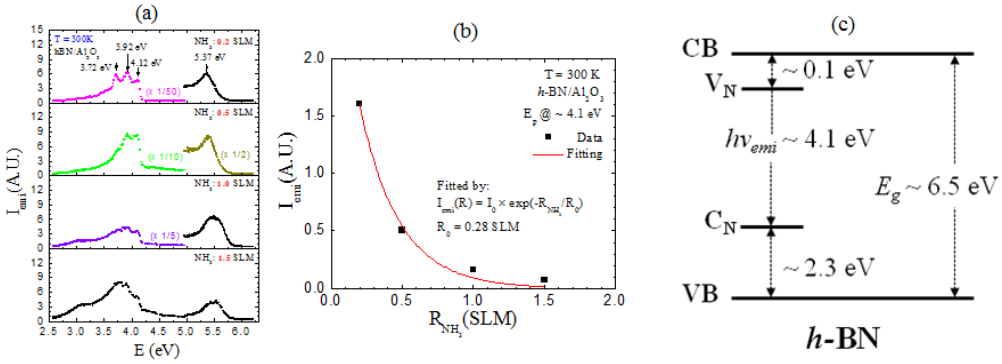

Figure 3. (a) 300 K PL spectra of *h*-BN epilayers grown under different NH_3 flow rates, (R_{NH_3}). (b) Integrated PL emission intensity of the DAP transition near 4.1 eV in *h*-BN as a function of R_{NH_3}. (c) Energy diagram showing the impurities and their energy levels involved in the DAP transition near 4.1 eV in *h*-BN [Publication #1].

provided an activation energy of ~ 0.1 eV for the shallow impurity involved in the DAP transition. The measured energy levels together with previous theoretical insights [4,5] on the formation energies of the impurities and defects in *h*-BN suggest that V_N and carbon impurities occupying the nitrogen sites (C_N), respectively, are the most probable shallow donor and deep acceptor impurities involved in this DAP transition. With the assignment of the involved impurities and determination of their energy levels, we are able to construct the energy diagram of the DAP transition near 4.1 eV in *h*-BN, as shown in Fig. 3(c). In Fig. 3(c), V_N and C_N are attributed to the shallow donor and deep acceptor involved in this DAP transition, respectively. Our results indicate that by monitoring the impurity related emission peaks in *h*-BN while varying the growth conditions, epilayers with improved optical qualities can be obtained.

Future Plans

1) *Epi-growth at high temperatures*. The strong B-N bond limits the migration of B atoms during the growth if the growth temperature is not high enough, leading to poor lateral homogeneity in the films. We will further develop high temperature growth processes for achieving *h*-BN epilayers with high growth rate, smooth surface morphology, and low dislocation and stacking-fault densities on various substrates.

2) *Optical characterization*. We will carry out time-resolved PL measurements to identify the mechanisms of optical transitions in materials grown under different conditions. In particular, studies of excitonic transitions in h-BN will be carried out. The basic optical properties of h-BN will be carefully studied to clarify the growth parameters that control their properties. Optical studies will be coupled with other advanced material characterization techniques, including variable temperature (10 K ≤ T ≤ 850 K) Hall effect, XRD, and optical absorption measurements.

3) *Doping and conductivity control*. In contrast to other members of III-nitride family, *p*-type *h*-BN is more readily obtained than n-type. We have demonstrated p-type conduction in *h*-BN via

Mg doping. It will be very interesting to explore suitable n-type dopants. The lateral and vertical transport properties will be measured to elucidate the effects of anisotropy in *h*-BN. The formation mechanisms and properties of native defects including B and N vacancies and their impact on the doping efficiency in *h*-BN will be probed. Methods to reduce or eliminate these native defects during MOCVD growth will be explored.

4) *Probing 2D properties* – Thin *h*-BN epilayers will be synthesized and the optical and electrical properties of *h*-BN will be investigated as its dimension scales from 3D to 2D.

References

[1] S. Nakamura, G. Fasol, and S. J. Pearton, "The blue laser diode: the complete story," Springer (2000).

[2] B. N. Pantha, R. Dahal, M. L. Nakarmi, N. Nepal, J. Li, J. Y. Lin, H. X. Jiang, Q. S. Paduano, and D. Weyburne, "Correlation between optoelectronic and structural properties and epilayer thickness of AlN," Appl. Phys. Lett. **90**, 241101 (2007).

[3] A. V. Paraskevov, J. Luminescence **132**, 2913 (2012).

[4] B. Huang and H. Lee, Phys. Rev. B **86**, 245406 (2012).

[5] C. Attaccalite, M. Bockstedte, A. Marini, A. Rubio, and L. Wirtz, Phys. Rev. B **83**, 144115 (2011).

[6] V. Wang, N. Ma, H. Mizuseki, and Y. Kawazoe, Solid State Comm. **152**, 816 (2012).

List of Publications (Last 2 years):

1. X. Z. Du, J. Li, J. Y. Lin, and H. X. Jiang, "The origin of deep-level impurity transitions in hexagonal boron nitride," Appl. Phys. Lett. 106, 021110 (2015).
2. T. C. Doan, J. Li, J. Y. Lin, and H. X. Jiang, "Charge carrier transport properties in layer structured hexagonal boron nitride," AIP Advances 4, 107126 (2014).
3. H. X. Jiang, and J. Y. Lin, "Hexagonal boron nitride for deep ultraviolet photonic devices," Semicon. Sci. Technol. 29, 084003 (2014); *invited review article*.
4. Q. Wang, S. Zhao, A. T. Connie, I. Shih, Z. Mi, T. Gonzalez, M. P. Andrews, X. Z. Du, J. Y. Lin, and H. X. Jiang, "Optical properties of strain-free AlN nanowires grown by molecular beam epitaxy on Si substrates," Appl. Phys. Lett. 104, 223107 (2014
5. T. C. Doan, S. Majety, S. Grendadier, J. Li, J. Y. Lin, and H. X. Jiang, "Fabrication and characterization of solid-state thermal neutron detectors based on hexagonal boron nitride epilayers," Nuclear Instruments and Methods in Physics Research Section A: Accelerators, Spectrometers, Detectors and Associated Equipment, 748C, 84 (2014).
6. X. Z. Du, C. D. Frye, J. H. Edgar, J. Y. Lin, and H. X. Jiang, "Temperature dependence of the energy bandgap of two-dimensional hexagonal boron nitride probed by excitonic photoluminescence ," J. Appl. Phys. 115, 053503 (2014).
7. S. Majety, T. C. Doan, J. Li, J. Y. Lin, and H. X. Jiang, "Electrical transport properties of Si-doped hexagonal boron nitride epilayers," AIP Advances 3, 122116 (2013).
8. X. K. Cao, B. Clubine, J. H. Edgar, J. Y. Lin, and H. X. Jiang, "Two-dimensional excitons in three-dimensional hexagonal boron nitride," Appl. Phys. Lett. 103, 191106 (2013).
9. S. Majety, J. Li, W. P. Zhao, B. Huang, S. H. Wei, J. Y. Lin, and H. X. Jiang, "Hexagonal boron nitride and 6H-SiC heterostructures," Appl. Phys. Lett. 102, 213505 (2013).
10. H. X. Jiang and J. Y. Lin, "Nitride micro-LEDs and beyond - a decade progress review," Optics Express 21, A475 (2013); *invited review article*.
11. X. K. Cao, S. Majety, J. Li, J. Y. Lin and H. X. Jiang, "Optoelectronic properties of hexagonal boron nitride epilayers," Proc. SPIE 8631, 863128 (2013); *invited*.

Program Title: Bridging Atomistic and Continuum Scales in Phase-Field Modeling of Stressed Polycrystalline Materials

Principal Investigator: Alain Karma
Address: Department of Physics and Center for Interdisciplinary Research on Complex Systems, Northeastern University, 360 Huntington Avenue, Boston, Massachusetts 02115
Email: a.karma@neu.edu

Program Scope

This research focuses on the development ofstate-of-the-art scale-bridging phase-field methodologies to understand the physical behavior of stressed polycrystalline materials relevant for energy, including both structural and functional materials. A primary focus is the investigation of materials interfaces and their interactions including solid-liquid interfaces, grain boundaries, compositional domain boundaries, and surfaces. This research takes advantage of a wealth of new observations from in situ imaging studies of those interfacesand recent advances in atomistic and continuum simulations. Conventional phase-field and phase-field-crystal (PFC) simulations are combinedwith molecular dynamics (MD) simulations in an effort to bridge quantitatively atomistic and continuum length and time scales. MD simulations provide a direct quantitative link to interatomic force fields while PFC simulations accessmuch longer diffusive time scales and provide a theoretical thermodynamics framework to understand generic behaviors. Specific phenomena under investigation include the complex interaction of grain and compositional domain boundaries in two-phase coherent solids with large misfit strain,fundamental mechanisms of curvature- and stress-driven grain boundary motion that impact the stability of nanocrystalline materials, the formation and stress-response of nanometer-thin intergranular liquid films at high homologous temperature, and the formation of bulknanocomposite andnanoporous structures by liquid metal dealloying.Multiscale modeling is expected to contribute new scientific understanding of interfacial processes relevant for the improved performance, design, and safety of diverse polycrystalline energy materials from structuralalloys for the automotive and aerospace industries to energy storage materials.

Recent progress

Morphological instability of grain boundaries in two-phase coherent solids

We have discovered computationally and characterized analytically a novel stress-driven morphological instability that strongly influences the coupled evolution of grain boundaries (GB) and compositional domain boundaries (CDB) in two-phase coherent solids. This instability is important for understanding the mechanical behavior of a large class of energy materials where GB interact with second phase precipitates, including Olivine used as electrode particles in Li-ion batteries and metallic alloys (e.g. GB serration in Ni-Al superalloys).The complex interactions between GBand second phase precipitateswasstudied in the simple configuration of a GB centered in a lamellar precipitate. Performing a linear stability analysis, we show that this morphology is unstable with respect to long wavelengthperturbations of the CDB. The instability is mediated by the elastic interactions between the GB and the CDB.A relationship between the growth rate and wavelength of the instability is derived, showing that the growth rate does not depends on the misorientation between grains as long as the GB couples with a shear stress. This analytical prediction is validated using two complementary simulation techniques, a non-linear elastic model (NLEM) [Geslin et al., Acta Mater. **71**, 80 (2014)] and an amplitude equation version of the phase-field crystal model [Spatschek and Karma, Phys. Rev. B**81**, 214201 (2010)]. As shown in Fig. 1.e, both simulations techniques show remarkable agreements with the analytical prediction for the growth rate function of the wave number. Moreover, the simulations show that,in non-linear stage, this instability produces an equilibrium configuration where dislocations from the initially planar GB decorate the precipitate and relax the misfit stresses (Fig 1.d). Those results are described in[Geslin, Wu, and Karma, Phys. Rev. Lett.,accepted, in press 2015].More simulations are being performed to investigate this instability for other relevant geometries (circular and cubic precipitates).

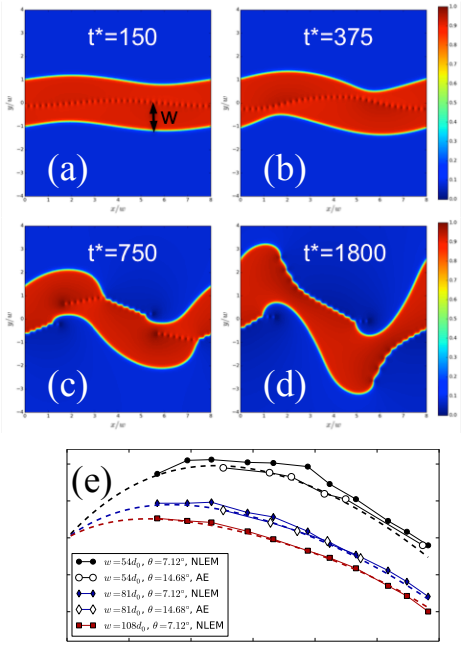

Fig. 1: (a-d) Snapshots ofsimulations illustrating the morphological instability of a GB centered in a lamellar precipitate. (e) Growth rate of the instability function of the wave number for different value of the width *w*. Comparison between analytical solution (dashed lines) and numerical results (symbols).

Stability of nanocrystallinematerials

Nanocrystalline (NC) materials, i.e. polycrystalline materials with a grain size in the range of ten to a few hundred nanometers, have attracted considerable interest because they exhibit a number of unique mechanical, chemical and electrical properties. However, the high GB

content can make NC materials structurally unstable, resulting in rapid grain growth and loss of properties. We have used large-scale molecular dynamics (MD) simulations to investigate basic mechanisms ofgrain growth infree-standing(001) thin films of NCcopper at 800K and 1250K (Fig. 2a-b). We find that the grain growth behavior departs markedly from the behavior predicted by the classical curvature-driven Mullins model. As compared to the prediction of this model, the grain size distribution in MD simulationsexhibits an excess of small grains, characterized by a shift of the peak of the distribution to small grain size (the so-called "ear" of the distribution), and an excess of very large grains, characterized by long "tail" of the distribution.While a qualitatively similar ear-and-tail distribution has been found experimentally to describe grain growth in thin metallic films and PFC simulations, the origin of this distribution has remained unknown.The MD simulations have allowed us to pinpoint for the first time the mechanism responsible for the stagnation of small grains, which underlies the ear of the distribution. Quantitative analysis of the evolution of the GB network reveals that the shrinkage of small grains is dramatically slowed down, or even stopped, by the geometrical coupling between normal GB motion and lattice translation [Karma et al, Phys. Rev. Lett.**109**, 095501 (2012)]. For a grain to shrink, lattice translation directions adjacent to each GB must be compatibleto allow GBs to move in a coordinate manner so as to produce a net grain rotation.However, for most small grains, directions conflict leading to "geometrical frustration". This mechanism is illustrated fora five-grain systeminFig. 2.d. In this example, the central grain shrinks initially bya dislocation dissociation-recombination mechanism([100]-type dislocations propagate along the GBs by dissociation recombination with [110]/2-type dislocations and become absorbed at triple junctions). This mechanism causes initially asymmetrical GBs surrounding the central grain to evolve towards lower energy symmetrical GBs. Because the lattice translation directions (represented by green arrows)associated with theinward motion of those symmetrical GB are conflicting, GB migration is stopped.Geometrically-frustrated grain growth stagnationalso occurs in the non–idealized grain growth simulations of Fig. 2.a-b.Theseprocesses are also affected by temperature. At higher temperature (1250K),geometrical frustration is found to be relieved by thermally-activated GB sliding, which facilitates GB normal motion without lattice translation and provides a natural explanation for the dependence of the grain growth exponent on temperature.

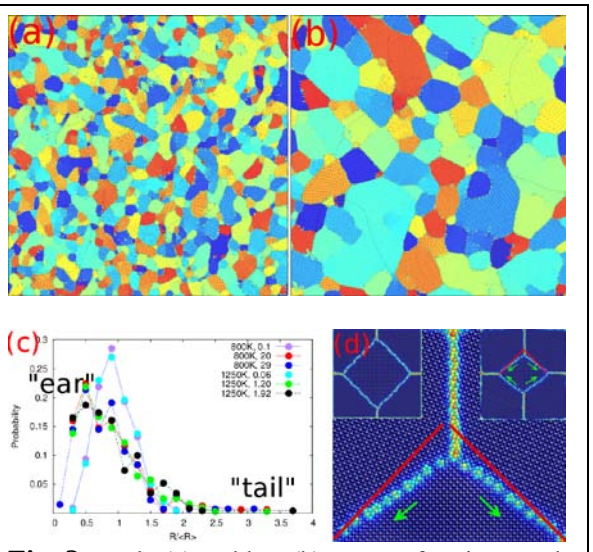

Fig. 2: Early (a) and late (b) stages of grain growth in molecular dynamics simulation of a (001)nanocrystalline thin Cu film at 800K. The color shows the grain disorientation (from -45° to 45°**)**. (c) Reduced grain size distribution at different times and temperatures showing an excess of small and large grains corresponding to an "ear" and "tail" of the distribution. (d) Five-grain simulation illustrating the mechanism of geometrical frustration. The red lines show the initial positions of the top GBs. The central grain stops shrinking because of the conflicting lattice translation directions shown with green arrows.

Bulk nanocomposite andnanoporous structure formation by liquid metal dealloying

Liquid metal dealloying has recently emerged as a novel method to produce bulk nanocomposite metallic structures with outstanding properties including high strength, high ductility, and high interfacial area. It has also been used recently used to produce bulk nanoporous silicon negative electrode material with high cyclability for Li-ion batteries. However the basic mechanisms that control the formation and behavior of those nanostructures are not well understood. We have developed a ternary alloy phase-field model of liquid metal dealloying to investigate the formation processes of these complex structures. The model relies on the coupling between the composition fields and an order parameter distinguishing the liquid and solid phases. This model was usedto investigate dealloying of tantalum-titanium (Ta-Ti) alloys by a copper (Cu) liquid bath. The comparison with experimental results is made possible by a collaboration with Jonah Erlebacher's group, specialized in the elaboration of nanoporous structures by liquid metal dealloying.

The phase-field simulations reveal that the initial formation stage of the nanoporous structurecan be seen as a surface spinodal decomposition between Ta-rich and Ta-poor regions along the interface (Fig. 3.a and e). The further dissolution of Ti can only proceeds in Ta-poor regions, leading to the penetration of the liquid in these regions (Fig. 3.b and f). At low Ta composition (e.g. 10%-Ta in Fig. 3a-d), the development of Rayleigh-Plateau instability leads to the formation of non-connected Ta-rich blobs. At intermediate Ta compositions (between 20% and 40%), we obtain a connected nanoporous structure (see Fig. 3.e-h).

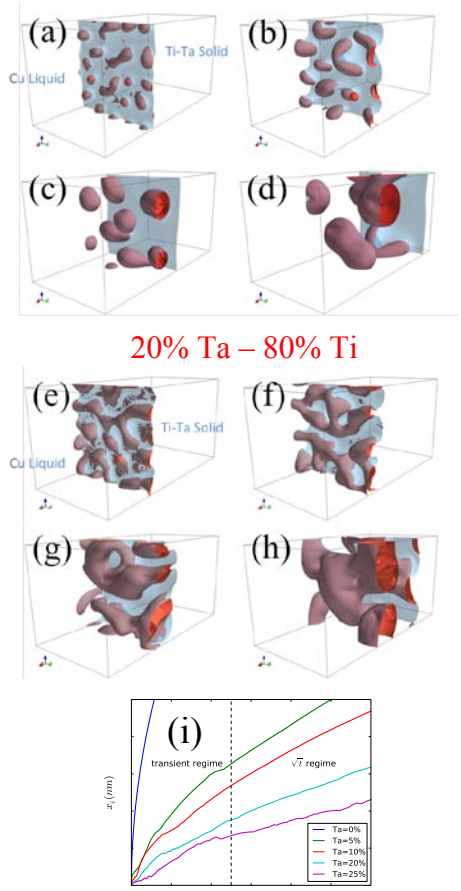

Fig. 3: (a-d) Phase-field simulations of liquid metaldealloyingof a 10%Ta-90%Ti alloy. The transparent blue surface represents the solid-liquid interface and the red domains are Ta-rich regions. (e-h) Simulated dealloying process for a 20%Ta-80%Ti alloy: Formation of a connected nanoporous structure. (i) Position of the interface vs. dealloying time revealing a $\sqrt{t}$ regime for different Ta composition in the solid.

At higher composition (greater or equal than 50%), the dealloying process is stopped by the accumulation of Ta at the interface. These three steps compare very well with the experimental observations of the same system. The dealloying kinetics has also been investigated using large scale 2D simulations (see Fig. 3.i). We note that the Ta content of the alloy slow down significantly the dissolution process. The kinetics quickly reaches a regime where the interface position evolves like $\sqrt{t}$. This behavior, characteristic of diffusion-limited kinetics, is attributed to the diffusion of Ti away from the dealloying front.

Experimental measurements show the existence of this regime during the dealloying process. Our phase-field model is able to reproduce all the characteristic features observed experimentally (mechanisms, morphology, kinetic).

Future Plan

Our future studies will be carried out in several directions. We will extend the investigation of the interaction between GBs and precipitate structures in two-phase coherent solids to include the effects of elastic anisotropy and different precipitate morphologies.We will pursue our phase-field study of liquid metal dealloying to better characterize the conditions (temperature and alloy compositions) leading to nanoporosity formation in the Ta-Ti-Cu system and investigate other systems (e.g the ternary Mg-Si-Bi ternary system used to produce nanoporous Si). In parallel, we will pursue our ongoing phase-field simulation study of grain-boundary premelting in metallic alloys and the further development of the phase-field-crystal method to incorporate quantitatively vacancy diffusion.

References to DOE sponsored publications (2012to 2015)

1. "Surface modes of coherent spinodal decomposition", M. Tang and A. Karma, *Phys. Rev. Lett.***108**, 265701 (2012).
2. "Coupled motion of asymmetrical tilt grain boundaries: Molecular dynamics and phase-field crystal simulations", Z.T. Trautt, A. Adland, A. Karma, and Y. Mishin,*ActaMaterialia***60**, 6528-6546 (2012).
3. "Relationship between Equilibrium Fluctuations and Shear-Coupled Motion of Grain Boundaries", A. Karma, Z.T. Trautt, and Y. Mishin, *Phys. Rev. Lett.***109**, 095501 (2012).
4. "Structural short-range forces between solid-melt interfaces", R. Spatschek, A. Adland, and A. Karma, *Phys. Rev.* B**87**, 024109 (2013).
5. "Phase-field-crystal study of grain boundary premelting and shearing in bcc iron", A. Adland, A. Karma, R. Spatschek, D. Buta, and M. Asta, *Phys. Rev.* B**87**, 024110 (2013).
6. "Unified Theoretical Framework for Polycrystalline Pattern Evolution", A. Adland, Y. Xu, and A. Karma, *Phys. Rev. Lett.* **110**, 265504 (2013).
7. "Phase-field modeling of grain-boundary premelting using obstacle potentials", V. SaiPavan Kumar Bhogireddy, C. Hüter, J. Neugebauer, I. Steinbach, A. Karma, and R. Spatschek, *Phys. Rev.* E**90**, 012401 (2014).
8. Ginzburg-Landau theory of the bcc-liquid interface kinetic coefficient, K.-A. Wu, C.-H. Wang, J.J. Hoyt, and A. Karma, *Phys. Rev.* B **91**, 014107 (2015).
9. "Morphological instability of grain boundaries in two-phase coherent solids", P.-A. Geslin, Y. Xu, and A. Karma, *Phys. Rev. Lett.* (accepted, in press 2015).

DOE award # DESC0003904, University of California, Irvine

Evaluating the Oxidative, Photothermal and Electrical Stability of Colloidal Nanocrystal Solids

PI: Matt Law
University of California, Irvine
Departments of Chemistry and Chemical Engineering and Materials Science
1120 Natural Sciences II, UC Irvine, Irvine, CA. 92697, lawm@uci.edu

Program Scope

IV-VI quantum dot (QD) solids are a novel class of granular electronic materials with great technological potential (e.g., in photodetectors, field-effect transistors (FETs), and solar cells), but their oxidative and thermal instability present a barrier to practical applications [1]. Poor stability is a fundamental issue facing many nanoscale materials due to high surface area and surface energy. Basic studies are needed to elucidate the most important mechanisms of degradation and develop robust countermeasures if QD materials are to become technologically important.

This project has determined the degradation mechanisms of IV-VI QD solids (primarily PbSe and PbS) and introduced new chemical strategies to drastically improve their performance, stability, and operating lifetimes [2-5]. Our approach is based on (1) detailed testing of QD thin film materials (principally FETs and solar cells) as a function of oxidative and thermal stress, and (2) using organic and inorganic approaches to link the QDs into strongly electronically coupled, high-mobility films, prevent their oxidation, and eliminate internal degrees of freedom that lead to film instability and degradation in response to electrical and thermal stress.

Stability against oxidation and thermal degradation is a major focus of this project. We have evaluated the stability of QD thin films and interfaces at temperatures less than 100°C (the regime most relevant to solar and transistor applications). Low-temperature oxidation and sintering of QD films have been investigated using optical absorption spectroscopy, Fourier transform infrared spectroscopy (FTIR), current-voltage scanning of transistors and solar cells, X-ray photoelectron spectroscopy, and scanning Kelvin probe microscopy (SKPM). SKPM is being used to map the potential profiles of operating QD FETs and solar cells as a function of illumination, air exposure, and temperature, which provides detailed information on how the work functions, potential drops and charge concentrations within these materials change with oxidation and other factors. We have pursued two strategies to fabricate QD films with stable electrical characteristics: (1) the use of robust molecular surface ligands [2], and (2) "matrix engineering," i.e., infilling the QD solid with metal oxide or metal sulfide matrices by low-temperature atomic layer deposition (ALD) to passivate surface states, prevent oxidation, lock the QDs into position, inhibit diffusion, and tune the height and width of the inter-QD potential barriers that govern charge transport [5,6].

Poor stability is a common feature of nanoscale electronic materials, yet stability is all too rarely the focus of basic research. Fundamental studies are therefore needed to elucidate the most important mechanisms of degradation and develop simple yet effective countermeasures. By revealing both how QD solids degrade in response to environmental stresses (oxidative, photothermal, and electric) and how to prevent this degradation, the project has greatly improved our ability to develop stable, high-performance QD materials for real-world applications.

Recent Progress

Over the past two years of the project, we have used scanning Kelvin probe microscopy (SKPM) to map the electrical potential across the cross section of operating PbS quantum dot (QD) solar cells as a function of applied bias and illumination. SKPM measures the applied voltage (V_{DC}) required to nullify the local electrostatic force (i.e., the potential difference) between a metallic AFM tip and a sample separated by a small air gap. V_{DC} is thus a measure of the local vacuum level difference between tip and sample. SKPM line profiles of PbS QD cells show a surprisingly thin space-charge region in *p*-type QD layers paired with *n*-type ZnO or TiO_2 window layers in a heterojunction configuration (Figure 1). We find that most of the applied potential is dropped in the *n*-type metal oxide layer, with very little in the QD layer. The QD space-charge region is thinner than 50 nm and the potential is flat across most of the QD film. The lack of electric field in the QD film shows that the QD layer is not fully depleted, contrary to the "depleted heterojunction" model that is now popular in the QD PV literature [7]. Instead, the space-charge region is thin and most of the photogenerated carriers reach the contacts via diffusion rather than drift. There are several possible ways to explain our results: (i) *pn* heterojunction model with $p >> n$; (ii) *pn* heterojunction model in which the QD layer contains mobile protons that partially screen the built-in field and narrow the space-charge region; (iii) selective contact model. Our work shows the importance of increasing the carrier diffusion length for improving cell efficiency. It also suggests that current models of QD solar cell operation should be

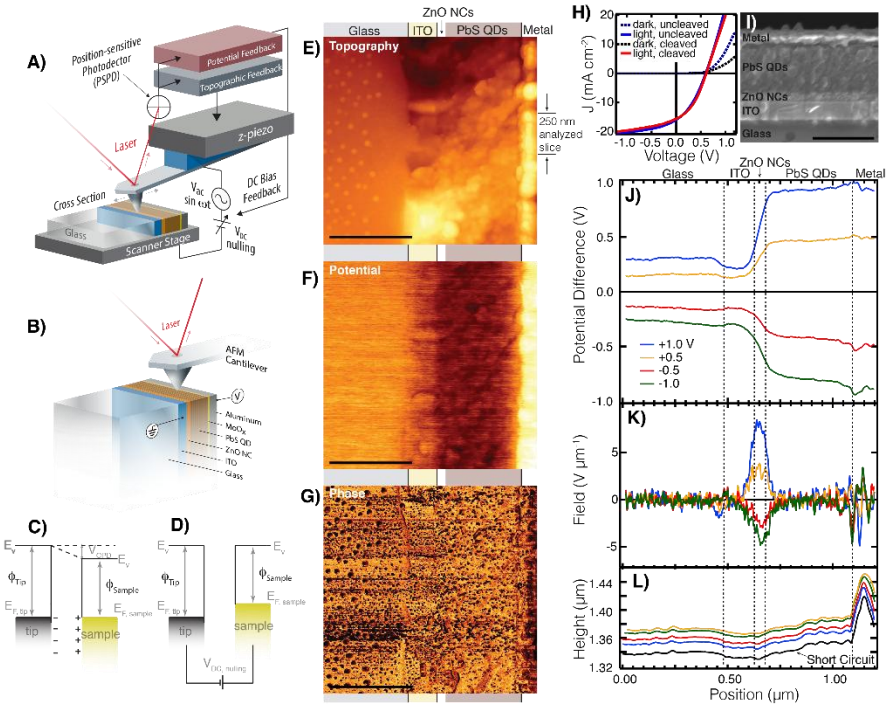

Figure 1. SKPM characterization of an operating PbS QD solar cell. (a) *Cartoon of the SKPM experimental setup.* ***(b)*** *A magnified view showing the experimental geometry and biasing arrangement.* ***(c)*** *Energy diagram for a tip-air-semiconductor system (ideal n-type semiconductor) in electrical contact at equilibrium.* ***(d)*** *Applying an external bias V_{DC} equal to the total vacuum level difference nullifies the tip-sample electrostatic force, thereby providing a measure of the local tip-sample potential difference.* ***(e)*** *Raw AFM topography,* ***(f)*** *potential difference (V_{DC}), and* ***(g)*** *phase images of a PbS QD solar cell cross section with the structure glass/ITO/ZnO NCs/PbS QDs/MoO_x/Al acquired at short circuit (V_{app} = 0 V) in the dark. The colored underlays demarcate the interfaces in the cross section and each horizontal scale bar is 500 nm.* ***(h)*** *J-V curves in the dark and at 1 sun illumination before and after cleaving the device.* ***(i)*** *SEM image of the device with all layers labeled. Scale bar is 500 nm.* ***(j)*** *Potential,* ***(k)*** *electric field, and* ***(l)*** *topography line profiles for various values of V_{app} in the dark, generated by averaging 250-nm thick slices of each image, as shown in* ***(e)****. Vertical dashed lines denote layer interfaces.*

reassessed and the possible role of mobile ions in determining cell electrostatics investigated in more detail. Finally, this work directly impacts the design of future QD solar cell architectures for enhanced photogenerated charge extraction.

In the past year, we have also demonstrated the first PbX QD field-effect transistors (FETs) that do not suffer from the bias-stress effect at room temperature. The bias-stress effect is an instability in which the drain current of a FET changes with time even at constant bias conditions. Usually this occurs when gate bias stress causes a progressive build-up of immobile charges near the dielectric/channel interfaces that screens the gate field, leading to drain current transients and shifts in threshold voltage. FETs with significant bias-stress effect are difficult to use in basic research and useless in practical technologies because such FETs do not hold their current. Unfortunately, all PbX FETs reported to date suffer from severe bias-stress effect that manifests as hysteresis in *I-V* curves. We have used our ALD matrix engineering strategy to eliminate the bias-stress effect in QD FETs, making the first high mobility, completely air stable, and completely bias-stress effect free PbX QD FETs. To achieve this, we used a pulse of H_2S gas to completely desorb volatile ligands coating the QDs, followed by infilling the QD film with amorphous alumina by low-temperature ALD. We determined that elimination of the bias-stress effect depends on complete ligand removal, the formation of a clean, well-passivated PbSe/PbS/alumina interface, and the sealing off of internal pore space to stop proton migration in the gate field. We elucidated two mechanisms for the bias-stress effect in these materials, both of which are inherent to the QDs rather than prosaic issues associated with the gate dielectric or FET contacts: (i) charge trapping / proton motion on the QD surface, and (ii) proton migration on the surface of the ALD oxide. It is unsurprising that high surface area, "messy" systems like QD solids contain mobile ions, but this has not been recognized by the community and mobile ions should have profound consequences for the operation of QD-based devices. Our development of the first high-mobility, environmentally stable, and transient-free QD FETs will help enable the practical use of QD films in FETs and solar cells.

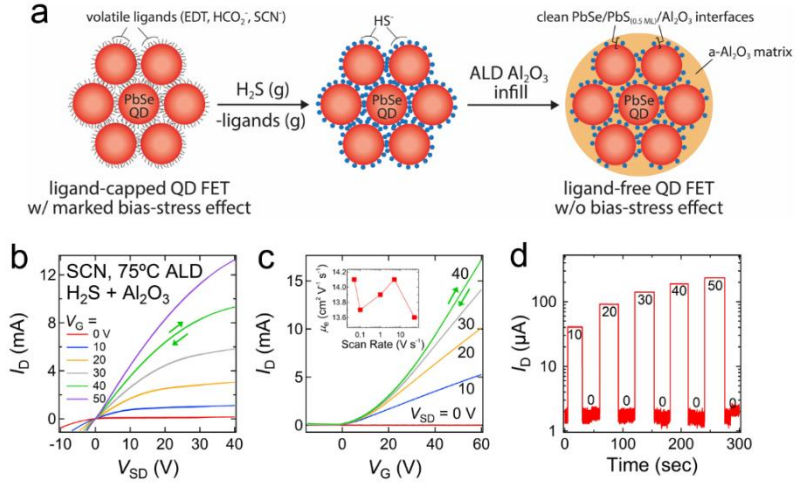

Figure 2. Design of bias-stress effect free QD FETs and example using SCN-capped PbSe QD films. (a) *Fabrication process. A single pulse of H_2S gas is used to protonate and completely remove a volatile organic ligand such as EDT, formate, or thiocyanate from the surface of the QDs. Deposition of alumina by low-temperature ALD then results in a ligand-free, atomically-clean PbSe/PbS/Al_2O_3 interface and a QD FET with negligible bias-stress transients at room temperature.* ***(b)*** *I_D-V_{SD} plots of a fully-infilled FET made from SCN-capped dots. There is no I-V hysteresis.* ***(c)*** *I_D-V_G plots. Inset shows a linear mobility of ~13.8 $cm^2\ V^{-1}\ s^{-1}$.* ***(d)*** *I_D-time plots showing the complete absence of bias-stress transients.*

Future Plans

Our major directions in the near future will include more in-depth and varied SKPM and EFM studies of working QD solar cells to determine their mechanisms of operation and to probe the real-time effects of oxidation, heat, light, and electric fields on the internal physics

of such cells. We will also use our high-mobility, air-stable, transient-free QD films made by ALD infilling to fabricate *p-n* heterojunction QD solar cells with record photocurrent and efficiency, with a short-term target of over 10%. We will extend our matrix engineering strategy to fabricate stable, high-mobility, and long diffusion length *n*-type and *p*-type QD solids with tunable doping, an important goal since doping in QD materials is poorly understood and uncontrolled. Finally, ionic transport in QD solids will be a new and exciting area of investigation originating from this project.

References

[1] Prospects of colloidal nanocrystals for electronic and optoelectronic applications. Talapin, D. V., Lee, J.-S., Kovalenko, M. V., Shevchenko, E. V. *Chem. Rev*. **110**, 389−458 (2010).
[2] p-Type PbSe and PbS quantum dot solids prepared with short-chain acids and diacids. Zarghami, M. H., Liu, Y., Gibbs, M., Gebremichael, E., Webster, C., Law, M. *ACS Nano* **4**, 2475-2485 (2010).
[3] Dependence of carrier mobility on nanocrystal size and ligand length in PbSe nanocrystal solids. Liu, Y., Gibbs, M., Puthussery, J., Gaik, S., Ihly, R., Hillhouse, H. W., Law, M. *Nano Letters* **10**, 1960-1969 (2010).
[4] The photothermal stability of PbS quantum dot solids. Ihly, R., Tolentino, J., Liu, Y., Gibbs, M., Law, M. *ACS Nano* **5**, 8175-8186 (2011).
[5] Robust, functional nanocrystal solids by infilling with atomic layer deposition. Liu, Y., Gibbs, M., Perkins, C. L., Zarghami, M. H., Bustamante, Jr., J., Law, M. *Nano Letters* **11**, 5349-5355 (2011).
[6] PbSe quantum dot field-effect transistors with air-stable electron mobilities above 7 cm^2 V^{-1} s^{-1}. Liu, Y., Tolentino, J., Gibbs, M., Ihly, R., Perkins, C. L., Liu, Y., Crawford, N., Hemminger, J. C., Law, M. *Nano Letters* **13**, 1578-1587 (2013).
[7] Depleted-heterojunction colloidal quantum dot solar cells. Pattantyus-Abraham, A. G., Kramer, I. J., Barkhouse, A. R., Wang, X., Konstantatos, G., Debnath, R., Levina, L., Raabe, I., Nazeeruddin, M. K., Grätzel, M., Sargent, E. H. *ACS Nano* **22**, 3374-80 (2010).

Journal Publications from DOE sponsored research in 2013-2015

1. PbSe quantum dot field-effect transistors with air-stable electron mobilities above 7 cm^2 V^{-1} s^{-1}. Liu, Y., Tolentino, J., Gibbs, M., Ihly, R., Perkins, C. L., Liu, Y., Crawford, N., Hemminger, J. C., Law, M. *Nano Letters*, **13**, 1578-1587 (2013).
2. Electrical potential mapping reveals dominant role of carrier diffusion in PbS quantum dot solar cells. Ihly, R., Nanayakkara, S. U., Gao, J., Zhang, J., Li, J., Nemmeth, W., Gibbs, M., Crisp, R., Law, M., Luther, J. M. *to be submitted.*
3. Elimination of bias-stress effect in ligand-free quantum dot field-effect transistors. Tolentino, J., Gibbs, M., Law, M. *to be submitted*.

Superconducting Materials

PI: Qiang Li
Condensed Matter Physics & Materials Science Department, Bldg. 480
Brookhaven National Laboratory, Upton, NY 11973-5000
631-344-4490, qiangli@bnl.gov

Program Scope

This program studies basic relationships between nanostructures and the macroscopic properties of superconductors. Both basic understanding and understanding of materials aspects for practical use are sought. Emphasis is on raising the critical temperature, T_c, and the critical current density, J_c, because they determine the limits to energy applications. Research activities focus on the responses of superconductivity and critical current to chemical, structural, and defect tuning in two classes of superconductors: (1) chalcogenides, and (2) cuprates. The key to increasing J_c is in controlling the pinning of magnetic vortices by defects in superconductors. In this program, defects are introduced precisely by controlled growth and ion irradiation. The goal is to create a landscape of tailored defects of desirable morphology and dimensions in superconductors that can produce the most effective vortex pinning in a broad range of temperatures and magnetic fields. Majority of materials are synthesized in thin film forms using an advanced pulsed laser deposition system capable of atomic layer-by-layer growth, and subsequently characterized via a range of techniques including transport, magneto-optical imaging, electron and optical spectroscopy, transmission electron microscopy, scanning tunneling microscopy, among others. We seek to understand and control the transport properties of superconducting materials by tackling a few key science issues, from the macroscopic to the atomic levels. Progress in the understanding of these two classes of materials could provide new strategies for enhancing T_c and designing new superconductors capable of enduring high magnetic fields and carrying high currents.

Recent Progress

A robust enhancement of T_c and J_c has been achieved in the $FeSe_{0.5}Te_{0.5}$ films irradiated with $1x10^{15}$ p/cm^2 dose of 190 KeV protons. The T_c^{zero} increased from 18.0 K to 18.5 K, while the self-field J_c was enhanced from 0.7 MA/cm^2 to 1.2 MA/cm^2, as shown in Figure 1. Extensive TEM analysis revealed that splayed cascade defects were produced by proton irradiation at this energy level. A modulation of compressive and tensile strain field was created in the vicinity of these defects, that leads to the enhancement of T_c in the irradiated

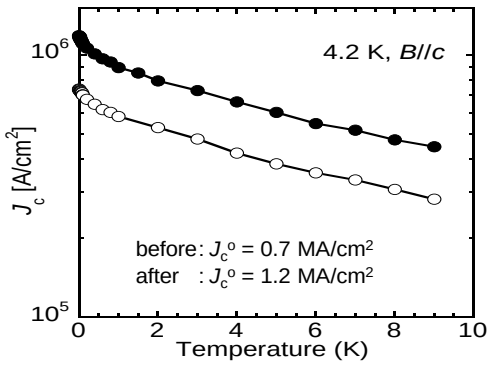

Figure 1 Temperature dependence of J_c of superconducting $FeSe_{0.5}Te_{0.5}$ films before and after 190 KeV proton irradiation

films, and strong vortex pinning, especially in high field and high temperature, resulting in an increase of J_c by one order of magnitude at 12 K over 6T. Simultaneous enhancement of T_c and J_c in superconductor was made possible for the first time by ion irradiation.

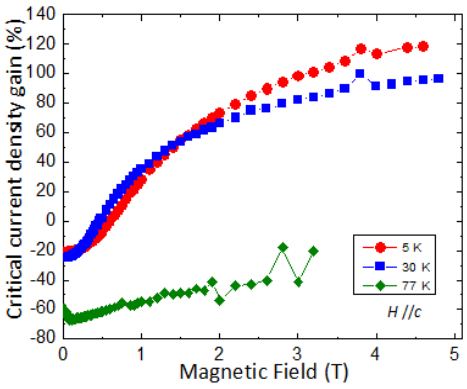

Figure 2 J_c grain in $YBa_2Cu_3O_7$ films at 5, 30, and 77 K after 18 MeV Au^{5+} irradiation

We observed a remarkable increase in J_c in $YBa_2Cu_3O_7$ films irradiated with 5-18 MeV Au^{5+}, as shown in Figure 2, and 1 MeV proton at 5 and 30 K. J_c enhancement increases monotonically with magnetic field. This observation suggests that point defects, created by 1–18 MeV ions, are effective pinning centers at low temperatures where vortex line is rather rigid. At 77 K, we observed an overall decrease in J_c in the irradiated samples, which is consistent with the view that point defects are not effective in pinning soft vortex lines in cuprate superconductors at elevated temperatures.

Grain boundary (GB) junctions were fabricated in the epitaxial $FeSe_{0.5}Te_{0.5}$ thin films on CeO_2 buffered [001] tilt $SrTiO_3$ bi-crystal substrates. J_c's across the junctions with different mis-orientation angles of 4º, 7º, 15º, 24º were measured at magnetic fields up to 30 T. It was found that the 4º and 7º junctions carry critical current densities comparable to that of the intra-grain film while those of the 15º and 24º junctions were suppressed drastically, as shown in Figure 3. A critical mis-orientation angle of 9º was identified that separates the low angle strong coupling region from the high angle weak link region. We found that the J_c across the grain boundary with a 24º mis-orientation angle are modulated by the magnetic field, indicating a Josephson effect. This junction is estimated to be in the intermediate-size regime with an effective transverse junction width $L \sim 2.6$-2.8 μm and a Josephson penetration depth $\lambda_J \sim 1.2$ μm. [Ref. 1]

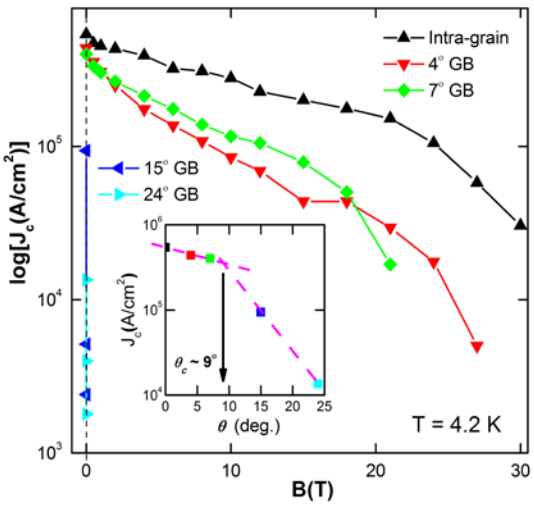

Figure 3 Field dependence of J_c ($B//c$) for the intra-grain and bi-crystal GB of $FeSe_{0.5}Te_{0.5}$ films at different misorientation angle θ at 4.2 K. Inset shows J_c's in self-field versus θ. A critical angle around 9º, which separates the low θ strong coupling region from the high θ weak link region, was identified by the arrow. (Ref. 1)

Although the cuprate high temperature superconductor (Cu-HTS) was discovered nearly thirty years ago, superconductors for high field applications are still based on low temperature superconductors (LTS), such as Nb_3Sn. The high anisotropies, brittle textures and high manufacturing costs, limit the applicability of the Cu-HTS. We demonstrated that the iron based superconductors, without most of the drawbacks of the cuprates, exhibit superior high field performances over LTS's at 4.2 K. [Ref. 2] J_c's above 10^6 A/cm^2 were observed in iron-chalcogenide $FeTe_{0.5}Se_{0.5}$ films grown on CeO_2 buffered single crystalline and bi-axial aligned Ni-W metal substrates. These robust films are capable of carrying record high J_c's exceeding 10^5 A/cm^2 under 30 T magnetic fields. In contrast to Cu-HTS, nearly isotropic J_c were observed at low temperatures and high fields in iron chalcogenides. This study opens new pathways for the potential high field applications of iron-based superconductors at liquid helium temperatures. [Ref. 2, 3] Recently, we performed magneto-optical image (MO) studies on proton irradiated and un-irradiated $FeTe_{0.5}Se_{0.5}$ thin films grown on $LaAlO_3$ (LAO) and Yttria-stabilized zirconia (YSZ) single-crystalline substrates. Typical roof-top patterns can be observed in the MO images of the thin films, from which homogeneous J_c over 1×10^6A cm^{-2} at 5 K was obtained. Magnetic flux penetration measurement reveals that the current is almost isotropically distributed in all thin films, as shown in Figure 3. [Ref. 4]

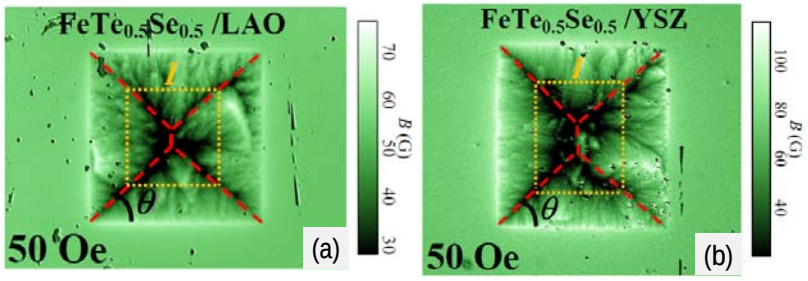

Figure 3 Magneto-optical images of flux penetrations into the $FeTe_{0.5}Se_{0.5}$ thin films grown on LAO and YSZ substrates at 5 K under 50 Oe magnetic fields. The red dashed lines in (a) and (b) show the current discontinuity lines, which cannot be crossed by vortices. The yellow dotted lines are the schematics of the current distributions in the thin films. [Ref. 4]

We found post-annealing of a polar (001) Ceria surface can produce stable surface reconstructions, which have markedly different surface activities for the growth of iron-chalcogenide and cuprate thin films on CeO_2 buffered substrates. $YBa_2Cu_3O_7$ film grown on (001) CeO_2 surface having the longest, fourfold period, reconstruction exhibits a twofold increase in J_c over surfaces with shorter period reconstructions. [Ref. 5] Iron chalcogenide thin films made with CeO_2 buffer are found to have record high J_c under high magnetic

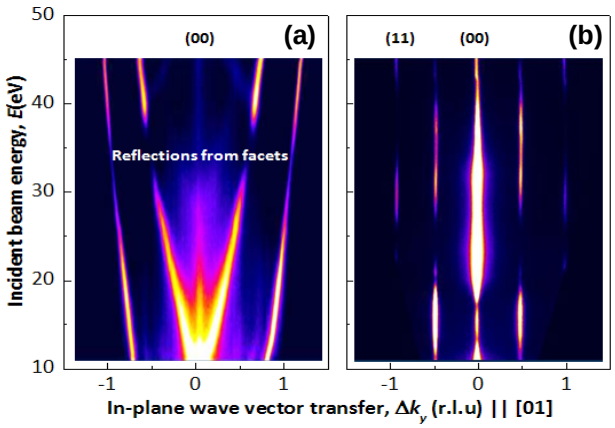

Figure 5 Reciprocal space maps of CeO_2 buffer surface obtained by micro-LEED, showing strong (111) faceting on the surface of as-deposited buffer (a) and sharp (001) termination on the post-processed buffer (b), [Ref. 5]

field. [Ref. 2] These findings opened a new avenue for catalysis mediated solid state synthesis of new complex materials.

Future Plans

A complete understanding of critical current and vortex pinning in superconductors requires studies of both elementary pinning and collective pinning mechanisms. With its atomic scale structural and spectroscopic imaging abilities, spectroscopy Scanning Tunneling Microscopy (STM) is an ideal tool for studying the elemental pinning processes in superconductors. Recently, superconducting gap map and vortex lattices of $CeCoIn_5$ have been measured by the BNL's Spectroscopic Imaging group [Ref. 6]. Detailed vortex arrangements can be used to understand the collective pinning mechanisms leading to various vortex states.

We plan to study the elemental pinning behavior in iron chalcogenide thin films by directly probing the interaction between vortices and defects, which will be introduced by controlled irradiation. A collaborative effort has been established which includes i) thin film synthesis, irradiation experiments, magnetic and transport measurement in our group (Li); ii) STM investigations by J. Lee and J. C. Davis (BNL's the Spectroscopic Imaging group) for electron scattering and spectroscopic properties of defects and matrix; iii) defect and local structural characterization by L. Wu and Y. Zhu (BNL's the Electron Microscopy group). These studies are expected to provide answers to two fundamental questions on vortex matter in superconductor:

1) What are the electronic structure of vortex and elementary pinning processes?
2) What is the relative role and strength of vortex-vortex interactions and vortex-defect interactions in various parts of the vortex phase diagram of iron based superconductors, and how does it respond to a different defect landscape?

References

1) W. Si, C. Zhang, X. Shi, T. Ozaki, J. Jaroszynski, and Q. Li "Grain boundary junctions of $FeSe_{0.5}Te_{0.5}$ thin films on $SrTiO_3$ bi-crystal substrates" *Appl. Phys. Lett*. **106**, 032602 (2015)
2) W. Si, S. Han, X. Shi, S. N. Ehrlich, J. Jaroszynski, A. Goyal & Q. Li "High current superconductivity in $FeSe_{0.5}Te_{0.5}$ -coated conductors at 30 tesla" *Nature Commun*. 4:1347 doi: 10.1038/ncomms2337 (2013).
3) Q. Li, W. Si and I. K Dimitrov, "Films of iron chalcogenides superconductors", *Rep. Prog. Phys*. **74** 124510 (2011).
4) Y. Sun, Y. Tsuchiya, S. Pyon, T. Tamegai, C. Zhang, T. Ozaki, & Q. Li "Magneto-optical characterizations of $FeTe_{0.5}Se_{0.5}$ thin films with critical current density over 1 $MA.cm^{-2}$" *Supercond. Sci. Technol*. **28** 015010 (2015)
5) V. F. Solovyov, T. Ozaki1, A. Atrei, L. Wu, A. Al-Mahboob, J. T. Sadowski, X. Tong, D. Nykypanchuk & Q. Li "Highly efficient solid state catalysis by reconstructed (001) Ceria surface" *Sci. Rep*. **4**, 4627; DOI:10.1038/srep04627 (2014).

6) M. P. Allan, J. C. Davis, et al "Imaging Cooper pairing of heavy fermions in $CeCoIn_5$" *Nature Physics* **9** 468 (2013)

Publications (supported by this FWP in 2013-2015)

1) W. Si, C. Zhang, X. Shi, T. Ozaki, J. Jaroszynski, and Q. Li "Grain boundary junctions of $FeSe_{0.5}Te_{0.5}$ thin films on $SrTiO_3$ bi-crystal substrates" *Appl. Phys. Lett*. **106**, 032602 (2015)

2) Y. Sun, Y. Tsuchiya, S. Pyon, T. Tamegai, C. Zhang, T. Ozaki, and Q. Li "Magneto-optical characterizations of $FeTe_{0.5}Se_{0.5}$ thin films with critical current density over 1 $MA.cm^{-2}$" *Supercond. Sci. Technol*. **28** 015010 (2015)

3) J. Wang, R. Zhong, S. Li, Y. Gan, Z. Xu, C. Zhang, T. Ozaki, M. Matsuda, Y. Zhao, Q. Li, G. Xu, G. Gu, J. M. Tranquada, R. J. Birgeneau, and Jinsheng Wen, "Substitution of Ni for Fe in superconducting $Fe_{0.98}Te_{0.5}Se_{0.5}$ depresses the normal-state conductivity but not the magnetic spectral weight" *Phys. Rev.* B **91**, 014501 (2015)

4) V. F. Solovyov, T. Ozaki1, A. Atrei, L. Wu, A. Al-Mahboob, J. T. Sadowski, X. Tong, D. Nykypanchuk and Q. Li "Highly efficient solid state catalysis by reconstructed (001) Ceria surface" *Sci. Rep*. **4**, 4627; DOI:10.1038/srep04627 (2014).

5) Y. M. Dai, A. Akrap, J. Schneeloch, R. D. Zhong, T. S. Liu, G. D. Gu, Q. Li, and C. C. Homes, "Spectral weight transfer in strongly correlated $Fe_{1.03}Te$" *Phys. Rev*. B **90**, 121114 (R) (2014)

6) X. Shi, X. Shi, Y. Li, Y. He, L. Chen, and Q. Li, "Enhanced power factor of higher manganese silicide via melt spin synthesis method" *J. of Appl. Phys*. **116**, 245104 (2014)

7) H. Hu, Y. Zhu, X. Shi, Q. Li, R. Zhong, J. A. Schneeloch, G. Gu, J. M. Tranquada, and S. J. L. Billinge, "Nanoscale coherent intergrowthlike defects in a crystal of $La_{1.9}Ca_{1.1}Cu_2O_{6+\delta}$ made superconducting by high-pressure oxygen annealing" *Phys. Rev*. B **90**, 134518 (2014)

8) H. Chi, H. Kim, J. Thomas, G. Shi, K. Sun, M. Abeykoon, E. Bozin, X. Shi, Q. Li, X. Shi, E. Kioupakis, A.Van der Ven, M. Kaviany, and C. Uher, "Low-temperature structural and transport anomalies in Cu_2Se" *Phys. Rev*. B **89**, 195209 (2014)

9) W. Si, S. Han, X. Shi, S. N. Ehrlich, J. Jaroszynski, A. Goyal & Q. Li "High current superconductivity in $FeSe_{0.5}Te_{0.5}$ -coated conductors at 30 tesla" *Nature Communications* 4:1347 doi: 10.1038/ncomms2337 (2013).

10) I. K. Dimitrov, W. D. Si, W. Ku, S. J. Han, and J. Jaroszynski "Unusual persistence of superconductivity against high magnetic fields in the strongly correlated iron-chalcogenide film $FeTe:O_x$" *Low Temperature Physics* **39**, 680 (2013)

11) V. F. Solovyov, I. Dimitrov, and Q. Li, "Growth of thick $YBa_2Cu_3O_7$ layers by barium fluoride" *Supercond. Sci. and Technol*. **26** 013001 (2013)

12) H. Liu, X. Shi, M. Kirkham, H. Wang, Q. Li, C. Uher, W. Q. Zhang, and L. D. Chen "Structure-transformation-induced abnormal thermoelectric properties in semiconductor copper selenide" *Materials Letters* **93** 121 (2013)

13) J. Wen, S. Li, Z. Xu, C. Zhang, M. Matsuda, O. Sobolev, J.-T. Park, A. Christianson, E. Bourret-Courchesne, Q. Li, G. Gu, D. Lee, J. M. Tranquada, G. Xu, and R. J. Birgeneau "Enhanced low-energy magnetic excitations via suppression of the itinerancy in $Fe_{0.98-z}Cu_zTe_{0.5}Se_{0.5}$" *Phys. Rev*. B **88**, 144509 (2013)

14) L. Wu, Q. Meng, C. Jooss, J. C. Zhang, H. Inada, D. Su, Q. Li, Y. Zhu "Origin of Phonon Glass–Electron Crystal Behavior in Thermoelectric Layered Cobaltate" *Advanced Functional Materials* **23**, 5728–5736 (2013).

15) R. D. Zhong, J. A. Schneeloch, X. Y. Shi, Z. J. Xu, C. Zhang, J. M. Tranquada, Q. Li, and G. D. Gu "Optimizing the superconducting transition temperature and upper critical field of $Sn_{1-x}In_xTe$" *Phys. Rev*. B **88**, 020505(R) (2013)

16) Z. Stegen, S. Han, J. Wu, A. K. Pramanik, M. Hucker, G. Gu, Q. Li, J. H. Park, G. S. Boebinger, and J. M. Tranquada, "Evolution of superconducting correlations within magnetic-field-decoupled $La_{2-x}Ba_xCuO_4$ (x = 0.095)" *Phys. Rev*. B **87**, 064509 (2013)

DOE award # DE-FG02-04ER46148, University of Utah

Effect of Mechanical Strain and Quantum Electronic Stress on Physical Behavior of Bulk Materials and on Growth Property of Solid Nanomembranes

PI: Feng Liu (fliu@eng.utah.edu)
Department of Materials Science & Engineering
University of Utah, Salt Lake City, UT 84112

Program Scope

This project encompasses four diverse but correlated research thrusts: (1) to continue our traditional efforts in the area of strain induced self-assembly of nanostructures in heteroepitaxial growth of thin films, (2) to expand a new research direction in exploring the "quantum electronic stress" effect, a new conceptual extension over the conventional mechanical stress effect we developed recently, (3) to foster a new research direction in studying the effect of strain on topological and electronic phases, such as topological insulator, of thin films, and (4) theoretical studies of group-IV nanomembranes in close collaboration with experiments by Prof. Lagally funded by the "Materials Synthesis and Processing" program of the same DOE-BES division. The common theme of our research efforts will remain focusing on fundamental understanding of stress/strain effect on physical behaviors of materials and on growth property of thin films. The focused specific topics in the four thrusts include: (1) Nonlinear elastic effects on nucleation and growth of strained islands inside and outside a patterned pit, (2) Quantum electronic stress induced solid-state structural phase transitions, (3) Effect of strain on topological and electronic phase transitions in Bi(111) and Sb(111) thin films. (4) Effect of strain on growth, structural, mechanical and transport properties of Si and other solid nanomembranes. Our theoretical/computational project will employ a multi-scale approach, combining several state-of-the-art theoretical and computational techniques, ranging from density-functional-theory based first-principles electronic structure calculations to continuum elasticity theoretical modeling. Broadly, our project will have direct technological impact on advancing electronic and optoelectronic materials for energy applications, to fulfill the mission of the Department of Energy.

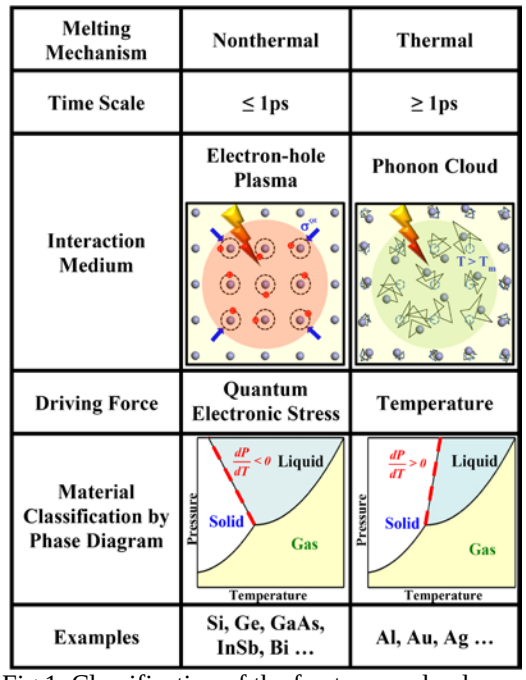

Fig.1. Classification of the femtosecond pulse laser induced ultrafast crystal-to-liquid phase transitions, under highfluence. The distinct time scale, interaction medium, driving force, phase diagram and examples are listed to distinguish nonthermal from thermal melting process.

Recent Progress

(1) **Quantum Hooke's Law to Classify Pulse Laser Induced Ultrafast Melting [1]**:Ultrafast crystal-to-liquid phase transition induced by femtosecond pulse laser excitation is an interesting material's behavior manifesting the complexity of light-matter interaction. It has been recognized there exist two types of such phase transitions: one occurs at a time scale shorter than a picosecond via a

nonthermal process mediated by electron-hole plasma formation; the other at a longer time scale via a thermal melting process mediated by electron-phonon interaction. However, it remains unclear what material would undergo which process and why? Recently, by exploiting the property of quantum electronic stress (QES) governed by quantum Hooke's law [1], we classify the transitions by two distinct classes of materials (Fig. 1): the faster nonthermal process can only occur in materials like ice having an anomalous phase diagram characterized with $dT_m/dP < 0$, where T_m is the melting temperature and P is pressure, above a high threshold laser fluence; while the slower thermal process may occur in all materials. Especially, the nonthermal transition is shown to be induced by the QES [1], acting like a negative internal pressure, which drives the crystal into a "super pressing" state to spontaneously transform into a higher-density liquid phase. Our findings significantly advance fundamental understanding of ultrafast crystal-to-liquid phase transitions, enabling quantitative a priori predictions.

(2) **Prediction of Organic Topological Insulators [6, 26-29]:**Topological insulators (TIs) are a recently discovered class of materials having insulating bulk electronic states but conducting boundary states distinguished by nontrivial topology. So far, several generations of TIs have been theoretically predicted and experimentally confirmed, all based on inorganic materials. Recently, we predicted the existence of a new family of two-dimensional organic TIs made of organometallic lattices [26-29], based on first-principles calculations and tight-binding model analyses. Designed by assembling molecular building blocks of organometallic compounds with strong spin-orbit coupling into a hexagonal and Kagome lattices (Fig. 2), these new classes of organic topological materials are shown to exhibit nontrivial topological edge states in both Dirac bands [26-29] and flat Chen bands (so-called fractional Chern insulator) [26,27], which are robust against significant lattice strain. Realization of half metallic state and anomalous quantum Hall effect in magnetic organic TIs with the inclusion of transition metal elements was also demonstrated [28]. We envision that organic topological materials will greatly broaden the scientific scope and technological impact of emerging topological materials.

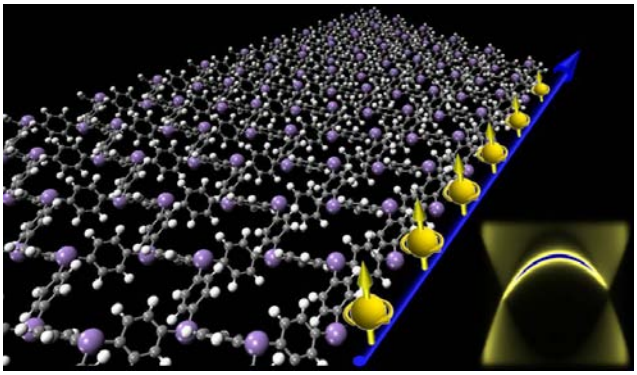

Fig. 2.Left: Atomic lattice of organometallic framework with the conducting edge spin current illustrated. Right: Electronic band structure showing topological edge state inside bulk band gap.

(3) **Epitaxial Growth of Large-gap Topological Quantum State on Semiconductor Substrate [3,4,7]:**Recently, we propose an approach to create topological quantum states on conventional semiconductor surfaces by epitaxial growth processes. For example, we show that Si(111) surface functionalized with 1/3 monolayer of halogen atoms exhibiting a trigonal superstructure, provides an ideal template for epitaxial growth of heavy metals like Bi which self-assemble into a hexagonal lattice with high kinetic and thermodynamic stability. Most remarkably, the Bi overlayer is 'atomically' bonded to but 'electronically' decoupled from the underlying Si substrate, exhibiting isolated QSH state with a large energy gap of 0.8 eV [4]. This surprising phenomenon is originated from an intriguing substrate orbital filtering effect, which critically select the orbital composition around the Fermi level leading to different topological phases. Furthermore, deposition of transition metal, e.g., W on the same template leads tothe formation of a new 2D material---sd^2 graphene, consisting of sd^2 hybridized atomicorbits in hexagonal lattice (Fig. 3). It is characterized with bond-centered electronic

hopping, which transforms the apparent atomic hexagonal lattice into the physics of Kagome lattice that exhibits room temperature quantum anomalous Hall state. We expect these significant findings to open up a new avenue to exploring novel topological quantum materials based on conventional semiconductor technology.

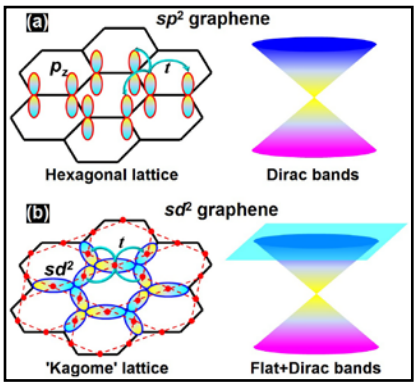

Fig. 3.Schematics of structural and electronic properties of (a) sp^2 graphene made of C and (b) sd^2 graphene made of W on Si. Electronic hopping (t) of C p_z-orbital in a hexagonal lattice (a, left panel) that leads to a Dirac band (a, right panel) is indicated. Also, hopping of bond-centered$sd^2\sigma$ state in a hexagonal lattice (b, left panel), which can be renormalized into hoping in a Kagome lattice (red dots and dashed lines in b, left panel) that leads to a Kagome band (b, right panel) is indicated.

Future Plans

We will continue to expand our current studies as described above, and the planned research topics in the next year include:

(1) Modeling vertical and lateral growth of Van der Waals 2D materials
(2) Search for new inorganic and organic topological materials
(3) Explore different epitaxial growth routes towards formation of topological quantum phases on semiconductor surfaces
(4) Continue the efforts of experimental collaborations.

Published Journal Publications of DOE sponsored research in 2013-2015

1. "Quantum Hooke's Law to Classify Pulse Laser Induced Ultrafast Melting", H. Hu, H. Ding and Feng Liu, *Sci. Rep.***5**, 8212 (2015).
2. "Silicon nanomembranes as a means to evaluate stress evolution in deposited thin films", A. M. Clausena, D. M. Paskiewicz, A. Sadeghiradb, J. Jakes, D. E. Savage, D. S. Stone, Feng Liu, M. G. Lagally, *Extreme Mechanics Letters***1**, 9 (2014).
3. "Half metal in two-dimensional hexagonal organometallic framework", H. Hu, Z. Wang and Feng Liu, *Nanoscale Research Letters***9**, 690 (2014).
4. "sd^2 Graphene: Kagome Band in Hexagonal lattice", M. Zhou, Z. Liu, W. Ming, Z. Wang, and Feng Liu, *Phys. Rev. Lett.* **113**, 236802 (2014).
5. "Epitaxial growth of large-gap quantum spin Hall insulator on semiconductor surface", M. Zhou, W. Ming, Z. Liu, Z. Wang, P. Li, Feng Liu, *Proc. Natl. Acad. Sci.*, **111**, 14378 (2014).
6. "Tuning Topological Edge States of Bi(111) Bilayer Film by Edge Adsorption", Z. F. Wang, Li Chen, and Feng Liu, *Nano Lett.*, **14**, 2879 (2014).
7. "Redox Control and High Conductivity of Nickel Bis(dithiolene) Complex π-Nanosheet: A Potential Organic Two-Dimensional Topological Insulator", T.Kambe, R. Sakamoto, T.Kusamoto, T. Pal, N. Fukui, K.Hoshiko, T.Shimojima, Z. Wang, T.Hirahara, K. Ishizaka, S. Hasegawa, Feng Liu, and H. Nishihara, *J. Am. Chem. Soc.*, **136**, 14357 (2014).
8. "Formation of quantum spin Hall state on Si surface and energy gap scaling with strength of spin orbit coupling", M. Zhou, W. Ming, Z. Liu, Z. Wang, Y. Yao, and Feng Liu, *Sci. Rep.***4**, 7102 (2014).
9. "Prediction of a Dirac state in monolayer TiB_2", L. Z. Zhang, Z. F. Wang, S. X. Du, H.-J. Gao, and Feng Liu, *Phys. Rev. B***90**, 161402(R) (2014).
10. "Giant room-temperature spin caloritronics in spin-semiconducting graphene nanoribbons", X. Chen, Y. Liu, B. L. Gu, W. Duan and Feng Liu, *Phys. Rev. B***90**, 121403(R) (2014).

11. “Quantum size effect on dielectric function of ultrathin metal film: a first-principles study of Al(1 1 1)”, W. Ming, S. Blair and Feng Liu, *J. Phys.: Condens. Matter***26**, 505302 (2004).
12. “Tuning nucleation density of metal island with charge doping of graphene substrate”, W. Ming and Feng Liu, *Appl. Phys. Lett*., **105**, 071609 (2014).
13. “Curved carbon nanotubes: From unique geometries to novel properties and peculiar applications”, L. Liu, Feng Liu, and J. Zhao, *Nano Res*. **7**, 626 (2014). (**Review**)
14. “Understanding graphene production by ionic surfactant exfoliation:A molecular dynamics simulation study”, P. Yang and Feng Liu, *J. Appl. Phys*. **116**, 014304 (2014).
15. “Density-functional-theory formulation of classical and quantum Hooke’s law”, H. Hu and Feng Liu, *Sci China Tech Sci*, **57**, 692 (2014) (**Invited review**)
16. “Orbit- and Atom-Resolved Spin Textures of Intrinsic, Extrinsic and Hybridized Dirac Cone States”, L. Miao, Z.F. Wang, C.L. Gao, C. Liu, Feng Liu, D. Qiang, J.F. Jia, *Phys. Rev. B***89**, 155116 (2014).
17. “Quantum Manifestation of Elastic Constants in Nanostructures”, M. Liu and Feng Liu, *Nanotechnology***25**, 135706 (2014).
18. “A large-area 15 nm graphene nanoribbon array patterned by a focused ion beam”, Y. Zhang, C. Hui, R. Sun, K. Li, K. He, X. Ma and Feng Liu, *Nanotechnology***25**, 135301 (2014).
19. “Strain tuning of native defect populations: the case of $Cu_2ZnSn(S,Se)_4$”, J. Zhu, Feng Liu and M. Scarpulla, *APL Materials*. **2**, 012110 (2014).
20. “A three-layer-mesh bridging domain for coupled atomistic–continuum simulations at finite temperature: Formulation and testing”, A. Sadeghirad, F. Liu, Comput. *Methods Appl. Mech. Engrg*. **268**, 299 (2014).
21. “Effect of surfactant Sb on In incorporation and thin film morphology of InGaN layers grown by organometallic vapor phase epitaxy”, J. L. Merrell, Feng Liu, and G. B. Stringfellow, *J. Crys. Growth*, **375**, 90 (2013).
22. “Effects of Li doping on H-diffusion in MgH2: A first-principles study”, W. Ming, Z. Z. Fang and Feng Liu, *J. Appl. Phys*. **114**, 243502 (2013).
23. “Strain-Engineered Surface Transport in Si(001): Complete Isolation of the Surface State via Tensile Strain”, M. Zhou, Z. Liu, Z. Wang, Z. Bai, Y. Feng, M. G. Lagally, and Feng Liu, *Phys. Rev. Lett*. **111**, 246801 (2013).
24. “First-Principles Calculations on the Effect of Doping and Biaxial Tensile Strain on Electron-Phonon Coupling in Graphene”, C. Si, W. Duan, Z. Liu, and Feng Liu, *Phys. Rev. Lett*. **111**, 196802 (2013).
25. “Spatially separated spin carriers in spin-semiconducting graphene nanoribbons”, Z. F. Wang, S. Jin and Feng Liu, *Phys. Rev. Lett*. **111**, 096803 (2013).
26. “Robustness of two-dimensional topological insulator states in bilayer bismuth against strain and electrical field”, L. Chen, Z. F. Wang, and Feng Liu, *Phys. Rev. B***87**, 235420 (2013).
27. “Prediction of a Two-Dimensional Organic Topological Insulator”, Z. F. Wang, Ninghai Su, and Feng Liu, *Nano Letters*, **13**, 2842 (2013).
28. “Flat Chern Band in a two-dimensional organometallic framework”, Z. Liu, Z. F. Wang, J.-W. Mei, Y. Wu and Feng Liu, *Phys. Rev. Lett*. **110**, 106804 (2013).
29. “Quantum anomalous hall effect in 2D organic topological insulator”, Z. F. Wang, Z. Liu and Feng Liu, *Phys. Rev. Lett*. **110**, 196801 (2013).
30. “Organic topological insulators in organometallic lattices”, Z. F. Wang, Zheng Liu and Feng Liu, *Nature Commun*. **4**, 1471 (2013).
31. “Quasiparticle Dynamics in Reshaped Helical Dirac Cone of Topological Insulators”, L. Miao, Z. F. Wang, W. Ming, M. Yao, M. Wang, F. Yang, F. Zhu, A. V. Fedorov, Z. Sun, C. L. Gao, C. Liu, Q. Xue, Feng Liu, D. Qian, J. Jia, PNAS, **110**, 2758 (2013).
32. “Creation of Helical Dirac Fermions by Interfacing Two Gapped Systems of Ordinary Fermions”, Z.F. Wang, M.-Y. Yao, W. Ming, L. Miao, F. Zhu, C. Liu, C. L. Gao. D. Qian, J.F. Jia, and Feng Liu, *Nature Commu*.,**4**, 1384 (2013).

Study of p-type ZnO and MgZnO Thin Films for Solid State Lighting

Jianlin Liu, Department of Electrical Engineering, University of California, Riverside

Program Scope

The objective of this project is to investigate p-type doping of ZnOand MgZnO thin films. ZnO has a direct band gap of 3.37eV with anexciton binding energy of 60 meV at room temperature. Moreover, the band gap can be tuned by alloying with Mg (MgZnO) and Cd(CdZnO). These properties would allow ZnO to be an excellent material for energy-saving light emitting devices. Nevertheless, the major difficulty is to control its p-type conductivity, namely, to achieve reliable and stable p-type ZnO and alloys. Intrinsic ZnO shows n-type conductivity as a result of the presence of shallow donor defects in the crystal. Many different dopants have been introduced to achieve p-type thin films, such as lithium(Li), sodium(Na), silver(Ag), phosphorous(P), nitrogen(N), antimony(Sb), arsenic(As), copper(Cu), etc. Recently, we have been investigating the scope for N and Cu doping to achieve reliable p-type ZnO and its alloys using RF plasma assisted molecular beam epitaxy (RF-MBE) system.

Recent Progress

Nitrogen-doped MgZnO thin film based random laser:

Nitrogen-doped $Mg_{0.12}Zn_{0.88}O$ thin film based metal-semiconductor-metal device was grown on c-plane sapphire substrate using RF-MBE. This film showed p-type behavior initially and turned into n-type after about one year. Concentric circular geometry MSM device structure was fabricated following the standard photolithography process. Ni/Au (20 nm/150 nm, metal-1) and Ti/Au (20 nm/150 nm, metal-2) were deposited on $Mg_{0.12}Zn_{0.88}O$:N layer as the contact metals for device-I. For device-II, Ni/Au (20 nm/150 nm) was used for both contacts.

Figure 1(a) shows x-ray diffraction (XRD) pattern of the $Mg_{0.12}Zn_{0.88}O$:N film. The top and bottom right inset in Fig. 1(a) show top and cross sectional view scanning electron microscopy (SEM) images of the film, respectively. The film exhibits columnar structures with many pits or air gaps in between and an average in-plane column size of ~200nm, which are evident in the SEM image. Figure 1(b) shows PL spectrum at RT of the $Mg_{0.12}Zn_{0.88}O$:N film. The excitonic near band edge peak is around 355nm (3.49eV) and deep level emissions are present in the spectrum.

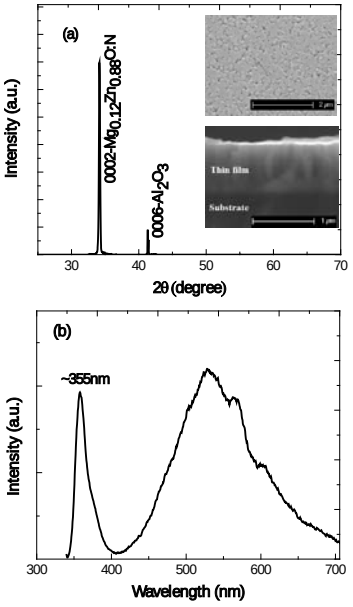

Figure 1.(a) XRD pattern of the $Mg_{0.12}Zn_{0.88}O$:N film. The top and bottom right inset show SEM images of the top surface and cross sectional view, respectively. (b) RT PL spectrumof the $Mg_{0.12}Zn_{0.88}O$:N film.

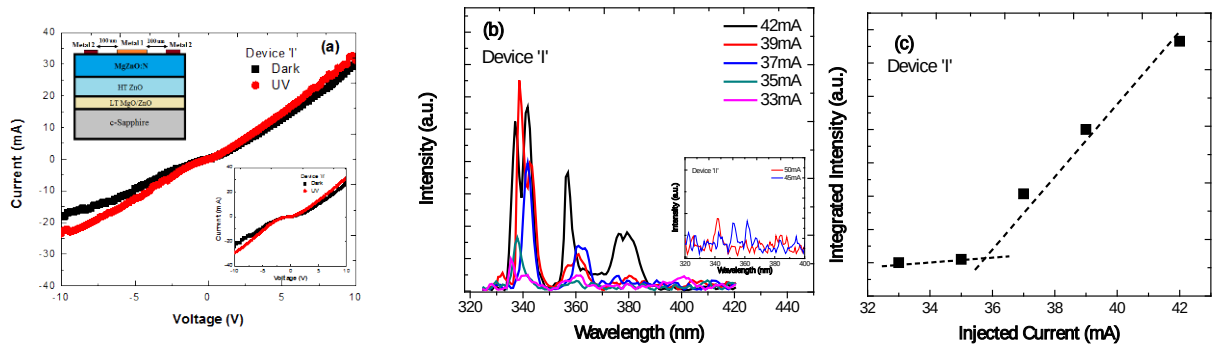

Figure 2. (a) I-Vcharacteristic in linear scale of the device-I under UV and dark. The top left inset shows the schematic of the device structure. The bottom right inset shows the I-V characteristic of the device-II, (b) EL spectra under different injection current at RT from device-I. The bottom right inset shows the EL spectra from device-II, (c) Integrated EL intensity at different injection current of device-I.

Figure 2(a) shows the I-V characteristics of the device-I with and without UV illumination. The bottom right inset shows the I-V characteristics of the device-II and top left inset shows cross sectional schematic of the device structure. The I-V curves shows almost symmetric nature under forward (positive voltage on Ni contact) and reverse biases, which is characteristic of MSM device.Figure 2(b) shows EL spectra with continuous dc current injection at room temperature from device-I. The inset shows the EL spectra from device-II. At low current injection (33-35 mA), the emission is broad and weak for device-I.With higher current injection (>37 mA), multiple emission peaks start to appear. The peaks are distributed mostly between 340-360 nm.Figure 2(c) shows the integrated light intensity as a function of injection current for device-I. A threshold current of around ~36 mA is evident. Light output power of ~15 nW was detected at 43 mA injection current.

Development of Copper-doped ZnO thin films:

Cu-doped p-type ZnO films are grown on c-sapphire substrates by RF-MBE. PL experiments reveal a shallow acceptor state at 0.15 eV above the valence band edge. Hall effect results indicate that a growth condition window is found for the formation of p-type ZnO thin films and the best conductivity is achieved with a high hole concentration of 1.54×10^{18} cm^{-3}, a low resistivity of 0.6 Ω cm and a moderate mobility of 6.65 $cm^2 V^{-1} s^{-1}$ at room temperature. For instance, Sample A, which was grown at a Cu cell temperature of 610 °C, shows n-type conductivity with a carrier concentration of 7.5×10^{17} cm^{-3} and a mobility of 11.7 $cm^2 V^{-1} s^{-1}$. With a Cu cell temperature of 605 ^oC (Sample B), the film exhibits p-type behavior with a hole concentration of 3.18×10^{17} cm^{-3} and a mobility of 4.3cm^2 V^{-1} s^{-1}. By decreasing the Cu cell temperature to 600 ^oC (Sample C), the carrier concentration increases to 1.54×10^{18} cm^{-3} while the mobility also increases to 6.65 $cm^2 V^{-1} s^{-1}$. Further decrease of the Cu cell temperature to 595 ^oC (Sample D) leads to the decrease of hole carrier concentration to 1.63×10^{17} cm^{-3} with a slightly lower mobility of 6.6 $cm^2 V^{-1} s^{-1}$.

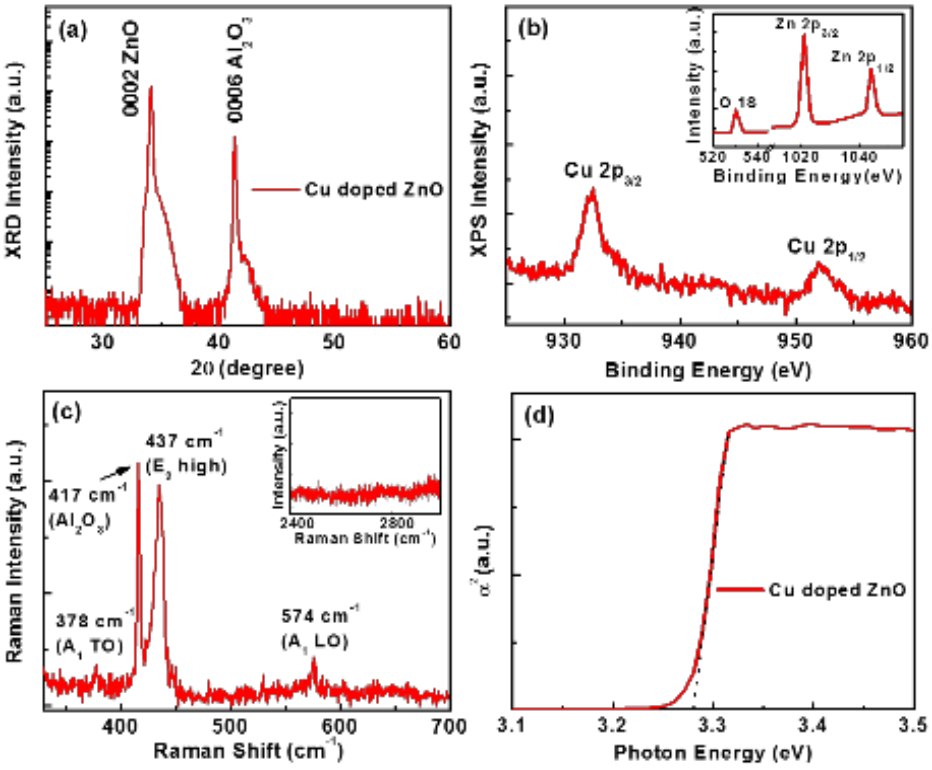

Figure 3. (a) XRD spectrum of p-type Cu-doped ZnO, (b) Cu 2p core-level XPS spectrum of Sample C (inset showing XPS spectrum for Zn 2p and O 1s), (c) Raman spectrum of Cu-doped ZnO, and inset is Raman spectrum showing no Cu-rich secondary phases, and (d) square of absorption coefficient (α^2).

Figure 3(a) shows an XRD spectrum of Cu-doped ZnO film (Sample C). The spectrum exhibits diffraction peaks for ZnO (0002) and Al_2O_3 (0006). The absence of other ZnO directions indicates that the ZnO film is single-crystalline in nature. Moreover, no diffraction signal originated from Cu and its compounds are observed within the detection level. Figure 3(b) shows a Cu 2p core level XPS spectrum of Cu-doped ZnO film (Sample C) with an inset indicating peaks relative to Zn and O. The incorporation of Cu dopant is determined by two prominent peaks at 932.4 eV and 952 eV corresponding to Cu $2p_{3/2}$ and Cu $2p_{1/2}$ spin-orbit splitting, respectively. Figure 3(c) shows Raman spectrum of Cu-doped ZnO film (Sample C). From the Raman spectrum of Cu-doped ZnO film, a strong Raman shift signal appears at 437 cm^{-1} due to the E_2 (high) mode of ZnO along with weak peaks at 378 and 574 cm^{-1}, which correspond to A_1 (TO) and A_1 (LO) modes of ZnO, respectively. The peak at 417 cm^{-1} is attributed to the optical phonon mode of the c-sapphiresubstrate. As seen from the inset, there is no signal corresponding to copper oxide or other copper compounds in the Raman spectrum, which is consistent with the XRD results that no secondary phases are present in the Cu-doped ZnO film. Figure 3(d) shows absorption spectrum of Sample C at room temperature. The absorption edge in the curve indicates an energy band gap of 3.27 eV (380 nm). The excitonic

resonance peak in the spectrum shows good optical quality and the single slope absorption edge ensures no significant phase mixing in the film.

MOS devices were fabricated to further study the p-type behavior of Cu-doped ZnO samples. The inset of Figure 4 shows the device structure, consisting of a metal gate (Au, 200 nm), Al_2O_3 (30 nm) and Cu-doped ZnO film (400 nm) on c-sapphire substrate. Capacitance-voltage (C-V) curves were measured at 300 K with a frequency of 100 kHz. For Samples B-D, by increasing the gate voltage from negative to positive values, the p-type Cu-doped ZnO film can accumulate holes (accumulation mode), then deplete holes (depletion mode), and finally fill with electrons on top of the Cu-doped ZnO film (inversion mode). In contrast, for Sample A, by decreasing the gate voltage from positive to negative values, the n-type film can accumulate electrons (accumulation mode), then deplete electrons (depletion mode), and finally fill with holes on top of the Cu-doped ZnO film (inversion mode). These trends of C-V curves further demonstrate the p-type conductivity of Cu-doped ZnO films.

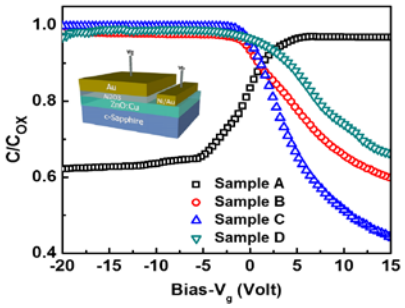

Figure 4. C-V characteristics of fabricated MOS capacitor (inset) devices utilizing Cu-doped ZnO (Samples A-D) as the semiconductor layer, Al_2O_3 as the oxide layer and Au as the metal layer.

Seebeck measurements on these Cu-doped ZnO samples were also carried out, exhibiting positive Seebeck coefficients for Samples B-D, which further confirms the p-type conductivity. However, most p-type samples were converted to n-type over a period of time, which is mostly due to the carrier compensation from hydrogen-based extrinsic donors of ZnO incorporated from ambient.

Future Plans

There is no question that p-type ZnO can be achieved. The p-type reliability is theunresolved issue. Our future plan is to find ways to achieve reliable p-type ZnO. Alternatively, we will study other wideband gap semiconductor materialsfor energy-saving solid state lighting and other technologies.

Publications (2013-present)

1. J. Huang, S. Chu, J. Y. Kong, L. Zhang, C. M. Schwarz, G. P. Wang, L. Chernyak, Z. H. Chen, and J. L. Liu, Advanced Optical Materials 1(2), 179(2013).
2. J. Huang, J. Qi, Z. L. Li, and J. L. Liu, Nanotechnology 24, 395203(2013).
3. M. M. Morshed, M. Suja, Z. Zuo, and J. L. Liu, Appl. Phys. Lett. 105, 211107 (2014).
4. M. M. Morshed, Z. Zuo, J. Huang, J. Zheng, Q. Lin, X. Yan, and J.L. Liu, Appl. Phys. A 117, 1467(2014).

5. J. Huang, M. Morshed, Z. Zuo, and J. L. Liu, Appl. Phys. Lett. 104, 131107 (2014).
6. M. M. Morshed, Z. Zuo, J. Huang, and J. L. Liu, Appl. Phys. A, 118, 817 (2015).

Polarized Neutron Scattering of Magnetic Nanoparticle Crystals

Sara A. Majetich, Physics Department, Carnegie Mellon University, Pittsburgh, PA 15213

Program Scope

The goal of the program is to understand the spin configurations within ordered assemblies of monodomain magnetic nanoparticles.

Recent Progress

Using small angle neutron scattering with polarization analysis, it is possible to obtain three dimensional magnetization information on a nanometer length scale [1]. This technique shows that "monodomain" particles can actually have more complex spin structures. While 10 nm $CoFe_2O_4$ nanoparticles appear to have the ideal full alignment of spins, the surface spins of similar Fe_3O_4 nanoparticles show coherent canting when a large magnetic field is applied, due to the competitions between exchange and Zeeman interactions [2].

Figure 1. Coherent canting of surface spins of Fe_3O_4 in a vertical magnetic field.

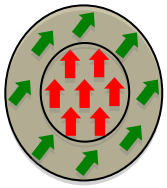

Future Plans

Future work includes investigation of small angle neutron scattering in $MnFe_2O_4$ nanoparticles, iand nelastic neutron scattering to study spin wave confinement effects.

References

1. K. L. Krycka, J. A. Borchers, J. A. Borchers, Y. Ijiri, W. C. Chen. S. M. Watson, M. Laver, T. R. Gentile, S. Harris, L. R. Dedon, J. J. Rhyne, and S. A. Majetich, Phys. Rev. Lett. **104** 207203 (2010).

2. K. Krycka, J. Borchers, Y. Ijiri, R. Booth, and S. Majetich, *J. Applied Crystallography* **45**, 554-565 (2012).

Publications

1. K. Hasz, Y. Ijiri, K. L. Krycka and J. A. Borchers, R. A. Booth, S. D. Oberdick, and S. A. Majetich, *Phys. Rev. B* **90**, 180405(R) (2014).

2. K. M. Chowdary and S. A. Majetich, *J. Phys. D: Appl. Phys.* **47**, 175001 (2014).

3. K. L. Krycka, J. A. Borchers, R. A. Booth, S. A. Majetich, Y. Ijiri, and J. J. Rhyne, *Phys. Rev. Lett.* **113**, 147203 (2014).

4. V. K. Sakharov, R. A. Booth, and S. A. Majetich, *J. Appl. Phys.* **115**, 17A517 (2014).

Acceptor Defects in ZnO and Related Materials

Matthew D. McCluskey[1] and Leah Bergman[2]

[1]Washington State University, Pullman, WA 99164-2814, mattmcc@wsu.edu

[2]University of Idaho, Moscow, ID 83844-0903, lbergman@uidaho.edu

Program Scope

Zinc oxide (ZnO) is an electronic material with desirable properties for a range of energy applications (Look, 2001; Janotti and Van de Walle, 2009; McCluskey and Jokela, 2009). ZnO is a wide band gap (3.4 eV) semiconductor that emits light in the near-UV region of the spectrum, with high efficiency. Despite its advantages, the lack of fundamental knowledge about dopants and defects presents an obstacle to the development of practical devices. Reliable *p*-type doping, required for high-performance transistors, lasers, or light-emitting diodes, has been elusive.

In this project, the fundamental properties of acceptor defects in ZnO and related materials are investigated. The results of optical and electrical characterization studies could provide the basis for the long-sought goal of reliable *p*-type doping of ZnO. More broadly, this investigation provides physical insight into defects in oxide semiconductors, in bulk crystals, thin films, and nanocrystals.

The project involves a coordinated program of synthesis and characterization at Washington State University and University of Idaho. Complementary experiments are performed at DOE user facilities, at Pacific Northwest National Laboratory and Lawrence Berkeley National Laboratory.

Recent Progress

Nanocrystals:In previous work (Teklemichael et al., 2011), we have shown that ZnO nanocrystals (~20 nm diameter) appear to contain hydrogenic acceptors as grown. In the present project, infrared and photoluminescence (PL) spectroscopy on 90-nm diameter nanocrystals suggest a relatively low acceptor binding energy (~0.4 eV) for these defects. A high-field (W-band) electron paramagnetic resonance (EPR) spectrum is shown in Fig. 1. The spectrum indicates two

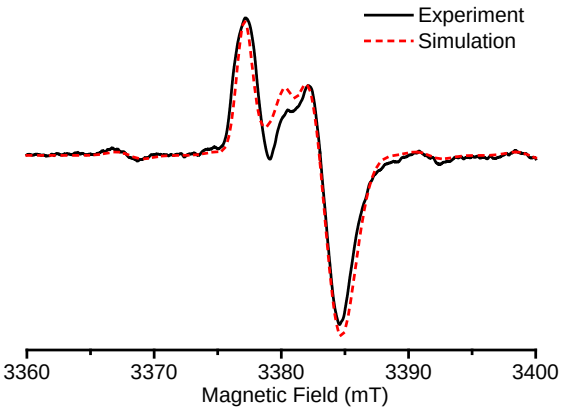

Fig. 1.Experimental (solid line) and modeled (dashed line) EPR spectra of ZnO nanocrystals taken at 77 K.

distinct defect centers. One has axial symmetry with $g_{//}$= 2.0056 and $g_{\perp}$= 2.0015, while the other is isotropic with g = 2.0035. From the fit, the axial defect is dominant. While the identity of this defect is unknown, the g values suggest that it is a zinc vacancy complex. This is important because, if the results hold, then zinc vacancies could provide a route to *p*-type conductivity.

Zinc vacancies: Motivated by the nanocrystal work, we are exploring how zinc vacancies introduce acceptor levels into bulk ZnO. We performed room-temperature PL excitation (PLE) experiments on laser-irradiated samples that contained isolated zinc vacancies. The green (2.4 eV) PL was monitored versus excitation photon energy. The irradiated samples show a strong PLE peak at 3.18 eV; i.e., excitation photons of 3.18 eV yield intense green PL (Fig. 2).The PLE peak was attributed to the excitation of an electron from the (0/-) acceptor level to the conduction-band minimum. The recapture of the electron then produced green PL. These results show that irradiation is a viable method for introducing isolated zinc vacancy acceptors into a near-surface region.

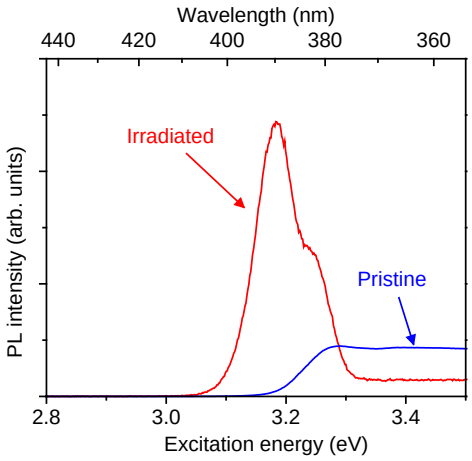

Fig. 2.Room-temperature PLE spectra of pristine ZnO and ZnO irradiated with high-intensity laser pulses.

Lithium acceptors:Substitutional lithium (Li_{Zn}) is a singleacceptor.From the width of its yellow PL band, Schirmer and Zwingel (1970) estimated the acceptor level to lie ~0.8 eV above the valence-band maximum. We developed a Li diffusion process that results in a high bulk Li concentration of ~10^{19} cm^{-3}. Van der Pauw measurements showedvery large resistivity at room temperature (~$10^{9}\Omega$ cm), consistent with deep-acceptor doping (Fig. 3). For temperatures > 400 K, the resistivity dropped significantly, due to bulk hole conduction. Modeling the data yielded an acceptor level of 0.86 eV. Although this level is deep, the result is important because it provides strong evidence for *p*-doping of ZnO.

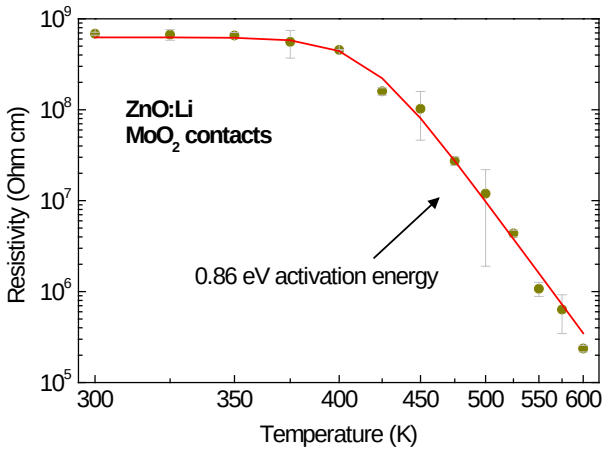

Fig. 3.Resistivity of ZnO:Li versus temperature. The solid line is a fit to a model with a hole activation energy of 0.86 eV.

Luminescence:In addition to controlling the conductivity, defects in ZnO have a major influence on the luminescent properties. These properties are important for solid-state lighting applications. In this project, we explored annealing conditions, with the aim of enhancing UV PL and understanding the underlying defect

processes. Thin-film ZnO samples were grown by sputtering on quartz substrates (1 hr, 250°C). Samples were annealed in O_2 and Ar for 1 hr at 900°C. As grown, samples have very weak UV PL at room temperature. After annealing in O_2, the UV luminescence increases, along with a band centered 2.18 eV (Fig. 4). This band is tentatively attributed to oxygen interstitials. The sample annealed in Ar also shows enhanced UV PL, but without the 2.18 eV band (Fig. 5).

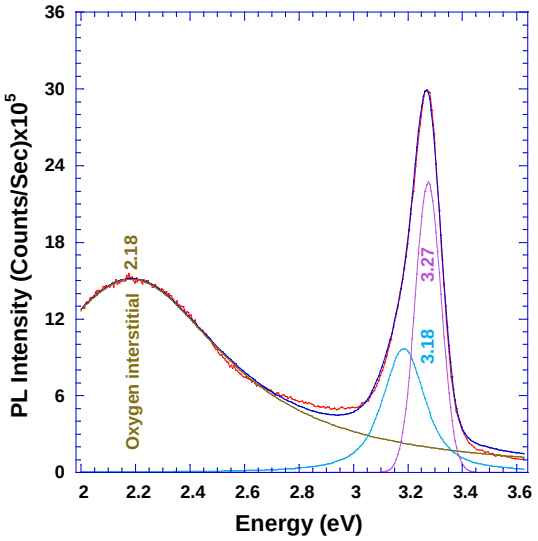

Fig. 4.Room-temperature PL spectrum of ZnO annealed in O_2.

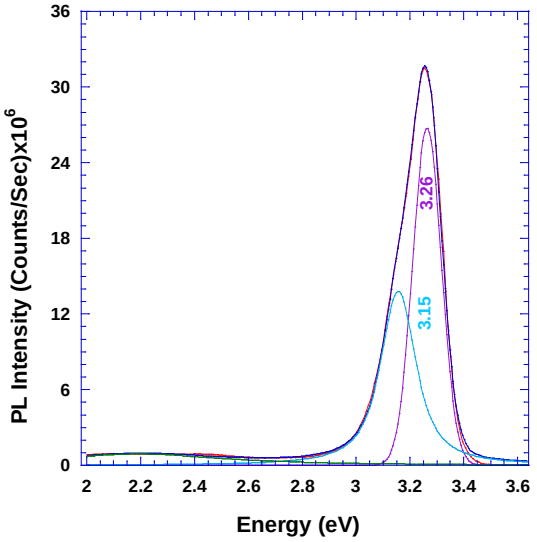

Fig. 5.Room-temperature PL spectrum of ZnO annealed in Ar.

Transmission: Using UV/visible spectroscopy, we have analyzed the Urbach tail of the band-gap absorption. This exponentially decaying sub-gap absorption feature is caused by defects and inhomogeneous strains. A transmission spectrum is shown in Fig. 6. The as-grown sample has a pronounced Urbach tail that broadens the absorption onset. The annealed samples, in contrast, show a sharp onset, suggesting a reduction in structural defects. These results are supported by low-temperature PL measurements, which show distinct peaks that arise from stacking faults. The results of this work provide insight into optical properties and are applicable to highly mismatched semiconductor alloys such as $ZnO_{1-x}S_x$.

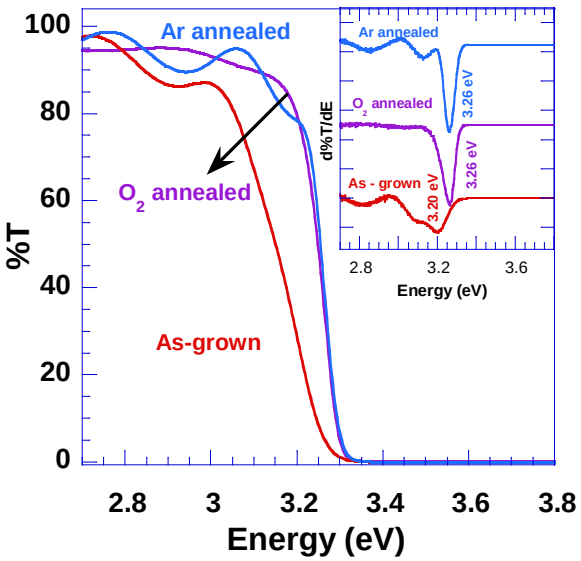

Fig. 6.Transmission spectra of ZnO films. Inset: Derivative of transmission versus energy.

Hydrogen complexes: Hydrogen is an important impurity because it passivates acceptors, potentially blocking *p*-type conductivity. To investigate this effect, we hydrogenated ZnO:Na by annealing in H_2 gas at 500°C for 60 hr. Using low-temperature (9 K) IR spectroscopy, we observed an O-H stretch mode at 3304 cm^{-1} (Fig. 7). Samples annealed in D_2 gas showed an O-D peak at 2466 cm^{-1}. The deuterated sample also showed a sideband at 2461 cm^{-1}. This sideband was tentatively attributed to a Fermi resonance between the stretch mode and the third harmonic of a wag mode. This is an accidental degeneracy: three times the O-D wag-mode frequency almost exactly equals the O-D stretch-mode frequency. The degeneracy causes the wag mode to acquire some stretch-like character and become IR active.

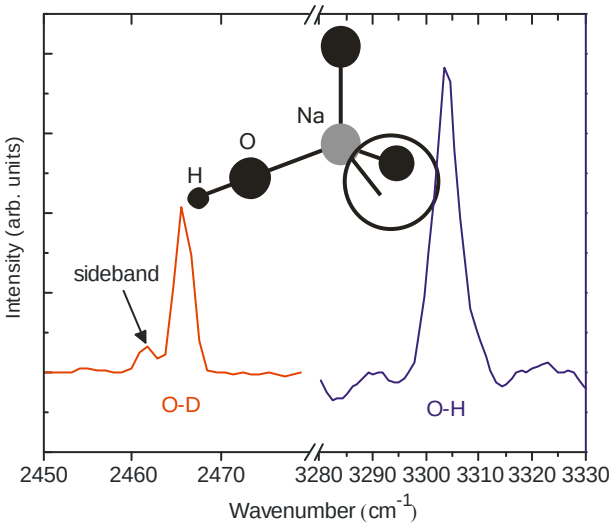

Fig. 7. IR transmission spectra of ZnO:Na annealed in hydrogen or deuterium.

Future Plans

We will pursue Li and Na doping of ZnO, complementing the Van der Pauw electrical measurements with Seebeck coefficient measurements. The Seebeck effect will determine the carrier type (holes versus electrons) unambiguously. In addition to bulk crystals, doping during sputtering will be investigated, with the aim of growing heavily doped, *p*-type thin films. Hydrogen, always an important impurity in these materials, will be studied with IR spectroscopy. Since hydrogen passivates acceptors, rendering them electrically neutral, achieving reliable *p*-type conductivity will require control over this omnipresent element.

References

A. Janotti and C.G. Van de Walle, *Rep. Prog. Phys.***72**, 126501 (2009).

D.C. Look,*Mater. Sci. Engin. B***80**, 383 (2001).

M.D.McCluskey and S.J. Jokela, *J. Appl. Phys.***106**, 071101 (2009).

O.F. Schirmer andD. Zwingel,*Solid State Commun.* **8**, 1559 (1970).

S.T. Teklemichael, W.M. HlaingOo, M.D. McCluskey, E.D. Walter, and D.W. Hoyt, *Appl. Phys. Lett.***98,** 232112 (2011).

Publications

E.H. Khan, M.H. Weber, and M.D. McCluskey, "Formation of isolated Zn vacancies in ZnO single crystals by absorption of ultraviolet radiation: A combined study using positron annihilation, photoluminescence, and mass spectroscopy," *Phys. Rev. Lett.***111**, 017401:1-5 (2013).

M.C. Tarun, F.A. Selim, and M.D. McCluskey, "Persistent photoconductivity in strontium titanate," *Phys. Rev. Lett.***111**, 187403:1-5 (2013).

J. Huso, J.L. Morrison, L. Bergman, and M.D. McCluskey, "Anharmonic resonant Raman modes in $Mg_{0.2}Zn_{0.8}O$," *Phys. Rev. B***87**, 125205:1-5 (2013).

N.S. Parmar, M.D. McCluskey, and K.G. Lynn, "Vibrational spectroscopy of Na-H complexes in ZnO," *Journal of Electronic Materials***42**, 3426-8 (2013).

F. Tuomisto, C. Rauch, M.R. Wagner, A. Hoffmann, S. Eisermann, B.K. Meyer, L. Kilanski, M.C. Tarun, and M.D. McCluskey, "Nitrogen and vacancy clusters in ZnO," *Journal of Materials Research***28**, 1977-83 (2013).

J. Huso, H. Che, D. Thapa, J.L. Morrison, M.G. Norton, and L. Bergman, "Phonon dynamics and anharmonicity in phase segregated structural domains of MgZnO film" *Appl. Phys. Lett.* **104**, 031908:1-5 (2014).

S.T. Teklemichael, M.D. McCluskey, G. Buchowicz, O.D. Dubon, and E.E. Haller, "Evidence for a shallow Cu acceptor in Si from infrared spectroscopy and photoconductivity," *Phys. Rev. B***90**, 165204:1-4 (2014).

F.A. Selim, D. Winarski, C.R. Varney, M.C. Tarun, Jianfeng Ji, and M.D. McCluskey, "Generation and characterization of point defects in $SrTiO_3$ and $Y_3Al_5O_{12}$," *Results in Physics***5,** 28-31 (2015).

M.D. McCluskey, C.D. Corolewski, J. Lv, M.C. Tarun, S.T. Teklemichael, E.D. Walter, M.G. Norton, K.W. Harrison, and S. Ha, "Acceptors in ZnO," *J. Appl. Phys.* (in press).

M.D. McCluskey, "Point defects in ZnO," in *Semiconductors in Semimetals*, ed. C. Jagadish, V. Privitera, L. Romano (Elsevier, 2015), Ch. 6 (in press).

J. Huso, H. Che, D. Thapa, AmrahCanul, M.D. McCluskey, and L. Bergman, "Phonon dynamics and Urbach energy studies of MgZnO alloys," *J. Appl. Phys.* (submitted).

N.S Parmar, C.D. Corolewski, M.D. McCluskey, and K.G. Lynn, "Potassium acceptor doping of ZnO crystals," *Appl. Phys. Lett.* (submitted).

Interfaces in Electronic and Structural Materials

Yuri Mishin, PI

Department of Physics and Astronomy
George Mason University, MSN 3F3
4400 University Drive, Fairfax, VA

Phone: 703-993-3984
Fax: 703-993-1269
Email: ymishin@gmu.edu

Program Scope

Development of new materials for future energy applications relies on progress in fundamental understanding of materials' interfaces and our ability to predict, design and control their properties. The objective of this program is to advance the fundamental understanding of interfaces, especially in materials subject to deformations and high temperatures, and to develop new methods for computational prediction of interface properties. During the renewed funding period that started in 2014, this program will focus on interfaces in thermoelectric materials using bismuth telluride Bi_2Te_3 as a model system. Specific goals include investigations of: (1) effect of crystallographic characteristics, applied stresses, temperatures and chemical composition on atomic structure, thermodynamic characteristics, mechanical strength and motion of internal interfaces in Bi_2Te_3 alloys, and (2) effect of interfaces on thermal conductivity of this material.

The main approach to achieving these goals is based on atomistic computer simulation methods, primarily molecular dynamics and a variety of Monte Carlo techniques. These methods are capable of delivering critical atomic-level information about the interface structures and predicting mechanical, thermodynamic and kinetic properties of interfaces. Extensive first principles calculations will be performed for calibration of a new many-body angular-dependent interatomic potential that will be developed for Bi_2Te_3 alloys in order to enable quantitative large-scale atomistic simulations. The results of the simulations will be validated against experimental data for grain boundary structures, mechanical and thermoelectric properties of Bi_2Te_3.

The project is expected to make a significant impact on the state of knowledge in interface science by improving the fundamental understanding of mechanical, thermal and dynamical properties of internal interfaces, especially in thermoelectric materials. This goal is revenant to the BES mission and is aligned with DOE's Grand Challenge of controlling matter away from equilibrium and the Basic Research Needs for solar energy utilization and electrical energy storage.

Recent Progress

1. Phase transformations at interfaces present a profound fundamental interest as complex examples of phase transitions in low-dimensional systems. We have developed a new methodology of atomistic simulations that has revealed multiple grain boundary phases and reversible first-order phase transformations between them. Furthermore, we have demonstrated that interface phase transformations can strongly impact transport properties, for example atomic diffusion along grain boundaries. Atomistic calculations of Ag diffusion in two different structural phases of a Cu grain boundary demonstrate excellent agreement with experimental measurements, providing the first convincing evidence for the existence of structural phase transformations in high-angle grain boundaries and demonstrate the possibility of their detection by boundary diffusion measurements and atomistic simulations. The interface phase

transformations can also influence electric and thermal resistance of interfaces and offer a means of achieving new properties via design optimal micrsotrostructures.

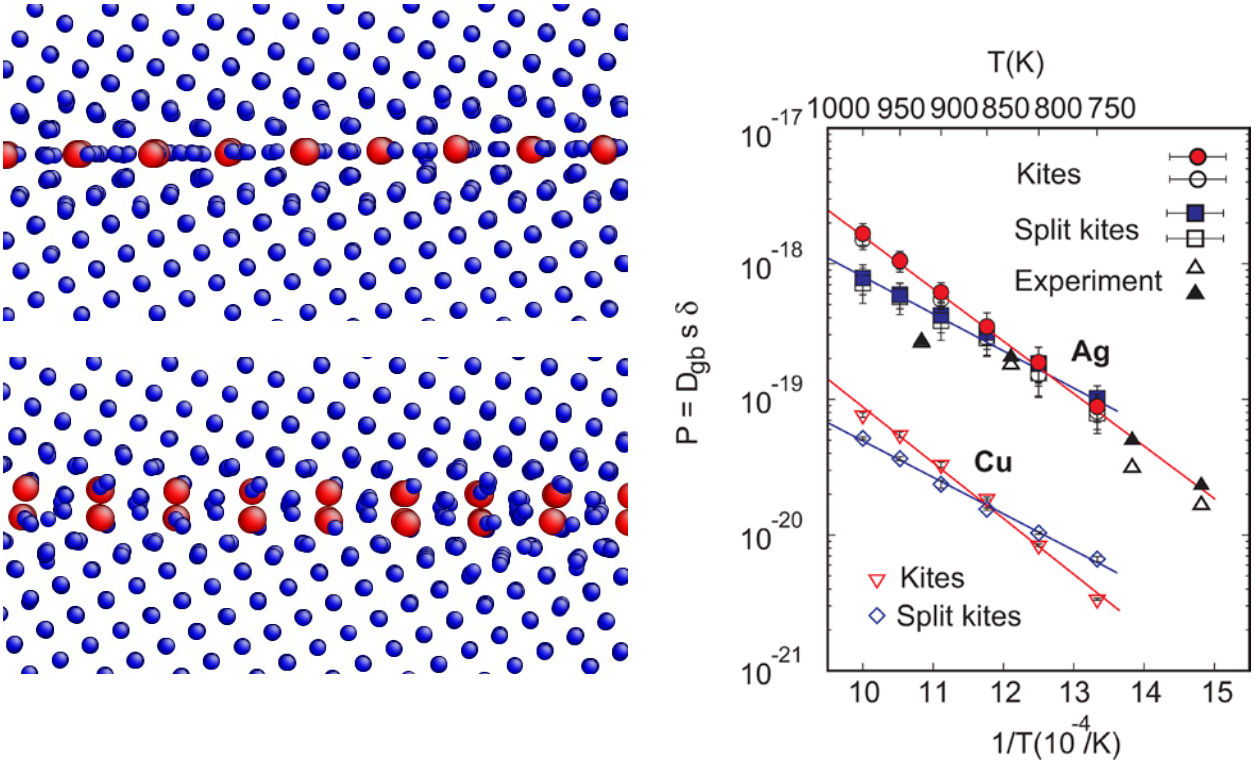

(a) (b)

(a) Two phases of segregated grain boundaries in copper: top – normal kite phase, bottom – split kite phase. (b) Diffusion coefficients of Cu and Ag in two grain boundary phases, demonstrating excellent agreement between computer simulations and experiment.

2. We have also studied the effect of GB phase transformations on GB diffusion. Recent diffusivity measurements in the symmetrical tilt Σ5(310) GB in copper [Divinski et al, PRB 2012] reported two distinct slopes on the Arrhenius plot of the diffusivity, suggesting a possible structural transformation in this GB. Contrary to the experiment, previous MD studies concluded that the diffusivity followed the Arrhenius law with a single slope. We have modified the methodology of the MD simulations allowing the number of atoms in the boundary to adjust in order to observe structural transformations at high temperatures. The diffusivities of the different GB structures have been calculated using both the traditional methodology based on the Einstein equation and a novel approach based on the Fisher model assuming type-C diffusion kinetics. This study provided a new understanding of the effect of structural transformations on GB diffusion coefficients at high temperatures. In addition, were were able to reproduce and understand the non-Arrhenius behavior of the GB diffusivity seen in experiments.

3. We have developed a rigorous thermodynamic theory of plane coherent solid-solid interfaces in multicomponent systems subject to non-hydrostatic mechanical stresses. The interstitial and substitutional chemical components are treated separately using chemical

potentials and diffusion potentials, respectively. All interface excess quantities have been derived using Cahn's generalized excess method without resorting to geometric dividing surfaces. This theory has been applied to GBs subject to non-hydrostatic elastic deformations. We have derived expressions for the GB free energy as the reversible work of GB formation under stress. We have also presented a generalized adsorption equation whose differential coefficients define the GB segregation, GB stress tensor, GB excess volume, and GB excess shear. The generalized adsorption equation generates a set of Maxwell relations describing cross effects between different GB properties. The theory has been applied to atomistic simulations of symmetrical tilt GBs in Cu and Cu-Ag alloys. Using a combination of MD and Monte Carlo methods, we computed a number of GB excess quantities and their dependencies on the applied stresses, temperature and chemical composition in the grains. We have also tested several Maxwell relations and obtain excellent agreement between the theory and simulations.

4. In collaboration with Prof. A. Karma (Northeastern University), we have studied equilibrium fluctuations of GBs by analytical methods and MD simulations. The proposed analytical expressions has been validated by MD simulations for symmetrical tilt GBs. This study demonstrates that equilibrium fluctuations can be used to extract the misorientation dependence of the GB mobility. The results shed light on fundamental relationships between equilibrium and non-equilibrium GB properties and provide new means to predict such properties.

5. The motion of curved GBs coupled to shear can produce grain rotation. We have studied the process of curvature-driven shrinkage and rotation of a cylindrical grain as a simple model of grain rotation in nano-crystalline materials. Geometrical rules of grain rotation have been derived, including high-angle misorientations and multiple coupling modes. At low temperatures, the coupling between GB migration and grain translation induces rotation of the grain towards higher or lower misorientation angles, depending on the initial misorientation. The grain rotation stops when the grain reaches a "frustration" angle at which the coupling factor changes sign. At very high temperatures, the grain rotation can cause GB premelting and eventually melting of the material. The dynamics of the GB motion and grain rotation have been studied as functions of the initial misorientation angle and temperature. The effects of imposed constraints blocking the grain rotation or exerting a cyclic torque have been examined. This work as recently been extended to more realistic structures, including a tricrystal composed of a cylindrical grain embedded at the center of a plane GB. The embedded grain shrinks by capillary forces and eventually vanishes. This process is often accompanied by rotation of the embedded grain in either a clockwise or counter-clockwise direction. Using the geometric theory of coupling between GB motion and grain translations, we proposed a model capable of predicting the direction of the grain rotation depending on the crystallographic parameters of the three grains. Full agreement has been found between the model predictions and the MD simulation results for both spontaneous grain shrinkage and in the presence of applied shear stresses. We are working on extending these results to polycrystalline materials.

6. Massive first-principle DFT calculations has been conducted for various crystalline structures of Bi and Te. The obtained first-principles database has been used to construct many-body angular-dependent interatomic potentials (ADP) for Bi and Te. The potentials accurately reproduce a wide range of properties of these elements, including structural energies, phase transformations, melting temperatures, phonon dispersion relations, thermal expansion, point defect formation and migration energies and many other properties. Work is currently underway to develop a similar first-principles database for developing the Bi-Te cross-interaction functions describing the Bi-Te binary system, particularly the bismuth telluride Bi_2Te_3.

Future Plans

We will continue the development of a first-principles database for the Bi-Te system. Having this database, we will development an accurate and reliable ADP interatomic potential for the binary Bi-Te system, focusing the bismuth telluride phase Bi_2Te_3. The potential will be tested for ability to reproduce thermodynamic, mechanical and physical properties of Bi_2Te_3 in close agreement with DFT and experimental data. In particular, the potential will be validated against experimental GB structures, as well as thermoelectric properties of Bi_2Te_3.

The new potential will be applied to study the effect of crystallographic characteristics, applied mechanical stresses, temperatures and chemical composition on the atomic structure, thermodynamic characteristics, mechanical strength and dynamics of internal interfaces in Bi_2Te_3 alloys. This will enables us to understand the effect of internal interfaces on thermal conductivity of this material and derive conclusion of the design of optimized microstructures for improved thermoelectric performance.

Publications of DOE sponsored research (2012-present)

1. Z. T. Trautt, Y. Mishin: Capillary-driven grain boundary motion and grain rotation in a tricrystal: A molecular dynamics study, *Acta Mater.***65**, 19-31 (2014)
2. T. Frolov, S. V. Divinski, M. Asta and Y. Mishin: Effect of interface phase transformations on diffusion and segregation in high-angle grain boundaries, *Phys. Rev. Letters***111**, 255502 (2013)
3. T. Frolov, D. Olmsted M. Asta and Y. Mishin: Structural phase transformations in metallic grain boundaries *Nature Communications* **4**, 1899 (2013)
4. A. Karma, Z. T. Trautt and Y. Mishin: Grain boundary fluctuations and coupling to shear deformation, *Phys. Rev. Letters***109**, 095501 (2012)
5. Z. T. Trautt, A. Adland, A. Karma and Y. Mishin: Coupled motion of asymmetrical tilt grain boundaries: molecular dynamics and phase field simulations, *Acta Mater.***60**, 6528-6546 (2012)
6. T. Frolov and Y. Mishin: Thermodynamics of coherent interfaces under mechanical stresses. I. Theory, *Phys. Rev.* B **85**, 224106 (2012)
7. T .Frolov and Y. Mishin: Thermodynamics of coherent interfaces under mechanical stresses. II. Application to atomistic simulation of grain boundaries, *Phys. Rev.* B **85**, 224107 (2012)
8. Z. T. Trautt and Y. Mishin: Grain boundary migration and grain rotation studied by molecular dynamics,*Acta Mater.***60**, 2407-2424 (2012)

“Colloidal Semiconductor Dense Films for Red, Green, and Blue Lasers”

Principal Investigator: ArtoNurmikko,
Brown University, School of Engineering, Providence, RI 02912
DOE Award DE-FG02-ER46387

Program Scope:The primary objective of this project is to create a solid thin film photonic material platform which uses low-cost wet chemistry based colloidal nanocrystal growth towards new classes of light emitters. Specifically, the project focuses on colloidal materials in the II-VI compound semiconductor and perovskite families in aiming to demonstrate stimulated emission and laser action across the ref, green, and blue. At basic physical level, for example, we seek to understand multiple physical properties of very dense, closely packed CdSe-based II-VI semiconductor colloidalquantum dot (CQD) core-shell solid thin films which we have now been shown to retain the high luminescence efficiencies (up to 90% and beyond) which the red, green, and blue (RGB) quantum dots exhibit in the starting high concentration solution form (Fig. 1 as recent progress). One major question is the nature of possible QD-QD interactions in dense films, whether by electronic or electromagnetic near field coupling.

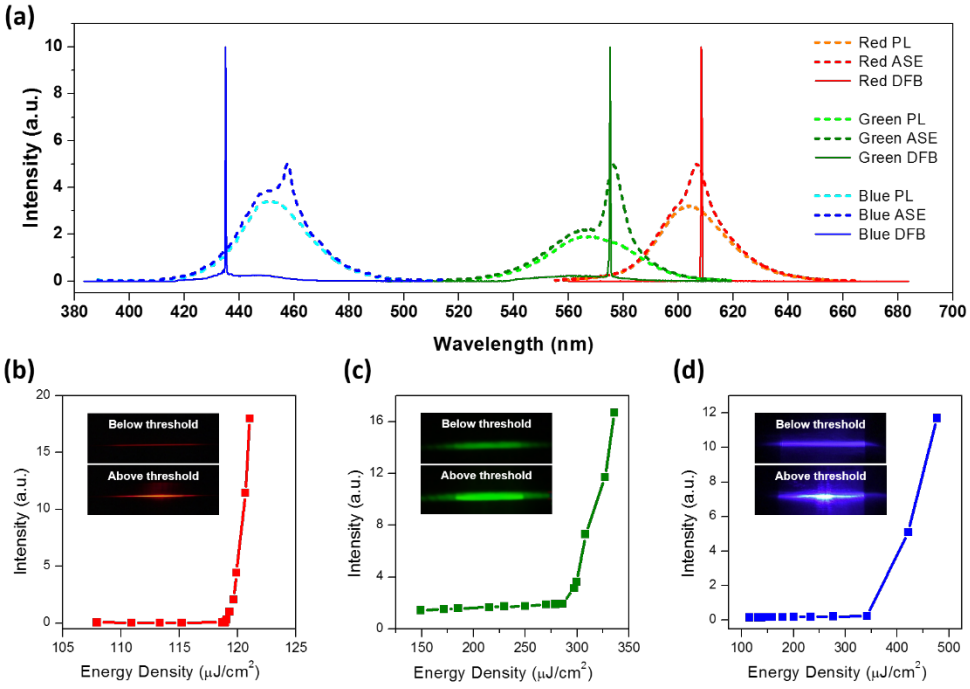

Fig. 1. (a) Spectral characteristics of RGB colloidal II-VI QD thin film optically pumped DFB lasers. Gain spectrum is controlled by the size of the CQDs, and obtained from single exciton-driven processes at room temperature. Solid lines represent the single mode output laser beams with high spatial coherence.

Recent Progress: We have broadened the material base and the optical feedback structures in the continuing pursuit of (nanofabricated) colloidal coherent emitters across the visible as follows: **Colloidal Quantum Dots (CQDs)**: With quantum confinement effect, the emission properties of the CQDs can be tuned to cover red, green, blue color with single material preparation by changing the nanocrystal size and thus exciton confinement energies (Fig 1). Recently, improved synthesis techniques for the II-VI CQDs have led to highly controlled size distribution so that single CQD spectroscopy and large ensembles of CQD in solis thin film form

show comparable luminescence linewidths – suggesting that we have reached near homogeneously broadened limits in this material system Fig 2.

Perovskite Inorganic-Organic Hybrids: With high absorption in the visible, long carrier diffusion length and low defect densities, organo-lead iodide ($CH_3NH_3PbI_3$) showpotential in photovoltaics. The large optical cross-section, low defect densities and slow Auger recombination rates could also make it a promising gain media for coherent emitters We have developed a capability of producing quality small grain (<100nm) $CH_3NH_3PbI_3$ nanocrystals (via specific solvent treatment) which have been deposited as thin films on both DFB and photonic crystal (PhC) substrates (see below).

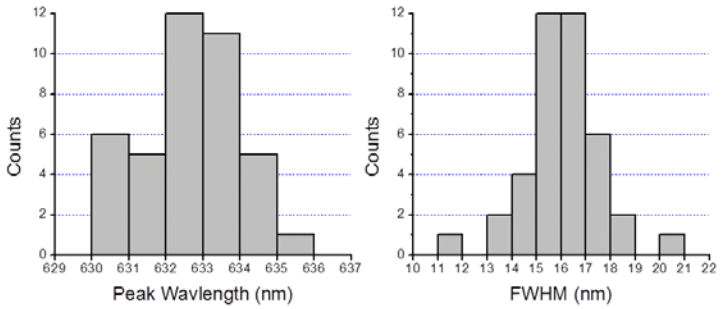

Figure 2: *Narrow distribution of emission wavelengths and linewidths from 40 individual CdSE/ZnCdSe CQDs at room temperature, displaying the highly monodisperse limit.*

Photonic Crystals (PhC): To assess and compare the colloidal quantum dots and solution grown perovskite nanocrystals as optical gain media, we have used electron-beam lithographically fabricated photonic quartz and glass substrates as templates. These in-plane two dimensional feedback structures offer high-Q cavity for laser application. The feedback mechanism is based on Bloch waves near the PhC band edge leads to Bragg reflections induced by periodic structure, which reduce the group velocity of photons to zero at Γ point. Figure 3 shows illustration of emission above the threshold of an optically pumped perovskite PhC device at three different PhC pitch values, where a well-defined and collimated spatially coherent beam was observed to emanate perpendicular the device plane. To our knowledge these are first such laser demonstrations.

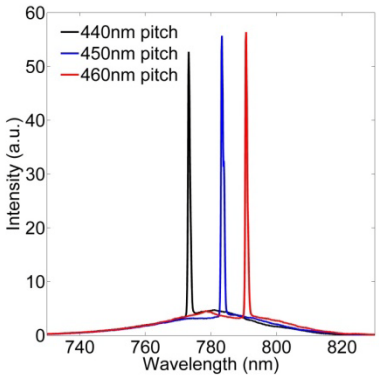

Figure 3: *Stimulated emission from PhC lasers with perovskite optical gain media*

Future Plans: Our future plans will include (a) building coherent 2-dimensional arrays of the photonic crystal (optically) pumped coherent sources for projecting complex coherent excitation patterns on photosensitive target media, and (b) extend the material basis to recently introduced CdSe-based nanoplatelets as new type of room temperature exciton gain media.

Publications: "Surface-emitting red, green, and blue colloidal quantum dot distributed feedback lasers", Roh, Kwangdong; Dang, Cuong; Lee, Joonhee; et al. OPTICS EXPRESS Volume: 22 Issue: 15 Pages: 18800-18806 Published: JUL 28 2014

DOE Award Number: DE-SC0005240, Boston College

Metamaterials as a Platform for the Development of Novel Materials for Energy Applications

PI: Prof. Willie J. Padilla

Program Scope

The proposed research builds on metamaterial absorbers and emitters demonstrated during the DOE-BES supported project (DE-SC0005240). As a primary objective of the proposed research, I have identified three main areas that are technologically relevant, practically realizable, and ideally suited to my expertise. While these three form the basis of the proposed research, it may be that even better ideas will be realized during the lifetime of the project, and that these ideas may be pursued in addition to or in place of the original ideas.

1) **Metamaterial absorbers** – The PI has demonstrated, in the previous effort, tailored metamaterial absorbers. There are, however, a number of fundamental unexplored phenomena regarding the absorption process. Graduate students and the PI will continue their investigation of the electromagnetic properties of metamaterial absorbers, initially at infrared wavelengths, then moving on to both longer (THz) and shorter (optical) wavelengths. The ability to tune the angular dependence and/or polarization state of the absorption process, for example, will be explored.
2) **Multi-band / broadband metamaterial emitters** – Metamaterials consisting of multi sub-unit cells can be utilized to tune emission over a broadband. However, the impact of scattering and generation of surface electromagnetic waves are examples of phenomena which may occur with periodicity and / or larger unit cell sizes, and remain unexplored. Graduate students and the PI will investigate the feasibility to which multiple unit-cell can contribute to emission while still maintaining desired electromagnetic properties. Iteration of various designs will take place within computation space in order to optimize metamaterials for a given energy range.
3) **Metamaterials for super blackbody emission** – For surfaces at a certain temperature the maximum emission is set by Planck's radiation law, i.e. it cannot be greater than an ideal blackbody. However for bodies or surfaces heated by a given constant input power, a tailored metamaterial surface can emit more power, in a narrow band, than an ideal blackbody surface. The physics underlying such a response will be theoretically and experimentally investigated and the extent that this phenomena can be utilized for potential energy applications will be explored.

These three materials operating at THz and Infrared wavelengths represent novel capabilities for MMs, and require precise design and fabrication. Below I outline the technical details behind my approach to achieve the design, fabrication, and characterization goals listed above for each of these materials. As previously mentioned, a complete basic research program

consisting of theory / design, modeling, characterization, and analysis will be followed in order to fully characterize the MMs, while at the same time minimizing iterations necessary to achieve the proposal goals.

Recent Progress

Dynamic 3 State Metamaterial

A three-state tunable metasurface that shows all wave-matter interaction states (Reflection, Transmission, and Absorption) in one device was demonstrated. Our initial work was performed at X-band (8 to 14 GHz). Working at microwave frequencies simplified the fabrication process allowing us focus on the fundamental science behind creating a switchable three-state system.

Schematic illustrations are shown in Fig. 1(a) & (b) reveal the design details of our ART metasurface. It is a 2-layer printed circuit board (PCB) structure with FR4 on bottom and structured Cu on top. All relevant parameters are defined in Fig. 1(a) & (b). The thickness of the FR4 and Cu are h_{di} = 1.55 mm and h_{Cu} = 17 ◎m. The unit cell is composed of a double ring resonator (as a single element) and a mirror of it (thus two elements). Varactor diodes are mounted in the gaps of the 2 rings. The 2 thick wires on the edge work as part of the resonator and the connecting wires for applying voltages to the diodes. The incident electric field is polarized along the thick wire with magnetic field perpendicular to the ring plane, as shown in Fig. 1(b).

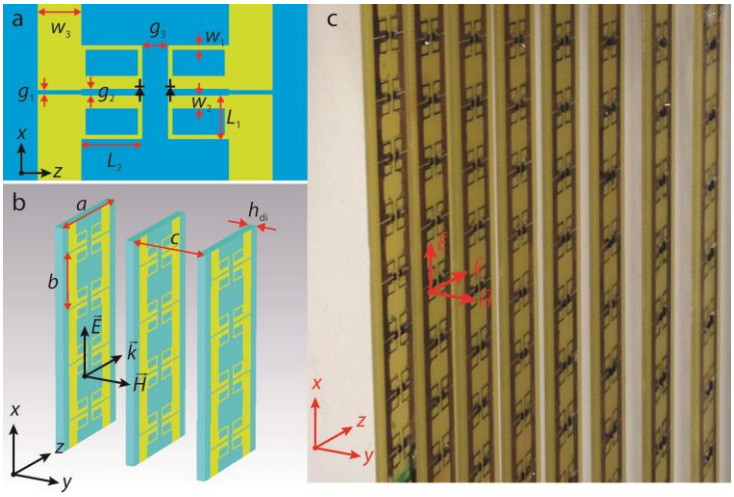

Figure 1 | Design and fabrication of a tunable metasurface. A) Top view of one unit cell of the tunable structure, with yellow corresponding to metal (Cu) and blue to dielectric (FR4). Locations of two mounted varactor diodes (Skyworks SMV 2019-079) are indicated by black diode symbols. **B)** Perspective view of a 4x3 array of the tunable metasurface, with polarization of incident light defined by black arrows. **C**) Optical image of a fabricated 10x8 array of the tunable metasurface.

The tuning was achieved by reverse biasing varactor diodes mounted onto the metasurface. By changing the capacitance of the varactor diodes, the impedance of the metasurface at one unique frequency is altered and thus the absorption, reflection and transmission spectra of the metasurface are tuned. S-parameter extraction is used to show the shifting of resonance peaks, and the extracted impedance results explain the 3-state tuning phenomena. The reverse voltage

varies in our simulation from 0 V to 21 V. The simulated transmission coefficient (S_{21}) shows shift of resonance peak from 7.4 GHz to 9.2 GHz with reverse bias increasing from 0 V to 21 V. The reflectance and absorbance spectra are shifting in an according way. Spectra of $|S_{21}|$ under tuning reversed bias are shown in Fig. 2(d). Our goal is to have a unique frequency (x axis) under which all A, R, T are high at different reverse biases (y axis). In Fig. 2 we plot the experimental (left panels) and simulated (right panels) results. In Fig. 2 (a) and (d) we plot the transmissivity (S21) as a function of frequency for a number of different applied voltages. The absorbance, reflectance, and transmittance is plotted in Fig. 2 (b) and (e) as a function of frequency. From Fig. 2 we can observe that at ~8.8 GHz, we realize a state with tunable high A, R, or T – the high reflectance occurring at 0 V, high absorbance at ~6 V and high transmittance at 21 V. In Fig. 2 (c) and (f) we plot the dependence of A, R, and T on the applied voltage.

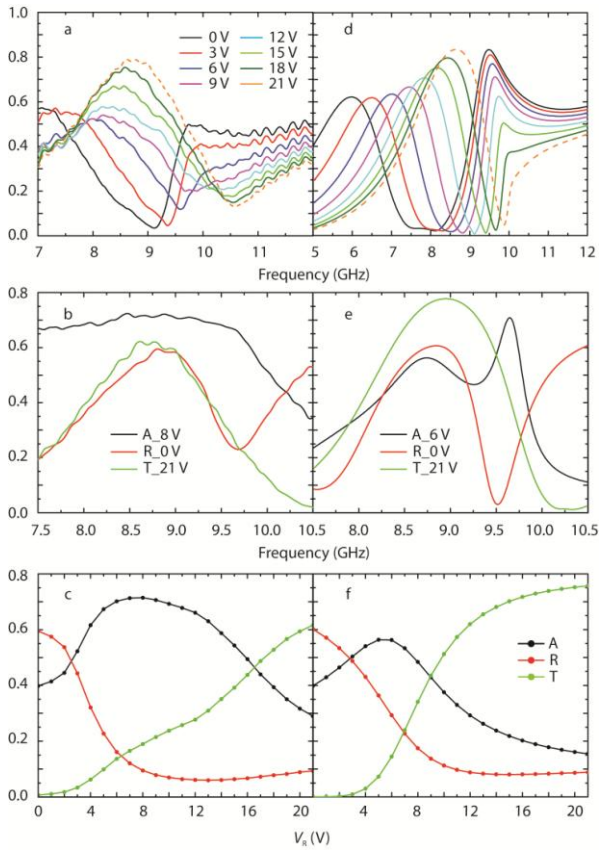

Figure 2 | Simulations and measurements of a 3-state "ART" tunable metasurface. A) Measured $|S_{21}|$ when tuning reverse bias from 0 to 21 V ($V_1 = V_2 = V_R$). B) measured absorbance (black) at 8 V; reflectance (red) at 0 V; transmittance (green) at 21 V. The spectra show at 8.8 GHz C) Absorbance, reflectance and transmittance *v.s.* voltage with fixed frequency (8.8 GHz). D) Simulated $|S_{21}|$ when tuning reverse bias from 0 to 21 V ($V_1 = V_2 = V_R$). E) simulated absorbance at 6 V; reflectance at 0 V; transmittance at 21 V. The spectra show at 8.8 GHz, their peaks coincide. F) Absorbance, reflectance and transmittance as a function of voltage with fixed frequency (8.8 GHz).

In addition to three-state operation, the structure can also work as a two-state switch. It can be designed to change between reflection and absorption as normal tunable MM. It can also be designed to be a transmission and absorption switch after optimizing the geometry. Without considering all the 3 states together, the 2 states devices can give better performance in tuning amplitude. As shown in our supplemental information, we designed an "AT" switch with around 90% absorption and transmission at 8.5 GHz.

One can envision that future versions of this tunable three-state device could be used to create smart windows for use in regions with large variation in their seasonal climates. The ability to

retain or reject heat as needed could offer significant reductions in energy used for heating and cooling.

Investigation into materials suitable for high temperature NIR Metamaterials

Metamaterial emitters for thermal photovoltaic (TPV) applications can be expected to be used at temperatures on the order of 1000K. At these temperatures however most of the properties and characteristics of traditionally used materials are not ideal. The temperatures will exceed the melting point for most metals and certain combinations of materials will form eutectic mixtures (i.e. silicon and gold).

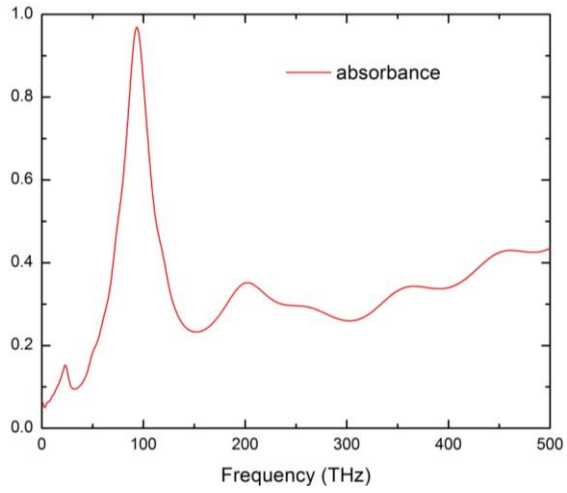

Figure 3 | Simulation results for our ITO metamaterial. The targeted wavelength for the peak absorption was 3 μm.

We have begun work on examining different materials for use in metamaterial absorbers/emitters. For conventional metamaterial designs we are looking at high melting point metals such as platinum and dielectrics such as aluminum oxide to prevent eutectic formation. The conductivity of these high melting point metals is lower than that of gold which impacts the MM response. Our Simulations and experimental results have shown that the absorption peak is broadened when using platinum. While these broader absorption/emissions peaks do offer a theoretical efficiency increases for TPV applications when compared to that of broadband emitters they are not as effective as narrow band responses targeted appropriately to the quantum efficiency of the thermal photovoltaic material.

We have also considered using Indium Tin Oxide (ITO) to create high temperature metamaterial absorbers – see Figure 3. Initial simulations suggest that ITO could offer the narrow band absorption response. Our ITO designs also show no higher order absorptive modes which can reduce the ultimate efficiency of a TPV system.

Future Plans

In the next year, we will continue work on design of an indium tin oxide (ITO) based metamaterial emitter. Samples will be fabricated and characterized using our FTIR spectrometer. We will examine the temperature dependent absorption and emission of the metamaterial. Using the results we will examine the predicted efficiency for a thermal photovoltaic system.

Tunable IR Metamaterials

We will design metamaterial structures responsive to IR wavelengths which can be dynamically tuned. Presently we are examining liquid crystals as the material to enable the tunable response.

Manuscripts submitted for publication

[1] Wen-Chen Chen, Machhindra Koirala, Xianliang Liu, Talmage Tyler, Kevin G. West, Christopher M. Bingham, Tatiana Starr, Anthony F. Starr, Nan M. Jokerst and Willie J. Padilla, "The Role of Plasmons in Metamaterial Absorbers," Submitted to Optics Express (2015).

[2] Xueyuan Wu and Willie Padilla, "Experimental realization of a three-state dynamic metamaterial surface," Submitted to Physical Review Letters (2015).

Extraordinary Responsive Magnetic Rare Earth Materials

Vitalij K. Pecharsky, L. Scott Chumbley, and Karl A. Gschneidner, Jr.
Ames Laboratory, Iowa State University, Ames, IA 50011-3020, vitkp@ameslab.gov

Program Scope

This research is focused on uncovering the underlying electronic, atomic, and microscopic interactions that result in an extraordinarily strong coupling between the magnetic and crystal lattices, and remarkable responsiveness to both strong (temperature and pressure) and weak (magnetic field) thermodynamic stimuli observed in some rare earth intermetallic materials. Selected model systems exhibit a number of diverse and unique properties associated with the magnetic ordering alone, magneto-volume, itinerant electron metamagnetic, and magnetic-martensitic transformations, which may or may not be driven by a reversible breaking and reforming of specific chemical bonds. In this effort, theory is intimately coupled with the state-of-the-art experiments to develop and validate phenomenological models of phase transformations that range from magneto-volume to magnetic-martensitic. Our ultimate goals are to *understand and manipulate* the responsiveness of materials that are sufficiently complex to facilitate control at length scales ranging from electronic interaction to atomistic and microstructural scales, yet remain simple enough to *develop predictive modeling tools*.

Recent Progress

To date, R_5T_4 compounds (R = rare earth element, T = group 14 element) are among the most studied families of intermetallics but our understanding of their physics continues to evolve. Earlier it was accepted that interchanging isoelectronic (ns^2p^2) Ge and Si has no effect on the average valence electron concentration; hence, the systematic variations of magnetism with x in $R_5(Si_xGe_{1-x})_4$ are driven nearly exclusively by chemical pressure. Our recent study shows, however, that volume contraction due to Si substitutions leads to an almost tenfold increase of Curie temperature (T_C) compared to the equivalent volume change by the applied hydrostatic pressure pointing to criticality of 5*d* - n*p* electronic interactions. By using x-ray spectroscopic and powder diffraction measurements coupled with density functional theory (DFT) calculations we have shown that a tenfold increase of T_C compared to the equivalent phase volume change by the applied hydrostatic pressure in $Gd_5(Si_xGe_{1-x})_4$ is electronically driven. Here, Si 3*p* – Gd 5*d* hybridization is stronger than Ge 4*p* – Gd 5*d*, and it becomes a critical factor in mediating indirect exchange interactions between the localized Gd 4*f* spins. This fundamental result highlights a strong sensitivity of T_C to the nature of *p-d* hybridization, *opening up opportunities for tailoring magnetism of these and other compounds* by tuning the 5*d* - n*p* hybridization *via* chemical substitutions.

Considering a second model system – $(R_{1-x}R_x')Al_2$ – we have established that the low temperature (T) anomalies observed in these systems are due to the variation of *both exchange and crystal field* splitting leading to anomalous intra-site correlated 4*f* and itinerant 5*d* states near the Fermi level, E_F. As predicted by DFT and validated experimentally, $HoAl_2$ undergoes a cubic to orthorhombic distortion at a spin reorientation transition below T_C, while $PrAl_2$ undergoes a cubic to tetragonal distortion at T_C. In addition to low energy 4*f* splitting, the 5*d* bands are split at E_F in $HoAl_2$. This band splitting competes with the exchange splitting near E_F and supports the structural distortion leading to spin reorientation in $HoAl_2$. Compared to $HoAl_2$, the 5*d* crystal field splitting in $Ho_{0.75}Er_{0.25}Al_2$ is weaker, which correlates with the gradual suppression of the spin reorientation transition in $(Ho_{1-x}Er_x)Al_2$ with x.

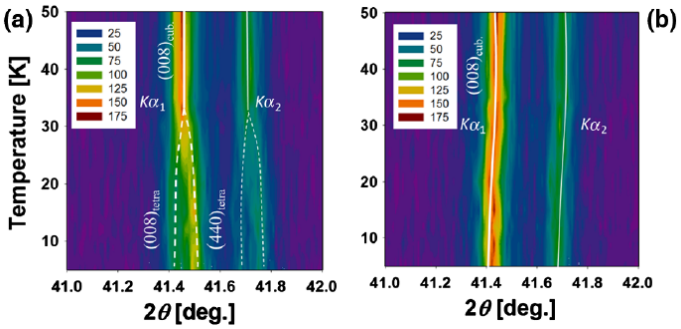

Fig. 1.Contour maps of the x-ray diffraction patterns of $PrAl_2$ measured in H= 0 (a) and H= 30 kOe (b) [476].

The strong 4*f* splitting close to E_F established from DFT confirms the low temperature anomaly and the structural distortion in $PrAl_2$. Interestingly, $PrAl_2$ recovers its cubic symmetry (Fig. 1) upon the application of an external magnetic field *via* lifting of the 4*f* crystal field splitting. The modification of the energy levels of the nuclear spin system due to the 4*f* band splitting gives rise to additional nuclear hyperfine splitting, resulting in higher Schottky heat capacity close to 0 K in the tetragonal $PrAl_2$ compared to the elemental Pr. The 4*f* crystal field splitting, which is the main reason of the tetragonal distortion in $PrAl_2$, is absent in $NdAl_2$ indicating no structural distortion in this compound.

Extended calculations of Er- and Tm-based series of mixed rare earth dialuminides reveal enhanced complexity: the effective quadrupolar moment (QM) of the lanthanides changes sign as a function of x, leading to a change in the sign of the anisotropy constant. The QMs change sign at compositions where the 4*f* and 5*d* crystal-field anomalies at E_F are expected. Sharp heat capacity anomalies occur at these concentrations because the quadrupolar interactions are effectively reduced to zero, giving rise to lattice instability due to higher order interactions and leading to first-order effects in the magnetically ordered state.

Future Plans

Rare earth materials provide a unique and fertile resource by allowing for a subtle yet precise control of crystallography, electronic structure, and magnetic properties of a compound. Knowledge of the mechanisms of phase changes driven by a minor stimulus, followed by a major perturbation of properties, is of interest for understanding nonlinear relationships in the free energy and is crucial for *guiding the discovery of advanced energy materials*. It is the latter goal that is the focus of this research, by building upon state-of-the-art synthesis, processing and

characterization, and integrating with theory, modeling, and computations gauged and refined against reliable experimental data.

In addition to the relatively well explored systems we consider new compounds that can be prepared by both *conventional* (thermal) and *unconventional* (mechanochemical redox) synthesis routes, whose basic science barely has been studied. At the electronic level, controlling interactions between the localized (4*f*) and itinerant (*spd*) electrons influences a number of effects associated with magnetic ordering, magnetic frustrations, magneto-volume, itinerant electron metamagnetic, and magnetic-martensitic transformations. At the microscopic scale, modification of strain-stress interactions between the matrix and impurity phases and lattice imperfections, such as interstitial inclusions, may provide additional levels of control. As a result, the availability of a diverse group of systems with closely related crystal structures adopting different magnetic ground states opens up a unique opportunity to resolve the recurring puzzle of the intrinsic relationships among the chemical composition, electronic, atomic and microscopic structures, and physical properties of intermetallic compounds, and will lead to a much richer physics than presently known. Consequently, new avenues for future energy-related applications of rare earth-based materials will be opened up *via* a judicious manipulations of chemical (electronic), crystallographic, and microscopic degrees of freedom.

The overall success of this research will be measured by advancements toward the following goals:

- Refining experimental and computational tools to isolate the mechanism(s) by which the magnetism of R sublattices can be affected by non-R atoms over the dominance of indirect exchange interactions;
- Reaching consistency in quantifying chemistry-structure-magnetic property relationships;
- Building a foundation towards predicting adjustments of the physical and chemical parameters critical in controlling the responsive behavior of magnetic materials;
- Developing cluster physics beyond traditional physical or chemical heterogeneity, and
- Delineating pathways to ensure impact on future energy-related technologies.

In the past, we showed how to selectively suppress FM (and enhance antiferromagnetic, AFM) states in some Gd-based compounds. The issues in focus next are: how to enhance FM in R_5T_4, and how to generalize our findings for other rare earth systems.Preliminary experiments show that when Sc replaces Gd in Gd_5Ge_4, the FM state of $(Gd_{1-x}Sc_x)_5Ge_4$ is enhanced up to at least $x = 0.2$. The effect of Sc on the magnetism of Gd_5Ge_4 goes beyond the trivial lattice compression and/or dilution effects, and Sc is magnetically active. 5*d*-3*d* hybridization may lead to a strong 4*f*-3*d* exchange and a sizeable Sc moment. Substitutions of Gd by Ti may show even a stronger effect compared to $(Gd_{1-x}Sc_x)_5Ge_4$. Hence, we will focus on the mechanisms

underlying the enhancement of ferromagnetism in R_5T_4 through tailoring magnetic R sites by Sc and Ti. To foster a more general understanding of magnetostructural transformations, we will include RScT, RAl_2, and RCo_2 families in addition to R_5T_4. The *expected outcome* is to understand the interplay between the localized 4*f* states and itinerant states of substituting elements and achieve a more complete control of the magnetic properties.

A unique opportunity to advance the physics of magnetic clusters is presented by a barely studied extended family of $R_{117}M_{52\pm x}T_{112\pm y}$compounds, where M = Cr, Fe or Co; T = Ge or Sn.They crystallize with giant unit cells that contain in excess of 10^3 atoms. The unit cells consist of several types of large ($10^1 - 10^2$ atoms) atomic clusters that are, nonetheless, arranged in the ordered manner. Interactions between and within the clusters give rise to unique magnetism. Compounds with different R, M and T will be examined by bulk measurements of polycrystals and, as needed, single crystals. Small angle neutron scattering will be employed to quantify correlation lengths, including their *T* and *H* dependencies. Total energy of various clusters will be probed by first-principles calculations and correlated with experiments. The analysis of the clusters' electronic structure and magnetism will give an invaluable insight into intrinsic properties of compounds with giant unit cells when the calculations of the whole unit cell may prove to be too difficult or even impossible to perform.

A common bottleneck that hinders practical applications of responsive materials, for example in magnetocaloric cooling, is lack of compounds that in weak, readily available magnetic fields exhibit substantial temperature and entropy changes. Using R_5T_4 and $La(Fe_{1-x}Si_x)_{13}$ model systems we will determine best chemical (doping, substitutions) and physical (strain, formation of defect structures) pathways to maximize $|(\partial M/\partial T)_H|$ at T_C while minimizing ΔH. In order to create a basic science foundation for precise manipulation of magnetostructural transformations in the three-dimensional coordinate space we will undertake a thorough experimental study of *T-H-P* diagrams of R_5T_4 and $LaFe_{13-x}Si_x$-based materials. For anisotropic R_5T_4 materials, uniaxial pressure is likely to be a more effective control parameter than hydrostatic pressure, which requires a much more extensive characterization effort using single crystals. The goal is to develop predictive tools making possible the creation of advanced rare earth materials with strong magnetocaloric effects attainable in weak magnetic fields.

Our preliminary experiments indicate that intermetallics can be prepared as nanoparticles by mechanochemical reduction of halides with alkali metals or their hydrides. Not only does this approach lead *to clean nanoparticles* that are nearly impossible to achieve by milling R-based alloys (due to heavy oxidation), but also this opens a pathway toward synthesis of single phase materials that form peritectically, and therefore require lengthy heat treatments. We will develop protocols for mechanochemical redox synthesis of R_5T_4, RCo_2 and RAl_2 and examine magnetostructural behaviors of clean nanoparticles. Results of this effort will have far-reaching implications for the science of other magnetic and functional materials, especially those that to date could not be prepared in a single phase and/or clean nanoparticulate state.

Publications

1. M. Khan, D. Paudyal, K.A. Gschneidner, Jr., and V.K. Pecharsky, "Magnetic properties of $Ho_{1-x}Er_xAl_2$ alloys," J. Appl. Phys. **113**, 17E106 (2013).

2. A. Provino, D. Paudyal, M. L. Fornasini, I. Dhiman, S. K. Dhar, A. Das, Y. Mudryk, P. Manfrinetti, and V. K. Pecharsky, "Unexpected crystal and magnetic structures in $MnCu_4In$ and $MnCu_4Sn$," Acta Mater.**61**, 2236 (2013).

3. J. Liu, D. Paudyal, Y. Mudryk, J. D. Zou, K. A. Gschneidner, Jr., and V. K. Pecharsky, "Unusual magnetic and structural transformations of $DyFe_4Ge_2$," Phys. Rev. B **88**, 014423 (2013).

4. Y.C. Tseng, D. Paudyal, Y. Mudryk, V. K. Pecharsky, K. A. Gschneidner, Jr, and D. Haskel,"Electronic contribution to the enhancement of the ferromagnetic ordering temperature by Si substitution in $Gd_5(Si_xGe_{1-x})_4$ system," Phys. Rev. B **88**, 054428 (2013).

5. D. Paudyal, A. K. Pathak, V. K. Pecharsky, and K. A. Gschneidner, Jr., "Understanding and prediction of electronic-structure-driven physical behaviors in rare-earth compounds," J. Phys.: Condens. Matter **25**, 396002 (2013).

6. A. K. Pathak, D. Paudyal, Y. Mudryk, V. K. Pecharsky, and K. A. Gschneidner, Jr., "Anomalous Schottky specific heat and structural distortion in ferromagnetic $PrAl_2$," Phys. Rev. Lett. **110**, 186405 (2013).

7. F. Bartolomé, C. M. Bonilla, J. Herrero-Albillos, I. Calvo, C. Castán, E. Weschke, D. Schmitz, D. Paudyal,Y. Mudryk, V. Pecharsky, K. A. Gschneidner, Jr., A. Stunnault, and L. M. García, "Short-range magnetic correlations and parimagnetism in RCo_2," The Eur. Phys. J. B **86**, 489 (2013).

8. Q. Cao, L. S. Chumbley, Y. Mudryk, M. Zou, V. K. Pecharsky, K.A. Gschneidner, Jr., "Effects of mechanical grinding and low temperature annealing on crystal structure of Er_5Si_4," J. Alloys. Compd. **556**, 127 (2013).

9. Y. Mudryk, P. Manfrinetti, V. Smetana, J. Liu, M. L. Fornasini, A. Provino, V. K. Pecharsky, G.J. Miller, K.A. Gschneidner, Jr., "Structural disorder and magnetism in rare-earth (*R*) $R_{117}Co_{54+x}Sn_{112\pm y}$," J. Alloys Compd. **557**, 252 (2013).

10. Y. Mudryk, V. K. Pecharsky, K. A. Gschneidner, Jr., "Unusual magnetic frustration in Lu-doped Gd_5Ge_4," J. Appl. Phys. **113**, 17E104 (2013).

11. C. L. Wang, J. D. Zou, J. Liu, Y. Mudryk, K. A. Gschneidner, Jr., Y. Long, V. Smetana, G. J. Miller, V. K. Pecharsky, "Crystal structure, magnetic properties, and the magnetocaloric effect of Gd_5Rh_4 and GdRh," J. Appl. Phys. **113**, 17A904.

12. K. Morrison, A. Dupas, Y. Mudryk, V. K. Pecharsky, K. A. Gschneidner, Jr., A.D. Caplin, and L.F. Cohen, "Identifying the critical point of the weakly first-order itinerant magnet $DyCo_2$ with complementary magnetization and calorimetric measurements," Phys. Rev. B **87**, 134421 (2013).

13. J. D. Zou, J. Liu, Y. Mudryk, V. K. Pecharsky, K. A. Gschneidner, "Ferromagnetic ordering and Griffiths-like phase behavior in $Gd_5Ge_{3.9}Al_{0.1}$," J. Appl. Phys. **114**, 063904 (2013).

14. N. Marcano, P. A. Algarabel, J. R. Fernandez, C. Magen, L. Morellon, N. K. Singh, K. A. Gschneidner, V. K. Pecharsky, and M. R. Ibarra, "Effects of pressure on the magnetic-structural and Griffiths-like transitions in Dy_5Si_3Ge," Phys. Rev. B **88**, 214429 (2013).

15. J. Liu, V. Smetana, K. A. Gschneidner, G. J. Miller, and V. K. Pecharsky, "The Crystal Structure and Magnetic Properties of $Pr_{117}Co_{56.7}Ge_{112}$," J. Appl. Phys. **113**, 17E120 (2013).

16. Q. Cao and L.S. Chumbley, "Characterization of second-phase platelets in a Gd_5Si_3 intermetallic compound," Microscopy **62**, 629 (2013).

17. W. W. Xie, S. Thimmaiah, J. Lamsal, J. Liu, T. W. Heitmann, D. Quirinale, A. I. Goldman, V. K. Pecharsky, and G. J. Miller, "β-Mn-type $Co_{8+x}Zn_{12-x}$ as a defect cubic laves phase: Site preferences, magnetism, and electronic structure," Inorg. Chem. **52**, 9399 (2013).

18. A. Provino, D. Paudyal, A. V. Morozkin, P. Manfrinetti, K. A. Gschneidner, Jr., "Systematics and anomalies in formation and crystal structures of RScSb and $R_3Sc_2Sb_3$ rare earth compounds," J. Alloys Compd. **587**, 783 (2014).

19. A. K. Pathak, D. Paudyal, K. A. Gschneidner, Jr., and V. K. Pecharsky, "Low temperature crystal structure and magnetic properties of RAl_2," J. Appl. Phys. **115**, 17E109 (2014).

20. A. Maurya, A. Thamizhavel, A. Provino, M. Pani, P. Manfrinetti, D. Paudyal, and S. Dhar, "Synthesis, crystal and electronic structure of the quaternary magnetic $EuTAl_4Si_2$ (T = Rh and Ir) compounds," Inorg. Chem. ***53***, 1443 (2014).

21. D. Paudyal, V. K. Pecharsky, and K. A. Gschneidner, Jr., "Electronic structure, magnetic properties, and magnetostructural transformations of rare earth dialuminides," J. Appl. Phys. **115**, 17E127 (2014).

22. M. L. Fornasini, D. Mazzone, A. Provino, M. Michetti, D. Paudyal, K. A. Gschneidner, Jr, and P. Manfrinetti; "New structures formed by $R_3Au_4Sn_3$, $R_5Au_8Sn_5$ and $R_3Au_6Sn_5$ compounds (R = rare earths)," Intermetallics **53**, 169 (2014).

23. A. K. Pathak, D. Paudyal, W. T. Jayasekara, S. Calder, A. Kreyssig, A. I. Goldman, K. A. Gschneidner, Jr., and V. K. Pecharsky, "Unexpected magnetism, Griffiths phase, and exchange bias in the mixed lanthanide $Pr_{0.6}Er_{0.4}Al_2$," Phys. Rev. B **89**, 224411 (2014).

24. S. Gupta, K. G. Suresh, A. K. Nigam, Y. Mudryk and D. Paudyal, V. K. Pecharsky and K.A. Gschneidner, Jr., "The nature of the first-order isostructural transition in GdRhSn," J. Alloys and Compounds **613**, 280 (2014).

25. C. M. Bonilla, D. Paudyal, J. Herrero-Albillos, V. K. Pecharsky, K. A. Gschneidner, Jr., L. M. Garcia, and F. Bartolome, "Formation of Co moment in the paramagnetic phase of RCo_2," IEEE Trans. Magn. **50**, 1700204 (2014).

26. C. Ritter, S. K. Dhar, R. Kulkarni, A. Provino, D. Paudyal, P. Manfrinetti, and K. A. Gschneidner Jr., "Electronically- and crystal-structure-driven magnetic structures and physical properties of RScSb (R = rare earth) compounds: a neutron diffraction, magnetization and heat capacity study," J. Phys.: Condens. Matter **26**, 366001 (2014).

27. J. M. Cadogan, D. H. Ryan, Y. Mudryk, V. K. Pecharsky, and K. A. Gschneidner, "On the Magnetic Order of Gd_5Ge_3," J. Appl. Phys. **115**, 17A901 (2014).

28. R. L. Hadimani, Y. Mudryk, T. E. Prost, V. K. Pecharsky, K. A. Gschneidner, and D. C. Jiles, "Growth and characterization of Pt-protected Gd_5Si_4 thin films," J. Appl. Phys. **115**, 17c113 (2014).

29. J. Liu, Y. Mudryk, J. D. Zou, V. K. Pecharsky, and K. A. Gschneidner, "Antiferromagnetic cluster spin-glass behavior in $Pr_{117}Co_{54.5}Sn_{115.2}$ - a compound with a giant unit cell," J. Alloys Compd. **600**, 101 (2014).

30. J. Liu, W. Xie, K.A. Gschneidner, Jr., G.J. Miller, and V.K. Pecharsky, "Spin-glass behavior in a giant unit cell compound $Tb_{117}Fe_{52}Ge_{113.8(1)}$," J. Phys.: Condens. Matter. **26**, 416003 (2014).

31. X.C. Zhong, Z.W. Liu, D.C. Zeng, K.A. Gschneidner, Jr., and V.K. Pecharsky, "Magnetocaloric effect of $Pr_2Fe_{17-x}Mn_x$ alloys," Rare Met. **33**, 552 (2014).

32. A. Provino, P. Manfrinetti, K. A. Gschneidner, S. K. Dhar, D. L. Schlagel, T. A. Lograsso, G. J. Miller, S. Thimmaiah, H. Wang, A. M. Russell, A. Becker, and Y. Mudryk, "Self-assembled nano- to micron-size fibers from molten $R_{11}Ni_4In_9$ intermetallics," Acta Mater. **73**, 27 (2014).

33. N. K. Singh, Y. Mudryk, V. K. Pecharsky, and K. A. Gschneidner, "In situ X-ray powder diffraction study of Ho_5Ge_4," J. Appl. Phys., **115**, 17e105 (2014).

34. S. H. Williams, D. W. Brown, B. Clausen, A. Russell, and K. A. Gschneidner, "Observations of a dynamical-to-kinematic diffraction transition in plastically deformed polycrystalline intermetallic YCu," Acta Mater. **70**, 307-315 (2014).

35. V. I. Zverev, A. M. Tishin, A. S. Chernyshov, Y. Mudryk, K. A. Gschneidner, and V. K. Pecharsky, "Magnetic and magnetothermal properties and the magnetic phase diagram of high purity single crystalline terbium along the easy magnetization direction," J. Phys.: Condens. Matter**26**, 066001 (2014).

36. Y. Mudryk, V.K. Pecharsky, and K.A. Gschneidner, Jr., "R_5T_4 compounds: An extraordinary versatile model system for the solid state science," in: J.-C. Bunzli and V.K. Pecharsky, Eds., Handbook on the Physics and Chemistry of Rare Earths **44**, 283 (Elsevier, 2014) and references therein.

37. A.K. Pathak, K.A. Gschneidner, Jr., and V.K. Pecharsky, "Negative to positive magnetoresistance and magnetocaloric effect in $Pr_{0.6}Er_{0.4}Al_2$," J. Alloys Compds. **621**, 411 (2015).

38. A.K. Pathak, K.A. Gschneidner, Jr., and V.K. Pecharsky, "The structural and magnetic properties of $Pr_{1-x}Er_xAl_2$," J. Appl. Phys. **117**, 17C107 (2015).

39. J.D. Zou, D. Paudyal, J. Liu, Y. Mudryk, V.K. Pecharsky, and K.A. Gschneidner, Jr., "Magnetostructural phase transformations in $Tb_{1-x}Mn_2$," J. Mater. Chem. C **3**, 2422 (2015).

40. J. Liu, V.K. Pecharsky, and K.A. Gschneidner, Jr., "Multiple phase transitions and magnetoresistance of $HoFe_4Ge_2$," J. Alloys Compds. **631**, 26 (2015).

Complex Hydrides – A New Frontier for Future Energy Applications

Vitalij K. Pecharsky, L. Scott Chumbley, Duane D. Johnson, and Marek Pruski
Ames Laboratory, Iowa State University, Ames, IA 50011-3020, vitkp@ameslab.gov

Program Scope

Hydrogen storage in solids is a mature scientific concept, and it remains one of the critical enabling materials technologies required to ensure a successful future transition from fossil carbon-based fuels to hydrogen, which is both a renewable and environmentally-benign energy carrier. Simple and complex light-metal hydrides, where up to six hydrogen atoms may coordinate the metal atom, support volumetric densities two to three times greater than the state-of-the-art compressed hydrogen at 700 bar, and have the potential to support reversible hydrogen storage systems exhibiting 1.8 to 2.5 kWh kg^{-1} gravimetric and 1.3 to 2.3 kWh l^{-1} volumetric energy densities. Importantly, hydrogen stored in a solid represents a safe, long-term solution to the distributed use of hydrogen in transportation when compared to compressed gas.

This project primarily utilizes mechanical energy to drive chemical transformations leading to formation of light-metal hydrides that contain 10 or more per cent hydrogen by weight and, therefore, are suitable for use in hydrogen storage systems in the future. Our *ultimate goal* is to create advanced hydrogen-containing materials by coupling mechanochemistry with advanced thermochemical, diffraction, microscopic, and solid-state nuclear magnetic resonance (SSNMR) characterization and state-of-the-art modeling based on the density functional theory. Our success will be measured by achieving the *following objectives*: i) established detailed mechanisms of both mechanochemical and thermochemical transformations in selected hydride systems, ii) identified pathways leading toward tailoring kinetic and thermodynamics properties and iii) demonstrated reversibility of potentially useful light-metal hydrides.

Recent Progress

Alane, AlH_3, meets all of the U.S. DOE technical targets for onboard storage for light-duty vehicles [1], except reversibility.We show that *pure* AlH_3 *can be prepared in quantitative yieldsatroom temperaturevia a fast mechanochemical transformation* (MT) as illustrated by (1) and (2a), which is a solvent-free alternative of the Schlesinger reaction. Formation of metallic Al, see Fig. 1a, is completely suppressed when the processing is performed above a critical hydrogen pressure, $p_c(H_2) \cong 200$ bar. A sample prepared at $p(H_2) = 250$ bar $> p_c(H_2)$ demonstrates a 99 % yield of AlH_3, see (1), (2a) and Fig. 1b, whereas that prepared at $p(H_2) = 100$ bar $< p_c(H_2)$ exhibits only a 40 % yield due to formation of metallic Al, see (1), (2b) and Fig. 1b. Noting that the equilibrium pressure of direct hydrogenation of Al at room temperature is

~10^4 bar [2], $p_c(H_2)$ of ~200 bar cannot inhibit the decomposition of nascent AlH_3. Indeed the same MT performed under $p_c(Ar) \cong 90$ bar and $p_c(He) \cong 125$ bar yields AlH_3 quantitatively. Further, by using $LiAlD_4$ and H_2 at $p(H_2) > p_c(H_2)$ we proved that gaseous H_2 remains chemically inert in this MT.

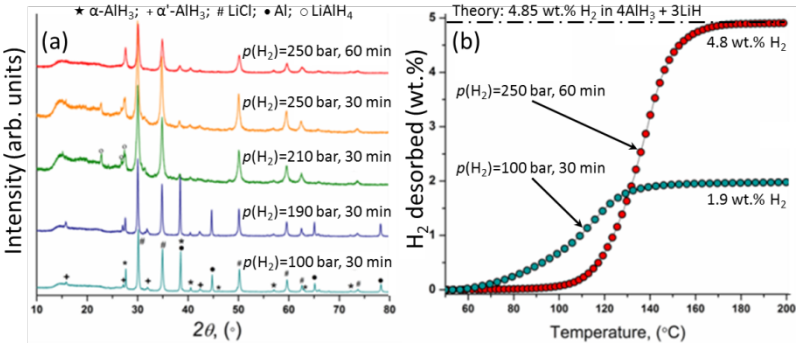

Fig. 1. (a) X-ray powder diffraction patterns of the products obtained after mechanochemical processing of $3LiAlH_4 + AlCl_3$ at 100 bar $\leq p(H_2) \leq$ 250 bar. (b) Temperature-programmed desorption (TPD) of as-prepared samples with ramping rate of 4 °C min^{-1}.

$$¾LiAlH_4 + AlCl_3 \rightarrow ¾LiAlCl_4 + AlH_3, \qquad p = any \qquad (1)$$

$$¾LiAlCl_4 + AlH_3 + {}^9/_4LiAlH_4 \rightarrow 4AlH_3 + 3LiCl, \qquad p > p_c \qquad (2a)$$

$$¾LiAlCl_4 + AlH_3 + {}^9/_4LiAlH_4 \rightarrow 2.4Al + 1.6AlH_3 + 3LiCl + 3.6H_2, \quad p < p_c \qquad (2b)$$

We examine the atomic processes of alane formation on Ti-doped Al (111) surface with(out) Ti doping. As shown inFig. 2a,the dissociative adsorption of H_2 on Al (111) costs energy: the formation of three atomically adsorbed H on Al (111) is 0.58 eV higher. The formation of alane pushes the energy further up, with alane adsorbing on a neighboring 3-fold hollow site, and leaves a surface Al vacancy behind. Overall, formation of alane on Al (111) is an endothermic reaction of 0.64 eV. If Al (111) already has an Al vacancy (e.g., as a result of ball-milling), the adsorption of 3H from dissocating ${}^3/_2H_2$ lowers the energy by 0.20 eV. Then, it needs to overcome 0.31 eV to form alane with an Al adatom. By introducing Ti on Al (111), seeFig. 2b, the Al vacancy formation energy is reduced to 0.46 eV. With Ti, the ${}^3/_2H_2$ dissociation is favored in both cases, an energy drop of 0.37 and 0.45 eV without and with Al vacancy, respectively. Then, the formation of AlH_3 is favored by a small energy drop of 0.08 eV in the vacancy case. Without a vacancy, alane can form with an energy drop of 0.10 eV if there

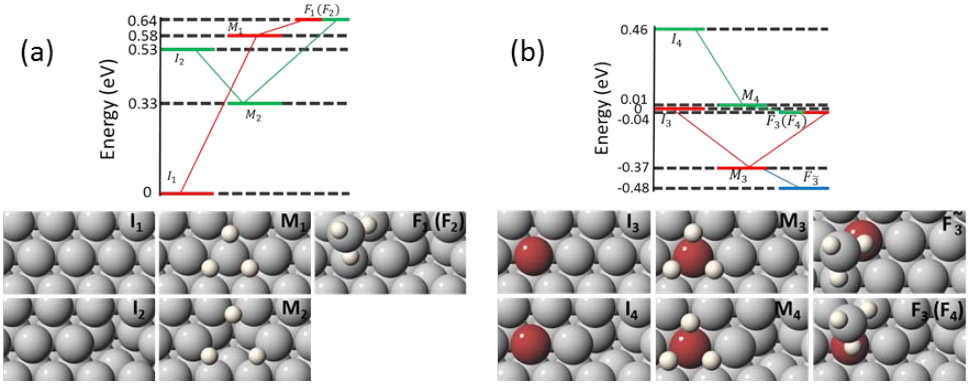

Fig. 2. Reaction diagram for formation of AlH_3on Al(111) (a) without, and (b) with Ti dopant. In each case, both the absence and presence of Al vacancy are considered.Relative energies of the initial (I), intermediate (M) and final (F) states are shown in the top panel and the corresponding atomic configurations are shown in the bottom panel. Gray, red and white spheres stand for Al, Ti and H, respectively.

is an activated Al adatom available by the vacancy creation at other places on the surface. Otherwise, a direct conversion to alane by creating a local Al vacancy costs 0.33 eV. With the avalability of an activated Al adatom diffusing on surface, *the formation of alane in both cases becomes endothermic*.

Future Plans

Our future research is unified under a versatile synthetic approach that utilizes mechanical energy to drive chemical transformations coupled with advanced characterization and modeling techniques. We focus on achieving the following objectives:

- Examine both mechanical energy- and thermal energy-driven chemical and phase transformations in selected metal hydride systems at and away from thermodynamic equilibrium; identify moieties and events critical to achieving reversibility of H_2 near room temperature and $p(H_2)$ lower than 200 bar.

- Using model systems develop mechanochemical tools suitable for enhancing kinetics and achieving favorable thermodynamics and superior reversibility in a broader class of complex metal hydrides.

- Create liquid-free and liquid-assisted mechanochemical strategies for high-yield, scalable, environmentally benign synthesis of alane (including direct hydrogenation of Al) and hybrid materials that contain complex metal hydrides and graphene.

- Establish nature of the products and intermediates, and mechanisms of the underlying interfacial phenomena and transport of species formed during (de)hydrogenation of graphene-based hybrids using state-of-the-art characterization and modeling methods.

- Advance and expand SSNMR characterization by employing dynamic nuclear polarization (DNP) to (hyper)polarize nuclear spins and by using the first spectrometer operating at ^1H resonance frequency of 1.5 GHz to enhance both sensitivity and resolution.

- Integrate experiment with first-principles theory to provide a fundamental understanding of the nature of metal-hydrogen bonding and formation, structure and stability of selected complex metal hydride systems, including effects of mechanical energy, temperature, and pressure in controlling the nature of hydrogen-metal bonds and, therefore the dehydrogenation and hydrogenation pathways.

Since each chemical element brings unique features into the progression of the Schlesinger-type metathesis reaction, we will explore mechanochemical synthesis of alane *via* reactions of binary or complex hydrides with other aluminum halides, e.g. NaH-AlX_3 (X = Cl, Br and I), MAlH_4-AlX_3 (M = Li, Na, X = Br, I). These systems, which are closely related to those described in Eqs.(1-2b) will be studied both experimentally and theoretically to understand both physical and chemical factors that are critical in controllingMTs.

Confirmed by SSNMR and gas-volumetric analyses, and in agreement with our theoretical predictions, ~2.4 % of AlH_3 forms as a result of mechanochemical processing of Al powder at $p(H_2) = 200$ bar. A major bottleneck in mechanochemical processing of Al or Al-rich intermetallic compounds is their ductility and, therefore, a strong tendency to cold-weld. Evidently, welding terminates the progress of gas-solid reaction, irrespective of the actual mechanism responsible for the direct hydrogenation of Al. We plan to investigate different process control agents that are not only capable of suppressing cold-welding, but may also make formation of AlH_3 at low hydrogen pressures thermodynamically favorable.

Following our preliminary experiments showing that the mechanochemical approach is suitable to create graphene-complex metal hydride nanostructures, we will achieve consistency in the preparation of high-quality graphene, create,and examine graphene/hydride composites with $LiBH_4$ and $LiAlH_4$. The (de)hydrogenation pathways of the prepared composites will be analyzed; relevant thermodynamic and kinetic parameters and nature of intermediates will be verified using first principles modeling, with experimental data serving as a benchmark for testing and improving our modeling tools.

Building upon successful x-ray scattering experiments [3], we will design, manufacture, and test mechanochemical tools suitable for real-time *in-situ* neutron scattering experiments. Proof-of-principle, real-time neutron scattering experiments will be performed on VULCAN [4], which offers easy access for installation of auxiliary equipment. The ultimate goal is to integrate mechanochemical experiment with NOMAD [4] to reliably detect nanocrystalline and amorphous phases in real time. Once fully developed and tested, this experimental capability is expected to have a strong impact not only on the mechanochemistry of hydrogen storage materials but on much broader mechanochemistry and mechanical alloying fields.

References

1. U.S. Department of Energy, Energy Efficiency and Renewable Energy. Fuel Cell Technologies Office. Multi-Year Research, Development, and Demonstration Plan. Program Activities for 2011-2020. Section 3.3. Hydrogen Storage, 2012 (Updated October 2014). http://energy.gov/sites/prod/files/2014/11/f19/fcto_myrdd_storage.pdf.

2. S. K. Konovalov and B. M. Bulychev, "The p,T-state diagram and solid-phase synthesis of aluminum hydride," Inorg. Chem. **34**, 172 (1995); J. Graetz, S. Chaudhuri, Y. Lee, T. Vogt, J. J. Reilly, "Pressure-induced structural and electronic changes in α-AlH_3," Phys. Rev. B **74**, 214114 (2006).

3. T, Friščić, I. Halasz, P.J. Beldon, A.M. Belenguer, F. Adams, S.A.J. Kimber, V. Honkimäki, and R.E. Dinnebier, "Real-time and in-situ monitoring of mechanochemical milling reactions," Nat. Chem. **5**, 66 (2013).

4. http://neutrons.ornl.gov/vulcan/; http://neutrons.ornl.gov/nomad/

Publications

1. S. Gupta, I. Z. Hlova, T. Kobayashi, R. V. Denys, F. Chen, I. Yu. Zavaliy, M. Pruski, and V. K. Pecharsky, "Facile synthesis and regeneration of $Mg(BH_4)_2$ by high energy reactive ball milling of MgB_2 Chem. Commun. **49**, 828 (2013).

2. R.V. Denys, I.Y. Zavaliy, V.V. Berezovets, V. Paul-Boncour, and V.K. Pecharsky, "Phase equilibria in the Mg-Ti-Ni system at 500 °C and hydrogenation properties of selected alloys," Intermetallics **32**, 167 (2013).

3. V.V. Berezovets, R.V. Denys, I.Y. Zavaliy, V. Paul-Boncour, and V.K. Pecharsky, "Characteristic features of the sorption-desorption of hydrogen by Mg-M-Ni (M = Al, Mn, Ti) ternary alloys," Mater. Sci. **49**, 159 (2013).

4. T. L. Tan, L. L. Wang, D. D. Johnson, and K. W. Bai, "Hydrogen deposition on Pt(111) during electrochemical hydrogen evolution from a first-principles multiadsorption-site study," J. Phys. Chem. C, **117**, 22696 (2013).

5. I. Z. Hlova, S. Gupta, J. F. Goldston, T. Kobayashi, M. Pruski, and V. K. Pecharsky, "Dry mechanochemical synthesis of alane from LiH and $AlCl_3$" Faraday Disc. **170**, 137 (2014).

6. S. Gupta, T. Kobayashi, I. Z. Hlova, J. F. Goldston, M. Pruski, and V. K. Pecharsky, "Solvent-free mechanochemical synthesis of alane, AlH_3: Effect of pressure on the reaction pathway," Green Chem., **16**, 4378 (2014).

7. S. Gupta, V.K. Pecharsky, T. Kobayashi, M. Pruski, and I. Z. Hlova, "Mechanochemical synthesis of Alane," Provisional application No. 61/939,156, filed with US PTO February 12 (2014); Converted to PCT application (EFS ID 21489037) February 12 (2015).

8. T. Kobayashi, S. Gupta, M. A. Caporini, V. K. Pecharsky, and M. Pruski, "Mechanism of solid-state thermolysis of ammonia borane: A ^{15}N NMR study using fast magic-angle spinning and dynamic nuclear polarization," J. Phys. Chem. C **118**, 19548 (2014).

9. J. M. Reich, L.-L. Wang, and D. D. Johnson, "H_2 Desorption from MgH_2 surfaces with steps and catalyst-dopants," J. Phys. Chem. C **118**, 6641 (2014).

10. N.A. Zarkevich, E.H. Majzoub, and D.D. Johnson, "Anisotropic thermal expansion in molecular solids: Theory and experiment on $LiBH_4$," Phys. Rev. B **89**, 134308 (2014).

Exploring the impact of the local environment on charge transfer states at molecular donor-acceptor heterojunctions

Barry P. Rand,[1,2] Antoine Kahn,[1] and Noel C. Giebink[3]

[1] Department of Electrical Engineering, Princeton University, Princeton, NJ 08544
[2] Andlinger Center for Energy and the Environment, Princeton University, Princeton, NJ 08544
[3] Department of Electrical Engineering, The Pennsylvania State University, University Park, PA 16802

Program Scope

Charge transfer from a donor-type to an acceptor-type molecule forms the basis for the photovoltaic effect observed within conjugated molecular systems. The charge transfer (CT) state is a bound geminate charge pair that defines an intermediate state in both charge generation and recombination processes. As such, the CT state possesses a binding energy ($\sim 10 k_b T$) that still needs to be overcome in order to produce a free charge pair. While some important realizations have been made concerning CT states recently regarding their role in limiting open-circuit voltage, there still remains a lack of fundamental knowledge regarding what controls CT state energy and the efficiency by which they may be dissociated, and whether or not Frenkel excitons become free charge via the formation of CT states. This research program sets out to comprehensively investigate the various nanoscale environmental factors that determine CT state behavior (dielectric, structural, dynamic, and energetic), as well as to quantify the their spatial extent and density of states (DOS) energetic distribution.

We will utilize sensitive spectral response measurements, impedance spectroscopy, X-ray scattering, and spectroscopic ellipsometry to probe the structure and optical response of thin films, as well as to extract dielectric properties. Surface-sensitive techniques such as ultraviolet photoelectron spectroscopy, inverse photoelectron spectroscopy, and X-ray photoelectron spectroscopy will be utilized to probe energy levels. Finally, time-resolved and steady-state photoluminescence (PL), electroluminescence (EL), electroabsorption, and pump-probe spectroscopy measurements will be used to probe CT state energetics and dynamics. In this way, the PIs assembled in this collaborative proposal represent a complementary team uniquely suited with the ability to transform our understanding of CT states.

Recent Progress

We have recently explored the dependence of CT energy, E_{CT}, on background dielectric constant and structure directly via EL, PL, external quantum efficiency (EQE), and absorption by varying the blend ratio of small molecule bulk heterojunction (BHJ) organic solar cells based on the donor N,N′-bis(1-naphthyl)-N,N′-diphenyl-1,1′-biphenyl-4,4′-diamine (NPD) and the acceptor C_{60}.[1] We observe a red-shift of E_{CT} with increasing C_{60} fraction (Fig. 1(a)), but find that modeling based on the accompanying change in dielectric constant via the solid-state solvation

effect can only explain the data at high (>50%) C_{60} loading (Fig. 1(c)). We attribute a higher than expected E_{CT} at low fullerene concentration to increased localization of the electron component of the CT state due to a reduction in average C_{60} crystallite size below 4 nm (Fig. 1(b)). Using electroabsorption spectroscopy, we observe a substantial increase in CT state polarizability beyond this threshold crystallite size indicative of increasing delocalization.

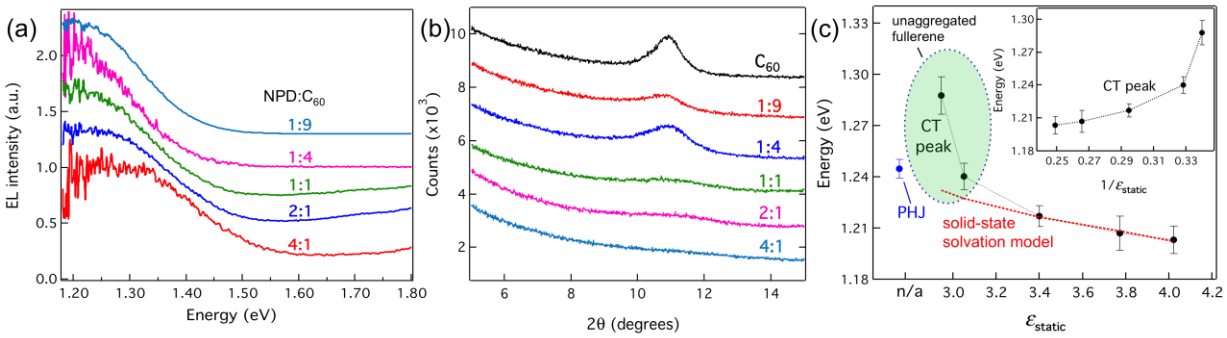

Figure 1. (a) Electroluminescence (EL) of co-evaporated layers of NPD:C_{60} with various concentrations as noted. (b) Grazing incidence X-ray diffraction (GIXRD) of NPD:C_{60} mixtures, showing that at C_{60} concentration <50%, crystallinity is strongly suppressed. (c) Charge transfer (CT) state energy as a function of background dielectric constant.

We have also been recently investigating donor-acceptor heterojunctions with significant differences in disorder. In one, micron-scale grains of rubrene[2] (see inset to Fig. 2) template a relatively highly ordered fullerene layer, whereas the other consists of amorphous rubrene with more disordered C_{60}. The CT states at each of these heterojunctions are markedly distinct, as shown in Fig. 2. The disordered one exhibits a single CT feature (similar to that typically observed) below the optical edges of the constituent materials (C_{60} defining the low energy absorption of the rubrene/C_{60} donor-acceptor pair), whereas the ordered interface unprecedentedly presents two features, the origin of which is currently being investigated via optical measurements such as spectral response and electroluminescence, as well as photoelectron spectroscopy.

Finally, we are making strides in identifying the width of the CT DOS together with its occupation function under normal solar cell operating conditions by exploring spectral shifts between CT PL and EL among various heterojunction materials and morphologies. Most device modeling to date assumes quasi-equilibrium Fermi-Dirac statistics in determining charge distributions and thus recombination rates at the DA interface; however, recent work[3] has called this into question, suggesting that occupation of the molecular site DOS is in fact far from equilibrium, particularly near the DA interface.

We are exploring the density of occupied states at the DA interface for small molecule solar cells consisting of NPD and C_{60} using pump-probe photocurrent spectroscopy in conjunction with CT electroluminescence and photoluminescence. Spectrally resolving the change in external quantum efficiency induced by steady-state background illumination, we observe characteristic changes in the low energy region dominated by CT absorption that differ strongly in the case of planar and bulk heterojunctions. We propose a model in which photocurrent generating CT absorptive transitions are bleached by charge carriers residing on molecules at the DA interface and show that it enables the interface DOS occupation function to be quantified directly. Taken together with bias and temperature dependent measurements, these results indicate that the occupation function depends strongly on DA interface morphology and is much farther from equilibrium in bulk heterojunction devices than in their planar heterojunction counterparts.

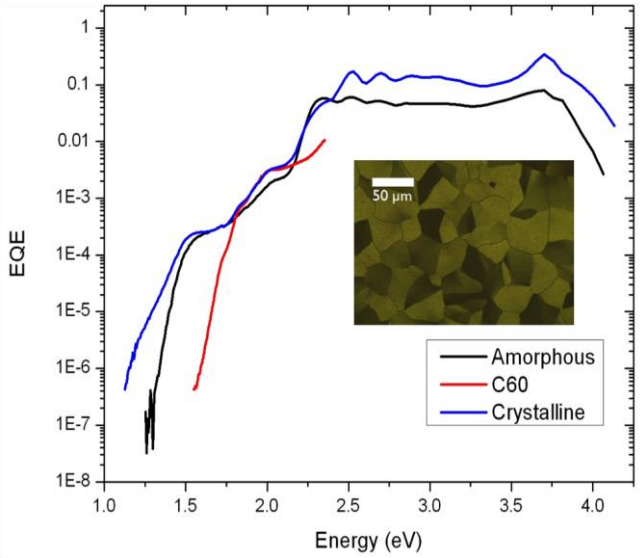

Figure 2. External quantum efficiency (EQE) as a function of incident photon energy for amorphous rubrene/C_{60} (black), crystalline rubrene/C_{60} (blue), and C_{60} (red). Any signal to lower energies from the C_{60} signal that defines the low energy Frenkel absorption edge of the rubrene/C_{60} heterojunction is charge transfer state absorption. Note that the crystalline heterojunction features 2 Gaussian features. Inset shows an optical micrograph of a crystalline rubrene film.

Independent assessment of this conclusion is provided by temperature-dependent CT photoluminescence (PL) data. Interpreting the spectral red-shift as a function of decreasing temperature within the framework of the generalized Planck equation for luminescent radiation enables us to quantify the change in effective luminescence temperature, T_{PL}, and compare it to the lattice (i.e. substrate) temperature, T_0. Figure 3(a) plots the log ratio of the CT emission spectra at different substrate temperatures relative to the room temperature spectrum. The linear relationship indicates that the data conform to the generalized Planck equation and extraction of the slope directly delivers T_{PL}, which is found to be dramatically higher in general than T_0.

This is in contrast to the same measurements carried out on GaAs, where the extracted T_{PL} and T_0 agree within ±0.1% over the entire temperature range. The results, summarized in Fig. 3(b), clearly show the difference between thermal GaAs luminescence and non-thermal CT luminescence. The non-equilibrium nature of charge distributions at the DA interface is expected to be a general phenomenon for disordered organic solar cells and has important implications for recombination and device modeling.

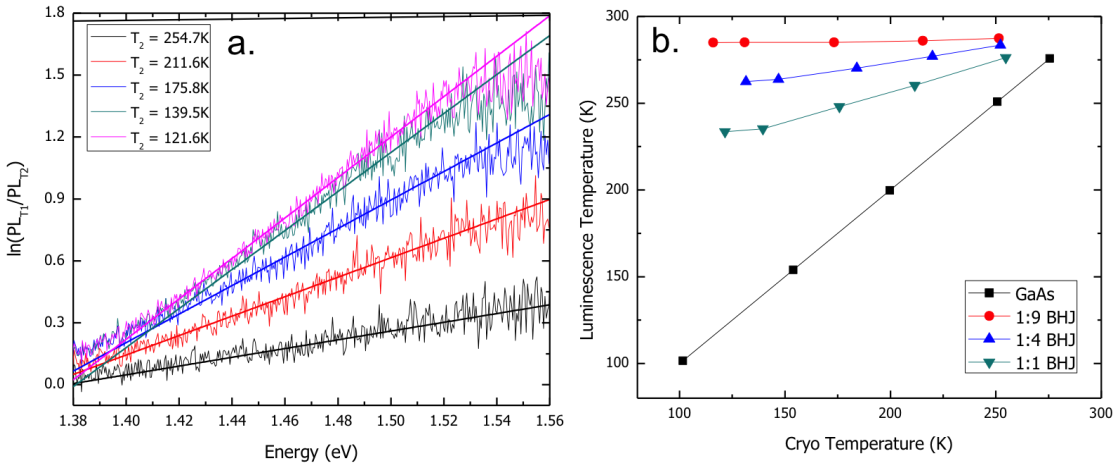

Figure 3 (a) Ratio of room temperate CT emission spectra to that obtained at lower temperatures for a 1:1 NPD:C_{60} bulk heterojunction blend film, with linear slope given by $\left(\boldsymbol{T_{PL}^{-1} - T_0^{-1}}\right)\boldsymbol{k_b^{-1}}$ according to the generalized Planck equation. (b) Luminescence temperatures extracted for several different blend ratios, demonstrating strongly non-thermal CT luminescence as compared to that obtained for GaAs.

Future Plans

As mentioned above, we are currently working on unambiguously assigning the origin of the 2 CT features in the highly crystalline rubrene/C_{60} heterojunction, through a combination of EL measurements and electron spectroscopy. Additionally, we are working on perturbed EQE measurements, where the perturbation consists of either a background light (broadband or monochromatic), voltage bias, or magnetic field (currently being set up). The combination of these efforts is expected to allow us to answer fundamental questions regarding the importance of excess driving energy, contribution of 'hot' CT states, and role of spin in the photogeneration process at molecular heterojunctions.

References

[1] B. Bernardo, D. Cheyns, B. Verreet, R.D. Schaller, B.P. Rand, N.C. Giebink, "Delocalization and dielectric screening of charge transfer states in organic photovoltaic cells," *Nature Commun.*, **5**, 3245 (2014).

[2] B. Verreet, P. Heremans, A. Stesmans, B.P. Rand, "Microcrystalline organic thin film solar cells," *Adv. Mater.*, **25**, 5504 (2013).

[3] A. Melianas, V, Pranculis, A. Devižis, V. Gulbinas, O. Inganäs, M. Kemerink, *Adv. Funct. Mater.* **24**, 4507 (2014).

Publications from DOE-sponsored research

E. Voroshazi, I. Cardinaletti, T. Conard, B.P. Rand, "Light-induced degradation of polymer:fullerene photovoltaic devices: An intrinsic or material-dependent failure mechanism?" *Adv. Energy Mater.*, **4**, 1400848 (2014).

SISGR: Defect Studies of CZTSSe & Related Thin Film Photovoltaic Materials
Michael A. Scarpulla, MSE & ECE Departments, University of Utah

Program Scope

The research objectives of this project center around investigations of the basic properties of Cu2ZnSn(S,Se)4¬ thin films especially the electronic defects in the bulk, at the interface with heterojunction partners, and at the polycrystalline grain boundaries. In the past 2 years we have carried out investigations in 1) measuring and understanding the electrical and compositional properties including grain boundaries in CZTSSe; 2) measuring and understanding electronic defects in CZTS, CZTSSe, and CZTSe thin films using electrical spectroscopies; 3) modeling the point defect equilibrium in CZTSSe; and 4) investigating defects at the CZTSSe surface which becomes the heterojunction interface with CdS.

The impact of this research is to generate basic but critical materials knowledge about an emerging alloy system that may be capable of photovoltaic efficiency on par with CdTe and CIGS but at lower cost and having the benefit of avoiding constraints on scale-up from rare and expensive elements using earth abundant elements.

Recent Progress

This project seeks fundamental understanding of the electronic states present in CZTSSe and their origins in the bulk or at structural defects and interfaces. We measure the electronic defects primarily in samples grown by leading collaborators using capacitive spectroscopy measurements such as deep level transient spectroscopy. As part of this, we are measuring and modeling the impedance of the samples to help identify the origins of the signals as true electronic defects as opposed to e.g. non-Ohmic back contacts. We are also studying the composition fluctuations on the mesoscale of 30 nm to 30 um (which should give resolution at the grain size) using transmission xray tomography and attempting to link this to observed electronic defects. Lastly, we are investigating bulk CZTS samples containing phase and grain and phase boundaries in order to understand how these structural defects manifest electronically.

Observation of Minority Electron Deep Defect in CZTSSe Capable of Explaining Observed Minority Carrier Lifetime

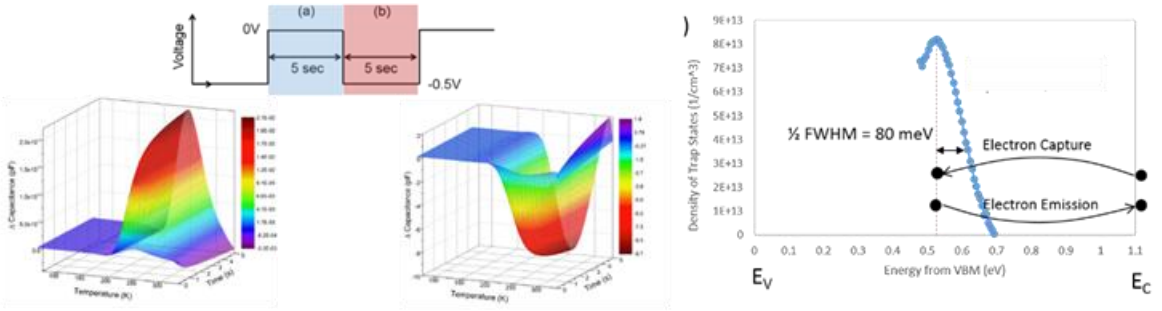

Figure 1 – (Left) Capacitance time transients after rising and falling voltage steps vs temperature. The relative magnitudes identify the process as electron capture and emission. (Right) Extracted density of trap energies.

We have used the powerful deep level transient spectroscopy (DLTS) technique to study traps and recombination centers in p-type Cu2ZnSnSSe4. We have for the first time observed using voltage and light pulsed DLTS signatures characteristic of minority electron interactions with deep levels (Figure 1). This is critical because there have been many reports of defects in

CZTSSe but linking them to recombination rates has not been established. In our study, we extracted the density of the states in space and energy as well as the electron cross section – thus we are able to estimate minority carrier lifetimes as well as including these defects in simulations to assess the impact on efficiency. We found that the number of these defects is near 1015 /cm3 in these nanoparticle ink CZTSSe films and the capture cross section of 2x1014 cm2 can account for the observed few-ns lifetime and about 1/3 of the unaccounted Voc deficit (near 400 mV) for CZTSSe. This means that at least in the samples studied the other sources of Voc loss cannot affect the bulk minority carrier lifetime – there must be other mechanisms. This rigorous accounting of the effect of different mechanisms is illuminating new paths for improving these materials. We are now investigating the presence of this defect in other films.

Equivalent Circuit Modeling for Thermal Admittance Spectroscopy Analysis of CZTSe

Admittance spectroscopy helps us to fully understand the time-dependent response of samples and discern artifact from true electronic defects. In order to more accurately analyze defect response we have created an equivalent AC circuit model including material and heterojunction physics which we use to fit admittance data from CZTSSe heterojunction samples. We find that the previously proposed mechanisms to explain the observed series resistance are quantitatively insufficient and that the main response reported by others as being related to trap states is most probably caused by a non-Ohmic back contact.

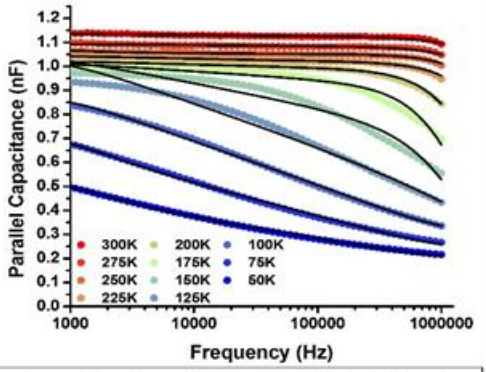

Figure 2 - Capacitance data fitted with the described equivalent circuit model.

Element Resolved Xray Tomography of CZTSe

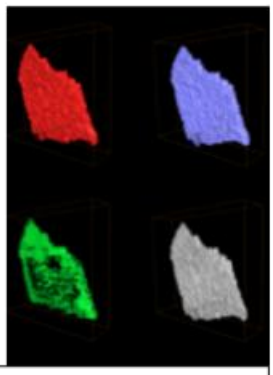

Figure 3 – Preliminary reconstructions of Cu, Zn, Sn, and Se (red, blue, green, gray).

Composition variation is expected in CZTSSe at the sub-grain level near grain boundaries for example. We have pushed the capabilities of beamline 6.2c at SSRL to attempt to reconstruct the composition of CZTSSe samples at the mesoscale in 3D with 50 nm voxels over flakes of thin film measuring tens of um (volumes containing hundreds of grains). We are the first research group to attempt to resolve relative compositional maps beyond binary (presence or absence of elements) using this technique. We will attempt to correlate composition fluctuations with electrical properties of the samples. In the next year, we will complete the tomographic reconstructions and optoelectronic measurements and correlate the two types of data.

Effects of KCN and NH4OH Etching on CZTSSe/CdS Interface

We investigated effects of KCN and NH4OH etching of the CZTSSe surface on the surface and grain boundary potentials of CZTSSe and CZTSe absorbers by KPFM and correlated these changes to heterojunction solar cell characteristics [1]. From CIGSe solar cell device processing, it is known empirically that KCN etching is beneficial – it is not a-priori obvious that

the same is true for CZTSSe thin films. Our results demonstrated that CZTSSe absorbers, especially after prolonged air exposure, possess an overlayer consisting oxide and airborne contamination layers. This overlayer was removed partially by NH4OH etching (as samples commonly experience as part of the chemical bath deposition of CdS) while KCN etching removes it completely. The characteristics of KCN- and NH4OH-etched CZTSSe solar cells demonstrated that KCN-etched solar cells outperformed their NH4OH-etched counterparts by increases in all device parameters – most obviously the short circuit current. In addition, quantum efficiency (QE) measurements demonstrate significant increase in long wavelength collection. Since the minority carrier diffusion length in CZTSSe is small, these data indicate that the KCN etching removes interface defect states that trap charge and thus allow the depletion width, within which the photocarrier collection is high, to extend deeper. Meanwhile, KPFM also show that GBs in KCN-etched CZTSSe absorbers are either negatively charged or neutral, whereas KCN-etching makes surface almost equipotential in CZTSe absorbers as evidenced by disappearance of positively charged GBs existed before etching.

CZTSSe Solar Cells with Al2O3 Passivation Layers

The key problem in making CZTSSe work as well in solar cells as other thin film materials is the very high open circuit voltage deficit. Voc measures the amount of stored free energy that can be achieved in a solar cell through the steady state population of photocarriers. As discussed above, we have found a recombination center that can account for approximately 1/3 of the Voc loss in CZTSSe. An additional 1/3 is believed to be caused by band tails [2]. Here we investigate the interface recombination and a possible way to reduce it using ALD surface modifications.

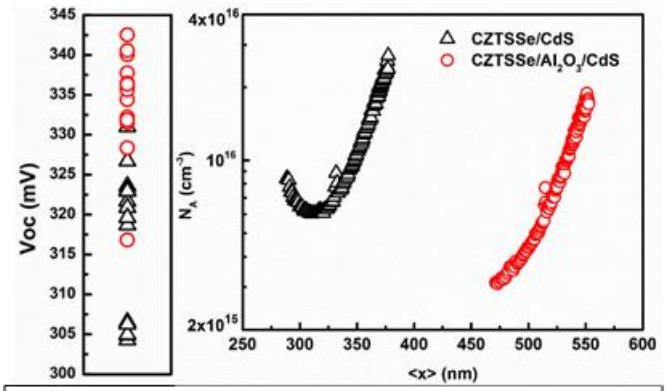

Figure 4 – (left) Open circuit voltage (Voc) of CZTSSe heterojunctions with (red circles) and without a thin ALD Al2O3 passivation layer between CZTSSe and CdS. (right) Corresponding C-V profiles showing evidence of reduced trapped charge at the passivated interface.

We investigated surface passivation effects of Al2O3 layer on CZTSSe solar cells as a way to remedy VOC deficit seen in these devices. For this purpose, CZTSSe devices with and without ALD deposited Al2O3 passivation layers (~ 1 nm) were fabricated and compared. KCN etching was used as a standard surface preparation method for both unpassivated and passivated CZTSSe devices, since our former study [1] clearly demonstrates positive effects of KCN etching on device performance. Characteristics of fabricated devices demonstrate increase in VOC of passivated devices as expected (Fig. 4). This is thought to be due to decrease in interface defect density in Al2O3 passivated devices as evidenced by lower hole concentration measured close to their junction region in these devices by capacitance-voltage (C-V) measurements (Fig. 5). A lower interface defect density in passivated devices results in wider depletion width as demonstrated by C-V and QE measurements. Overall, CZTSSe surface passivation by Al2O3 demonstrate positive results; however, further research is necessary to address observed issues such as lower fill factor seen in passivated devices due to increased series resistance. Currently, we are working on a manuscript to report this study.

Future Plans

In this last year of this project, we will concentrate on wrapping up the ongoing efforts into publications. We are continuing defect spectroscopies on CZTSSe films obtained from collaborators at IBM (solution processed), NREL (coevaporated), IMEC (sputtered and annealed), and Purdue (nanoparticle inks) in order to determine the uniqueness or universality of the minority electron trap we discovered across films prepared by different means. Through a successful user proposal at the Molecular Foundry at LBNL, we have initiated a project that will allow us to investigate the lateral transport of photocurrent at the sub-grain level. Experiments will be undertaken in April 2015. We will complete papers on the x-ray tomography, admittance spectroscopy, and interface passivation.

References

[1] M.E. Erkan, et al. Solar Energy Materials and Solar Cells, 136(0), 78-85.
[2] T. Gokmen, et al. Applied Physics Letters, 105(3), 033903.

Publications 2013-2015

M.E. Erkan, V.C. I. Repins, and M.A. Scarpulla. Interplay between surface preparation and device performance in CZTSSe solar cells: Effects of KCN and NH4OH etching.
Solar Energy Materials & Solar Cells, 78-85 (2015). dx.doi.org/10.1016/j.solmat.2015.01.006

H. Du, F. Yan, M. Young, B. To, C.S. Jiang, P. Dippo, D. Kuciauskas, Z. Chi, E.A. Lund, C. Hancock, W.M. Hlaing-Oo, M.A. Scarpulla and G. Teeter. Investigation of combinatorial coevaporated thin film Cu2ZnSnS4. I. Temperature effect, crystalline phases, morphology, and photoluminescence.
Journal of Applied Physics 115, 173502 (2014); dx.doi.org/10.1063/1.4871664

E.A. Lund, H. Du, W.M. Hlaing-Oo, G. Teeter, and M.A. Scarpulla. Investigation of combinatorial coevaporated thin film Cu2ZnSnS4 (II): Beneficial cation arrangement in Cu-rich growth.
Journal of Applied Physics 115, 173503 (2014); dx.doi.org/10.1063/1.4871665

A. Nagaoka, H. Miyake, T. Taniyama, K. Kakimoto, Y. Nose, M.A. Scarpulla, and K. Yoshino. Effects of sodium on electrical properties in Cu2ZnSnS4 single crystal.
Applied Physics Letters 104, 152101 (2014). dx.doi.org/10.1063/1.4871208

J. Zhu, F. Liu, and M.A. Scarpulla. Strain tuning of native defect populations: The case of Cu2ZnSn(S,Se)4
APL Materials 2 012110 (2014). dx.doi.org/10.1063/1.4863076

V. Kosyak, N.B. Mortazavi-Amiri, A.V. Postnikov, and M.A. Scarpulla. A Quasichemical Model of Native Point Defect Equilibrium in Cu2ZnSnS4 (CZTS) and Application to One-Zone Annealing
Journal of Applied Physics, 114 124501 (2013). dx.doi.org/10.1063/1.4819206

DOE award # DE-FG02-07ER46377, University of Texas at Austin

Thermal Transport in Two-Dimensional Layered Nanostructures

PI: Prof. Li Shi, University of Texas at Austin, lishi@mail.utexas.edu

Collaborator: Prof. Cronin, University of Southern California

Program Scope

This project is one of the three tasks of a collaborative program, Phonon and Electron Transport in Pristine Two-Dimensional Layered Nanostructures and Heterostructures. This joint program aims to elucidate the transport and conversion processes of energy carriers (phonons and electrons) in a new class of two-dimensional (2D) materials with novel structures, functionalities, and properties. The structure-property relationships resulting from the proposed research can serve as the basis for designing high-performance electronic devices and energy conversion devices employing these 2D materials. The scope of this specific task is to investigate phonon transport and thermal properties of 2D layered nanostructures, such as graphene, ultrathin graphite, h-BN, and MoS_2.

Recent Progress

Scattering of Phonons by High-Concentration Isotopic Impurities in Ultrathin Graphite

Phonon scattering by isotopic impurities is an important mechanism for manipulating the thermal conductivity, κ, of high κ materials that are actively investigated for thermal management applications. Isotope impurity scattering in the low concentration, independent scattering regime is relatively well understood. In comparison, the isotope impurity scattering in the high concentration regime has remained elusive. In this regime, whether and how interference among the scattered lattice waves can play an important role in the measured thermal conductivity is one of the central topics in recent phonon transport investigations.

In this work, we have studied the effects of isotope impurity

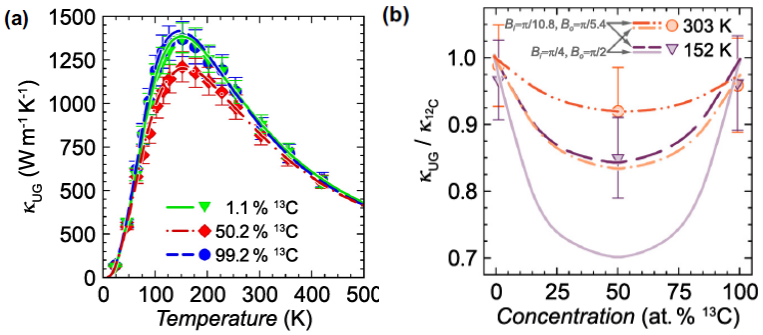

Figure 1. (a) Solid thermal conductivity of the UG (κ_{UG}) versus temperature for ^{13}C concentration of 1.1% (green down triangles), 50.2% (red diamonds), and 99.2% (blue circles). The lines are the calculated thermal conductivity for different ^{13}C concentrations. (b) Calculated solid thermal conductivity normalized by the theoretical value for isotopically pure ^{12}C graphite ($\kappa_{UG}/\kappa 12_C$) as a function of ^{13}C isotopic concentration at temperatures of 152 K (purple down triangles) and 303 K (orange circles). In one calcualtion, the isotope scattering coefficient B is taken from the indepednet scattering model to be B_i= π/4 given for the in-plane mode and B_o = π/2 for the out-of-plane modes. In another calculaiton, the two B coefficients are reduced to B_i= π/10.8 for the in-plane mode and B_o = π/5.4 in order to match the experimental data.

scattering on the measured thermal conductivity of high-quality ultrathin graphite (UG) samples with both low and high isotope impurity concentrations. The peak thermal conductivity of the UG samples occurs at a temperature close to 150 K, and is reduced in a UG sample with about 50 at.% ^{13}C and 50 at.% ^{12}C compared to two other UG samples with 1.1 and 99.2 at.% ^{13}C, respectively. However, our analysis suggests that the reduction is well below those predicted by an independent, incoherent isotope scattering model derived from perturbation theory, although the phonon dispersion of the isotopically disordered graphite can still be obtained from the virtual crystal approximation with the use of an average mass. Such discrepancy is in agreement with recent theoretical predictions of the effects of multiple scattering of phonons by high-concentration isotope impurities in low-dimensional systems.

Reexamination of Basal Plane Thermal Conductivity of Suspended Few-Layer Graphene Samples Measured by Electro-Thermal Micro-Bridge Methods

While elimination of inter-layer scattering is expected to result in increased basal-plane thermal conductivity of suspended clean graphene compared to the graphite value, it is now known that interaction with a disordered support can suppress the basal plane thermal conductivity of supported graphene below the graphite value. However, it still remains an intriguing question why the thermal conductivity of suspended graphene measured by several electro-thermal methods is lower than the graphite value.

In this work, we have measured the basal-plane thermal conductivity of a suspended bilayer graphene samplewith the use of a suspended electro-thermalbridge method in the temperature (T) range between 40 and 400 K. The measurement results are analyzed together with those obtained in two prior works with different electro-thermal bridge devices to evaluate and eliminate the errors caused by the thermal contact resistance. The analysis suggests that the existing measurement data have not revealed the failure of Fourier's law, as the measured thermal resistance increases with the suspended length nearly linearly. The thermal contact resistance is obtained by extrapolating the thermal resistance data to vanishing suspended length, and used to obtain the thermal interface conductance for graphene transferred to the measurement device. With the contact thermal resistance accounted for, the results show that the thermal conductivity of the suspended graphene samples obtained by exfoliation and chemical vapor deposition (CVD) can approach those of the natural graphite source and highly oriented pyrolytic graphite (HOPG), respectively, at above room

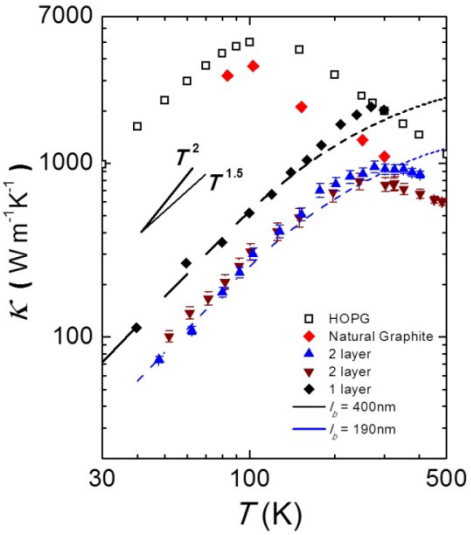

Figure 2. Basal plane thermal conductivity (κ) of the suspended 2-layer (blue triangle) exfoliated graphene samples measured in this work, in comparison to the data of a exfoliated bi-layer graphene sample(brown down triangles)measured by Pettes *et al*,[1]a CVD single layer graphene sample (black diamond) measured by Xu *et al*,[4]HOPGin Touloukian *et al*,[6] and natural graphite measured by Sadeghi *et al*.[7] The black and blue dashed lines are the calculation results for a constant scattering mean free path of 400 and 200 nm, respectively. The two solid lines show the T^2 and $T^{1.5}$dependence.

temperature (Fig. 2).

However, the low-temperature thermal conductivity of the suspended graphene samples is still considerably lower, with the peak thermal conductivity shifted to a much higher temperature, than the graphite values. The low-temperature thermal conductivity values can be fitted with a constant mean free path value (Fig. 2), which is considerably larger than the lateral dimension and the grain size of the graphene sample. In addition, the as-obtained fitting result is lower than the measured thermal conductivity of two samples in the temperature range between 200 K and 300 K. This behavior suggests that the mean free paths of relatively high frequency phonons that make an important contribution to the peak thermal conductivity are larger than those of low-frequency phonons that dominate the low-temperature thermal conductivity. Such frequency-dependence of the phonon mean free path is opposite to those expected for phonon-phonon scattering, phonon-point defect scattering, and phonon-lateral boundary scattering, and is in agreement with an earlier theory of phonon transmission and scattering at the interface between graphene and an amorphous support. As there are polymer residues on the surface of such suspended graphene samples prepared by a polymer-assisted transfer technique, these results lead to the conclusion that phonon scattering by polymer residues instead of phonon-lateral boundary scattering is the dominate scattering mechanism, and such scattering is characterized with increasing mean free path with increasing frequency.

Basal-Plane Thermal Conductivity of Few-Layer Molybdenum Disulfide

Molybdenum disulfide (MoS_2), one of the transition metal dichalcogenides, has attracted considerable interest recently as one of the candidate materials for future-generation electronic devices. For materials used in high-performance electronic devices, high thermal conductivity is desirable for spreading the Joule heat generated locally so as to reduce the local hot spot temperature. While past studies have clarified the phonon transport mechanisms behind the thickness-dependent and environment-sensitive thermal conductivity of few-layer graphene and h-BN, the

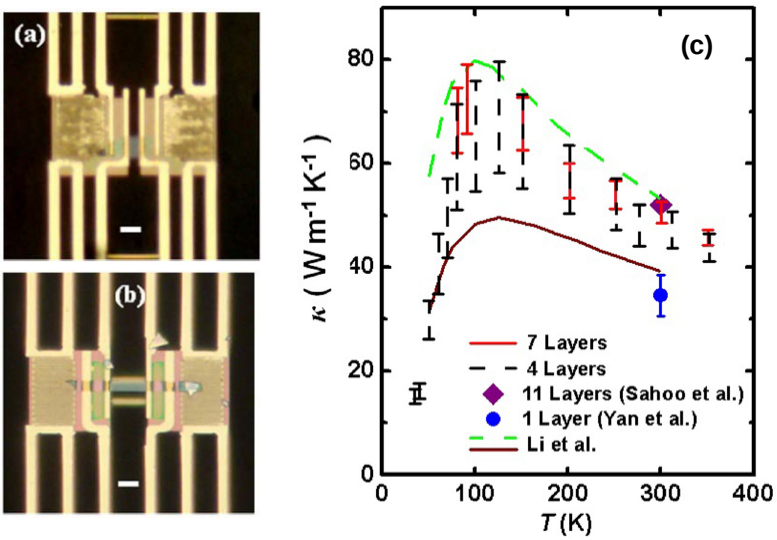

Figure 3. (a-b) Optical micrographs of two few-layer MoS_2 samples, each suspended between two SiN_x membranes with integrated resistance thermometers. Scale bars are 5 μm. (c) Thermal conductivity of the 4- (black dashed vertical lines) and 7- (red solid vertical lines) layer MoS_2 samples as a function of temperature. Shown for comparison are the measured room-temperature values of a 11 layer MoS_2 sample (purple diamond) and a monolayer MoS_2 sample (blue circle) reported by Sahoo et al.[2] and Yan et al.,[3] respectively, and the thermal conductivity calculated by Li et al.[5] with the boundary scattering length assumed to be 200 nm (green dashed line) and 100 nm (brown solid line), respectively.

thickness dependence of the basal plane thermal conductivity of other 2D layered materials including MoS_2 remain mostly unknown.

In this work, we have measured the basal-plane thermal conductivity of a four-layer and a seven-layer MoS_2 samples with the use of a suspended device in the temperature range between 40 and 350 K. The results are shown in Fig. 3. The measured apparent thermal conductivity is 37 and 45 $Wm^{-1}K^{-1}$ at room temperature for the 4 layer and 7 layer samples, respectively. For the two samples, the peak thermal conductivity is observed at a temperature close to 120 K, above which the measured thermal conductivity is dominated by intrinsic phonon-phonon scattering. Even when phonon-phonon scattering becomes dominant as temperature increases to room temperature and above, however, phonon scattering by disorders on the top and bottom surfaces of the suspended few-layer MoS_2 samples still play an important role and results in an increasing basal plane thermal conductivity with increasing layer thickness. Although the room-temperature thermal conductivity measured for the 4 layer and 7 layer MoS_2 samples is smaller than those of graphene and bulk Si, these values are still considerably higher than those of Si thin films or nanowires of the same thickness. This relatively high thermal conductivity of the few-layer thin 2D samples origins from the anisotropic phonon dispersion, which yields a phonon-surface scattering mean free path on the order of the sample thickness multiplied by the large anisotropy ratio in the group velocity of the 2D layered materials.

Future Plans

In the next year, we will employ a new four-probe thermal transport measurement method to measure the intrinsic thermal conductance of clean, suspended few-layer 2D samples, and collaborate in thermoelectric measurements of 2D heterostructures.

References

1. M. T. Pettes, I. S. Jo, Z. Yao and L. Shi, Nano Letters **11** (3), 1195-1200 (2011).
2. S. Sahoo, A. P. S. Gaur, M. Ahmadi, M. J. F. Guinel and R. S. Katiyar, J Phys Chem C **117** (17), 9042 (2013).
3. R. Yan, J. R. Simpson, S. Bertolazzi, J. Brivio, M. Watson, X. Wu, A. Kis, T. Luo, A. R. H. Walker and H. G. Xing, Acs Nano **8** (1), 986 (2014).
4. X. Xu, L. F. C. Pereira, Y. Wang, J. Wu, K. Zhang, X. Zhao, S. Bae, C. Tinh Bui, R. Xie, J. T. L. Thong, B. H. Hong, K. P. Loh, D. Donadio, B. Li and B. Özyilmaz, Nat Commun **5**, 3689 (2014).
5. W. Li, J. Carrete and N. Mingo, Appl Phys Lett **103**, 253103 (2013).
6. Y. S. Touloukian, R. W. Powell, C. Y. Ho and P. G. Klemens, New York, IFI/Plenum (1970).
7. M. M. Sadeghi, I. Jo and L. Shi, P Natl Acad Sci USA **110** (41), 16321-16326 (2013).

Publications

1. M. M. Sadeghi, I. Jo, L. Shi, “Phonon-Interface Scattering in Multi-layered Graphene on an Amorphous Support,” Proceedings of the National Academy of Sciences 110, 16321–16326 (2013)

2. D. G. Cahill, P. V. Braun, G. Chen, S. H. Fan, K. E. Goodson, P. Keblinski, W. P. King, G. D. Mahan, A. Majumdar, H. J. Maris, S. R. Phillpot, E. Pop, L. Shi, “Nanoscale Thermal Transport II: 2003-2012,” Applied Physics Reviews 1, 011305 (2014)

3. C. C. Chen, Z. Li, L. Shi, S. B. Cronin, “Thermal Interface Conductance across a Graphene/Hexagonal Boron Nitride Heterojunction,” Applied Physics Letters 104, 081908 (2014)

4. I. Jo, M. T. Pettes, E. Ou, W. Wu, L. Shi, “Basal-plane thermal conductivity of few-layer molybdenum disulfide”, Applied Physics Letters 104, 201902 (2014)

5. C.-C. Chen, Z. Li, L. Shi, S. B. Cronin, “Thermoelectric Transport Across Graphene/Hexagonal Boron Nitride/Graphene Heterostructures”, Nano Research, 1-7 (2014)

6. A. L. Moore, L. Shi, “Emerging Challenges and Materials for Thermal Management of Electronics,” Materials Today 17, 163 - 174 (2014)

7. M. T. Pettes, M. M. Sadeghi, H. X. Ji, I. Jo, W. Wu, R. S. Ruoff, L. Shi, “Phonon Scattering by High-Concentration Isotopic Impurities in Ultrathin Graphite,” Physical Review B, 91, 035429 (2015)

Metamaterials

Costas M. Soukoulis, Thomas Koschny, Jigang Wang
Ames Laboratory, Iowa State University, Ames, Iowa.

Program Scope

Many of the technologies, that underpin our economy and enable our standard of living, depend on advanced materials. Therefore, the engine for progress in many disciplines is the discovery and understanding of new materials, and their properties. Metamaterials are novel artificial materials that enable the realization of innovative properties unattainable in naturally existing materials. This program explores theoretical understanding, analysis, development, fabrication, and experimental characterization of electromagnetic metamaterials, and investigates their feasibility for various applications. In view of the complexity of electromagnetic interactions in metamaterials, the combination of theory, state-of-the-art models and computational techniques are essential to understand these structures, and we collaborate with experimentalists to fabricate and characterize some of these materials.

Recent Progress

Graphene for THz Applications: Graphene — a one-atom-thick continuous sheet of carbon atoms — has special properties that make it a desirable material for manipulating terahertz waves. THz applications operate at frequencies between microwave and far infrared. Some metamaterials could benefit by replacing the metals currently used in fabrication with graphene. Indeed, graphene provides a number of advantages over metals including that its properties offer the unprecedented ability to tune the electrical response for a given applications. Graphene also offers the advantage of a potential enhancement of terahertz wave confinement [2]. Experimental data have shown significantly higher electrical losses than has been estimated by theoretical work, showing there is more research that needs to be done to make metamaterial devices from graphene. We have published [1] an analysis and comparison of gold-

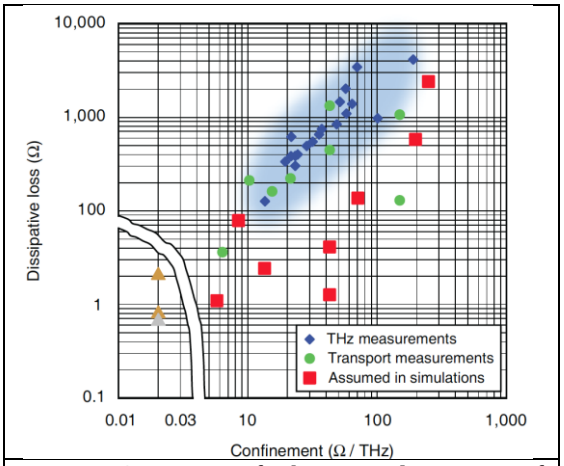

Fig. 1. Overview of sheet conductivities of graphene as found in current literature, classified according to the figures-of-merit dissipative loss and confinement [1].

and graphene-based resonator nanostructures for THz metamaterials and an ultrathin graphene-based modulator.

Broadband THz Radiation from Split-Ring-Resonator Metamaterials: The terahertz spectral range of the electromagnetic spectrum—from about 100 GHz to 15 THz—has long been a challenging region in between the successful technological realms of electronics and photonics, because of the lack of efficient and compact sources and detectors for terahertz radiation. In the past few decades, however, the development of technologies like quantum-cascade lasers, terahertz wave generation through nonlinear crystals, and terahertz time-domain spectroscopy has enabled the exploration of terahertz science and the rapid rise of terahertz imaging and spectroscopy for, amongst others, biomedical and security applications. *One key challenge is to develop ultrafast few-cycle THz pulses with extraordinary stability and a gapless spectrum covering the entire THz region.* We have developed [3] an approach based on meta-atoms called split-ring resonators (SRRs). By tailoring their size, these can exhibit a strong magnetic response to any desired frequency in the THz to infrared spectrum. We demonstrated [3] efficient single-cycle broadband THz generation, ranging from about 0.1–4 THz from a thin layer of split-ring resonators by pumping at the telecommunication wavelength of 1.5um (200 THz). This only 40nm thick metamaterial THz emitter performed as well as traditional emitters (ZnTe) that are thousands of times thicker (0.2mm or 1mm). The terahertz emission originates from exciting the magnetic-dipole resonance of the SRR and quickly decreases under off-resonance pumping. This, together with pump polarization dependence and power scaling of the terahertz emission, identifies the role of optically induced nonlinear currents in split-ring resonators. In comparison with theory, we have shown [3] a giant sheet nonlinear susceptibility that far exceeds known thin films and bulk inorganic materials such as ZnTe. Our approach provides a potential solution to bridge the "*THz technology gap*" by solving the four key challenges in the THz emitter technology: *efficiency*; *broadband spectrum*; *compact size* and *tunability*. In summary, we have shown that a single nanometer-scale layer of SRRs merges nonlinear metamaterials and THz science/technology,

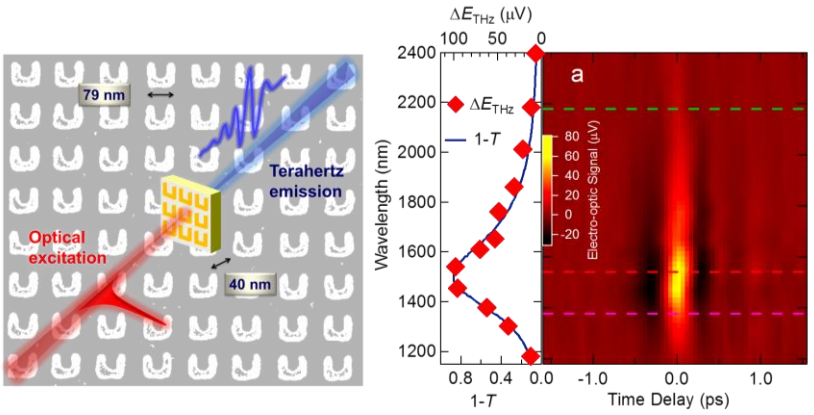

Fig. 2. (Left) Schematic showing broadband THz generation from SRRs by pumping the magnetic resonance of SRRs with 1500 nm, 140fs ultrafast laser pulse. The gray background patterns are the actual electron micrograph of SRRs. (Right) False-color plot of generated THz pulse power vs. pump wavelength and pump-probe delay. On-resonance pumping at 1500 nm gives rise to maximum THz emission. *T* is the measured unpumped transmission of the SRRs around their magnetic-dipole resonance [3].

representing a new platform for exploring artificial magnetism induced nonlinear THz generation.

Gigahertz metamaterials resonators with large quality factors: Metamaterials can create media with properties unattainable in nature, but mitigating dissipation is a key challenge for their further development. Here, we demonstrate a low-loss metamaterial by exploiting dark bound states in dielectric inclusions coupled to the external waves by small nonresonant metallic antennas. We experimentally demonstrate a dispersion-engineered metamaterial based on a meta-atom made from alumina, and show that its resonance has a much larger quality factor than metal-based meta-atoms [4]. Finally, we show that our dielectric meta-atom can be used to create sheet metamaterials with negative permittivity or permeability [4]. In the future, the dielectric meta-atoms can also be straightforwardly scaled to terahertz and optical frequencies, where high-performance dielectrics, such as silicon and fused silica, can be leveraged and even higher quality factors can be expected.

Future Plans

Advances in understanding the mechanisms that can minimize loss are critical for future applications, such as solar energy harvesting, biological and THz imaging. We will develop new dielectric resonators that enable low-loss optical metamaterials, study optimal resonator designs and their intricate coupling to gain and radiation field to enable practical loss-compensated metamaterials, and create novel lasing structures that are analog to spasers, but allow more control, higher Q-factors and lower lasing thresholds. Metal-based metamaterials can have huge nonlinearities, much stronger than in natural materials. We will design and fabricate metamaterials with large, tailored nonlinear optical properties for advanced THz generation. We will explore dynamically photo-imprinted metasurfaces on suitable semiconductor and graphene substrates to provide unprecedented control of THz waves like dynamic spectral filters, switches and spatial modulation. Finally, we will characterize the physical properties of metamaterials and develop necessary advanced optical characterization techniques.

Dielectric resonances in the dark states, as metamaterials resonators with controllable electromagnetic response and low loss: We will develop novel low-loss resonator structures optical MMs, which are based on dark dielectric bound states, specifically, dark Mie resonances in silicon discs, which will give both negative ε and μ, and will be fabricated. We will also develop dielectric metamaterials for THz frequencies based on bound state in GaAs films that are photo-imprinted to provide mode configuration and radiative coupling. These dielectric resonant structures may allow for surmounting the limitations of highly lossy metallic metamaterial resonators and enabling low-loss metamaterials at optical frequencies.

Dynamic, tunable, nonlinear and switchable metamaterials: We will explore, theoretically and experimentally, dynamically photo-imprinted MM structures on suitable

photoconductive semiconductor substrates to provide unprecedented control of THz waves like spectral filters, perfect absorbers, switches and spatial modulation. Photo-induced sheet conductivities on GaAs surfaces have proven to exceed the best available samples of graphene while still providing tunability and well confined surface plasmons, potentially allowing for photo-imprinted resonant metasurfaces and plasmonics. We will develop THz generation in resonant MMs and optimize resonator designs for stronger nonlinear response. We will experimentally explore the THz properties of intercalated multilayer graphene, which shows promise of behaving like decoupled stacks of individual graphene layers. If so, it could reach and exceed the effective bulk conductance of 30nm noble metal films and provide a lower loss alternative conductor in THz metamaterials at nm thickness. Finally, we will explore tunable, mutually biased, dielectric insulated multilayer graphene stacks for THz modulators with large modulation ratio.

Active metamaterials with loss compensation and lasing: We will study optimal resonator designs and coupling of gain and radiated field to enable practical loss-compensated MMs. We will develop novel types of lasers and light sources based on lasing into dark surface states that are weakly coupled to radiative emission by small, non-resonant, purpose-designed scatterers providing radiative dipole moments. These structures are analog to spasers but allow for more control, higher Q-factors, and lower lasing thresholds.

Development of computational tools: We will develop further our self-consistent FDTD calculations for non-linear and gain materials, enabling realistic simulations that include spontaneous emission and noise to model luminescence and the transition from luminescence to lasing and allow comparison with experimental data. The simulation tools will provide guidance to the experiment on how full loss compensation and lasing/spasing can be achieved.

References

[1] P. Tassin, Th. Koschny, and C. M. Soukoulis, "Graphene for terahertz applications," *Science* **341**, 620 (2013).

[2] N. Shen, P. Tassin, Th. Koschny and C. M. Soukoulis, "Comparison of gold- and graphene-based resonant nanostructures for THz metamaterials and an ultrathin graphene-based modulator," *Phys. Rev. B.* 90, 115437 (2014).

[3] L. Luo, I. Chatzakis, J. Wang, F. B. P. Niesler, M. Wegener, T. Koschny, and C. M. Soukoulis, "Broadband Terahertz Generation from Metamaterials," *Nature Commun.* **5**, 3055 (2014).

[4] A. Jain, P. Tassin, Th. Koschny and C. M. Soukoulis, "Large quality factor in sheet metamaterials made from dielectric meta-atoms," *Phys. Rev. Lett.* **112**, 117403 (2014).

Publications

1. I. Chatzakis, P. Tassin, L. Luo, N. H. Shen, L. Zhang, J. G. Wang, T. Koschny, and C. M. Soukoulis, "One- and Two-Dimensional Photo-Imprinted Diffraction Gratings for Manipulating Terahertz Waves," *Applied Physics Letters*, **103**, 043101 (2013).
2. Lei Zhang, Th. Koschny and C. M. Soukoulis, "Creating double negative index materials using the Babinet principle with one metasurface," *Phys. Rev. B* **87**, 045101 (2013).
3. Y. C. Fan, Z. Y. Wei, H. Q. Li, H. Chen, and C. M. Soukoulis, "Low-Loss and High-Q Planar Metamaterial with Toroidal Moment," *Physical Review B*, **87**, 115417 (2013).
4. V. Ginis, P. Tassin, C. M. Soukoulis, and I. Veretennicoff, "Enhancing Optical Gradient Forces with Metamaterials," *Physical Review Letters*, **110**, 057401 (2013).
5. N. H. Shen, T. Koschny, M. Kafesaki, and C. M. Soukoulis, "Robust Wedge Demonstration to Optical Negative Index Metamaterials," *Applied Physics Letters*, **102**, 241915 (2013).
6. P. Tassin, T. Koschny, and C. M. Soukoulis, "Graphene for Terahertz Applications," *Science*, **341**, 620-621 (2013).
7. B. Dastmalchi, P. Tassin, T. Koschny, and C. M. Soukoulis, "Strong Group-Velocity Dispersion Compensation with Phase-Engineered Sheet Metamaterials," *Physical Review B*, **89**, 115123 (2014).
8. L. Luo, I. Chatzakis, J. G. Wang, F. B. P. Niesler, M. Wegener, T. Koschny, and C. M. Soukoulis, "Broadband Terahertz Generation from Metamaterials," *Nature Communications*, **5**, 3055 (2014).
9. A. Jain, P. Tassin, T. Koschny, and C. M. Soukoulis, "Large Quality Factor in Sheet Metamaterials Made from Dark Dielectric Meta-Atoms," *Physical Review Letters*, **112**, 117403 (2014).
10. N. H. Shen, P. Tassin, T. Koschny, and C. M. Soukoulis, "Comparison of gold- and graphene-based resonant nanostructures for THz metamaterials and ultrathin graphene-based modulator," *Physical Review B*, **90**, 115437 (2014).
11. Z. Huang, S. Droulias, T. Koschny, and C. M. Soukoulis, "Mechanism of the Metallic Metamaterials coupled to the Gain Material," *Optics Express*, **22**, 28596-28605 (2014).
12. C. M. Soukoulis, T. Koschny, P. Tassin, N. H. Shen, and B. Dastmalchi, "What is a good conductor for metamaterials or plasmonics," *Nanophotonics*, (2014).
13. Y. Fan, N. Shen, Th. Koschny and C. M. Soukoulis, "Tunable terahertz meta-surface with graphene cut-wires," *ACS Photonics* **2**, 151 (2015).
14. A. A. Basharin, C. Mavidis, M. Kafesaki, E. N. Economou, and C. M. Soukoulis, "Epsilon near Zero Based Phenomena in Metamaterials," *Physical Review B*, **87**, 155130 (2013).
15. M. Massaouti, A. A. Basharin, M. Kafesaki, M. F. Acosta, R. I. Merino, V. M. Orera, E. N. Economou, C. M. Soukoulis, and S. Tzortzakis, "Eutectic Epsilon-near-Zero Metamaterial Terahertz Waveguides," *Optics Letters*, **38**, 1140-1142 (2013).
16. F. H. Shi, Y. H. Chen, P. Han, and C. M. Soukoulis, "Investigation of One-Dimensional Photonic Bandgap Structures Containing Lossy Double-Negative Metamaterials through the Bloch Impedance," *Journal of the Optical Society of America B-Optical Physics*, **30**, 1473-1478 (2013).
17. J. Zheng, Y. H. Chen, Z. F. Chen, X. G. Wang, P. Han, Z. H. Yong, Y. Wang, C. W. Leung, and C. M. Soukoulis, "Investigation of Interface States in Single-Negative

Metamaterial Layered Structures Based on the Phase Properties," *Optics Express*, **21**, 16742-16752 (2013).
18. Y. C. Fan, Z. Y. Wei, H. Q. Li, H. Chen, and C. M. Soukoulis, "Photonic Band Gap of a Graphene-Embedded Quarter-Wave Stack," *Physical Review B*, **88**, 241403 (2013).
19. J. Zhang, T. Li, J. Wang, and J. Schmalian, "Post-Transient Relaxation in Graphene after an Intense Laser Pulse," *European Physical Journal-Special Topics*, **222**, 1263-1270 (2013).
20. J. H. Zhang, J. Schmalian, T. Q. Li, and J. G. Wang, "Transient Charge and Energy Balance in Graphene Induced by Ultrafast Photoexcitation," *Journal of Physics-Condensed Matter*, **25**,
21. A. Patz, T. Q. Li, S. Ran, R. M. Fernandes, J. Schmalian, S. L. Bud'ko, P. C. Canfield, I. E. Perakis, and J. G. Wang, "Ultrafast Observation of Critical Nematic Fluctuations and Giant Magnetoelastic Coupling in Iron Pnictides," *Nature Communications*, **5**, 3229 (2014).
22. S. Droulias, C. Fietz, P. Zhang, T. Koschny, and C. M. Soukoulis, "Lasing Threshold Control in Two-Dimensional Photonic Crystals with Gain," *Optics Express*, **22**, 19302-19313 (2014).
23. M. Kafesaki, A. A. Basharin, E. N. Economou, and C. M. Soukoulis, "THz Metamaterials Made of Phonon-Polariton Materials," *Photonics and Nanostructures-Fundamentals and Applications*, **12**, 376-386 (2014).
24. G. Kenanakis, R. Zhao, N. Katsarakis, M. Kafesaki, C. M. Soukoulis, and E. N. Economou, "Optically Controllable THz Chiral Metamaterials," *Optics Express*, **22**, 12149-12159 (2014).
25. A. C. Tasolamprou, Lei Zhang, M. Kafesaki, T. Koschny, and C. M. Soukoulis, "Experimentally Excellent Beaming in a Two-layer Dielectric Structure," *Optics Express*, **22**, 23147-23152 (2014).

Project Title: Ground state magnetism and cooperative phenomena in correlated electron oxide materials

Principal Investigator: Prof. Hariharan Srikanth
University of South Florida, Department of Physics, ISA 2019
4202 East Fowler Ave, Tampa, FL 33620
E-mail: sharihar@usf.edu

Co-Principal Investigator: Dr. Manh-Huong Phan
University of South Florida, Department of Physics, ISA 2019
4202 East Fowler Ave, Tampa, FL 33620
E-mail: phanm@usf.edu

Project Participants (USF): Paula Lampen (Ph.D student), Vijaysankar Kalappattil (Ph.D student), Dr. Raja Das (Postdoctoral fellow).

Project Collaborators (Rutgers University): Dr. H.T. Yi and Prof. S.W. Cheong (Director, Rutgers Center for Emergent Materials)

Other Collaborators: Prof. David Mandrus (The University of Tennessee) and Prof. Chris Leighton (The University of Minnesota)

Program Scope:

Transition-metal oxides exhibit rich complexity in their fundamental physical properties determined by the intricate interplay between structural, electronic and magnetic degrees of freedom. The overall goal of our DOE funded project is to investigate the fundamental physics of magnetism in bulk and nanostructured oxides that exhibit spin frustration either due to structural configuration or unusual phenomena arising from geometry and electron correlation effects. We have demonstrated the importance of combining conventional DC and AC magnetic susceptibility measurements with relatively unconventional RF transverse susceptibility (TS) and magnetocaloric effect (MCE) methods to probe the ground state magnetic properties and glassy behavior in a wide variety of complex oxide systems, including single crystalline and nano-crystalline $Ca_3Co_2O_6$, single crystalline $La_{0.5}Sr_{0.5}MnO_3$ nanowires, and $SrFe_{12}O_{19}/La_{1-x}Ca_xMnO_3$ (SFO/LCMO) hard-soft phase composites. Other research efforts include the exploration of exotic magnetism in other strongly coupled systems, such as core/shell $Fe/\gamma\text{-}Fe_2O_3$ nanoparticles, hollow $\gamma\text{-}Fe_2O_3$ nanoparticles, $Au\text{-}Fe_3O_4$ nanoparticles and $La_{0.7}Pr_{0.25}Co_2P_2$ single crystals that share some similar and novel phenomena. These studies yield new insights into the ground state magnetism and spin-glass-like phenomena and demonstrate the important effects of reduced dimensionality in correlated electron materials.

We present here representative results in $Ca_3Co_2O_6$ having Ising-like spin chains arranged on a triangular lattice geometry and $EuTiO_3$ - a G-type antiferromagnet showing quantum paraelectricity and complex magnetism in single crystalline and nanocrystalline forms.

Recent Progress:

1. A new magnetic phase diagram for the quasi-one-dimensional (1D) spin chain compound $Ca_3Co_2O_6$

The magnetic behavior of the spin chain cobaltite $Ca_3Co_2O_6$ combines geometric frustration with intrinsic low-dimensionality, giving rise to complex physical phenomena that continue to attract a great deal of interest. $Ca_3Co_2O_6$ consists of face sharing CoO_6 trigonal prisms and CoO_6 octahedra alternating along the *c*-axis to form chains. Ferromagnetic coupling along the chains and weak antiferromagnetic coupling between nearest- and next-nearest-neighbor chains through a helical exchange pathway establish a long-wavelength spin-density wave (SDW) ground state along the *c*-axis [1]. Although the question of the true ground state of this complex frustrated spin chain system and its temperature- and time-variation has been highly scrutinized, less work has been undertaken on the field dependence of the magnetic order at intermediate temperatures. Several phase diagrams can be found in the literature based on bulk magnetization [2] and muon spin relaxation measurements [3]. However, these studies do not take into account the current understanding of the SDW ground state or the more recently described low temperature short-

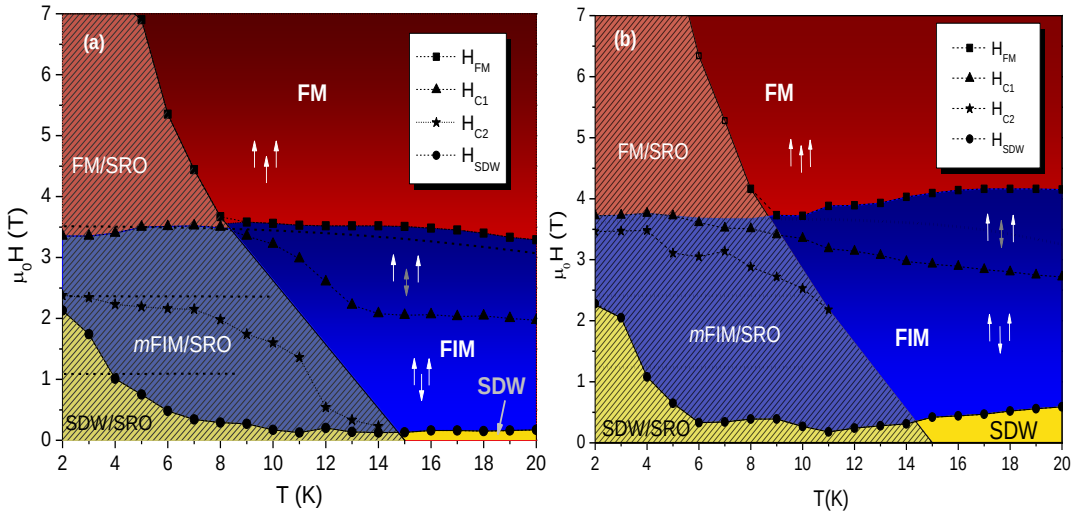

Figure 1: Magnetic phase diagrams including ferromagnetic (FM), ferrimagnetic (FIM), metastable FIM (*m*FIM), short-range-order (SRO), and spin-density wave (SDW) phases for (a) single crystal sample and (b) powder sample. Dashed lines represent locations of the magnetization steps taken from *M* (*H*) curves.

range order (SRO) phase [4].

We have applied the magnetic field and temperature dependence of magnetic entropy change as a probe of the magnetic states of $Ca_3Co_2O_6$ to establish a new and more comprehensive magnetic phase diagram for this exotic system. The $Ca_3Co_2O_6$ single crystals synthesized using a flux technique were provided by Prof. Cheong's group at Rutgers University, while the nanocrystaline samples were synthesized using the advanced sol-gel method in our laboratory at USF. Based on the temperature- and field-dependent magnetic entropy change in $Ca_3Co_2O_6$ we have contructed new phase diagrams for both single crystalline and polycrystalline samples (Figure 1a,b). Between H_{C1} and H_{FM}, the entropy of the system increases during the flipping process of the third spin chain in the up-up-down configuration. Short-range correlations with an antiferromagnetic character are present below 15 K and grow in volume fraction as the temperature is lowered, resulting in a crossover from ΔS_M (H) < 0 to ΔS_M (H) > 0 at 12 K. A line

bordering the region in which the SRO phase contributes significantly to the magnetic behavior is extrapolated between the point at which H_{FM} begins to increase and the emergence of H_{C2} – a local maximum in ΔS_M (H) due to field-induced disorder in chains aligned in opposition to the applied field. This ΔS_M – based analysis produces a phase diagram that reflects the current understanding of the role of SDW and SRO phases in $Ca_3Co_2O_6$, and extends results to temperatures below the onset of slow dynamics (~10 K). We resolve sub-features of the FIM phase for the first time including the field extent of conversion between the up-up-down and up-up-up configurations at high temperature and a critical field H_{C2} at which a maximum entropy occurs in the metastable FIM region. The interesting features of the phase diagram are robust with respect to sample morphology, as can be seen from a similar phase diagram obtained in sol-gel derived sub-micron powders. In this case we note a shift toward higher field in several features, including the SDW crossover, as the number of pinning sites increases with grain boundary density.

Overall, our study provides new physical insights into the complex nature of magnetic interactions and collective phenomena in geometrically frustrated quasi 1D magnets like $Ca_3Co_2O_6$. The main findings have been reported in Physical Review B (*Lampen et al., Phys. Rev. B* ***89****, 144414, 2014*). We are currently investigating the effects of reduced dimentionality (nanostructuring, grain boundaries) on the low-temperature spin dynamics and related magnetization relaxation processes in $Ca_3Co_2O_6$.

2. Ferromagnetic clustering in $EuTiO_3$:

A search for new multiferroic materials with large magnetoelectric effects continues to generate new physics underlying the interaction between spin, polar, and structural degrees of freedom. The electric field control of magnetic moments or the magnetic field control of electrical polarization through the magnetoelectric effect is of great importance due to prospective applications in magnetic memory storage, spintronic, and sensing devices [5]. $EuTiO_3$ is a quantum paraelectric with a G-type antiferromagnetic structure below T_N ~5.5 K. Recently, $EuTiO_3$ has received growing attention in the scientific community since it exhibits a strong magnetoelectric coupling around T_N, where the dielectric constant exhibits an unusual drop [6]. Ferroelectric and ferromagnetic orderings are realized in thin films of $EuTiO_3$ due to biaxial strain and spin-phonon cupling [7]. $EuTiO_3$ undergoes a structural transition from the high-temperature cubic to the low-temperature tetragonal structure due to an oxygen octrahedral rotation instability. However, the critical temperatures reported for this transition range from 160 K to 308 K [7,8]. The magnetic properties of $EuTiO_3$ have been studied in polycrystalline, single crystalline, and thin film samples, however the nature of the structural transition and the

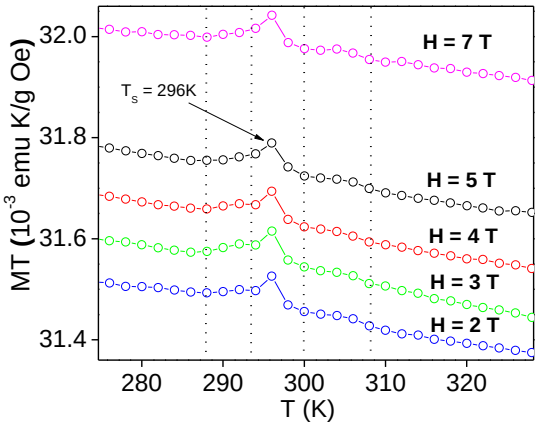

Figure 2: Temperature dependence of *MT* in the 275-325 K range for different applied fields. The peak at ~296 K is defined as a structural phase transition temperature (T_S), which clearly shows no variation with applied field. The dotted lines below and above the T_S may represent the extended range of short-range ordered ferromagnetic clusters.

formation and low temperature freezing of ferromagnetic clusters remain controversial. Discrepancies arise primarily from differences in sample quality and impurities.

To resolve this important issue, we have performed systematic DC and AC magnetization studies on high-quality single crystals of $EuTiO_3$, which were grown in Prof. Mandrus' laboratory at University of Tennessee-Knoxville. The structural transition of $EuTiO_3$ is clearly observed as a peak in the *MT* vs. *T* curves at ~296 K (Figure 2). In constrast to previously performed specific heat and thermal expansion experiments that suggested a field-dependent broad structural transition, we have observed for the first time a clear structural transtion directly from DC magnetization measurements in high-quality $EuTiO_3$, and demonstrated that this structural transition is magnetic field independent (Figure 2). Consistent with resonant ultrasound experiments, the second anomaly at ~136 K is observed as an intercept of the high- and low-temperature linear regimes in the *MT* vs. *T* curves, which is attributed to the formation of dynamically correlated ferromagnetic clusters due to increased spin-lattice coupling. Our AC susceptibility measurements show signatures of the freezing of ferromagnetic clusters at ~35 K, which has not previously been reported. Our analysis based on a critical power law yields a relaxation time of $\sim 10^{-6}$ s, demonstrating significant interaction among ferromagnetic clusters. Neutron diffraction experiments are currently underway to confirm these findings.

Future plans:

In addition to continuing our studies on the ground state magnetic properties of bulk and nanostructured complex oxides, including spin chain compounds of the form $Ca_3Co_{2-x}Mn_xO_6$ (x = 0.0, 0.1, 0.2, 0.4, 0.8, and 1.0) and bilayer manganites of the form $La_{2-2x}Sr_{1+2x}Mn_2O_7$ (x = 0.1, 0.3, 0.4, 0.5, and 0.6), we will also extend our efforts to address some of the outstanding issues in rare-earth cobalt arsenides (RCo_2As_2), rare-earth pyrochlores ($R_2Ru_2O_7$), and thin films of $VTiO_3$. Each of these systems is of considerable current interest with unresolved issues that we are well-suited to address through our unique combination of DC and AC magnetization, TS and MCE studies coupled with neutron scattering and other local structural probes. Spin-Seebeck effect (SSE) is an important property in the emergent field of "spin caloritronics" which lends itself to the study of the interplay between spin, charge, and heat. We are currently setting up experiments to perform longitudinal and transverse SSE measurements in ferromagnetic metals, semiconductors, and insulators. Our future plans include the synthesis of core-shell and hybrid nanoparticles in our lab and the characterization of their interface magnetism through collaborative work. Surface magnetism in complex oxide nanostructures is largely unexplored and not well understood. Our research efforts over the next year will be targeted towards elucidating these emergent aspects of correlated magnetic oxide physics.

References:

[1] S. Agrestini et al., Phys. Rev. Lett. **101**, 097207 (2008).
[2] A. Maignan et al., Eur. Phys. J. B **15**, 657 (2000)
[3] S. Takeshita et al., J. Phys. Chem. Solids **68**, 2174 (2007)
[4] S. Agrestini et al., Phys. Rev. Lett. **106**, 197204 (2011)
[5] W. Eerenstein et al., Nature **442**, 759 (2006).
[6] T. Katsufuji et al., Phys. Rev. B **64**, 054415 (2001).
[7] J. H. Lee et al., Nature **466**, 954 (2010).
[8] P. G. Reuvekamp et al., **90**, 104105 (2014).

Publications:

List of papers acknowledging DoE grant support during the 2-year period (2013-2014):

(Students and postdocs' names are italicized, PI and co-PI names are in bold)

1. "Macroscopic phase diagram and magnetocaloric study of metamagnetic transitions in the spin chain system $Ca_3Co_2O_6$" - *P. Lampen, N.S. Bingham*, **M.H. Phan**, H.T. Yi, S.W. Cheong, and **H. Srikanth, *Physical Review B* 89**, 144414 (2014)
2. "Heisenberg-like ferromagnetism in 3*d*-4*f* intermetallic $La_{0.7}Pr_{0.25}Co_2P_2$ with localized Co moments" - *P. Lampen*, **M.H. Phan**, P. Chai, M. Shatruk, and **H. Srikanth**, ***Physical Review B***, **90**, 174404 (2014)
3. "Tuning Exchange Bias in Fe/γ -Fe_2O_3 Core-Shell Nanoparticles: Impacts of Interface and Surface Spins" - *H. Khurshid*, P. Mukherjee, **M. H. Phan**, and **H. Srikanth**, ***Applied Physics Letters* 104**, 072407 (2014)
4. "Exchange Bias in Au-Fe_3O_4 Composite Nanoparticles'' - *S. Chandra*, *N.A. Frey*, **M.H. Phan**, S. Srinath, M.A. Garcia, Y. Lee, C. Wang, S. Sun, O. Iglesias, and **H. Srikanth, *Nanotechnology* 25**, 055702 (2014)
5. "Enhanced Magnetism in Highly Ordered Magnetite Nanoparticle-filled Nanohole Arrays" - B. Duong, *H. Khurshid*, P. Gangopadhyay, *J. Devkota*, *K. Stojak*, **H. Srikanth**, L. Tetard, R. Norwood, N. Peyghambarian, **M.H. Phan**, and J. Thomas, ***Small* 10**, 2840 (2014)
6. "Magnetocaloric effect and critical behavior in $Pr_{0.5}Sr_{0.5}MnO_3$: An analysis of the validity of the Maxwell relation and the nature of phase transitions" - R. Caballero-Flores, *N.S. Bingham*, **M.H. Phan**, M.A. Torija, C. Leighton, V. Franco, A. Conde, and **H. Srikanth, *Journal of Physics: Condensed Matter* 26**, 286001 (2014)
7. "Inverse magnetocaloric and exchange bias effects in single crystalline $La_{0:5}Sr_{0:5}MnO_3$ nanowires" – *S. Chandra*, *A. Biswas*, S. Datta, B. Ghosh, A. K. Raychaudhuri and **H. Srikanth**, ***Nanotechnology* 24**, 505712 (2013)
8. "Universality in the entropy change for the inverse magnetocaloric effect" - *A. Biswas*, *S. Chandra*, T. Samanta, B. Ghosh, **M.H. Phan**, A. K. Raychaudhuri, I. Das, and **H. Srikanth**, ***Physical Review B*** 87:134420 (2013)
9. "Magnetic entropy change in core/shell and hollow nanoparticles" – *S. Chandra*, *A. Biswas*, *H. Khurshid*, W. Li, G. C. Hadjipanayis and **H. Srikanth**, ***Journal of Physics: Condensed Matter* 25**, 426003 (2013)
10. "Synthesis, structure and magnetic properties of $SrFe_{12}O_{19}$/ $La_{1-x}Ca_xMnO_3$ hard/soft phase composites" - D.T.M. Hue, *P. Lampen*, T.V. Manh, V.D. Viet, H.D. Chinh, **H. Srikanth**, and **M.H. Phan, *Journal of Applied Physics*** 114, 123901 (2013)
11. "The scaling and universality of conventional and inverse magnetocaloric effects in Heusler alloys" – A. Biswas, P. Zhang, T-L Phan, T. D. Thanh, N. H. Dan, S. C. Yu, **H. Srikanth**, and **M.H. Phan**, ***Applied Physics Letters* 103**,162410 (2013)
12. "Influence of magnetic field on critical behavior near a first order transition in optimally doped manganites: The case of $La_{1-x}Ca_xMnO_3$ (x = 0.2, 0.3, and 0.4)" - P. Zhang, *P. Lampen*, T.L. Phan, and S.C. Yu, T. D. Thanh, N. H. Dan, V. D. Lam, **H. Srikanth**, and **M.H. Phan**, ***Journal of Magnetism and Magnetic Materials*** 348, 146 (2013)
13. "Impact of structural disorder on the magnetic ordering and magnetocaloric response of amorphous Gd-based microwires" - *A. Biswas*, Y.Y. Yu, *N.S. Bingham*, H. Wang, F. Qin, J.F.

Sun, S.C. Yu, V. Franco, **H. Srikanth**, and **M.H. Phan**, ***Journal of Applied Physics*** 115, 17A318 (2014)

14. "Enhanced magnetism and ferroelectricity in epitaxial $Pb(Zr_{0.52}Ti_{0.48})O_3/CoFe_2O_4/La_{0.7}Sr_{0.3}MnO_3$ multiferroic heterostructures grown using dual-laser ablation technique" - D. Mukherjee, M. Hordagoda, *P. Lampen*, **M.H. Phan**, **H. Srikanth**, S. Witanachchi, and P. Mukherjee, **Journal of Applied Physics** 115, 17D707 (2014)

15. "Impacts of first-order magnetic transition and phase coexistence on the universal behavior of inverse magnetocaloric effect," - *A. Biswas*, T. L. Phan, N. H. Dan, S. C. Yu, **M.H. Phan**, and **H. Srikanth**, ***Journal of Applied Physics*** 115, 17A907 (2014)

16. "Growth and Physical Property Study of Single Nanowire (Diameter ~45nm) of Half Doped Manganite" – S. Datta, *S. Chandra*, S. Samanta, K. Das, **H. Srikanth**, and Barnali Ghosh, ***Journal of Nanomaterials*** 2013 (http://dx.doi.org/10.1155/2013/162315)

Probing Coherent States of Light and Matter in Two-Dimensional Semiconductors

Nathaniel P. Stern
Department of Physics and Astronomy
Northwestern University

Program Scope

The ability to enhance light-matter interactions in engineered optical environments is well-established in micro- and nano-photonics, but this capability has not yet been seriously exploited for coherent phenomena in two-dimensional (2D) semiconductors despite their rich correlations between spin, momentum, and light.The objective of this program is to investigate cavity-enhanced optical coupling between photonic resonators and monolayer semiconductors such as transition metal dichalcogenides. When reduced to a single atomic layer, the band structure of these materials displays degenerate valleys in momentum space that can be separately addressed by polarized light [1,2]. The scope of this research is to explore a fundamentally new regime of interfacing photons with nano-materials using excitations of specific valley quantum number, potentially revealing new avenues for probing coherent phenomena in layered 2D systems. Drawing on progress in photonics, nanoscale materials, and quantum optics, our approach combines monolayer material synthesis with solid-state quantum optics and on-chip photonic device circuits to realize valley-sensitive quantum manipulation using light.

This project currently focuses on several primary directions. We study mechanisms of valley-specific light-matter coupling in monolayer semiconductors. Enabling this, we seek to advance strategies for integrating these materials into dielectric photonic resonators with exquisite control over the material's optical environment. Further, we investigate new methods of probing coherent phenomena in 2D materials using light-matter excitations. The ability to engineer light-matter interactions with layered nanomaterials will have long-term impact by advancing possibilities for controlling matter using light, such as through coherent control of valley states and exploiting symmetries of low-dimensional materials in integrated photonic and polaritonic devices.

Recent Progress

Observing exciton-polaritons in two-dimensional semiconductors: Treating the interaction between light and semiconductors using quantum mechanical language, photons and coupled electron-hole pair excitations (*excitons*) interact by exchanging a quantum of energy between the matter and optical fields. The strength of this interaction is denoted as g. When the energies of these excitations are nearly degenerate, the system is best described as a hybrid quantum particle that is both light and matter [3]. The interacting composite system, called an *exciton-polariton*, can be identified through an anti-crossing of its energy dispersion. The aim of this task is to

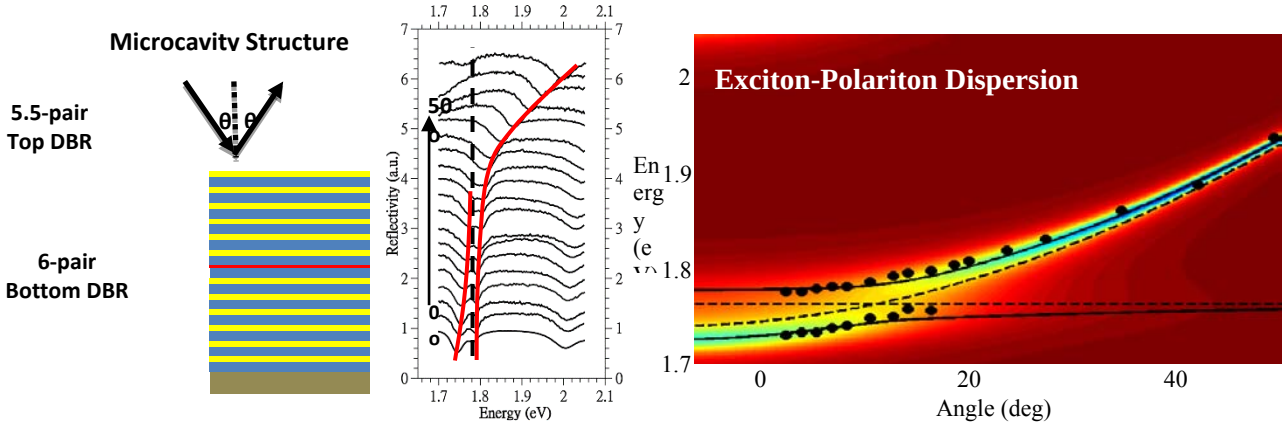

Figure 1:*Left* - MoS_2 is deposited by CVD in a dielectric DBR microcavity. *Middle* - Reflectivity measured as a function of angle maps the energy dispersion relation of exciton-polaritons. *Right* - The anti-crossing and Rabi splitting of 38 +/- 8 meV reveal hybrid light-matter states in monolayer semiconductors.

measure these exciton-polaritons in transition-metal dichalcogenides such as MoS_2. In addition to having strong interactions with light, these materials have the possibility to support new valley quantum numbers that can couple to light polarization.

Creating a strongly-coupled exciton-polariton system requires enhancing the interaction *g* above the loss rate of light and matter fields. This is achieved using an optical microcavity integrating layered 2D atomic sheetsinto dielectric multilayer stacks. We use plasma enhanced chemical vapor deposition (PECVD) to deposit distributed Bragg reflector (DBR) mirrors made of silicon nitride and silicon dioxide multilayers, standard facility recipes, with alternating indices of refraction. We then deposit a large-area monolayer MoS_2 sheet grown by CVD on the DBR and deposit the remaining mirror on top. Vapor deposition on the DBR proceeds similarly to SiO_2 substrates, but the growth quality is not as high (**Fig. 1**). Exciton resonance in photoluminescence is shifted on DBR cavities. The reason for this is unclear, but we hypothesize that it is related to surface quality and roughness from the PECVD process.

We have obtained measurements of the exciton-polaritonenergy dispersion using angle-resolved white light reflectivity for spectral and resonance sensitivity. Changing the incident angle modifies the resonance condition for the optical cavity, allowing tuning along the exciton-polariton dispersion curve (**Fig. 1**). The expected anti-crossing is observed and the Rabi splitting is extracted. We measure the coupling constant to be g = 25 +/ 4 meV. This value is of similar order of magnitude as predicted by our calculations. This measurement of exciton-polariton splitting in MoS_2 is consistent with other recent reports in the literature [4].We have investigated gel-transfer techniques to assemble microcavity structures using several approaches to best achieve measurable exciton-polariton coupling in 2D semiconductors. Our results highlight that achieving hybrid light-matter states in MoS_2 is straightforward given the large optical interactions. This ease is promising for achieving even more interesting hybrid optical states in microcavities with integrated monolayer nanomaterials such as topologically protectedexciton-polariton edge states.

Integration of monolayer semiconductors with photonics: The ability to manipulate valleys using light polarization in monolayer semiconductors suggests that near-field evanescent light in photonics can be used to enable new probes of fundamental valley physics. At the same time, these materials can bring new functionality to photonic devices because of their sensitivity to polarization afforded by the inversion asymmetry of their crystal lattices. The aim of this task is to advance strategies for integrating monolayer semiconductors with a planar photonics platform. Because evanescent fields can exhibit optical helicity [5], they may offer a novel method to control spin and valley polarization in integrated photonic circuits. We are investigating using a photonic ring resonator architecture as the basis for controlling photon interactions with valley polarized excitons in monolayer semiconductors.

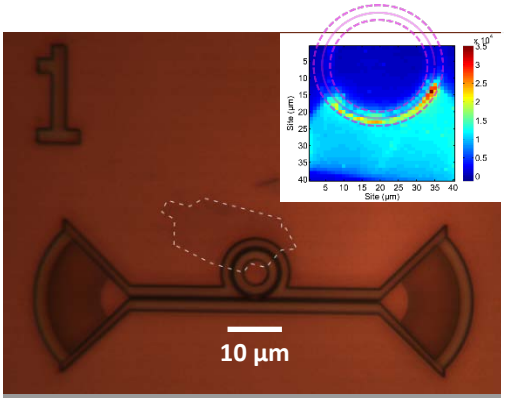

Figure 2: Visco-elastic layer transfer of MoS_2 onto a microring photonic ring resonator. Luminescence is persevered after transfer (inset). Coupling between device and material is confirmed by a reduction in quality factor (not shown).

Because of low loss in the visible spectrum and the ability for high quality factors, silicon nitride is used as the waveguide material. Simultaneous requirements of size and smoothness in fabrication necessitate using high-resolution electron beam lithography for fabrication of the ring resonators, which is performed in collaboration with Argonne National Laboratory. Dry transfer techniques can reliably place a large monolayer of MoS_2 on photonic ring resonators analogous to graphene transfer methods (**Fig. 2**) [6]. Optical quality of the monolayer after transfer is confirmed by scanning photoluminescence measurements, whereas coupling between the material and optical modes is validated by observing a reduction in the quality factor of the resonator.

High-mobility carriers at monolayer/multilayer interfaces: There is a vigorous effort in the literature to investigate electronic properties in heterostructures composed of layered 2D semiconductor nanomaterials. Our efforts to integrate monolayer semiconductors into opto-electronic devices have led us to discover enhanced transport along 1D interfaces in homojunctions of layered materials. Progress in our processing methods have enabled us to identify and to contact interfaces between monolayers and multilayers of MoS_2. Using these techniques, we identified attached monolayer/multilayer flakes of MoS_2 and separately patterned them into composite and control devices (**Fig. 3**). Photoexcitation measurementsreveal that this

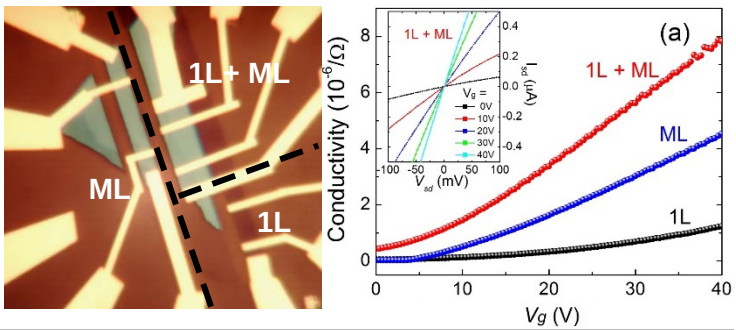

Figure 3: Homo-interfaces of monolayer and multilayer MoS_2 are fabricated (left). Interfaces show increased photoexcitation under illumination and higher conductivity (right).

interface has significant band-bending, which leads to enhanced photocurrents. Electrical characterization of this interface reveals increased conductivity and mobility of the interface electrons of up to ~1000 cm^2/Vs [7]. Measurement of high-mobility electrons is important for breaking the mobility limit in MoS_2, which can be significant for achieving interesting quantum and valley transport phenomena in opto-electronic experiments.

Future Plans

The early progress evident in recent results for this project are promising for future directions studying optical phenomena in layered nanomaterials. The general directions will be continued in future work. For exciton-polaritons in 2D materials, work will focus on observing valley-dependent cavity phenomena multilayer cavities and evanescently coupled photonic resonators. Strong exciton-polariton coupling will be extended to more diverse 2D nanomaterials to compare efficiency of light-matter coupling. Cavity enhancement of stark shifts will also be explored. We will try to develop coupling of helicity in evanescent fields to optical transitions in materials. Such coupling, observed in atomic systems, would be very useful for manipulating valley polarization in planar photonic devices. Initial measurements will focus on characterizing MoS_2 coupling to ring resonators to confirm that the material can be integrated with SiN photonics. We will continue optical experiments on homojunctions to investigate the origin of the enhanced mobility that we observed. Collaborative interactions with the DOE's Argonne National Laboratory will be increased for both faster sample fabrication and also additional measurement approaches to coupling light and 2D materials with high resolutions.

References

[1] D. Xiao, G.-B. Liu, W. Feng, X. Xu, and W. Yao. "Coupled spin and valley physicsin monolayers of MoS_2 and other group-VI dichalcogenides," *Phys. Rev. Lett*. **108**, 96802 (2012).

[2] K. F. Mak, K. He, J. Shan, and T. F. Heinz. "Control of valley polarization in monolayer MoS2 by optical helicity," *Nature Nano.***7**, 494 (2012).

[3] S. Pau, G. Björk, J. Jacobson, H. Cau, and Y. Yamamoto. "Microcavityexciton-polariton splitting in the linear regime," *Phys. Rev. B***51**, 14437 (1995).

[4] X. Liu, T. Galfsky, Z. Sun, F. Xia, E. Lin, Y. Lee, S. Kena-Cohen, and V. Menon. "Strong light–matter coupling in two-dimensional atomic crystals," *Nature Photonics* **9**, 30 (2015).

[5] E. J. Lenferink, G. Wei, and N. P. Stern. "Coherent optical non-reciprocity in axisymmetric resonators," *Opt. Express***22**, 16099 (2014).

[6] N. Gruhler, C. Benz, H. Jang, J.-H. Ahn, R. Danneau, and W. H. P. Pernice. "High-quality Si_3N_4 circuits as a platform for graphene-based nanophotonic devices," *Opt. Express* 21, 31678 (2013).

[7] Y. Jia, T. K. Stanev, E. J. Lenferink, and N. P. Stern. "High-Mobility Charge Accumulation at a Monolayer/Multilayer Homo-interface in MoS_2" *submitted*, *under review* (2015).

Publications

1. Ying Jia, Teodor K. Stanev, Erik J. Lenferink, and Nathaniel P. Stern. “High-Mobility Charge Accumulation at a Monolayer/Multilayer Homo-interface in MoS_2” *submitted*, *under review* (2015).

DOE Award # DE-SC0007043

Georgia State University Research Foundation

Quantum Nanoplasmonics Theory

Mark I. Stockman, PI, Vadym Apalkov, co-PI

Date of Report: March 8, 2015

Research period covered by the Report: May 15, 2013 – March 8, 2015.

Overall during this grant period, the grant provided a major support that resulted in publications of Refs. [1-6]. The following publications received a supplementary support from the grant for the period of this Report: Refs. [7-13]. Preliminary results have been published on spaser as a versatile diagnostic and theranostic tool in cancer diagnostics and treatment [14].

1 Program Scope

This is a program of fundamental theoretical studies. The main focus is on ultrafast and strong field quantum phenomena in nanostructured and nanofilm solids induced by ultrashort and intense laser pulses. The following three major subprojects comprise the main scope of this program:

1. *Novel Quantum Nanooptics and Nanoplasmonics: Phenomena in Condensed Matter in Strong Ultrafast Fields.* Advanced laser sources presently allow generation of femtosecond optical pulses with only one full optical oscillation, highly-stabilized phase, and the field strength exceeding that of crystal fields, on the order of several V/Å. We study theoretically novel phenomena caused by such fields. Among them, reversible (non-damaging) excitation of currents in dielectrics. We examine relation of these phenomena to fundamental properties of adiabaticity and time-reversal symmetry. We also incorporate novel two dimensional materials, such as graphene, in strong optical fields where unique effects fundamentally different from three-dimensional solids are envisioned. We also consider solids subjected to strong visible/near-IR fields and attosecond XUV pulses. We expect that the strong fields will create highly nonequilibrium electron distributions in momentum space of the crystals, which the XUV pulses will transfer to free space revealing ultrafast, subfemtosecond electron dynamics. Our goal is to establish fundamental limits for the fastest optoelectronic signal processing ("attosecond transistors"), which require wideband material systems with dielectrics replacing semiconductors of contemporary electronics.
2. *Ultrafast Quantum Nanoplasmonics with Hot Electrons.* We develop theory of novel phenomena based on relaxation of plasmons to hot electrons in the process of adiabatic nanofocusing in plasmonic tapers. In such a taper, surface plasmon polariton propagate toward the apex adiabatically following the local radius of the cone progressively slowing down and forming a plasmonic hot spot at the apex. Because such polaritons are dark waves and do not decay into free-space photons, the only primary channel of relaxation for them is dephasing into hot-electron pairs. Correspondingly, there also will be a hot spot of hot electrons at the apex. Our goal is to theoretically investigate this phenomenon as a source of nanometer-size subfemtosecond electron current pulses that can be injected into semiconductors or organic molecules via Schottky diode formed by the plasmonic taper. We propose to establish fundamental limits for the ultimate spatio-temporal concentration of the electron injection. Such injection is promising for use in ultrafast nanoscopy and nanospectroscopy.
3. *Novel Nanospasers in Quantum Regime.* Spaser was introduced by us as nanometer-scale generator and amplifier of nanolocalized optical fields. Spaser consists of a resonator, which is a metal plasmonic nanoparticle supporting the required modes and providing the feedback required for generation, and the gain medium, usually containing dye molecules or direct bandgap semiconductors. Here we propose to

theoretically investigate novel spasers. One of such proposed spasers has a graphene nanopatch as the resonator on a stack of quantum wells, which under electrical pumping provide gain. We will investigate feasibility of such a spaser and describe its kinetics and properties of local fields it generates. We will also introduce other new spasers including those where a graphene patch serves as a resonator and two-dimensional chalcogenides are sandwiched with it to provide gain under optical pumping. We propose to introduce yet another novel spaser, which physically is a nanocrystal of a topological insulator. In such a nanocrystal, the bulk is a narrow-band semiconductor, which will provide gain under optical pumping, while the surface is a two-dimensional metal with expected plasmonic behavior. We expect that such a nanocrystal under optical pumping will develop spasing generating coherent surface plasmons.

2 Brief Description of Accomplishments

In this Section, we highlight a few main, key achievements of this Grant period.

1.1. Hot-electron nanoscopy using adiabatic compression of surface plasmons [1]

Surface plasmon polaritons are a central concept in nanoplasmonics and have been exploited to develop ultrasensitive chemical detection platforms, as well as imaging and spectroscopic techniques at the nanoscale. Surface plasmons can decay to form highly energetic (or hot) electrons in a process that is usually thought to be parasitic for applications, because it limits the lifetime and propagation length of surface plasmons and therefore has an adverse influence on the functionality of nanoplasmonic devices. Recently, however, it has been shown that hot electrons produced by surface plasmon decay can be harnessed to produce useful work in photodetection, catalysis and solar energy conversion. Nevertheless, the surface-plasmon-to-hot-electron conversion efficiency has been below 1% in all cases. In this article we show that adiabatic focusing of surface plasmons on a Schottky diode-terminated tapered tip of nanoscale dimensions allows for a plasmon-to-hot-electron conversion efficiency of ~30%, which is an absolute record. We further demonstrate that, with such high efficiency, hot electrons can be used for a new nanoscopy technique based on an atomic force microscopy set-up. We show that this hot-electron nanoscopy preserves the chemical sensitivity of the scanned surface and has a spatial resolution below 50 nm, with margins for improvement.

1.2. Attosecond Metrology: From Electron Capture to Future Signal Processing [5]

The accurate measurement of time lies at the heart of experimental science, and is relevant to everyday life. Extending chronoscopy to ever shorter timescales has been the key to gaining real-time insights into microscopic phenomena, ranging from vital biological processes to the dynamics underlying high technologies. The generation of isolated attosecond pulses in 2001 allowed the fastest of all motions outside the nucleus — electron dynamics in atomic systems — to be captured. Attosecond metrology has provided access to several hitherto immeasurably fast electron phenomena in atoms, molecules and solids. The fundamental importance of electron processes for the physical and life sciences, technology and medicine has rendered the young field of attosecond science one of the most dynamically expanding research fields of the new millennium. In this work, we consider the fundamental concepts underlying attosecond measurement and control techniques. Among their many potential applications, we focus on the exploration of the fundamental speed limit of electronic signal processing. This endeavor relies on ultimate-speed electron metrology, as provided by attosecond technology.

1.3. All-Color Spasers with Ultralow Thresholds [11]

In this work, we report on the first demonstration of broadband tunable, single-mode plasmonic nanolasers (spasers) emitting in the full visible spectrum. These spasers are based on a single metal/oxide/semiconductor nanostructure platform comprising of InGaN/GaN semiconductor nanorods supported on an Al_2O_3 (sapphire)-capped epitaxial Ag film. In particular, all-color lasing in sub-

diffraction plasmonic resonators is achieved via a novel mechanism based on a property of weak size dependence inherent in spasers. This has been explained theoretically. Moreover, we have successfully reduced the continuous-wave (CW) lasing thresholds to ultrasmall values for all three primary colors and have clearly demonstrated the possibility of "thresholdless" spasing for the blue plasmonic nanolaser.

2. Future Plans

We intend to capitalize on the progress achieved and further develop the field of quantum nanoplasmonics theory. One of the promising directions in the future research will be quantum theory of graphene in strong ultrafast laser fields. We also intend to broaden this direction by considering also other quasi-two-dimensional materials such as silicene and germanine. We will also be developing quantum theory of other two-dimensional materials in strong fields including those with semiconductor behavior. We also plan to consider topological insulators in strong fields. We will continue developing quantum theory of spaser. In particular, we will develop theory of spaser as a source of optical energy, ultrabright label, and efficient absorber. Preliminary results related to these spaser application have just been published as a preprint [14].

3. List of People Working on this Project

1. Mark I. Stockman, PhD, DSc, Professor of Physics; PI of the Project. The percentage of support (for this research) received from this grant: 50%
2. Vadym Apalkov, PhD, Associate Professor of Physics; co-PI of this project. The percentage of support (for this research) received from this grant: 40%
3. Hamed Koochaki (graduate student). The percentage of support (for this research) received from this grant: 30%

Note: There have been a significant number of international collaborators who greatly contributed to the project but have not obtained a support from the grant.

4. Estimate of the unexpended funds at the end of the budget period

There will be no unexpended funds at the end of the current grant period

5. References

1. A. Giugni, B. Torre, A. Toma, M. Francardi, M. Malerba, A. Alabastri, R. Proietti Zaccaria, M. I. Stockman, and E. Di Fabrizio, *Hot-Electron Nanoscopy Using Adiabatic Compression of Surface Plasmons*, Nat. Nano **8**, 845-852 (2013).
2. M. I. Stockman, *Spaser, Plasmonic Amplification, and Loss Compensation*, in *Active Plasmonics and Tuneable Plasmonic Metamaterials*, edited by A. V. Zayats and S. Maier (John Wiley and Sons, Hoboken, NJ, 2013).
3. M. I. Stockman, *Lasing Spaser in Two-Dimensional Plasmonic Crystals*, NPG Asia Mater **5**, e71-e71 (2013).
4. M. I. Stockman, *Nanoplasmonics: From Present into Future*, in *Plasmonics: Theory and Applications*, edited by T. V. Shahbazyan and M. I. Stockman (Springer, Dordrecht, Heidelberg, New York, London, 2013), Vol. 15, p. 1-101.
5. F. Krausz and M. I. Stockman, *Attosecond Metrology: From Electron Capture to Future Signal Processing*, Nat. Phot. **8**, 205-213 (2014).
6. M. I. Stockman, *Nanoplasmonics: Fundamentals and Applications*, in *Nano-Structures for Optics and Photonics* (Springer Netherlands, 2015), p. 3-102.

7. V. Apalkov and M. I. Stockman, *Proposed Graphene Nanospaser*, Light Sci. Appl. **3**, e191-1-6 (2014).
8. H. K. Kelardeh, V. Apalkov, and M. I. Stockman, *Wannier-Stark States of Graphene in Strong Electric Field*, Phys. Rev. B **90**, 085313-1-11 (2014).
9. S. Ghimire, G. Ndabashimiye, A. D. DiChiara, E. Sistrunk, M. I. Stockman, P. Agostini, L. F. DiMauro, and D. A. Reis, *Strong-Field and Attosecond Physics in Solids*, Journal of Physics B: Atomic, Molecular and Optical Physics **47**, 204030-1-10 (2014).
10. T. Higuchi, M. I. Stockman, and P. Hommelhoff, *Strong-Field Perspective on High-Harmonic Radiation from Bulk Solids*, Phys. Rev. Lett. **113**, 213901-1-5 (2014).
11. Y.-J. Lu, C.-Y. Wang, J. Kim, H.-Y. Chen, M.-Y. Lu, Y.-C. Chen, W.-H. Chang, L.-J. Chen, M. I. Stockman, C.-K. Shih, and S. Gwo, *All-Color Plasmonic Nanolasers with Ultralow Thresholds: Autotuning Mechanism for Single-Mode Lasing*, Nano Lett. **14**, 4381–4388 (2014).
12. H. K. Kelardeh, V. Apalkov, and M. I. Stockman, *Graphene in Ultrafast and Superstrong Laser Fields*, Phys. Rev. B **91**, 045439-1-8 (2015).
13. T. Paasch-Colberg, A. Schiffrin, N. Karpowicz, S. Kruchinin, Saglam Ozge, S. Keiber, O. Razskazovskaya, S. Muhlbrandt, A. Alnaser, M. Kubel, V. Apalkov, D. Gerster, J. Reichert, T. Wittmann, J. V. Barth, M. I. Stockman, R. Ernstorfer, V. S. Yakovlev, R. Kienberger, and F. Krausz, *Solid-State Light-Phase Detector*, Nat. Phot. **8**, 214–218 (2014).
14. E. I. Galanzha, R. Weingold, D. A. Nedosekin, M. Sarimollaoglu, A. S. Kuchyanov, R. G. Parkhomenko, A. I. Plekhanov, M. I. Stockman, and V. P. Zharov, *Spaser as Novel Versatile Biomedical Tool*, arXiv:1501.00342, 1-33 (2015).

Understanding Structure-Property Relationships in Ferroelectric Oxides

Trevor A. Tyson, Department of Physics
New Jersey Institute of Technology, Newark NJ 07102-1982
Email: tyson@njit.edu

DOE Award DE-FG02-07ER46402, New Jersey Institute of Technology

Abstract and Program Scope

Ferroelectric oxides exhibit intriguing properties and may also support magnetic states leading to so called multiferrroic properties. Ferroelectric as a separate class are making possible non-volatile storage system with high information storage capacities requiring low power. The coupled systems which exhibit both magnetic and ferroelectric behavior materials show promise to lead to devices in which ferromagnetic memory can be written with magnetic fields or magnetic bits can be written by an electric field. The work conducted in our research focuses on single phase materials. We are exploring the complex low temperature behavior of the hexagonal layered $RMnO_3$ (R= rare earth, Y and Sc) system following the detailed structural changes which occurred on crossing into the magnetic states. This analysis is also being extended to the small-ion E-phase systems. Moving towards materials with possible device applications, we are examining nano-scale materials as a path toward high density storage. Detailed studies of atomic level mechanisms behind the coupling of ferroelectricity and magnetism in system systems with strong coupling of polarization and magnetization will be conducted. In depth measurement of the structural properties and dynamics will be conducted over a range of length scales from atomic to mesoscopic scale using x-ray absorption spectroscopy, x-ray diffuse scattering, x-ray and neutron pair distribution analysis and high resolution x-ray diffraction. These measurements are being done for varying temperatures, magnetic fields and external pressures. The multiple length scale synchrotron and neutron sources based measurements may assist in developing more detailed models of these materials and possibly lead to device applications. **Work published over the last two years under this grant is given in the last section.**

ResearchResults

A. Polar State in $SrTiO_3$ Nanoparticles

Monodispersed strontium titanatenanoparticles were prepared and studied in detail. It is found that ~10 nm as-prepared stoichiometric nanoparticles are in a polar structural state (with possibly ferroelectric properties) over a broad temperature range [3]. Our recent high pressure diffraction measurements also reveal that the new structural state in nanoscale is stable for pressure up to ~13 GPa. A tetragonal structure, with possible reduction of the electronic hybridization is found as the particle size is reduced. In the 10 nm particles, no change in the local Ti-off centering is seen between 20 and 300 K. The results indicate that nanoscale motifs of $SrTiO_3$ may be utilized in data storage as assembled nano-particle arrays in applications where chemical stability, temperature stability and low toxicity are critical issues.

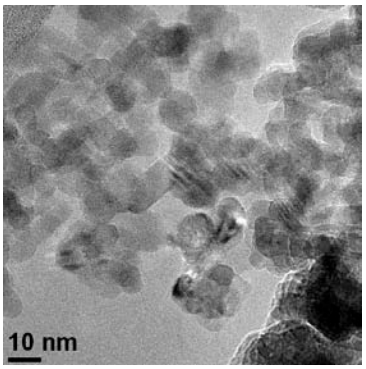

Fig. 1.TEM images of the ~10 nm sampleof $SrTiO_3$show a small variation in particle size for each particle yielding a narrow size distribution (10.1 ± 1.1 nm). Similar morphology was found for the 82 nm and 112 nm particles studied.

In Fig. 1, we show TEM images of the nanoparticle powders (i.e. measuring 10.1 ± 1.1 nm, 82.6 ± 9.1 nm, and 112.5 ± 14 nm, respectively) noting that the scale for the ~10 nm sample is different from that of the other samples. Detailed studies indicate that the particles are single phase, as revealed by both x-ray diffraction and electron diffraction measurements. The morphology of the particles is cube-like with a tight variation in particle size of approximately 10%.Mn K-edge spectroscopic measurementsreveal an asymmetric Ti-O distribution in the 10 nm system and Raman scattering reveals polar mode (Fig. 2). In addition, high resolution x-ray diffraction measurements were conducted to probe for tetragonal distortions. Total scattering (Bragg+Diffuse) hard x-ray pair distribution function measurements were conducted to examine the Sr:Ti ratioindependently. Theresults indicate that nanoparticles are stoichiometric (variation inTi valance less than 0.05 units), withreduction in hybridization of the O p and Ti d bands and O p with Sr d bands as particle size is reduced and reveal that the 10 nn sample exhibits a non-negligible tetragonal splitting with a= 3.9142(3) Å and c = 3.9118(6) Å.No change in the local Ti-off centering is seen between 20 and 300 K.The mechanism driving these changes with particle size is not yet understood, but the results may encourage more detailed experimental work and as well as theoretical investigations.

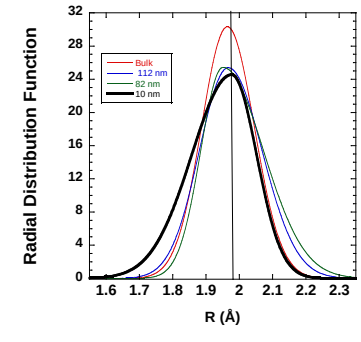

(a)

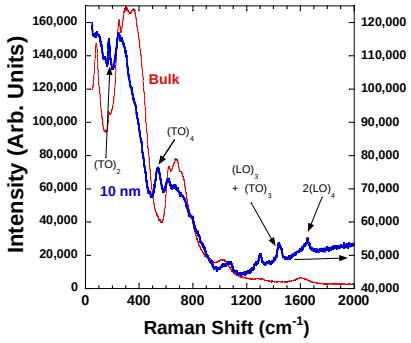

(b)

Fig. 2.(a) XAFS derived radial distribution function ($SrTiO_3$) for the first shell Ti-O peak extracted from the fitting for all four samples. We note the high degree of asymmetry in the 10 nm sample consistent with a polar structure. (b) Raman spectra for Bulk $SrTiO_3$ and the 10 nm sample. We observed polar modes $(TO)_2$, $(LO)_3$, and $(TO)_4$ in the 10 nm sample. The peaks above ~800 cm^{-1} are due to two-phonon excitations.

B. Nature of the Structure of E-Phase Perovskite Multiferroics

Although coupling of magnetization and polarization is known to exist in o-$R$$MnO_3$ (perovskites) probing the properties on multiple length scales will provide a clearer picture of the nature of the electric polarization by specifying its true origin (electronic and/or atomic) and possibly provide paths to enable enhancement and increased coupling with magnetic fields. Few experimental studies have explored the changes in structure near the magnetic transition temperature in detail. No systematic structural study, on multiple length scales, of the E-phase perovskites has been conducted covering local, short range, andlong rangestructure. In addition, no systematic and direct comparison of DFT calculations with predicted structural changes in simple E phase systems with only Mn magnetic sties has been done. In the current work [5], perovskite $ScMnO_3$ was prepared and detailed temperature-dependent x-ray absorption measurements (XAFS), pair distribution function (PDF) measurements and single crystal diffractions measurements were done extending down to temperatures near 10 K. DFT modeling was conducted for comparison and predicted large displacement of the Mn ions (twice the predicted value for the $LuMnO_3$ system). The DFT models predict that this system ($ScMnO_3$) also possesses E-phase magnetic order, as expected. However, the measurements reveal no significant local or long range distortions and contradict the predicted results of

DFT models, revealing that DFT does not properly account for the spin- lattice coupling in these oxides and possibly predicts the incorrect magnetic order at low temperatures. Similar structural measurements and modeling were conducted on perovskite $LuMnO_3$, yielding the same conclusions.

Specifically, structural measurements on multiple length scales were conducted on a new perovskite (see Ref .[5]), $ScMnO_3$, and onorthorhombic $LuMnO_3$ as a benchmark. Complementary density functional theory (DFT) calculations were carried out, and predict that $ScMnO_3$possesses E-phase magnetic orderat low temperature with displacements of the Mn sites (relative to the high temperature state) of ~0.07 Å, compared to ~0.04 Å predicted for $LuMnO_3$. However, detailed local, intermediate and long-range structural measurements by x-ray pair distribution function analysis, single crystal x-ray diffraction and x-ray absorption spectroscopy, find no local or long-range distortions on crossing into the low temperature E-phase of the magnetically ordered state. The measurements on E-magnetic phase perovskite systems place upper limits on any structural changes to be at most one order of magnitude lower than density functional theory predictions and suggest that this theoretical approach does not properly account for the spin-lattice coupling in these oxides and may possibly predict the incorrect magnetic order at low temperatures. The results suggest that the electronic contribution to the electrical polarization dominates and should be more accurately treated in theoretical models.

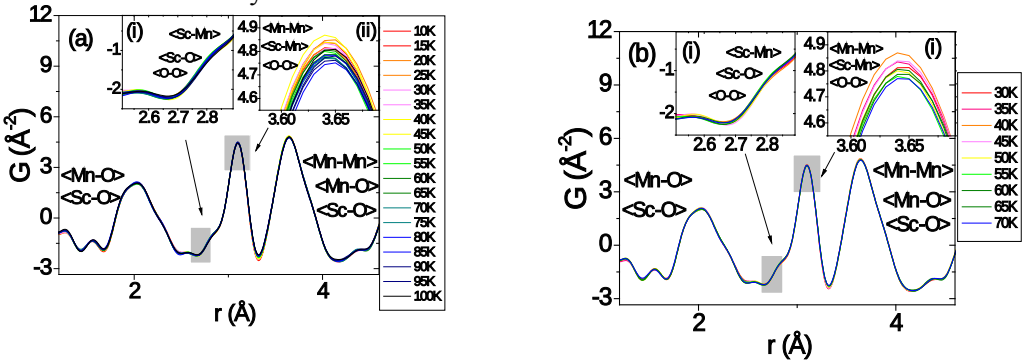

Fig. 3. (a) Radial distribution function derived from temperature dependent x-ray scattering measurements (PDF, Ref [5])) reveal no significant change in the local structure with temperature (10 to 100 K) and (b) specifically on crossing into the magnetically ordered phase near 50 K. Combined with XAFS and single crystal measurements over the same temperature range, the results predict that the DFT derived prediction of ionic displacement are too large by at least an order of magnitude.

C. Pressure Dependent Structural Changes and Electrical Polarization in Perovskite $RMnO_3$

High pressure x-ray diffraction (XRD) measurements on $RMnO_3$ (*R*=Dy, Ho and Lu) reveals that varying structural changes occurs for different *R* ions. Large lattice changes (orthorhombic strain) occur in $DyMnO_3$ and $HoMnO_3$while theJahn-Teller (JT) distortion remains stable. On the other hand, in the small R-ion system $LuMnO_3$Mn-O bond distortions are observed in the region 4-8 GPa with the broad minimum in the JT distortion. High pressure IR measurements indicate that a phonon near 390 cm^{-1} corresponding to the complex motion of the Mn and O ions changes anomalously for $LuMnO_3$. It softens in the 4-8 GPa region, which is consistent with the structural change in Mn-O bonds and then hardens at high pressures. By contrast, the phonons continuously harden with increasing pressure for $DyMnO_3$ and $HoMnO_3$. DFT calculations show that the *E*-phase $LuMnO_3$ is the most stable phase up to the 10 GPa pressure examined. Simulations indicate that the distinct structural change under pressure in $LuMnO_3$ can possibly be used to optimize the electric polarization by pressure/strain. See Ref. [1] for details.DFTsimulations predict that isotropic pressures enhance the polarization in both $HoMnO_3$and $LuMnO_3$.

D. Probing the Microscopic Level Origin of Magnetic Field Coupled Polarization in $RAl_3(BO_3)_4$

Detailed exploration of the properties of $HoAl_3(BO_3)_4$ including temperature and magnetic field dependent heat capacity measurements, pressure and temperature dependent x-ray diffraction measurements, x-ray pair distribution measurements and temperature and magnetic field dependent x-ray absorption fine structure measurements were combined with density functional calculations to develop a detailed understanding of the microscopic level mechanism behind the large electric polarization induced by magnetic fields. A low temperature local distortion or continuous lowering of symmetry is found to occur below ~50 K, concomitant with the onset of magnetic order. At low temperatures, no significant change in the HoO_6polyhedra is seen to occur with magnetic fields, however, magnetic fields are found to enhance correlations between near neighbor HoO_6polyhedra via the BO_3 planes. The stiff lattice (Bulk modulus found to be ~ 200 GPa by high pressure XRD measurements) enables these strong spin lattice coupling.

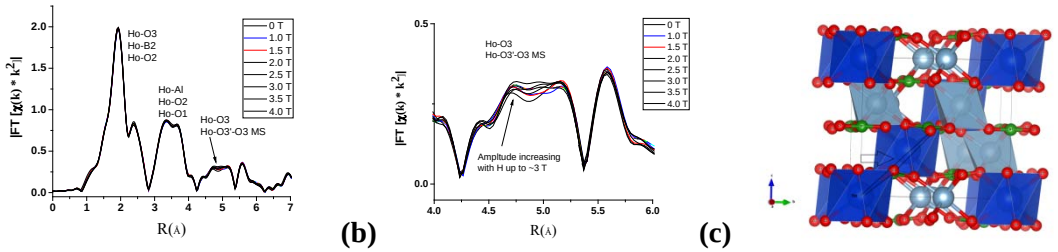

Fig. 4.XAFS structure function (Fourier transform of fine structure times k^2) taken at 5 K for magnetic fields varying from 0 T to 4 T in (a). Note that significant changes occur in the region near ~5 Å with the largest change corresponding to the field increasing from 0 T to 3 T. Measurements for magnetic fields between 4 and 8 T show no significant changes. ExpandedXAFS structure function for the 0 T to 4 T data are shown in (b). In panel (c) the single scattering path Ho-O3 and multiple scattering path Ho-O3'-O3associated with the peak are shown. This strong variation at low field 0 to ~3T is related enhanced coupling of neighboring HoO_6polyhedra via the BO_3 planes.

Future Plans for this Project

For the nanoscale $SrTiO_3$ system, we plan to systematically study the particle size variation of the polar state via electrical measurements and detailed structural measurements and complement these results with theoretical models tounderstand the physicsorigin ofthis phenomena. For the E-phase and other perovskite $RMnO_3$ systems, we will explore the pressure dependent of the local and long range structure in order to ascertain how to enhance electric polarization with strain or external pressure. DFT simulations of the magnetic ordering as a function pressure willalso be conducted. We plan to complete our exploration of the dependence of magnetic ordering temperature on the structure of the hexagonal $RMnO_3$ system by examining the temperature dependent structure of the small ion systems such as hexagonal $InMnO_3$ (T_N ~120 K) and $ScMnO_3$ (T_N ~130 K, compared with $YMnO_3$ with T_N ~70 K) and their alloys in order to find ways to increase T_N and the coupling between the magnetization and electric polarization. The nature of the high temperature onset of ferroelectricity will be examined structurally. To understand the origin of the strong coupling of magnetization and polarization in $HoAl_3(BO_3)_4$, we will conduct high pressure structural studies to probe the magnetic orders and net polarization to determine how they are modified with changes in bond distances.To understand the longer range structure in this materials, total x-ray and Neutron scattering (diffuse + Bragg Scattering) on powder samples will be conducted between 4 K and 300 K to complement the XAFS studies already carried out. Modeling of the data will be used to determine the correct unit cells, space groups and local distortions as a function of temperature from the low temperature magnetic ordered phases. DFT based simulations of phonon DOS will be compared with neutron scattering measurements to look for low energy phonons.

PublicationsUnder this Grant (Last Two Years)

[1] T. Wu, T. A. Tyson, H. Chen, P. Gao, T. Yu, Z. Chen, Z. Liu, K. H. Ahn, X. Wang and S.-W. Cheong, "*Pressure Dependent Structural Changes and Predicted Electrical Polarization in Perovskite RMnO3*", submitted to Phys. Rev. B. (seearXiv link arxiv.org/pdf/1403.7998).

[2] M.-R. Li, M. Retuerto, Z. Deng, T. Sarkar, J. Sanchez-Benitez, M. C. Croft, T. S. Dasgupta, T. Das, T. A. Tyson, D. Walker, and M. Greenblatt, *"Strong Electron Hybridization and Fermi-to-Non-Fermi Liquid Transition in $LaCu_3Ir_4O_{12}$"*, Chem. Mater. **27**, 211 (2015).

[3] T. A. Tyson, T. Yu, M. Croft, M. E. Scofield. D. Bobb-Semple, J. Tao, C. Jaye, D. Fischer and S. S. Wong, "*Polar State in Freestanding Strontium Titanate Nanoparticles"*, Appl. Phys. Lett. **105**, 091901 (2014).

[4] T. Yu, T. A. Tyson, P. Gao, T. Wu, X. Hong, S. Ghose, and Y.-S. Chen, *"Structural changes related to the magnetic transitions in hexagonal InMnO3"*, Phys. Rev. B. **90**, 174106 (2014).

[5] T. Yu, T. A. Tyson, H. Y. Chen, A. M. M. Abeykoon, Y.-S. Chen and K. H. Ahn ,*"Absence of significant structural changes near the magnetic ordering temperature in small-ion rare earth perovskite RMnO3"*, J. Phys.: Condens. Matter **26,** 495402 (2014).

[6] H. Chen, T. Yu, P. Gao, J. Bai, J. Tao, T. A. Tyson, L. Wang, and R. Lalancette, *"Synthesis and Structure in Perovskite-Type ScMnO3",* Inorganic Chemistry **52**, 9692 (2013).

[7] T. Wu, T. A. Tyson, J. Bai, K. Pandya, C. Jaye and D. Fischer, *"On the Origin of Enhanced Thermoelectricity in Fe doped $Ca_3Co_4O_9$ ", J. Mat. Chem C. **1**, 4114 (2013).*

[8] T. Yu, P. Gao, T. Wu, T. A. Tyson, and R. Lalancette, *"Ferroelectricity in Single Crystal InMnO3",* Appl. Phys. Lett.***102**, 172901 (2013).*

[9] T. Wu, T. A. Tyson, H. Chen, J. Bai, H. Wang, and C. Jaye, *"A structural change in $Ca_3Co_4O_9$ associated with enhanced thermoelectric properties", J. Phys. Cond. Mat. **24**, 455602 (2012).*

[10] X. Luo, Y. S. Oh, A. Sirenko, P. Gao, T. A. Tyson, K. Char, and S. W. Cheong, *"High Carrier Mobility in Transparent Ba1-xLaxSnO Crystals with Wide Band Gap*", Appl. Phys. Lett. **100**, 172112 (2012).

[11] T. A. Tyson, T. Yu, S. J. Han, M. Croft, G. D. Gu, I. K. Dimitrov and Q. Li, "*Local structure of the superconductor K0.8Fe1.6+xSe2: evidence of large structural disorder*", Phys. Rev. B **85**, 024504 (2012).

Mesoscale Interfacial Dynamics in MagnetoelectricNanocomposites

Dwight Viehland, Materials Science and Engineering, Virginia Tech

Shashank Priya, Mechanical Engineering, Virginia Tech

Program Scope

This research program at Virginia Tech focuses on investigating the mesoscale physics and chemistry of two-phase (magnetostrictive and piezoelectric) magnetoelectric (*ME) epitaxial oxide layers.* The specific objectives are to: (1) Develop self-assembling magnetostrictive/piezoelectric nanocomposites having near-periodic nanostructures with giant magnetoelectricity. (2) Develop complex and patterned 3-D ME structures where one might be able to demonstrate the effect of orientation and size effects on ME coupling leading to controlled E-field tuning of the magnetization. (3) Extend the two-phase self-assembly approach to other multifunctional systems, with the goal of developing new and unique combinatorial properties. (4) Develop miniaturized integrated ME layers with self-biasing features.

Recent Progress

In the last several years, two phase nano-composites of magnetostrictive and piezoelectric materials were synthesized as epitaxial thin layers. In thin layers, we wanted to engineer *nano-structures by self-assembly of multi-phases* via minimizing the strain energy caused by lattice misfits between phases, and correspondingly that between phases and substrate in the case of layers. All of these variables affect the *micro-elasticity* by changing the phase distribution, orientation relationships, interface bonding, and defect chemistry.

In the course of these investigations, we have made the following contributions:

(i) Engineered magnetic shape anisotropy in $BiFeO_3$-$CoFe_2O_4$ self-assembled thin films [1]. Various phase architectures of self-assembled $BiFeO_3$-$CoFe_2O_4$ (BFO-CFO) thin films have been deposited on differently oriented $SrTiO_3$ (STO) and $Pb(Mg_{1/3}Nb_{2/3})O_3$-xat%$PbTiO_3$ (PMN-x%PT) substrates. CFO forms segregated rectangular, strip and triangular nanopillars embedded in a coherent BFO matrix on (001), (110) and (111) oriented substrates, respectively (see Fig.1a). These studies established a detailed relationship of magnetic anisotropy with specific shape and dimensions of ordered magnetic arrays. The results suggest a way to effectively control the magnetic anisotropy in patterned ferromagnetic oxide arrays with tunable shape, aspect ratio and elastic strain conditions of the nanostructures.

(ii) Achieved volatile and nonvolatile magnetic easy-axis rotation in epitaxial ferromagnetic thin films on ferroelectric single crystal substrates (see Fig.1b) [2,3]. We have explored the relationship between phase transformation and magnetoelectric effect by depositing epitaxial Mn-doped $CoFe_2O_4$ (MCFO) films on <011> oriented $Pb(Mg,Nb)O_3$-$PbTiO_3$ (PMN-PT). A giant in-plane (IP) uniaxial strain in MCFO film was induced by electric field due to dramatic lattice parameter change trigged by a rhombohedral to orthorhombic phase transition, rotating the magnetic easy axis from IP <0-11> to IP <100>. The phase transformation can be either reversible or irreversible, resulting in volatile and/or nonvolatile magnetic easy axis rotations respectively.

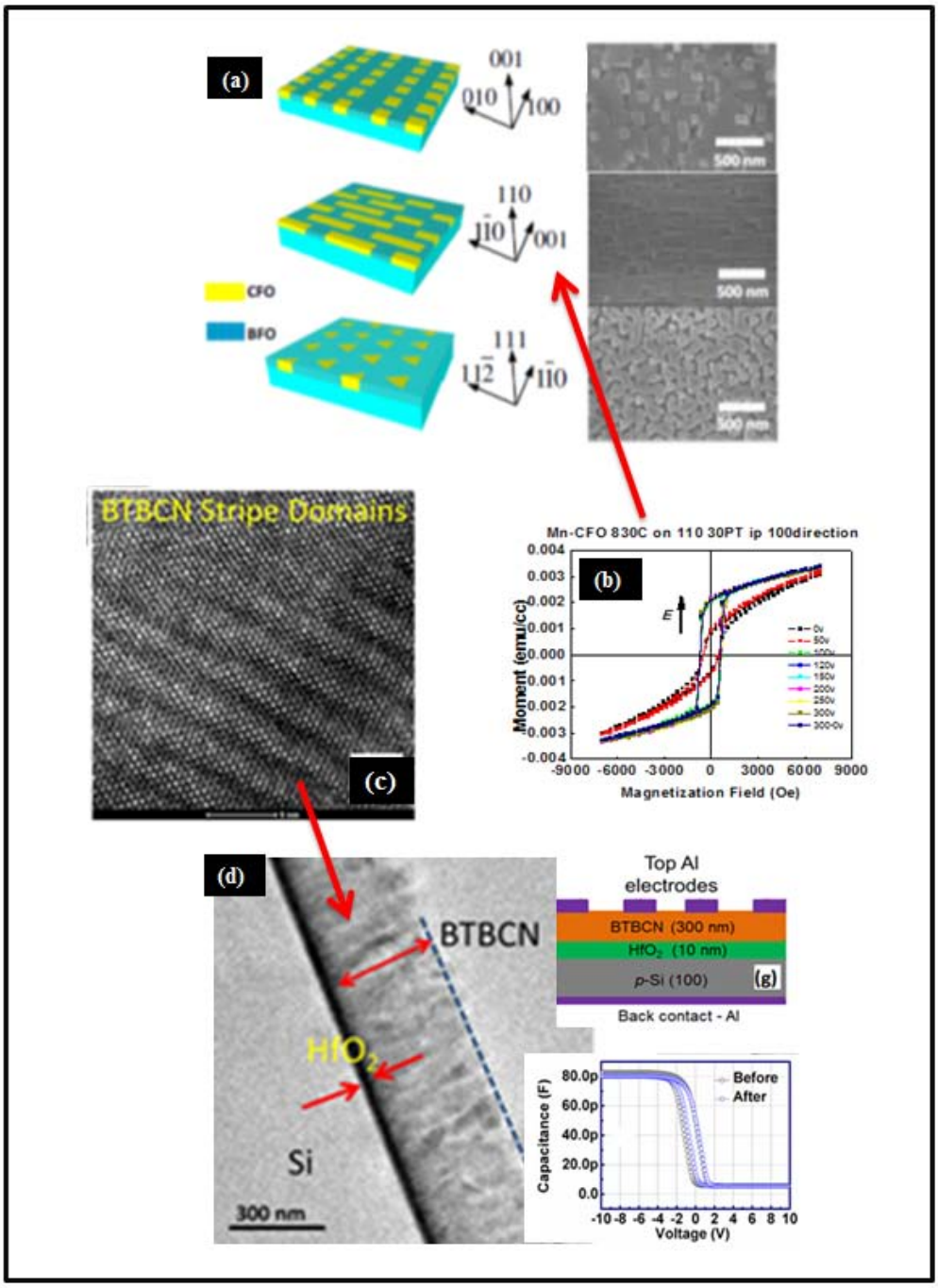

Figure 1. (a) Illustration of how CFO forms segregated rectangular, strip and triangular nanopillars embedded in a coherent BFO matrix on (001), (110) and (111) oriented substrates, respectively [1]; (b) electrical tunability of the magnetization curve of Mn-doped CFO grown on (110) PMN-x%PT substrates [2,3]; (c) HRTEM image of BT-BCN stripe nano-domains, which is helpful for fast switching; and(d) Cross-sectional TEM image of BT-BCN on HfO_2 buffered Si. Both the interfaces were found to be smooth and uniform. High resolution TEM image of the BT-BCN and HfO_2 interface along with elemental mapping of the BT-BCN/HfO_2/Si interfaces using high resolution EDS-TEM showed that there were no interfacial defects or any traceable inter-diffusion of Si; schematic of Al/BT-BCN/HfO_2/p-Si NVM; and electrical characteristics revealing good ferroelectric characteristics and memory window.

(iii) Provided fundamental understanding of the nature of magnetoelectric coupling in single phase solid solutions that lead to the design of multiferroic memory structures. The challenge of growth and alignment of perovskite (1-x)$BaTiO_3$-x$Ba(Cu_{1/3}Nb_{2/3})O_3$ (BT-BCN) thin films on HfO_2 buffered Si for non-volatile memory (NVM) was successfully met, as shown in Figs. 1 (c) and (d). Piezoelectric force microscopy (PFM), x-ray diffraction, and high resolution transmission electron microscopy demonstrated ferroelectricity in BT-BCN thin films. PFM revealed a 180^o phase change under external voltage, demonstrating domain reversal and its effectiveness for NVM. X-ray photoelectron microscopy showed band alignments between atomic-layer deposited HfO_2 and pulsed-laser deposited BT-BCN films. Programming and erasing operations were explained on the basis of the band-alignments. The structure offers a large memory window, low leakage current, and high and low capacitance values that were easily distinguishable even after ~10^6 s, indicating strong charge storage potential.

(iv) Successfully developed co-fired textured magnetostrictive/ piezoelectric/ magnetostrictive (M/P/M) laminate structures with Ag inner electrodes that exhibited self-biased characteristic. Compositions corresponding to $Pb(Mg_{1/3}Nb_{2/3})O_3$-32.5$PbTiO_3$ [PMN-PT] and $(Ni_{0.6}Cu_{0.2}Zn_{0.2})Fe_2O_3$ [NCZF] were used as piezoelectric and magnetostrictive materials respectively. Low relative permittivity <001> BT micro-crystals (ε_r= 130) were selected as templates. The in-plane magnetostrictioncoeffficient (λ_{11}) was measured in-parallel to an applied magnetic bias H_{DC} by a strain gauge method, andthe in-plane piezomagnetic coefficient ($q_{ij}= d\lambda_{ij}/dH$) was computed from the measured results, demonstrating an inherent hysteresis. The experiments illustrate the role of interfacial coupling on the ME coefficient. Silver electrode layer has much larger thermal expansion coefficient (~18 ppm) than that of piezoelectric phase (~2 ppm) and ferrites (~10 ppm), and thermal conductivity of Ag is much higher than that of piezoelectric phase and ferrite. Differential thermal expansion and thermal conductivity could result in built-in interface strain which can be modulated to assist the strain transfer mechanism and hysteretic response. We plan to conduct detailed STEM analysis measuring the charge gradient across the multi-phase interfaces to establish the correlation among the intrinsic and extrinsic variables.

Future Plans

1) Self-bias ME structures: We are investigating the self-biased magnetoelectric effect in homogenous two-phase magnetostrictive-piezoelectric (Ni-PZT) laminate structures. Experimental results illustrate the method for tuning the magnitude of self-bias effect via geometry effect and provide understanding behind the hysteretic changes. The self-biased response was found to be directly related to the nature of magnetization and can be tuned by variation in demagnetization state and the resultant differential magnetic flux distribution. In comparison with the functionally graded structure, the simple bilayer Ni-PZT self-biased laminate structure provides several advantages. To achieve this bilayer structure at the scale required for the device control, growth and optimization of high quality PZT film on magnetostrictive Ni substrate is important. Our preliminary results indicate that PZT film can be successfully synthesized on metal substrate by optimizing the growth condition and preventing the substrate oxidation. We are continuing to optimize the growth conditions and in parallel have started to quantify the local effects that control the origin of non-linearity. Our initial results

based upon the piezoresponse microscopy combined with the electrical measurements has shown the unique nature of the domain wall width in controlling the hysteretic behavior.

2) Finer two phase nanostructures with better control of phase distribution: We will try to develop smoother and flatter atomic surfaces on substrates that have been terminated for the deposition of two phase thin layers with nanostructures. Such finely tuned substrates could have significant implications in controlling the size, shape and phase distribution of vertically integrated ME nanocomposites, ME nano-chessboard structures, and vertically integrated two phases multifunctional systems (such as ZnO-CFO, ZnO-BTO, SBN-YIG). With highly ordered nano-structure aligned in out-of-plane direction, the elastic coupling between two phases are expected much stronger than any other two phase ME composites in use.

3) Integration of single phase multiferroic on semi-conducting Nb-doped $SrTiO_3$ and understand the nature of ME coupling: We were successful in demonstrating the resistive non-volatile memory effect in BT-BFO ($BaTiO_3$ – $BiFeO_3$) epitaxial thin-films grown on semiconducting Nb:STO substrates. The initial structures have shown excellent write-read memory properties by invoking polarization inversion as shown in Fig. 2. We have also demonstrated that the structure has excellent retention and switching capabilities, which pushes this technology one more step towards the realization of a meaningful future generation ReRAM device. The device operates at very low voltage of ± 1.10 V and offers high ON/OFF ratio of 1000, fast switching and excellent retention and endurance properties. The band alignment between the BT-BFO and the Nb:STOheterojunction was found to be type-II staggered type, and the operating principle and electrical transport properties of memory devices were explained. The BT-BFO/Nb:STO memory devices suppresses the cross-talk between adjacent memory cells due to the use of semiconducting Nb:STO substrate instead of metal electrode. Moreover, the BT-BFO/Nb:STOheterojunction is found to be an efficient detector for UV-detection and its fast response. The half-wave rectifier circuit was constructed using BT-BFO and it shows an excellent performance in presence of low and high-frequency signals. The obtained results provide a new pathway towards design of future generation multifunctional electronic devices such as low-power and fast switching ReRAMs, optoelectronic detectors, and high-frequency signal processors. Furthermore, the BT-BFO material shows excellent photovoltaic properties; therefore, the optical read-write ultrafast memories can also be realized. Currently, we are characterizing these structures under varying optical, magnetic and electrical conditions and hope to provide some new understanding on ME coupling that is different from the conventional strain-mediated response. These alternative approaches for ME coupling will be of higher relevance in the nanoscale structures.

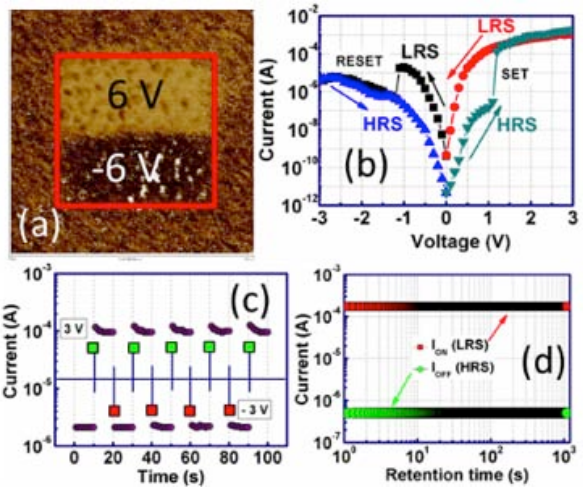

Figure 2: *(a) Memory read-write micrograph, (b) HRS-LRS-HRS current switching, (c) current switching, and (d) charge retention property*

4) *Deposition of multiferroic materials on piezoelectric substrates with memristor characteristics*: We are in the process of developing various multiferroic oxide solid solutions

onto piezoelectric crystal substrates. Our goal is to develop heterostructures that have more than two (2) stable magnetic states that can be addressed by electric field.

Publication

1. Kundu, S., Maurya, D., Clavel, M., Zhou, Y., Halder, N. N., Hudait, M. K., Banerji, P., Priya, S., Integration of lead-free ferroelectric thin films on HfO_2/Si (100) for high performance non-volatile memory applications, Scientific Reports, Vol. 5, pp. 8494 (2015).
2. M. K. Hudait, M. Clavel, Y. Zhu, P. Goley, S. Kundu, D. Maurya, and S. Priya. Integration of $SrTiO_3$ on Crystallographically Oriented Epitaxial Germanium for Low-power Device Applications, ACS Appl. Mater. Interface DOI: 10.1021/am509172 (2015).
3. Yan Zhu, Deepam Maurya, Shashank Priya, and Mantu K. Hudait. Tensile-Strained NanoscaleGe/In0.16Ga0.84As Heterostructure for Tunnel Field-Effect Transistor, ACS Appl. Mater. Interfaces, 6, 4947–4953 (2014).
4. Yuan Zhou, Yongke Yan, and Shashank Priya. Cofired magnetoelectric transformer, Applied Physics Letters, 104, 232906 (2014).
5. Y. Zhang, Z. Wang, Y. Wang, C. Luo, J.F. Li, and D. Viehland, "Electric-field induced strain modulation of magnetization in Fe-Ga/Pb(Mg1/3Nb2/3)- PbTiO3 magnetoelectricheterostructures" Journal of Applied Physics 115, 084101; doi: 10.1063/1.4866495 (2014).
6. Y. Zhu, N. Jain, M. K. Hudait, D. Maurya, R. Varghese and S. Priya "X-ray photoelectron spectroscopy analysis and band offset determination of CeO_2 deposited on epitaxial (100), (110), and (111)Ge" (J. Vac. Sci. Technol. B 32, 2014, 011217)
7. N. Jain, Y. Zhu, D. Maurya, R. Varghese, S. Priya and M. K. Hudait "Interfacial band alignment and structural properties of nanoscale TiO_2 thin films for integration with epitaxial crystallographic oriented germanium" (J. Appl. Phys. 115, 2014, 024303)
8. Y. Zhou and S. Priya, "Near-flat self-biased magnetoelectric response in geometry gradient composite" (Journal of Applied Physics, In press 2014).
9. Z. Wang, Y. Li, W. Ge, R. Viswan, J.F. Li, and D. Viehland, "Monolithic magnetoelectricheterostructure with enhanced ferroelectric and piezoelectric properties and tunable magnetic properties" Materials Letters vol. 113, pages 159-162 (2013).
10. Wang, ZG; Li, YX; Viswan, R; Hu, BL; Harris, VG; Li, JF; Viehland, D, "Engineered Magnetic Shape Anisotropy in BiFeO3-CoFe2O4 Self-assembled Thin Films", ACS Nano ACS Nano vol. 7, issue:4, Pages: 3447-3456 (2013).
11. Y. Zhou, C. S. Park, C. H. Wu, D. Maurya, M. Murayama, A. Kumar, R. S. Katiyar, and S. Priya "Microstructure and surface morphology evolution of pulsed laser deposited piezoelectric BaTiO3 films" (Journal of Materials Chemistry C, 1(39), 6308, 2013).

.

Thermodynamic, Kinetic and Electrochemical Studies on Mixed Proton, Oxygen Ion and Electron (Hole) Conductors

Anil V. Virkar, University of Utah

Program Scope

The scope of the project is to ivestigate multi-species, coupled transport in mixed proton, oxygen ion electron (hole) conductors which are candidates for fuel cells, electrolyzers and reversible cells for electrochemical energy conversion and storage. The work also includes studies on transport in cationconducting materials which have implications for sodium-sulfur and lithium-ion batteries. The work is experimental and theoretical. Transport theory is developed within the framework of linear non-equilibrium thermodynamics.

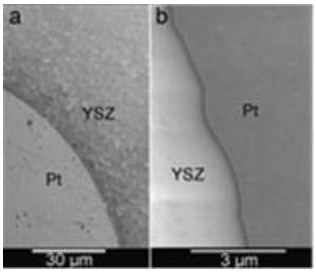

Embedded Pt probe inside a dense yttria-stabilized zirconia electrolyte

Recent Progress

Recent work has been on: (a) Calculation and measurement of chemical potentials of neutral species in ion conducting materials under equilibrium and non-equilibrium conditions. (b) Investigation of point defect distributions in oxygen ion conductors under thermodynamic non-equilibrium conditions where cation distribution is frozen and anions adjust to it. (c) Chemical potentials of neutral species depend upon low level electronic conductivity in electrolytes. We have developed a novel method involving embedded electrode to measure electronic conductivity of oxygen ion conductors at exceptionally low temperatures.This method allows the measurement of electronic conductivity without polarizing the sample unlike in prior studies [1,2].

Future Plans

1) To investigate local thermodynamics in ion conducting materials under transport (systems removed from equilibrium). The materials of interest include: (i) Mixed proton, oxygen ion and electron/hole conductors; (ii) Predominantly oxygen ion conductors, (iii) Cation conductors.
2) To synthesize ion conducting materials far removed from equilibrium.
3) To model and make property measurements on ion-conducting materials far removed from equilibrium.
4) To measure local thermodynamics and transport properties using embedded probes.

References

1) J. H. Park and R. Blumenthal, *J. Electrochem. Soc*., **136** 2867 (1989).
2) I. Valov, V. Ruhrup, R. Klein, T.-C. Rodel, A. Stork, S. Berendts, M. Dogan, H.-D. Weimhofer, M. Lerch and J. Janek, *Solid State Ionics*, **180** 1463 (2009).

Publications

1) J. H. Wright, A. V. Virkar, Q. Liu, and F. Chen, "Electrical characterization and water sensitivity of $Sr_2Fe_{1.5}Mo_{0.5}O_{6-\square}$ as a possible solid oxide fuel cell electrode", *J. Power Sources*, **237** 13-18 (2013). http://dx.doi.org/10.1016/j.jpowsour.2013.02.079

2) P. Parthasarathy and A. V. Virkar, "Vapor phase conversion of α-alumina + zirconia composites into sodium ion conducting Na-β"-alumina + zirconia solid electrolytes", *J. Electrochem.Soc.*, **160** (11) A2268-A2280 (2013).http://dx.doi.org/10.1149/2.095311jes

3) P. Parthasarathy and A. V. Virkar, "Electrochemical Ostwald ripening of Pt and Ag catalysts supported on carbon", *J. Power Sources*, **234** 82-90 (2013).

http://dx.doi.org/10.1016/j.jpowsour.2013.01.115

4) L. Zhang, F. Liu and A. V. Virkar, "Electrochemical measurements on cells, I: Simulation of potential distribution with an embedded probe", *ECS Trans.*, **58** (3) 79-91 (2013).

http://dx.doi.org/10.1149/05803.0079ecst

5) J. H. Koh, R. Abbaraju, P. Parthasarathy, and A. V. Virkar, "Design and synthesis of degradation-resistant core-shell catalysts for proton exchange membrane fuel cells", *J. Power Sources*, **261** 271-277 (2014). http://dx.doi.org/10.1016/j.jpowsour.2014.03.102

6) A. V. Virkar, H-T.Lim, and G. Tao, "Failure of solid oxide fuel cells by electrochemically induced pressure", *Procedia IUTAM*, **10** 328-337 (2014).

http://dx.doi.org/10.1016/j.piutam.2014.01.028

7) L. Zhang, L. Zhu, F. Liu and A. V. Virkar, "Improved grain boundary conductivity by post annealing: Minimizing vacancy depletion through non-equilibrium distribution of immobile species", *ECS Trans*., **61** (1) 139-150 (2014). http://dx.doi.org/10.1149/06101.0139ecst

8) L. Zhu, L. Zhang, F. Zhao and A. V. Virkar, "Concepts for ultra-high power density solid oxide fuel cells (SOFC)", *ECS Trans.*, **61** (1) 177-190 (2014). http://dx.doi.org/10.1149/06101.0177ecst

9) L. Zhu, L. Zhang, and A. V. Virkar, "Measurement of ionic and electronic conductivities of yttria-stabilized zirconia by an embedded electrode method", *J. Electrochem.Soc*., **162** (3) F298-F309 (2015).http://dx.doi.org/10.1149/2.0691503jes

Nanocrystal-based Dyads for Solar to Electric Energy Conversion

David N. Beratan, Chemistry Department, Duke University, Durham NC

Ron Naaman, Chemical Physics, Weizmann Institute of Science, Rehovot ISRAEL

David H. Waldeck, Chemistry Department, University of Pittsburgh, Pittsburgh PA

Program Scope

We are exploring nanoparticle-based materials that promise to provide a systematic and modular approach to creating a new generation of solar energy conversion devices. The project team (comprised of researchers at U. Pittsburgh, Duke Univ., and the Weizmann Institute of Science) is working to develop a systematic and quantitative approach to creating supramolecular assemblies of linked nanoparticles that function as charge transfer elements. Figure 1 illustrates features of a bulk heterojunction device architecture, in which sets of semiconductor nanoparticles self-organize at the interface of two photoconductive polymer phases. Our goal is to identify properties of the charge transfer elements and their assemblies that will allow such a device to capture the entire available range of solar irradiance and to efficiently transduce the absorbed energy to separated charges. The structure that is illustrated in Figure 1 is composed mainly of interfaces.

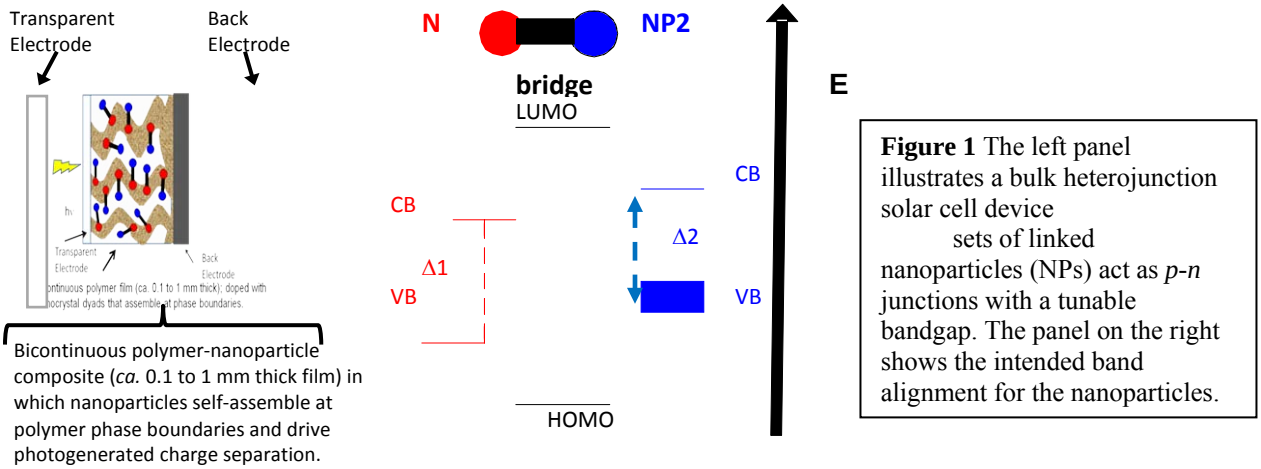

Figure 1 The left panel illustrates a bulk heterojunction solar cell device sets of linked nanoparticles (NPs) act as *p-n* junctions with a tunable bandgap. The panel on the right shows the intended band alignment for the nanoparticles.

Over the past few years, our team has experimentally and computationally explored the important NP-ligand interactions and NP-electrode interactions that control the energy level placements [1,2]. These studies have included the determination of the valence band edge (HOMO) and conduction band edge (LUMO) positions by both electrochemical methods and photoemission spectroscopy, as well as their comparison with density functional theory calculations of the structural and electronic properties of ligand capped $Cd_{33}Se_{33}$ and $Cd_{33}Te_{33}$ nanoclusters Currently, we are exploring how to engineer the NP/NP interfaces and the NP/CP interfaces to enhance charge separation and inhibit charge recombination. Particular foci of our effort are aimed at understanding the importance of energy-level gradients [2], built-in electrostatic potentials [3] and symmetry/chirality properties [4] to improve the charge-separation efficiency in inorganic-organic hybrid structures.

Recent Progress

Electric-field Effect on the Charge Transfer between Semiconductor Nanoparticles and Conjugated Polymers: Excitonic solar cells, such as organic bulk heterojunction devices, use donor-acceptor (D-A) energy offsets to facilitate electron-hole pair dissociation, whereasconventional *p-n* junction solar cells employ an internal electric field. We explored howto combine these two strategiesby using a model system (see Fig. 2), which consisted of the conjugated co-polymer (PDPPPV, donor) and CdTe semiconductor nanoparticles (NPs, acceptor). By placing charged functional groups on the polymer side chains (R) and NP surface ligands (L) during synthesis, we obtain positively(+) and negatively(-) charged polymers and NPs. If the oppositely-charged polymer and NP are mixed together in solution, they form electrostatic aggregates in which an internal electrostatic field exists at the polymer-NP (D-A) interface. In this way, we examined whether the direction of the internal field affects the charge separation driven by the D-A energy offsets (see Fig. 2). For instance, the (+)NP/(-)PDPPPV aggregates should have a favorable internal field that drives charge transfer in the same direction as the D-A energy offsets; see below. However, reversing the surface charge on both NP and PDPPPV, i.e., (-)NP/(+)PDPPPV, results in an unfavorable internal field direction that fails to align with the D-A energy offsets, and this latter case not charge transfer occurs.

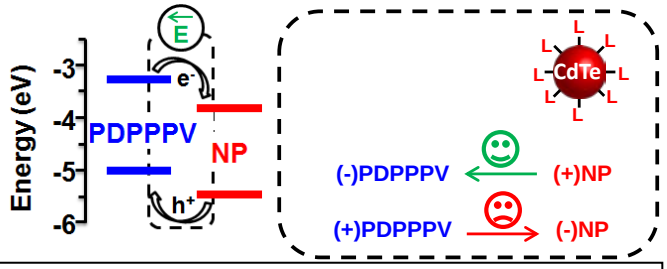

Figure 2. An energy diagram and internal electric field scheme are shown.

Figure 3 shows transient absorption spectroscopy and spectro-electrochemistry (Fig. 3) for the assembly in whichphotoinduced hole transfer occurs from (+)NP to (-)PDPPPV and produces the (-)PDPPPV radical cation, (-)PDPPPV(h). Fig. 3A shows the NIR transient absorption spectra for the (+)NP/(-)PDPPPV assembly, in which a broad transient absorption, centered at 910 nm,arises because of the absorption of (-)PDPPPV(h). Figure 3B shows a similar absorption feature arising in the NIR region as a (-)PDPPPV film is electrochemically oxidized to produce (-)PDPPPV(h). Thus, this work suggests that a dual-charge-separating force can be created at the D-A heterojunction by combining the internal field and the energy offsets.

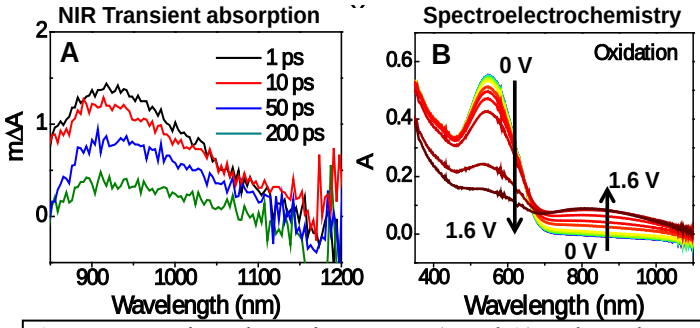

Figure 3. Transient absorption spectra (panel A) and steady-state absorption spectra (panel B) of the (-)PDPPPV radical cation are shown. See text for further details.

Chiral- Induced Spin Selectivity: We have begun a series of studies that are aimed at examining the use of chiral organic linker molecules between nanoparticles and between nanoparticles and electrodes for inducing vectorial charge transfer. Recently [5], we showed that monolayer films of oligopeptides display a spin selectivity per unit length much larger than that of nucleic acids. These studies examined the spin polarization of transmitted electrons by three different methods: photoemission spectroscopy for energies above the vacuum level, electrochemical voltammetry

for tunneling of electrons below the vacuum level through 2-D films of oligopeptides, and single molecule conductance for tunneling through single molecules. Figure 4 shows a plot of the measured spin polarization as a function of length for three different types of photoemission measurements and for the electrochemical measurements. The length dependence and the absolute spin polarization are similar for both energy regimes. Single molecule conductance studies provide an effective charge transport barrier of 0.5 eV between the two spin channels.In concert with this study, we have prepared chiral CdSe and CdTe NPs through a ligand exchange procedure from oleic acid to L or D cysteine, and we are using them to study how the chirality affects the charge transfer efficiency on Ni and Au/Ni electrodes as a function of the direction of an external applied magnetic field.

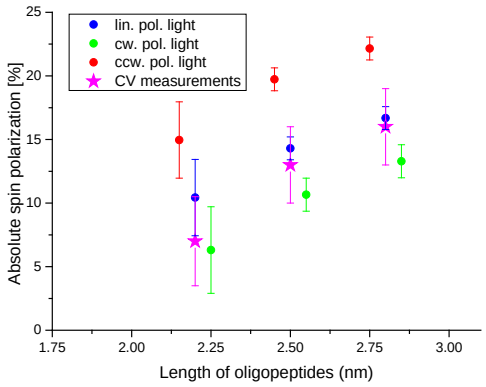

Figure 4: The length dependence of the absolute value of the longitudinal spin polarization. The results for the photoelectrons are shown for clockwise and counter clockwise circular polarized (green and red respectively) and for linear polarized light (blue). The spin polarization, in the electrochemical study, of the faradaic current at 0.13 V and 0.28 V is shown as pink stars. The sign of the polarization in the photoelectron signal was negative, while in the case of the electrochemical studies it was not determined.

Dependence of charge transfer on the number of chemical contacts and electron tunneling pathways: In recent experiments we have examined the photoinduced charge transfer between CdSe nanoparticles (NPs) and a gold substrate, when the NPs are attached to the gold via self-assembled monolayers of alkanedithiols (DT)of various lengths. Two methods were applied for measuring the charge transfer yield, surface photovoltage (SPV) and temperature dependent photoluminescence. The results demonstrate a net transfer of electrons from the NPs to the gold, under constant illumination. Interestingly the data reveal that the monolayer comprised of ten carbon methylene chains displays an unusually efficient electron transfer, which is attributed to the high local density resulting in multiple links between the NPs and the substrate [to be submitted].

A quantitative understanding of these data and a wide range of charge transfer phenomena in complex systems requires that we develop a theoretical framework to describe the delivery of multiple electrons. When electrons move over long distances through high barriers, where the probability for thermal population of oxidized or reduced bridge-localized states is very small, the electrons will tunnel from the donor (D) to acceptor (A), facilitated by bridge-mediated superexchange interactions. We have

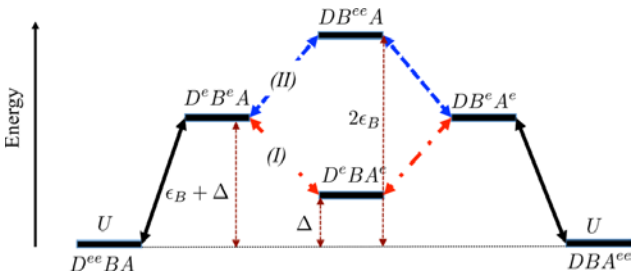

Fig 5: Schematic diagram for two electron superexchange.

developed simple superexchange models for two-electron transfer and explored how the bridge structure and energetics influence multielectron superexchange; in particular comparing two-electron superexchange with single-electron superexchange. In contrast to one-electron superexchange, two-electron superexchange involves both one- and two-electron virtual intermediate states, the number of virtual intermediates increases very rapidly with system size, and multiple classes of pathways interfere with one another. Multielectron superexchange introduces interference between singly and doubly oxidized (or reduced) bridge virtual states, so that even simple linear donor–bridge–acceptor systems have pathway topologies that resemble those seen for one-electron superexchange through bridges with multiple parallel pathways.

Future Plans

The work plan for the next year will continue to proceed on multiple fronts.

- We are pursuing efforts to incorporate favorable photonic bandgap engineering into composite nanoparticle films and quantifying their energy level structure through UPS and electrochemistry experiments.
- We will expand our studies into examining how chiral linking groups can be used to inhibit electron-hole recombination for both chiral conducting polymers and chiral nanoparticles.
- We will finalize our studies of how we may control the relative admixture of through-bond and through-space tunneling between linked NPs as a function of radius, capping groups, and surface polarization.
- We will develop coarse-grained models to assist in the design of NP pairs that favor charge separation and slow charge recombination, and we will begin to transfer these ideas to all-atom simulation to test the robustness of the concepts at the same time that they are being tested experimentally.

References

1. For example, see a) A.E. Kuznetsov and D.N. Beratan, J. Phys. Chem. C, 118, 7094-7109 (2014); b) B. P. Bloom, L.-B. Zhao, Y. Wang, D. H. Waldeck, D. N. Beratan, P. Zhang, and R.Liu J. Phys. Chem. C. (2013) 22401−22411; c) Y. Wang, Z. Xie, G. Gotesman, L. Wang, B.P. Bloom, T. Z. Markus, D. Oron, R. Naaman, and D. H. Waldeck J. Phys. Chem. C *116* (2012) 17464-17472.
2. Y. Wang, L. Wang, and D. H. Waldeck J. Phys. Chem. C 115 (2011) 18136-18141.
3. a) Y. Wang, K. Liu, P. Mukherjee, D. A. Hines, P. Santra, H. Y. Shen, P. Kamat, and D. H. Waldeck Phys. Chem. Chem. Phys. ***16*** (2014), 5066 – 5070; b) M. Wu, P. Mukherjee, D. N. Lamont, and D. H. Waldeck J. Phys. Chem. C ***114*** (2010) 5751-5759. doi: 10.1021/jp9098667
4. a) R. Naaman and D. H. Waldeck J. Phys. Chem. Lett ***3*** (2012) 2178-2187; b) R. Naaman and D. H. Waldeck, "Spintronics and Chirality: Spin Selectivity in Electron Transport Through Chiral Molecules" Ann. Rev. Phys. Chem. 66, (2015) in press.
5. M. Kettner, B. Gohler, H. Zacharias, D. Mishra, V. Kiran, R. Naaman, D. H. Waldeck, S. Sek, J. Pawlowski, and J. Juhaniewicz J. Phys. Chem. C., (2015) ASAP.

Publications

1.A. Migliore, R. Naaman, D.N. Beratan, "*Sensing of molecules using quantum dynamics"* submitted (2015).

2. R. Naaman and D. H. Waldeck, *"Spintronics and Chirality: Spin Selectivity in Electron Transport Through Chiral Molecules"* Ann. Rev. Phys. Chem. 66, (2015) in press.

3J. Lin, D. Balamurugan, P. Zhang, S.S. Skourtis, and D.N. Beratan, *"Two electron transfer pathways,"* J. Phys. Chem. B., in press (2015) (Newton/Miller Festschrift).

4. M. Kettner, B. Gohler, H. Zacharias, D. Mishra, V. Kiran, R. Naaman, D. H. Waldeck, S. Sek, J. Pawlowski, and J. Juhaniewicz*"Spin Filtering in Electron Transport through Chiral Oligopeptides"* J. Phys. Chem. C., (2015) doi:10.1021/jp509974z

5. B. Ding, Y. Wang, P.S. Huang, D. H. Waldeck, J.-K.Lee, *"Depleted Bulk Heterojunctions in Thermally Annealed PbS Quantum Dot Solar Cells"* J. Phys. Chem. C 118 (2014) 14749-14758.

6. A.E. Kuznetsov and D.N. Beratan, *"Structural and electronic $Cd_{33}Se_{33}$ and $Cd_{33}Te_{33}$ quantum dots,"* J. Phys. Chem. C, 118, 7094-7109 (2014).

7.B. Ding, T. Gao, Y. Wang, D.H. Waldeck, P. Leub, J.-K. Lee *"Synergistic Effect of Surface Plasmonic Particles in PbS/TiO2 Heterojunction Solar Cells"*Solar Energy Materials and Solar Cells 128 (2014) 386-393.

8. Y. Wang, K. Liu, P. Mukherjee, D. A. Hines, P. Santra, H. Y. Shen, P. Kamat, and D. H. Waldeck *"Driving Charge Separation for Hybrid Solar Cells: Photo-induced Hole Transfer in Conjugated Copolymer and Semiconductor Nanoparticle Assemblies"*Phys. Chem. Chem. Phys. 16 (2014), 5066 – 5070

9.B. P. Bloom, L.-B. Zhao, Y. Wang, D. H. Waldeck, D. N. Beratan, P. Zhang, and R.Liu"*Ligand Induced Changes in the Characteristic Size Dependent Electronic Energies of CdSe Nanoparticles"* J. Phys. Chem. C. (2013) 22401−22411

10. Sivan Kober, GiladGotesman, Ron Naaman, *"Surprising Molecular Length Dependence in Conduction through a Hybrid Organic-Inorganic System",* J. Phys. Chem. Lett. **4**, 2041−2045 (2013).

DOE Award DE-SC0006647, Cornell University
Charge Transfer Across the Boundary of Photon-Harvesting Nanocrystals
PI: Frank Wise, Department of Applied Physics
Co-PI's: Tobias Hanrath, Jim Engstrom
Department of Chemical and Biochemical Engineering
Cornell University, Ithaca, NY 14853
frank.wise@cornell.edu

Program Scope

The goal of this project is to understand the fundamental processes that govern interfacial charge transfer across nanocrystal (NC) boundaries. We carry out fundamental studies of charge transport in NC assemblies, and from NCs into other semiconductor materials with two principal objectives: (1) to understand and controlelectronic structure and transport properties across nanoscale interfaces, and (2) to createconfined-but-connected nanostructures that balance quantum-confinement and –couplingfor optimized light capture and charge transport. Major themes include the role of dimensionality in charge and energy transport and the physical and chemical properties of NC surfaces. The work is done in the context of photovoltaic devices, but the knowledge that we gain will also be relevant to a variety of settings, including molecular electronics, sensors, light emitters, and electrocatalysis.

Recent Progress

Square Superlattice of PbS Nanocubes

Conventional synthesis of cube-shaped lead-salt NCs is limited to >10-nm sizes. We created sub-10-nm PbS nanocubes by reacting quasi-spherical NCs with $(NH_4)_2S$, which leads to preferential growth of the (111) facets and reshapes quasi-spherical NCs into cubes. With short ligands such as octylamine, the PbS cubes organize into simple-square superlattices (Fig. 1), wherethe electronic coupling is expected to be higher than in assemblies of quasi-spherical NCs (Publication 4 below).

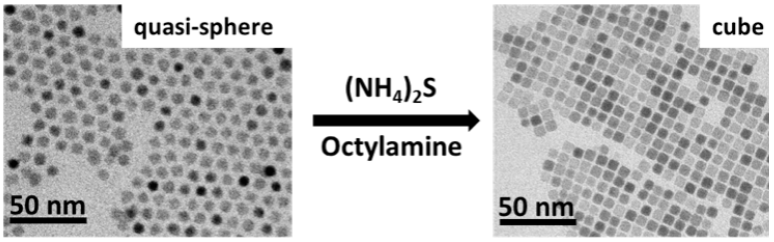

Fig. 1. Octylamine-passivated cubic PbSNCs readily organize into simple square superlattices.

Atomically-CoherentPbSeNanocrystal Superlattices

Recently, the fabrication of quasi-two-dimensional superlattices of oriented NCs with epitaxial inter-dot connections was reported by our group and one other group [1,2]. Such "atomically-coherent" assemblies can exhibit square or honeycomb symmetry. Atomistic tight-binding calculations of the electronic states of the square superlattices of cadmium-salt and lead-salt NCs imply promising transport properties [3].

Our general approach to create interconnected nanostructures combines the directed assembly and epitaxial attachment of colloidal NCs at fluid interfaces (Fig.2). This approach

allows us to assemble the NCs into superstructures with predefined symmetries (*e.g.* square, honeycomb, or linear, wire-like assemblies) and to connect neighboring NCs through exposed facets.

Advances in our understanding of the complex interrelationships of nanocrystal self-assembly, ligand displacement, particle fusion and solvent evaporation have allowed us to form confined-but-connected structures with an unprecedented degree of structural fidelity. Fig. 3 shows a large square superlattice in which proximate PbSe nanocrystals are epitaxially connected through their {100} facets. Superlattice order with a correlation distance more than 100 nm is revealed by x-ray scattering and high-resolution electron microscopy

Variable-temperature measurements of field-effect transistor structures indicate that charge-carrier transport in these films is thermally-activated, with a delocalization length of ~10 nm. These results are consistent with calculations (Publication 6), which underscores the critical role of energy and structural disorders on the properties of the assembly.

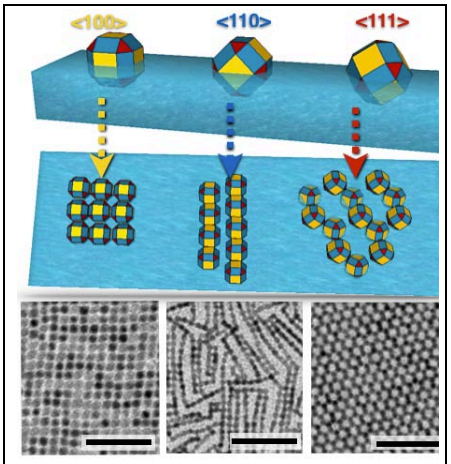

Fig.2. Creation of NC superlattice polymorphs with programmable structures. NC orientation (top) and multi-particle interactions at the fluid interface (middle) dictate the NC superstructure. TEM images of square, line, and hexagonal structures. Scale bars: 50nm (bottom).

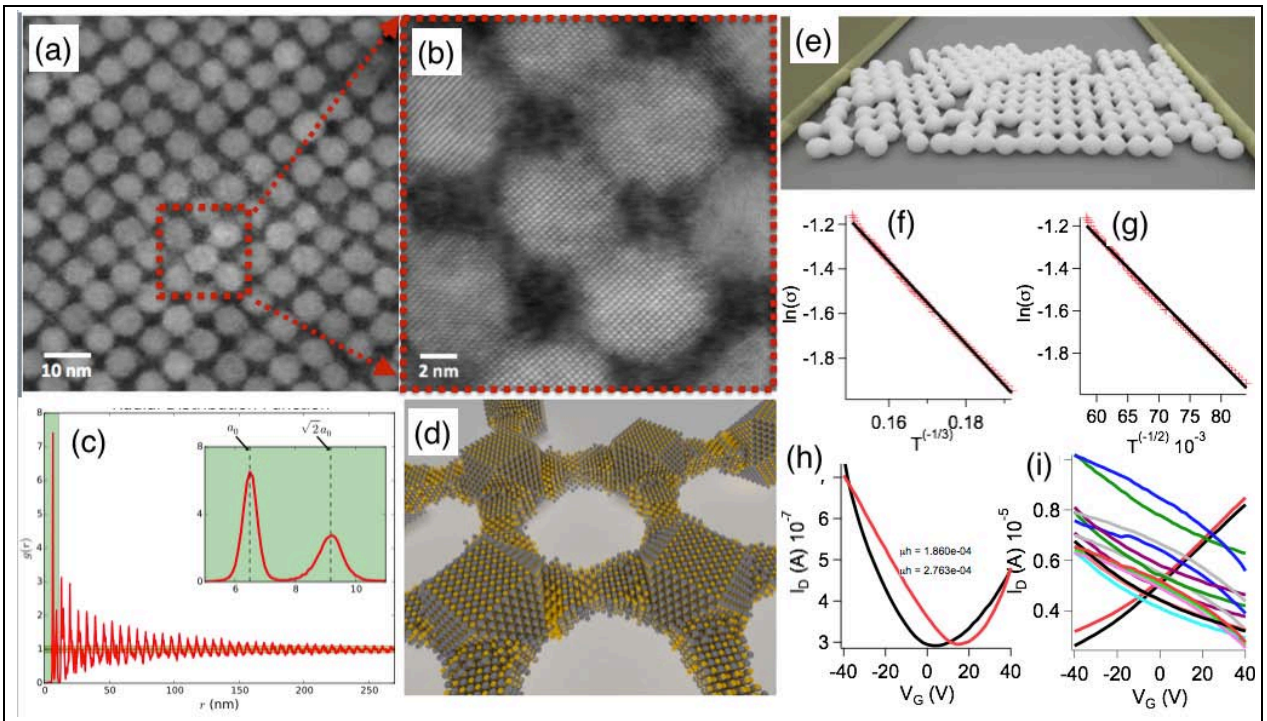

Fig.3.Epitaxially connected square PbSe superlattice (a) low-resolution and (b) high-resolution micrographs illustrate the structural fidelity of the superlattice. (c) the pair-distribution function confirms a correlation distance of more than 100 nm. (d) atomistic model of PbSe NCs connected through their {100} facets. (e) field-effect transistor device structure, (f,g) variable –temperature conductivity fits to Mott 2D and Efros-Shklovskiivariable range hopping, (h,i) the majority carrier (n-type, p-type or ambipolar) can be modulated through changes in the surface chemistry of the PbSe NC film.

Nanocrystal Surface Treatments

Ideally, NC surfaces would be terminated with atoms or molecules that passivate all surface defects while allowing strong electronic coupling of adjacent NCs. We have shown that ligand removal by ammonium sulfide treatment, followed by iodine treatment, can produce improved surfaces by creation of a thin shell of lead iodide. A smallconcentration of large NCs are added to thin films of small NCs to assess electron transport in the films [4]. A larger ratioof photoluminescence from the large NCs to that from the small NCs(PL_{large}/PL_{small}) indicates stronger inter-particle coupling, while a longer luminescence lifetime indicates reduced trap density. Our treated films exhibit both improved electron transport and reduced defect density compared to previous films (Fig. 4).

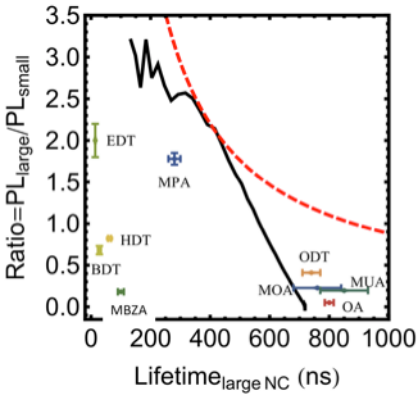

Fig.4. Luminescence ratio vs. lifetime for NC films treated by ammonium sulfide and iodine (black line). Data points for films with indicated ligands are also shown. Better films will be closer to the top right corner of the graph. The dashed red line is for a constant product of luminescence ratio and lifetime.

Development of high-pressure probe/reaction cell

We have completed the installation of the high-pressure probe/reaction cell (*i.e.*, micro-reactor, Fig. 5(a)) that we areusing in examinations of ALD infiltration reactions on NC thin films, which include ligand-displacement and exchange reactions. The probeis capable of: (i) producing reaction conditions (partial pressures, temperature) useful for vapor phase surface modification and/or thin film deposition, (ii) *in situ*, real-time measurement of thin film electrical properties, in the dark and under illumination, and (iii) fast, *in vacuo*transfer of the thin film sample to an adjacent chamber for surface analysis using X-ray photoelectron spectroscopy (XPS) and related techniques. The probe is designed to confine the gas phase reactants to a zone of ~ 1.5 cm dia. using the flow of an inert curtain gas (Fig. 5(b)).

We have used the probe in a number of experiments that demonstrate its versatility. In terms of gases that can be used in ligand exchange reactions we have exposed substrates to both ethylene diamine, $NH_2(CH_2)_2NH_2$, and ethanedithiol, $SH(CH_2)_2SH$. We have exposed a thin film of PbSnanocrystals to a flow of molecular iodine, I_2. In these experiments we were able to show that by controlling the partial pressure of I_2 and the time of exposure we could control the amount of the near surface layers that were converted to PbI_x. Finally, we have demonstrated the ability to conduct ALD, in this case, the growth of ZrO_2 using $Zr[N(CH_3)(CH_2CH_3)]_4$ and H_2O as reactants [Fig. 5(c)].

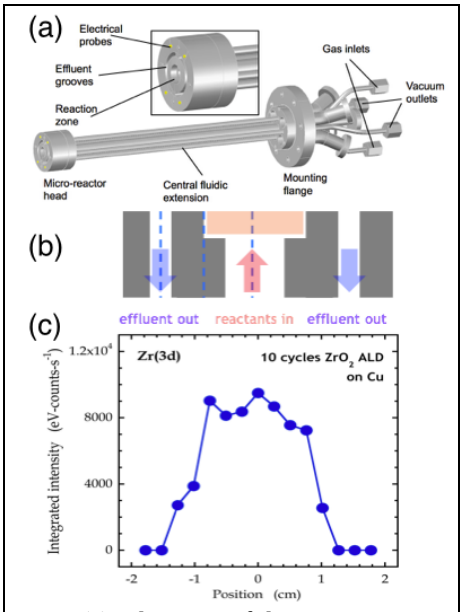

Fig. 5 (a) schematic of the micro-reactor for spatially-confined ALD (b) flow profile and and (c) photoemission from a thin film ofZr (3d)

Future Plans

Our plans for the near future include the following:

- Systematic structural, electronic, and optical characterization of the atomically-coherent structures will be completed.
- Measurements of the conductivity and mobility of the superlattices in field-effect transistor structures will be performed, and the results compared to theoretical predictions.
- Treated nanocrystal films will be assessed in photovoltaic devices.
- We will continue to investigate ALD infiltration reactions on NC thin films, includingligand displacement and exchange reactions.
- We will conduct experiments involving *in situ*, real-time measurement of thin film electrical properties, in the dark and under illumination, using the micro-reactor probe.

References

1. W. H. Evers *et al.*, "Low-Dimensional Semiconductor Superlattices Formed by Geometric Control Over Nanocrystal Attachment," *Nano Lett.*13, 2317 (2013).
2. W. J. Baumgardner, K. Whitham, T. Hanrath, "Confined-but-Connected Quantum Solids *via* Controlled Ligand Displacement," *Nano Lett.* 13, 3225 (2013).
3. E. Kalesaki*et al.*, "Electronic Structure of Atomically Coherent Square Semiconductor Superlattices with Dimensionality Below Two"*Phys. Rev. B* 88, 115431 (2013).
4. D. Zhitomirsky*et al.*, "Measuring Charge Carrier Diffusion in Coupled Colloidal Quantum Dot Solids," *ACS Nano* 7,5282 (2013).
5. C. Schliehe*et al.*, "Ultrathin PbS Sheets by Two-Dimensional Oriented Attachment," *Science* 329, 550 (2010).

Publications under DOE-BES support 2013-present

1. W. J. Baumgardner, K. Whitham, T. Hanrath, "Confined-but-Connected Quantum Solids *via* Controlled Ligand Displacement," *Nano Lett.* 13, 3225 (2013).
2. B.-R. Hyun, J. J. Choi, K. L. Seyler, L. Sun, T. Hanrath, and F. W. Wise, "Heterojunction PbS Nanocrystal Solar Cells with Oxide Charge-Transport Layers," *ACS Nano* 7, 10938 (2013).
3. K. Bian, B. T. Richards, H. Yang, W. Bassett, F. Wise, Z. Wang and T. Hanrath, "Optical properties of PbS nanocrystal quantum dots at ambient and elevated pressure," *Phys. Chem. Chem. Phys*. 16, 8515 (2014).
4. H. Zhang, J. Yang, and F. W. Wise, "Sub-10-nm monodisperse PbS cubes by post-synthesis shape engineering," *Phys. Chem. Chem. Phys.* 16, 14640 (2014).
5. B. Park, K. Whitham, K. Bian, Y.-F. Lim, and T. Hanrath, "Probing Surface States in PbS Nanocrystal Films Using Pentacene Field Effect Transistors: Controlling Carrier Concentration and Charge Transport in Pentacene," *Phys. Chem. Chem. Phys.* 16, 25729 (2014).
6. J. Yang and F. W. Wise, "Effects of disorder on electronic properties of nanocrystal assemblies," *J. Phys. Chem. C***119**, 3338 (2015).

Metal-Insulator Phase Transition: Science and Applications

Junqiao Wu

University of California, Berkeley, and Lawrence Berkeley National Laboratory

Program Scope

This is a DOE Early Career Award granted in 2011. This project seeks to uncover novel physics and develop new applications from the metal-insulator phase transition (MIT) in vanadium dioxide (VO_2) and related materials. VO_2 undergoes the VO_2 undergoes the first-order MIT at 341K, accompanied by a structural phase transition from the monoclinic, insulating (I) phase at low temperatures to the tetragonal, metallic (M) phase at high temperatures. In typical large-size bulk and/or polycrystalline VO_2 films having a high density of crystal defects and/or clamping strain, the MIT typically progresses via gradual evolution of microscopic M/I domain structures [1]. As a result, intrinsic properties of the pure M and I phases can be hidden from measurements due to ensemble averaging over the M/I domains. The large (>1%) spontaneous strain associated with the MIT may cause cracks and fatigue in VO_2 films, which are responsible for degraded electronic, thermal and electrothermal transport properties. Single-crystal VO_2 nanobeams that we developed [2, 3], on the other hand, can be made free standing [4, 5] or subjected to uniform uniaxial strain [4, 6]. The lack of extended structural defects in these materials enables them to support single-domain, abrupt MIT, allowing unambiguous assignment of the intrinsic M- and I-phase properties. By exploiting the MIT of these samples and related materials, we discover new physics and develop novel, nano-micro scale tools and devices to achieve unprecedented functionalities or capabilities for various energy technologies.

Recent Progress

1. We showed that the Wiedemann-Franz (WF) law is violated across the MIT in VO_2. In an electrically conductive solid, the WF law requires the electronic contribution to thermal conductivity to be proportional to the product of electrical conductivity and absolute temperature, where the ratio is the Lorenz number (L), typically not much different from the Sommerfeld value L_0. The WF law reflects a basic property of Fermi liquid where charge and heat are both carried by the same quasiparticles that both experience elastic scattering. At temperatures below the Debye temperature, the WF law has been experimentally shown to be robust in conventional conductors, with violations theoretically predicted [7-10] or experimentally observed in strongly correlated electron systems [11-19] or Luttinger liquids [20]. We observed dramatic breakdown of the WF law in VO_2, in which L nearly vanishes at the MIT temperature, where the electronic thermal conductivity amounts to only < ~ 5% of the value expected from the WF law. Interestingly, doping VO_2 with W partially recovers the WF law. Manuscript is in preparation (2015) [21].
2. We developed a VO_2 nanowire-based microthermometer for quantitative evaluation of electron beam heating. This microthermometer can serve as a thermal flow meter to investigate sample heating from the incident electron beam inside electron microscopes. Owing to its small size the vanadium dioxide nanowire-based microthermometer has a large measurement range and high sensitivity, making it a good candidate to explore the temperature environment of small spaces or to monitor the temperature of tiny, nanoscale objects. Published at Nature Commun., 5, 4986 (2014) [22].
3. We directly observed nanoscale Peltier and Joule effects at metal-insulator domain walls in vanadium dioxide nanobeams. Published at Nano Lett., 14, 2394(2014) [23].

4. We discovered monolayer behavior in bulk ReS_2 due to electronic and vibrational decoupling. Such vanishing interlayer coupling enables probing of two-dimensional-like systems without the need for monolayers. Published at Nature Commun., 5, 3252 (2014) [24].
5. We demonstrated powerful, multifunctional torsional micro muscles activated by phase transition. These torsional muscles combine multiple functions as torsional actuators, micro catapults, proximity sensors, as well as memristors. Being able to sense a distanced object and then respond by rotating to a different configuration, the torsional muscles simulate active neuromuscular systems with all-inorganic materials. Published at Adv. Mater. 26, 1746 (2014) [25].
6. We discovered a temperature-gated thermal rectification effect for active heat flow control using asymmetric VO_2 nanowires. To the best of our knowledge, this is the first demonstration of solid-state active-thermal devices with a large rectification (~ 20%) in the rectifier state. This temperature-gated rectifier can have substantial implications ranging from autonomous thermal management of heating and cooling systems to efficient thermal energy conversion and storage. Published at Nano Lett., 14, 4867 (2014) [26].
7. We developed a new way to gate free carrier density and light emission in monolayer semiconductors with physisorption of gas molecules. Over 100 times modulation of light emission efficiency of two-dimensional semiconducting chalcogenides was observed by physical adsorption of O_2 and/or H_2O molecules, while inert gases do not cause such effect. The O_2 and/or H_2O pressure acts quantitatively as an instantaneously reversible "molecular gating" force, providing orders of magnitude broader control of carrier density and light emission than conventional electric field gating. Unique and universal in 2D semiconductors, the effect offers a new mechanism for modulating electronic interactions and implementing optical devices. Published at Nano Lett., 13, 2831 (2013) [27].

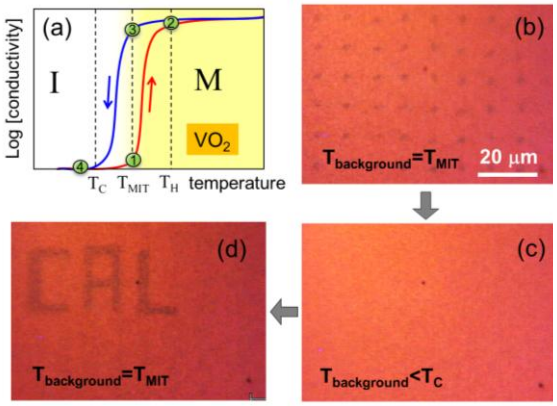

Fig.1. Photothermally rewritable metamaterials by micro-printing the metal-insulator phase transition (MIT) of a VO_2 film. (a) Schematic showing the MIT of a VO_2 film nominally occurring at T_{MIT} = 67°C but with a hysteresis of width $|T_H - T_C|$ ~ 10°C. (b) Heating a ~ 200nm-thick film to $T_{background} = T_{MIT}$, a focused laser writes a pattern of metallic phase (M, darker) onto the insulating phase (I, brighter) of VO_2. (c) Cooling the film to $T_{background} < T_C$ completely erases the M-phase pattern. (d) Heating the film back to $T_{background} = T_{MIT}$, a different M-phase pattern is written onto the same area. (K. Dong et al, unpublished (2015))

Future Plans

Utilizing the MIT in VO_2 and related materials, we will work toward an exciting new topic: 4D metamaterials --- reconfigurable 3D micro-printing of metal-insulator phase transition. We will develop photonic metamaterials that are rewritable and constructed in three dimensions, both functionalities being unprecedented but much needed in metamaterials research. Ultimately, dynamic 3D holographic imaging, for example, could be achieved using these metamaterials.

We will create these metamaterials by laser writing microstructures of metallic (M) phase inside the insulating (I) phase of a VO_2 film. As a strongly correlated electron material, VO_2 undergoes the MIT at T_{MIT} =

67°C but with a hysteresis of width $|T_H - T_C| \sim 10^oC$ (Fig.1(a)). Globally heating a VO_2 film to $T_{background} = T_{MIT}$, the film would be still in the I phase; a focused laser then photothermally writes a pattern of M phase onto the I phase. Due to the hysteresis of the MIT, the pattern would stay even if the laser is turned off, thus stabilizing the M pattern embedded in the I phase. Owing to the large contrast in nearly all physical properties between the M and I phases, the system acts as a photonic metamaterial that could diffract and scatter infrared and microwave light with the desired angle, phase shift and amplitude. Cooling the film to $T_{background} < T_C$ completely erases the M pattern, and heating the film back to $T_{background} = T_{MIT}$, a different M pattern can be written onto the same area, thus enabling rapid switching between different metamaterial configurations for desired functionalities. In the next step, we will use optics to focus the laser at different depths in the VO_2 film, so as to introduce another variation in the out-of-plane direction for 3D micro-pattering of the M phase. Taken together, a reconfigurable material can be created in three dimensions (hence the term "4D"), bringing unprecedented functionalities for manipulation of light in the infrared to microwave spectrum.

It is anticipated that a prototype of metamaterial will be demonstrated based on the MIT of VO_2 which transmits and reflects microwave beams with desired phase shifts, and the metamaterial can be repeatedly written and erased with a laser beam. Performance metrics such as spectral response, spatial resolution, maximum phase shift amount, and speed and endurance of the reconfiguration will be quantified. Feasibility of writing truly 3D metallic structures inside an insulating matrix will be tested, which paves the way to micro-printing for 3D metamaterials.

References

1 M. M. Qazilbash, et al., Science **318**, 1750 (2007).
2 B. S. Guiton, et al., J. Am. Chem. Soc. **127**, 498 (2005).
3 J. Wu, et al., Nano Lett. **6**, 2313 (2006).
4 J. Wei, et al., Nature Nanotech. **4**, 420 (2009).
5 J. Cao, et al., Nature Nanotech. **4**, 732 (2009).
6 J. H. Park, et al., Nature **500**, 431 (2013).
7 C. L. Kane, et al., Phys. Rev. Lett. **76**, 3192 (1996).
8 K. S. Kim, et al., Phys. Rev. Lett. **102**, 156404 (2009).
9 A. Garg, et al., Phys. Rev. Lett. **103**, 096402 (2009).
10 R. Mahajan, et al., Phys. Rev. B **88**, 125107 (2013).
11 Y. Zhang, et al., Phys. Rev. Lett. **84**, 2219 (2000).
12 C. Proust, et al., Phys. Rev. B **72**, 214511 (2005).
13 N. Doiron-Leyraud, et al., Phys. Rev. Lett. **97**, 207001 (2006).
14 M. A. Tanatar, et al., Science **316**, 1320 (2007).
15 X. F. Sun, et al., Phys. Rev. B **80**, 104510 (2009).
16 H. Pfau, et al., Nature **484**, 493 (2012).
17 Y. Machida, et al., Phys. Rev. Lett. **110**, 236402 (2013).
18 J. K. Dong, et al., Phys. Rev. Lett. **110**, 176402 (2013).
19 J. P. Reid, et al., arXiv:1309.6315 (2014).
20 N. Wakeham, et al., Nature Commun. **2**, 396 (2011).
21 S. Lee, et al., In preparation (2015).
22 H. Guo, et al., Nature Commun. **5**, 4986 (2014).
23 T. Favaloro, et al., Nano Lett. **14**, 2394 (2014).
24 S. Tongay, et al., Nature Commun. **5**, 3252 (2014).
25 K. Liu, et al., Adv. Mater. **26**, 1746 (2014).

[26] J. Zhu, et al., Nano Lett. **14**, 4867 (2014).
[27] S. Tongay, et al., Nano Lett. **13**, 2831 (2013).

Publications (resulting from work supported by the grant over the previous two years)

1. H. Guo, M. I. Khan, C. Cheng, W. Fan, C. Dames, J. Wu and A. M. Minor, VO2 nanowire-based microthermometer for quantitative evaluation of electron beam heating, Nature Commun., 5, 4986 (2014).
2. Tela Favaloro*, Joonki Suh*, Bjorn Vermeersch, Kai Liu, Yijia Gu, Long-Qing Chen, Kevin X. Wang, Junqiao Wu, Ali Shakouri, Direct observation of nanoscale Peltier and Joule effects at metal-insulator domain walls in vanadium dioxide nanobeams, Nano Lett., 14, 2394(2014).
3. Sefaattin Tongay, Hasan Sahin, Changhyun Ko, Alex Luce, Wen Fan, Kai Liu,Jian Zhou, Ying-Sheng Huang, Ching-Hwa Ho, Jinyuan Yan, D. Frank Ogletree, Shaul Aloni, Jie Ji, Shushen Li, Jingbo Li, F. M. Peeters, and Junqiao Wu, Monolayer behaviour in bulk ReS2 due to electronic and vibrational decoupling, Nature Commun., 5, 3252 (2014).
4. Kai Liu, Chun Cheng, Joonki Suh, Robert Tang-Kong, Deyi Fu,Sangwook Lee, Jian Zhou, Leon O. Chua, Junqiao Wu, Powerful, Multifunctional Torsional Micro Muscles Activated by Phase Transition, Adv. Mater. 26, 1746-1750 (2014).
5. Jia Zhu, Kedar Hippalgaonkar, Sheng Shen, Kevin Wang, Junqiao Wu, Xiaobo Yin, Arun Majumdar and Xiang Zhang, Temperature-Gated Thermal Rectifier for Active Heat Flow Control, Nano Lett., 14, 4867-4872 (2014).
6. Xiuqing Meng, Sefaattin Tongay, Jun Kang, Zhanghui Chen, Fengmin Wu, Shu-Shen Li, Jian-Bai Xia, Jingbo Li and Junqiao Wu, Stable p- and n-type doping of few-layer graphene/graphite, Carbon, 57, 507 (2013).
7. Sefaattin Tongay, Jian Zhou, Can Ataca, Jonathan Liu, Jeong Seuk Kang, Tyler S. Matthews, Long You, Jingbo Li, Jeffrey C. Grossman and Junqiao Wu, Broad-range modulation of light emission in two-dimensional semiconductors by molecular physi-sorption gating, Nano Lett., 13, 2831 (2013).
8. Sefaattin Tongay, Jian Zhou, Can Ataca, Kelvin Lo, Jingbo Li, Jeffrey C. Grossman, and Junqiao Wu, Thermally driven crossover from indirect toward direct bandgap in 2D semiconductors: MoSe2 versus MoS2,Nano Lett., 12, 5576 (2012).

Materials Design for Dye-Sensitized Photoelectrodes: from Solar Cells, to Solar Fuels and Solar Batteries

Yiying Wu, Department of Chemistry and Biochemistry, Ohio State University, Columbus, Ohio

Program Scope

This project is to design and synthesize materials for dye-sensitized solar cells, solar fuels and solar batteries. A major challenge in developing efficient p-type dye-sensitized solar cells (p-DSCs) is the lack of p-type wide-bandgap semiconductors with good transparency and high hole mobility. Our prior results have clearly shown that $CuGaO_2$ holds a great promise as the p-type semiconductor in p-DSCs. Therefore, in this renewal proposal, *we will systematically investigate Cu(I)-based p-type delafossite semiconductors including $CuAlO_2$, $CuGaO_2$ and $CuScO_2$. The goal is to understand the basic chemistry and crystallization process in the hydrothermal synthesis of these delafossite nanocrystals, determine their band energies, and measure the charge carrier dynamics at the semiconductor/dye/electrolyte interface.* The results will be important not only for dye-sensitized solar cells, but also for other fields such as transparent electronics, organic photovoltaics and photoelectrochemical cells for solar fuels.

Recent Progress

1: Solar Battery

--- M. Yu, X. Ren, L. Ma, Y. Wu*, "Integrating a Redox-Coupled Dye-Sensitized Photoelectrode into a Lithium-Oxygen Battery for Photo-Assisted Charging", *Nature Communications* 2014, 5:5111 (doi: 10.1038/ncomms6111).

The concept of "solar battery" represents an interesting direction of solar fuels based on the integration of photoelectrochemistry into battery redox chemistry. This recent work describes an interesting photo-assisted charging approach to address the overpotential challenge in Li-O_2 batteries (Figure 1). The novelty is in the use of a redox couple to integrate a dye-sensitized photoelectrode with the oxygen electrode in a

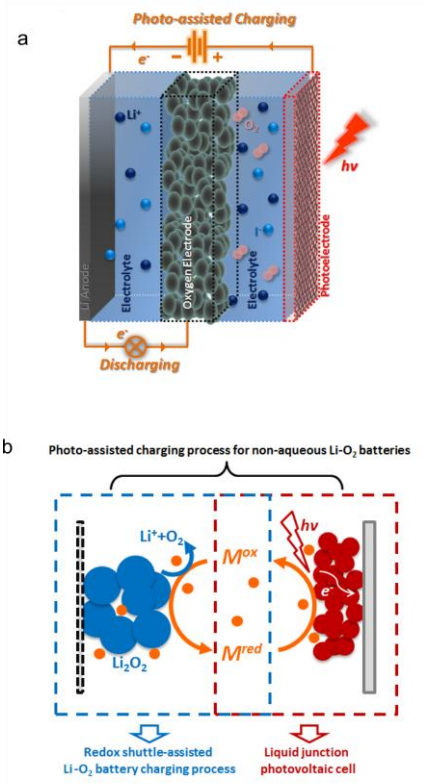

Figure 1: (**a**). Scheme of a three-electrode solar-battery; (**b**). Proposed photoelectrochemical mechanism of the photo-assisted charging process.

Li-O_2 battery. This is a unique way to utilize the solar energy to compensate the energy cost in the charging process. I am enthusiastic of this work. It shows an elegant example on how to use photoelectrochemical approaches to solve battery challenges, and represents a new direction in battery research. The concept of "solar battery" will be of broad interest to both the solar cell community and the battery community.

2: Understanding hydrothermal crystallization of $CuGaO_2$ nanocrystals

-- M. Yu, T. Draskovic, Y. Wu*, "Understanding the Crystallization Mechanism of Delafossite CuGaO2 for Controlled Hydrothermal Synthesis of Nanoparticles and Nanoplates", *Inorganic Chemistry*, **2014**, *53* (11), pp 5845–5851(DOI: 10.1021/ic500747x).

-- M. Yu, T. Draskovic, Y. Wu*, "Cu(I)-based Delafossite Compounds as Photocathodes in p-type Dye-Sensitized Solar Cells", *Physical Chemistry Chemical Physics* (Perspective) **2014**,16, 5026-5033. (**DOI:** 10.1039/C3CP55457K)

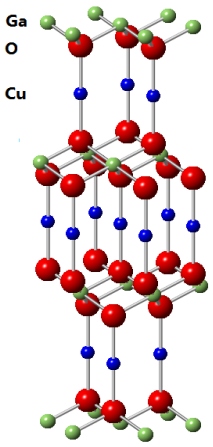

Figure 2: crystal structure of $CuGaO_2$.

In our previous study, the $CuGaO_2$-based p-DSCs have shown higher open-circuit voltages and better charge transport than the NiO-based ones. However, the large particle size of $CuGaO_2$ limits the photocurrent density. For p-DSCs, nanoparticles are desirable for efficient dye loading. Therefore, developing synthetic methods of delafossite $CuGaO_2$ with controlled sizes is important for achieving their potential. We have systematically studied the phase formation and crystal growth mechanism of delafossite $CuGaO_2$ under hydrothermal conditions. We have revealed that the stabilization of Cu^I cations in aqueous solution and the controlling of the hydrolysis of Ga^{III} species are two crucial factors that determine the phase formation. Moreover, the oriented attachment (OA) growth is proposed as the crystal growth mechanism to explain the formation of large $CuGaO_2$ nanoplates. By suppressing this OA process, we have successfully synthesized delafossite $CuGaO_2$ nanoparticles that are 20 nm in size for the first time. Considering the structural and chemical similarities between the Cu-based delafossite series compounds, the understanding of the hydrothermal chemistry and crystallization mechanism of $CuGaO_2$ should also benefit syntheses of other similar delafossites such as $CuAlO_2$ and $CuScO_2$ that have potential applications for p-DSCs.

d-4: Design of dye molecules incluing a panchromatic cyclometalated Ru(II) dye O18

-- M. He, Z. Ji, Z. Huang, Y. Wu*, "Molecular Orbital Engineering of a Panchromatic Cyclometalated Ru(II) Dye for p-Type Dye-Sensitized Solar Cells", *J. Phys. Chem. C.* (invited Article in honor of the Michael Graetzel Festschrift), **2014**, *118* (30), pp 16518–16525. (**DOI:** 10.1021/jp4117694)

-- Kevin A. Click, Damian R. Beauchamp, Benjamin R. Garrett, Zhongjie Huang, Christopher M. Hadad and Yiying Wu*, " Double-Acceptor as a Superior Organic Dye Design for p-Type DSSCs: High Photocurrents and Observed Light Soaking Effect", *Physical Chemistry Chemical Physics*, 2014, 16, 26103--26111 . (DOI: 10.1039/C4CP04010D)

Dye sensitizers are crucial for achieving high efficiency in p-DSCs. Following our early work on using cyclometalated Ru(II) complexes as sensitizers for p-DSCs, we report a panchromatic cyclometalated Ru(II) dye **O18** with the absorption tail extending to 800 nm and enhanced molar extinction coefficients. (Figure 3) In comparison to our previous best-performing **O3**, the π-conjugated system of 2,2'-bipyridyl (bpy) ligands in **O18** is extended, resulting in the stabilization of the lowest unoccupied molecular orbital (LUMO) and the increase of the absorption cross section in O18.

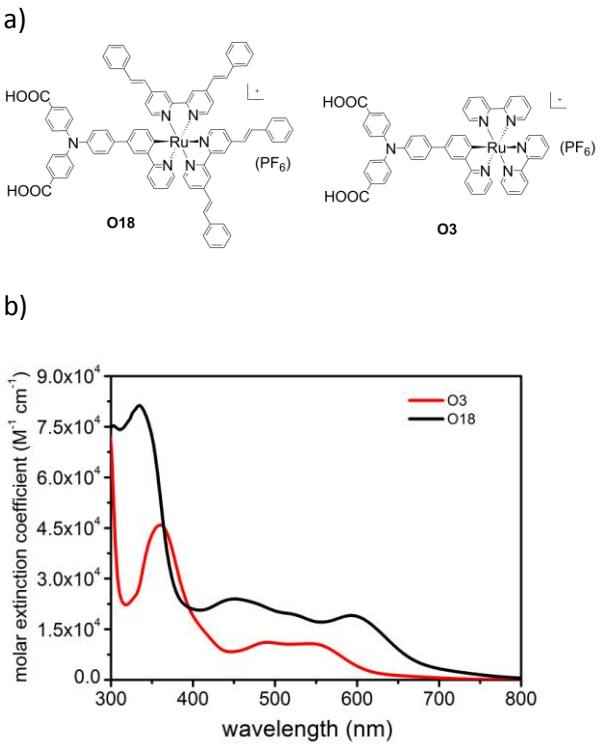

Figure 3: (a) Structures of cyclometalated Ru(II) dyes O18 and O3; b) absorption spectra of O3 and O18 in DMF.

We then carried out side-by-side comparison of p-type NiO solar cells using **O3** and **O18**. Under the same NiO film thickness, **O18**-based NiO solar cells showed much more improved short-circuit currents than **O3**-based NiO solar cells. The optimized O18-based NiO solar cells show short-circuit currents up to 3.43 mA/cm^2 and efficiencies up to 0.104%, which are the best among all cyclometalated-Ru(II)-sensitized p-type NiO solar cells. We also carried out femtosecond transient absorption spectroscopy to elucidate the electron transfer process in the dye/NiO interface. **O3** and **O18** show geminate recombination time constants of 1.7 and 1.1 ns, respectively, both of which decreased by 1 order of magnitude compared to our previous report.

Future Plans

Solar fuels and solar batteries represent the future direction of this project. Our plans include: (1) expanding the solar battery project into semiconductor photoelectrochemistry and flow batteries; (2) investigating hydrogen evolution catalysts with high turn-over frequency so that the reaction rate can match the electron flux from the dye-sensitized photoelectrodes; and (3) investigating the properties of delafossites.

Publications

1. Kevin A. Click, Damian R. Beauchamp, Benjamin R. Garrett, Zhongjie Huang, Christopher M. Hadad and Yiying Wu*, " Double-Acceptor as a Superior Organic Dye Design for p-Type DSSCs: High Photocurrents and Observed Light Soaking Effect", *Physical Chemistry Chemical Physics*, 2014, 16, 26103--26111 . (DOI: 10.1039/C4CP04010D)
2. M. Yu, X. Ren, L. Ma, Y. Wu*, "Integrating a Redox-Coupled Dye-Sensitized Photoelectrode into a Lithium-Oxygen Battery for Photo-Assisted Charging", *Nature Communications* 2014, 5:5111 (doi: 10.1038/ncomms6111).
3. M. Yu, T. Draskovic, Y. Wu*, "Understanding the Crystallization Mechanism of Delafossite CuGaO2 for Controlled Hydrothermal Synthesis of Nanoparticles and Nanoplates", *Inorganic Chemistry*, **2014**, *53* (11), pp 5845–5851(DOI: 10.1021/ic500747x).
4. M. He, Z. Ji, Z. Huang, Y. Wu*, "Molecular Orbital Engineering of a Panchromatic Cyclometalated Ru(II) Dye for p-Type Dye-Sensitized Solar Cells", *J. Phys. Chem. C.* (invited Article in honor of the Michael Graetzel Festschrift), **2014**, *118* (30), pp 16518–16525. (**DOI:** 10.1021/jp4117694)
5. M. Yu, T. Draskovic, Y. Wu*, "Cu(I)-based Delafossite Compounds as Photocathodes in p-type Dye-Sensitized Solar Cells", *Physical Chemistry Chemical Physics* (Perspective) **2014**,16, 5026-5033. (**DOI:** 10.1039/C3CP55457K)
6. J. Ahmed, C.K. Blakely, J. Prakash, S.R. Bruno, M. Yu, Y. Wu, V.V. Poltavets*, "Scalable synthesis of delafossite CuAlO2 nanoparticles for p-type dye-sensitized solar cell applications", *Journal of Alloys and Compounds* **2014**, 591, pp 275–279. (DOI: 10.1016/j.jallcom.2013.12.199).
7. Z. Ji, Y. Wu*, "Photoinduced Electron Transfer Dynamics of Cyclometalated Ruthenium(II)-Naphthalenediimide Dyad at NiO Photocathode", *J. Phys. Chem. C* **2013**, *117* (36), pp 18315–18324. (**DOI:** 10.1021/jp405659m).
8. Z. Ji, G. Natu, Y. Wu*, "Cyclometalated ruthenium sensitizers bearing triphenylamino group for p-type NiO dye-sensitized solar cells", *ACS Applied Materials and Interfaces* **2013**, *5* (17), pp 8641–8648. (**DOI:** 10.1021/am402263q).
9. Z. Ji, M. He, Z. Huang, U. Ozkan, Y. Wu*, "Photostable p-Type Dye-Sensitized Photoelectrochemical Cells for Water Reduction", *J. Am. Chem. Soc*. **2013**, 135 (32), pp 11696–11699. (DOI: 10.1021/ja404525e).

Polymeric Multiferroics

Shenqiang Ren, University of Kansas
Manfred Wuttig, University of Maryland, College Park

Program Scope

The goal of this project is to investigate room temperature magnetism andmagnetoelectric coupling of polymeric multiferroics. A new family of organic charge-transfer complexes has been emerged as a fascinating opportunity for the development of all-organic electrics and spintronics due to its weak hyperfine interaction and low spin-orbit coupling; nevertheless, direct observations of room temperature magnetic spin ordering have yet to be accomplished in organic charge-transfer complexes. Furthermore, room temperature magnetoelectric coupling effect hitherto known multiferroics, is anticipated in organic donor-acceptor complexes because of magnetic field effects on charge-transfer dipoles, yet this is also unexplored. The PIs seek to fundamental understanding of the synthetic control of organic complexes to demonstrate and explore room temperature multiferroicity.

Recent Progress

Finding 1: Spin resonance and magnetoelectricbehavior of polymeric multiferroics.

The magnetoelectric coupling effect could yield entirely new multifunctional organic material paradigms.[1-6]A significant change of electron spin resonance (ESR) is observed (Figure 1a and 1b) under external electric field, which indicates the increase of susceptibility. Taking into account the effect of thermally excited triplet bipolaron (with spin) from singlet ones (no spin), the total susceptibility can be expressed as: $\chi = \chi_p + \chi_{bp-T} \propto \frac{n_p}{T}\mu_B^2 + \frac{n_{bp-T}}{T}(2\mu_B)^2$.[7] Therefore, temperature dependent susceptibility is determined by the competition between thermally excited triplet bipolaron from singlet ones and Curie's law. If the singlet bipolaron comprises the majority (Figure 1c, red line), the susceptibility increases first and then decreases with temperature. As the temperature increases, singlet bipolarons could transfer into the triplet states to enhance the susceptibility. Our calculations confirm that thermally excited triplet bipolarons dominate the susceptibility at temperatures below 150 K, and then by Curie's law at temperatures above 150 K, which matches experimental results (Figure 1d). However, if singlet bipolarons are in the minority (Figure 1c, black and blue lines), few triplet bipolarons are transferred from singlet states.

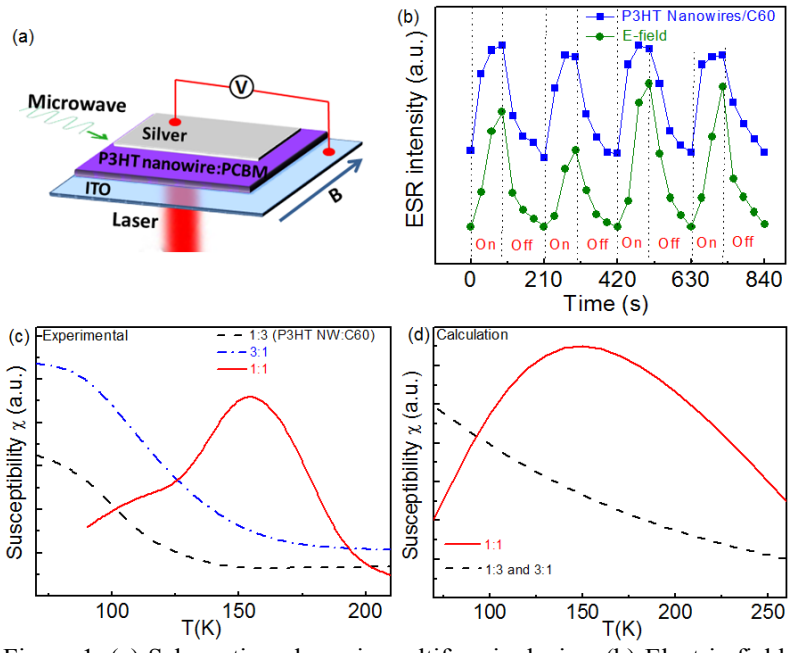

Figure 1. (a) Schematic polymeric multiferroic device. (b) Electric field controlled ESR. (c) and (d) Temperature dependent magnetic susceptibility of experimental and theoretical results, respectively.

Therefore, the susceptibility decreases with temperature based on Curie's law. Temperature dependent susceptibility is controlled by the ratio tunability between polaron and bipolaron.

Finding 2: Multiferroic charge transfer co-crystals.

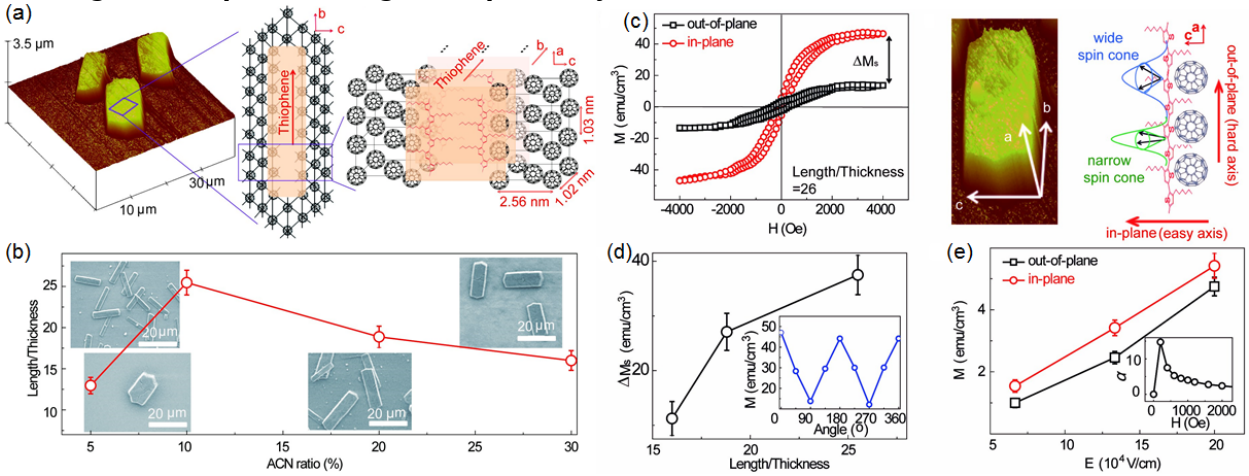

Figure 2. The structure and growth control of SCTCs. (a) Three-dimensional atomic force microscope (AFM) image of supramolecular co-crystal. (b) The dimensions and corresponding SEM images of supramolecular co-crystals at5%, 10%, 20% and 30% polar solvent loading ratios. (c) Anisotropy of magnetization, and the in-plane and out-of-plane magnetic hysteresis (M-H) loops of supramolecular co-crystal thin films. (d) the dimension control of SCTCs on magnetization, and (e) ME coupling in SCTCs.

Here, we describe three-dimensional supramolecular assembly and co-crystallization of thiophene donor and polymerized fullerene acceptor as the prototypical supramolecular charge-transfer co-crystals (SCTCs). Figure 2a shows three-dimensional atomic force microscope (AFM) image of SCTCs based on the co-crystallization of thiophene donor and polymerized C_{60} acceptor. The overall dimensions of SCTCs require a hierarchical organization and long-range non-covalent interactions between the thiophene donor and C_{60} acceptor, where the segregation stacking between the donor and acceptor molecules can be adjusted by the polar solvent loading ratios (Figure2b). The crystallized thiophene donor exhibits the monoclinic structure with the lattice constant a=1.660 nm, b=0.780 nm and c=0.863 nm, while the polymerized C_{60} acceptor adopts face-centered cubic (fcc) structure with the lattice constant 1.415 nm. The diffraction superimposes to each other between (200)-thiophene and (111)-C_{60} with a lattice mismatch less than 1.57%, meaning that a stable interfacial configuration is formed between (200)-thiophene and (111)-C_{60} structure within the co-crystals (Figure2a).

Ferromagnetism is observed in SCTCs, and the magnetic hysteresis loops were employed to elucidate the anisotropy of magnetization within SCTCs between in-plane (easy axis) and out-of-plane (hard axis) directions, as shown in Fig. 2c. The charge-lattice coupling within the crystallized thiophene nanowire chain gives rise to the spin density wave leading to the spontaneous magnetization of SCTCs. A strong (weak) charge-lattice coupling would induce a narrow (wide) spin cone, which promotes the alignment of spins within the narrow (wide) spin cone along easy (hard) axis.[8]In comparison, a decreased charge density or length/thickness ratio would broaden the spin cone along the hard axis and promote its magnetization, which narrows the ΔM_s difference between the easy axis and hard axis (Fig. 2d). Furthermore, by tuning the angle of applied magnetic field (when magnetic field is parallel to the *b*-*c* plane or the easy axis, the angle θ is set as 0^o or 180^o as shown in the inset of Fig. 2d), the saturation magnetization exhibits an angle-dependent behavior between the in-plane (easy axis) and out-of-plane (hard

axis) directions, which confirms the angular dependent spin cone orientation effect within the low symmetry of co-crystals.[9] Considering the induction of electric polarizationby spin current in the spin-current model,[10] we demonstrate room temperaturemagnetoelectric (ME) coupling effect, as shown in Fig. 2e. The tunable polarization by external magnetic field further confirms the ME coupling in supramolecular charge-transfer co-crystals (the inset of Fig.2e) as resulting from the increased triplet exciton density through external magnetic field controlled conversion from singlet to triplet charge-transfer. The optimal ME coupling coefficient α=0.148 V cm^{-1} Oe^{-1} ($\Delta E=\alpha\Delta H$) is achieved under 200 Oe bias magnetic field.To understand the origin of magnetism in SCTCs, simulations were carried out by the spin unrestricted density functional theory (DFT) framework with the GGA-PBE functionals implemented in the VASP package. The C_{60}intercalationbetween the side chains of the thiophene enhancescharge-transfer interactions to increase the density of charges in thiophenenanowires. Our results indicate that the observed magnetism likely originates from the charged crystalline thiophene nanowires. The ground state is spin-unpolarized due to the degenerate spin up and spin down energy levels. By introducing positive charges into the thiophene crystal through charge-transfer, a splitting of energy level between spin up and spin down, which results in a net magnetic moment.

Finding 3: Ultra-Low Fatigue Shape Memory Alloy Films

We discovered an ultra-low fatigue shape memory alloy system based on TiNiCuwhere Ti_2Cu precipitates mediate up to ten million complete and reproducible transformation cycles. Figure 3 compares the stress-strain curves of two NiTiCu films displaying very different fatigue characteristics. We propose that this difference andthe ultra-low fatigue of $Ti_{54}Ni_{34}Cu_{12}$films, is determined by the presence and/or absence of Ti_2Cu precipitates and the ensuing dual Austenite, B2↔Ti_2Cu↔Martensite, B19, epitaxy shown in Fig. 4. On the basis of refined X-ray (performed at APS) and TEM diffraction data we propose a scenario leading to the low fatigue state in the Ti-rich sample: Ti_2Cu coherently precipitate in the B2 matrix. The B2 matrix transforms completely to B19 aided by the simultaneous Ti_2Cu/B19 epitaxies. The B19/Ti_2Cu epitaxy provides an internal stress pattern, which stabilizes the B19 phase at low temperatures. During stress cycling, the equivalent epitaxy stabilizesalternatingly the B2 phase. At each temperature andstress the transforming phases attain equilibrium by forming a compatible morphology directed by the internal epitaxy-generated stress distribution. Complete transformation is attained at each cycle as the epitaxial stresses are reversible. Hence, we propose that the epitaxially promoted completion of the B2↔B19 phase transformation creates the low fatigue state of the $Ti_{54}Ni_{34}Cu_{12}$films. The Ti_2Cu precipitates act like

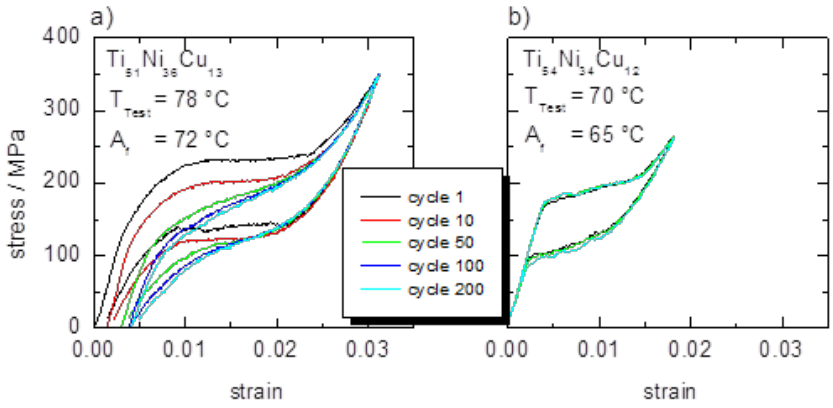

Figure 3. Stress-strain curves of tensile fatigue tests performed up to 200 cycles at test temperatures, T_{Test} larger than Austenite finish temperature A_f noted in the panels. Fatigue characteristics of near equiatomic $Ti_{51}Ni_{36}Cu_{13}$ (sample 1) films with strong fatigue behavior and mechanically stable $Ti_{54}Ni_{34}Cu_{12}$ (sample 2) films are shown.

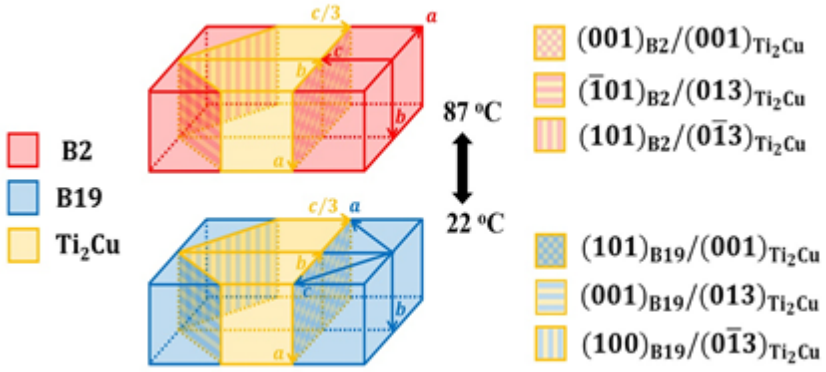

Figure 4: B2↔Ti_2Cu↔B19 epitaxies in $Ti_{54}Ni_{34}Cu_{12}$, sample 2. Color coding is shown on the left. The smallest misfit strains, calculated on the basis of lattice parameters, are

$$\varepsilon_{\parallel}[(001)_{B2}/(001)_{Ti_2Cu}] = \frac{2a(B2)}{2b(Ti_2Cu)} - 1 = 2.80\%, \quad \varepsilon_{\perp}[(001)_{B2}/(001)_{Ti_2Cu}] = \frac{b(B2)}{a(Ti_2Cu)} - 1 = 2.80\%,$$

$$\varepsilon_{\parallel}[(100)_{B19}/(0\bar{1}3)_{Ti_2Cu}] = \frac{c(B19)}{\sqrt{b^2 + (c/3)^2}(Ti,Cu)} - 1 = -1.28\%, \quad \varepsilon_{\perp}[(100)_{B19}/(0\bar{1}3)_{Ti_2Cu}] = \frac{b(B19)}{a(Ti_2Cu)} - 1 = -1.70\%.$$

sentinels assuring that the B2↔B19 transformation proceeds toward completion at each cycle. The transformation will return the film to a stress state and morphology, compatible with the pristine state. The decrease of the anisotropic peak broadening of the epitaxy-effected XRD peaks indicates trainability.

Future Plans

The co-existence of ferroelectricity and ferromagnetism in polymeric multiferroics opens up a host of new functionalities that are absent in each of the individual component. The future plans include the following:

1) magneto-dielectric coupling effect under high frequency;
2) room temperature magnetic and electric field effects;
3) magneto-transport behavior of multiferroic charge-transfer crystals;
4) further evaluations of the ultra-low fatigue in these off-stoichiometry NiTi alloy films.

References

(1) Narymbetov, B.; etc, Origin of ferromagnetic exchange interactions in a fullerene-organic compound. *Nature***2000**, *407*, 883.

(2) Mizoguchi, K.; etc, Pressure effect in TDAE-C_{60} ferromagnet: Mechanism and polymerization. *Phys. Rev. B***2001**, *63*, 140417.

(3) Mihailovic, D.; Arcon, D.; Venturini, P.; Blinc, R.; Omerzu, A.; Cevc, P., Orientational and Magnetic Ordering of Buckyballs in TDAE-C_{60}. *Science***1995**, *268*, 400.

(4) Deligiannakis, Y.; etc, Direct Observation of Electron Spin Density on TDAE Cations in the Ferromagnetic State of Solid TDAE-C_{60}. *Phys. Rev. Lett.***1999**, *83*, 1435.

(5) Kagawa, F.; Horiuchi, S.; Tokunaga, M.; Fujioka, J.; Tokura, Y., Ferroelectricity in a one-dimensional organic quantum magnet. *Nat. Phys.***2010**, *6*, 169.

(6) Lunkenheimer, P.; etc, Multiferroicity in an organic charge-transfer salt that is suggestive of electric-dipole-driven magnetism. *Nat. Mater.***2012**, *11*, 755.

(7) Qin, W.; Jasion, D.; Chen, X.; Wuttig, M.; Ren, S., Charge-Transfer Magnetoelectrics of Polymeric Multiferroics. *ACS Nano***2014**, *8*, 3671.

(8) Armstrong, J. N.; Hua, S. Z.; Chopra, H. D., Anisotropic Curie temperature materials. *Phys. Status Solidi B***2013**, *250*, 387.

(9) Callen, E. R., Anisotropic Magnetization. *J. Appl. Phys.***1960**, *31*, S149.

(10) Katsura, H.; Nagaosa, N.; Balatsky, A. V., Spin Current and Magnetoelectric Effect in Noncollinear Magnets. *Phys. Rev. Lett.***2005**, *95*, 057205.

Publications

1) Chluba, C.; Ge, W.; Miranda, R.; Strobel, J.; Kienle, L.; Quandt, E.; Wuttig, M.Ultra-Low Fatigue TiNiCuShape Memory Alloy Films, Under Review, ***Science,*** 2015.
2)Qin, W.; Chen, X; Li, H.; Gong, M.; Kirkeminde, A.; Yuan, G.; Grossman, J.; Wuttig, M.; Ren, S. Room temperature multiferroicity of supramolecular charge-transfer co-crystals. Under Review,***NatureCommunications,*** 2015.
3)Qin, W.; Gong, M.; Shastry, T.; Hersam, M.; Ren, S. Charge-transfer induced magnetic field effects of nano-carbon heterojunctions. ***Nature - Scientific Report,***2014, 4, 6126.
4)Qin, W.; Gong, M.; Chen, X.; Shastry, T. A.; Sakidja, R.; Yuan, G.; Hersam, M. C.; Wuttig, M.; Ren, S. Multiferroicity of carbon-based charge-transfer magnets. ***Advanced Materials,***2014, DOI: 10.1002/adma.201403396.
5) Qin, W.; Jasion, D.; Chen, X.; Wuttig, M.; Ren, S. Charge-Transfer Magnetoelectrics of Polymeric Multiferroics. ***ACS Nano***, 8, 3671, (2014).
6) Qin, W.; Lohrman. J.; Ren, S. Magnetic and Optoelectronic Properties of Gold Nanocluster-ThiopheneAssembly.***AngewandteChemie International Edition***, DOI: 10.1002/anie.201402685, (2014).
7) Hong, C.; Jin, X.;Totleben, J.;Lohrman, J.; Harak E.; Subramaniam, B.;Chaudhari, RV.; Ren, S. Graphene Oxide Stabilized Cu2O for Shape Selective Nanocatalysis. ***Journal of Materials Chemistry A***, 2, 7147(2014).
8) Gong, M.; Kirkeminde, A.; Kumar, N.; Zhao, H.; Ren, S. Ionic-Passivated FeS_2 Photocapacitors for Energy Conversion and Storage, ***Chemical Communications***, 49, 9260 (2013).

Enhancement of spin-lattice coupling in nanoengineered oxide films and heterostructures by laser MBE

Xiaoxing Xi, Department of Physics, Temple University, Philadelphia, PA 19122

Program Scope

The objective of the proposed research is to investigate the enhancement of magnetoelectric coupling innanoengineered oxide films and heterostructures that are predicted to show strongmagnetoelectriccoupling via control of oxygen octahedron rotations. The main focus of the project is theshort-period superlattices of $(BaTiO_3)_n/(CaMnO_3)_n$, which have been predicted by first-principlescalculations to exhibit interface-induced giant magnetoelectric coupling. The film growth technique is the atomic layer-by-layergrowth using laser MBE from separate oxide targets (for example, growing $SrTiO_3$from SrO andTiO_2targets). The atomiclayer-by-layer mode of the laser MBE growth is superior to the conventional laser MBE in achievingstoichiometry control, and it is more suitable for the synthesis of the short-period superlattices. Structural, ferroelectric, and magnetic characterizations areperformed to study the magnetoelectric coupling in these samples.

Recent Progress

1.$BaTiO_3$ and $CaMnO_3$ films grown from BaO, TiO_2, CaO, and MO_2 targets

First-principles calculations predictthatshort-period superlattices of $(BaTiO_3)_n/(CaMnO_3)_n$exhibit interface-induced giant magnetoelectric coupling via control of oxygen octahedron rotations [1]. Success in experimentally confirming this prediction will require a highly accurate control of the film sub-unit cell layering sequence and stoichiometry in each atomic layer. The atomic layer-by-layer growth method by laser MBE from separate oxide targets provides a solution to grow such a complex system.

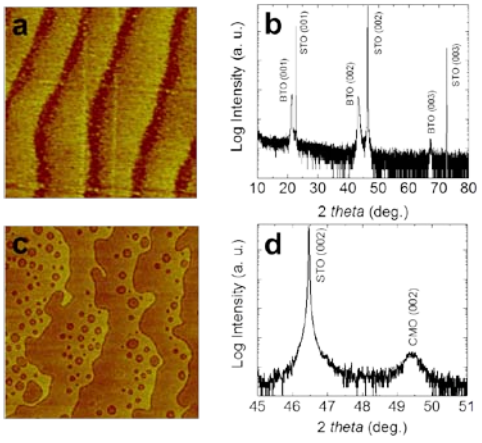

Figure 1| a) AFM image and b) XRD *theta*-2 *theta* scan of a 30 nm $BaTiO_3$ film grown from BaO and TiO_2 targets on $SrTiO_3$ substrate. c) AFM image and d) XRD *theta*-2 *theta* scan of a 30 nm $CaMnO_3$ film grown from CaO and MnO_2 targets on $SrTiO_3$ substrate.

The starting point of building the $(BaTiO_3)_n/(CaMnO_3)_n$ short-period superlatticesis to construct $BaTiO_3$ films and $CaMnO_3$ films separately in an atomic layer-by-layer manner. Figure 1a shows an AFM image over a 2 um x 2 um area of a 30 nm stoichiometric $BaTiO_3$film grown on a $SrTiO_3$ substrate by laser ablating BaO and TiO_2 targets sequentially. Atomically flat surface was achieved with step height of 1 u.c. and Rq=0.2 nm. In the x-ray diffraction (XRD)spectrum in Fig. 1b, only sharp peaks for the $BaTiO_3$ film wereobserved besides the substrate peaks, indicating a single phase structure. The same approach has also been applied on the growth of $CaMnO_3$ films. Figure 1c shows an AFM imageover a 10 um x 10 um area of a 30 nm $CaMnO_3$ film grown by laser ablating CaO and MnO_2 targets sequentially. Atomically flat surface with step height 1 u.c. and rms roughness of 0.2 nm was achieved in this system as well. In Fig. 1d, the XRD θ-2θ scan again shows the phase purityof the film.

2.$(BaTiO_3)_1/(CaMnO_3)_1$superlattices

With the confidence of growing the two construction blocks $BaTiO_3$ and $CaMnO_3$ separately and maintaining both the structure purity and surface smoothness in them, a 80 u.c. $(BaTiO_3)_1/(CaMnO_3)_1$superlatticewas grown on a $SrTiO_3$ substrate. Figure 2a shows a schematic of the superlattice. As indicated in the schematic, the superlattice was constructed in an atomic layer-by-layer manner, namely, in a sequence of BaO-TiO_2-CaO-MnO_2. The sequence repeats itself for 80 times. Figure 2b shows the RHEED intensity oscillation during the growth of the superlattice. Each oscillation period (one bigger oscillation and one smaller oscillation for the specular spot, and one oscillation and a relatively flat part for the diffracted spot) indicates the growth of 1 u.c. of the superlattice. Such a repeatable oscillation pattern lasts during the entire 80 u.c. superlattice growth process, indicating the repeated atomic layer construction sequence.

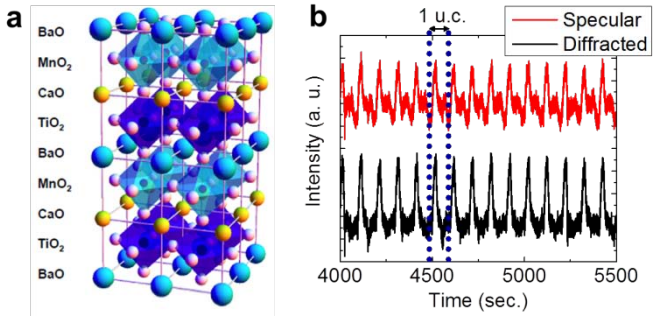

Figure 2| a) A schematic of the $(BaTiO_3)_1/(CaMnO_3)_1$superlattice,b) RHEED intensity oscillations during the growth of a $(BaTiO_3)_1/(CaMnO_3)_1$superlattice film on a $SrTiO_3$ substrate.

3.$LaAlO_3/SrTiO_3$interface with different $LaAlO_3$stoichiometry

The atomic layer-by-layer deposition by laser MBE from separate oxide targets allows for stoichiometry control not available when ablating from a single compound target. An excellent example is the growth of $LaAlO_3/SrTiO_3$interface with different $LaAlO_3$stoichiometry from La_2O_3 andAl_2O_3 targets. Since the first report of the 2D electron gas formation at the $LaAlO_3/SrTiO_3$ interface [2], most published results have been produced byPLD/laser MBE from single $LaAlO_3$ target.Recent studies show that the stoichiometry is a key factor in the interface properties [3]. PLD/laser MBE from single $LaAlO_3$target relies on tuning growth pressure and laser energy density to achieve stoichiometry, which may simultaneously introduce extrinsic defects. $LaAlO_3/SrTiO_3$ interfaces fabricated at different groupsoften showed contradictory results. Growing $LaAlO_3$ films one atomic layer at a time from LaO and Al_2O_3 targets, we tune the stoichiometry by varying the numbers of laser pulses used to ablate each target without changing the growth conditions. Using our method, the 2D growth modewas mainteined up to 38 mTorr. At such oxygen pressure,a 3D island growth is normally observed in the traditional PLD growthfrom a $LaAlO_3$target [4]. Figure 3 shows the dependence of a) sheet resistance, b) carrier density, c) hall mobility on temperature, for $LaAlO_3$films of different stoichiometry. In our process,as shown in Fig. 3b, high carrier density similar to theoretical prediction (~2 x 10^{14} cm^{-2})was achieved. The high oxygen pressure during the growth help to eliminate potential oxygen

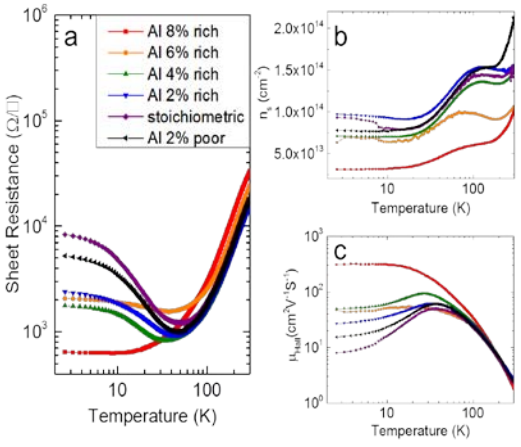

Figure 3| Transport properties of a series of 10 u.c. epitaxial $LaAlO_3$films with different stoichiometry on$SrTiO_3$ substrates. a)Sheet resistance, b) carrier density, andc) mobility, as a function of temperature.

vacancy in the$SrTiO_3$ substrate.In contrast, the traditional PLD growth from a $LaAlO_3$target at high oxygen pressure leads to drastically reducedcarrier density [5].

4.Growth of Ruddlesden-Popper compound $La_5Ni_4O_{13}$

The atomic layer-by-layer growth method by laser MBE was further testedby the growth of a sample from RP series of $La_{n+1}Ni_nO_{3n+1}$, with *n*=4. Figure4a shows a schematic of this $La_5Ni_4O_{16}$ structure, and Fig.4b shows the RHEED diffraction spot oscillations during the growth of 4 u.c. $La_5Ni_4O_{16}$ on $LaAlO_3$ substrate. RHEED oscillations maintained the shape and intensity during the growth of 50 u.c. film.As shown in Fig. 4c, XRD θ-2θ scan confirmed the phase purity of the50 u.c. $La_5Ni_4O_{16}$ film by showing all the RP phase-related x-ray diffraction peaks from (0010) to (0028) without peak splitting.The n>=4 RP $La_{n+1}Ni_nO_{3n+1}$compounds have never been reported in the literature.

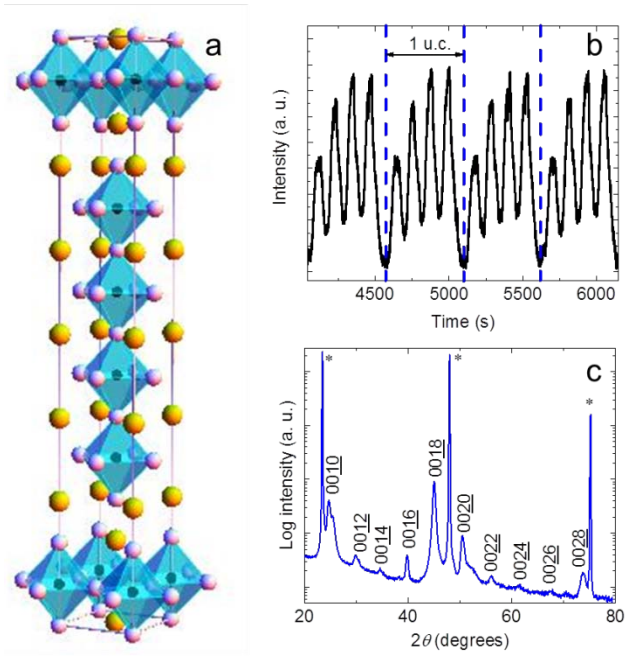

Figure 4| RP phase of $La_{n+1}Ni_nO_{3n+1}$ (n=4). a) A schematic of $La_5Ni_4O_{13}$ phase.b) RHEED oscillations during the growth of a $La_5Ni_4O_{13}$ film on $LaAlO_3$ substrate. c) XRD *theta*-2 *theta* scan of the $La_5Ni_4O_{13}$ film.

Future Plans

1. Complete the publications of results on Atomic Layer-by-Layer Growth by Laser MBE from Separate Oxide Targets, which includes the examples of $LaAlO_3/SrTiO_3$interface with different $LaAlO_3$stoichiometryand Growth of Ruddlesden-Popper compound $La_5Ni_4O_{13}$,and on Epitaxial Strain and Its Relaxation at the $LaAlO_3/SrTiO_3$ Interface.
2. Optimize the growth of $(BaTiO_3)_n/(CaMnO_3)_n$superlatticesand measure their structural, ferroelectric, and magnetic properties to explore the interface-induced giant magnetoelectric couplingpredicted by first-principles calculations.

References

[1]Hongwei Wang *et al., EPL* **100,** 17005 (2012).
[2]A. Ohtomo and H. Y. Hwang,*Nature* 427, 423 (2004).
[3] M.P. Warusawithana*et al.*, *NatureCommun.*4, 2351 (2013).
[4] Ariando*et al.*,*NatureCommun*. 2, 188 (2011).
[5] A. Brinkman *et al.*,*NatureMater.*6, 493 (2007).

Publications

1. Q. Y. Lei, G. Z. Liu, X. X. Xi, "Structural Characterization of Homoepitaxial $SrTiO_3$ Films Grown by Pulsed Laser Deposition",*Integr. Ferroelectrics*141:1, 128-133(2013)
2. M. Golalikhani1, Q. Y. Lei, G. Chen, J. E. Spanier, H. Ghassemi, C. L. Johnson, M. L. Taheri,

and X. X. Xi, “Stoichiometry of $LaAlO_3$ films grown on $SrTiO_3$ by pulsed laser deposition”, *J. Appl. Phys.* **114**, 027008 (2013).
3.Qingyu Lei, Maryam Golalikhani, Guozhen Liu, Dongyue Yang, Ke Chen, Bruce Davison, Andrew Farrar, Dmitri Tenne, Suilin Shi, Fuqiang Huang, Rakesh Singh, JiandongGuo, D. G. Schlom, Xiaoxing Xi,“Building nanoscale oxide thin films and heterostructures by laser molecular beam epitaxy using separate targets”, *in preparation*.
4. Guozhen Liu, Ke Chen, Qingyu Lei, Dongyue Yang, and X. X. Xi, “Epitaxial Strain and Its Relaxation at the $LaAlO_3/SrTiO_3$ Interface”, *in preparation*.

Sub-wavelength Metamaterial Physics and Applications

Xiang Zhang

Materials Sciences Division, Lawrence Berkeley National Laboratory

Department of Mechanical Engineering, University of California, Berkeley

Program Scope

The spectacular on-going development of metamaterials provides an exciting gateway to realize unique and unprecedented optical properties and functionalities not existing in natural materials. Our program is setup to explore novel physics in optical metamaterials. The fundamental discoveries from the proposed research will have profound impact on a wide range of applications in accord with DOE's strategic plans, such as high speed optical communications, imaging and nanophotonics for energy conversion with high efficiency.

Recent Progress

In recent years, metamaterials have shown novel nonlinear properties such as phase-mismatch-free nonlinear generation, new quasi-phase matching capabilities and large nonlinear susceptibilities. However, the understanding of nonlinear metamaterials is still in its infancy, with no general conclusion on the relationship between linear and nonlinear properties. The key question is then whether one can determine the nonlinear behavior of these artificial materials from their exotic linear behavior. We show that it is possible to predict the relative nonlinear susceptibility of large classes of metamaterials using nonlinear scattering theory[1], which allows efficient design of metamaterials with strong nonlinearity for important applications such as coherent Raman sensing, entangled photon generation and frequency conversion.

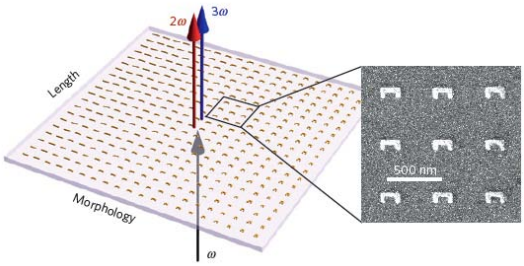

Nonlinear scanning confocal experiment used to demonstrate nonlinear scattering theory. DOI: 10.1038/NMAT4214 (2015)

Future Plans

We will use the developed experimental and theoretical methods to predict and demonstrate other perturbative parametric processes in nanostructures, including multiple-wave mixing and parametric down-conversion in arbitrary nanostructures.

References

1. Roke, S., Bonn, M. &Petukhov, A. V. Nonlinear optical scattering: The concept of effective susceptibility. Phys. Rev. B 70, 115106 (2004).

Publications

- Xiaobo Yin, Ziliang Ye, Junsuk Rho, Yuan Wang, Xiang Zhang, "Photonic Spin Hall Effect at Metasurfaces", **Science**, 339, 1405-1407 (2013).
- Xiaobo Yin & Xiang Zhang, "Unidirectional light propagation at exceptional points", **Nature Materials**, 12, 175-177 (2013).
- Haim Suchowski, Kevin O'Brien, Zi Jing Wong, Alessandro Salandrino, Xiaobo Yin, Xiang Zhang, "Phase Mismatch–Free Nonlinear Propagation in Optical Zero-Index Materials", **Science**, 342, 1223-1226 (2013).
- Ziliang Ye, Ting Cao, Kevin O'Brien, Hanyu Zhu, Xiaobo Yin, Yuan Wang, Steven G. Louie & Xiang Zhang, "Probing excitonic dark states in single-layer tungsten disulphide," **Nature**, 513, 214-218 (2014).
- Kevin O'Brien, N. D. Lanzillotti-Kimura, Junsuk Rho, Haim Suchowski, Xiaobo Yin, and Xiang Zhang, "Ultrafast acousto-plasmonic control and sensing in complex nanostructures," **Nature Communications**, 5, 4042 (2014).
- HamidrezaRamezani, Hao-Kun Li, Yuan Wang, and Xiang Zhang, "Unidirectional Spectral Singularities", **Physical Review Letters**, 113, 263905 (2014).
- Kevin O'Brien, Haim Suchowski, Junsuk Rho, Alessandro Salandrino, BoubacarKante, Xiaobo Yin & Xiang Zhang, "Predicting nonlinear properties of metamaterials from the linear response", **Nature Materials**, AOP.DOI: 10.1038/NMAT4214 (2015).

Tailoring Thermal Radiative Properties with Doped-Silicon Nanowires

Zhuomin Zhang zhuomin.zhang@me.gatech.edu
George W. Woodruff School of Mechanical Engineering
Georgia Institute of Technology, Atlanta, GA 30332

Program Scope

Aligned doped-silicon nanowire (D-SiNW) arrays form a hyperbolic metamaterial in the mid-infrared and have unique thermal radiative properties, such as broadband omnidirectional absorption, low-loss negative refraction, etc. A combined theoretical and experimental investigation will be performed to characterize D-SiNW arrays and other metamaterials for tailoring thermal radiative properties. Both the finite-difference time-domain method and the effective medium theory will be used to study wave propagation, energy density, and radiation absorption in the inhomogeneous medium. Near-field thermal radiation between anisotropic materials with hyperbolic dispersions will also be predicted for potential application in energy harvesting. This project aims at realizing D-SiNW-based metamaterials for thermal radiation control as well as for near-field imaging in the mid-infrared region. Other metamaterials, such as graphene, multilayered structures, and gratings or the combination will also be considered.

The activities and findings summarized below focus on the theoretical calculations that help the fundamental understanding of nanoscale thermal radiation. Fabrication and characterization of the D-SiNW structures are still underway.

Recent Progress

Low-loss, all-angle negative refraction can be achieved in the mid-infrared region using D-SiNW arrays with a hyperbolic dispersion. Three mechanisms contribute to such unique phenomenon: loss-enhanced transmission, impedance matching, and absence of resonances [1]. Potential applications include enhanced near-field radiative transfer, local cooling, thermal imaging, and design of infrared flat lenses and collimators. In the far field, broadband and tunable absorption has been predicted in the mid-infrared based on D-SiNWs [2]. Nanostructured materials can greatly enhance radiative heat transfer at nanometer distances, especially with D-Si nanowires and nanoholes due to the nature of their hyperbolic dispersion, which results in broadband near-field heat flux enhancement [3].

Metallodielectric photonic crystals can also exhibit hyperbolic dispersions and propagating waves may exist at extremely large lateral wavevectors and resulting in greatly enhanced near-field radiative heat transfer. However, one of the concerns is that this could also give rise to large lateral displacement and penetration depth of the photon energy. Energy streamlines trace the direction of the Poynting vector inside the structure to depict the propagation of evanescent waves. The energy streamlines can also be used to describe the flow of electromagnetic energy through a structure when wave propagation does not follow ray optics (i.e., geometric optics). Bright et al. [4] obtained expressions for the dyadic Green's functions in uniaxial anisotropic effective media, separated by a small vacuum gap according to the fluctuation-dissipation theorem. Surprisingly large lateral displacement of the energy streamlines has been demonstrated in the emitter, from about –5000 to + 5000 times the vacuum gap distance. The mechanisms have been elucidated using doped silicon with a lossless dielectric as the periodic multilayered

structure whose anisotropic dielectric functions are described by the effective medium theory (EMT). The potentially large penetration depth and lateral shift of photons associated with hyperbolic metamaterials suggest that both lateral and vertical characteristic dimensions need be sufficiently large for the structure to be treated as one-dimensional [4]. Homogenization based on EMT has been widely used both in the far field to predict the optical properties and in the near field to predict the heat flux. The characteristic thermal wavelength given by Wien's law is indeed much longer than the dimension of the unit cell. However, in the near field, large wavevector modes featured with small effective wavelength can effectively tunnel through the vacuum gap and often dominate the radiative energy transfer. The applicability of EMT for near-field radiation has been evaluated by comparison with exact solutions for metallodielectric multilayered metamaterials, and quantitative criteria have been obtained for both the hyperbolic modes and surface modes [5]. In addition to D-Si nanostructures, carbon nanotubes and graphite also exhibit hyperbolic dispersion and can enhance near-field thermal radiation [6].

Graphene has attracted great attention in nanoelectronics, plasmonics, and energy harvesting. Large near-field radiative heat transfer between graphene-covered corrugated silica (SiO_2) has been demonstrated using the exact scattering theory [7]. The radiative heat flux between graphene-covered submicron SiO_2 grating and bulk SiO_2 at the gap distance of d = 100 nm is shown in Fig. 1 as a function of the graphene chemical potential. In the calculation, the temperatures of the emitter and receiver are set at 310 K and 290 K, respectively. The period of the grating is 500 nm, and the depth and width of the trench are 500 nm and 300 nm, respectively. The heat flux for graphene-covered gratings can be nearly six times as high as that between bulk silica. The underlying mechanism is mainly attributed to the improved photon tunneling of modes away from SiO_2 phonon resonance bands due to graphene plasmons.

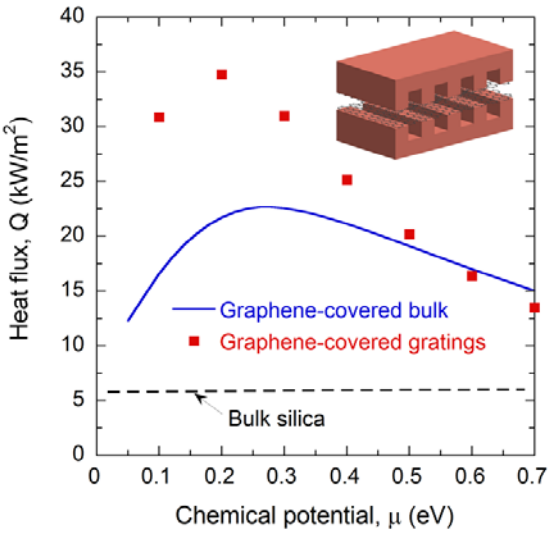

Fig. 1. Predicted heat flux between graphene-covered gratings, graphene-covered bulk silica, and bulk silica at a gap spacing d = 100 nm as a function of the chemical potential of graphene [7].

It was postulated that graphene sheets covering broadband hyperbolic substrates can further improve near-field photon transport by extending the number of tunneling evanescent modes. Figure 2(a) illustrates two graphene-covered semi-infinite D-SiNW arrays separated by a vacuum gap. The near-field transmission coefficient contour is shown in Fig. 2(b) in terms of the angular frequency and parallel wavevector component β, divided by the wavevector in free space k_0. In the calculation, the temperatures of both the emitter and receiver are near room temperature, the doping concentration of the D-SiNWs is 10^{20} cm^{-3} with a filling ratio of 0.02, the chemical potential of graphene is 0.3 eV, and the vacuum spacing d is 200 nm. The transmission coefficient is close to unity across a broad frequency range up to 1.5×10^{14} rad/s and a large wavevector space up to $20k_0$. All the photons emitted in this regime will be absorbed, which gives a blackbody behavior in the near field. As a result, the calculated heat transfer coefficient of this hybrid structure is much greater than that for plain D-SiNWs or suspended graphene sheets alone [8].

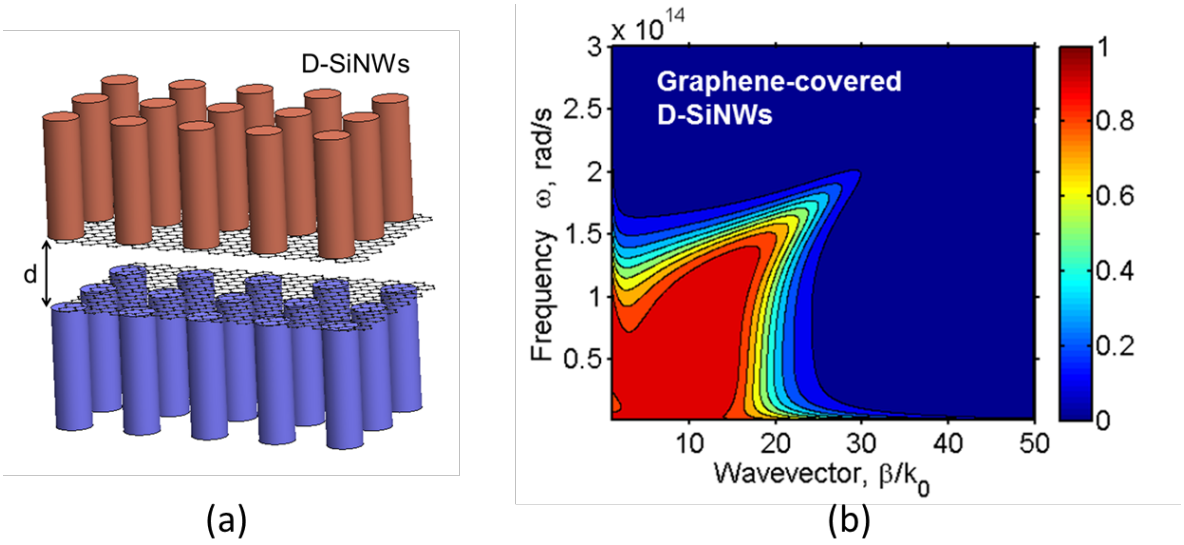

Fig. 2. (a) Illustration of the graphene-covered semi-infinite D-SiNW arrays separated by a vacuum gap *d*. (b) Contour plot of the TM polarization tunneling transmission coefficient of doped graphene (μ = 0.3 eV) on D-SiNWs separated by a 200 nm vacuum gap. The broad triangular region of near-unity transmission attests to the hybridization of hyperbolic and surface plasmon modes [8].

In addition to enhancing near-field radiative transfer, it is shown that covering graphene on top of a Ag grating or 2D pillar array will improve both the magnitude and coherence of the transmitted infrared radiation [9]. The underlying mechanism of this anomalous blocking-assisted transmission is attributed to the excitation of localized magnetic resonances, as demonstrated by comparison of an effective circuit model with the rigorous coupled-wave simulation. Strong electromagnetic fields exist inside the slit region when magnetic resonances are excited. The transmission enhancement is alignment-free and can be actively tuned by changing the chemical potential of graphene through electric gating. The findings discussed above suggest possibilities for more efficient contactless thermal management and photon energy harvesting based on graphene-covered metamaterials in both the near- and far-field regimes [7-9].

Extensive studies have also been carried out through this project on how to improve the efficiency of near-field thermophotovoltaic (TPV) systems using a back-side reflector, design of far-field TPV emitters based on a 2D tungsten metamaterials, design of broadband infrared polarizers with extremely high extinction ratios, materials and structures for near-field thermal rectifiers, as well as experimental investigations of the spectral radiative properties of thin films and subwavelength structures [10-19].

Future Plans

Experiments are underway to demonstrate broadband and tunable absorption from the near- to mid-infrared region based on doped silicon nanowires. Low-cost nanosphere lithography is used to fabricate silicon nanowires with various diameters and lengths. Introduction of phosphorous with different levels of concentration will be done through the diffusion of P_2O_5 at 1100 °C to dope the silicon nanowires with phosphorous atoms. The absorptance of the fabricated silicon nanowires on silicon substrates will be measured using facilities in the PI's lab. Further theoretical investigation is also undergoing to simulate near-field heat flux and forces between nanostructures.

Publications (supported by the DOE-BES contract)

1. X.L. Liu and Z.M. Zhang, "Metal-free low-loss negative refraction in the mid-infrared region," Appl. Phys. Lett. **103**, 103101 (2013).
2. X.L. Liu, L.P. Wang, and Z.M. Zhang, "Wideband tunable omnidirectional infrared absorbers based on doped-silicon nanowire arrays," J. Heat Transfer **135**, 061602 (2013).
3. X.L. Liu, R.Z. Zhang, and Z.M. Zhang, "Near-field radiative heat transfer with doped-silicon nanostructured metamaterials," Int. J. Heat Mass Transfer, **73**, 389 (2014).
4. T.J. Bright, X.L. Liu, and Z.M. Zhang, "Energy streamlines in near-field radiative heat transfer between hyperbolic metamaterials," Opt. Express **22**(S4), A1112 (2014).
5. X.L. Liu, T.J. Bright, and Z.M. Zhang, Z.M., "Application conditions of effective medium theory in near-field radiative heat transfer between multilayered metamaterials," J. Heat Transfer **136**, 092703 (2014).
6. X.L. Liu, R.Z. Zhang, and Z.M. Zhang, "Near-field thermal radiation between hyperbolic metamaterials: Graphite and carbon nanotubes," Appl. Phys. Lett. **103**, 213102 (2013).
7. X.L. Liu and Z.M. Zhang, "Graphene-assisted near-field radiative heat transfer between corrugated polar materials," Appl. Phys. Lett. **104**, 251911 (2014).
8. X.L. Liu, R.Z. Zhang, and Z.M. Zhang, "Near-perfect photon tunneling by hybridizing graphene plasmons and hyperbolic modes," ACS Photonics **1**, 785 (2014).
9. X.L. Liu, B. Zhao, and Z.M. Zhang, "Blocking-assisted infrared transmission of subwavelength metallic gratings by graphene," J. Opt. **17**, 035004 (2015).
10. T.J. Bright, L.P. Wang, and Z.M. Zhang, "Performance of near-field thermophotovoltaic cells enhanced with a backside reflector," J. Heat Transfer **136**, 062701 (2014).
11. B. Zhao, L.P. Wang, Y. Shuai, and Z.M. Zhang, "Thermophotovoltaic emitters based on a two-dimensional grating/thin-film nanostructure," Int. J. Heat Mass Transfer **67**, 637 (2013).
12. B. Zhao and Z.M. Zhang, "Study of magnetic polaritons in deep gratings for thermal emission control," J. Quant. Spectrosc. Radiat. Transfer **135**, 81 (2014).
13. L.P. Wang and Z.M. Zhang, "Thermal rectification enabled by near-field radiative heat transfer between intrinsic silicon and other materials," Nanoscale Microscale Thermophys. Eng. **17**, 337 (2013).
14. X.L. Liu, B. Zhao, and Z.M. Zhang, "Wide-angle near infrared polarizer with extremely high extinction ratio," Opt. Express **21**, 10502 (2013).
15. H. Wang, X.L. Liu, L.P. Wang, and Z.M. Zhang, "Anisotropic optical properties of silicon nanowire arrays based on the effective medium approximation," Int. J. Therm. Sci. **65**, 62 (2013).
16. L.P. Wang and Z.M. Zhang, "Measurement of coherent thermal emission due to magnetic polaritons in subwavelength microstructures," J. Heat Transfer **135**, 091014 (2013).
17. H. Wang, X.L. Liu, and Z.M. Zhang, "Absorption coefficient of crystalline silicon at wavelengths from 500 nm to 1000 nm," Int. J. Thermophys. **34**, 213 (2013).
18. J.I. Watjen, T.J. Bright, Z.M. Zhang, C. Muratore, and A.A. Voevodin, "Spectral radiative properties of tungsten thin films," Int. J. Heat Mass Transfer **61**, 106 (2013).
19. T.J. Bright, J.I. Watjen, Z.M. Zhang, et al. "Infrared optical properties of amorphous and nanocrystalline Ta_2O_5 thin films," J. Appl. Phys. **114**, 083515 (2013).

Author Index

Author Index

Participant List

Participant List

Name	Organization	E-mail Address
Ager, Joel	Lawrence Berkeley National Laboratory	jwager@lbl.gov
Alberi, Kirstin	National Renewable Energy Laboratory	Kirstin.Alberi@nrel.gov
Anlage, Steven	University of Maryland	anlage@umd.edu
Atwater, Harry	California Institute of Technology	haa@caltech.edu
Balke, Nina	Oak Ridge National Laboratory	balken@ornl.gov
Barnett, Scott	Northwestern University	s-barnett@northwestern.edu
Bergman, Leah	University of Idaho	lbergman@uidaho.edu
Boehme, Christoph	University of Utah	boehme@physics.utah.edu
Brener, Igal	Sandia National Laboratories	ibrener@sandia.gov
Ceder, Gerbrand	Massachusetts Institute of Technology	gceder@mit.edu
Chen, Youping	University of Florida	ypchen2@ufl.edu
Chen, Gang	Massachusetts Institute of Technology	kekex@mit.edu
Chiang, Yet-Ming	Massachusetts Institute of Technology	ychiang@mit.edu
Chien, Chia-Ling	Johns Hopkins University	clchien@jhu.edu
Chrzan, Daryl	University of California, Berkeley/LBNL	dcchrzan@berkeley.edu
Click, Tammy	ORISE	tammy.click@orau.org
Cohn, Joshua	University of Miami	cohn@physics.miami.edu
Crommie, Michael	University of California, Berkeley	crommie@berkeley.edu
Cronin, Stephen	University of Southern California	scronin@usc.edu
Eastman, Jeffrey	Argonne National Laboratory	jeastman@anl.gov
Efros, Alexander	U.S. Naval Research Laboratory	Efros.Alexander@nrl.navy.mil
Egami, Takeshi	University of Tennessee/ORNL	egami@utk.edu
Fan, Sanhui	Stanford University	Shanhui@stanford.edu
Fecko, Chris	U.S. Department of Energy	christopher.fecko@science.doe.gov
Giebink, Noel	Penn State University	ncg2@psu.edu
Gokirmak, Ali	University of Connecticut	ali.gokirmak@uconn.edu
Horwitz, James	U.S. Department of Energy	james.horwitz@science.doe.gov
Jena, Purusottam	Virginia Commonwealth University	pjena@vcu.edu
Jiang, Hongxing	Texas Tech University	hx.jiang@ttu.edu
Karma, Alain	Northeastern University	a.karma@neu.edu
Knezevic, Irena	University of Wisconsin - Madison	irena.knezevic@wisc.edu
Kortan, Refik	U.S. Department of Energy	refik.kortan@science.doe.gov

Koschny, Thomas	Ames Lab, Iowa State University	koschny@ameslab.gov
Law, Matt	University of California, Irvine	lawm@uci.edu
Leone, Stephen	LBNL/University of California, Berkeley	srl@berkeley.edu
Li, Qiang	Brookhaven National Laboratory	qiangli@bnl.gov
Lin , Shawn-Yu	Rensselaer Polytechnic Institute	sylin@rpi.edu
Liu, Feng	University of Utah	fliu@eng.utah.edu
Liu, Jianlin	University of California, Riverside	jianlin@ece.ucr.edu
Ma, Evan	Johns Hopkins University	ema@jhu.edu
Majetich, Sara	Carnegie Mellon University	sara@cmu.edu
Malko, Anton	The University of Texas at Dallas	anton.malko@utdallas.edu
Maroudas, Dimitrios	University of Massachusetts, Amherst	maroudas@ecs.umass.edu
Mascarenhas, Angelo	National Renewable Energy Laboratory	angelo.mascarenhas@nrel.gov
McCluskey, Matthew	Washington State University	mattmcc@wsu.edu
Mishin, Yuri	George Mason University	ymishin@gmu.edu
Nurmikko, Arto	Brown University	Arto_Nurmikko@brown.edu
Padilla, Willie	Duke University	willie.padilla@duke.edu
Pecharsky, Vitalij	Ames Laboratory/Iowa State University	vitkp@ameslab.gov
Priya, Shashank	Virginia Tech	spriya@vt.edu
Rand, Barry	Princeton University	brand@princeton.edu
Ren, Shenqiang	University of Kansas	shenqiang@ku.edu
Ren, Zhifeng	University of Houston	zren@uh.edu
Sandhu, Sunil	Stanford University	sunil.sandhu@stanford.edu
Scarpulla, Michael	University of Utah	scarpulla@eng.utah.edu
Severs, Linda	ORISE	linda.severs@orau.org
Shi, Jing	University of California, Riverside	jing.shi@ucr.edu
Shi, Li	The University of Texas at Austin	Lishi@mail.utexas.edu
Smalyukh, Ivan	University of Colorado	ivan.smalyukh@colorado.edu
Srikanth, Hariharan	University of South Florida	sharihar@usf.edu
Stadler, Shane	Louisiana State University	stadler@phys.lsu.edu
Stern, Nathaniel	Northwestern University	n-stern@northwestern.edu
Stockman, Mark	Georgia State University	mstockman@gsu.edu
Suzuki, Yuri	Stanford University	ysuzuki1@stanford.edu
Tang, Ming	Rice University	mingtang@rice.edu
Tyson, Trevor	New Jersey Institute of Technology	tyson@njit.edu
Van de Walle, Chris	University of California, Santa Barbara	vandewalle@mrl.ucsb.edu
Viehland, Dwight	Virginia Tech	Viehland@mse.vt.edu

Virkar, Anil	University of Utah	anil.virkar@utah.edu
Waldeck, David	University of Pittsburgh	dave@pitt.edu
Wang, Zhong Lin (ZL)	Georgia Institute of Technology	zlwang@gatech.edu
Willets, Katherine	Temple University	kwillets@temple.edu
Wise, Frank	Cornell University	frank.wise@cornell.edu
Wong, Stanislaus	Brookhaven National Laboratory	sswong@bnl.gov
Wu, Junqiao	University of California, Berkeley	wuj@berkeley.edu
Wu, Yiying	Ohio State University	wu@chemistry.ohio-state.edu
Wuttig, Manfred	University of Maryland	wuttig@umd.edu
Xi, Xiaoxing	Temple University	xiaoxing@temple.edu
Yap, Yoke Khin	Michigan Technological University	ykyap@mtu.edu
Zhang, Xiang	LBNL/University of California, Berkeley	xzhang4@lbl.gov / xzhang@me.berkeley.edu
Zhang, Zhuomin	Georgia Tech	zhuomin.zhang@me.gatech.edu
Zhou, Miao	University of Utah	phy.miaozhou@gmail.com
Zidan, Ragaiy	Savannah River National Laboratory	ragaiy.zidan@srnl.doe.gov